



# PEM Fuel Cells

Theory and  
Practice

---

FRANO BARBIR

# Foreword

There are two key problems with continued use of fossil fuels, which meet about 80% of the world energy demand today. The first problem is that they are limited in amount and sooner or later will be depleted. According to the estimates by petroleum companies, the production of the most conveniently utilizable fossil fuels, petroleum and natural gas, will peak sometime between the years 2015 and 2020 and then begin to decrease. This means that there will be a gap between demand and production of fluid fuels, beginning around 2015.

The second problem is that fossil fuels are causing serious environmental problems, such as global warming, climate changes, melting of ice caps, rising sea levels, acid rains, pollution, ozone layer depletion, oil spills, forest and agricultural land damage caused by surface mining of coal, and so on. It is estimated that the worldwide environmental damage adds up to some five trillion dollars per year.

Early in the 1970s Hydrogen Energy System had been proposed as a solution for these two interconnected global problems. Since then, during the last quarter of last century, through research and development work in universities and research laboratories around the world, foundations of the Hydrogen Energy System have been established. Earlier this century, conversion to the Hydrogen Economy began.

Hydrogen is an excellent energy carrier with many unique properties. It is the lightest, most efficient, and cleanest fuel. One of its unique properties is that through electrochemical processes, it can be converted to electricity in fuel cells with higher efficiencies than conversion of fossil fuels to mechanical energy in internal combustion engines or to electrical energy in thermal power plants. This unique property of hydrogen has made hydrogen fuel cells the automotive power plant of choice for car companies. It has also made fuel cells the power plant of choice for companies manufacturing power plants for the future. The reason for higher efficiency of hydrogen fuel cells is that they are electrochemical engines, not heat engines, and as such they are not subject to Carnot Cycle limitations. Consequently, it is expected that during the present century fuel cells will

replace the heat engines (viz., internal combustion engines, steam turbines, and gas turbines) as hydrogen replaces fossil fuels.

Research has been conducted and is currently being conducted into several types of fuel cells, such as alkaline fuel cells, proton exchange membrane (PEM) fuel cells, phosphoric acid fuel cells, molten carbonate fuel cells, solid oxide fuel cells, and so forth. Some of them are already commercialized, whereas others are close to commercialization. They are expected to find applications in almost every energy utilizing plant and/or device, from power plants to cars and homes, from laptop computers to mobile phones.

PEM fuel cells in particular have desirable properties. They operate at relatively low temperatures, which makes them easier to contain and reduces thermal losses. They are also smaller in volume and lighter in weight, which make them perfect for automotive and portable applications. That is why all the hydrogen fuelled buses and cars on the market by major companies are powered by PEM fuel cells and why about 90% of fuel cell research and development work involves PEM fuel cells. Consequently, today's and tomorrow's engineers engaged in energy engineering should be thoroughly knowledgeable in PEM fuel cells, just as the energy engineers of yesterday had to have thorough knowledge of heat engines.

The author of this book *PEM Fuel Cells: Theory and Practice*, Dr. Frano Barbir, is a well-established Hydrogen Energy scientist. After receiving his Ph.D. degree in Hydrogen Energy, he has been closely involved in PEM fuel cell research and development work in fuel cell companies. He has also seen the need for educating engineers in fuel cell technologies. As a result, he has developed and taught senior/graduate level courses on fuel cells in two universities. Consequently, he is well qualified to write an authoritative textbook on PEM fuel cells. The book starts with the fundamentals of PEM fuel cells, and then covers materials, operations, modeling, design, and applications. It is a well-written, comprehensive, and well-laid-out look into PEM fuel cells.

Consequently, I strongly recommend this textbook on PEM fuel cells to all senior/graduate level engineering students whether they are mechanical, electrical, chemical, industrial, environmental, or energy engineers, who are studying energy conversion and energy applications. The library of any engineer and researcher involved in power generation, vehicle automotive power plants, and power units for portable systems would also be well served by this textbook.

*Dr. T. Nejat Veziroğlu*  
*Director*

*UNIDO-International Centre for Hydrogen Energy Technologies*  
*Istanbul, Turkey*  
*February 2005*

# Preface and Acknowledgments

The idea for this book came about many years ago. Over the years of working as an engineer, researcher, scientist, and a company executive, I gave numerous presentations about fuel cell technology, progress, and perspectives. I immensely enjoyed preparing the presentations, organizing my thoughts and views, and supporting them with facts and graphics. In doing so I always had an audience in mind. I tailored my presentations to suit the audience and designed them to be simple and easy to follow. This book is a direct result of those numerous presentations. I take pleasure in sharing my enthusiasm about this new and exciting technology, and I particularly treasure teaching this new technology to the next generation—young engineers I have worked with, and the students I have had the opportunity to advise and teach. After all, they will be the ones implementing this technology and benefiting from it.

For nine years I worked for Energy Partners, a small, privately owned company in West Palm Beach, Florida. It was an amazing educational experience: a sandbox for the engineers. Instead of learning from books (at that time there were no books on fuel cells) we learned from the fuel cell itself. We started with a working fuel cell, a cubic foot magic box that sometimes had a mind of its own. My job was to make it do what we wanted it to do. In order to do that, I had to learn everything about fuel cells: their theory, materials, components, design, operation, diagnostics, supporting system, and so on—everything I did not get a chance to learn while I was in school. Of course, I could not have done it alone. I enjoyed sharing what I had learned with my young colleagues as much as I enjoyed learning together with them. Soon, we made the world's first PEM fuel cell-powered passenger automobile, followed by an extended golf-cart/people transporter, and several utility vehicles (John Deere Gators). Every new vehicle was leaps and bounds better than the previous one, and through this process I accumulated knowledge. It is unfortunate that at one time we were expected to start making profit, which the fuel cell technology was not yet capable of. Not at that time. Nevertheless, I am grateful to Mr. John H. Perry, Jr., the owner of Energy Partners, for allowing me to have such fun and to learn so much.

In my career I had a chance to work with and learn from many outstanding engineers and scientists, and I would like to take this opportunity to thank them:

- Prof. T. Nejat Veziroğlu, professor at University of Miami, and now the Director of UNIDO-International Centre for Hydrogen Energy Technologies, for inspiring me with the idea of hydrogen economy, in the times when hydrogen economy was more like science fiction, and for being my mentor all these years;
- Late Prof. Harold J. Plass, Jr., then professor at University of Miami, for teaching me simplicity in engineering analyses;
- Late Prof. Howard T. Odum, then professor at University of Florida, Gainesville, for overwhelming depth and clarity of his visions;
- Floyd Marken, then chief engineer at Energy Partners, for his wisdom and common sense engineering;
- Dr. Mario Nadal, then principal electrical engineer at Energy Partners, for numerous lunch discussions and for taking care of the electrical side of the fuel cell system with such ease that I never felt the urge to get involved in electrical aspects of fuel cell engineering;
- Dr. Hongtan Liu, professor at University of Miami, my colleague and friend from student days, for coming to work with me and our pioneering work in applying CFD techniques in fuel cell modeling;
- Vince Petraglia, then vice president of Energy Partners, for sharing his wealth of fuel cell experience and wisdom, summarized in the following statement: “A fuel cell is sensitive to change of every its color”;
- Dr. George Joy, then president of Energy Partners, for believing in me and including me in the company management team;
- Trent Molter, one of the founders of Proton Energy Systems, and now my colleague at Connecticut Global Fuel Cell Center, for giving me the opportunity to come to Connecticut with my team of engineers, and for a wealth of information about fuel cells in their early days.

A very special thanks go to people who made direct contributions in writing this book, namely:

- Dr. Wilson Chiu, assistant professor at University of Connecticut, who contributed a good chunk of the Chapter 7 Fuel Cell Modeling;
- Niloufar Fekrazad, graduate student at University of Connecticut, who also contributed to the Fuel Cell Modeling chapter;
- Xinting Wang and Richard Fu, graduate students at University of Connecticut, who willingly dug for various data whenever I needed them;

- Dr. Haluk Görgün, postdoctoral researcher at Connecticut Global Fuel Cell Center, for enthusiastically running the lab while I was busy finishing this book, and for contributing to Section 9.4 Electrical Subsystem;
- Ana Barbir, my daughter, and also an engineer, who proofread most of my manuscript in its various stages of development, corrected my English grammar, and made many useful comments on how to improve it.

These acknowledgments would not be complete without thanking my wife Georgia, my life companion of thirty-something years, for taking care of all other aspects of our lives while I was involved in writing this book. Without her constant encouragement and support this book would never have happened. This book is dedicated to her.

*Frano Barbir  
University of Connecticut  
Storrs, CT  
February 2005*

# CHAPTER 1

## 1. Introduction

### 1.1. What Is a Fuel Cell?

A fuel cell is an electrochemical energy converter that converts chemical energy of fuel directly into DC electricity. Typically, a process of electricity generation from fuels involves several energy conversion steps, namely:

1. combustion of fuel converts chemical energy of fuel into heat,
2. this heat is then used to boil water and generate steam,
3. steam is used to run a turbine in a process that converts thermal energy into mechanical energy, and finally
4. mechanical energy is used to run a generator that generates electricity.

A fuel cell circumvents all these processes and generates electricity in a single step without involving any moving parts (Figure 1-1). It is this simplicity that attracts attention. Such a device must be simpler, thus less expensive and far more efficient than the four-step process previously depicted. Is it really? Today—not really! Or better, not yet. But fuel cells are still being developed. This book intends to provide a basis for engineering of fuel cell devices. It includes state-of-the-art designs and materials (as they exist at the time of this writing), which are likely to change in the future as this technology continues to develop (perhaps even sooner than the students using this book as a textbook get jobs in the fuel cell industry). However, the engineering basis will not change, at least not dramatically and not so quickly. The knowledge of engineering principles will allow future fuel cell engineers to adopt these new designs and new materials and, we hope, come up with even newer designs and materials. This is what the purpose of an engineering education should be. This book will not teach the principles of thermodynamics, catalysis, electrochemistry, heat transfer, fluid mechanics, or electricity conduction, but it will apply those engineering disciplines in the engineering of a fuel cell as an energy conversion device.

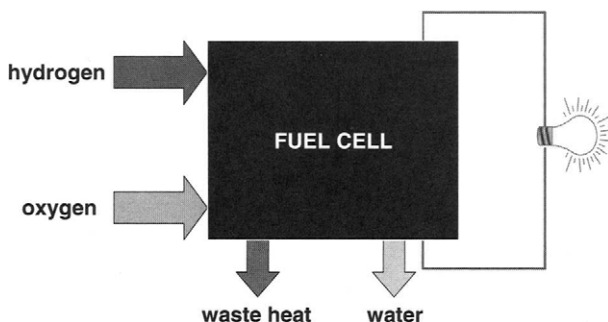


FIGURE 1-1. Fuel cell generates DC electricity from fuel in one step.

The efficiency of an energy conversion process is one of the most important aspects of that conversion. Some typical questions are usually tackled by engineering textbooks: How much energy of one kind is required to generate one unit of energy of another kind? What is the theoretical limit? How close we can come to that limit in practical applications? This last question is where most engineering textbooks fail—in providing practical results and real—not theoretical—efficiencies. As an example, let us examine the Carnot process or the Carnot engine. Every engineering student should know that the Carnot process is the most efficient process to operate between given temperatures. The fact that such an engine cannot be made, and even if it could be made it would have to operate infinitesimally slow to allow the heat transfer processes to happen with no losses, is maybe mentioned in some textbooks. But the fact that such an engine would be very efficient at generating no power is never emphasized enough. Yes, the famous Carnot engine would have to operate at the efficiencies lower than the famous Carnot efficiency in order to generate useful power. This book emphasizes the efficiency. But not only the theoretical efficiency, but the efficiency of practical, power-generating devices. That is why there is a subsection on efficiency in almost every chapter. The chapter on Fuel Cell Thermodynamics deals with theoretical fuel cell efficiencies. As important as it is to learn about the Carnot efficiency, it is equally important to learn about theoretical limits in fuel cells. The chapter on Fuel Cell Electrochemistry introduces various losses that are unavoidable because of the physical properties of the materials involved. These losses obviously have an effect on the efficiency of energy conversion. The chapter on Fuel Cell Systems discusses various supporting devices that are needed to get the fuel cell going. Most of those devices need power, which means that some of the power produced by a fuel cell would be used to run those supporting devices, and therefore less net power would actually be delivered by the fuel cell system. This means that the practical efficiency will

be somewhat lower than the theoretical one. How much lower? That would depend on the system configuration, design, and selection of auxiliary components. And finally, the efficiency of an energy conversion device in a practical application will probably depend on how that device is being used. Does it run all the time at constant power output or does the power output vary? If it varies, how much and how often? These are the reasons why the efficiency is discussed in almost every chapter of this book.

Another important aspect of an energy conversion process is the cost. It is the cost of produced energy that matters in practical applications. Obviously, this cost depends greatly on the efficiency of the energy conversion process and the cost of the consumed (or thermodynamically, the more correct term would be "converted") energy. The cost of the energy conversion device itself must also be taken into account. The cost of any device depends on the cost of the materials and the efforts (labor) involved to process those materials and make the components, and finally to assemble those components into a working device. Unfortunately, there is not enough information available on fuel cell costs, either materials or labor. One of the reasons the fuel cells are expensive is that they are not being mass produced. And one of the reasons they are not being mass produced is that their markets are limited because they are expensive. This "chicken and egg" problem is typical for any new technology.

This book will interweave the theory and practice of the fuel cell and fuel cell system design, engineering, and applications. This book will not provide a recipe on how to build the best possible fuel cell, but it will give an engineering student an understanding of the basic processes and materials inside a fuel cell. It will also supply enough tools and instructions on how to use them, to design a fuel cell or a fuel cell system, or how to select a fuel cell for a particular application. This book does not provide a direct answer to all fuel cell-related questions, but it provides the engineering tools needed to find those answers.

A fuel cell is in some aspects similar to a battery. It has an electrolyte, and negative and positive electrodes (Figure 1-2), and it generates DC electricity through electrochemical reactions. However, unlike a battery, a fuel cell requires a constant supply of fuel and oxidant. Also, unlike in a battery, the electrodes in a fuel cell do not undergo chemical changes. Batteries generate electricity by the electrochemical reactions that involve the materials that are already in batteries. Because of this, a battery may be discharged, which happens when the materials that participate in the electrochemical reactions are depleted. Some batteries are rechargeable, which means that the electrochemical reactions may proceed in reverse when external electricity is applied—a process of recharging the battery. A fuel cell cannot be discharged as long as the reactants—fuel and oxidant—are supplied. Typical reactants for fuel cells are hydrogen and oxygen; however, neither has to be in its pure form. Hydrogen may be present either in a mixture with other gases (such as CO<sub>2</sub>, N<sub>2</sub>, CO), or in hydrocarbons such

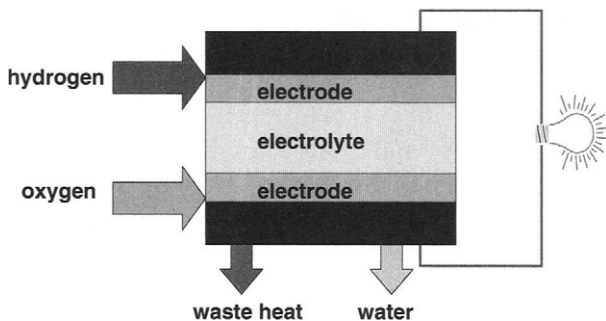


FIGURE 1-2. A fuel cell is similar to a battery in that it has electrodes and an electrolyte, but it needs a fuel and oxidant supply and it generates waste heat and water.

as natural gas,  $\text{CH}_4$ , or even in liquid hydrocarbons such as methanol,  $\text{CH}_3\text{OH}$ . Ambient air contains enough oxygen to be used in fuel cells. Yet another difference between a fuel cell and a battery is that a fuel cell generates by-products: waste heat and water, and the system is required to manage those (a battery also generates some heat but at a much lower rate that usually does not require any special or additional equipment).

## 1.2. A Very Brief History of Fuel Cells

The timeline of fuel cell development history is shown in Figure 1-3. The discovery of the fuel cell operating principle—the gaseous fuels that generate electricity, is attributed to Sir William Grove in 1839 [1], although it appears that a Swiss scientist Christian F. Shoenbein independently discovered the very same effect at about the same time (or even a year before) [2]. However, in spite of sporadic attempts to make a practical device, the fuel cell, or the “gaseous voltaic battery” as it was called by Grove [3], remained nothing more than a scientific curiosity for almost a century. E. Chen, in *Fuel Cells Technology Handbook* [4], provides a very detailed description of these early fuel cell developments. It was another Englishman, Francis T. Bacon, who started working on practical fuel cells in 1937, and he developed a 6 kW fuel cell by the end of the 1950s. However, the first practical fuel cell applications were in the U.S. Space Program. General Electric developed the first polymer membrane fuel cells that were used in the Gemini Program in the early 1960s. This was followed by the Apollo Space Program, which used the fuel cells to generate electricity for life support, guidance, and communications. These fuel cells were built by Pratt and Whitney based on license taken on Bacon’s patents (Figure 1-4).

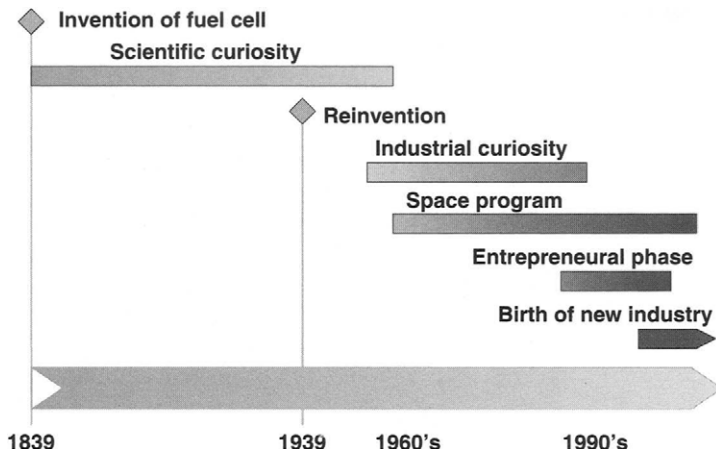


FIGURE 1-3. Fuel cell history timeline.

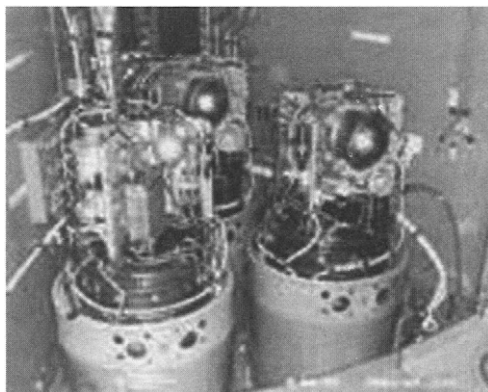


FIGURE 1-4. Apollo fuel cells. {Courtesy of UTC Fuel Cells.}

In the mid-1960s General Motors experimented with a fuel cell-powered van (these fuel cells were developed by Union Carbide). Although fuel cells have continued to be successfully used in the U.S. Space Program until today, they were again "forgotten" for terrestrial applications until the early 1990s. In 1989, Perry Energy Systems, a division of Perry Technologies, working with Ballard, a then emerging Canadian company, successfully demonstrated a polymer electrolyte membrane (PEM) fuel cell-powered submarine (Figure 1-5). In 1993, Ballard Power Systems demonstrated fuel cell-powered buses. Energy Partners, a successor of Perry Energy Systems,

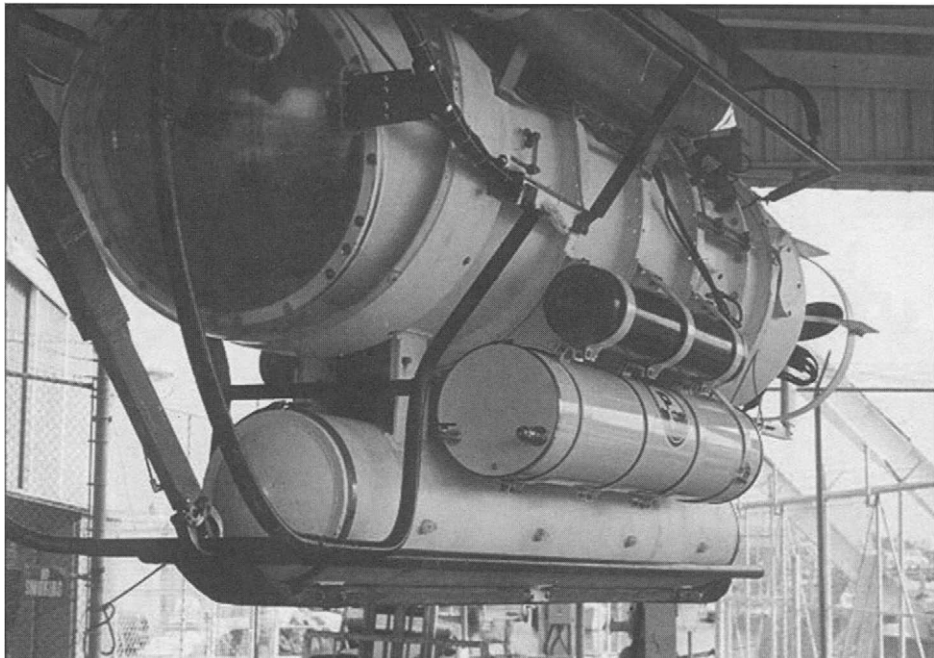


FIGURE 1-5. PC1401 by Perry Group powered by PEM fuel cells (1989). (Courtesy of Teledyne Energy Systems.)

demonstrated the first passenger car running on PEM fuel cells in 1993 (Figure 1-6) [5]. The car companies, supported by the U.S. Department of Energy, picked up on this activity and by the end of the century almost every car manufacturer had built and demonstrated a fuel cell-powered vehicle. A new industry was born. The stocks of fuel cell companies, such as Ballard and PlugPower, soared in early 2000 (Figure 1-7), based on a promise of a new energy revolution (eventually in 2001 they came down with the rest of the market). The number of fuel cell-related patents worldwide, but primarily in the United States and Japan, is increasing dramatically (Figure 1-8) [6,7], showing continuous interest and involvement of the scientific and engineering community.

### 1.3. Types of Fuel Cells

Fuel cells can be grouped by the type of electrolyte they use, namely:

- Alkaline fuel cells (AFC) use concentrated (85 wt%) KOH as the electrolyte for high temperature operation ( $250^{\circ}\text{C}$ ) and less concentrated (35–50 wt%) for lower temperature operation ( $<120^{\circ}\text{C}$ ). The

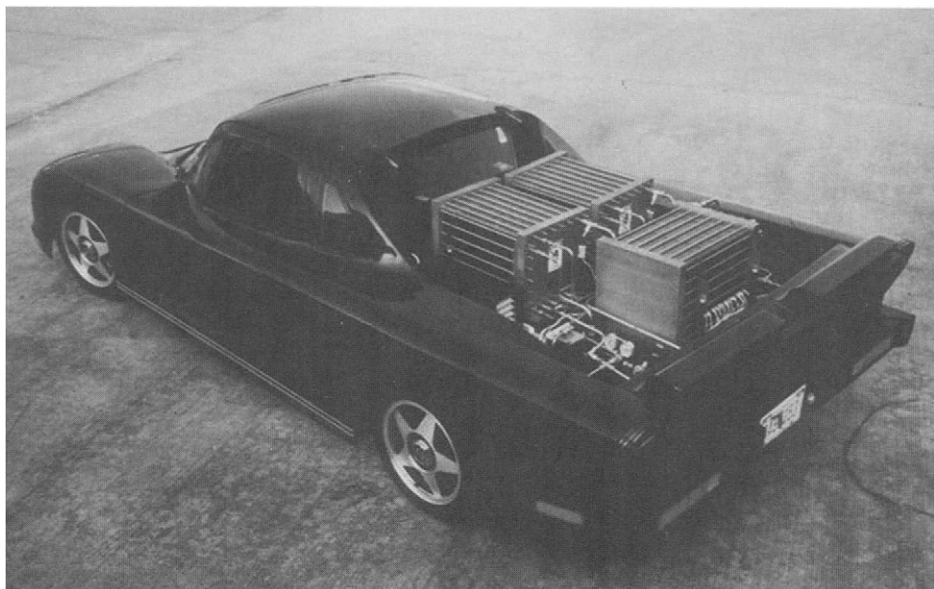


FIGURE 1-6. Energy Partners' GreenCar, the first PEM fuel cell-powered passenger automobile, 1993. (Courtesy of Teledyne Energy Systems.)

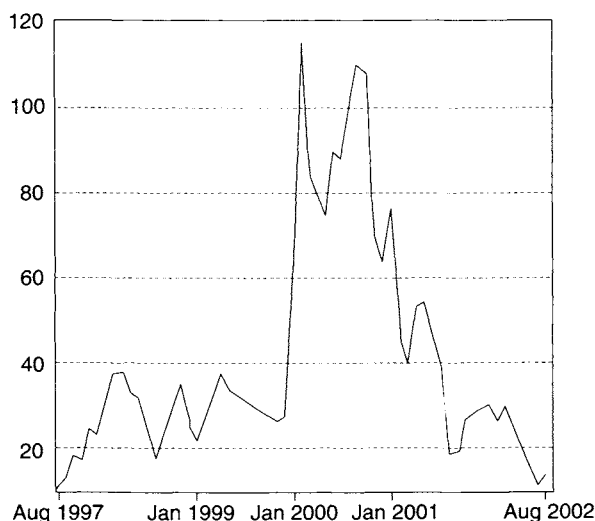


FIGURE 1-7. The stocks of fuel cell companies soared in early 2000 (example of Ballard).

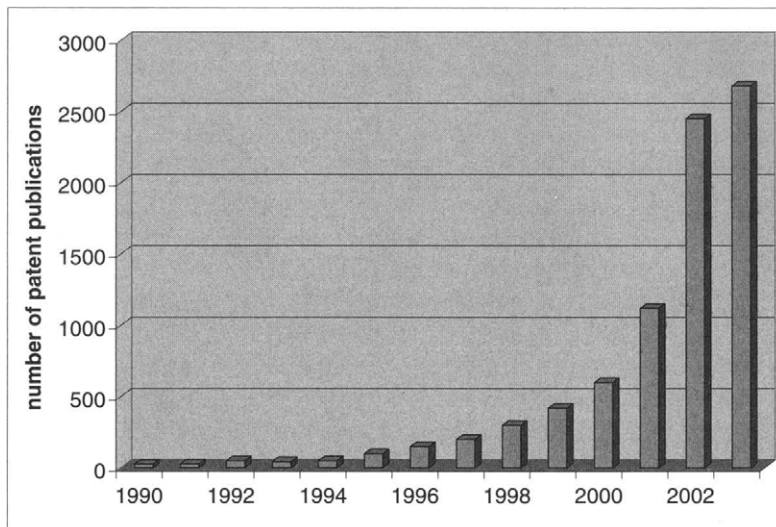


FIGURE 1-8. Fuel cell patent publications per year worldwide. (Adapted from [6] and [7].)

electrolyte is retained in a matrix (usually asbestos), and a wide range of electrocatalysts can be used (such as Ni, Ag, metal oxides, and noble metals). This fuel cell is intolerant to CO<sub>2</sub> present in either fuel or oxidant. Alkaline fuel cells have been used in the space program (Apollo and Space Shuttle) since the 1960s.

- Polymer electrolyte membrane or proton exchange membrane fuel cells (PEMFC) use a thin ( $\leq 50\text{ }\mu\text{m}$ ) proton conductive polymer membrane (such as perfluorosulfonated acid polymer) as the electrolyte. The catalyst is typically platinum supported on carbon with loadings of about  $0.3\text{ mg/cm}^2$ , or, if the hydrogen feed contains minute amounts of CO, Pt-Ru alloys are used. Operating temperature is typically between 60 and  $80^\circ\text{C}$ . PEM fuel cells are a serious candidate for automotive applications, but also for small-scale distributed stationary power generation, and for portable power applications as well.
- Phosphoric acid fuel cells (PAFC) use concentrated phosphoric acid (~100%) as the electrolyte. The matrix used to retain the acid is usually SiC, and the electrocatalyst in both the anode and the cathode is platinum. Operating temperature is typically between 150 and  $220^\circ\text{C}$ . Phosphoric acid fuel cells are already semicommercially available in container packages (200kW) for stationary electricity generation (UTC Fuel Cells). Hundreds of units have been installed all over the world.

- Molten carbonate fuel cells (MCFC) have the electrolyte composed of a combination of alkali (Li, Na, K) carbonates, which is retained in a ceramic matrix of  $\text{LiAlO}_2$ . Operating temperatures are between 600 and 700°C where the carbonates form a highly conductive molten salt, with carbonate ions providing ionic conduction. At such high operating temperatures, noble metal catalysts are typically not required. These fuel cells are in the precommercial/demonstration stage for stationary power generation.
- Solid oxide fuel cells (SOFC) use a solid, nonporous metal oxide, usually  $\text{Y}_2\text{O}_3$ -stabilized  $\text{ZrO}_2$  (YSZ) as the electrolyte. These cells operate at 800 to 1000°C where ionic conduction by oxygen ions takes place. Similar to MCFC, these fuel cells are in the pre-commercial/demonstration stage for stationary power generation, although smaller units are being developed for portable power and auxiliary power in automobiles.

Figure 1-9 summarizes the basic principles and electrochemical reactions in various fuel cell types.

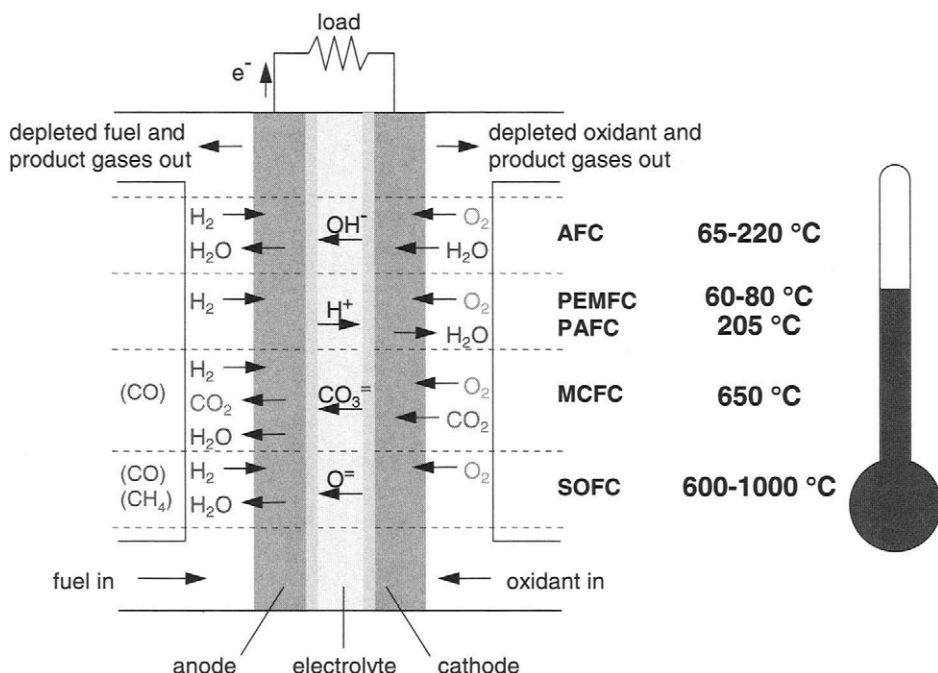


FIGURE 1-9. Types of fuel cells, their reactions and operating temperatures.

Sometimes, a direct methanol fuel cell (DMFC) is categorized as yet another type of fuel cell; however, according to the previous categorization (based on electrolyte), it is essentially a polymer membrane fuel cell that uses methanol instead of hydrogen as a fuel.

## 1.4. How Does a PEM Fuel Cell Work?

Although some general engineering principles may be applicable to all fuel cell types, this book is about PEM fuel cells, their operation, design, and applications. PEM stands for polymer electrolyte membrane or proton exchange membrane. Sometimes, they are also called polymer membrane fuel cells, or just membrane fuel cells. In the early days (1960s) they were known as solid polymer electrolyte (SPE) fuel cells. This technology has drawn the most attention because of its simplicity, viability, quick start-up, and the fact that it has been demonstrated in almost any conceivable application, as shown in the following sections.

At the heart of a PEM fuel cell is a polymer membrane that has some unique capabilities. It is impermeable to gases but it conducts protons (hence the name, proton exchange membrane). The membrane that acts as the electrolyte is squeezed between the two porous, electrically conductive electrodes. These electrodes are typically made out of carbon cloth or carbon fiber paper. At the interface between the porous electrode and the polymer membrane there is a layer with catalyst particles, typically platinum supported on carbon. A schematic diagram of cell configuration and basic operating principles is shown in Figure 1-10. Chapter 4 deals in greater detail with those major fuel cell components, their materials, and their properties.

Electrochemical reactions happen at the surface of the catalyst at the interface between the electrolyte and the membrane. Hydrogen, which is fed on one side of the membrane, splits into its primary constituents—protons and electrons. Each hydrogen atom consists of one electron and one proton. Protons travel through the membrane, whereas the electrons travel through electrically conductive electrodes, through current collectors, and through the outside circuit where they perform useful work and come back to the other side of the membrane. At the catalyst sites between the membrane and the other electrode they meet with the protons that went through the membrane and oxygen that is fed on that side of the membrane. Water is created in the electrochemical reaction, and then pushed out of the cell with excess flow of oxygen. The net result of these simultaneous reactions is current of electrons through an external circuit—direct electrical current.

The hydrogen side is negative and it is called the anode, whereas the oxygen side of the fuel cell is positive and it is called the cathode.

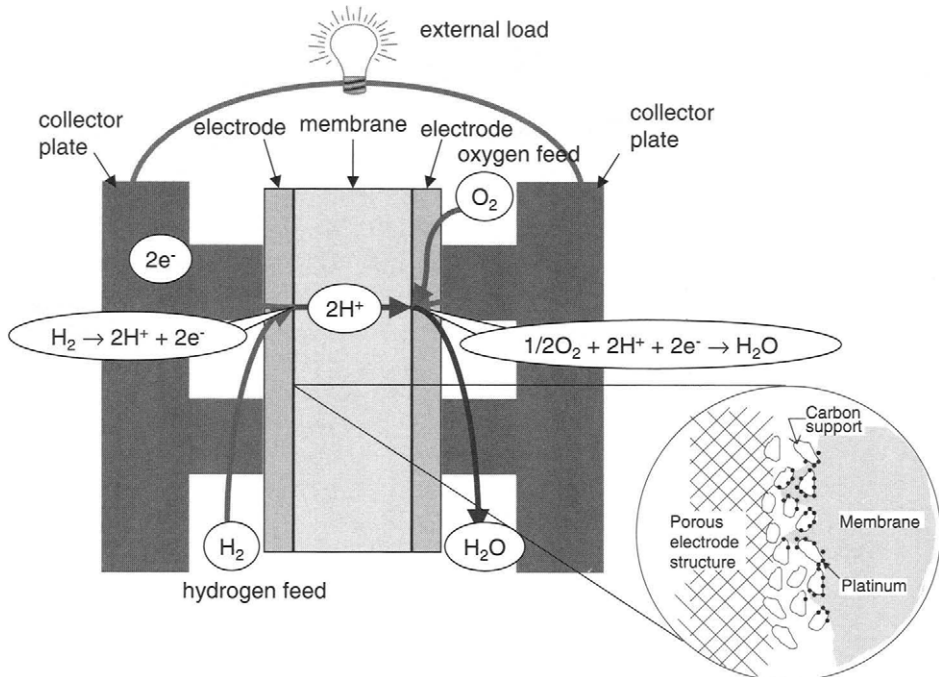


FIGURE 1-10. The basic principle of operation of a PEM fuel cell.

Chapters 4 and 5 explain in greater detail all the processes involved in making the fuel cell work. Because each cell generates about 1 V, as will be shown subsequently, more cells are needed in series to generate some practical voltages. Depending on application, the output voltage may be between 6 V and 200 V or even more. How the cells are stacked up, and what the issues are in stack design, is discussed in Chapter 6.

A fuel cell stack needs a supporting system (as explained in Chapter 9) to:

- Handle the supply of reactant gases and their exhaust, including the products;
- Take care of waste heat and maintain the stack temperature;
- Regulate and condition power output;
- Monitor the stack vital parameters; and
- Control the start-up, operation, and shutdown of the stack and system components.

## 1.5. Why Do We Need Fuel Cells?

Fuel cells are a very promising energy technology with a myriad of possible applications as discussed next and in greater detail in Chapter 10. Fuel cells have many properties that make them attractive when compared with the existing, conventional energy conversion technologies, namely:

- Promise of high efficiency—Because the fuel cell efficiency is much higher than the efficiency of internal combustion engines, fuel cells are attractive for automobile applications. Also, fuel cell efficiency is higher than the efficiency of conventional power plants, and therefore the fuel cells may be used for decentralized power generation. However, new energy conversion technologies, such as hybrid electric vehicles and combined cycle power plants, also have high conversion efficiencies.
- Promise of low or zero emissions—Fuel cells operating on hydrogen generate zero emissions—the only exhaust is unused air and water. This may be attractive not only for transportation but also for many indoor applications, as well as submarines. However, hydrogen is not a readily available fuel, and if a fuel cell is equipped with a fuel processor to generate hydrogen, or if methanol is used instead of hydrogen, some emissions are generated, including carbon dioxide. In general, these emissions are lower than those of comparable conventional energy conversion technologies.
- Issue of national security—Fuel cells use hydrogen as fuel. Although hydrogen is not a readily available fuel it may be produced from indigenous sources, either by electrolysis of water or by reforming hydrocarbon fuels. Use of indigenous sources (renewable energy, nuclear, biomass, coal or natural gas) to generate hydrogen may significantly reduce dependence on foreign oil, which would have an impact on national security. However, widespread use of hydrogen would require establishing a hydrogen infrastructure or the so-called hydrogen economy, which will be discussed in Chapter 11.
- Simplicity and promise of low cost—Fuel cells are extremely simple. They are made in layers of repetitive components, and they have no moving parts. Because of this, they have the potential to be mass produced at a cost comparable to that of existing energy conversion technologies or even lower. To date, the fuel cells are still expensive for either automotive or stationary power generation, primarily because of use of expensive materials, such as sulfonated fluoropolymers used as proton exchanged membrane, and noble metals, such as platinum or ruthenium, used as catalysts. Mass production techniques must still be developed for fabrication of fuel cell components and for the stack and system assembly.

- No moving parts and promise of long life—Because a fuel cell does not have any moving parts, it may be expected to exhibit a long life. Current fuel cell technology may reach the lifetime acceptable for automotive applications (3000–5000 hours), but their durability must be improved by an order of magnitude for use in stationary power generation (where the requirement is >40,000–80,000 hours).
- Modular—Fuel cells are by their nature modular—more power may be generated simply by adding more cells. Mass produced fuel cells may be significantly less expensive than traditional power plants. Instead of building big power plants, which must be planned well in advance, and whose permitting process may be extremely cumbersome, it may be cost-effective to gradually increase generation capacity by adding smaller fuel cells to the grid. Such a concept of distributed generation may not only be cost-effective but also may significantly improve reliability of the power supply.
- Quiet—Fuel cells are inherently quiet, which may make them attractive for a variety of applications, such as portable power, backup power, and military applications.
- Size and weight—Fuel cells may be made in a variety of sizes—from microwatts to megawatts—which makes them useful in a variety of applications, from powering electronic devices to powering entire buildings. The size and weight of automotive fuel cells approaches those of internal combustion engines, and the size and weight of small fuel cells may offer advantage over the competing technologies, such as batteries for electronic devices.

## 1.6. Fuel Cell Applications

Because of their attractive properties, fuel cells have already been developed and demonstrated in the following applications (some of which are shown in Figure 1-11):

- Automobiles—Almost every car manufacturer has already developed and demonstrated at least one prototype vehicle, and many have already gone through several generations of fuel cell vehicles. Some car manufacturers are working on their own fuel cell technology (General Motors, Toyota, Honda), and some buy fuel cell stacks and systems from fuel cell developers such as Ballard, UTC Fuel Cells, and DeNora (DaimlerChrysler, Ford, Nissan, Mazda, Hyundai, Fiat, Volkswagen).
- Scooters and bicycles—Several companies (Palcan, Asian Pacific, Manhattan Scientific) have demonstrated fuel cell-powered scooters and bicycles using either hydrogen stored in metal hydrides or methanol in direct methanol fuel cells.

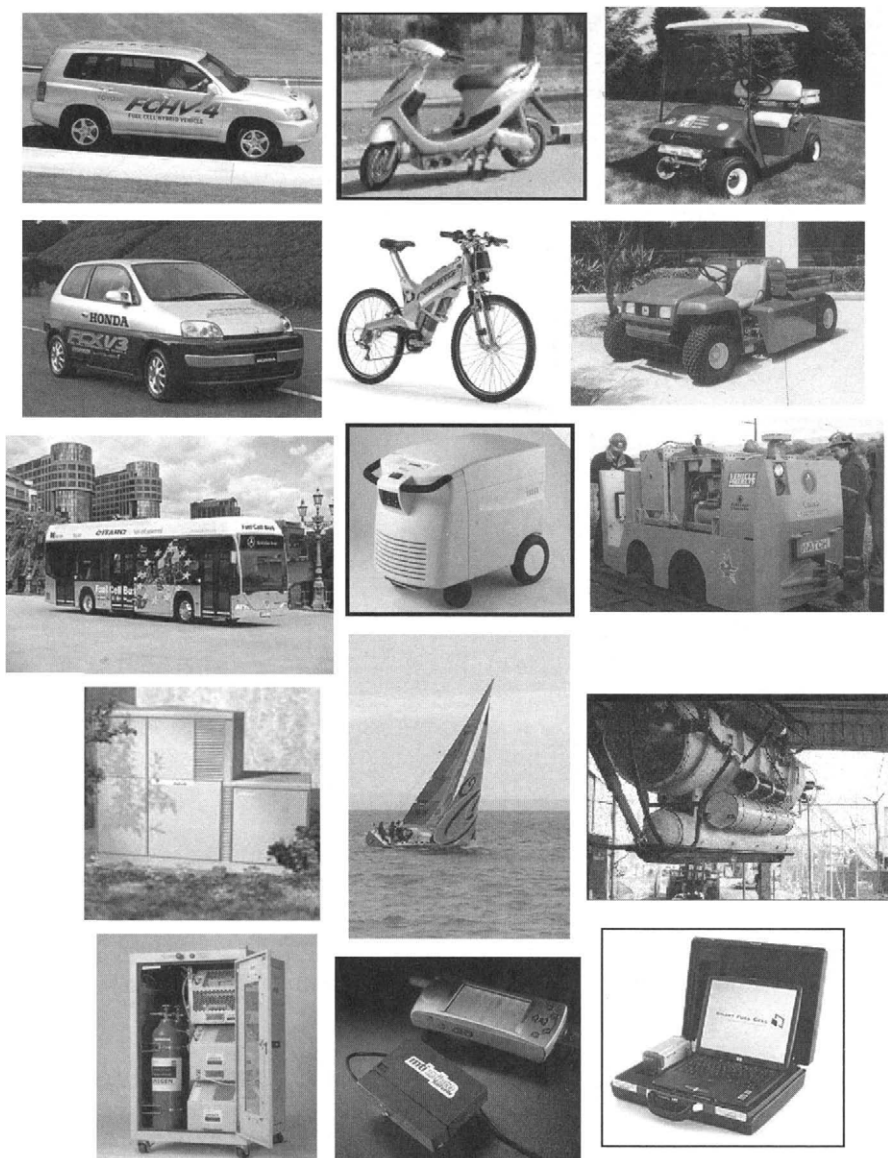


FIGURE 1-11. Collage of fuel cell applications and demonstrations to date (mid-2004). (Courtesy of Toyota, Asian Pacific Fuel Cell Technologies, Schatz Energy Center—Humboldt State University, Honda, Aprilia, Teledyne Energy Systems, Daimler-Chrysler, Ballard Power Systems, Fuel Cell Propulsion Institute, Plug Power, MTU, Teledyne Energy Systems, Proton Energy Systems, MTI Micro Fuel Cells and Smart Fuel Cells.)

- Golf carts—Energy Partners demonstrated a fuel cell-powered golf cart in 1994 (it was used in Olympic Village at the 1996 Olympic Games in Atlanta). Schatz Energy Center developed fuel cell-powered golf carts to be used in the city of Palm Desert in California.
- Utility vehicles—Energy Partners converted three John Deere Gator utility vehicles to fuel cell power [8] and demonstrated them in service at Palm Springs airport (1996). John Deere is working with Hydrogenics, Canada, on development of fuel cell-powered electric utility vehicles, including those for lawn maintenance.
- Distributed power generation—Several companies are working on development of small (1–10 kW) fuel cell power systems intended to be used in homes. Some of them are combined with boilers to provide both electricity and heat (PlugPower with Vaillant, and Ballard with Ebara).
- Backup power—Ballard announced plans to commercialize 1 kW backup power generators in cooperation with Coleman (2000), but then bought back the technology and continued to sell the units (2002). Proton Energy Systems demonstrated regenerative fuel cells combining its own PEM electrolyzer technology with Ballard's Nexa units [9]. A regenerative fuel cell generates its own hydrogen during periods when electricity is available.
- Portable power—Many companies (MTI, Motorola, NEC, Fuji, Matsushita, Medis, Manhattan Scientific, Polyfuel) are developing miniature fuel cells as battery replacements for various consumer and military electronic devices. Because of fuel storage issues, most of them use methanol in either direct methanol fuel cells or through microreformer in regular PEM fuel cells.
- Space—Fuel cells continue to be used in the U.S. Space Program, providing power on the space orbiters. Although this proven technology is of the alkaline type, NASA announced plans to use PEM fuel cells in the future.
- Airplanes—in November 2001 Boeing announced that it was modifying a small single-engine airplane by replacing its engine with fuel cells and an electric motor that would turn a conventional propeller. Test flights are scheduled to begin in early 2004, and are being conducted with the intention of using fuel cells as auxiliary power units on jet airliners in the future.
- Locomotives—Propulsion Research Institute started a consortium that demonstrated a fuel cell-powered locomotive for mining operations (the fuel cell was built by DeNora).
- Boats—MTU Friedrichschaffhausen demonstrated a sailboat on lake Constanze (2004) powered by a 20 kW fuel cell, developed jointly with Ballard.

- Underwater vehicles—In 1989 Perry Technologies successfully tested the first commercial fuel cell-powered submarine, the two-person observation submersible PC-1401, using Ballard's fuel cell [10]. Siemens has been successfully providing fuel cell engines for large submarines used by the German, Canadian, Italian, and Greek Navies.

## References

1. Grove, W. R., On Voltaic Series and the Combination of Gases by Platinum, *London and Edinburgh Philosophical Magazine and Journal of Science*, Series 3, 14, 127-130-420, 1839.
2. Bossel, U., *The Birth of the Fuel Cell 1835-1845* (European Fuel Cell Forum, Oberrohrdorf, Switzerland, 2000).
3. Grove, W. R., On a Gaseous Voltaic Battery, *London and Edinburgh Philosophical Magazine and Journal of Science*, Series 3, 21, 417-420, 1842.
4. Chen, E., History, in G. Hoogers (editor), *Fuel Cell Technology Handbook* (CRC Press, Boca Raton, FL, 2003).
5. Nadal, M. and F. Barbir, Development of a Hybrid Fuel Cell/Battery Powered Electric Vehicle, in D. L Block and T. N. Veziroglu (editors), *Hydrogen Energy Progress X*, Vol. 3 (International Association for Hydrogen Energy, Coral Gables, FL, 1994) pp. 1427-1440.
6. Stone C. and A. E. Morrison, From Curiosity to "Power to Change the World," *Solid State Ionics*, Vol. 152-153, 2002, pp. 1-13
7. Fuel Cell Today, <http://www.fuelcelltoday.com> (accessed August 2004).
8. Barbir, F., M. Nadal and M. Fuchs, Fuel Cell Powered Utility Vehicles, Proc. Portable Fuel Cell Conference, (Ed.) F. Buchi, pp. 113-126, Lucerne, Switzerland, June 1999.
9. Barbir, F., S. Nomikos, and M. Lillis, Practical Experiences with Regenerative Fuel Cell Systems, in *Proc. 2003 Fuel Cell Seminar* (Miami Beach, FL, 2003).
10. Blomen, L. J. M. J. and M. N. Mugerwa, *Fuel Cell Systems* (New York, Plenum Press, 1993).

# CHAPTER 2

## 2. Fuel Cell Basic Chemistry and Thermodynamics

A fuel cell is an electrochemical energy converter—it converts chemical energy of fuel, typically hydrogen, directly into electrical energy. As such, it must obey the laws of thermodynamics.

### 2.1. Basic Reactions

The electrochemical reactions in fuel cells happen simultaneously on both sides of the membrane—the anode and the cathode. The basic fuel cell reactions are:

At the anode:



At the cathode:



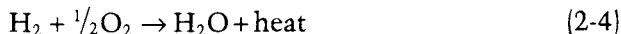
Overall:



These reactions may have several intermediate steps, and there may be some (unwanted) side reactions, but for now these reactions accurately describe the main processes in a fuel cell.

### 2.2. Heat of Reaction

The overall reaction (Equation 2-3) is the same as the reaction of hydrogen combustion. Combustion is an exothermic process, which means that there is energy released in the process:



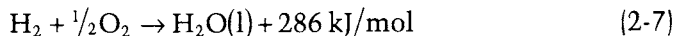
The heat (or enthalpy) of a chemical reaction is the difference between the heats of formation of products and reactants. For the previous Equation (2-4) this means:

$$\Delta H = (h_f)_{\text{H}_2\text{O}} - (h_f)_{\text{H}_2} - \frac{1}{2}(h_f)_{\text{O}_2} \quad (2-5)$$

Heat of formation of liquid water is  $-286 \text{ kJ mol}^{-1}$  (at  $25^\circ\text{C}$ ) and heat of formation of elements is by definition equal to zero. Therefore:

$$\Delta H = (h_f)_{\text{H}_2\text{O}} - (h_f)_{\text{H}_2} - \frac{1}{2}(h_f)_{\text{O}_2} = -286 \text{ kJ/g} - 0 - 0 = -286 \text{ kJ mol}^{-1} \quad (2-6)$$

Note that the negative sign for enthalpy of a chemical reaction, by convention, means that heat is being released in the reaction, that is, this is an exothermic reaction. Equation (2-4) may now be rewritten as:

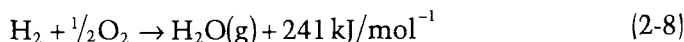


Here a positive sign is used because the enthalpy is placed on the right side of the reaction, clearly meaning a product of the reaction.

This equation is valid at  $25^\circ\text{C}$  only, meaning that both the reactant gases and the product water are at  $25^\circ\text{C}$ . At  $25^\circ\text{C}$ , and atmospheric pressure, water is in liquid form.

### 2.3. Higher and Lower Heating Value of Hydrogen

The enthalpy of hydrogen combustion reaction (Equation 2-7) (*i.e.*,  $286 \text{ kJ mol}^{-1}$ ) is also called the hydrogen's heating value. It is the amount of heat that may be generated by a complete combustion of 1 mol of hydrogen. The measurement of a heating value is conducted in a calorimetric bomb. If 1 mol of hydrogen is enclosed in a calorimetric bomb with  $\frac{1}{2}$  mol of oxygen, ignited, fully combusted, and allowed to cool down to  $25^\circ\text{C}$ , at atmospheric pressure there will be only liquid water left in the bomb (Figure 2-1). The measurement should show that  $286 \text{ kJ}$  of heat was released. This is known as hydrogen's higher heating value. However, if hydrogen is combusted with sufficient excess of oxygen (or air) and allowed to cool down to  $25^\circ\text{C}$ , the product water will be in the form of vapor mixed with unburned oxygen and/or nitrogen in case that air was used (Figure 2-2). The measurement should show that less heat was released, exactly  $241 \text{ kJ}$ . This is known as hydrogen's lower heating value.



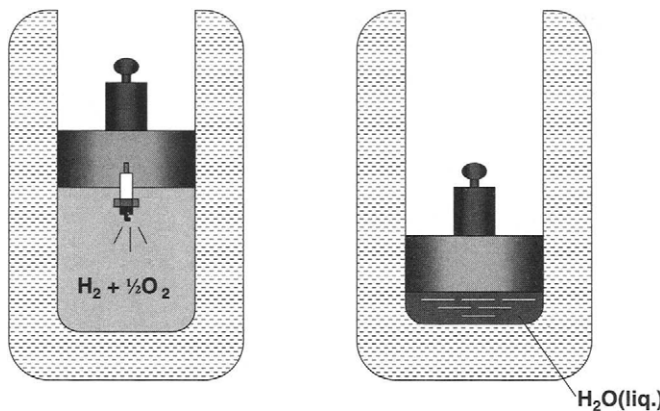


FIGURE 2-1. Combustion of  $H_2 + \frac{1}{2}O_2$  in a calorimetric bomb—measurement of higher heating value.

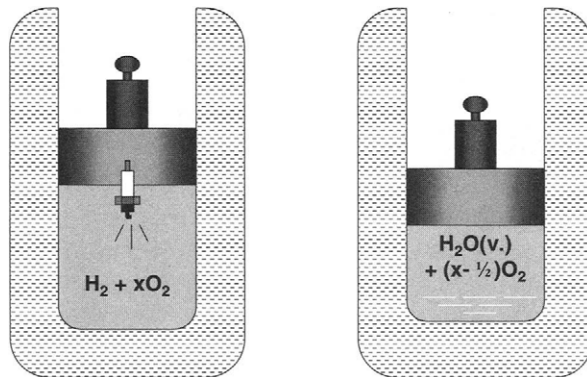


FIGURE 2-2. Combustion of  $H_2$  with excess  $O_2$  in a calorimetric bomb—measurement of lower heating value.

The difference between higher and lower heating value is the heat of evaporation of water (at 25°C):

$$H_{fg} = 286 - 241 = 45 \text{ kJ mol}^{-1} \quad (2-9)$$

## 2.4. Theoretical Electrical Work

Because there is no combustion in a fuel cell, what is the relevance of hydrogen's heating value (higher or lower) to a fuel cell? Hydrogen heating value is used as a measure of energy input in a fuel cell. This is the

maximum amount of (thermal) energy that may be extracted from hydrogen. However, electricity is produced in a fuel cell. Can all the energy input be converted into electricity? Obviously not! In every chemical reaction some entropy is produced, and because of that, a portion of the hydrogen's higher heating value cannot be converted into useful work—electricity. The portion of the reaction enthalpy (or hydrogen's higher heating value) that can be converted to electricity in a fuel cell corresponds to Gibbs free energy and is given by the following equation:

$$\Delta G = \Delta H - T\Delta S \quad (2-10)$$

In other words, there are some irreversible losses in energy conversion due to creation of entropy,  $\Delta S$ .

Similarly, as  $\Delta H$  for the reaction (Equation 2-4) is the difference between the heats of formation of products and reactants (Equation 2-5),  $\Delta S$  is the difference between entropies of products and reactants:

$$\Delta S = (s_f)_{H_2O} - (s_f)_{H_2} - \frac{1}{2}(s_f)_{O_2} \quad (2-11)$$

The values of  $h_f$  and  $s_f$  for reaction reactants and products at ambient pressure and 25°C are shown in Table 2-1 [1].

Therefore, at 25°C, out of 286.02 kJ mol<sup>-1</sup> of available energy, 237.34 kJ mol<sup>-1</sup> can be converted into electrical energy and the remaining 48.68 kJ mol<sup>-1</sup> is converted into heat. At temperatures other than 25°C, these values are different as shown in Section 2.6.

## 2.5. Theoretical Fuel Cell Potential

In general, electrical work is a product of charge and potential:

$$W_{el} = qE \quad (2-12)$$

where:

$W_{el}$  = electrical work (J mol<sup>-1</sup>)

$q$  = charge (Coulombs mol<sup>-1</sup>)

$E$  = potential (Volts)

TABLE 2-1  
Enthalpies and Entropies of Formation for Fuel Cell Reactants and Products

	$h_f$ (kJ mol <sup>-1</sup> )	$s_f$ (kJ mol <sup>-1</sup> K <sup>-1</sup> )
Hydrogen, H <sub>2</sub>	0	0.13066
Oxygen, O <sub>2</sub>	0	0.20517
Water (liquid), H <sub>2</sub> O (l)	-286.02	0.06996
WATER (vapor), H <sub>2</sub> O (g)	-241.98	0.18884

The total charge transferred in a fuel cell reaction (Equations 2-1 through 2-3) per mol of H<sub>2</sub> consumed is equal to:

$$q = n N_{\text{Avg}} q_{\text{el}} \quad (2-13)$$

where:

$n$  = number of electrons per molecule of H<sub>2</sub> = 2 electrons per molecule

$N_{\text{Avg}}$  = number of molecules per mole (Avogadro's number) =  $6.022 \times 10^{23}$  molecules/mol

$q_{\text{el}}$  = charge of 1 electron =  $1.602 \times 10^{-19}$  Coulombs/electron

The product of Avogadro's number and charge of 1 electron is known as Faraday's constant:

$$F = 96,485 \text{ Coulombs/electron-mol}$$

Electrical work is therefore:

$$W_{\text{el}} = nFE \quad (2-14)$$

As mentioned previously, the maximum amount of electrical energy generated in a fuel cell corresponds to Gibbs free energy, ΔG:

$$W_{\text{el}} = -\Delta G \quad (2-15)$$

The theoretical potential of fuel cell is then:

$$E = \frac{-\Delta G}{nF} \quad (2-16)$$

Because ΔG, n, and F are all known, the theoretical fuel cell potential of hydrogen/oxygen can also be calculated:

$$E = \frac{-\Delta G}{nF} = \frac{237,340 \text{ J mol}^{-1}}{2 \cdot 96,485 \text{ Asmol}^{-1}} = 1.23 \text{ Volts} \quad (2-17)$$

At 25°C, the theoretical hydrogen/oxygen fuel cell potential is 1.23 Volts.

## 2.6. Effect of Temperature

The theoretical cell potential changes with temperature. Substituting Equation (2-10) into (2-16) yields:

$$E = -\left( \frac{\Delta H}{nF} - \frac{T\Delta S}{nF} \right) \quad (2-18)$$

Obviously, an increase in the cell temperature results in a lower theoretical cell potential. Note that both  $\Delta H$  and  $\Delta S$  are negative (see Table 2-2). In addition, both  $\Delta H$  and  $\Delta S$  are functions of temperature:

$$h_T = h_{298.15} + \int_{298.15}^T c_p dT \quad (2-19)$$

$$s_T = s_{298.15} + \int_{298.15}^T \frac{1}{T} c_p dT \quad (2-20)$$

Specific heat of any gas is also a function of temperature (Figure 2-3). An empirical relationship may be used [2]:

$$c_p = a + bT + cT^2 \quad (2-21)$$

where  $a$ ,  $b$ , and  $c$  are the empirical coefficients, different for each gas as shown in Table 2-3.

TABLE 2-2  
Enthalpies, Entropies and Gibbs Free Energy for Hydrogen Oxidation Processes

	$\Delta H \text{ (kJ mol}^{-1}\text{)}$	$\Delta S \text{ (kJ mol}^{-1} \text{ K}^{-1}\text{)}$	$\Delta G \text{ (kJ mol}^{-1}\text{)}$
$\text{H}_2 + \frac{1}{2}\text{O}_2 \rightarrow \text{H}_2\text{O(l)}$	-286.02	-0.1633	-237.34
$\text{H}_2 + \frac{1}{2}\text{O}_2 \rightarrow \text{H}_2\text{O(g)}$	-241.98	-0.0444	-228.74

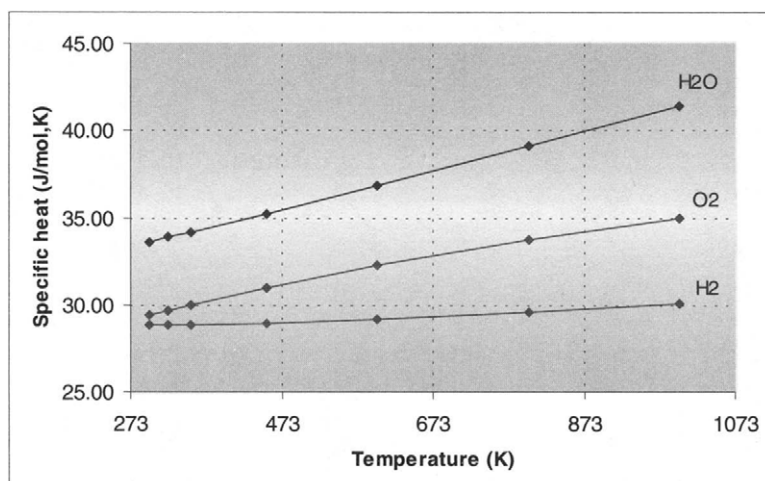


FIGURE 2-3. Specific heat,  $C_p$ , as a function of temperature for hydrogen, oxygen, and water vapor.

Substituting Equation (2-21) into Equations (2-19) and (2-20) and integrating yields:

$$\Delta H_T = \Delta H_{298.15} + \Delta a(T - 298.15) + \Delta b \frac{(T^2 - 298.15^2)}{2} + \Delta c \frac{(T^3 - 298.15^3)}{3} \quad (2-22)$$

$$\Delta S_T = \Delta S_{298.15} + \Delta a \ln\left(\frac{T}{298.15}\right) + \Delta b(T - 298.15) + \Delta c \frac{(T^2 - 298.15^2)}{2} \quad (2-23)$$

where  $\Delta a$ ,  $\Delta b$ , and  $\Delta c$  are the differences between the coefficients  $a$ ,  $b$ , and  $c$ , respectively, for products and reactants, that is:

$$\begin{aligned} \Delta a &= a_{H_2O} - a_{H_2} - \frac{1}{2}a_{O_2} \\ \Delta b &= b_{H_2O} - b_{H_2} - \frac{1}{2}b_{O_2} \\ \Delta c &= c_{H_2O} - c_{H_2} - \frac{1}{2}c_{O_2} \end{aligned} \quad (2-24)$$

At temperatures below 100°C, changes of  $C_p$ ,  $\Delta H$ , and  $\Delta S$  are very small (Table 2-4), but at higher temperatures, such as those experienced in solid oxide fuel cells, they must not be neglected. As shown in Table 2-4 and Figure 2-4, the theoretical cell potential decreases with temperature. However, in operating fuel cells, in general, a higher cell temperature results in a higher cell potential. This is because the voltage losses in operating fuel cells decrease with temperature, and this more than compensates for the loss of theoretical cell potential.

TABLE 2-3  
The Coefficients for Temperature Dependency of  $C_p$ , in  $J\text{mol}^{-1}\text{K}^{-1}$ , from [2]

	<i>a</i>	<i>b</i>	<i>c</i>
H <sub>2</sub>	28.91404	-0.00084	2.01E-06
O <sub>2</sub>	25.84512	0.012987	-3.9E-06
H <sub>2</sub> O (g)	30.62644	0.009621	1.18E-06

TABLE 2-4  
Change of Enthalpy, Gibbs Free Energy, and Entropy of Hydrogen/Oxygen Fuel Cell Reaction (in  $\text{kJ mol}^{-1}\text{K}^{-1}$ ) with Temperature and Resulting Theoretical Cell Potential

T(K)	$\Delta H$	$\Delta G$	$\Delta S$	$E_{th}$ (V)
298.15	-286.02	-237.34	-0.16328	1.230
333.15	-284.85	-231.63	-0.15975	1.200
353.15	-284.18	-228.42	-0.15791	1.184
373.15	-283.52	-225.24	-0.15617	1.167

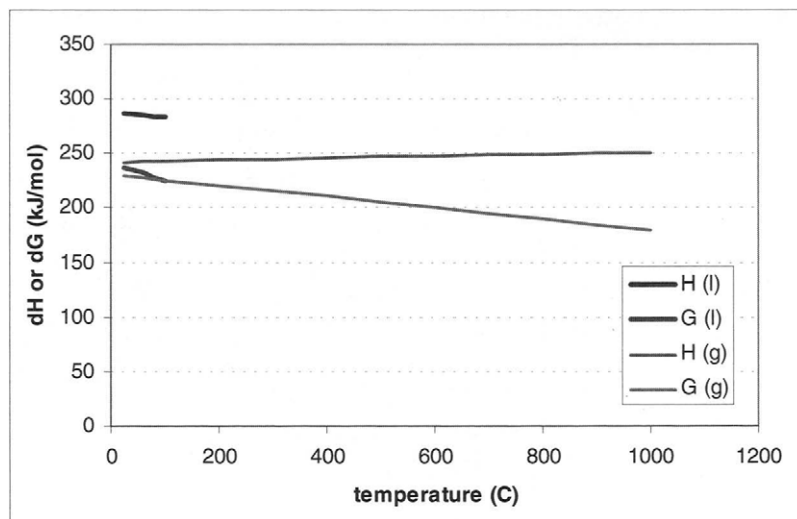


FIGURE 2-4. Enthalpy and Gibbs free energy of hydrogen/oxygen fuel cell as a function of temperature.

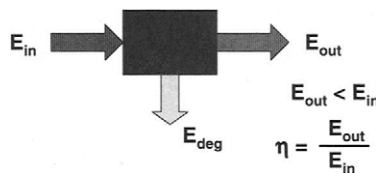


FIGURE 2-5. Efficiency of any energy conversion process.

## 2.7. Theoretical Fuel Cell Efficiency

The efficiency of any energy conversion device is defined as the ratio between useful energy output and energy input (Figure 2-5).

In case of a fuel cell, the useful energy output is the electrical energy produced, and energy input is the enthalpy of hydrogen, that is, hydrogen's higher heating value (Figure 2-6). Assuming that all of the Gibbs free energy can be converted into electrical energy, the maximum possible (theoretical) efficiency of a fuel cell is:

$$\eta = \Delta G / \Delta H = 237.34 / 286.02 = 83\% \quad (2-25)$$

Very often, hydrogen's lower heating value is used to express the fuel cell efficiency, not only because it results in a higher number, but also to compare it with the fuel cell's competitor—the internal combustion engine,

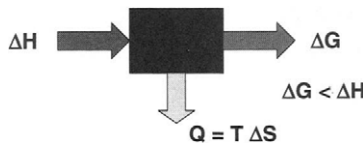


FIGURE 2-6. Energy inputs and outputs for a fuel cell as an energy conversion device.

whose efficiency has traditionally been expressed with lower heating value of fuel. In that case the maximum theoretical fuel cell efficiency would be:

$$\eta = \Delta G / \Delta H_{LHV} = 228.74 / 241.98 = 94.5\% \quad (2-26)$$

The use of lower heating value, both in the fuel cell and especially in the internal combustion engine, is justified by water vapor being produced in the process, so the difference between higher and lower heating value (heat of evaporation) cannot be used anyway. Although the use of both lower and higher heating values in expressing the efficiency of an energy conversion device is appropriate (as long as it is specified which heating value has been used), the use of lower heating value may become confusing. In the late 1990s the manufacturers of condensing boilers in Germany were claiming that their boilers were more than 100% efficient, because they were using the lower heating value of fuel as a measure of energy input. Lower heating value does not account for the heat of condensation of product water, but in this case the heat of condensation was indeed utilized because those were condensing boilers. It is therefore thermodynamically more correct to use the higher heating value, because it accounts for all the energy available, and it is consistent with the definition of the efficiency as shown in Figure 2-5.

If both  $\Delta G$  and  $\Delta H$  in Equation (2-25) are divided by  $nF$ , the fuel cell efficiency may be expressed as a ratio of two potentials:

$$\eta = \frac{-\Delta G}{-\Delta H} = \frac{\frac{-\Delta G}{nF}}{\frac{-\Delta H}{nF}} = \frac{1.23}{1.482} = 0.83 \quad (2-27)$$

where:

$\frac{-\Delta G}{nF} = 1.23V$  is the theoretical cell potential, and

$\frac{-\Delta H}{nF} = 1.482 V$  is the potential corresponding to hydrogen's higher heating value, or the thermoneutral potential.

As will be shown in the following sections, the fuel cell efficiency is always proportional to the cell potential and may be calculated as a ratio of the cell potential and the potential corresponding to hydrogen's higher heating value, that is, 1.482 V. The potential corresponding to the lower heating value is 1.254 V.

## 2.8. Carnot Efficiency Myth

Carnot efficiency is the maximum efficiency that a heat engine may have operating between the two temperatures (Figure 2-7).

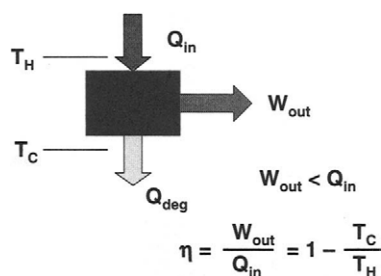


FIGURE 2-7. Carnot process efficiency.

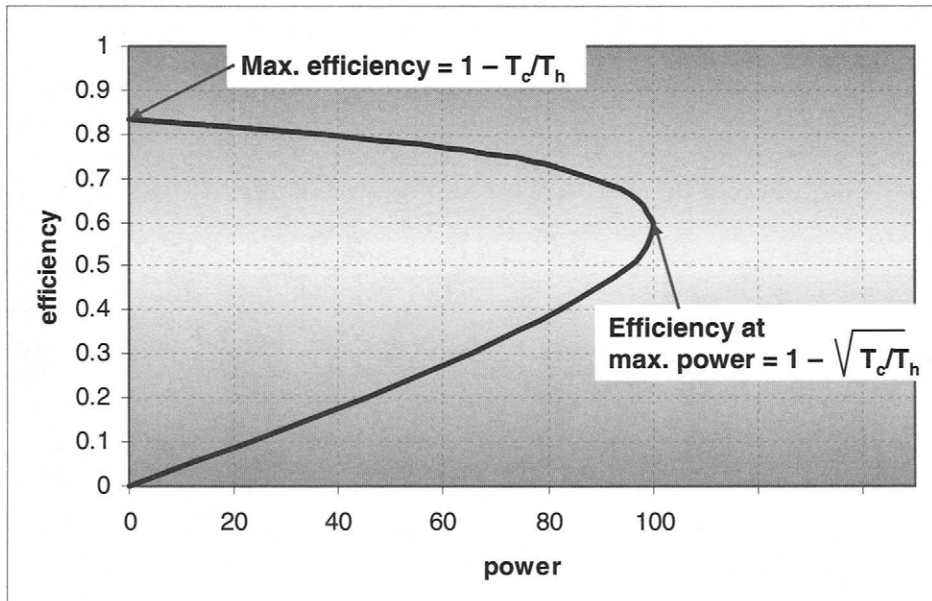


FIGURE 2-8. Efficiency vs power curve for a hypothetical Carnot engine.

The Carnot efficiency has little practical value. It is a maximum theoretical efficiency of a hypothetical engine. Even if such an engine could be constructed, it would have to be operated at infinitesimally low velocities to allow the heat transfer to occur. It would be very efficient, but it would generate no power (Figure 2-8), thus it would be useless. The same applies to the theoretical fuel cell efficiency. The fuel cell operating at theoretical efficiency would generate no current, and therefore it would be of no practical value.

It may be shown [3] that the efficiency at maximum power of a Carnot engine is:

$$\eta = 1 - \sqrt{\frac{T_C}{T_H}} \quad (2-28)$$

The Carnot efficiency does not apply to fuel cells because a fuel cell is not a heat engine, but rather an electrochemical energy converter. For this reason a fuel cell operating at low temperature, for example 60°C, and discarding heat into the environment at 25°C, may have an efficiency significantly higher than any heat engine operating between the same two temperatures (Figure 2-9). The theoretical efficiency of high temperature fuel cells may be lower than the theoretical (Carnot) efficiency of a heat engine operating between the same temperatures (Figure 2-9). Some may argue that for any hydrogen/oxygen or hydrogen/air system the high temperature source is the temperature of hydrogen/oxygen flame and that in this case no fuel cell efficiency can exceed the Carnot efficiency of an engine using this flame as the heat source. Although this may be correct, it has no relevance to the fuel cell where there is no flame and the theoretical efficiency is determined by the ratio between Gibbs free energy and enthalpy of the hydrogen/oxygen reaction regardless of the hydrogen/oxygen flame temperature.

## 2.9. Effect of Pressure

All of the previous equations were valid at atmospheric pressure. However, a fuel cell may operate at any pressure, typically from atmospheric all the way up to 6–7 bar. For an isothermal process, and with a little bit of basic thermodynamics [4], the change in Gibbs free energy may be shown to be:

$$dG = V_m dP \quad (2-29)$$

where:

$V_m$  = molar volume,  $\text{m}^3 \text{mol}^{-1}$

$P$  = pressure, Pa

For an ideal gas:

$$PV_m = RT \quad (2-30)$$

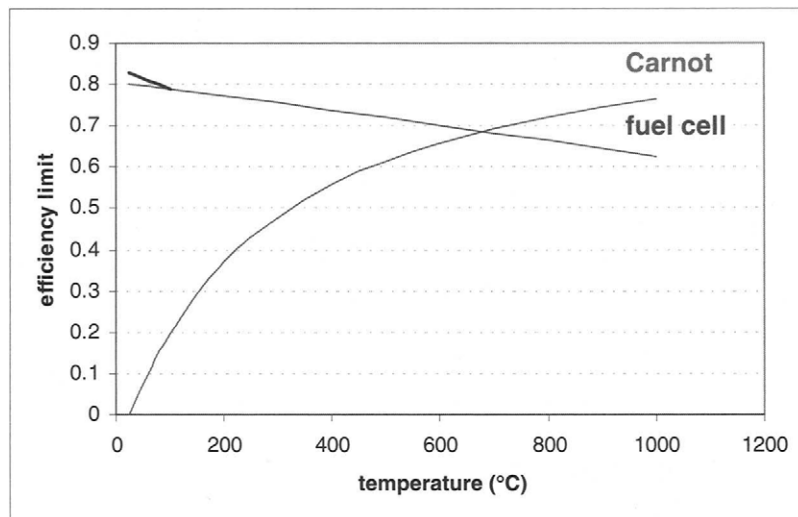


FIGURE 2-9. Theoretical efficiencies of Carnot engine and fuel cell as a function of temperature.

Therefore:

$$dG = RT \frac{dP}{P} \quad (2-31)$$

After integration:

$$G = G_0 + RT \ln\left(\frac{P}{P_0}\right) \quad (2-32)$$

Where  $G_0$  is Gibbs free energy at standard temperature and pressure ( $25^\circ\text{C}$  and 1 atm), and  $P_0$  is the reference or standard pressure (1 atm).

For any chemical reaction:



The change in Gibbs free energy is the change between products and reactants:

$$\Delta G = mG_C + nG_D - jG_A - kG_B \quad (2-34)$$

After substituting into Equation (2-32):

$$\Delta G = \Delta G_0 + RT \ln \left[ \frac{\left( \frac{P_C}{P_0} \right)^m \left( \frac{P_D}{P_0} \right)^n}{\left( \frac{P_A}{P_0} \right)^j \left( \frac{P_B}{P_0} \right)^k} \right] \quad (2-35)$$

This is known as the Nernst equation, where  $P$  is the partial pressure of the reactant or product species and  $P_0$  is the reference pressure (i.e., 1 atm or 101.25 kPa).

For the hydrogen/oxygen fuel cell reaction, the Nernst equation becomes:

$$\Delta G = \Delta G_0 + RT \ln\left(\frac{P_{H_2O}}{P_{H_2} P_{O_2}^{0.5}}\right) \quad (2-36)$$

By introducing Equation (2-18) into Equation (2-36):

$$E = E_0 + \frac{RT}{nF} \ln\left(\frac{P_{H_2} P_{O_2}^{0.5}}{P_{H_2O}}\right) \quad (2-37)$$

Note that the previous equations are only valid for gaseous products and reactants. When liquid water is produced in a fuel cell,  $P_{H_2O} = 1$ . From Equation (2-37) it follows that at higher reactant pressures the cell potential is higher. Also, if the reactants are diluted, for example, if air is used instead of pure oxygen, their partial pressure is proportional to their concentration and consequently the cell potential is lower. In case of air vs oxygen, the theoretical voltage loss/gain is:

$$\Delta E = E_{O_2} - E_{Air} = \frac{RT}{nF} \ln\left(\frac{P_{O_2}}{P_{Air}}\right)^{0.5} = \frac{RT}{nF} \ln\left(\frac{1}{0.21}\right)^{0.5} \quad (2-38)$$

At 80°C this voltage gain/loss becomes 0.012 V. In practice, this is much higher, as will be discussed in Chapter 3.

## 2.10. Summary

The ideal cell potential, if all Gibbs free energy is utilized, is:

$$E_{25C,1atm} = \frac{-\Delta G}{nF} = \frac{237,340}{2,96,485} \frac{J mol^{-1}}{As mol^{-1}} = 1.23 \text{ Volts} \quad (2-39)$$

Cell potential is a function of temperature and pressure:

$$E_{T,P} = -\left(\frac{\Delta H}{nF} - \frac{T\Delta S}{nF}\right) + \frac{RT}{nF} \ln\left[\frac{P_{H_2} P_{O_2}^{0.5}}{P_{H_2O}}\right] \quad (2-40)$$

Ignoring the changes of  $dH$  and  $dS$  with temperature (which has a very small error for temperatures below 100°C), this equation becomes:

$$E_{T,P} = 1.482 - 0.000845T + 0.0000431T \ln(P_{H_2} P_{O_2}^{0.5}) \quad (2-41)$$

For example, a hydrogen/air fuel cell, operating at 60°C with reactant gases at atmospheric pressure and with liquid water as a product, is expected to have a potential of:

$$\begin{aligned} E_{T,P} &= 1.482 - 0.000845 \times 333.15 + 0.0000431 \times 333.15 \ln(1 \times 0.21^{0.5}) \\ &= 1.482 - 0.282 - 0.011 = 1.189 \text{ V} \end{aligned} \quad (2-42)$$

Note that oxygen concentration (by volume) in air is 21%, and therefore the oxygen partial pressure in this case is 21% of the atmospheric pressure.

The ideal fuel cell efficiency is:

$$\eta = \Delta G / \Delta H = 237.34 / 286.02 = 83\% \quad (2-43)$$

or:

$$\eta = E_0 / 1.482 \text{ V} = 1.23 / 1.482 = 83\%$$

The ideal efficiency decreases with the temperature. For example, at 60°C the ideal efficiency of a hydrogen/air fuel cell is:

$$\eta = E_0 / 1.482 \text{ V} = 1.189 / 1.482 = 80\%$$

## References

1. Weast, R. C. (editor), *CRC Handbook of Chemistry and Physics* (CRC Press, Boca Raton, FL, 1988).
2. Hirschenhofer, J. H., D. B. Stauffer, and R. R. Engleman, *Fuel Cells: A Handbook* (Revision 3) (U.S. Department of Energy, Morgantown Energy Technology Center, DOE/METC-94/1006, January 1994).
3. Kurzon, F. L. and B. Ahlborn, Efficiency of a Carnot Engine at Maximum Power Output, *American Journal of Physics*, Vol. 43, 1975, pp. 22–24.
4. Chen, E., Thermodynamics and Electrochemical Kinetics, in G. Hoogers (editor), *Fuel Cell Technology Handbook* (CRC Press, Boca Raton, FL, 2003).

## Problems

### Problem No. 1:

Derive Equation (2-29) starting from  $G = H - TS$ . Explain assumptions.

**Problem No. 2:**

For a hydrogen/air fuel cell operating at 60°C with reactant gases at atmospheric pressure and with liquid water as a product, calculate the theoretical cell potential taking into account the changes of reaction enthalpy and entropy with temperature (Equations 2-22 and 2-23).

**Problem No. 3:**

For a hydrogen/air fuel cell operating at 600°C with reactant gases at atmospheric pressure and with gaseous water as a product, calculate the theoretical cell potential taking into account the changes of reaction enthalpy and entropy with temperature (Equations 2-22 and 2-23). Repeat the same process ignoring those changes and compare the results.

**Problem No. 4:**

Calculate the expected difference in theoretical cell potential between a hydrogen/oxygen fuel cell operating at 80°C and 5 bar (both reactant gases) and the same fuel cell operating at atmospheric pressure. What if the pressure is increased to 25 bar?

**Quiz**

1. Fuel cell is:
  - a) a device that stores fuel
  - b) a device that converts fuel into electricity
  - c) a device that generates fuel
2. Fuel cell catalyst serves to:
  - a) make good electric contacts
  - b) make the electrochemical reactions happen
  - c) generate internal electrical current
3. Fuel cell catalyst must be:
  - a) electrically conductive
  - b) an electrical insulator
  - c) electrically conductive or an insulator—it does not matter
4. Porous fuel cell electrode is porous:
  - a) so that the fuel cell may be made lightweight
  - b) so that it can allow transfer of electrons (through solid) and gases (through voids)
  - c) it does not have to be porous

5. Fuel cells must be stacked in order to:

- a) generate more current than a single cell of the same active area
- b) generate same current as a single cell of the same active area but at a higher voltage
- c) generate both more current and higher voltage than a single cell of the same active area

6. Heating value of fuel is:

- a) a measure of how much heat can be generated in a fuel cell
- b) a measure of how much electricity can be generated in a fuel cell
- c) a measure of how much heat can be generated if the fuel is combusted (not necessarily in a fuel cell)

7. Fuel cell:

- a) is always more efficient than a Carnot cycle
- b) has approximately the same efficiency as a Carnot cycle
- c) ideal efficiency may be compared with a Carnot cycle and it may be higher or lower than the Carnot efficiency, depending on the temperature

8. Theoretical fuel cell potential:

- a) is higher at higher hydrogen or oxygen pressure
- b) is lower at higher hydrogen pressure
- c) does not depend on pressure

9. Theoretical fuel cell potential:

- a) is higher at higher temperatures
- b) is lower at higher temperatures
- c) does not depend on temperature

10. Fuel cell efficiency is:

- a) proportional to its voltage
- b) inversely proportional to its voltage
- c) proportional to the square of voltage divided by heat generating rate

# CHAPTER 3

## 3. Fuel Cell Electrochemistry

### 3.1. Electrode Kinetics

A fuel cell is an electrochemical energy converter. Its operation is based on the following electrochemical reactions happening simultaneously on the anode and the cathode:

At the anode:



At the cathode:



More precisely, the reactions happen on an interface between the ionically conductive electrolyte and electrically conductive electrode. Because there are gases involved in fuel cell electrochemical reactions, the electrodes must be porous allowing the gases to arrive to, as well as product water to leave the reaction sites. Note that these are the overall reactions and that in both cases there are several intermediary sequential and parallel steps involved.

#### 3.1.1. Reaction Rate

Electrochemical reactions involve both a transfer of electrical charge and a change in Gibbs energy [1]. The rate of an electrochemical reaction is determined by an activation energy barrier that the charge must overcome in moving from electrolyte to a solid electrode or vice versa. The speed at which an electrochemical reaction proceeds on the electrode surface is the rate at which the electrons are released or “consumed,” which is the electrical current. Current density is the current (of electrons or ions) per unit area of the surface. From Faraday’s Law it follows that current density is proportional to the charge transferred and the consumption of reactant per unit area:

$$i = nF j \quad (3-3)$$

where  $nF$  is the charge transferred (Coulombs mol<sup>-1</sup>) and  $j$  is the flux of reactant per unit area (mols<sup>-1</sup> cm<sup>-2</sup>).

Therefore, the reaction rate may be easily measured by a current-measuring device placed external to the cell. However, the measured current or current density is actually the net current, that is, the difference between forward and reverse current on the electrode. In general, an electrochemical reaction involves either oxidation or reduction of the species:



In a hydrogen/oxygen fuel cell the anode reaction is oxidation of hydrogen, in which hydrogen is stripped of its electrons, and the products of this reaction are protons and electrons. The cathode reaction is oxygen reduction and water is generated as a product.

On an electrode at equilibrium conditions, that is, when no external current is being generated, both processes, oxidation and reduction, occur at equal rates:



The consumption of the reactant species is proportional to their surface concentration. For the forward reaction of Equation (3-6), which is the reaction described by Equation (3-5), the flux is:

$$j_f = k_f C_{\text{Ox}} \quad (3-7)$$

where:

$k_f$  = forward reaction (reduction) rate coefficient, and  
 $C_{\text{Ox}}$  = surface concentration of the reacting species

Similarly, for the backward reaction of Equation (3-6), which is the reaction described by Equation (3-4), the flux is:

$$j_b = k_b C_{\text{Rd}} \quad (3-8)$$

where:

$k_b$  = backward reaction (oxidation) rate coefficient, and  
 $C_{\text{Rd}}$  = surface concentration of reacting species

Each of these two reactions either releases or consumes electrons. The net current generated is the difference between the electrons released and consumed:

$$i = nF(k_f C_{\text{Ox}} - k_b C_{\text{Rd}}) \quad (3-9)$$

At equilibrium, the net current is equal to zero, although the reaction proceeds in both directions simultaneously. The rate at which these reactions proceed at equilibrium is called the exchange current density.

### 3.1.2. Reaction Constants; Transfer Coefficient

From the Transition State Theory [2], it may be shown that the reaction rate coefficient for an electrochemical reaction is a function of the Gibbs free energy [1]:

$$k = \frac{k_B T}{h} \exp\left(\frac{-\Delta G}{RT}\right) \quad (3-10)$$

where:

$$\begin{aligned} k_B &= \text{Boltzmann's constant} \\ h &= \text{Planck's constant} \end{aligned}$$

The Gibbs free energy for electrochemical reactions may be considered to consist of both chemical and electrical terms [1]. In that case, for a reduction reaction:

$$\Delta G = \Delta G_{\text{ch}} + \alpha_{\text{Rd}} F E \quad (3-11)$$

and for an oxidation reaction:

$$\Delta G = \Delta G_{\text{ch}} - \alpha_{\text{Ox}} F E \quad (3-12)$$

The subscript "ch" denotes the chemical component of the Gibbs free energy,  $\alpha$  is a transfer coefficient,  $F$  is the Faraday's constant, and  $E$  is the potential. There is a fair amount of confusion in the literature concerning the transfer coefficient,  $\alpha$ , and the symmetry factor,  $\beta$ , that is sometimes used. The symmetry factor,  $\beta$ , may be used strictly for a single-step reaction involving a single electron ( $n = 1$ ). Its value is theoretically between 0 and 1, but most typically for the reactions on a metallic surface it is around 0.5. The way in which  $\beta$  is defined requires that the sum of the symmetry factors in the anodic and cathodic direction be unity; if it is  $\beta$  for the reduction reaction it must be  $(1 - \beta)$  for the reverse, oxidation reaction.

However, both electrochemical reactions in a fuel cell, namely oxygen reduction and hydrogen oxidation, involve more than one step and more

than one electron. In that case, at steady state, the rate of all steps must be equal, and it is determined by the slowest step in the sequence, which is referred to as the rate-determining step. In order to describe a multistep process, instead of the symmetry factor,  $\beta$ , a rather experimental parameter is used, which is called the transfer coefficient,  $\alpha$ . Note that in this case  $\alpha_{\text{Rd}} + \alpha_{\text{Ox}}$  does not necessarily have to be equal to unity. Actually, in general  $(\alpha_{\text{Rd}} + \alpha_{\text{Ox}}) = n/v$ , where  $n$  is the number of electrons transferred in the overall reaction and  $v$  is the stoichiometric number defined as the number of times the rate-determining step must occur for the overall reaction to occur once [3].

The forward (reduction) and backward (oxidation) reaction rate coefficients in Equation (3-9) are then respectively:

$$k_f = k_{0,f} \exp\left[\frac{-\alpha_{\text{Rd}}FE}{RT}\right] \quad (3-13)$$

$$k_b = k_{0,b} \exp\left[\frac{\alpha_{\text{Ox}}FE}{RT}\right] \quad (3-14)$$

### 3.1.3. Current Potential Relationship—Butler–Volmer Equation

By introducing into Equation (3-9) the net current, density is obtained:

$$i = nF \left\{ k_{0,f} C_{\text{Ox}} \exp\left[\frac{-\alpha_{\text{Rd}}FE}{RT}\right] - k_{0,b} C_{\text{Rd}} \exp\left[\frac{\alpha_{\text{Ox}}FE}{RT}\right] \right\} \quad (3-15)$$

At equilibrium, the potential is  $E_r$ , and the net current is equal to zero, although the reaction proceeds in both directions simultaneously. The rate at which these reactions proceed at equilibrium is called the exchange current density [1,4]:

$$i_0 = nFk_{0,f}C_{\text{Ox}} \exp\left[\frac{-\alpha_{\text{Rd}}FE_r}{RT}\right] = nFk_{0,b}C_{\text{Rd}} \exp\left[\frac{\alpha_{\text{Ox}}FE_r}{RT}\right] \quad (3-16)$$

By combining the Equations (3-15) and (3-16), a relationship between the current density and potential is obtained:

$$i = i_0 \left\{ \exp\left[\frac{-\alpha_{\text{Rd}}F(E - E_r)}{RT}\right] - \exp\left[\frac{\alpha_{\text{Ox}}F(E - E_r)}{RT}\right] \right\} \quad (3-17)$$

This is known as the Butler–Volmer equation, where  $E_r$  is the reversible or equilibrium potential. Note that the reversible or equilibrium potential at the fuel cell anode is 0 V by definition [5], and the reversible potential at the fuel cell cathode is 1.229 V (at 25°C and atmospheric pressure) and it does vary with temperature and pressure as shown in Chapter 2. The

difference between the electrode potential and the reversible potential is called overpotential. It is the potential difference required to generate current.

The Butler–Volmer Equation (3-17) is valid for both anode and cathode reaction in a fuel cell:

$$i_a = i_{0,a} \left\{ \exp \left[ \frac{-\alpha_{Rd,a} F(E_a - E_{r,a})}{RT} \right] - \exp \left[ \frac{\alpha_{Ox,a} F(E_a - E_{r,a})}{RT} \right] \right\} \quad (3-18)$$

and

$$i_c = i_{0,c} \left\{ \exp \left[ \frac{-\alpha_{Rd,c} F(E_c - E_{r,c})}{RT} \right] - \exp \left[ \frac{\alpha_{Ox,c} F(E_c - E_{r,c})}{RT} \right] \right\} \quad (3-19)$$

The overpotential on the anode is positive ( $E_a > E_{r,a}$ ), which makes the first term of the Equation (3-18) negligible in comparison with the second term, that is, the oxidation current is predominant and the equation may be reduced to:

$$i_a = -i_{0,a} \exp \left[ \frac{\alpha_{Ox,a} F(E_a - E_{r,a})}{RT} \right] \quad (3-20)$$

Note that the resulting current has a negative sign, which denotes that the electrons are leaving the electrode (net oxidation reaction).

Similarly, the overpotential on the cathode is negative ( $E_c < E_{r,c}$ ), which makes the first term of the Equation (3-19) much larger than the second term, that is, the reduction current is predominant and the equation may be reduced to:

$$i_c = i_{0,c} \exp \left[ \frac{-\alpha_{Rd,c} F(E_c - E_{r,c})}{RT} \right] \quad (3-21)$$

The transfer coefficients in the previous equations for hydrogen/oxygen fuel cells using Pt catalyst seem to have value around 1. Note that in some literature there is an  $n$  parameter in the previous equations [1,5] denoting the number of electrons involved. Clearly, on the fuel cell anode side  $n = 2$ , and on the cathode side,  $n = 4$ . In that case it is the product of  $n\alpha$  that has value around 1. Larminie and Dicks [6] list a value of  $\alpha = 0.5$  for the hydrogen fuel cell anode (with two electrons involved) and  $\alpha = 0.1$  to 0.5 for the cathode. Newman [7] specifies  $\alpha$  in range between 0.2 and 2.

### 3.1.4. Exchange Current Density

Exchange current density,  $i_0$ , in electrochemical reactions is analogous to the rate constant in chemical reactions. Unlike the rate constants, exchange current density is concentration dependent (as can be seen

directly from Equation 3-16]. It is also a function of temperature (from Equation 3-10). The effective exchange current density (per unit of electrode geometrical area) is also a function of electrode catalyst loading and catalyst specific surface area. If the reference exchange current density (at reference temperature and pressure) is given per actual catalyst surface area, then the effective exchange current density at any temperature and pressure is given by the following equation [8]:

$$i_0 = i_0^{\text{ref}} a_c L_c \left( \frac{P_r}{P_r^{\text{ref}}} \right)^{\gamma} \exp \left[ -\frac{E_C}{RT} \left( 1 - \frac{T}{T_{\text{ref}}} \right) \right] \quad (3-22)$$

where:

- $i_0^{\text{ref}}$  = reference exchange current density (at reference temperature and pressure, typically 25°C and 101.25 kPa) per unit catalyst surface area,  $\text{A cm}^{-2} \text{Pt}$ ,
- $a_c$  = catalyst specific area (theoretical limit for Pt catalyst is  $2400 \text{ cm}^2 \text{mg}^{-1}$ , but state-of-the-art catalyst has about 600–1000  $\text{cm}^2 \text{mg}^{-1}$ , which is further reduced by incorporation of catalyst in the electrode structures by up to 30%).
- $L_c$  = catalyst loading (state-of-the-art electrodes have 0.3–0.5  $\text{mg Pt cm}^{-2}$ ; lower loadings are possible but would result in lower cell voltages).
- $P_r$  = reactant partial pressure, kPa
- $P_r^{\text{ref}}$  = reference pressure, kPa
- $\gamma$  = pressure coefficient (0.5 to 1.0)
- $E_C$  = activation energy,  $66 \text{ kJ mol}^{-1}$  for oxygen reduction on Pt [8]
- $R$  = gas constant,  $8.314 \text{ J mol}^{-1} \text{ K}^{-1}$
- $T$  = temperature, K
- $T_{\text{ref}}$  = reference temperature, 298.15 K

The product  $a_c L_c$  is also called electrode roughness, meaning the catalyst surface area,  $\text{cm}^2$ , per electrode geometric area,  $\text{cm}^2$ . Instead of the ratio of partial pressures, a ratio of concentrations at the catalyst surface may be used as well.

Exchange current density is a measure of an electrode's readiness to proceed with the electrochemical reaction. If the exchange current density is high, the surface of the electrode is more active. In a hydrogen/oxygen fuel cell, the exchange current density at the anode is much larger (several orders of magnitudes) than at the cathode. The higher the exchange current density, the lower the energy barrier that the charge must overcome moving from electrolyte to the catalyst surface and vice versa. In other words, the higher the exchange current density, the more current is generated at any overpotential.

Because the anode exchange current density in hydrogen/oxygen fuel cells is several orders of magnitudes larger than the cathode current density

( $\sim 10^{-4}$  vs  $\sim 10^{-9} \text{ A cm}^{-2} \text{ Pt}$ , at  $25^\circ\text{C}$  and  $1 \text{ atm}$ ), the overpotential on the cathode is much larger than the anode overpotential. For that reason, very often the cell potential—current relationship is approximated solely by Equation (3-21).

### 3.2. Voltage Losses

If a fuel cell is supplied with reactant gases, but the electrical circuit is not closed (Figure 3-1a), it will not generate any current, and one would expect the cell potential to be at, or at least close to, the theoretical cell potential for given conditions (temperature, pressure, and concentration of reactants). However, in practice this potential, called the open circuit potential, is significantly lower than the theoretical potential, usually less than 1 V. This suggests that there are some losses in the fuel cell even when no external current is generated. When the electrical circuit is closed with a load (such as a resistor) in it, as shown in Figure 3-1b, the potential is expected to drop even further as a function of current being generated, due to unavoidable losses. There are different kinds of voltage losses in a fuel cell caused by the following factors:

- kinetics of the electrochemical reactions
- internal electrical and ionic resistance
- difficulties in getting the reactants to reaction sites
- internal (stray) currents
- crossover of reactants

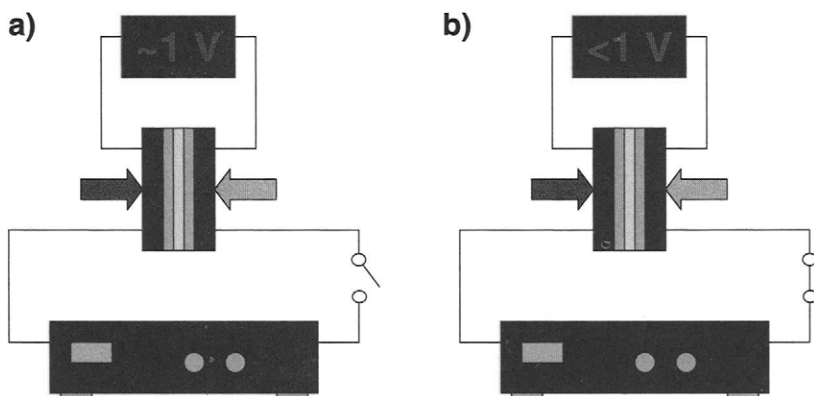


FIGURE 3-1. Fuel cell with a load: a) in open circuit; b) load connected.

Although mechanical and electrical engineers prefer to use voltage losses, (electro)chemical engineers use terms such as polarization or overpotential. They all have the same physical meaning—difference between the electrode potential and the equilibrium potential. From the electrochemical engineer's point of view, this difference is the driver for the reaction, and from a mechanical or electrical engineer's point of view, this represents the loss of voltage and power.

### 3.2.1. Activation Polarization

Some voltage difference from equilibrium is needed to get the electrochemical reaction going, as shown previously (Equation 3-17). This is called activation polarization, and it is associated with sluggish electrode kinetics. The higher the exchange current density, the lower the activation polarization losses. These losses happen at both anode and cathode; however, oxygen reduction requires much higher overpotentials, that is, it is a much slower reaction than hydrogen oxidation.

As discussed earlier, at relatively high negative overpotentials (*i.e.*, potentials lower than the equilibrium potential), such as those at the fuel cell cathode, the first term in the Butler–Volmer equation becomes predominant, which allows for expression of potential as a function of current density (from Equation 3-21):

$$\Delta V_{act,c} = E_{r,c} - E_c = \frac{RT}{\alpha_c F} \ln\left(\frac{i}{i_{0,c}}\right) \quad (3-23)$$

Figure 3-2 shows typical activation polarization for oxygen reduction on Pt.

Similarly, at the anode at positive overpotentials (*i.e.*, higher than the equilibrium potential) the second term in the Butler–Volmer equation becomes predominant:

$$\Delta V_{act,a} = E_a - E_{r,a} = \frac{RT}{\alpha_a F} \ln\left(\frac{i}{i_{0,a}}\right) \quad (3-24)$$

Note that by definition, in electrochemistry, the reversible potential of the hydrogen oxidation reaction is zero at all temperatures [5]. That is why the standard hydrogen electrode is used as a reference electrode. Therefore, for hydrogen anodes  $E_{r,a} = 0\text{ V}$ . Activation polarization of the hydrogen oxidation reaction is much smaller than activation polarization of the oxygen reduction reaction.

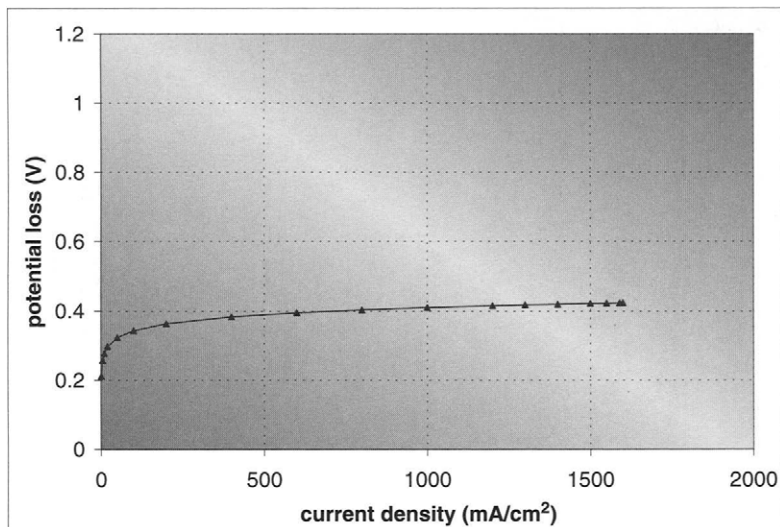


FIGURE 3-2. Voltage loss due to polarization activation.

A simplified way to show the activation losses is to use the so-called Tafel equation:

$$\Delta V_{act} = a + b \log(i) \quad (3-25)$$

where

$$a = -2.3 \frac{RT}{\alpha F} \log(i_o), \text{ and } b = 2.3 \frac{RT}{\alpha F}.$$

Term  $b$  is called the Tafel slope.

Note that at any given temperature the Tafel slope depends solely on transfer coefficient,  $\alpha$ . For  $\alpha = 1$ , the Tafel slope at 60°C is ~60 mV per decade, what is typically found for oxygen reduction on Pt.

If voltage-current relationship is plotted in a logarithmic scale, the main parameters,  $a$ ,  $b$ , and  $i_o$ , are easily detectable (Figure 3-3).

If these activation polarizations were the only losses in a fuel cell, the cell potential would be:

$$E_{cell} = E_c - E_a = E_r - \Delta V_{act,c} - \Delta V_{act,a} \quad (3-26)$$

$$E_{cell} = E_r - \frac{RT}{\alpha_c F} \ln\left(\frac{i}{i_{o,c}}\right) - \frac{RT}{\alpha_a F} \ln\left(\frac{i}{i_{o,a}}\right) \quad (3-27)$$

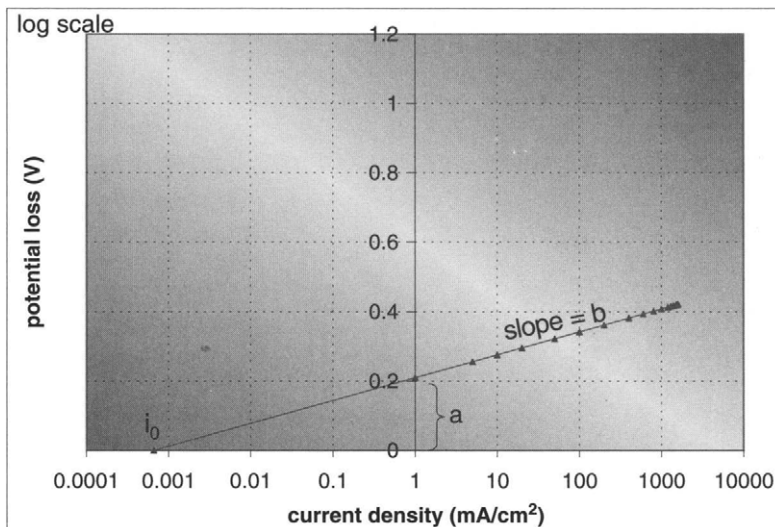


FIGURE 3-3. Potential loss due to activation polarization in log scale.

If anode polarization is neglected, the previous equation becomes:

$$E_{\text{cell}} = E_t - \frac{RT}{\alpha F} \ln\left(\frac{i}{i_0}\right) \quad (3-28)$$

which has the same form as the Tafel Equation (3-25).

### 3.2.2. Internal Currents and Crossover Losses

Although the electrolyte, a polymer membrane, is not electrically conductive and is practically impermeable to reactant gases, some small amount of hydrogen will diffuse from anode to cathode, and some electrons may also find a "shortcut" through the membranes. Because each hydrogen molecule contains two electrons, this fuel crossover and the so-called internal currents are essentially equivalent. Each hydrogen molecule that diffuses through the polymer electrolyte membrane and reacts with oxygen on the cathode side of the fuel cell results in two fewer electrons in the generated current of electrons that travels through an external circuit. These losses may appear insignificant in fuel cell operation, because the rate of hydrogen permeation or electron crossover is several orders of magnitude lower than hydrogen consumption rate or total electrical current generated. However, when the fuel cell is at open circuit potential or when it operates at very low current densities, these losses may have a dramatic effect on cell potential, as shown in Figure 3-4.

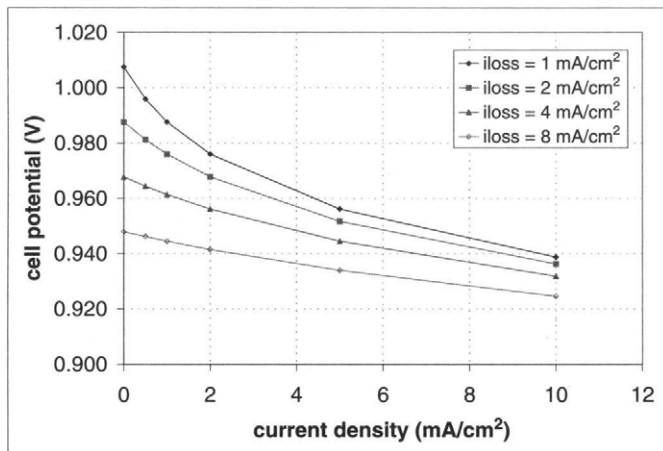


FIGURE 3-4. Effect of internal currents and/or hydrogen crossover loss on open circuit potential.

The total electrical current is the sum of external (useful) current and current losses due to fuel crossover and internal currents:

$$I = I_{\text{ext}} + I_{\text{loss}} \quad (3-29)$$

Current divided by the electrode active area, A, is current density, A/cm<sup>2</sup>:

$$i = \frac{I}{A} \quad (3-30)$$

Therefore:

$$i = i_{\text{ext}} + i_{\text{loss}} \quad (3-31)$$

If this total current density is used in the equation that approximates the cell potential (Equation 3-28), the following equation results:

$$E_{\text{cell}} = E_r - \frac{RT}{\alpha F} \ln \left( \frac{i_{\text{ext}} + i_{\text{loss}}}{i_0} \right) \quad (3-32)$$

Therefore, even if the external current is equal to zero, such as at open circuit, the cell voltage may be significantly lower than the reversible cell potential for given conditions. Indeed, open circuit potential of hydrogen/air fuel cells is typically below 1 V, most likely about 0.94 to 0.97 V (depending on operating pressure).

$$E_{\text{cell,OCV}} = E_r - \frac{RT}{\alpha F} \ln \left( \frac{i_{\text{loss}}}{i_0} \right) \quad (3-33)$$

Although hydrogen crossover and internal currents are equivalent, they physically have different effects in a fuel cell. The loss of electrons occurs after the electrochemical reaction has taken place and therefore the effect on both anode and cathode activation polarization would have the effect as depicted by Equation (3-32). Hydrogen that permeates through the membrane does not participate in the electrochemical reaction on the anode side, and in that case the total current resulting from the electrochemical reaction would be the same as the external current. However, hydrogen that permeates through the membrane to the cathode side may react with oxygen on the surface of the catalyst in reaction  $H_2 + \frac{1}{2}O_2 \rightarrow H_2O$ , and as a result would "depolarize" the cathode, that is, reduce the cathode (and cell) potential. Equations (3-32) and (3-33) are therefore only an approximation.

In addition, oxygen may permeate through the membrane as well, although the oxygen permeation rate is much lower than the hydrogen permeation rate. The effect on fuel cell performance would be similar to that of hydrogen crossover loss, but in this case the anode would be "depolarized."

Hydrogen crossover is a function of membrane permeability, membrane thickness, and hydrogen partial pressure (*i.e.*, hydrogen concentration) difference across the membrane, as the main driving force. A very low open circuit potential (significantly below 0.9 V) may indicate either a hydrogen leak or an electrical short.

As the fuel cell starts generating current, hydrogen concentration in the catalyst layer decreases, which reduces the driving force for hydrogen permeation through the membrane. That is one of the reasons these losses are mainly negligible at operating currents.

### 3.2.3. Ohmic (Resistive) Losses

Ohmic losses occur because of resistance to the flow of ions in the electrolyte and resistance to the flow of electrons through the electrically conductive fuel cell components. These losses can be expressed by Ohm's law:

$$\Delta V_{\text{ohm}} = iR_i \quad (3-34)$$

where:

$i$  = current density,  $\text{A cm}^{-2}$ , and

$R_i$  = total cell internal resistance (which includes ionic, electronic, and contact resistance,  $\Omega \text{cm}^2$ ):

$$R_i = R_{i,i} + R_{i,e} + R_{i,c} \quad (3-35)$$

Electronic resistance is almost negligible, even when graphite or graphite/polymer composites are used as current collectors. Ionic and

contact resistances are approximately of the same order of magnitude [8,9]. Both will be discussed later in Chapter 4. Typical values for  $R_i$  are between 0.1 and  $0.2\Omega\text{cm}^2$ . Figure 3-5 shows typical resistive losses in the fuel cell ( $R_i = 0.15\Omega\text{cm}^2$ ). Note that Figure 3-5 is in the same scale as Figure 3-6 for an easy comparison of the magnitude of these losses.

### 3.2.4. Concentration Polarization

Concentration polarization occurs when a reactant is rapidly consumed at the electrode by the electrochemical reaction so that concentration gradients are established. We learned before that the electrochemical reaction potential changes with partial pressure of the reactants, and this relationship is given by the Nernst equation:

$$\Delta V = \frac{RT}{nF} \ln\left(\frac{C_B}{C_s}\right) \quad (3-36)$$

where:

$C_B$  = bulk concentration of reactant,  $\text{mol cm}^{-3}$

$C_s$  = concentration of reactant at the surface of the catalyst,  $\text{mol cm}^{-3}$

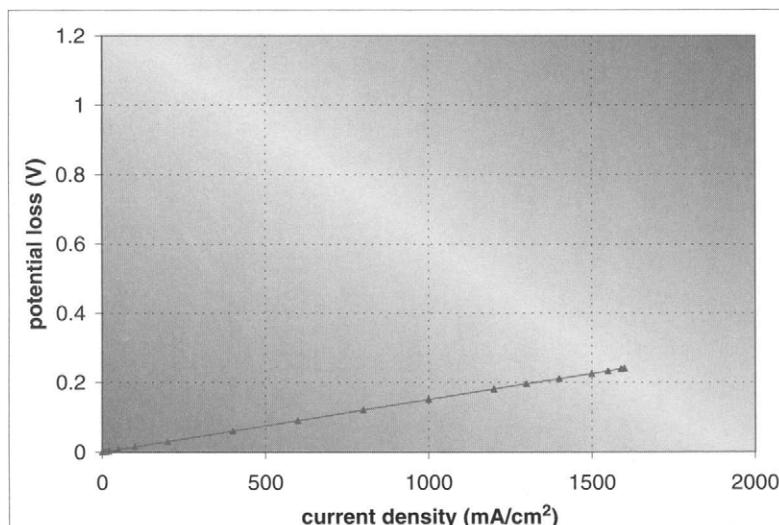


FIGURE 3-5. Resistive (ohmic) losses in the fuel cell ( $R_i = 0.15\Omega\text{-cm}^2$ ).

According to Fick's Law, the flux of reactant is proportional to concentration gradient:

$$N = \frac{D \cdot (C_B - C_S)}{\delta} A \quad (3-37)$$

where:

$N$  = flux of reactants,  $\text{mol s}^{-1}$

$D$  = diffusion coefficient of the reacting species,  $\text{cm}^2 \text{s}^{-1}$

$A$  = electrode active area,  $\text{cm}^2$

$\delta$  = diffusion distance, cm

In steady state, the rate at which the reactant species is consumed in the electrochemical reaction is equal to the diffusion flux (Equation 3-3):

$$N = \frac{I}{nF} \quad (3-38)$$

By combining Equations (3-37) and (3-38), the following relationship is obtained:

$$i = \frac{nF \cdot D \cdot (C_B - C_S)}{\delta} \quad (3-39)$$

The reactant concentration at the catalyst surface thus depends on current density—the higher the current density, the lower the surface concentration. The surface concentration reaches zero when the rate of consumption exceeds the diffusion rate—the reactant is consumed faster than it can reach the surface. Current density at which this happens is called the limiting current density. A fuel cell cannot produce more than the limiting current because there are no reactants at the catalyst surface. Therefore, for  $C_S = 0$ ,  $i = i_L$ , and the limiting current density is then:

$$i_L = \frac{nFDC_B}{\delta} \quad (3-40)$$

By combining Equations (3-36), (3-39), and (3-40), a relationship for voltage loss due to concentration polarization is obtained:

$$\Delta V_{\text{conc}} = \frac{RT}{nF} \ln\left(\frac{i_L}{i_L - i}\right) \quad (3-41)$$

The previous equation would result in a sharp drop of cell potential as the limiting current is approached (as shown in Figure 3-6). However, because of nonuniform conditions over the porous electrode area, the limiting current is almost never experienced in practical fuel cells. In order to experience a sharp drop of cell potential when the limiting current density is

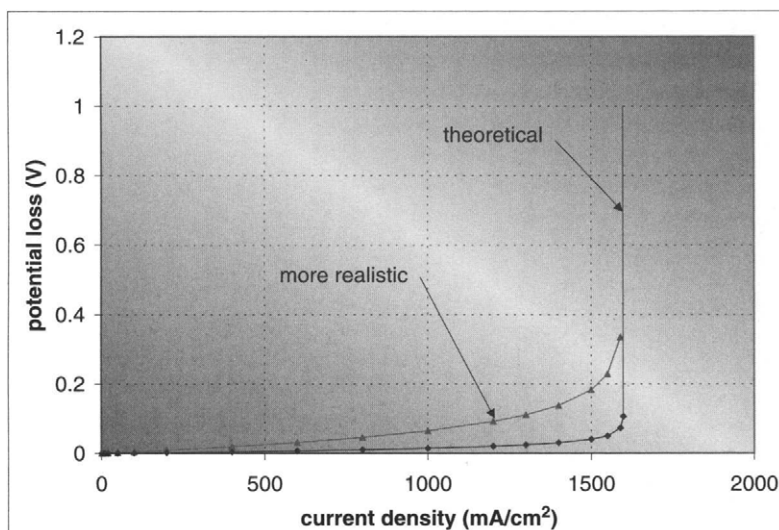


FIGURE 3-6. Concentration polarization losses in the fuel cell.

reached, the current density would have to be uniform over the entire electrode surface, which is almost never the case. There will be some areas that would reach the limiting current density sooner than other areas. Limiting current density may be experienced at either cathode or anode.

Another reason why a sharp distinguished drop in cell voltage at limiting current does not show in practical fuel cells is that the exchange current density is a function of concentration of reactant at the catalyst surface,  $C_s$ . As the current density approaches limiting current density, the surface concentration, and consequently the exchange current density, approaches zero (as follows from Equation 3-22), which causes additional voltage loss, as follows from Equation (3-27) or Equation (3-28).

An empirical equation better describes the polarization losses, as suggested by Kim *et al.* [10]:

$$\Delta V_{\text{conc}} = c \cdot \exp\left(\frac{i}{d}\right) \quad (3-42)$$

where  $c$  and  $d$  are empirical coefficients (values of  $c = 3 \times 10^{-5} \text{ V}$  and  $d = 0.125 \text{ A cm}^{-2}$  have been suggested [6]).

### 3.3. Cell Potential—Polarization Curve

Figure 3-7 shows the proportions between the three types of losses in the fuel cell. Activation losses are by far the largest losses at any current density.

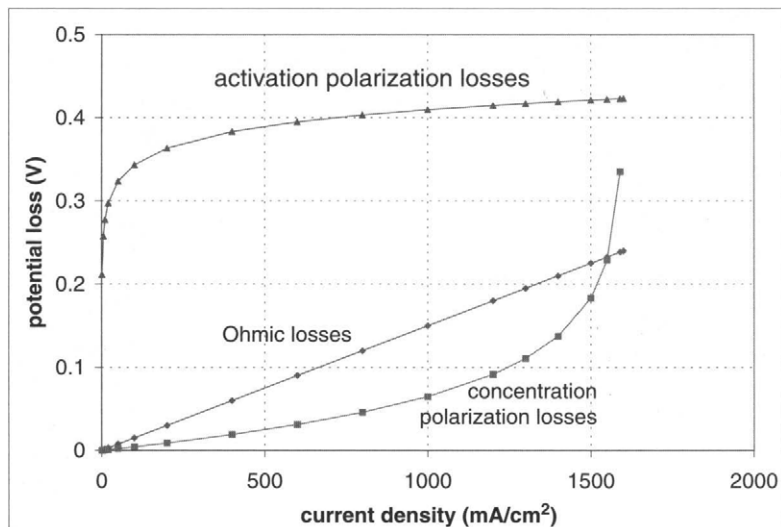


FIGURE 3-7. Voltage losses in the fuel cell.

Activation and concentration polarization can occur at both anode and cathode. The cell voltage is therefore:

$$V_{\text{cell}} = E_r - (\Delta V_{\text{act}} + \Delta V_{\text{conc}})_a - (\Delta V_{\text{act}} + \Delta V_{\text{conc}})_c - \Delta V_{\text{ohm}} \quad (3-43)$$

By introducing Equations (3-23), (3-24), (3-34), and (3-41) into Equation (3-43), a relationship between fuel cell potential and current density, the so-called fuel cell polarization curve, is obtained:

$$\begin{aligned} E_{\text{cell}} = & E_{r,T,p} - \frac{RT}{\alpha_c F} \ln\left(\frac{i}{i_{0,c}}\right) - \frac{RT}{\alpha_a F} \ln\left(\frac{i}{i_{0,a}}\right) \\ & - \frac{RT}{nF} \ln\left(\frac{i_{L,c}}{i_{L,c} - i}\right) - \frac{RT}{nF} \ln\left(\frac{i_{L,a}}{i_{L,a} - i}\right) - iR_i \end{aligned} \quad (3-44)$$

In addition, Equation (3-32) may be taken into account, which would account for hydrogen crossover and internal current losses.

$$\begin{aligned} E_{\text{cell}} = & E_{r,T,p} - \frac{RT}{\alpha_c F} \ln\left(\frac{i_{\text{ext}} + i_{\text{loss}}}{i_{0,c}}\right) - \frac{RT}{\alpha_a F} \ln\left(\frac{i_{\text{ext}} + i_{\text{loss}}}{i_{0,a}}\right) \\ & - \frac{RT}{nF} \ln\left(\frac{i_{L,c}}{i_{L,c} - i_{\text{ext}} - i_{\text{loss}}}\right) - \frac{RT}{nF} \ln\left(\frac{i_{L,a}}{i_{L,a} - i_{\text{ext}} - i_{\text{loss}}}\right) \\ & - (i_{\text{ext}} + i_{\text{loss}})R_{i,i} - i_{\text{ext}}(R_{i,e} + R_{i,c}) \end{aligned} \quad (3-45)$$

An additional complication is that the exchange current densities, as well as hydrogen crossover losses, are proportional to local reactant concentration in the catalyst layer, which decreases with increased reaction rate, that is, increased current density. If a similar argument is used as in Equations (3-35) through (3-40), which assumes a linear decrease of reactant concentration with increased current density, the following equations may be derived:

$$i_{\text{loss}}(i_{\text{ext}}) = i_{\text{loss}}^{\text{ref}} \frac{i_L - i_{\text{ext}}}{i_L + i_{\text{loss}}^{\text{ref}}} \quad (3-46)$$

and

$$i_0(i_{\text{ext}}) = \frac{i_0^{\text{ref}}}{i_L} (i_L - i_{\text{ext}} - i_{\text{loss}}) \quad (3-47)$$

where  $i_{\text{loss}}^{\text{ref}}$  is the current loss when the surface concentration is equal to bulk concentration. Similarly,  $i_0^{\text{ref}}$  is defined as the exchange current density when the surface concentration is equal to bulk concentration. Note that in case of hydrogen crossover or internal current loss, the surface concentration may not be equal to bulk concentration when there is no external current ( $i_{\text{ext}} = 0$ ).

A sufficiently accurate approximation of the fuel cell polarization curve may be obtained by the following equation:

$$E_{\text{cell}} = E_{r,T,P} - \frac{RT}{\alpha F} \ln\left(\frac{i}{i_0}\right) - \frac{RT}{nF} \ln\left(\frac{i_L}{i_L - i}\right) - iR_i \quad (3-48)$$

that has the same form and same parameters as Equation (3-44), but assumes that the anode losses are negligible compared with the cathode losses. If the anode activation losses cannot be ignored, the fuel cell polarization curve may still be expressed with the previous Equation (3-48), but in that case:

$$\frac{1}{\alpha} = \frac{1}{\alpha_a} + \frac{1}{\alpha_c} \quad \text{and} \quad i_0 = i_{0,a}^{\alpha \alpha_a} \cdot i_{0,c}^{\alpha \alpha_c}$$

Figure 3-8 shows how the cell polarization curve is formed, by subtracting the activation polarization losses, ohmic losses, and concentration polarization losses from the equilibrium potential. Anode and cathode activation losses are lumped together, but, as mentioned before, a majority of the losses occur on the cathode because of sluggishness of the oxygen reduction reaction.

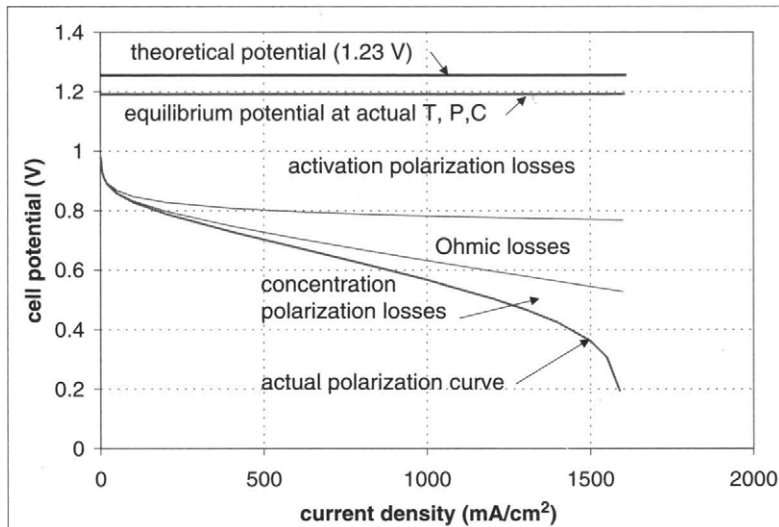


FIGURE 3-8. Voltage losses in fuel cell and resulting polarization curve.

### 3.4. Distribution of Potential Across A Fuel Cell

Figure 3-9 illustrates potential distribution in a hydrogen/air fuel cell over the cell cross-section [8]. At open circuit, when there is no current being generated, the anode is at reference or zero potential and the cathode is at the potential corresponding to the reversible potential at given temperature, pressure, and oxygen concentration. As soon as the current is being generated, the cell potential, measured as the difference between cathode and anode solid phase potentials (solid phase means electrically conductive parts), drops because of various losses as discussed earlier.

Note that the cell potential is equal to the reversible cell potential (or the equilibrium potential,  $E_{eq}$ ) reduced by the potential losses:

$$E_{cell} = E_r - E_{loss} \quad (3-49)$$

where the losses are composed of activation and concentration polarization on both anode and cathode and of ohmic losses as discussed earlier:

$$E_{loss} = (\Delta V_{act} + \Delta V_{conc})_a + (\Delta V_{act} + \Delta V_{conc})_c + \Delta V_{ohm} \quad (3-50)$$

The cell potential is equal to the difference between the cathode and the anode solid state potentials:

$$E_{cell} = E_c - E_a \quad (3-51)$$

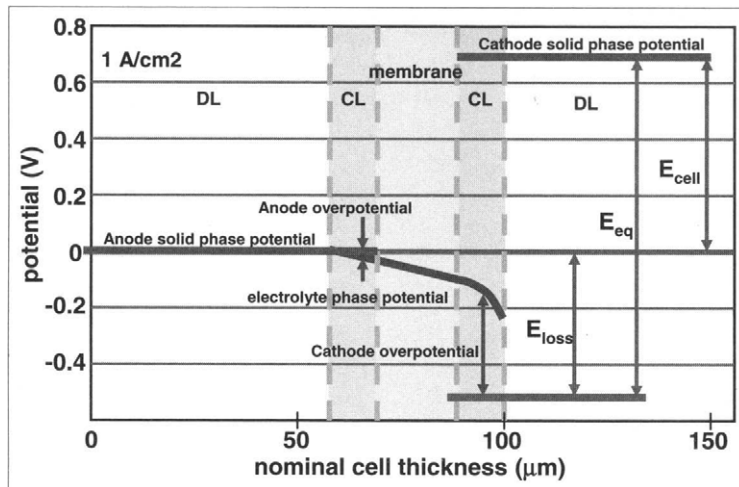


FIGURE 3-9. Potential distribution in fuel cell cross-section.

where the cathode potential is:

$$E_c = E_{r,c} - (\Delta V_{act} + \Delta V_{conc})_c \quad (3-52)$$

and the anode potential is:

$$E_a = E_{r,a} + (\Delta V_{act} + \Delta V_{conc})_a \quad (3-53)$$

$$E_{r,a} = 0 \text{ (by definition)}$$

All these potentials may be tracked down in Figure 3-9.

### 3.5. Sensitivity of Parameters in Polarization Curve

A polarization curve is the most important characteristic of a fuel cell and its performance. It has numerous parameters even in its shorter version (Equation 3-48):

$$E_{cell} = E_{r,T,P} - \frac{RT}{\alpha F} \ln\left(\frac{i + i_{loss}}{i_0}\right) - \frac{RT}{nF} \ln\left(\frac{i_L}{i_L - i}\right) - iR_i \quad (3-54)$$

It would be useful to see what effect each of the parameters has on the polarization curve shape. As a baseline, the following parameters were

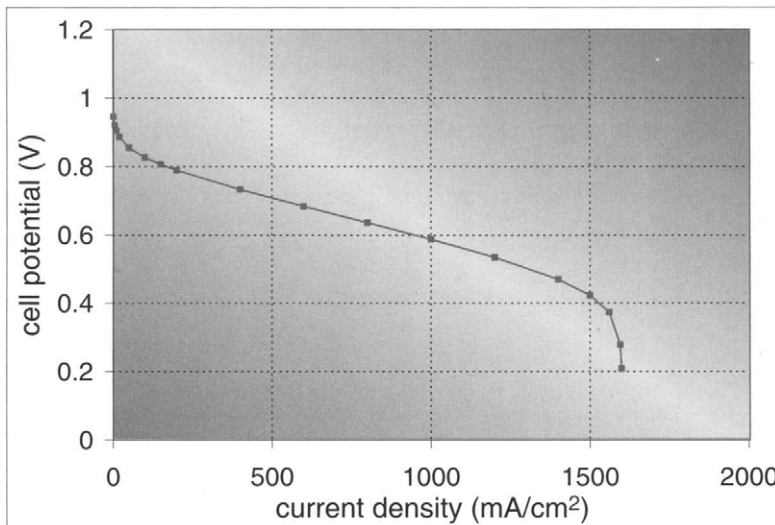


FIGURE 3-10. A typical fuel cell polarization curve.

selected that resulted in a realistic fuel cell polarization curve (Figure 3-10):

Fuel: Hydrogen

Oxidant: Air

Temperature: 333 K

Pressure: 101.3 kPa (atmospheric)

Gas constant, R:  $8.314 \text{ J mol}^{-1} \text{ K}^{-1}$

Transfer coefficient,  $\alpha$ : 1

Number of electrons involved, n: 2

Faraday's constant, F:  $96,485 \text{ C mol}^{-1}$

Current loss,  $i_{\text{loss}}$ :  $0.002 \text{ A cm}^{-2}$

Reference exchange current density,  $i_0$ :  $3 \times 10^{-6} \text{ A cm}^{-2}$

Limiting current density,  $i_L$ :  $1.6 \text{ A cm}^{-2}$

Internal resistance,  $R_i$ :  $0.15 \text{ Ohm}\cdot\text{cm}^2$

When the previous numerical values are plugged into Equation (3-54), the following baseline polarization curve results as shown in Figure 3-10.

### 3.5.1. Effect of Transfer Coefficient/Tafel Slope

The transfer coefficient,  $\alpha$ , has a strong effect on fuel cell performance. Although its typical value is about 1 (note that some books use  $\alpha n$  instead of just  $\alpha$ ; in that case  $\alpha n \approx 1$ ), Figure 3-11 shows fuel cell performance with  $\alpha = 0.5$  and  $\alpha = 1.5$ .

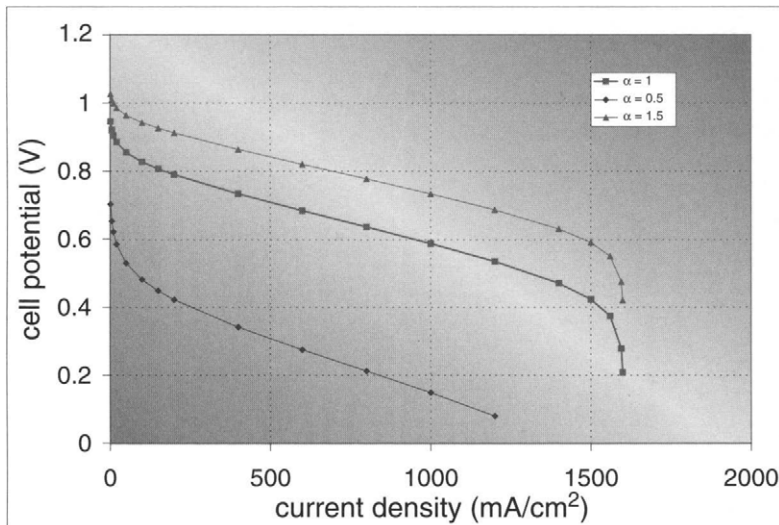


FIGURE 3-11. Effect of transfer coefficient on fuel cell performance.

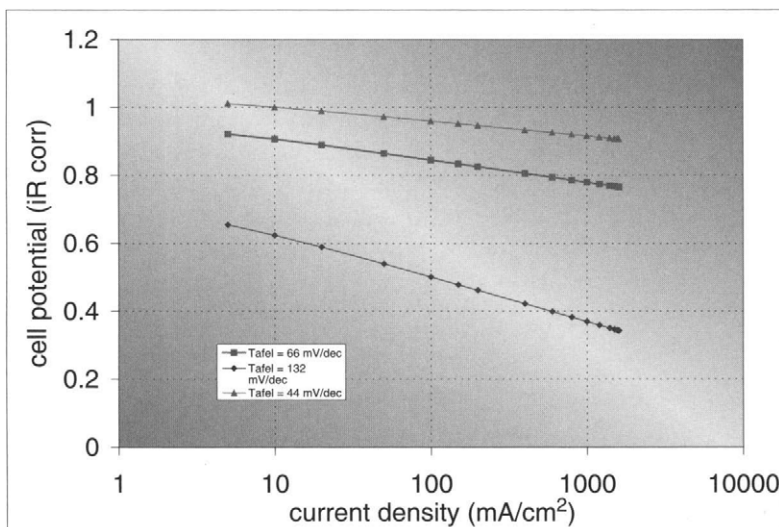


FIGURE 3-12. Effect of Tafel slope on fuel cell polarization curve.

Transfer coefficient is the determining factor for the Tafel slope. The Tafel slope is a parameter in Equation (3-25) defined as:

$$b = 2.3 \frac{RT}{\alpha F} .$$

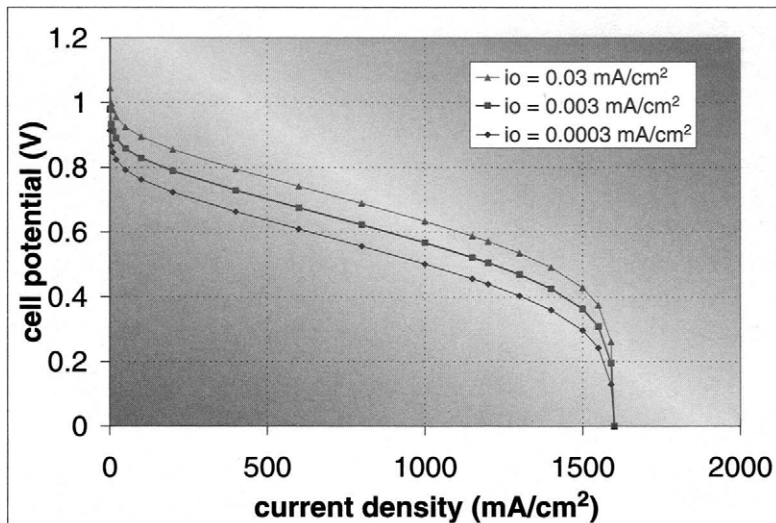


FIGURE 3-13. Effect of exchange current density on fuel cell polarization curve.

With the previous numerical values the Tafel slope is 0.066 V/decade, which is a typical value for hydrogen/oxygen fuel cells. For  $\alpha = 0.5$  and  $\alpha = 1.5$  the Tafel slope is 0.132 and 0.44 V/decade. Figure 3-12 shows the polarization curves for three different values of the Tafel slope. For convenience, the curves are plotted in the log scale, with the cell potential corrected for resistive losses, and concentration polarization losses have been neglected. In that case the polarization curve becomes a straight line. Higher Tafel slopes result in lower performance.

### 3.5.2. Effect of Exchange Current Density

Figure 3-13 shows polarization curves for three different values of exchange current density. For each order of magnitude higher exchange current density, the entire curve is shifted up approximately by the value of  $b$ , that is, Tafel slope.

### 3.5.3. Effect of Hydrogen Crossover and Internal Current Loss

As already discussed, hydrogen crossover and internal current losses have an effect only at very low current densities (Figure 3-14). These losses reduce the cell's open circuit potential and the potential at current densities below  $100 \text{ mA/cm}^2$ . Even an order of magnitude higher losses do not have a significantly larger effect.

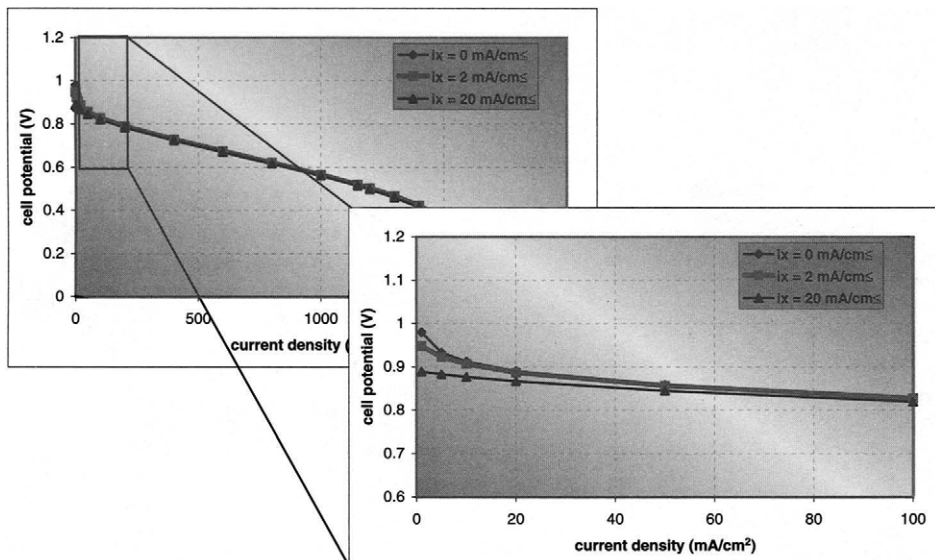


FIGURE 3-14. The effect of internal currents and/or hydrogen crossover on the fuel cell polarization curve.

### 3.5.4. Effect of Internal Resistance

Resistive or Ohmic losses are directly proportional to current density. The departure from the baseline becomes noticeable as the current density increases (Figure 3-15).

### 3.5.5. Effect of Limiting Current Density

Limiting current density only has an effect at very high current densities approaching the limiting current density (Figure 3-16). At low current densities there is almost no effect, that is, the three polarization curves for three different limiting currents fall on top of each other.

### 3.5.6. Effect of Operating Pressure

An increase in cell operating pressure results in higher cell potential due to:

- a) The Nernst equation,

$$E = E_0 + \frac{RT}{nF} \ln\left(\frac{P_{H_2} P_{O_2}^{0.5}}{P_{H_2O}}\right) \quad (3-55)$$

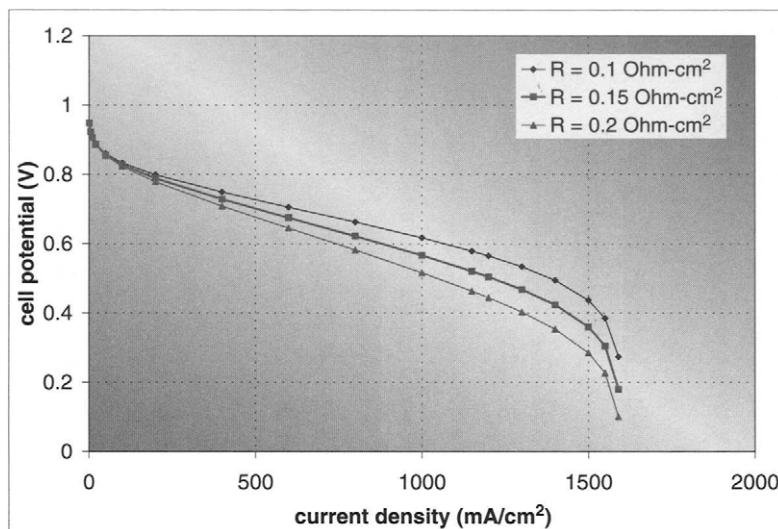


FIGURE 3-15. Effect of cell internal resistance on its polarization curve.

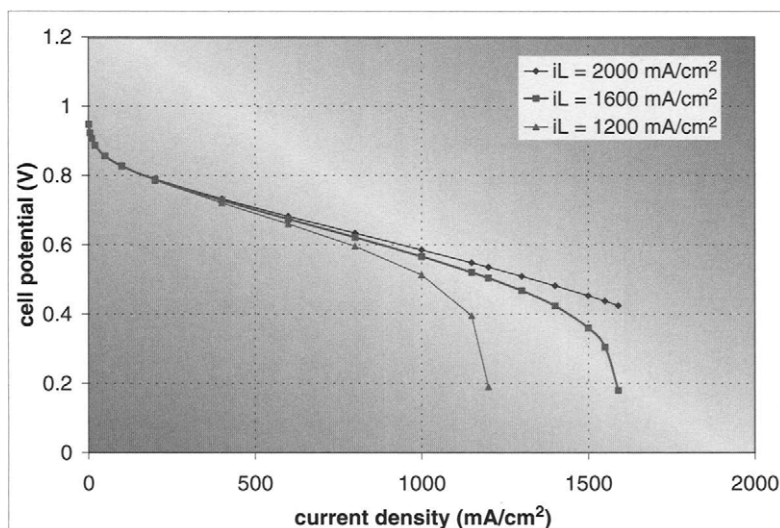


FIGURE 3-16. Effect of limiting current density on fuel cell polarization curve.

- b) An increase in exchange current density due to increased concentration of reactant gases in the electrode(s). Remember, exchange current density is proportional to surface concentration (Equation 3-16), which in turn is directly proportional to pressure. Exchange current density at pressure different from reference/ambient pressure, as shown in Equation (3-22), is:

$$i_0 = i_0^{\text{ref}} \left( \frac{P}{P_0} \right)^{\gamma} \quad (3-56)$$

The cell potential gain at elevated pressure is:

$$\Delta V = \frac{RT}{nF} \ln \left[ \left( \frac{P_{H_2}}{P_0} \right) \left( \frac{P_{O_2}}{P_0} \right)^{0.5} \right] + \frac{RT}{\alpha F} \ln \left( \frac{P}{P_0} \right) \quad (3-57)$$

For given conditions, the gain resulting from a pressure increase from atmospheric to 200 kPa is 34 mV, and from atmospheric to 300 kPa it is 55 mV. This gain applies to any current density, which results in an elevated polarization curve at elevated pressures, as shown in Figure 3-17. In addition, elevated pressure may have an effect on limiting current density by improving mass transfer of gaseous species.

### 3.5.7. Air vs Oxygen

A similar effect may be expected if pure oxygen is used instead of air. Because oxygen concentration in air is only 21%, operation with pure

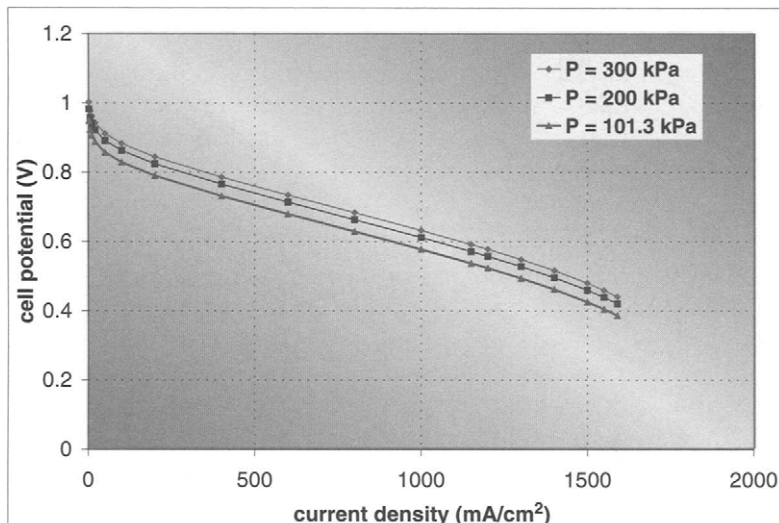


FIGURE 3-17. Effect of operating pressure on fuel cell polarization curve.

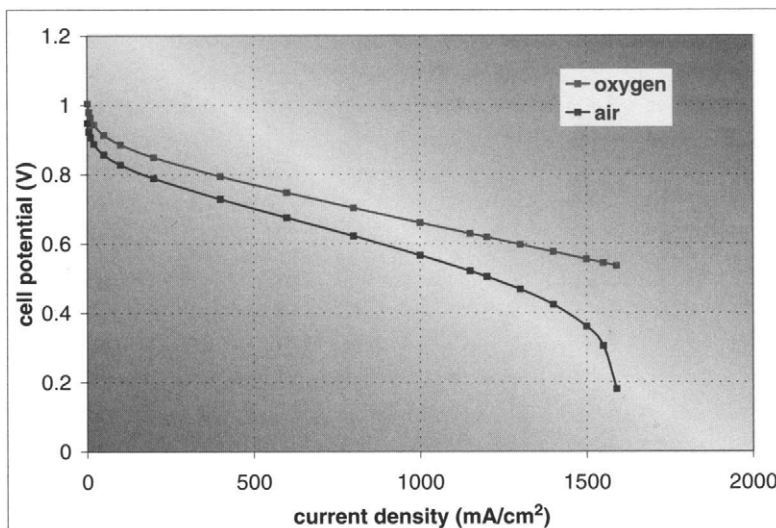


FIGURE 3-18. Effect of oxygen concentration on fuel cell polarization curve.

oxygen results in a gain similar to elevating the air pressure by a factor of  $1/0.21$ .

The gain is:

$$\Delta V = \frac{RT}{nF} \ln \left[ \left( \frac{1}{0.21} \right)^{0.5} \right] + \frac{RT}{\alpha F} \ln \left( \frac{1}{0.21} \right) \quad (3-58)$$

At given conditions, the calculated gain is 56 mV. In addition, operation with pure oxygen usually eliminates concentration polarization, as shown in Figure 3-18. Comparison of polarization curves between pure oxygen and oxygen mixtures with nitrogen or helium is used for diagnostic purposes to study concentration polarization.

### 3.5.8. Effect of Operating Temperature

Fuel cell performance usually improves with elevated temperature, although this cannot be predicted simply by the equations describing the polarization curve derived previously. Increased temperature results in potential loss due to  $T\Delta S/nF$  (Equation 2.18 and Table 2.4). It also results in a higher Tafel slope, which in turn results in potential loss (Figure 3-12). However, increased temperature results in exponentially higher exchange current density (from Equation 3-22) and significantly improves mass transport properties. Figure 3-19 shows the results of an experiment in which the cell temperature gradually increased from  $-10^{\circ}\text{C}$  to  $60^{\circ}\text{C}$ , and the resulting polarization curves clearly indicate voltage gain with increased temperature [11].

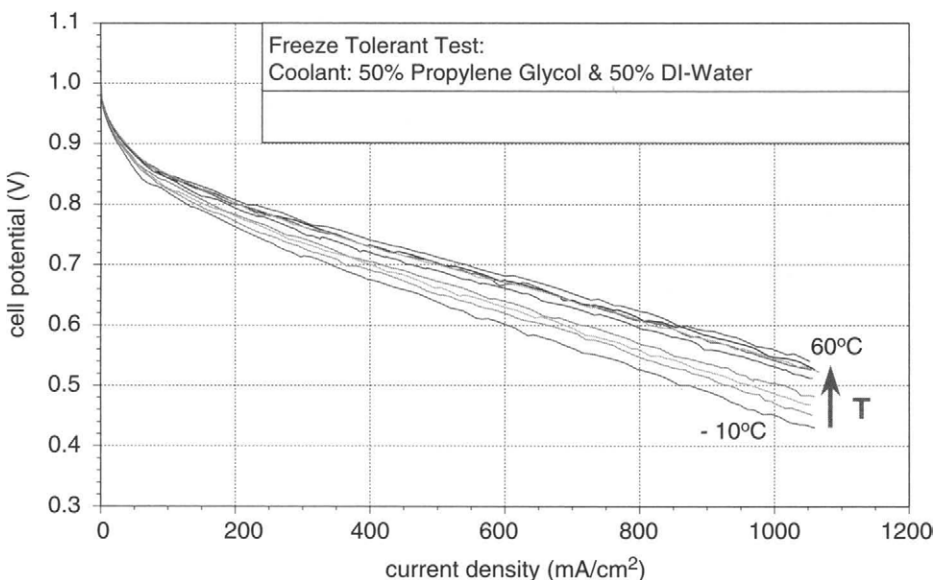


FIGURE 3-19. Effect of operating temperature on fuel cell polarization curve [11].

### 3.6. Fuel Cell Efficiency

The fuel cell efficiency is defined as a ratio between the electricity produced and hydrogen consumed. Of course, both must be in same units, such as Watts or kilowatts.

$$\eta = \frac{W_{el}}{W_{H_2}} \quad (3-59)$$

Electricity produced is simply a product between voltage and current.

$$W_{el} = I \cdot V \quad (3-60)$$

where  $I$  is the current in Amperes and  $V$  is the cell potential in Volts. Hydrogen consumed is (according to Faraday's Law) directly proportional to current:

$$N_{H_2} = \frac{I}{nF} \quad (3-61)$$

where  $N_{H_2}$  is in  $\text{mol s}^{-1}$ , and

$$W_{H_2} = \Delta H \frac{I}{nF} \quad (3-62)$$

where:

$W_{H_2}$  = energy value of hydrogen consumed in Joules per second (Watts),  
 $\Delta H$  = hydrogen's higher heating value (286 kJ mol<sup>-1</sup>).

It should be noted that  $\Delta H/nF$  has dimension of Volts, and for  $\Delta H = 286 \text{ kJ/mol}$  it has a value of 1.482 V, which is the so-called thermoneutral potential.

By combining Equations (3-59) through (3-62), the fuel cell efficiency is simply directly proportional to cell potential:

$$\eta = \frac{V}{1.482} \quad (3-63)$$

Sometimes, instead of hydrogen's higher heating value (HHV),  $\Delta H = 286 \text{ kJ/mol}$ , the lower heating value (LHV) is used ( $\Delta H_{LHV} = 241 \text{ kJ/mol}$ ). The difference between the higher and lower heating value is the heat of product water condensation. Because the product water may leave the fuel cell in either form, that is, as liquid or as vapor, both values are correct; however, the type of heating value used to calculate the efficiency must be specified. The lower heating value efficiency is:

$$\eta_{LHV} = \frac{V}{1.254} \quad (3-64)$$

If some hydrogen is lost either because of hydrogen diffusion through the membrane, or because of combining with oxygen that diffused through the membrane, or because of internal currents, hydrogen consumption will be higher than that corresponding to generated current (Equation 3-61). Consequently, the fuel cell efficiency would be somewhat lower than given by Equation (3-63). Typically, this loss is very low, in the order of magnitude of a few mA/cm<sup>2</sup>, and therefore it affects the fuel cell efficiency only at very low current densities (as shown in Figure 3-14). The fuel cell efficiency is then a product of voltage efficiency and current efficiency:

$$\eta = \frac{V}{1.482} \frac{i}{(i + i_{loss})} \quad (3-65)$$

If hydrogen is supplied to the cell in excess of that required for the reaction stoichiometry, this excess will leave the fuel cell unused. In case of pure hydrogen, this excess may be recirculated back into the stack so it does not change the fuel cell efficiency (not accounting for the power needed for hydrogen recirculation pump), but if hydrogen is not pure (such as in reformate gas feed), unused hydrogen leaves the fuel cell and does not participate in the electrochemical reaction. The fuel cell efficiency is then:

$$\eta = \frac{V}{1.482} \eta_{fu} \quad (3-66)$$

where  $\eta_{fu}$  is fuel utilization, which is equal to  $1/S_{H_2}$ , where  $S_{H_2}$  is the hydrogen stoichiometric ratio, that is, the ratio between the amount of hydrogen actually supplied to the fuel cell and that consumed in the electrochemical reaction:

$$S_{H_2} = \frac{N_{H_2,act}}{N_{H_2,theor}} = \frac{nF}{I} N_{H_2,act} \quad (3-67)$$

Well-designed fuel cells may operate with 83% to 85% fuel utilization when operated with reformate, and above 90% when operated with pure hydrogen. Note that the current efficiency term in (Equation 3-65) is included in fuel utilization,  $\eta_{fu}$  in Equation (3-66).

### 3.7. Implications and Use of Fuel Cell Polarization Curve

Polarization curve is the most important characteristic of a fuel cell. It may be used for diagnostic purposes, as well as for sizing and control of a fuel cell. In addition to potential-current relationship, other information about the fuel cell may also become available just by rearranging the potential-current data.

#### 3.7.1. Other Curves Resulting from Polarization Curve

For example, Power is a product of potential and current (Equation 3-60). Similarly, power density (in W/cm<sup>2</sup>) is a product of potential and current density:

$$w = V \cdot i \quad (3-68)$$

Power density vs current density may be plotted together with the polarization curve on the same diagram (Figure 3-20). Such a plot shows that

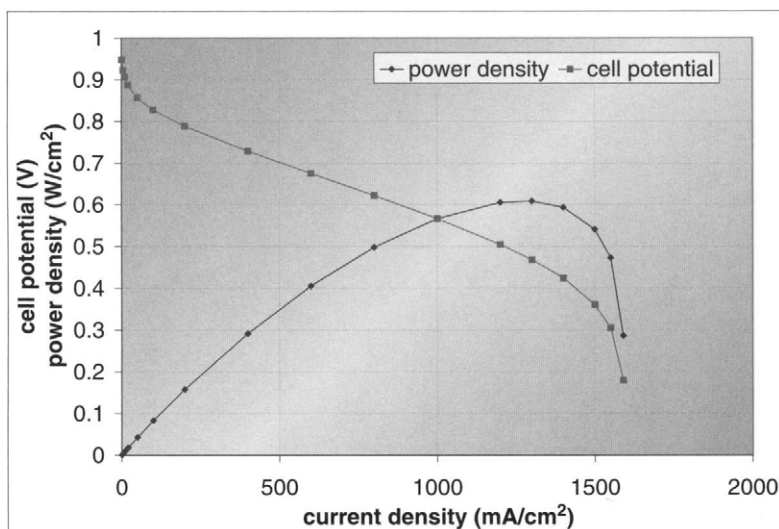


FIGURE 3-20. Typical fuel cell polarization curve and resulting power curve.

there is a maximum power density a fuel cell may reach. It does not make sense to operate a fuel cell at a point beyond this maximum power point, because the same power output may be obtained at a lower current and higher potential. Although the graph in Figure 3-20 shows maximum power density of about  $0.6\text{ W/cm}^2$ , power densities in excess of  $1\text{ W/cm}^2$  have been reported with PEM fuel cells.

If cell potential is plotted vs power density (Figure 3-21), the same information is available—there is a maximum power that the cell can reach. Because the fuel cell efficiency is directly proportional to the cell potential (Equations 3-63 and 3-65), the same graph shows a very useful piece of information—a relationship between the cell efficiency and power density. For a fuel cell with a polarization curve as shown in Figure 3-20, the maximum power is reached at efficiency of 33%. This is significantly lower than the maximum theoretical fuel cell efficiency of 83%. A higher efficiency may be reached with the same fuel cell, but at significantly lower power densities. This means that for a required power output a fuel cell may be made larger (with a larger active area) and more efficient, or more compact but less efficient, by selecting the operating point anywhere on the polarization curve or on the efficiency–power density plot. Typically, a fuel cell is rarely sized anywhere close to the maximum power density. More commonly, the operating point is selected at cell potential around 0.7V. For the graph in Figure 3-21, this would result in power density of  $0.36\text{ W/cm}^2$  and efficiency of 47%. For applications where a higher efficiency is required, a higher nominal cell potential may be selected (0.8V)

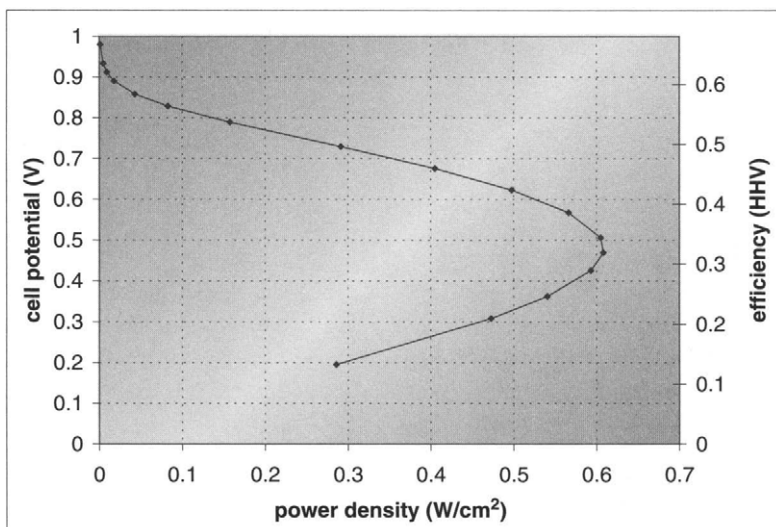


FIGURE 3-21. Cell potential vs power density for a fuel cell with the polarization curve from Figure 3-20.

or higher), which would result in a 55% to 60% efficient fuel cell, but the power density would be  $<0.1 \text{ W/cm}^2$ . Similarly, for applications where fuel cell size is important, a lower nominal cell potential may be selected (around 0.6V), which would result in a higher power density, that is, a smaller fuel cell.

Although Figure 3-21 shows that fuel cell efficiency above 60% may be possible, albeit at very low current and power densities, in practice that is rarely the case. At very low current densities, hydrogen crossover and internal current losses, although very small, become important, and the efficiency-power curve flattens. For the particular case, a maximum efficiency of ~55% is reached (Figure 3-22).

### 3.7.2. Linear Approximation of Polarization Curve

Sometimes, quick calculations regarding fuel cell efficiency-power-size relationships need to be made. Unlike an equation that describes the fuel cell polarization curve (such as Equation 3-54), a linear approximation may be easily manipulated. For most fuel cells and their practical operating range, a linear approximation is actually a very good fit, as shown in Figure 3-23.

Linear polarization curve has the following form:

$$V_{\text{cell}} = V_0 - k \cdot i \quad (3-69)$$

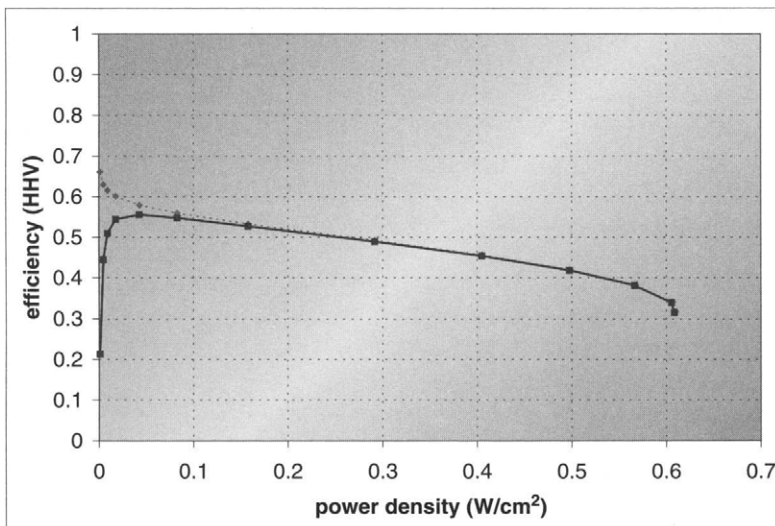


FIGURE 3-22. Fuel cell efficiency vs power density curve; solid line with and dashed line without internal current and/or hydrogen crossover losses.

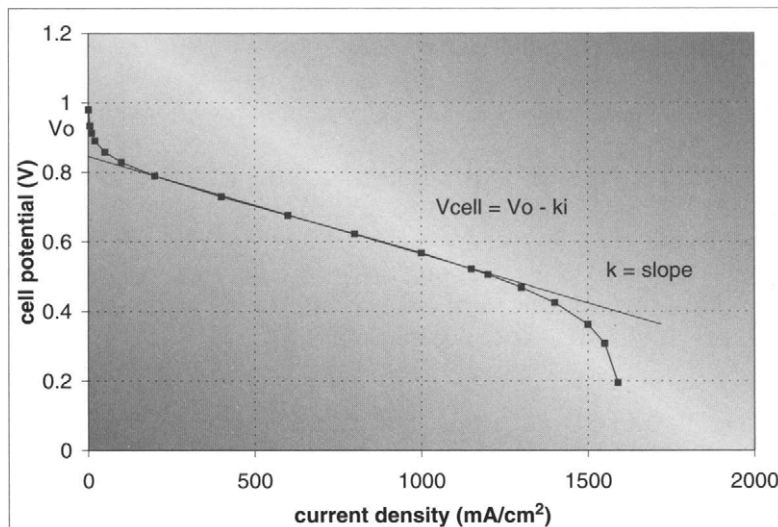


FIGURE 3-23. Linearization of a fuel cell polarization curve.

where  $V_0$  is the intercept (actual open circuit voltage is always higher), and  $k$  is the slope of the curve. In that case current density is:

$$i = \frac{V_0 - V_{cell}}{k} \quad (3-70)$$

and power density as a function of cell potential is:

$$w = \frac{V_{cell}(V_0 - V_{cell})}{k} \quad (3-71)$$

It can be shown that the maximum power density of:

$$w_{max} = \frac{V_0^2}{4k} \quad (3-72)$$

is reached at cell potential:

$$V_{cell}|_{w_{max}} = \frac{V_0}{2} \quad (3-73)$$

### 3.7.3. Use of Polarization Curve for Fuel Cell Sizing

#### Example

$H_2/Air$  fuel cell polarization curve is given with the following parameters:

$$\begin{aligned}\alpha &= 1 \\ i_0 &= 0.001 \text{ mA cm}^{-2} \\ R_i &= 0.2 \Omega \text{ cm}^2\end{aligned}$$

Operating conditions:

$$\begin{aligned}T &= 60^\circ\text{C} \\ P &= 101.3 \text{ kPa}\end{aligned}$$

Operating point is selected at 0.6 V.

Active area is 100 cm<sup>2</sup>.

a) Calculate nominal power output.

*Solution:*

Power output is:

$$\begin{aligned}W_{el} &= V_{cell} \times i \times A \\ V_{cell} &= 0.6 \text{ V} \\ A &= 100 \text{ cm}^2 \\ i &= ?\end{aligned}$$

Current density must be determined from the polarization curve. Because no hydrogen crossover and internal current losses and no limiting current are given, the fuel cell polarization curve may be calculated from:

$$V_{cell} = E_r - \frac{RT}{\alpha F} \ln\left(\frac{i}{i_0}\right) - iR_i$$

where:

$$\begin{aligned}V_{cell} &= 0.6 \text{ V} \\ E_{r,P,T} &= 1.482 - 0.000845T + 0.0000431T \ln(P_{H_2}P_{O_2}^{0.5}) = 1.482 - 0.000845 \\ &\quad \times 333.15 + 0.0000431 \times 333.15 \times \ln(0.21)^{0.5} = 1.189 \text{ V} \\ R &= 8.314 \text{ J mol}^{-1} \text{ K}^{-1} \\ T &= 60^\circ\text{C} = 333.15 \text{ K} \\ \alpha &= 1 \\ n &= 2 \\ F &= 96,485 \text{ C mol}^{-1} \\ i_0 &= 0.001 \text{ mA cm}^{-2} \\ R_i &= 0.2 \Omega \text{ cm}^2\end{aligned}$$

Current density cannot be explicitly calculated from the previous equation.

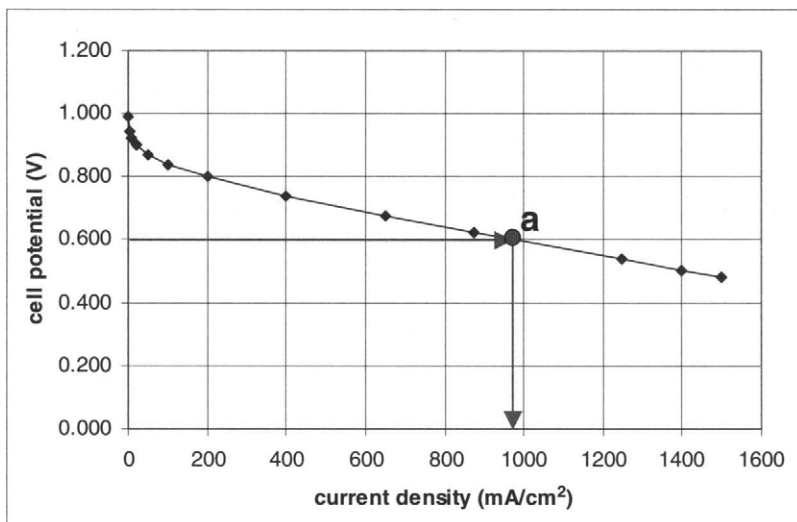


FIGURE 3-24. Resulting polarization curve and operating point *a* for the example.

It can be calculated:

- a) graphically by plotting the polarization curve
- b) by iteration
- c) by linear approximation

This fuel cell's polarization curve with graphical solution for current density at 0.6 V is shown in Figure 3-24.

The resulting current density at 0.6 V is:

$$i = 970 \text{ mA cm}^{-2}$$

Fuel cell power output is then:

$$W_{el} = V_{cell} \times i \times A = 0.6 \times 0.970 \times 100 = \underline{\underline{58.2 \text{ W}}}$$

- b) The engineers improved fuel cell performance by improving internal resistance to  $R_i = 0.15 \text{ Ohm}\cdot\text{cm}^2$ . Calculate power gain at 0.6 V.

*Solution:*

A new polarization curve is shown in Figure 3-25. From there, the new current density is:

$$i = 1.25 \text{ A cm}^{-2}$$

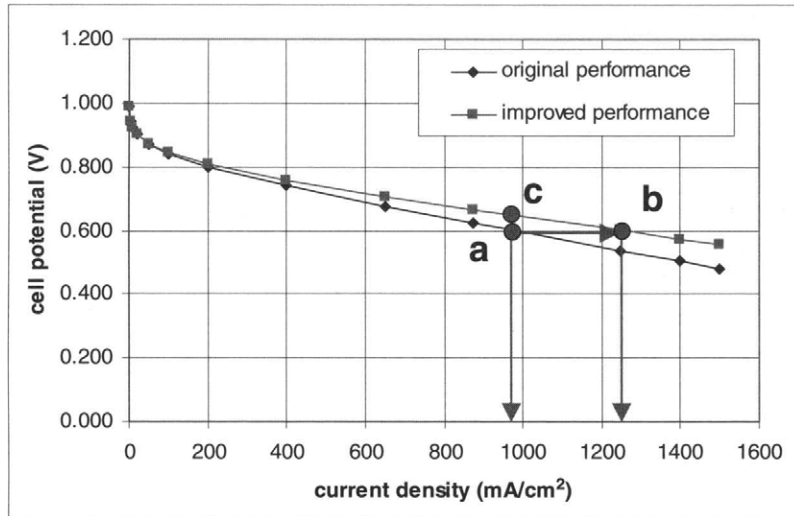


FIGURE 3-25. Improved polarization curve and operating points *b* and *c* for the example.

New fuel cell power output is:

$$W_{el} = V_{cell} \times i \times A = 0.6 \times 1.25 \times 100 = 75.0 \text{ W}$$

Power gain is:

$$\Delta W = 75.0 \text{ W} - 58.2 \text{ W} = \underline{\underline{16.8 \text{ W or } 28.9\%}}$$

- c) The engineers found out that there was not enough air flow to operate this fuel cell at a higher current density. Calculate the power and efficiency gain if the improved fuel cell is to be operated at the original current density.

*Solution:*

$$V_{cell} = E_r - \frac{RT}{\alpha F} \ln\left(\frac{i}{i_0}\right) - iR_i$$

$$V_{cell} = 1.189 - \frac{8.314 \times 333.15}{1 \times 96,485} \ln\left(\frac{970}{0.001}\right) - 0.97 \times 0.15 = 0.648 \text{ V}$$

New fuel cell power output is:

$$W_{el} = V_{cell} \times i \times A = 0.648 \times 0.97 \times 100 = 62.9 \text{ W}$$

Power gain is:

$$\Delta W = 62.9 \text{ W} - 58.2 \text{ W} = \underline{\underline{4.7 \text{ W or } 8\%}}$$

The efficiency before improvement was:

$$\eta = V_{cell}/1.482 = 0.6/1.482 = 0.405$$

The efficiency after improvement is:

$$\eta = V_{cell}/1.482 = 0.648/1.482 = 0.437$$

- d) The engineers realized that there is no need for additional power. Calculate the efficiency gain if the improved fuel cell is to be operated at the original power output.

Fuel cell power output is:

$$58.2 = V_{cell} \times i \times 100$$

Another  $V_{cell}$ - $i$  relationship is obtained from the polarization curve:

$$V_{cell} = 1.189 - \frac{8.314 \times 333.15}{1 \times 96,485} \ln\left(\frac{i}{0.001}\right) - i \times 0.15$$

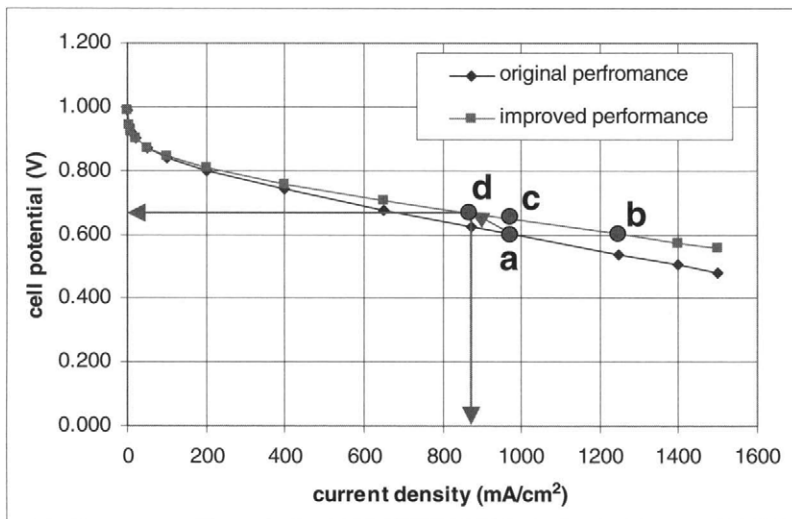


FIGURE 3-26. Operating point *d* for the example.

Again, by iteration or graphically the solution is:

$$\begin{aligned} V_{\text{cell}} &= 0.666 \text{ V} \\ i &= 875 \text{ mA cm}^{-2} \end{aligned}$$

Note that points "a" and "d" (the original and new operating points) in Figure 3-26 lay on two different polarization curves but on the same constant power line.

The new efficiency is:

$$\eta = V_{\text{cell}} / 1.482 = 0.666 / 1.482 = \underline{\underline{0.449}}$$

## References

- Chen, E., Thermodynamics and Electrochemical Kinetics, in G. Hoogers (editor), *Fuel Cell Technology Handbook* (CRC Press, Boca Raton, FL, 2003).
- Atkins, P. W., *Physical Chemistry*, Sixth ed. (Oxford University Press, Oxford, 1998).
- Gileadi, E., *Electrode Kinetics for Chemists, Chemical Engineers and Material Scientists* (VCH Publishers, New York, 1993).
- Bockris, J.O'M. and S. Srinivasan, *Fuel Cells: Their Electrochemistry* (McGraw-Hill, New York, 1969).
- Bard, A. J. and L. R. Faulkner, *Electrochemical Methods* (John Wiley & Sons, New York, 1980).
- Larminie, J. and A. Dicks, *Fuel Cell Systems Explained*, Second ed. (John Wiley & Sons, Chichester, England, 2003).
- Newman, J. S., *Electrochemical Systems*, Second ed. (Prentice Hall, Englewood Cliffs, NJ, 1991).
- Gasteiger, H. A., W. Gu, R. Makharia, and M. F. Matthias, *Catalyst Utilization and Mass Transfer Limitations in the Polymer Electrolyte Fuel Cells*, Tutorial (Electrochemical Society Meeting, Orlando, FL, 2003).
- Barbir, F., J. Braun, and J. Neutzler, Properties of Molded Graphite Bi-Polar Plates for PEM Fuel Cells, *International Journal on New Materials for Electrochemical Systems*, No. 2, 1999, pp. 197–200.
- Kim, J., S.-M. Lee, S. Srinivasan, and C. E. Chamberlain, Modeling of Proton Exchange Fuel Cell Performance with an Empirical Equation, *Journal of Electrochemical Society*, Vol. 142, No. 8, 1995, pp. 2670–2674.
- Fuchs, M. and F. Barbir, *Development of Advanced, Low-Cost PEM Fuel Cell Stack and System Design for Operation on Reformate Used in Vehicle Power Systems*, *Transportation Fuel Cell Power Systems, 2000 Annual Progress Report* (U.S. Department of Energy, Office of Advanced Automotive Technologies, Washington, D.C., October 2000) pp. 79–84.

## Problems

### Problem No. 1:

A fuel cell operates at 60°C and ambient pressure. Exchange current density,  $i_0$  is 0.005 mA/cm<sup>2</sup>. Assume charge transfer coefficient to be 0.5.

- a) Calculate the activation voltage losses at 1.5 A/cm<sup>2</sup>.
- b) If the resistive losses at 1.5 A/cm<sup>2</sup> are  $\frac{1}{2}$  of the activation losses, calculate the cell resistance,  $R_i$ .
- c) Assume no concentration polarization losses and calculate cell voltage at 1.5 A/cm<sup>2</sup>, at 1 A/cm<sup>2</sup>, and at 0.5 A/cm<sup>2</sup>.

### Problem No. 2:

A fuel cell voltage of 0.8 V was measured at 0.2 A/cm<sup>2</sup> and 0.6 V at 0.8 A/cm<sup>2</sup>. The size of the fuel cell is 100 cm<sup>2</sup>. Approximate the fuel cell with a linear polarization curve ( $V = V_0 - k \cdot i$ ). Calculate:

- a) maximum power output
- b) cell voltage and current density at  $\frac{1}{2}$  maximum power
- c) efficiency at maximum power
- d) efficiency at  $\frac{1}{2}$  maximum power

### Problem No. 3:

Cathode exchange current density is  $1 \times 10^{-10}$  A/cm<sup>2</sup> of Pt surface (measured with oxygen at 25°C and atmospheric pressure). Calculate the expected current density at 0.9 V (iR corrected) if an MEA is prepared with catalyst specific surface area of 640 cm<sup>2</sup>/mg and with Pt loading of 0.4 mg/cm<sup>2</sup>, and the cell operates with H<sub>2</sub>/Air at 60°C and 300 kPa. What potential gain may be expected at same current density if the Pt loading on the cathode is increased to 2 mg/cm<sup>2</sup>?

### Problem No. 4:

H<sub>2</sub>/O<sub>2</sub> fuel cell has the following polarization curve parameters:  $i_0 = 0.003$ ,  $\alpha = 0.5$ ,  $R_i = 0.15$  Ohm·cm<sup>2</sup>. The fuel cell operates at 65°C and 1 bar.

- a) Calculate the cell voltage at 1 A/cm<sup>2</sup>.
- b) Calculate voltage gain if the cell is to be operated at 6 bar (take into account both the ideal voltage gain and increase in exchange current density proportional to pressure increase).

### Problem No. 5:

A H<sub>2</sub>/Air fuel cell operates at 80°C and 1 atm. Exchange current density at these conditions is 0.0012 mA per cm<sup>2</sup> of the electrode area. Pt loading is 0.4 mg/cm<sup>2</sup>. The charge transfer coefficient is 0.5. Electrode area is 100 cm<sup>2</sup>.

- a) Calculate the theoretical cell voltage for these conditions.
- b) When the voltmeter is connected to this fuel cell it shows an open circuit voltage of 0.975 V. Calculate current density loss due to hydrogen crossover or due to internal currents.

#### Problem No. 6:

Hydrogen flow rate into a 100-cm<sup>2</sup> fuel cell is 0.0018 g/s. What is the limiting current density?

#### Problem No. 7:

A 100-cm<sup>2</sup> hydrogen/oxygen fuel cell operates at 0.5 A/cm<sup>2</sup> and 0.7 V. Hydrogen flow rate is kept proportional to current generated at stoichiometric ratio of 1.5. Hydrogen crossover and internal current loss account for 2 mA/cm<sup>2</sup>.

- a) Calculate the fuel cell efficiency at these conditions.
- b) Hydrogen flow rate at the entrance.
- c) Hydrogen flow rate at the fuel cell exit.

#### Problem No. 8:

What is the oxygen concentration at the catalyst surface (in mol/cm<sup>3</sup>) when the fuel cell from Problem 5 reaches the limiting current (Pt loading is 0.4 mg/cm<sup>2</sup>, gas diffusion layer thickness is 0.3 mm, gas diffusion porosity is 0.7, effective oxygen diffusion coefficient is 0.14 cm<sup>2</sup>/s, velocity in the channel is 75 cm/s)?

### Quiz

1. The largest voltage losses in a fuel cell in normal operation are due to:
  - a) activation
  - b) concentration/mass transport difficulties
  - c) resistance
2. Higher exchange current density:
  - a) means more voltage losses
  - b) means less voltage losses
  - c) has nothing to do with voltage losses
3. Concentration polarization means:
  - a) concentration of reactants at the catalyst site is too high
  - b) reactants reach the catalyst site at an insufficient rate
  - c) reactants flow rate is higher than it should be

4. Resistance in a fuel cell is:
  - a) ionic resistance through the membrane
  - b) electric resistance through electrically conductive parts
  - c) both ionic and electric
5. Leak of hydrogen through a membrane would:
  - a) reduce the fuel cell voltage, particularly at low or no external currents
  - b) increase the cell voltage
  - c) increase the cell current
6. Pressure increase in a fuel cell typically results in:
  - a) voltage gain
  - b) voltage loss
  - c) lower efficiency
7. Higher Pt loading typically:
  - a) does not change the cell voltage
  - b) results in voltage loss
  - c) results in voltage gain
8. iR corrected cell voltage is:
  - a) cell voltage plus voltage loss attributable to resistance
  - b) cell voltage minus voltage loss attributable to resistance
  - c) resistance loss plus activation voltage losses
9. Selecting an operating point on the polarization curve of a fuel cell at a higher voltage means:
  - a) more power output than the same size fuel cell with a lower selected nominal cell voltage
  - b) larger fuel cell for the same power output
  - c) higher current density
10. A fuel cell runs on H<sub>2</sub> and air and generates 10W. If pure O<sub>2</sub> is used to replace the air, and current and voltage are adjusted so that the fuel cell continues to deliver 10W, the fuel cell would:
  - a) operate at higher current than before O<sub>2</sub> introduction
  - b) operate at lower current than before O<sub>2</sub> introduction
  - c) initially show an increase in cell potential but then it would come back to the original current and cell voltage so that the power output does not change

# CHAPTER 4

## 4. Main Cell Components, Materials Properties and Processes

### 4.1. Cell Description

The heart of a fuel cell is a polymer, proton-conductive membrane. On both sides of the membrane there is a porous electrode. The electrodes must be porous because the reactant gases are fed from the back and must reach the interface between the electrodes and the membrane, where the electrochemical reactions take place in the so-called catalyst layers, or more precisely, on the catalyst surface. Technically, the catalyst layer may be a part of the porous electrode or part of the membrane, depending on the manufacturing process. The multilayer assembly of the membrane sandwiched between the two electrodes is commonly called the membrane electrode assembly or MEA. The MEA is then sandwiched between the collector/separator plates—"collector" because they collect and conduct electrical current, and "separator" because in multicell configuration they separate the gases in the adjacent cells. At the same time, in multicell configuration they physically/electrically connect the cathode of one cell to the anode of the adjacent cell, and that is why they are also called the bipolar plates. They provide the pathways for flow of reactant gases (so-called flow fields), and they also provide the cell structural rigidity.

The following processes take place inside the fuel cell (the numbers correspond to those in Figure 4-1):

1. Gas flow through the channels; some convective flows may be induced in the porous layers.
2. Gas diffusion through porous media.
3. Electrochemical reactions, including all the intermediary steps.
4. Proton transport through proton-conductive polymer membrane.
5. Electron conduction through electrically conductive cell components.

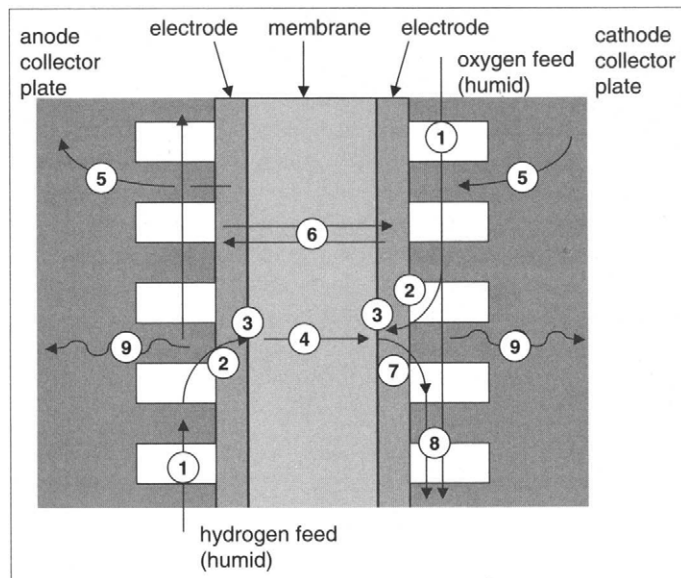


FIGURE 4-1. Main cell components (not in scale) and processes.

6. Water transport through polymer membrane including both electrochemical drag and back diffusion.
7. Water transport (both vapor and liquid) through porous catalyst layer and gas diffusion layers.
8. Two-phase flow of unused gas carrying water droplets.
9. Heat transfer, including both conduction through solid components of the cell and convection to reactant gases and cooling medium.

Obviously, the design of the components and properties of materials must accommodate the above-listed processes with minimum obstruction and losses. Because in some of the components more than one process takes place, very often with conflicting requirements, the properties and the design must be optimized. For example, the gas diffusion layer must be optimized so that the reactant gas may easily diffuse, yet at the same time that water, which travels in the opposite direction, does not accumulate in the pores. On top of that, the diffusion layer (or current collector layer as it is sometimes called) must be both electrically and thermally conductive. Similar requirements may be established for almost every fuel cell component. Although a fuel cell seems to be a very simple device, numerous processes take place simultaneously. It is therefore important to understand those processes, their mutual interdependence, and their dependence on components design and materials properties.

*First fuel cell law:* One cannot change only one parameter in a fuel cell—change of one parameter causes a change in at least two other parameters, and at least one of them has an opposite effect of the one expected to be seen.

## 4.2. Membrane

A fuel cell membrane must exhibit relatively high proton conductivity, must present an adequate barrier to mixing of fuel and reactant gases, and must be chemically and mechanically stable in the fuel cell environment [1]. Typically, the membranes for PEM fuel cells are made of perfluorocarbon-sulfonic acid ionomer (PSA). This is essentially a copolymer of tetrafluorethylene (TFE) and various perfluorosulfonate monomers. The best-known membrane material is Nafion™ made by Dupont, which uses perfluoro-sulfonylfluoride ethyl-propyl-vinyl ether (PSEPVE). Figure 4-2 shows the chemical structure of perfluorosulfonate ionomer such as Nafion™. Similar materials have been developed and sold as either a commercial or development product by other manufacturers such as Asahi Glass (Flemion), Asahi Chemical (Aciplex), Chlorine Engineers ("C" membrane), and Dow Chemical. W.L. Gore and Associates have developed a composite membrane made up of a Teflon-like component providing mechanical strength and dimensional stability and a perfluorosulfonic acid component providing protonic conductivity.

The  $\text{SO}_3\text{H}$  group is ionically bonded, and so the end of the side chain is actually an  $\text{SO}_3^-$  ion with  $\text{H}^+$  ion. This is why such structure is called ionomer. Because of their ionic nature, the ends of the side chains tend to cluster within the overall structure of the membrane. Although the

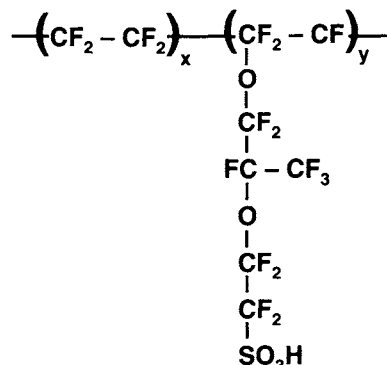


FIGURE 4-2. Structure of PFSA polymer (Nafion™).

Teflon-like backbone is highly hydrophobic, the sulphonic acid at the end of the side chain is highly hydrophylic. The hydrophylic regions are created around the clusters of sulphonated side chains. This is why this kind of material absorbs relatively large amounts of water (in some cases up to 50% by weight). H<sup>+</sup> ions movement within well-hydrated regions makes these materials proton conductive.

Nafion™ membranes come extruded in different sizes and thicknesses. They are marked with a letter N, followed by a 3- or 4-digit number. The first 2 digits represent equivalent weight divided by 100, and the last digit or two is the membrane thickness in mills (1 mill = 1/1000 inch = 0.0254 mm). Nafion™ is available in several thicknesses, namely 2, 3.5, 5, 7, and 10 mills (50, 89, 127, 178, 254 µm, respectively). For example, Nafion™ N117 has equivalent weight of 1100 and it is 7 mills (0.178 mm) thick. The equivalent weight (EW) in g eq<sup>-1</sup> of a polymer membrane can be expressed with the following equation:

$$EW = 100n + 446 \quad (4-1)$$

where n is the number of TFE groups on average per PSEPVE monomer [2].

EW is practically a measure of ionic concentration within the ionomer. Typical EW for Nafion™ membranes is 1100, although materials with EW as low as 700 have been synthesized and studied. Copolymers with EW greater than approximately 1500 g eq<sup>-1</sup> do not have ionic conductivity sufficient for practical fuel cell applications.

#### 4.2.1. Water Uptake

The protonic conductivity of a polymer membrane is strongly dependent on membrane structure and its water content. The water content in membrane is usually expressed as grams of water per gram of polymer dry weight, or as number of water molecules per sulfonic acid groups present in the polymer,  $\lambda = N(H_2O)/N(SO_3H)$ . The maximum amount of water in the membrane strongly depends on the state of water used to equilibrate the membrane. It has been noticed that a Nafion membrane equilibrated with liquid water (*i.e.*, boiled in water) takes roughly up to 22 water molecules per sulfonate group, whereas the maximum water uptake from the vapor phase is only about 14 water molecules per sulfonate group. In addition, water uptake from the liquid phase is dependent on the membrane pre-treatment. Zawodzinski *et al.* [3,4] have shown that water uptake after the membrane had been completely dried out at 105°C is significantly smaller than if the membrane had been dried out at room temperature;  $\lambda = 12$  to 16 depending on the temperature of rehydration for the membrane previously dried out at 105°C vs  $\lambda = 22$  and independent of the temperature of rehydration for the membrane previously dried at room temperature. This may be explained by the polymer morphological changes at elevated tem-

peratures. Indeed, for an experimental Dow membrane, which has a somewhat higher glass transition temperature than Nafion<sup>TM</sup>, the effect of drying the membrane at 105°C is less pronounced than for Nafion<sup>TM</sup> membrane, that is, after rehydration at 80°C the membrane exhibited the same water uptake ( $\lambda = 25$ ) as the membrane previously dried out at room temperature.

Water uptake from the vapor phase may be more relevant for fuel cell operation, where the reactant gases are humidified and water is present in the vapor phase. The shape of a generic isotherm for ion-exchange polymers is shown in Figure 4-3. It may be noticed that there are two distinct steps in water sorption from the gas phase, namely:

- a) at low vapor activity region,  $a_{H_2O} = 0.15\text{--}0.75$ , water uptake increases to about  $\lambda = 5$ , and
- b) at high vapor activity region,  $a_{H_2O} = 0.75\text{--}1.0$ , water uptake increases sharply to about 14.4-

The first step corresponds to uptake of water by solvation by the ions in the membrane, whereas the second step corresponds to water that fills the pores and swells the polymer. It is important to notice that the resulting water uptake from the fully saturated vapor phase (with  $a_{H_2O} = 1$ ) is significantly lower than that from the liquid phase (also  $a_{H_2O} = 1$ ), that is,  $\lambda = 14$  vs  $\lambda = 22$ , respectively. This phenomenon was first reported in 1903 by Schroeder, and is therefore called Schroeder's paradox [1]. A possible explanation of this difference in uptake from vapor and liquid phases is that sorption from the vapor phase involves condensation of water inside the polymer, most probably on the strongly hydrophobic polymer backbone, and the resulting uptake is lower than if sorption and imbibition occurred directly from the liquid phase [1].

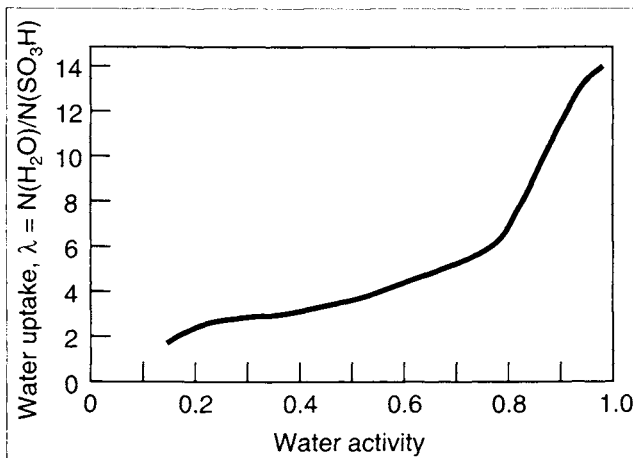


FIGURE 4-3. Water uptake in proton conductive membranes at 30°C [4].

Based on experimental results, Zawodzinski *et al.* [4] fit a polynomial equation to obtain a relationship between water activity on the faces of the membrane and water content:

$$\lambda = 0.043 + 17.18a - 39.85a^2 + 36a^3 \quad (4-2)$$

where  $a$  is water activity defined as  $p/p_{\text{sat}}$ , where  $p$  is water partial pressure, and  $p_{\text{sat}}$  is the saturation pressure at given temperature.

#### 4.2.2. Physical Properties

Water uptake results in the membrane swelling and changes its dimensions, which is a very significant factor for fuel cell design and assembly. From Table 4-1 that shows some critical Nafion™ membrane properties at various water contents [2,5], it can be seen that the dimensional changes are in the order of magnitude of 10%, which must be taken into account in cell design and during the installation of the membrane in the cell.

In 1995, W.L. Gore and Associates, Inc. introduced the Gore-Select membrane, a new microreinforced expanded polytetrafluoroethylene (ePTFE) polymer electrolyte membrane targeted specifically toward PEMFC applications [6]. The microreinforcements allow Gore-Select membranes to utilize ionomers that do not have sufficient mechanical properties (*i.e.*, ionomers with EW <1000). These membranes exhibit much higher strength, better dimensional stability, lower gas permeability, and higher conductivity than comparable nonreinforced Nafion membranes [6].

#### 4.2.3. Protonic Conductivity

Protonic conductivity is the most important function of the polymer membranes used in fuel cells. The charge carrier density in an ionomeric proton

TABLE 4-1  
Mechanical Properties of Nafion™ Membranes (1100 EW)

Property	50% RH, 23°C	Water Soaked, 23°C	Water Soaked, 100°C
Thickness change (%) <sup>1</sup>	—	10	14
Linear expansion (%) <sup>1</sup>	—	10	15
Tensile modulus (MPa)	249	114	64
Tensile strength (MPa) <sup>2</sup>	43	34	25
	32	26	24
Elongation at break (%) <sup>2</sup>	225	200	180
	310	275	240

<sup>1</sup> Relative to thickness and linear expansion at 50% RH and 23°C.

<sup>2</sup> When two numbers are given, the upper one refers to the properties in machine direction and the lower one to transverse direction.

conductive membrane of EW 1100 is similar to that in 1 M aqueous sulfuric acid solution. Remarkably, proton mobility in a fully hydrated membrane is only one order of magnitude lower than the proton mobility in aqueous sulfuric acid solution. As a result, the protonic conductivity of fully hydrated membrane is about  $0.1 \text{ S cm}^{-1}$  at room temperature. The conductivity of PFSA membranes is a strong function of water content and temperature (Figures 4-4 and 4-5). Above  $\lambda = 5$ , the relationship between water content and protonic conductivity is almost linear. Below  $\lambda = 5$ , there is very little water uptake (Figure 4-3), which may suggest that there is not enough water in the clusters around the ends of the sulphonated side chains

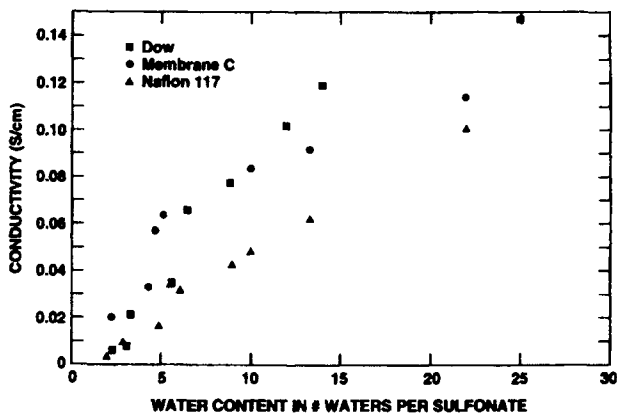


FIGURE 4-4. Conductivity of various proton conductive membranes at  $30^\circ\text{C}$  as a function of state of membrane hydration [4]. (Reprinted by permission of the Electrochemical Society)

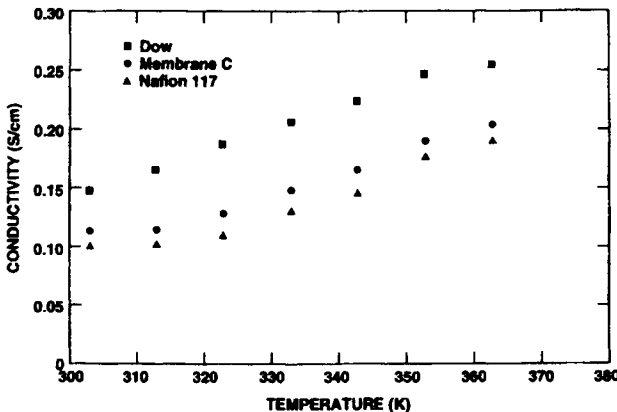


FIGURE 4-5. Conductivity of various proton conductive membranes immersed in water as a function of temperature [4]. (Reprinted by permission of the Electrochemical Society)

and that because of that protons are sequestered by the sulphonate groups. Note that conductivity at  $\lambda = 14$  (membrane equilibrated with water vapor) is about  $0.06 \text{ S cm}^{-1}$ . Protonic conductivity dramatically increases with temperature (Figure 4-5) and at  $80^\circ\text{C}$  reaches  $0.18 \text{ S cm}^{-1}$  for a membrane immersed in water. Based on these measurements, Springer *et al.* [7] correlated the ionic conductivity (in  $\text{S cm}^{-1}$ ) to water content and temperature with the following expression:

$$\kappa = (0.005139\lambda - 0.00326) \exp\left[1268\left(\frac{1}{303} - \frac{1}{T}\right)\right] \quad (4-3)$$

Zawodzinski [8] has suggested that there are several possible ways of ionic conductivity of Nafion-like materials (Figure 4-6):

- At very low water contents ( $\lambda \sim 2-4$ ), hydronium ions ( $\text{H}_3\text{O}^+$ ) move via vehicle mechanism.
- As the water content increases ( $\lambda \sim 5-14$ ), easier movement of hydronium ions is facilitated.
- At fully hydrated membranes ( $\lambda > 14$ ), water in interfacial regions screens weakly bound water from ion-dipole interactions, and both water and ions move freely.

#### 4.2.4. Water Transport

There are several mechanisms of water transport across a polymer membrane. Water is produced on the cathode side as the result of the

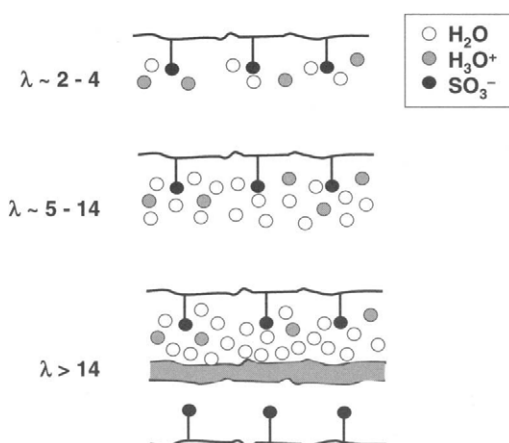


FIGURE 4-6. Mechanisms of water and hydronium ions movement through PFSA ionomer at various hydration levels, as suggested by Zawodzinski [8].

electrochemical reaction [Equation 2.2]. The rate of water generation (in  $\text{mol s}^{-1} \text{cm}^{-2}$ ) is:

$$N_{\text{H}_2\text{O,gen}} = \frac{i}{2F} \quad (4-4)$$

where  $i$  is current density ( $\text{A/cm}^2$ ), and  $F$  is Faraday's constant.

Water is dragged from the anode to the cathode by protons moving through the electrolyte as described previously. This is called electroosmotic drag. The flux of water due to electroosmotic drag (in  $\text{mol s}^{-1} \text{cm}^{-2}$ ) is:

$$N_{\text{H}_2\text{O,drag}} = \xi(\lambda) \frac{i}{F} \quad (4-5)$$

where  $\xi$  is the electroosmotic drag coefficient defined as number of water molecules per proton. In general, this coefficient is a function of membrane hydration ( $\lambda$ ). This number has been reported over the years with considerable variation [1], depending on the method of measurement and data fitting. One way to measure the electroosmotic drag is to pass current through the membrane and monitor the level of a water column [9]. Using this method, Le Conti *et al.* [9] reported drag coefficients in the range of 2–3 water molecules per proton for membrane water content in the range of  $15 \leq \lambda \leq 25$ . They concluded that the drag coefficient decreases linearly with water content of the immersed membranes. Zawodzinski *et al.* [4] used the same method and measured a drag coefficient of 2.5 for fully hydrated and immersed Nafion<sup>TM</sup> 1100 membranes. At  $\lambda = 11$  the drag coefficient was measured to be  $0.9 \text{ N}(\text{H}_2\text{O})/\text{N}(\text{H}^+)$ .

An electrochemical method was developed by Fuller and Newman [10] based on electrochemical potential that arises across a membrane sample exposed at each side to different water activities. In that case the electrochemical drag is:

$$\xi(\lambda) = \frac{F\Delta\Phi}{RT \log \frac{a_{\text{H}_2\text{O},r}}{a_{\text{H}_2\text{O},l}}} \quad (4-6)$$

where  $\Delta\Phi$  is the measured potential,  $a_{\text{H}_2\text{O}}$  is water activity, and subscripts r and l refer to the right and left sides of the membrane. This method is suitable for vapor-equilibrated membranes. Fuller and Newman [10] reported an essentially constant drag coefficient of  $1.4 \text{ N}(\text{H}_2\text{O})/\text{N}(\text{H}^+)$  in the range of  $5 \leq \lambda \leq 14$ . In the range  $0 \leq \lambda \leq 5$ , the coefficient gradually drops to zero. Zawodzinski *et al.* [11] used a wider range of water activities and found a drag coefficient of  $1.0 \text{ N}(\text{H}_2\text{O})/\text{N}(\text{H}^+)$  in the range of  $1.4 \leq \lambda \leq 14$ .

Water generation and electroosmotic drag would create a large concentration gradient across the membrane. Because of this gradient, some

water diffuses back from the cathode to the anode. The rate of water diffusion (in  $\text{mol s}^{-1} \text{cm}^{-2}$ ) is:

$$N_{\text{H}_2\text{O,diff}} = D(\lambda) \frac{\Delta c}{\Delta z} \quad (4-7)$$

where  $D$  is the water diffusion coefficient in ionomer of water content  $\lambda$ , and  $\Delta c/\Delta z$  is a water concentration gradient along the  $z$ -direction (through the membrane). Measurement of diffusion coefficient of water through a polymer membrane is not simple. Several methods have been applied, such as:

- Water uptake dynamics, used by Yeo and Eisenberg [12], which resulted in diffusion coefficient in the range of  $1 \times 10^{-6}$  to  $10 \times 10^{-6} \text{ cm}^2 \text{s}^{-1}$ , increasing with temperature in the range of 0–99°C, with activation energy of  $18.8 \text{ kJ mol}^{-1}$ . Similar results were also reported by Eisman [13].
- Radiotracer and electrochemical techniques, developed by Verbrugge and coworkers [14], which resulted in self-diffusion coefficient of water in the range of  $6$ – $10 \times 10^{-6} \text{ cm}^2 \text{s}^{-1}$  in fully hydrated Nafion membranes at room temperature.
- Pulsed field gradient neutron magnetic resonance (NMR) used by Slade *et al.* [15] and Zawodzinski *et al.* [16] resulted in self-diffusion coefficients of water close to  $10 \times 10^{-6} \text{ cm}^2 \text{s}^{-1}$  for fully hydrated Nafion samples. Zawodzinski *et al.* [16] also measured the self-diffusion coefficients in Nafion membranes equilibrated with water vapor and found that the diffusion coefficient decreases from  $6 \times 10^{-6} \text{ cm}^2 \text{s}^{-1}$  to  $0.6 \times 10^{-6} \text{ cm}^2 \text{s}^{-1}$  as water content in the membrane decreased from  $\lambda = 14$  to  $\lambda = 2$  (these measurements were conducted at 30°C).

It should be noted that the radiotracer and pulsed field gradient NMR techniques measure the self-diffusion coefficient of water,  $D_s$ , rather than the Fickian or interdiffusion coefficient of water through the polymer membrane,  $D$ , and some correction is required, because it is the Fickian water diffusion coefficient that is the proper transport property to use in macroscopic studies of water diffusion [17]. The relationship is:

$$D = \frac{\partial(\ln a)}{\partial(\ln C)} D_s \quad (4-8)$$

where  $a$  is the thermodynamic activity of water and  $C$  is water concentration or  $\lambda$ .

Motupally *et al.* [18] studied water transport in Nafion membranes, and, by comparing the variation in literature values of water diffusion coef-

ficients with their own experiments and the results of Zawodzinski *et al.* [16], suggested the following relationships:

$$D(\lambda) = 3.1 \times 10^{-3} \lambda (e^{0.28\lambda} - 1) \exp\left(\frac{-2436}{T}\right) \quad \text{for } 0 < \lambda < 3 \quad (4-9)$$

$$D(\lambda) = 4.17 \times 10^{-4} \lambda (161e^{-\lambda} + 1) \exp\left(\frac{-2436}{T}\right) \quad \text{for } 3 < \lambda < 17 \quad (4-10)$$

In addition to diffusion due to concentration gradient, water may be hydraulically pushed from one side of the membrane to the other if there is a pressure difference between the cathode and the anode. The rate of hydraulic permeation (in  $\text{mol s}^{-1} \text{cm}^{-2}$ ) is [1]:

$$N_{H2O,hyd} = k_{hyd}(\lambda) \frac{\Delta P}{\Delta z} \quad (4-11)$$

where  $k_{hyd}$  is the hydraulic permeability coefficient of the membrane of water content  $\lambda$ , and  $\Delta P/\Delta z$  is a pressure gradient along the  $z$ -direction (through the membrane).

For a thin membrane, water back diffusion may be sufficient to counteract the anode-drying effect due to the electroosmotic drag. However, for a thicker membrane, drying may occur on the anode side. This was very vividly demonstrated by Büchi and Scherer [19], who created thick membranes by combining several layers of Nafion membranes. They showed that the membrane resistance is independent of current density for the membranes up to  $120\mu\text{m}$ , but it does increase for thicker membranes (Figure 4-7).

Because the thicker membranes consisted of several layers, it was possible to measure the resistance of individual layers. The only layer that exhibited resistance increase with current density was the layer next to the anode (Figure 4-8). This clearly indicates that drying as a result of electroosmotic drag occurred close to the anode, because back diffusion was not sufficient to counteract the electroosmotic drag.

Janssen and Overvelde [20] studied the net water transport in an operating fuel cell with Nafion 105 and 112 membranes and found the effective drag (net water transport across the membrane) to be much smaller than reported previously. The values of  $-0.3$  to  $+0.1$  were reported (negative values refer to the back diffusion being higher than the electroosmotic drag), and were found to greatly depend on anode humidification. No significant dependence was found on reactants stoichiometry and pressure differential, indicating that the hydraulic permeation may be negligible for these membranes. As expected, Nafion 112 membrane exhibited somewhat lower net drag than thicker Nafion 105 membrane.

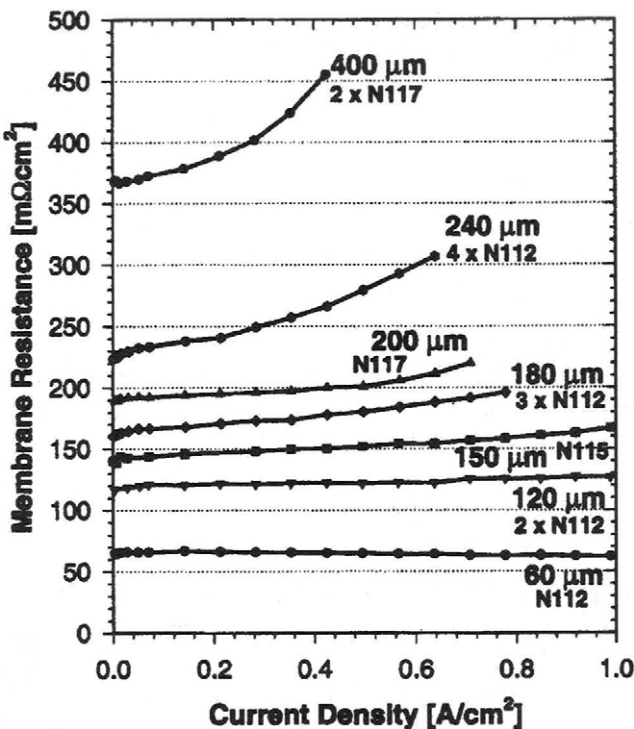


FIGURE 4-7. *In situ* resistance of Nafion membranes with different thicknesses as function of current density (cell temperature 60°C) [19]. (Reprinted by permission of the Electrochemical Society)

#### 4.2.5. Gas Permeation

In principle, the membrane should be impermeable to reactant species, in order to prevent their mixing before they have had a chance to participate in the electrochemical reaction. However, because of the membrane's essentially porous structure, its water content and solubility of hydrogen and oxygen in water, some gas does permeate through the membrane.

Permeability is a product of diffusivity and solubility:

$$P_m = D \times S \quad (4-12)$$

Because diffusivity is expressed in cm<sup>2</sup>s<sup>-1</sup> and solubility in molcm<sup>-3</sup>Pa<sup>-1</sup>, permeability would have unit of molcm s<sup>-1</sup>cm<sup>-2</sup>Pa<sup>-1</sup>. A common unit for permeability is Barrer.

$$1 \text{ Barrer} = 10^{-10} \text{ cm}^3 \text{ cm s}^{-1} \text{ cm}^{-2} \text{ cmHg}^{-1}$$

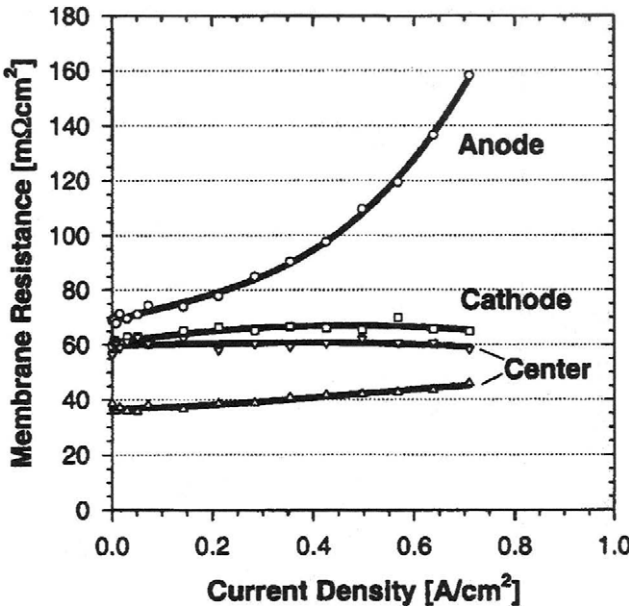


FIGURE 4-8. Resistance of the membrane layers in  $\text{H}_2/\text{O}_2$  fuel cell with four Nafion 112 layers as a function of current density (cell temperature 60°C) [19]. (Reprinted by permission of the Electrochemical Society)

Solubility of hydrogen in Nafion is  $S_{\text{H}_2} = 2.2 \times 10^{-10} \text{ mol cm}^{-3} \text{ Pa}^{-1}$  [21] and is fairly independent of temperature, and diffusivity is a function of temperature [21,22]:

$$D_{\text{H}_2} = 0.0041 \exp\left(-\frac{2602}{T}\right) \quad (4-13)$$

The oxygen solubility (in  $\text{mol cm}^{-3} \text{ Pa}^{-1}$ ) is a function of temperature, and it is given by the following equation [22,23]:

$$S_{\text{O}_2} = 7.43 \times 10^{-12} \exp\left(\frac{666}{T}\right) \quad (4-14)$$

Oxygen diffusivity (in  $\text{cm}^2 \text{s}^{-1}$ ) is [21,22]:

$$D_{\text{O}_2} = 0.0031 \exp\left(-\frac{2768}{T}\right) \quad (4-15)$$

Permeabilities of various gases through dry Nafion is shown in Figure 4-9 [24]. As expected, hydrogen has one order of magnitude higher

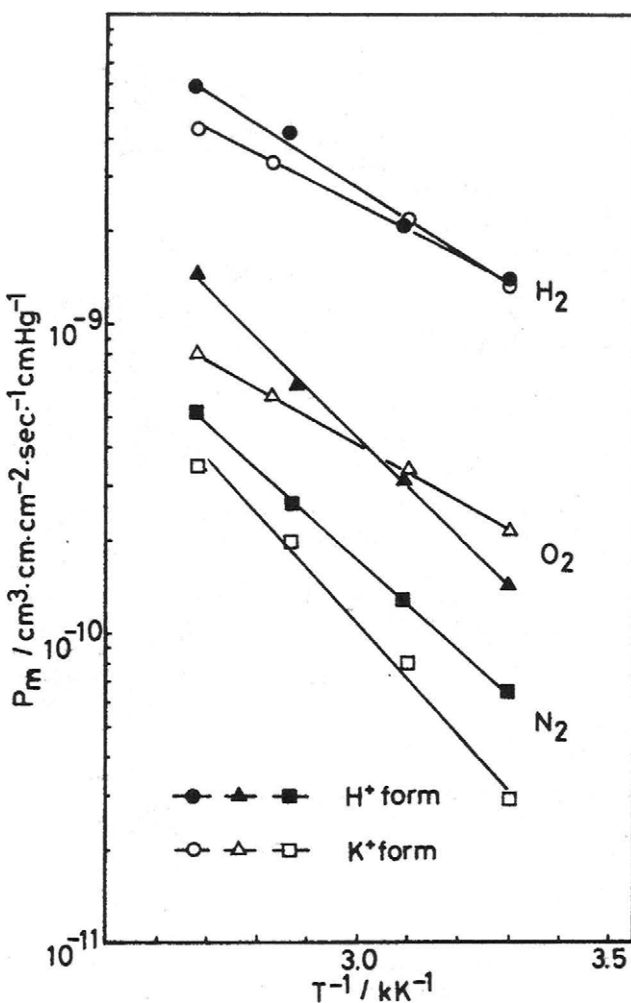


FIGURE 4-9. Permeability of hydrogen, oxygen, and nitrogen for Nafion 125 membrane [24]. (Reprinted by permission of the Electrochemical Society)

permeability than oxygen. Permeability through wet Nafion is another order of magnitude higher, as shown in Figure 4-10. Expectedly, permeation through wet Nafion is somewhat lower than permeation through water, and permeation through dry Nafion is somewhat lower than permeation through Teflon.

#### *Example:*

Calculate hydrogen permeability in Barrers through Nafion at 25°C and 101.3 kPa (1 atm).

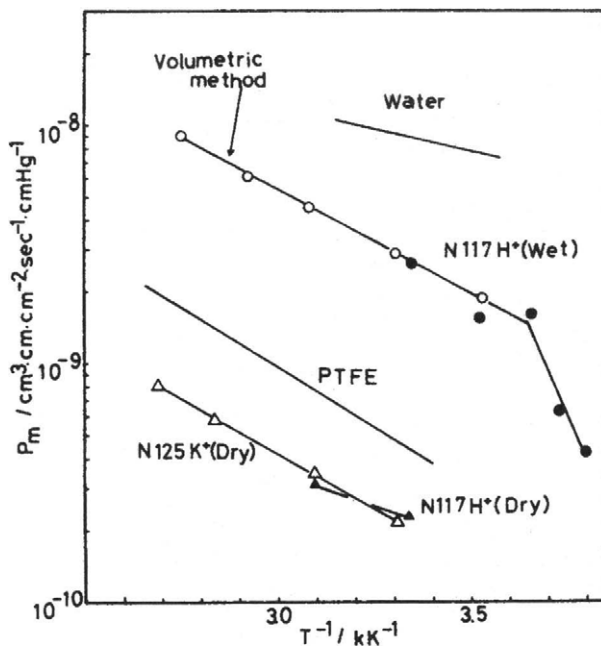


FIGURE 4-10. Permeability of oxygen through dried and hydrated Nafion membranes [24]. (Reprinted by permission of the Electrochemical Society)

*Solution:*

At 25°C (298.15 K) hydrogen diffusivity is:

$$D_{\text{H}_2} = 0.0041 \exp\left(-\frac{2602}{298.15}\right) = 6.65 \times 10^{-7} \text{ cm}^2 \text{ s}^{-1}$$

Hydrogen permeability is a product of diffusivity and permeability:

$$\begin{aligned} P_m &= 6.65 \times 10^{-7} \text{ cm}^2 \text{ s}^{-1} \times 2.2 \times 10^{-10} \text{ mol cm}^{-3} \text{ Pa}^{-1} \\ &= 1.44 \times 10^{-16} \text{ mol cm s}^{-1} \text{ cm}^{-2} \text{ Pa}^{-1} \end{aligned}$$

Molar volume (cm<sup>3</sup> mol<sup>-1</sup>) for any gas is:

$$v_m = \frac{RT}{P}$$

where:

R = universal gas constant = 8.314 J mol<sup>-1</sup> K<sup>-1</sup>

P = pressure = 101,300 Pa

T = temperature = 298.15 K

$$v_m = \frac{8.314 \times 298.15}{101,300} = 0.02447 \text{ m}^3\text{mol}^{-1} = 24,470 \text{ cm}^3\text{mol}^{-1}$$

Permeability of hydrogen through Nafion at 25°C and 101.3 kPa (1 atm) is therefore:

$$P_m = 1.44 \times 10^{-16} \text{ mol cm s}^{-1} \text{cm}^{-2} \text{Pa}^{-1} \times 24,470 \text{ cm}^3 \text{mol}^{-1} \times 1350 \text{ Pa/cmHg} \\ = 47.7 \times 10^{-10} \text{ cm}^3 \text{cm s}^{-1} \text{cm}^{-2} \text{cmHg}^{-1} = \underline{\underline{47.7 \text{ Barrers}}}$$

The permeation rate, in addition to permeability, obviously should be proportional to pressure and the area of the membrane, and inversely proportional to membrane thickness. The permeation rate is then:

$$N_{\text{gas}} = P_m \frac{AP}{d} \quad (4-16)$$

For example, the permeation rate of hydrogen through 100 cm<sup>2</sup> of Nafion 112 at 25°C and 300 kPa is:

$$N_{\text{gas}} = 1.44 \times 10^{-16} \times \frac{100 \times 300 \times 10^3}{50.8 \times 10^{-4}} = 8.5 \times 10^{-7} \text{ mol s}^{-1}$$

Hydrogen permeation may also be expressed in A cm<sup>-2</sup>:

$$N_{\text{H}_2} = \frac{I}{2F} \Rightarrow i = \frac{2FN_{\text{H}_2}}{A} = \frac{2 \times 96,485 \times 8.5 \times 10^{-7}}{100} = 0.0016 \text{ A cm}^{-2}$$

### 4.3. Electrode

A fuel cell electrode is essentially a thin catalyst layer pressed between the ionomer membrane and porous, electrically conductive substrate. It is the layer where the electrochemical reactions take place. More precisely, the electrochemical reactions take place on the catalyst surface. Because there are three kinds of species that participate in the electrochemical reactions, namely gases, electrons and protons, the reactions can take place on a portion of the catalyst surface where all three species have access. Elec-

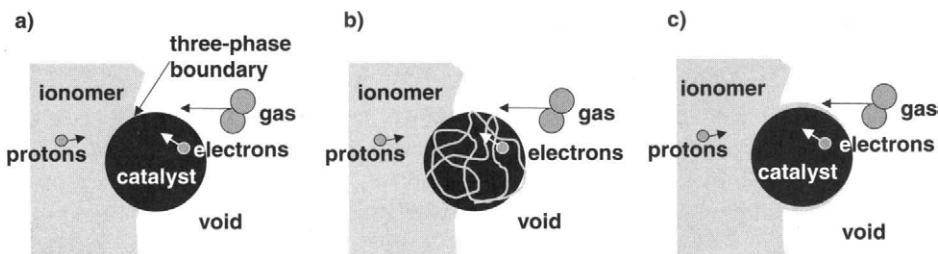


FIGURE 4-11. Graphical representation of the reaction sites.

trons travel through electrically conductive solids, including the catalyst itself, but it is important that the catalyst particles are somehow electrically connected to the substrate. Protons travel through ionomer; therefore the catalyst must be in intimate contact with the ionomer. And finally, the reactant gases travel only through voids; therefore the electrode must be porous to allow gases to travel to the reaction sites. At the same time, product water must be effectively removed; otherwise the electrode would flood and prevent oxygen access.

As shown graphically in Figure 4-11a, the reactions take place at the three-phase boundary, namely ionomer, solid, and void phases. However, this boundary has an infinitesimally small area (essentially it is a line not an area) that would result in infinitely large current densities. In practice, because some gas may permeate through the polymer, the reaction zone is larger than a single three-phase boundary line. The reaction zone may be enlarged by either "roughening" the surface of the membrane or by incorporating ionomer in the catalyst layer (as shown in Figure 4-11b). In an extreme case, the entire catalyst surface may be covered by a thin ionomer layer (Figure 4-11c), except for some allowance for electrical contacts. Obviously, the ratios between the catalyst area covered by ionomer to catalyst area opened to void to catalyst area contacting other catalyst particles or electrically conductive support must be optimized.

The most common catalyst in PEM fuel cells for both oxygen reduction and hydrogen oxidation reactions is platinum. In the early days of PEMFC development large amounts of Pt catalyst were used (up to  $28 \text{ mg cm}^{-2}$ ). In the late 1990s, with the use of supported catalyst structure, this was reduced to  $0.3\text{--}0.4 \text{ mg cm}^{-2}$ . It is the catalyst surface area that matters, not the weight, so it is important to have small platinum particles ( $4 \text{ nm}$  or smaller) with large surface area finely dispersed on the surface of catalyst support, typically carbon powders (cca  $40 \text{ nm}$ ) with high mesoporous area ( $>75 \text{ m}^2 \text{ g}^{-1}$ ). Typical support material is Vulcan XC72R by Cabot, but other carbons such as Black Pearls BP 2000, Ketjen Black Intl., or Chevron Shawinigan have been used.

To minimize the cell potential losses due to the rate of proton transport and reactant gas permeation in the depth of the electrocatalyst layer, this layer should be made reasonably thin. At the same time, the metal active surface area should be maximized, for which the Pt particles should be as small as possible. For the first reason, higher Pt/C ratios should be selected (>40% by wt.); however, smaller Pt particles and consequently larger metal areas are achieved with lower loading (as shown in Table 4-2). Paganin *et al.* [25] found that the cell's performance remained virtually unchanged when the Pt/C ratio was varied from 10% to 40% with a Pt loading of  $0.4 \text{ mg/cm}^2$ . However, the performance deteriorated as the Pt/C ratio was increased beyond 40%. This indicates a negligible change in the active catalyst area between Pt/C ratios of 10% and 40% and significant decrease in catalyst active area beyond 40% Pt/C (also seen in Table 4-2). Table 4-2 shows the achievable catalyst active area for various Pt/carbon compositions [26] (using Ketjen Carbon Black-supported electrocatalyst).

In general, higher Pt loading results in voltage gain (Figure 4-12) [27], assuming equal utilization and reasonable thickness of the catalyst layer. However, when current density is calculated per area of Pt surface then there is almost no difference in performance, that is, all the polarization curves fall on top of each other (Figure 4-13) [27]. Note that the Tafel slope is about  $70 \text{ mV/decade}$ .

The key to improving the PEM fuel cell performance is not in increasing the Pt loading, but rather in increasing Pt utilization in the catalyst layer.

The catalyst surface active area may be greatly increased if ionomer is included in the catalyst layer either by painting it with solubilized PFSA in a mixture of alcohols and water or preferably by premixing catalyst and ionomer in a process of forming the catalyst layer. Zawodzinski *et al.* [28] have shown that there is an optimum amount of ionomer in the catalyst layer—around 28% by weight (Figure 4-14). Similar findings were reported by Qi and Kaufman [29] and Sasikumar *et al.* [30].

TABLE 4-2  
Achievable Pt Active Area for Various Pt/Carbon Compositions Using Ketjen Carbon Black-Supported Catalyst [26]

wt. % Pt on Carbon	XRD Pt Crystallite Size, nm	Active Area* $\text{m}^2/\text{g Pt}$
40	2.2	120
50	2.5	105
60	3.2	88
70	4.5	62
unsupported Pt black	5.5–6	20–25

\* CO chemisorption.

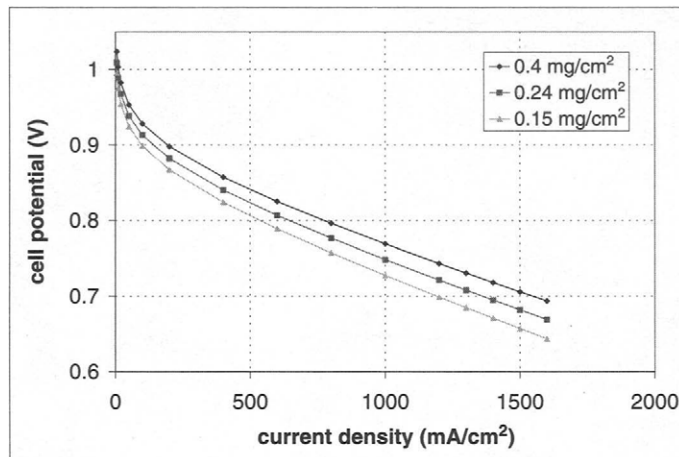


FIGURE 4-12. Effect of Pt loading on fuel cell polarization curve (H<sub>2</sub>/O<sub>2</sub> fuel cell).

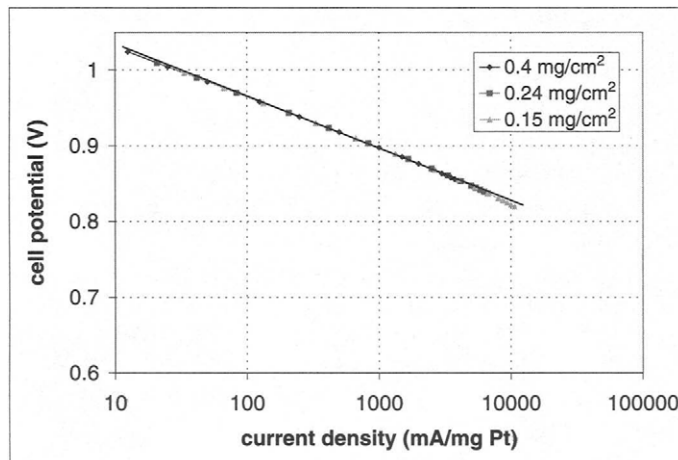


FIGURE 4-13. Cell performance per unit of Pt electrocatalyst.

In principle, there are two ways of preparation of catalyst layer and its attachment to the ionomer membrane. Such a combination of membrane and catalyst layers is called the membrane electrode assembly or MEA. The first way of preparing an MEA is to deposit the catalyst layer to the porous substrate, the so-called gas diffusion layer, typically carbon fiber paper or carbon cloth, and then hot-press it to the membrane. The second

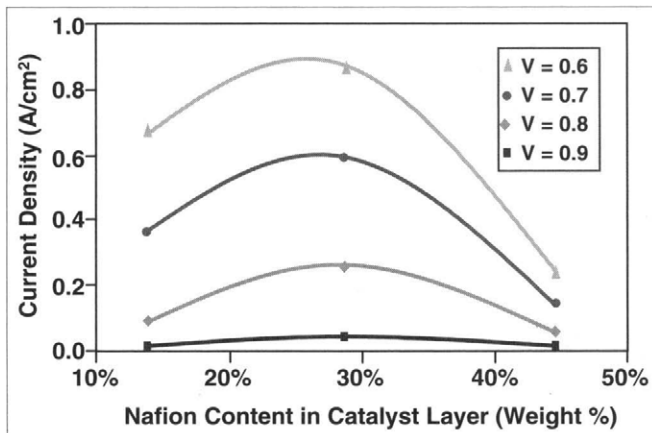


FIGURE 4-14. Effect of Nafion content in catalyst layer on fuel cell performance [28].

method of preparing an MEA is application of the catalyst layers directly to the membrane, forming a so-called three-layer MEA or catalyzed membrane. A gas diffusion layer may be added later, either as an additional step in MEA preparation (in that case a five-layer MEA is formed) or in a process of stack assembly.

Several methods have been developed for deposition of a catalyst layer on either the porous substrate or the membrane, such as spreading, spraying, sputtering, painting, screen printing, decaling, electrodeposition, evaporative deposition, and impregnation reduction. There are several manufacturers of MEAs, such as Dupont, 3M, Johnson Matthey, W.L. Gore & Associates, and Umicore (previously dmc<sup>2</sup> and Degussa). Their manufacturing processes are typically trade secrets.

At present there are no alternative cathode electrocatalysts to platinum. Some platinum alloy electrocatalysts prepared on traditional carbon black supports offer a 25 mV performance gain compared with Pt electrocatalysts. However, only the more stable Pt-based metal alloys, such as PtCr, PtZr, or PtTi, can be used in PEMFC, due to dissolution of the base metal by the perfluorinated sulfonic acid in the electrocatalyst layer and membrane [26]. The focus of the continued search for the elusive electrocatalyst for oxygen reduction in acid environment should be on development of materials with required stability and greater activity than Pt.

#### 4.4. Gas Diffusion Layer

A layer between the catalyst layer and bipolar plates is called a gas diffusion layer, electrode substrate, or diffusor/current collector. Although it does not directly participate in the electrochemical reactions, a gas diffusion layer in PEM fuel cells has several important functions:

- It provides a pathway for reactant gases from the flow field channels to the catalyst layer, allowing them access to the entire active area (not just to those adjacent to the channels).
- It provides a pathway for product water from the catalyst layer to the flow field channels.
- It electrically connects the catalyst layer to the bipolar plate, allowing the electrons to complete the electrical circuit.
- It also serves to conduct heat generated in the electrochemical reactions in the catalyst layer to the bipolar plate, which has means for heat removal (as will be discussed in Chapter 6).
- It provides mechanical support to the MEA, preventing it from sagging into the flow field channels.

The required properties of the gas diffusion layer follow from its functions:

- It must be sufficiently porous to allow flow of both reactant gases and product water (note that these fluxes are in opposite direction). Depending on the design of the flow field, diffusion in both through-plane and in-plane is important.
- It must be both electrically and thermally conductive, again in both through-plane and in-plane. Interfacial or contact resistance is typically more important than bulk conductivity.
- Because the catalyst layer is made of discrete small particles, the pores of the gas diffusion layer facing the catalyst layer must not be too big.
- It must be sufficiently rigid to support the “flimsy” MEA. However, it must have some flexibility to maintain good electrical contacts.

These somewhat conflicting requirements are best met by carbon fiber-based materials such as carbon fiber papers and woven carbon fabrics or cloths. Table 4-3 shows the properties of typical gas diffusion layers made of carbon paper and carbon cloth, as reported by various manufacturers.

From Table 4.3. it follows that the thickness of various gas diffusion materials varies between 0.017 to 0.04 cm, density varies between 0.21 to  $0.73 \text{ g cm}^{-3}$  and porosity varies between 70% and 80%.

**TABLE 4-3**  
Properties of Typical Fuel Cell Gas Diffusion Layers

Company	Material Carbon Fiber Papers	Thickness cm	Density g/cm³	Weight g/m²	Porosity %	Electrical Resistivity	
						Through Plane Ohmcm	In-Plane Ohmcm
Toray	TGP-H-060	0.019	0.44	84	78	0.080	0.0058
	TGP-H-090	0.028	0.44	123	78	0.080	0.0056
	TGP-H-120	0.037	0.45	167	78	0.080	0.0047
Spectracorp	2050-A	0.026	0.48	125		2.692	0.012
	2050-L	0.02	0.46	92		7.500	0.022
	2050-HF	0.026	0.46	120		3.462	0.014
Ballard	AvCarb P50	0.0172	0.28	48		0.564	
	AvCarb P50T	0.0172	0.28	48		0.564	
SGL Carbon	10-BA	0.038	0.22	84	88	0.263	
	10-BB	0.042	0.30	125	84	0.357	
	20-BA	0.022	0.30	65	83	0.455	
	20-BC	0.026	0.42	110	76	0.538	
	21-BA	0.02	0.21	42	88	0.550	
	21-BC	0.026	0.37	95	79	0.577	
	30-BA	0.031	0.31	95	81	0.323	
	30-BC	0.033	0.42	140	77	0.394	
	31-BA	0.03	0.22	65		0.317	
	31-BC	0.034	0.35	120	82	0.441	
E-TEK	LT 1100-N	0.018	0.50	90		0.360	
	LT 1200-W	0.0275	0.73	200		0.410	
	LT 1400-W	0.04	0.53	210		0.500	
	LT 2500-W	0.043	0.56	240		0.550	
Carbon cloth	AvCarb	0.038	0.31	118		0.132	
Ballard	1071 HCB*						0.009

\*Measurements performed and reported by General Motors [31].

#### 4.4.1. Treatments and Coatings

Diffusion media are generally made hydrophobic to avoid flooding in their bulk. Typically, both cathode and anode gas diffusion media are PTFE treated. A wide range of PTFE loadings have been used in PEMFC diffusion media (5% to 30%), most typically by dipping the diffusion media into a PTFE solution followed by drying and sintering.

Hydrophobic properties of gas diffusion media are rarely reported by the manufacturers. These properties are often tailored to a specific cell design, and must be measured and correlated to the cell performance. Typically, this involves the measurement of contact angle on the surface by either a Sessile drop method or Wilhelmy methods.

Figure 4-15 shows a fuel cell performance with treated and untreated cathode diffusion media [31]. The untreated one was susceptible to flooding, especially at higher current densities.

In addition, the interface with the adjacent catalyst layer may also be fitted with a coating or a microporous layer to ensure better electrical contacts as well as efficient water transport in and out of the diffusion layer. This layer (or layers) consists of carbon or graphite particles mixed with PTFE binder. The resulting pores are between 0.1 and 0.5  $\mu\text{m}$ , thus much smaller than the pore size of the carbon fiber papers (20–50  $\mu\text{m}$ ). Figure 4-16 shows a nonwoven gas diffusion media with a microporous layer on top of it. The small pore size helps in improving the electrical contacts with the adjacent catalyst layer. However, the primary role of this microporous layer is to facilitate effective wicking of liquid water from the cathode cat-

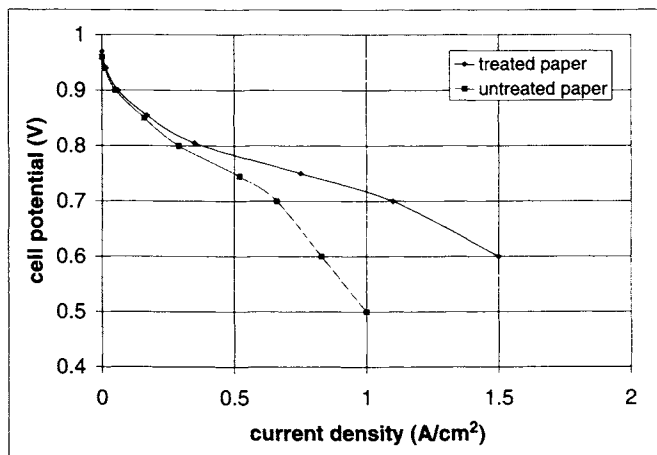


FIGURE 4-15. Fuel cell performance with treated and untreated carbon fiber paper [31].  $50\text{ cm}^2$ ,  $\text{H}_2/\text{Air}$ ;  $80^\circ\text{C}$ ,  $270\text{ kPa}$ , 2.0/2.0 stoichiometry, 100%/50% an/ca relative humidity.



FIGURE 4-16. A nonwoven gas diffusion media with a microporous layer on top of it.

alyst layer into the diffusion media, resulting in much smaller water droplets less likely to clog and flood the gas diffusion media bulk.

#### 4.4.2. Porosity

Gas diffusion media are by definition porous. Porosity is typically between 70% and 80% as shown in Table 4-3. Porosity of a gas diffusion layer may be easily calculated from its areal weight, thickness, and the density of the solid phase (for carbon-based materials,  $\rho_{\text{real}}$  varies between 1.6 and  $1.95 \text{ g cm}^{-3}$ ). The porosity,  $\epsilon$ , also depends on the compressed thickness:

$$\epsilon = 1 - \frac{W_A}{\rho_{\text{real}} d} \quad (4-17)$$

where:

$W_A$  = areal weight ( $\text{g cm}^{-2}$ )

$\rho_{\text{real}}$  = solid phase density

$d$  = thickness (either compressed or uncompressed)

Porosity may be measured by mercury porosimetry or by capillary flow porometry [31].

#### 4.4.3. Electrical Conductivity

One of the functions of the gas diffusion layer is to connect electrically the catalyst layer with the bipolar plate. Because only a portion of the bipolar plate makes the contact (the other portion is open for access of reactant gases), the gas diffusion layer bridges the channels and redistributes electrical current. Because of this, both through-plane and in-plane resistivities of gas diffusion material are important. Through-plane resistivity,  $\rho_z$ , often includes both bulk and contact resistance, depending on the method used in measurements. It is obvious from data in Table 4-3 that some manufacturers (Toray for example) report true through-plane resistivity, measured for example with mercury contacts to eliminate contact resistance, whereas others applied a method that included the contact resistance. Mathias *et al.* [31] measured through-plane resistivity of Toray TGP-H-060 and confirmed the manufacturer's data of  $0.08 \Omega\text{cm}$ . They also measured the total through-plane resistance of  $0.009 \Omega\text{cm}^2$ , which if divided by the thickness ( $0.019 \text{ cm}$ ) would result in  $0.473 \Omega\text{cm}$  (which is close to data reported by other manufacturers in Table 4-3). In-plane resistivity of common gas diffusion media,  $\rho_{xy}$ , typically measured by a four-point probe method, is typically about an order of magnitude lower than the through-plane value. The relevance of through-plane and in-plane resistivity is discussed in Chapter 6, Stack Design, and the importance of contact resistance between the gas diffusion layer and bipolar plates is discussed in this chapter, in the section 4.5. Bi-Polar Plates.

#### 4.4.4. Compressibility

In a fuel cell, a gas diffusion layer is compressed to minimize the contact resistance losses. Both carbon papers and carbon cloths are relatively soft and easily deformable materials. Cloth is more compressible than paper, as can be seen from Figure 4-17. When exposed to a cyclic compression test they both exhibit a weakening of the material—the first compression stress-strain curve is different than the one resulting from subsequent cycles [31].

#### 4.4.5. Permeability

Effective diffusion coefficients in typical PEMFC diffusion media include the effects of material porosity and tortuosity. In most cases they reflect bulk as opposed to Knudsen diffusion, because the pore diameters are several orders of magnitude higher than the mean free path of gas molecules. However, Knudsen diffusion may be prevalent in microporous layers

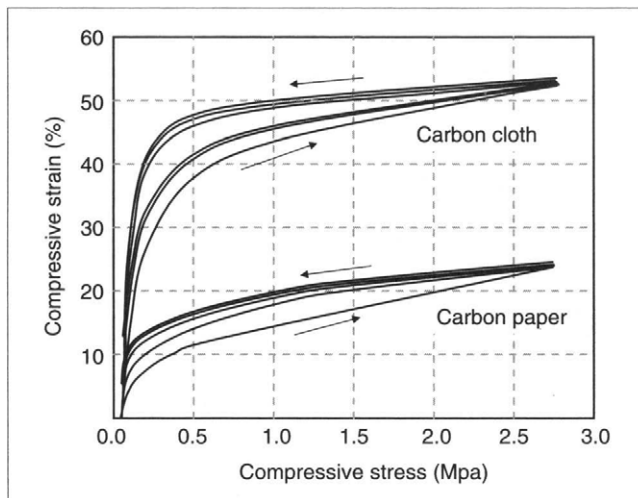


FIGURE 4-17. Stress-strain curves for carbon paper (Toray TGP-H-060) and carbon cloth (Textron 1071HCB), from [31].

where the pore size can approach the gas molecule mean free path. Convective flow resistance of the diffusion media is given as either a Gurley number or a Darcy coefficient. The Gurley number is the time required to pass a specified volume of flow through a sample at a given pressure drop. The Darcy coefficient relates to the pressure drop, which according to Darcy's law is proportional to the volumetric flow rate:

$$Q = K_D \frac{A}{\mu l} \Delta P \quad (4-18)$$

where:

$Q$  = volumetric flow rate,  $\text{m}^3 \text{s}^{-1}$

$K_D$  = Darcy coefficient,  $\text{m}^2$

$A$  = cross-sectional area perpendicular to the flow,  $\text{m}^2$

$\mu$  = gas viscosity,  $\text{kg m}^{-1} \text{s}^{-1}$

$l$  = length of the path (thickness of diffusion media),  $\text{m}$

$\Delta P$  = pressure drop,  $\text{Pa}$

For an uncompressed Toray TGP-H-060 carbon fiber paper, the Darcy coefficient of  $5\text{--}10 \times 10^{-12} \text{ m}^2$  has been reported [31]. Approximately the same value has been reported for in-plane flow through the same material compressed to 75% of its original thickness [31].

#### 4.5. Bipolar Plates

In a single-cell configuration (such as the one shown in Figure 4-1) there are no bipolar plates. The two plates on each side of the membrane electrode assembly may be considered as two halves of a bipolar plate. The fully functioning bipolar plates are essential for multicell configurations (as shown in Figure 4-18), by electrically connecting the anode of one cell to the cathode of the adjacent cell.

The bipolar collector/separator plates have several functions in a fuel cell stack. Their required properties follow from their functions, namely:

- They connect cells electrically in series—therefore, they must be electrically conductive.
- They separate the gases in adjacent cells—therefore, they must be impermeable to gases.
- They provide structural support for the stack—therefore, they must have adequate strength, yet they must be lightweight.
- They conduct heat from active cells to the cooling cells or conduits—therefore, they must be thermally conductive.
- They typically house the flow field channels—therefore, they must be conformable.

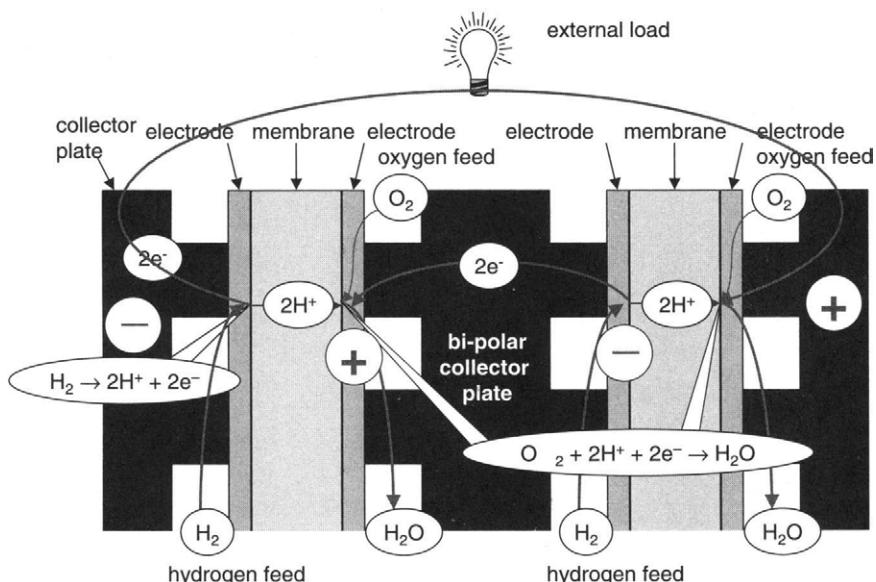


FIGURE 4-18. Bipolar plate connects and separates two adjacent cells.

**TABLE 4-4**  
Bi-polar Plate Design Criteria [32]

Property	Requirements	Comment
Electrical conductivity	$>100 \text{ S cm}^{-1}$	Bulk conductivity
Corrosion rate	$<16 \mu\text{A cm}^{-2}$	
Hydrogen permeability	$<2 \times 10^{-6} \text{ cm}^3 \text{ cm}^{-2} \text{ s}^{-1}$	@80°C, 3 atm
Compressive strength	$>2 \text{ MPa}$	
Thermal conductivity	$>20 \text{ W/mK}$	Strong function of stack design—some some designs may require higher thermal conductivity
Tolerance	$<0.05 \text{ mm}$	
Cost	$<\$10/\text{kW}$	Including both material and fabrication
Weight	$<1 \text{ kg/kW}$	

In addition, they must be corrosion resistant in the fuel cell environment, yet they must not be made out of "exotic" and expensive materials. To keep the cost down not only must the material be inexpensive, but also the manufacturing process must be suitable for mass production.

Some of the abovementioned requirements may contradict each other; therefore, selection of the material involves an optimization process. The resulting material may not be the best in any of the property categories, but it is the one that best satisfies the optimization criteria (typically the lowest cost per kWh of electricity produced). Table 4-4 summarizes bipolar plate design criteria.

#### 4.5.1. Materials

One of the first materials used for PEM fuel cell bipolar plates was graphite, primarily because of its demonstrated chemical stability in the fuel cell environment. Graphite is inherently porous, which may be detrimental in fuel cell applications. Those plates therefore must be impregnated to make them impermeable. This material is still used in laboratory fuel cells (primarily in single cells). However, machining of graphite plates is not an easy task and may be prohibitively expensive for most fuel cell applications. It should be mentioned that one fuel cell manufacturer (UTC Fuel Cells) uses porous graphite plates for water management inside the fuel cell stack.

In general, two families of materials have been used for fuel cell bipolar plates, namely graphite based (including graphite/composite) and metallic.

### *Metallic Plates*

The bipolar plates are exposed to a very corrosive environment inside a fuel cell (pH 2 to 3 and temperature 60°C to 80°C). Typical metals such as aluminum, steel, titanium, or nickel would corrode in a fuel cell environment, and dissolved metal ions would diffuse into the ionomer membrane, resulting in lowering of ionic conductivity and reducing the fuel cell life. In addition, a corrosion layer on the surface of a bipolar plate would increase electrical resistance. Because of these issues, metallic plates must be adequately coated with a noncorrosive yet electrically conductive layer, such as graphite, diamond-like carbon, conductive polymer, organic self-assembled polymers, noble metals, metal nitrides, metal carbides, indium doped tin oxide, and so on. The effectiveness of the coating in protecting the bipolar plate from the corrosive PEM fuel cell environment depends on (i) corrosion resistance of coating, (ii) micropores and microcracks in the coating layer, and (iii) difference between the coefficient of thermal expansion of the base material and coating. Metallic plates are suitable for mass manufacturing (stamping, embossing), and because they can be made very thin (<1 mm), result in compact and lightweight stacks. The need for protective coating and the problems associated with those in fuel cell operation are the major drawback for the metallic plates in PEM fuel cells.

### *Graphite-Composite Plates*

Carbon composite bipolar plates have been made using thermoplastics (polypropylene, polyethylene, or polyvinylidenefluoride) or thermoset resins (phenolic, epoxies, and vinyl esters) with fillers (such as carbon/graphite powder, carbon black, or coke-graphite) and with or without fiber reinforcements. These materials are typically chemically stable in fuel cell environment, although some thermosets may leach and consequently deteriorate. Depending on the rheological properties of these materials they are suitable for compression molding, transfer molding, or injection molding. Very often, a careful optimization of the material's composition and properties is required involving a trade-off between manufacturability (*i.e.*, cost) and functional properties (*i.e.*, electrical conductivity). For example, a replacement of a compression-molded material with bulk resistivity of 2.9 mOhm-cm with an injection-molded material with bulk resistivity of 26 mOhm-cm has been considered [33] because of the improvements in manufacturing speed (20 seconds of cycle time for injection molding vs 20 minutes for thermoplastic compression molding). Important properties that must be considered in designing and manufacturing of graphite/composite bipolar plates are tolerances, warping, and skinning effect (accumulation of polymer at the surface of the plate as a result of the molding process). High-speed molding processes can meet the cost targets, and the materials (graphite and polymer) are not expensive. These plates, especially those with fluoropolymers, have unsurpassed

chemical stability in the fuel cell environment. However, they are bulky (minimum thickness ~2 mm), and relatively brittle (which may be a problem for high-speed automated stack assembly processes). Although their electrical conductivity is several orders of magnitude lower than the conductivity of the metallic plates, the bulk resistive losses are in the order of magnitude of several millivolts.

#### *Composite Graphite/Metallic Plates*

A sandwich of two embossed graphite foils with a thin metallic sheet in between has been patented by Ballard [34]. This concept combines the advantages of both graphite (corrosion resistance) and metallic plates (impermeability and structural rigidity), and results in a lightweight, durable, and easy-to-manufacture bipolar plate. It should also be mentioned that graphite foil has very low contact resistance, due to its conformability.

#### 4.5.2. Properties

The most important properties of various metallic and graphite/composite bipolar plate materials are summarized in Tables 4-5 and 4-6, respectively.

TABLE 4-5  
Selected Properties of Metallic Bi-polar Plate Materials [35]

Property	Unit	Materials			
		SS	Al	Ti	Ni
Density	$\text{g cm}^{-3}$	7.95	2.7	4.55	8.94
Bulk el. conductivity	$\text{S cm}^{-1}$	14,000	377,000	23,000	146,000
Thermal conductivity	$\text{W m}^{-1} \text{K}^{-1}$	15	223	17	60.7
Thermal expansion	$\mu\text{m m}^{-1} \text{K}^{-1}$	18.5	24	8.5	13

TABLE 4-6  
Selected Properties of Some Graphite/Composite Bi-polar Plate Materials

Property	Unit	Materials and Manufacturers			
		graphite POCO	BBP 4 SGL	PPG 86 SGL	BMC940 BMC
Density	$\text{g cm}^{-3}$	1.78	1.97	1.85	1.82
Bulk el. conductivity	$\text{S cm}^{-1}$	680	200	56	100
Thermal conductivity	$\text{W m}^{-1} \text{K}^{-1}$	95	20.5	14	19.2
Thermal expansion	$\mu\text{m m}^{-1} \text{K}^{-1}$	7.9	3.2	27	30
Tensile strength	MPa	60			30
Flexural strength	MPa	90	50	35	40
Compressive strength	MPa	145	76	50	

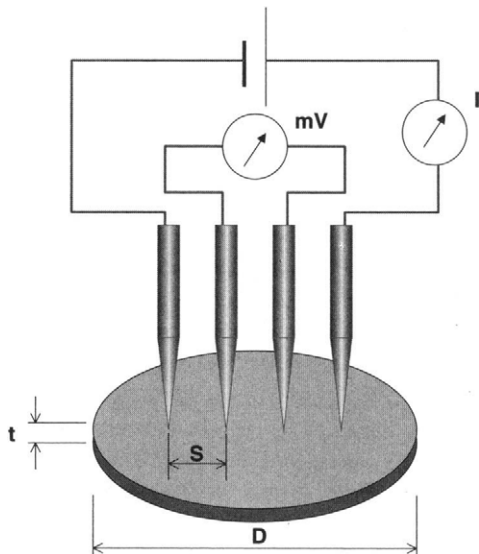


FIGURE 4-19. Experimental setup for measuring sample resistivity with four-point probe method [33].

One of the most important properties of the fuel cell bipolar plates is their electrical conductivity. One should distinguish between the bulk and total conductivity or resistivity, the latter including both bulk and interfacial contact components. In an actual fuel cell stack, contact (interfacial) resistance is more important than bulk resistance.

Bulk electrical resistivity of the plates may be measured with a four-point probe method for sheet resistivity as described by Smits [36]. The experimental setup is shown in Figure 4-19. This method allows measurement of bulk resistivity of thin plates by applying a geometry-dependent correction factor to the measured value of voltage drop and applied current:

$$\rho = k \frac{V}{I} t \quad (4-19)$$

where:

$\rho$  = resistivity ( $\Omega\text{cm}$ )

$k$  = correction factor, function of  $D/S$  and  $t/S$ , where  $D$  = sample diameter,  $S$  = spacing of probes, and  $t$  = sample thickness; values for correction factor are tabulated in Table 4-7 [36].

$V$  = measured voltage (V)

$I$  = applied current (A)

$t$  = sample thickness (cm)

**TABLE 4-7**

Correction Factor for Bulk Resistivity Measurement of Thin Round Samples with Four-Point Probe [36]

D/S	t/S									
	<0.4	0.4	0.5	0.6	0.7	0.8	1	1.25	1.666	2
3	2.2662	2.2651	2.2603	2.2476	2.2240	2.1882	2.0881	1.9240	1.6373	1.4359
4	2.9289	2.9274	2.9213	2.9049	2.8744	2.8281	2.6987	2.4866	2.1161	1.8558
5	3.3625	3.3608	3.3538	3.3349	3.3000	3.2468	3.0982	2.8548	2.4294	2.1305
7.5	3.9273	3.9253	3.9171	3.8951	3.8543	3.7922	3.6186	3.3343	2.8375	2.4883
10	4.1716	4.1695	4.1608	4.1374	4.0940	4.0281	3.8437	3.5417	3.0140	2.6431
15	4.3646	4.3624	4.3533	4.3288	4.2834	4.2145	4.0215	3.7055	3.1534	2.7654
20	4.4364	4.4342	4.4249	4.4000	4.3539	4.2838	4.0877	3.7665	3.2053	2.8109
40	4.5076	4.5053	4.4959	4.4706	4.4238	4.3525	4.1533	3.8270	3.2567	2.8560
$\infty$	4.5324	4.5301	4.5206	4.4952	4.4481	4.3765	4.1762	3.8480	3.2747	2.8717

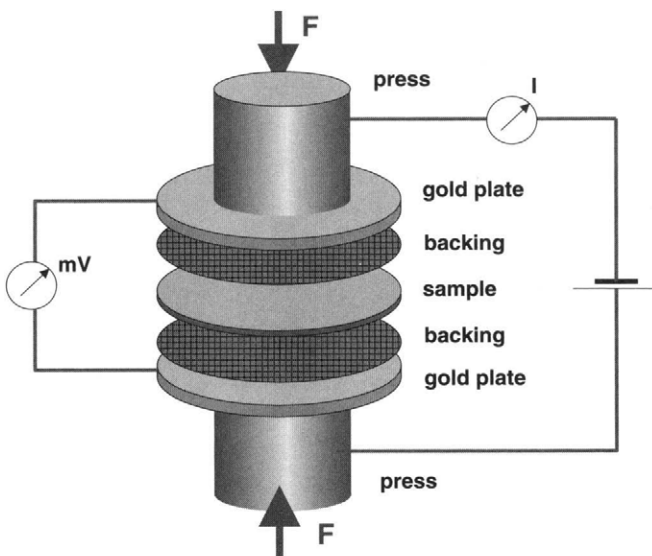


FIGURE 4-20. Schematic diagram of experimental setup for measuring total (contact and bulk) resistance of graphite and molded graphite composite samples, including electrode-backing layers [33, 37].

However, bulk resistivity is not a significant source of voltage loss in fuel cells, even for relatively high-resistivity plates. For example, a 3-mm thick molded graphite/composite plate with bulk resistivity as high as  $8 \text{ m}\Omega\text{cm}$  would result in about  $2.4 \text{ mV}$  voltage loss at  $1 \text{ A}/\text{cm}^2$ . Much higher resistance results from the interfacial contacts, such as between the bipolar plate and the gas diffusion layer.

The interfacial contact resistance may be determined by sandwiching a bipolar plate between the two gas diffusion layers [37] (or a gas diffusion layer between the two bipolar plates [38]), and then passing electrical current through the sandwich and measuring voltage drop (see Figure 4-20). The total voltage drop (or resistance,  $R = V/I$ ) in this experiment is a strong function of clamping pressure. There are several serial resistances in this experiment, namely contact resistance between the gold contact plates and the gas diffusion media,  $R_{\text{Au-GDL}}$ , bulk (through-plane) resistance of the gas diffusion media,  $R_{\text{GDL}}$ , contact resistance between the gas diffusion media and bipolar plate,  $R_{\text{GDL-BP}}$ , and bulk resistance of the bipolar plate,  $R_{\text{BP}}$ , as illustrated in Figure 4-21:

$$R_{\text{mes}} = 2R_{\text{Au-GDL}} + 2R_{\text{GDL}} + 2R_{\text{GDL-BP}} + R_{\text{BP}} \quad (4-20)$$

The bulk resistance of the gas diffusion media,  $R_{\text{GDL}}$ , and of the bipolar plate,  $R_{\text{BP}}$ , should be known from independent measurements or from

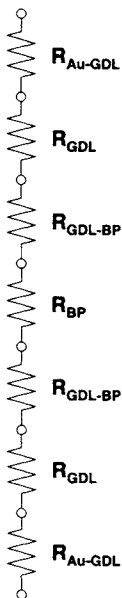


FIGURE 4-21. Resistances involved in measurement from Figure 4-20.

manufacturer's specifications, and the unwanted contact resistance between the gold contact plate and gas diffusion media may be determined by an additional measurement involving just the gas diffusion media between the two gold contact plates:

$$R'_{\text{mes}} = 2R_{\text{Au-GDL}} + R_{\text{GDL}} \quad (4-21)$$

The contact resistance is then:

$$R_{\text{GDL-BP}} = (R_{\text{mes}} - R'_{\text{mes}} - R_{\text{BP}} - R_{\text{GDL}})/2 \quad (4-22)$$

Bulk resistance of the bipolar plate and the gas diffusion media should be independent of the clamping force, but the contact resistance is obviously a strong function of the clamping force. Figure 4-22 shows the contact resistance for several gas diffusion media [38]. At 2 MPa, contact resistance for carbon fiber paper is about 3 mΩcm. Carbon cloth has lower contact resistance, that is, about 2 mΩcm. Almost identical results were reported by Mathias *et al.* [31] using a slightly different measuring procedure.

Interfacial contact resistance depends not only on contact (clamping) pressure, but also on the surface characteristics and the effective conductivities of the two surfaces in contact. Using the fractal geometric descrip-

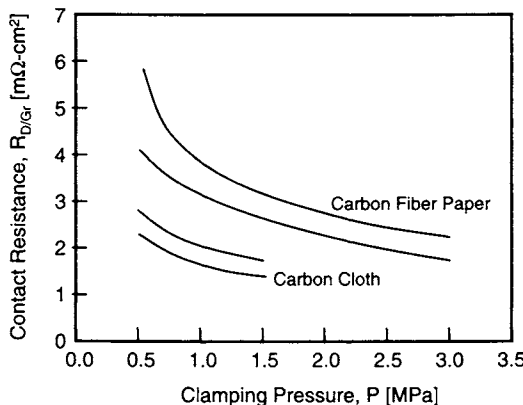


FIGURE 4-22. Results of the contact resistance measurements between the gas diffusion media and graphite composite bipolar plate. From [38].

tion of surface topographies, Majumdar and Tien [38] arrived at a relationship between the contact resistance and clamping pressure. Mishra *et al.* [38] modified the Majumdar-Tien relationship to fit the case of a relatively soft material, such as gas diffusion layer, with hard material, such as bipolar plate:

$$R = \frac{A_a K G^{D-1}}{\kappa L^D} \left[ \frac{D}{(2-D)p^*} \right]^{\frac{D}{2}} \quad (4-23)$$

where:

$R$  = contact resistance,  $\Omega \cdot m^2$

$A_a$  = apparent contact area at the interface,  $m^2$

$K$  = geometric constant

$G$  = topography of a surface profile,  $m$

$D$  = fractal dimension of a surface profile

$\kappa$  = effective electrical conductivity of two surfaces,  $S \cdot m^{-1}$

$$\frac{1}{\kappa} = \frac{1}{2} \left( \frac{1}{\kappa_1} + \frac{1}{\kappa_2} \right)$$

$L$  = scan length,  $m$

$p^*$  = dimensionless clamping pressure (ratio of actual clamping pressure and compressive modulus of gas diffusion layer)

After obtaining the geometric parameters from the surface profilometric scans and plugging them in Equation (4-21), Mishra *et al.* [37] obtained reasonably good agreements with measurements of contact resistance.

## References

1. Gottesfeld, S. and T. A. Zawodzinski, Polymer Electrolyte Fuel Cells, in R. C. Alkire, H. Gerischer, D. M. Kolb, and C. W. Tobias (editors), *Advances in Electrochemical Science and Engineering*, Vol. 5 (Wiley-VCH, New York, 1997).
2. Doyle, M. and G. Rajendran, Perfluorinated Membranes, in W. Vielstich, A. Lamm, and H. A. Gastegier (editors), *Handbook of Fuel Cells, Fundamentals, Technology and Applications*, Vol. 3 *Fuel Cell Technology and Applications* (John Wiley & Sons, New York, 2003), pp. 351–395.
3. Zawodzinski, Jr., T. A., C. Deroiun, S. Radzinski, R. J. Sherman, T. Springer, and S. Gottesfeld, Water Uptake By and Transport Through Nafion 117 Membranes, *Journal of the Electrochemical Society*, Vol. 140, 1993, p. 1041.
4. Zawodzinski, Jr., T. A., C. Lopez, R. Jestel, J. Valerio, and S. Gottesfeld, A Comparative Study of Water Uptake By and Transport Through Ionomeric Fuel Cell Membranes, *Journal of the Electrochemical Society*, Vol. 140, 1993, p. 1981.
5. Nafion product sheet, Dupont NAE101, February 2004.
6. Cleghorn, S., J. Kolde, and W. Liu, Catalyst Coated Composite Membranes, in W. Vielstich, A. Lamm, and H. A. Gastegier (editors), *Handbook of Fuel Cells, Fundamentals, Technology and Applications*, Vol. 3 *Fuel Cell Technology and Applications* (John Wiley & Sons, New York, 2003), pp. 566–575.
7. Springer, T. E., T. A. Zawodzinski, and S. Gottesfeld, Polymer Electrolyte Fuel Cell Model, *Journal of the Electrochemical Society*, Vol. 138, No. 8, 1991, pp. 2334–2342.
8. Zawodzinski, T. A., *Membranes Performance and Evaluation*, NSF Workshop on Engineering Fundamentals of Low Temperature PEM Fuel Cells (Arlington, VA, November 2001) ([http://electrochem.cwru.edu/NSF/presentations/NSF\\_Tom-Zawodzinsk\\_Membranes.pdf](http://electrochem.cwru.edu/NSF/presentations/NSF_Tom-Zawodzinsk_Membranes.pdf)).
9. La Conti, A. B., A. R. Fragala, J. R. Boyack, Solid Polymer Electrolyte Electrochemical Cells: Electrode and Other Materials Considerations, in J. D. E. McIntyre, S. Srinivasan, and F. G. Will (editors), *Electrode Materials and Processes for Energy Conversion and Storage*, in *Proc. the Electrochemical Society*, PV 77-6 (Pennington, NJ, 1977), p. 354.
10. Fuller, T. and J. Newman, Experimental Determination of the Transport Number of Water in Nafion 117 Membrane, *Journal of the Electrochemical Society*, Vol. 139, 1992, p. 1332.
11. Zawodzinski, Jr., T. A., T. Springer, F. Uribe, and S. Gottesfeld, Characterization of polymer electrolytes for fuel cell applications, *Solid State Ionics*, Vol. 60, 1993, p. 199.
12. Yeo, S. C. and A. Eisenberg, Physical properties and supermolecular structure of perfluorinated ion-containing (nafion) polymers, *Journal of Applied Polymer Science*, Vol. 21, 1977, p. 875.
13. Eisman, G. A., The physical and mechanical properties of a new perfluorosulfonic acid ionomer for use as a separator/membrane in proton exchange

- processes, in J. W. Van Zee, R. E. White, K. Kinoshita, and H. S. Burney (editors), *Diaphragms, Separators, and Ion Exchange Membranes*, in *Proc. the Electrochemical Society*, PV 86-13 (Pennington, NJ, 1986) pp. 156–171.
- 14. Verbruge, M., Methanol Diffusion in Perfluorinated Ion-Exchange Membranes, *Journal of the Electrochemical Society*, Vol. 136, 1989, p. 417.
  - 15. Slade, R. C. T., A. Hardwick, and P. G. Dickens, Investigation of H<sup>+</sup> motion in NAFION film by pulsed <sup>1</sup>H NMR and A.C. conductivity measurements, *Solid State Ionics*, Vols 9–10, Part 2, 1983, p. 1093.
  - 16. Zawodzinski, Jr., T. A., M. Neeman, L. Sillerud, and S. Gottesfeld, Determination of water diffusion coefficients in perfluorosulfonate ionomeric membranes, *Journal of Physical Chemistry*, Vol. 95, 1991, p. 6040.
  - 17. Newman, J., *Electrochemical Systems* (Prentice Hall, Englewood Cliffs, NJ, 1991).
  - 18. Motupally, S., A. J. Becker, and J. W. Weidner, Diffusion of Water in Nafion 115 Membranes, *Journal of the Electrochemical Society*, Vol. 147, 2000, p. 3171.
  - 19. Buchi, F. N. and G. G. Scherer, Investigation of the Transversal Water Profile in Nafion Membranes in Polymer Electrolyte Fuel Cells, *Journal of the Electrochemical Society*, Vol. 148, No. 3, 2000, pp. A181–A188.
  - 20. Janssen, G. J. M. and M. L. J. Overvelde, Water transport in the proton-exchange-membrane fuel cell: measurements of the effective drag coefficient, *Journal of Power Sources*, Vol. 101, 2001, pp. 117–125.
  - 21. Jeo, R. S. and J. McBreen, Transport Properties of Nafion Membranes in Electrochemically Regenerative Hydrogen/Halogen Cells, *Journal of the Electrochemical Society*, Vol. 126, 1979, p. 1682.
  - 22. Ogumi, Z., Z. Takehara, and S. Yoshizawa, Gas Permeation in SPE Method, *Journal of the Electrochemical Society*, Vol. 131, 1984, p. 769.
  - 23. Bernardi, D. M. and M. W. Verbrugge, A Mathematical Model of the Solid-Polymer-Electrolyte Fuel Cell, *Journal of the Electrochemical Society*, Vol. 139, 1992, p. 2477.
  - 24. Sakai, T. H. Takeraka and E. Torikai, Gas Diffusion in the Dried and Hydrated Nafions, *Journal of the Electrochemical Society*, Vol. 133, No. 1, 1986, pp. 88–92.
  - 25. Paganin, V. A., E. A. Ticianelli, and E. R. Gonzales, Development and electrochemical studies of gas diffusion electrodes for polymer electrolyte fuel cells, *Journal of Applied Electrochemistry*, Vol. 26, 1996, pp. 297–304.
  - 26. Ralph, T. R. and M. P. Hogarth, Catalysis for Low Temperature Fuel Cells, Part I: The Cathode Challenges, *Platinum Metals Review*, Vol. 46, No. 1, 2002, pp. 3–14.
  - 27. Gasteiger, H. A., W. Gu, R. Makharia, and M. F. Mathias, Catalyst Utilization and Mass Transfer Limitations in the Polymer Electrolyte Fuel Cells, *Electrochemical Society Meeting* (Orlando, FL, September 2003).
  - 28. F. Uribe, T. Zawodzinski, J. Valerio, G. Bender, F. Garzon, A. Saab, T. Rockward, P. Adcock, J. Xie, and W. Smith, Fuel cell electrode optimization for operation on reformatte and air, in *Proc. 2002 Fuel Cells Lab R&D Meeting, DOE Fuel Cells for Transportation Program* (Golden, CO, May 9, 2002).
  - 29. Qi, Z. and A. Kaufman, Low Pt loading high performance cathodes for PEM fuel cells, *Journal of Power Sources*, Vol. 113, 2003, pp. 37–43.

30. Sasikumar, G., J. W. Ihm, and H. Ryu, Dependence of optimum Nafion content in catalyst layer on platinum loading, *Journal of Power Sources*, Vol. 132, 2004, pp. 11–17.
31. Mathias, M. F., J. Roth, J. Fleming, and W. Lehnert, Diffusion Media Materials and Characterization, in W. Vielstich, A. Lamm, and H. A. Gasteiger (editors), *Handbook of Fuel Cells, Fundamentals, Technology and Applications*, Vol. 3 *Fuel Cell Technology and Applications* (John Wiley & Sons, New York, 2003) pp. 517–537.
32. U.S. Department of Energy, *Transportation Fuel Cell Power Systems, 2000 Annual Progress Report* (U.S. Department of Energy, Washington, D.C., 2000).
33. Barbir, F. and J. Braun, Development of Low Cost Bi-Polar Plates for PEM Fuel Cells, in *Proc. Fuel Cell 2000 Research & Development, Strategic Research Institute Conference* (Philadelphia, September 2000).
34. Wilkinson, D. P., G. J. Lamont, H. H. Voss, and C. Schwab, Method of fabricating an embossed fluid flow field plate, U.S. Patent #5, 527, 363, 1996.
35. MatWeb Materials Properties Data, <http://www.matweb.com> (accessed October 2004.)
36. Smits, F. M., Measurement of Sheet Resistivities with the Four-Point Probe, *Bell System Technical Journal*, May 1958, pp. 711–718.
37. Barbir, F., J. Braun, and J. Neutzler, Properties of Molded Graphite Bi-Polar Plates for PEM Fuel Cells, *International Journal on New Materials for Electrochemical Systems*, No. 2, 1999, pp. 197–200.
38. Mishra, V., F. Yang, and R. Pitchumani, Electrical Contact Resistance Between Gas Diffusion Layers and Bi-Polar Plates in a PEM Fuel Cell, in *Proc. 2<sup>nd</sup> International Conference on Fuel Cell Science, Engineering and Technology* (Rochester NY, 2004).
39. Majumdar, A. and C. L. Tien, Fractal Network Model for Contact Conductance, Joint ASME/AIChE National Heat Transfer Conference, (Philadelphia, PA, 1989), pp. 1–9.

## Problems

### Problem No. 1:

Nafion conductivity is 0.1 S/cm when fully hydrated.

- a) Calculate the resistance of Nafion 117 membrane.
- b) Calculate the resistance of two Nafion 112 layers; assume no interfacial resistance.
- c) If water level in one of the two Nafion 112 layers drops to 50% of the fully hydrated level, calculate the total resistance through both layers.

### Problem No. 2:

Fuel cell operating conditions are:

Temperature = 80°C, Pressure = 300 kPa, both gases fully saturated.

Calculate cell ionic resistance and hydrogen crossover for two different membranes, namely Nafion 112 and 117.

**Problem No. 3:**

Resistance measurement of a 65-cm<sup>2</sup> fuel cell with Nafion membrane shows 2.61 mOhm. The reactant gases are fully saturated at cell operating temperature of 70°C. Estimate the membrane thickness assuming that 2/3<case fraction> of the above resistance is protonic resistance.

**Problem No. 4:**

Calculate:

- a) Permeability of hydrogen at 60°C.
- b) What would be the permeation rate through 200 cm<sup>2</sup> of Nafion 115 if the pressure of hydrogen is 300 kPa?
- c) What would be the equivalent current loss?

**Problem No. 5:**

A fuel cell is put together that has 10 cells, 300-cm<sup>2</sup> active area each, using Nafion 115. Before it can be operated it must be checked for leaks.

- a) What would be an acceptable hydrogen leak rate (if the test is performed at room temperature and at pressure of 0.5 bar above atmospheric)? Assume that Nafion is fully saturated.
- b) If Nafion was dry after assembly, would you expect higher or lower permeation rate than if it was wet?
- c) What would be the permeation rate in operation when the operating temperature is 80°C and the operating pressure is 200 kPa?
- d) What would be the equivalent current loss?

**Problem No. 6:**

Two fuel cells of equal active area operate at same operating conditions ( $H_2/O_2$ , 80°C, 1 atm, both gases fully humidified) and generate same current. However, cell #1 has 30 mV higher potential than cell #2. The only possible difference between the two cells is the catalyst loading. The first cell has Pt loading of 0.4 mg/cm<sup>2</sup> Pt. What is the Pt loading of cell #2?

**Problem No. 7:**

If 1% of the cars produced in the world use PEM fuel cells with platinum loading of 0.1 mg/cm<sup>2</sup>, what would be the annual demand for platinum? See if you can compare it with today's world platinum consumption. (Assume 75 kW fuel cell per car with operation at 1.3 A/cm<sup>2</sup> at 0.65 V per cell.)

## Quiz

1. Nafion works in fuel cells because:
  - a) it is so thin
  - b) it is full of water
  - c) it conducts protons
2. Higher water content in Nafion membrane results in:
  - a) higher ionic conductivity
  - b) lower ionic conductance because the membrane becomes thicker
  - c) higher ionic resistivity
3. Membrane thickness has an effect on:
  - a) ionic conductance
  - b) gas permeation
  - c) both ionic conductance and gas permeation
4. Smaller catalyst particles results in:
  - a) more surface area, thus higher exchange current density
  - b) thicker catalyst layer
  - c) higher catalyst loading
5. In a gas diffusion layer on the cathode (air) side:
  - a) oxygen and water flow in opposite directions
  - b) oxygen and water flow in the same direction
  - c) oxygen and water mix together
6. Bipolar plate bulk resistance is a:
  - a) function of its thickness
  - b) function of material conductivity
  - c) function of both thickness and conductivity
7. The advantage of graphite-based bipolar plates over metallic plates is:
  - a) better conductivity
  - b) better corrosion resistance
  - c) lighter weight
8. Catalyst loading is:
  - a) a process of loading the catalyst on the support particles
  - b) quantity of catalyst per unit electrode geometric area
  - c) quantity of catalyst per cell

9. Electroosmotic drag:

- a) moves water from anode to cathode
- b) moves water from cathode to anode
- c) moves water in both directions as a function of pressure difference

10. Contact or clamping pressure has effect on:

- a) bulk resistance of the bipolar plate
- b) resistance in the membrane
- c) interfacial resistance

# CHAPTER 5

## 5. Fuel Cell Operating Conditions

### 5.1. Operating Pressure

A fuel cell may be operated at ambient pressure or it may be pressurized. As we have already learned, a fuel cell gains some potential when the pressure is increased (Figure 5-1 for example), but as illustrated in Chapter 9, the net gain, when the compression power is taken into account, is at least questionable. The issue of pressurization is also related to the issue of water management, and therefore must be addressed from a system perspective.

When a fuel cell is fed the reactant gases from a pressurized tank, its pressure is controlled by a backpressure regulator placed at the outlet (Figure 5-2a). This pressure regulator keeps the desired, preset pressure at the fuel cell outlet. Very often, in laboratory settings, the inlet pressure is not even recorded. The inlet pressure is always higher because of inevitable pressure drop in tiny channels inside the fuel cell. However, when the reactant gas (for example, air) is fed to a fuel cell by a mechanical device, a blower or a compressor, which is the case in any practical system, it is the inlet pressure that matters (Figure 5-2b). The compressor or the blower must be capable of delivering the required flow rate at desired pressure. The backpressure regulator may still be used to pressurize the cell, or if no back-pressure regulator is used, the gas leaves the cell at atmospheric pressure. Note that atmospheric pressure may vary too, depending on weather conditions or elevation (many fuel cell experiments reported by the Los Alamos National Laboratory are actually conducted at substandard pressure, because of elevation).

### 5.2. Operating Temperature

The cell temperature is another operating parameter that may be selected and preset. In general, a higher operating temperature results in higher cell potential; however, for each fuel cell design there is an optimal

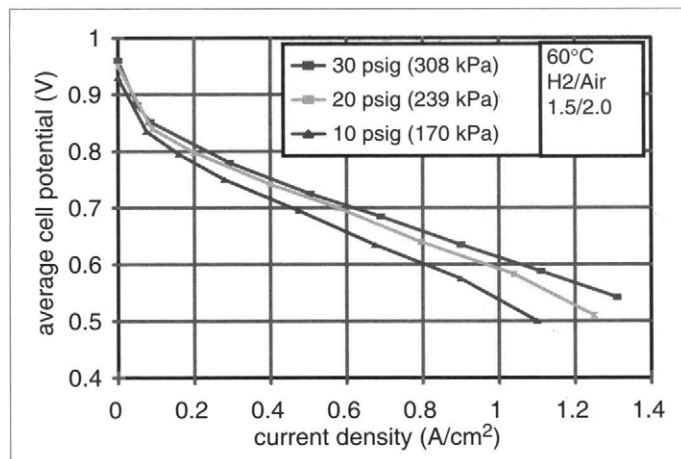


FIGURE 5-1. Fuel cell performance at various operating pressures [1].

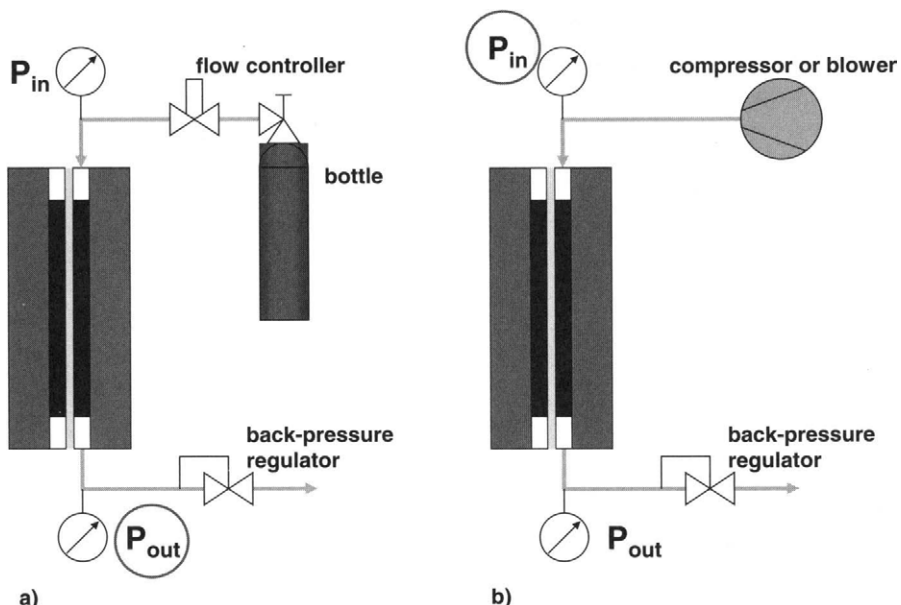


FIGURE 5-2. Fuel cell operating pressure as a function of reactant gas supply; a) supply from a high-pressure tank, b) supply by a mechanical device, a compressor or blower.

temperature. As already shown in Figure 3-19, a PEM fuel cell does not have to be heated up to the operating temperature in order to become operational.

The operating temperature of practical fuel cells, similarly to operating pressure, must be selected from the system perspective, taking into account not only the cell performance, but also the system requirements, particularly the size and parasitic power requirements of the heat management subsystem. A fuel cell generates heat as a by-product of the electrochemical reaction. To maintain the desired temperature, heat must be taken away from a fuel cell. Some heat dissipates from the outer surface of the fuel cell and some must be taken away with a cooling system. Medium that takes away the heat may be air, water, or a special coolant. The inner design of the fuel cell must allow the heat transfer to occur. Sometimes, small fuel cells need a heater to reach the operating temperature. In these fuel cells so much heat is being taken away from the outer surface that an additional heater is required. This of course is not very practical, but it is sometimes necessary for testing of fuel cells at a desired temperature.

The following is the fuel cell heat balance:

$$Q_{\text{gen}} + Q_{\text{react,in}} = Q_{\text{dis}} + Q_{\text{react,out}} + Q_{\text{cool}} \quad (5-1)$$

In other words, the heat generated in the fuel cell, plus the heat brought into the cell with reactant gases, is taken away from the cell by heat dissipation from the cell surface to the surrounding, by the reactant gases leaving the cell, and by the coolant.

The temperature inside a fuel cell may not be uniform; it may vary from inlet to outlet, from inside out, or from cathode to anode. So which temperature is the cell temperature? The cell temperature may be approximated by the following temperatures, which are much easier to measure than the cell temperature:

- surface temperature
- temperature of air leaving the cell
- temperature of coolant leaving the cell

Because of finite temperature differences needed for heat transfer inside a fuel cell, none of the above is exactly the cell operating temperature. The surface temperature is clearly lower than the temperature inside a fuel cell in a case when the fuel cell is heating itself, and it is actually higher than the inside temperature if the fuel cell is heated with the heating pads on its surface. Because most of the losses in the fuel cell may be associated with the cathode reaction, the temperature of air exiting the fuel cell is a good approximation of the cell operating temperature, although again the temperature inside a fuel cell must be at least slightly higher than the air temperature. In a case when the cell temperature is maintained by the flow of coolant through the cell, the coolant outlet temperature may be

used as the operating temperature. The accuracy of these approximations depends on thermal conductivity of the cell materials and air and coolant flow rates.

### 5.3. Reactants Flow Rates

The reactants flow rate at the inlet of a fuel cell must be equal to or higher than the rate at which those reactants are being consumed in the cell. The rates (in  $\text{mol s}^{-1}$ ) at which hydrogen and oxygen are consumed and water is generated are determined by Faraday's Law:

$$\dot{N}_{\text{H}_2} = \frac{I}{2F} \quad (5-2)$$

$$\dot{N}_{\text{O}_2} = \frac{I}{4F} \quad (5-3)$$

$$\dot{N}_{\text{H}_2\text{O}} = \frac{I}{2F} \quad (5-4)$$

where:

$\dot{N}$  = consumption rate ( $\text{mol s}^{-1}$ )

I = current (A)

F = Faraday's constant ( $\text{C mol}^{-1}$ )

The mass flow rates of reactants consumption (in  $\text{g s}^{-1}$ ) are then:

$$\dot{m}_{\text{H}_2} = \frac{I}{2F} M_{\text{H}_2} \quad (5-5)$$

$$\dot{m}_{\text{O}_2} = \frac{I}{4F} M_{\text{O}_2} \quad (5-6)$$

The mass flow rate of water generation (in  $\text{g s}^{-1}$ ) is:

$$\dot{m}_{\text{H}_2\text{O}} = \frac{I}{2F} M_{\text{H}_2\text{O}} \quad (5-7)$$

Most often, the flow rates of gases are expressed in standard liters per minute (slpm). Standard liter is a quantity of gas that would occupy 1 liter of volume at standard conditions, namely atmospheric pressure, 101.3 kPa, and 15°C. Note that most chemical handbooks and textbooks refer to 25°C as standard or reference temperature, but in technical fluid mechanics standard temperature is 15°C (although some books use 20°C and some

use 70°F]. To avoid confusion with standard temperatures, in Europe it is common to use normal liter or normal m<sup>3</sup>, where the temperature has been normalized to 0°C.

For any ideal gas, mols and volumes are directly related by the equation of state:

$$PV = NRT \quad (5-8)$$

Molar volume is:

$$v_m = \frac{V}{N} = \frac{RT}{P} \quad (5-9)$$

At standard conditions, that is, atmospheric pressure and 15°C, molar volume is:

$$\begin{aligned} v_m &= \frac{RT}{P} = \frac{8.314 \times 288.15}{101,300} = 0.02365 \text{ m}^3 \text{ mol}^{-1} \\ &= 23.65 \text{ l mol}^{-1} = 23,650 \text{ cm}^3 \text{ mol}^{-1} \end{aligned}$$

The volumetric flow rates of reactants consumption (in standard liters per minute or slpm) are:

$$\dot{V}_{H_2} = 23.65 \times 60 \times \frac{I}{2F} \quad (5-10)$$

$$\dot{V}_{O_2} = 23.65 \times 60 \times \frac{I}{4F} \quad (5-11)$$

Consumption of the reactants, hydrogen and oxygen, and water generation in the fuel cell is summarized in Table 5-1.

The reactants may, and in some cases must, be supplied in excess of consumption. For example, this is always necessary on the cathode side where water is produced and must be carried out from the cell with excess

TABLE 5-1  
Reactants Consumption and Water Generation (per Amp and per Cell)

	<i>Hydrogen Consumption</i>	<i>Oxygen Consumption</i>	<i>Water Generation (liq.)</i>
<i>mols<sup>-1</sup></i>	$5.18 \times 10^{-6}$	$2.59 \times 10^{-6}$	$5.18 \times 10^{-6}$
<i>gs<sup>-1</sup></i>	$10.4 \times 10^{-6}$	$82.9 \times 10^{-6}$	$93.3 \times 10^{-6}$
<i>cm<sup>3</sup>s<sup>-1</sup></i>	0.1225	0.06125	$93.3 \times 10^{-6}$
<i>slpm</i>	0.00735	0.003675	N/A
<i>Nm<sup>3</sup>h<sup>-1</sup></i>	$0.418 \times 10^{-3}$	$0.209 \times 10^{-3}$	N/A

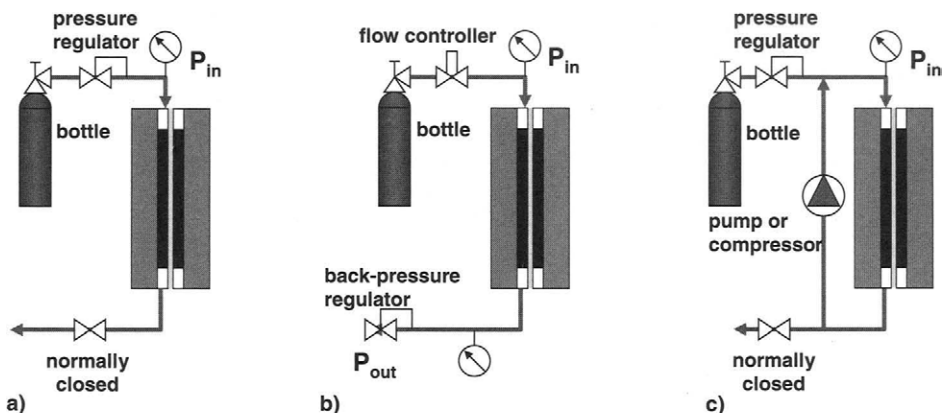


FIGURE 5-3. Modes of reactant supply: a) dead-end mode, b) flow-through mode, and c) recirculation mode.

flow. The ratio between the actual flow rate of a reactant at the cell inlet and the consumption rate of that reactant is called the stoichiometric ratio,  $S$ .

$$S = \frac{\dot{N}_{act}}{\dot{N}_{cons}} = \frac{\dot{m}_{act}}{\dot{m}_{cons}} = \frac{\dot{V}_{act}}{\dot{V}_{cons}} \quad (5-12)$$

Hydrogen may be supplied at the exact rate at which it is being consumed, in so-called dead-end mode (Figure 5-3a). If hydrogen is available at elevated pressure, such as in a high-pressure storage tank, the dead-end mode does not require any controls, that is, hydrogen is being supplied as it is being consumed. In a dead-end mode  $S = 1$ . If hydrogen loss due to crossover permeation or internal currents is taken into account then the hydrogen flow rate at the fuel cell inlet is slightly higher than the consumption rate corresponding to the electrical current being generated:

$$S = \frac{\dot{N}_{cons} + \dot{N}_{loss}}{\dot{N}_{cons}} > 1 \quad (5-13)$$

Fuel utilization is reverse of stoichiometric ratio:

$$\eta_{fu} = \frac{1}{S} \quad (5-14)$$

Even in a dead-end mode, hydrogen has to be periodically purged, because of accumulation of inerts or water. The frequency and duration of purges depends on purity of hydrogen, rate of nitrogen permeation through mem-

brane, and water net transport through the membrane. In calculating the fuel cell efficiency, the loss of hydrogen due to purging must be taken into account through fuel utilization.

$$\eta_{fu} = \frac{\dot{N}_{cons}}{\dot{N}_{cons} + \dot{N}_{loss} + \dot{N}_{prg} \tau_{prg} f_{prg}} \quad (5-15)$$

where:

- $\dot{N}_{loss}$  = rate of hydrogen loss ( $\text{mol s}^{-1}$ )
- $\dot{N}_{prg}$  = rate of hydrogen purge ( $\text{mol s}^{-1}$ )
- $\tau_{prg}$  = duration of hydrogen purge (s)
- $f_{prg}$  = frequency of purges ( $\text{s}^{-1}$ )

Instead of purging, hydrogen may be supplied in excess ( $S > 1$ ) in so-called flow-through mode (Figure 5-3b). In that case fuel utilization is given by Equation 5-14. Air is almost always supplied in a flow-through mode, with stoichiometry about  $S = 2$  or higher. In case of pure reactants (hydrogen and/or oxygen), a recirculation mode may be utilized (Figure 5-3c). In this case the unused gas is returned to the inlet by a pump or a compressor, or sometimes a passive device such as an ejector (based on a Venturi tube) may be employed. Note that in case of recirculation, a cell may operate at stoichiometric ratio much higher than 1, but because unused reactant (hydrogen or oxygen) is not wasted but returned for consumption back to the cell inlet, fuel or oxidant utilization on a system level is high (close to 1).

Fuel utilization in various modes of operation is summarized below.  
In dead-end and recirculation mode:

$$\eta_{fu} = \frac{\dot{N}_{cons}}{\dot{N}_{cons} + \dot{N}_{loss}} \quad (5-16)$$

dead-end mode with purging:

$$\eta_{fu} = \frac{\dot{N}_{cons}}{\dot{N}_{cons} + \dot{N}_{loss} + \dot{N}_{prg} \tau_{prg} f_{prg}} \quad (5-17)$$

flow-through mode:

$$\eta_{fu} = \frac{\dot{N}_{cons}}{\dot{N}_{act}} \quad (5-18)$$

In general, higher flow rates result in better fuel cell performance. Although pure hydrogen may be supplied in a dead-end mode ( $S \approx 1$ ) or with a stoichiometry slightly higher than 1 (1.1 to 1.2), hydrogen in a mixture of gases

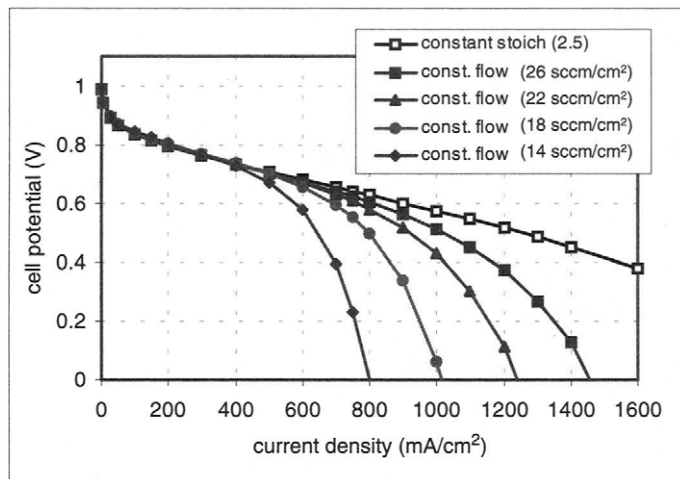


FIGURE 5-4. Fuel cell performance at different air flow rates.

(such as that coming out of a fuel processor) must be supplied with higher stoichiometries (1.1 to 1.5). The exact flow rate is actually a design variable. If the flow rate is too high the efficiency will be low (because hydrogen would be wasted), and if the flow rate is too low the fuel cell performance may suffer.

Similarly, for pure oxygen flow rate, the required stoichiometry is between 1.2 and 1.5, but when air is used, typical stoichiometry is 2 or higher. Although higher air flow rates result in better fuel cell performance, as shown in Figure 5-4, the air flow rate is also a design variable. Air is supplied to the cell by means of a blower or a compressor (depending on operating pressure) whose power consumption is directly proportional to the flow rate. Therefore, at higher air flow rates the fuel cell may perform better, but power consumption of a blower or particularly of a compressor may significantly affect the system efficiency. This is discussed in Chapter 9 in greater detail.

There are at least two reasons why fuel cell performance improves with excess air flow rate, namely:

1. Higher flow rate helps remove product water from the cell.
2. Higher flow rates keep oxygen concentration high.

Because oxygen is being consumed in the cell, its concentration at the cell outlet depends on the flow rate. If air is supplied at exact stoichiometric ratio ( $S = 1$ ), all the oxygen in the supplied air will be consumed in the fuel cell, that is, oxygen concentration in air exhaust will be zero. The higher the flow rate, the higher the oxygen concentration at the outlet and throughout the cell is going to be, as shown in Figure 5-5.

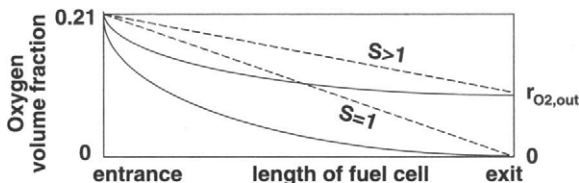


FIGURE 5-5. Oxygen volume or molar fraction through a fuel cell (dashed lines represent an ideal case where the rate of oxygen consumption is constant, and solid lines are more realistic, because the consumption rate is a function of oxygen concentration).

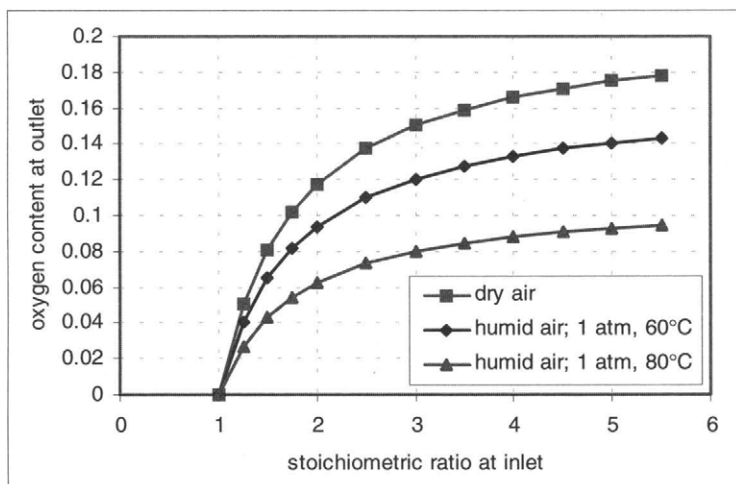


FIGURE 5-6. Oxygen content (by vol.) at the fuel cell outlet as a function of stoichiometric ratio.

If oxygen volume or molar fraction at the fuel cell inlet is  $r_{O_2,in}$ , then the oxygen volume or molar fraction at the outlet is:

$$r_{O_2,out} = \frac{S-1}{\frac{S}{r_{O_2,in}} - 1} \quad (5-19)$$

From Figure 5-6 it is clear that oxygen content at the outlet rapidly diminishes with stoichiometric ratios below 2. Because air at the outlet is almost always saturated with water vapor, oxygen content is even lower than it would be in dry air. For example, oxygen content at the fuel cell outlet at atmospheric pressure and 80°C operating with a stoichiometric ratio of 2 would be only 6%. An increase of stoichiometric ratio to 3 would result in oxygen content increasing to 8%. Above the stoichiometric ratio of 3 the

curve levels off, and little gain in oxygen concentration and fuel cell performance is achieved.

## 5.4. Reactants Humidity

Because the membrane requires water to maintain protonic conductivity, as shown in Chapter 4, both reactant gases typically must be humidified before entering the cell. In some cases they have to be saturated, but in some cases excess humidity is needed on the anode side and less-than-saturated conditions may be sufficient on the cathode side.

Humidity ratio is a ratio between the amount of water vapor present in a gas stream and the amount of dry gas. Humidity mass ratio (grams of water vapor/grams of dry gas) is:

$$x = \frac{G_v}{G_a} \quad (5-20)$$

Humidity molar ratio (mols of water vapor/mols of dry gas) is:

$$\chi = \frac{N_v}{N_a} \quad (5-21)$$

The relationship between mass and molar humidity ratios is:

$$x = \frac{M_w}{M_a} \chi \quad (5-22)$$

Molar ratio of gases is the same as a ratio of partial pressures:

$$\chi = \frac{p_v}{p_a} = \frac{p_v}{P - p_v} \quad (5-23)$$

where P is the total pressure and  $p_v$  and  $p_a$  are the partial pressures of vapor and gas, respectively.

Relative humidity is a ratio between the water vapor partial pressure,  $p_v$ , and saturation pressure,  $p_{vs}$ , which is the maximum amount of water vapor that can be present in gas for given conditions:

$$\phi = \frac{p_v}{p_{vs}} \quad (5-24)$$

Saturation pressure is a function of temperature only. The values of saturation pressure may be found in thermodynamic tables. *ASHRAE Funda-*

mentals [2] provides an equation that allows us to calculate the saturation pressure (in Pa) for any given temperature between 0°C and 100°C:

$$p_{vs} = e^{aT^{-1} + b + cT + dT^2 + eT^3 + f \ln(T)} \quad (5-25)$$

where a, b, c, d, e, and f are the coefficients:

$$a = -5800.2206$$

$$b = 1.3914993$$

$$c = -0.048640239$$

$$d = 0.41764768 \times 10^{-4}$$

$$e = -0.14452093 \times 10^{-7}$$

$$f = 6.5459673$$

The humidity ratios may be expressed in terms of relative humidity, saturation pressure, and total pressure, by combining the Equations (5-22), (5-23), and (5-24):

$$x = \frac{M_w}{M_a} \frac{\varphi p_{vs}}{P - \varphi p_{vs}} \quad (5-26)$$

and

$$\chi = \frac{\varphi p_{vs}}{P - \varphi p_{vs}} \quad (5-27)$$

Figure 5-7 shows the water vapor content in gas at different temperatures and pressures. As it follows from Equation (5-27), at lower pressure a gas can contain more water vapor, and as it follows from Equations (5-25) and

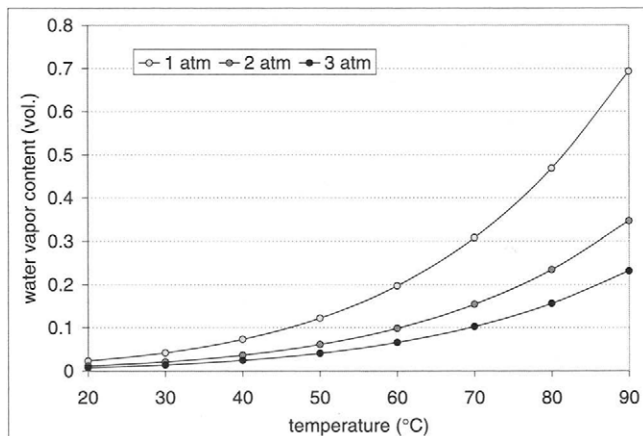


FIGURE 5-7. Water vapor content in a gas at different pressures and temperatures.

(5-27), water content in gas increases exponentially with temperature. At 80% and ambient pressure, water content in air is close to 50%. Water vapor content by volume is:

$$r_{H_2O,v} = \frac{\chi}{\chi + 1} = \frac{\varphi P_{vs}}{P} \quad (5-28)$$

Enthalpy of dry gas is:

$$h_g = c_{pg}t \quad (5-29)$$

where:

$h_g$  = enthalpy of dry gas,  $J g^{-1}$

$c_{pg}$  = specific heat of gas,  $J g^{-1} K^{-1}$

$t$  = temperature in  $^{\circ}C$

Note that this equation allows the use of degrees Celsius, by assuming that a reference zero state is at  $0^{\circ}C$  (*i.e.*,  $h_0 = 0$ ), and 1 degree of temperature difference on Celsius scale is equal to 1 degree Kelvin.

Enthalpy of water vapor is [3]:

$$h_v = c_{pv}t + h_{fg} \quad (5-30)$$

where  $h_{fg}$  = heat of evaporation =  $2500 J g^{-1}$  at  $0^{\circ}C$ .

Enthalpy of moist gas is then [3]:

$$h_{vg} = c_{pg}t + x(c_{pv}t + h_{fg}) \quad (5-31)$$

and the unit is Joules per gram of dry gas.

Enthalpy of liquid water is:

$$h_w = c_{pw}t \quad (5-32)$$

If the gas contains both water vapor and liquid water, such as may be the case at the fuel cell outlet, its enthalpy is [3]:

$$h_{vg} = c_{pg}t + x_v(c_{pv}t + h_{fg}) + x_w c_{pw}t \quad (5-33)$$

where  $x_v$  = water vapor content (in grams of vapor per gram of dry gas) and  $x_w$  = liquid water content (in grams of liquid water per gram of dry gas). The total water content is:

$$x = x_v + x_w \quad (5-34)$$

Note that when  $x_w = 0$  then  $x = x_v$ , and when  $x_w > 0$  then  $x_v = x_{vs}$  (when there is liquid water present in gas, gas is already saturated with vapor).

The processes with moist gas are best seen in an h-x diagram, or a so-called Mollier diagram (Figure 5-8) [3], where the x-axis is tilted by:

$$\left( \frac{dh}{dx} \right)_{t=0^\circ\text{C}} = h_{fg} \quad (5-35)$$

The saturation line divides the diagram in two distinct regions, namely the unsaturated region above the saturation line and fog (mist) region below the saturation line (Figure 5-8). The state of moist gas is determined by its temperature and relative humidity, or temperature and water content, or temperature and dew point. Dew point is the temperature at which all the water vapor present in gas would condense.

The reactant gases in PEM fuel cells are typically humidified. Most commonly, both reactant gases are required to be saturated at the cell operating temperature, although there are cell and MEA designs that require either subsaturated conditions or oversaturation. The process of humidification may be as simple as water or steam injection. In either case, to get from a dry gas or from ambient temperature air to fully saturated gas at cell operating temperature, both water and heat are required. Injection of water in relatively dry gas would result in saturation at a temperature lower than that of starting air and water (as shown in Figure 5-9).

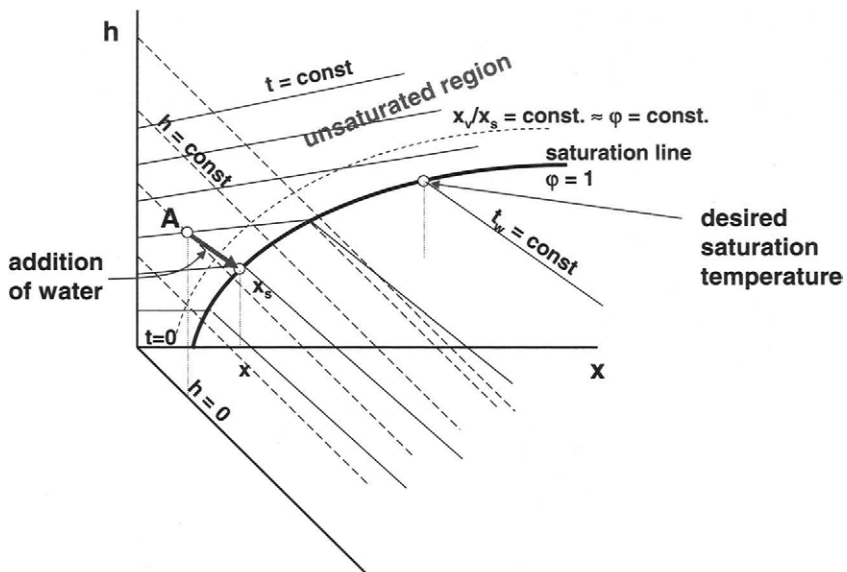


FIGURE 5-8. Mollier h-x diagram for moist air.

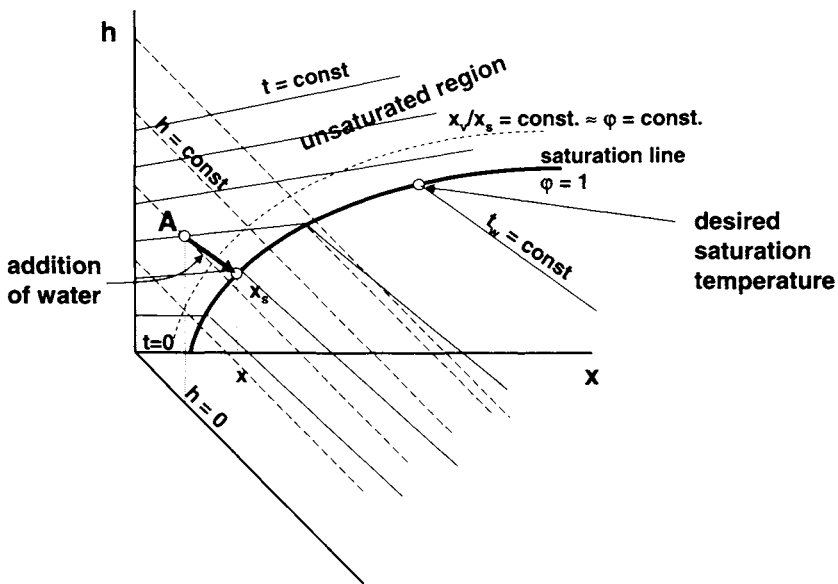


FIGURE 5-9. Illustration of humidification process in an h-x diagram.

The amount of heat required for humidification may be quite significant, especially if ambient pressure air is to be saturated at relatively high temperatures.

*Example:*

A fuel cell with 300-cm<sup>2</sup> active area operates at 0.6 A/cm<sup>2</sup> and 0.65 V. Air is supplied at stoichiometric ratio of 2 and at a pressure of 1.15 bar, and it is humidified by injecting hot water (60°C) just before the stack inlet. Ambient air conditions are 1 bar, 20°C, and 60% RH. The requirement is to saturate the air at cell operating temperature of 60°C. Calculate the air flow rate, the amount of water required for 100% humidification of air at the inlet, and heat required for humidification.

Oxygen consumption is (Equation 5-3):

$$\dot{N}_{O_2, \text{cons}} = \frac{I}{4F} = \frac{0.6 \text{ A cm}^{-2} \times 300 \text{ cm}^2}{4 \times 96,485} = 0.466 \times 10^{-3} \text{ mol s}^{-1}$$

Oxygen flow rate at cell inlet is (Equation 5-12):

$$\dot{N}_{O_2, \text{act}} = S \dot{N}_{O_2, \text{cons}} = 2 \times 0.466 \times 10^{-3} = 0.933 \times 10^{-3} \text{ mol s}^{-1}$$

Air flow rate at cell inlet is:

$$\dot{N}_{\text{air}} = N_{\text{O}_2, \text{act}} \frac{1}{r_{\text{O}_2}} = \frac{1.933 \times 10^{-3}}{0.21} = 4.44 \times 10^{-3} \text{ mol s}^{-1}$$

$$\dot{m}_{\text{air}} = \dot{N}_{\text{air}} m_{\text{air}} = 4.44 \times 10^{-3} \text{ mol s}^{-1} \times 28.85 \text{ g mol}^{-1} = 0.128 \text{ g s}^{-1} \quad \underline{\text{Answer}}$$

where  $m_{\text{air}}$  = molecular weight of air  $\approx 0.21 \times 32 + 0.79 \times 28 = 28.85 \text{ g s}^{-1}$ .

The amount of water in air at cell inlet (saturated at 1.15 bar and 60°C) is (from Equation 5-20):

$$\dot{m}_{\text{H}_2\text{O}} = x_s \dot{m}_{\text{air}}$$

where  $x_s$  is water content in air at saturation, that is,  $\varphi = 1$  (from Equation 5-26):

$$x_s = \frac{m_{\text{H}_2\text{O}}}{m_{\text{air}}} \frac{p_{\text{vs}}}{P - p_{\text{vs}}}$$

where  $p_{\text{vs}}$  is saturation pressure at 60°C (from Equation 5-25) and  $P$  is total pressure, 1.15 bar = 115 kPa.

$$p_{\text{vs}} = e^{aT^{-1} + b + cT + dT^2 + eT^3 + f \ln(T)} = 19.944 \text{ kPa} \quad (\text{for } T = 333.15 \text{ K})$$

$$x_s = \frac{m_{\text{H}_2\text{O}}}{m_{\text{air}}} \frac{p_{\text{vs}}}{P - p_{\text{vs}}} = \frac{18}{28.85} \frac{19.944}{115 - 19.944} = 0.131 \text{ g}_{\text{H}_2\text{O}} / \text{g}_{\text{air}}$$

$$\dot{m}_{\text{H}_2\text{O}} = x_s \dot{m}_{\text{air}} = 0.131 \text{ g}_{\text{H}_2\text{O}} / \text{g}_{\text{air}} \times 0.128 \text{ g}_{\text{air}} \text{ s}^{-1} = 0.0168 \text{ g}_{\text{H}_2\text{O}} \text{ s}^{-1}$$

Ambient air already has some water in it (60% relative humidity at 20°C):

$$x_s = \frac{m_{\text{H}_2\text{O}}}{m_{\text{air}}} \frac{\varphi p_{\text{vs}}}{P - \varphi p_{\text{vs}}} = \frac{18}{28.85} \frac{0.6 \times 2.339}{100 - 0.6 \times 2.339} = 0.00888 \text{ g}_{\text{H}_2\text{O}} / \text{g}_{\text{air}}$$

$$\dot{m}_{\text{H}_2\text{O}} = x_s \dot{m}_{\text{air}} = 0.00888 \text{ g}_{\text{H}_2\text{O}} / \text{g}_{\text{air}} \times 0.128 \text{ g}_{\text{air}} \text{ s}^{-1} = 0.0011 \text{ g}_{\text{H}_2\text{O}} \text{ s}^{-1}$$

Therefore, the amount of water needed for humidification of air at cell inlet is:

$$\dot{m}_{\text{H}_2\text{O}} = 0.0168 - 0.0011 = 0.0157 \text{ g}_{\text{H}_2\text{O}} \text{ s}^{-1} \quad \underline{\text{Answer}}$$

Heat required for humidification may be calculated from heat balance:

$$H_{\text{air,in}} + H_{\text{H}_2\text{O,in}} + Q = H_{\text{air,out}} \Rightarrow Q = H_{\text{air,out}} - H_{\text{air,in}} - H_{\text{H}_2\text{O,in}}$$

Enthalpy of wet/moist air is (Equation 5-31):

$$h_{\text{vair}} = c_{p,\text{air}}t + x(c_{p,v}t + h_{fg})$$

$$\begin{aligned}\text{Humidified air: } h_{\text{vair}} &= 1.01 \times 60 + 0.131 \times (1.87 \times 60 + 2500) \\ &= 402.8 \text{ J g}^{-1}\end{aligned}$$

$$\begin{aligned}\text{Ambient air: } h_{\text{vair}} &= 1.01 \times 20 + 0.00888 \times (1.87 \times 20 + 2500) \\ &= 42.73 \text{ J g}^{-1}\end{aligned}$$

$$\text{Water: } h_{\text{H}_2\text{O}} = c_{p,w}t = 4.18 \times 60 = 250.8 \text{ J g}^{-1}$$

$$\begin{aligned}Q &= 402.8 \text{ J g}^{-1} \times 0.128 \text{ g/s} - 42.73 \text{ J g}^{-1} \times 0.128 \text{ g s}^{-1} - 250.8 \text{ J g}^{-1} \times 0.0157 \text{ g s}^{-1} \\ &= 51.56 \text{ W} - 5.47 \text{ W} - 3.94 \text{ W} = \underline{\underline{42.15 \text{ W}}} \quad \text{Answer}\end{aligned}$$

Just for comparison:

$$\begin{aligned}\text{Cell electricity generation: } W_{\text{el}} &= I \times V = 0.6 \text{ A cm}^{-2} \times 300 \text{ cm}^2 \times 0.65 \text{ V} \\ &= 117 \text{ W}\end{aligned}$$

$$\text{Cell efficiency: } \eta = V/1.482 = 0.65/1.482 = 0.439$$

$$\text{Heat generation by the cell: } Q = 117/0.439 - 117 = 149.5 \text{ W}$$

$$\text{Water generation rate: } \dot{m}_{\text{H}_2\text{O}} = \frac{I}{2F} M_{\text{H}_2\text{O}} = \frac{0.6 \times 300}{2 \times 96,485} 18 = 0.0168 \text{ g s}^{-1}$$

The fuel cell from this example thus generates more than enough heat and just about enough water needed for humidification of incoming air. With a clever system design it would be possible to capture both heat and water generated by the cell and use it for humidification of incoming air.

Figure 5-10. shows the conditions at which a fuel cell generates enough water for humidification of both air and hydrogen (assuming both gases are completely dry before humidification). Above the line for given

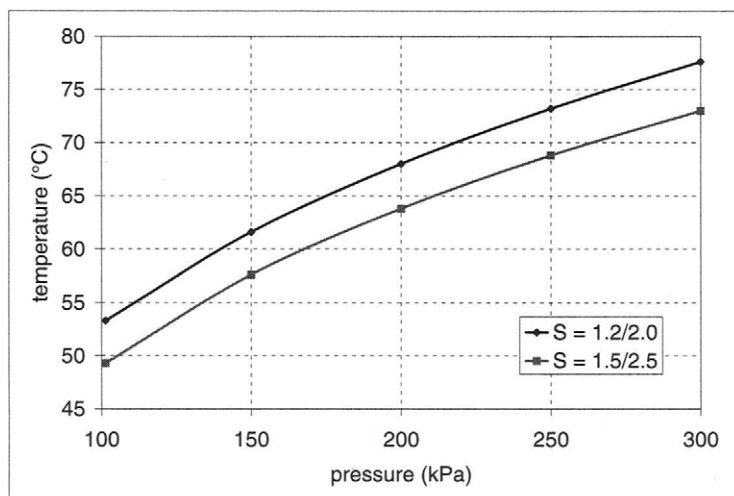


FIGURE 5-10. Temperatures and pressures at which a fuel cell generates enough water to humidify both hydrogen and air inlet streams.

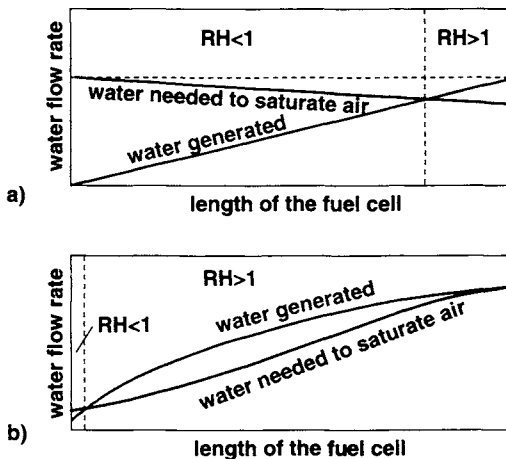


FIGURE 5-11. Water profiles in fuel cell: a) assuming uniform current density distribution and isothermal conditions; b) assuming realistic current density distribution and air temperature increase from inlet to outlet.

stoichiometry ratios, the need for humidification of reactant gases is greater than the amount of water generated in the stack.

A logical question arises: If a fuel cell generates enough water on the cathode side, why does air have to be humidified before entering the cell? In general, air humidification is needed to prevent drying of the portion of the membrane near the air inlet. Figure 5-11a shows that although there is enough water generated in the cell, air in most of the cell is undersaturated. However, the conditions in Figure 5-11a are not very realistic:

- Air is assumed to enter the cell dry and heated at the cell operating temperature.
- The cell is isothermal.
- There is no pressure drop.
- Water generation rate (*i.e.*, reaction rate) is constant.

When more realistic conditions are applied, the water profiles in the cell change dramatically as shown in Figure 5-11b. Conditions are selected so that the product water is sufficient to saturate air at the fuel cell exit. Air enters the cell at ambient conditions, relatively dry. At low temperatures (20°C to 30°C), small amounts of water are needed to saturate air, and the product water is more than sufficient. As the air is heated up and its pressure decreases, it needs more and more water. With careful design of air passages and heat transfer inside the fuel cell, it is possible to match the two water profiles even more closely.

Figure 5-12 shows the inlet air water content required to saturate air at the fuel cell outlet for typical air flows. Conditions above the line would

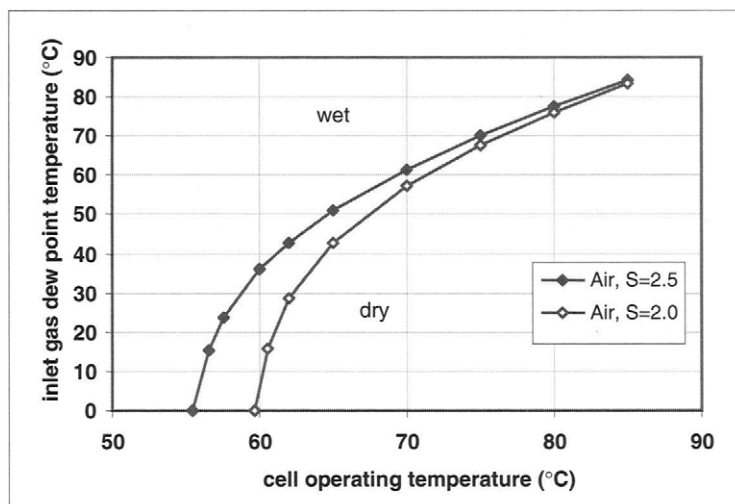


FIGURE 5-12. Water content in air at inlet (specified as dew point) required to result in saturated conditions at the fuel cell outlet.

result in liquid water at the outlet, whereas conditions below the line would result in undersaturated air at the outlet.

## 5.5. Fuel Cell Mass Balance

Fuel cell mass balance requires that the sum of all mass inputs must be equal to the sum of all mass outputs. The inputs are the flows of fuel and oxidant plus water vapor present in those gases. The outputs are the flows of unused fuel and oxidant, plus water vapor present in those gases, plus any liquid water present in either fuel or oxidant exhaust.

$$\sum (\dot{m}_i)_{in} = \sum (\dot{m}_i)_{out} \quad (5-36)$$

where  $i$  are the species, namely  $H_2$ ,  $O_2$ ,  $N_2$ ,  $H_2O(g)$ , and  $H_2O(l)$ . In cases when hydrogen is fed from a fuel processor, other species may also be present and must be accounted for in the energy balance, such as  $CO_2$  and small amounts of  $CO$ ,  $CH_4$ , and others.

### 5.5.1. Inlet Flow Rates

All the flow rates at inlet are proportional to current and number of cells. Because the cell power output is:

$$W_{el} = n_{cell} V_{cell} I \quad (5-37)$$

All the flows are also proportional to power output and inversely proportional to cell voltage:

$$I \cdot n_{cell} = \frac{W_{el}}{V_{cell}} \quad (5-38)$$

Hydrogen mass flow rate ( $\text{g s}^{-1}$ ) is:

$$\dot{m}_{H_2in} = S_{H_2} \dot{m}_{H_2,cons} = S_{H_2} \frac{M_{H_2}}{2F} I \cdot n_{cell} \quad (5-39)$$

If hydrogen is in a gas mixture, with  $r_{H_2}$  volume and mol fraction, then the mixture flow rate is:

$$\dot{m}_{fuel} = \frac{S_{H_2}}{r_{H_2}} \frac{M_{fuel}}{2F} I \cdot n_{cell} \quad (5-40)$$

Oxygen mass flow rate ( $\text{g s}^{-1}$ ) is:

$$\dot{m}_{O_2in} = S_{O_2} \dot{m}_{O_2,cons} = S_{O_2} \frac{M_{O_2}}{4F} I \cdot n_{cell} \quad (5-41)$$

Air mass flow rate ( $\text{g s}^{-1}$ ) is:

$$\dot{m}_{Airin} = \frac{S_{O_2}}{r_{O_2}} \frac{M_{Air}}{4F} I \cdot n_{cell} \quad (5-42)$$

Nitrogen mass flow rate ( $\text{g s}^{-1}$ ) is:

$$\dot{m}_{N_2in} = S_{O_2} \frac{M_{N_2}}{4F} \frac{1 - r_{O_2in}}{r_{O_2in}} I \cdot n_{cell} \quad (5-43)$$

Water vapor in hydrogen inlet ( $\text{g s}^{-1}$ ) is:

$$\dot{m}_{H_2OinH_2in} = S_{H_2} \frac{M_{H_2O}}{2F} \frac{\varphi_{an} P_{vs(T_{an,in})}}{P_{an} - \varphi_{an} P_{vs(T_{an,in})}} I \cdot n_{cell} \quad (5-44)$$

Water vapor in fuel inlet ( $\text{g s}^{-1}$ ) is:

$$\dot{m}_{H_2O,fuelin} = \frac{S_{H_2}}{r_{H_2}} \frac{M_{H_2O}}{2F} \frac{\varphi_{an} P_{vs(T_{an,in})}}{P_{an} - \varphi_{an} P_{vs(T_{an,in})}} I \cdot n_{cell} \quad (5-45)$$

Water vapor in oxygen inlet ( $\text{g s}^{-1}$ ) is:

$$\dot{m}_{H2OinO2in} = S_{O2} \frac{M_{H2O}}{4F} \frac{\varphi_{ca} P_{vs(T_{ca,in})}}{P_{ca} - \varphi_{ca} P_{vs(T_{ca,in})}} I \cdot n_{cell} \quad (5-46)$$

Water vapor in air inlet ( $\text{g s}^{-1}$ ) is:

$$\dot{m}_{H2OinAirin} = \frac{S_{O2}}{r_{O2}} \frac{M_{H2O}}{4F} \frac{\varphi_{ca} P_{vs(T_{ca,in})}}{P_{ca} - \varphi_{ca} P_{vs(T_{ca,in})}} I \cdot n_{cell} \quad (5-47)$$

### 5.5.2. Outlet Flow Rates

The equations for the outlet mass flow rates must account for reactants consumption, water generation, and water net transport across the membrane.

The unused hydrogen flow rate is:

$$\dot{m}_{H2out} = (S_{H2} - 1) \frac{M_{H2}}{2F} I \cdot n_{cell} \quad (5-48)$$

The water content in hydrogen exhaust is equal to water brought into the cell with hydrogen inlet minus the net water transport across the membrane. As discussed in Chapter 3, water gets “pumped” from anode to cathode because of electroosmotic drag. At the same time, some water diffuses back because of water concentration gradient and because of pressure differential. The net water transport is then the difference between these two fluxes.

$$\dot{m}_{H2OinH2out} = \dot{m}_{H2OinH2in} - \dot{m}_{H2OED} + \dot{m}_{H2OBD} \quad (5-49)$$

Electroosmotic drag is proportional to current, just like any other flow in or out of the fuel cell (Equation 4-5). The proportionality constant,  $\xi$ , represents a number of water molecules per proton. When  $\xi = 1$ , each proton is accompanied by one water molecule to form  $H_3O^+$ .

$$\dot{m}_{H2OED} = \xi \frac{M_{H2O}}{F} I \cdot n_{cell} \quad (5-50)$$

Back diffusion of water depends on water concentration on both sides of the membrane, water diffusivity through the membrane, and membrane thickness. Because water concentration is not uniform, it is not easy to explicitly calculate back diffusion for the entire cell or a stack of cells. For the sake of mass balance, back diffusion may be expressed as a fraction,  $\beta$ , of electroosmotic drag. When  $\beta = 1$ , back diffusion is equal to electroosmotic drag, that is, there is no net water transport across the membrane. The coefficient  $\beta$  may be determined experimentally by carefully condensing and measuring water content in both anode and cathode exhaust streams.

$$\dot{m}_{H2OBD} = \beta \dot{m}_{H2OED} = \beta \xi \frac{M_{H2O}}{F} I \cdot n_{cell} \quad (5-51)$$

Depending on the hydrogen flow rate, that is, stoichiometry, and conditions at the outlet (temperature and pressure), water at hydrogen exhaust may be present as vapor only, or liquid water may be present after the gas is saturated with water vapor. The water vapor content/flux at anode outlet is the smaller of total water flux at anode outlet and the maximum amount the exhaust gas can carry (saturation):

$$\dot{m}_{H2OinH2out,V} = \min \left[ (S_{H2} - 1) \frac{M_{H2O}}{2F} \frac{P_{vs(T_{out,an})}}{P_{an} - \Delta P_{an} - P_{vs(T_{out,an})}} I \cdot n_{cell}, m_{H2OinH2out} \right] \quad (5-52)$$

where  $\Delta P_{an}$  is the pressure drop on the anode side, that is, the difference in pressure between the inlet and outlet.

The amount of liquid water, if any, is the difference between the total water present at the exhaust and water vapor:

$$\dot{m}_{H2OinH2out,L} = m_{H2OinH2out} - \dot{m}_{H2OinH2out,V} \quad (5-53)$$

A similar set of equations may be applied for the cathode exhaust. Oxygen flow rate at the outlet, that is, unused oxygen, is equal to oxygen supplied at the inlet minus oxygen consumed in the fuel electrochemical reaction:

$$\dot{m}_{O2out} = (S_{O2} - 1) \frac{M_{O2}}{4F} I \cdot n_{cell} \quad (5-54)$$

Nitrogen flow rate at the exit is the same as the flow rate at the inlet, because nitrogen does not participate in the fuel cell reaction:

$$\dot{m}_{N2out} = \dot{m}_{N2in} = S_{O2} \frac{M_{N2}}{4F} \frac{1 - r_{O2in}}{r_{O2in}} I \cdot n_{cell} \quad (5-55)$$

Depleted air flow rate is then simply a sum of oxygen and nitrogen flow rates:

$$\dot{m}_{Airout} = \left[ (S_{O2} - 1) M_{O2} + S_{O2} \frac{1 - r_{O2in}}{r_{O2in}} M_{N2} \right] \frac{I \cdot n_{cell}}{4F} \quad (5-56)$$

Note that the oxygen volume fraction at the outlet is inevitably lower than the inlet volume fraction:

$$\frac{r_{O_2,out}}{r_{O_2,in}} = \frac{S_{O_2} - 1}{\frac{S_{O_2}}{r_{O_2,in}} - 1} \quad (5-57)$$

Both  $r_{O_2,in}$  and  $r_{O_2,out}$  refer to volume or molar fractions in dry air. The actual volume fraction in humid air is lower (see Figure 5-6):

$$r_{O_2,out}^* = \frac{S_{O_2} - 1}{\frac{S_{O_2}}{r_{O_2,in}} - 1} \left( 1 - \frac{\varphi p_{vs}}{P} \right) \quad (5-58)$$

Water content in the cathode exhaust is equal to the amount of water brought in the cell by humid air at the inlet, plus water generated in the cell and plus the net water transport across the membrane, that is, the difference between electroosmotic drag and water back diffusion:

$$\dot{m}_{H_2OinAirout} = \dot{m}_{H_2OinAirin} + \dot{m}_{H_2Ogen} + \dot{m}_{H_2OED} - \dot{m}_{H_2OBD} \quad (5-59)$$

Depending on the oxygen/air flow rate, that is, stoichiometry, and conditions at the outlet (temperature and pressure), water at cathode exhaust may be present as vapor only, or liquid water may be present after the gas is saturated with water vapor. The water vapor content/flux at cathode outlet is the smaller of total water flux at cathode outlet and the maximum amount the exhaust gas can carry (saturation):

$$\dot{m}_{H_2OinAirout,V} = \min \left[ \frac{S_{O_2} - r_{O_2,in}}{r_{O_2,in}} \frac{M_{H_2O}}{4F} \frac{P_{vs(T_{out,ca})}}{P_{ca} - \Delta P_{ca} - P_{vs(T_{out,ca})}} I \cdot n_{cell} \dot{m}_{H_2OinAirout} \right] \quad (5-60)$$

where  $\Delta P_{ca}$  is the pressure drop on the cathode side, that is, the difference in pressure between the inlet and outlet.

The amount of liquid water, if any, is the difference between the total water present at the exhaust and water vapor:

$$\dot{m}_{H_2OinAirout,L} = \dot{m}_{H_2OinAirout} - \dot{m}_{H_2OinAirout,V} \quad (5-61)$$

The previous set of equations (5-36 through 5-60) represents the fuel cell mass balance. For a given set of inlet conditions (temperatures, pressures, flow rates, relative humidities), and some known or estimated stack performance characteristics (such as current, pressure drop, temperature difference, electroosmotic drag, and back diffusion), it allows one to calculate the flow rates and particularly water conditions at the outlet, or it may be used to tailor the inlet conditions so that desired conditions at the outlet are obtained, as demonstrated in an example at the end of this chapter.

## 5.6. Fuel Cell Energy Balance

Fuel cell energy balance requires that the sum of all energy inputs must be equal to the sum of all energy outputs:

$$\sum (H_i)_{in} = W_{el} + \sum (H_i)_{out} + Q \quad (5-62)$$

The inputs are the enthalpies of all the flows into the fuel cell, namely fuel and oxidant, plus enthalpy of water vapor present in those gases. The outputs are:

- a) electric power produced;
- b) enthalpies of all the flows out of the fuel cell, namely unused fuel and oxidant, plus enthalpy of water vapor present in those gases, plus enthalpy of any liquid water present in either fuel or oxidant exhaust; and
- c) heat flux out of the fuel cell, both controlled through a cooling medium and uncontrolled because of heat dissipation (radiation and convection) from the fuel cell surface to the surroundings.

For each dry gas or a mixture of dry gases, the enthalpy (in  $\text{J s}^{-1}$ ) is:

$$H = \dot{m}c_p t \quad (5-63)$$

where:

$\dot{m}$  = mass flow rate of that gas or mixture ( $\text{g s}^{-1}$ )

$c_p$  = specific heat ( $\text{J g}^{-1} \text{K}^{-1}$ )

$t$  = temperature in  $^{\circ}\text{C}$

Note that the use of degrees Celsius implies that  $0^{\circ}\text{C}$  has been selected as a reference state for all enthalpies.

If a gas is combustible, that is, it has a heating value, its enthalpy is then:

$$H = \dot{m}(c_p t + h_{HHV}^0) \quad (5-64)$$

where  $h_{HHV}^0$  is the higher heating value of that gas ( $\text{J g}^{-1}$ ) at  $0^{\circ}\text{C}$ . Typically, heating values are reported and tabulated at  $25^{\circ}\text{C}$ . The difference between the heating value at  $25^{\circ}\text{C}$  and  $0^{\circ}\text{C}$  is the difference between the enthalpies of reactants and products at those two temperatures. For hydrogen it is:

$$h_{HHV}^0 = h_{HHV}^{25} - \left( c_{p,H_2} + \frac{1}{2} \frac{M_{O_2}}{M_{H_2}} c_{p,O_2} - \frac{M_{H_2O}}{M_{H_2}} c_{p,H_2O(l)} \right) \cdot 25 \quad (5-65)$$

Enthalpy of water vapor is (from Equation 5-30):

$$H = \dot{m}_{H_2O(g)}(c_{p,H_2O(g)}t + h_{fg}^0) \quad (5-66)$$

Enthalpy of liquid water is:

$$H = \dot{m}_{H_2O(l)}c_{p,H_2O(l)}t \quad (5-67)$$

Some properties of the species commonly found in fuel cell inlets and outlets are listed in Table 5-2.

The use of mass and energy balance equations is demonstrated in the following example.

*Example:*

A hydrogen/air fuel cell may be cooled by evaporative cooling by injecting liquid water at the air inlet and having the air flow rate sufficiently high. For a fuel cell that generates 1 kW at 0.7 V, find the required oxygen stoichiometric ratio and injected liquid water flow rate (g/s) so that the outlet air is fully saturated at 65°C (and there is no liquid water at the outlet) and that no additional cooling or heating of the fuel cell is required. Air is supplied at room temperature (20°C) with 70% relative humidity. Hydrogen is supplied in a dead-end mode at room temperature (20°C) and dry. Assume that the net water transport through the membrane is sufficient to maintain saturated conditions in the anode chamber at 65°C. Inlet pressure is 120 kPa (for both air and hydrogen); air outlet pressure is atmospheric.

Water balance is:

$$\dot{m}_{H_2OinAirin} + \dot{m}_{H_2OInject} + \dot{m}_{H_2Ogen} = \dot{m}_{H_2OinAirOut,V}$$

TABLE 5-2  
Properties of Some Gases and Liquids

	Molecular Weight ( $gmol^{-1}$ )	Specific Heat ( $Jg^{-1}K^{-1}$ )	Higher Heating Value ( $Jg^{-1}$ )
Hydrogen, H <sub>2</sub>	2.0158	14.2	141,900
Oxygen, O <sub>2</sub>	31.9988	0.913	
Nitrogen, N <sub>2</sub>	28.0134	1.04	
Air	28.848	1.01	
Water vapor, H <sub>2</sub> O (g)	18.0152	1.87	
Water, H <sub>2</sub> O (l)	18.0152	4.18	
Carbon monoxide	28.0105	1.1	10,100
Carbon dioxide	44.0099	0.84	
Methane	16.0427	2.18	55,500
Methanol (l)	32.04	2.5	22,700

Water in air in is (Equation 5-47):

$$\dot{m}_{H_2OinAirin} = \frac{S_{O_2}}{r_{O_2}} \frac{M_{H_2O}}{4F} \frac{\varphi_{ca} P_{vs(T_{ca,in})}}{P_{ca} - \varphi_{ca} P_{vs(T_{ca,in})}} I \cdot n_{cell}$$

$$r_{O_2} = 0.2095$$

$$M_{H_2O} = 18.015 \text{ (from Table 5-2)}$$

$$F = 96,485 \text{ As mol}^{-1}$$

$$\varphi_{ca} = 70\%$$

$$P_{vs} = e^{aT^{-1} + b + cT + dT^2 + eT^3 + f \ln(T)}; T = 293.15; P_{vs} = 2.339 \text{ kPa}$$

$$I \cdot n_{cell} = W/V = 1000 \text{ W}/0.7 \text{ V} = 1428.6 \text{ Amps}$$

$$\dot{m}_{H_2OinAirin} = 0.004397 S_{O_2} \text{ g s}^{-1}$$

Water generated is (Equation 5-7):

$$\dot{m}_{H_2O,gen} = \frac{I}{2F} M_{H_2O} = \frac{1,428.6}{2 \times 96,485} 18.015 = 0.1333 \text{ g s}^{-1}$$

Water vapor in air out is (from Equation 5-60):

$$\dot{m}_{H_2OinAirout,V} = \left[ \frac{S_{O_2} - r_{O_2,in}}{r_{O_2,in}} \frac{M_{H_2O}}{4F} \frac{P_{vs(T_{out,ca})}}{P_{ca} - \Delta P_{ca} - P_{vs(T_{out,ca})}} I \cdot n_{cell} \right]$$

$$P_{vs} = e^{aT^{-1} + b + cT + dT^2 + eT^3 + f \ln(T)}; T = 65^\circ\text{C} = 338.15 \text{ K}; P_{vs} = 25.04 \text{ kPa}$$

$$P_{ca} - \Delta P_{ca} = 101.3 \text{ kPa}$$

$$\dot{m}_{H_2OinAirout,V} = 0.1044 S_{O_2} - 0.02188 \text{ g s}^{-1}$$

Water balance is therefore:

$$0.004397 S_{O_2} + \dot{m}_{H_2OinInject} + 0.1333 = 0.1044 S_{O_2} - 0.02188$$

or after rearranging:

$$\dot{m}_{H_2OinInject} - 0.1 S_{O_2} + 0.15518 = 0 \quad (\text{Equation E1})$$

Energy balance is:

$$H_{H_2in} + H_{Airin} + H_{H_2OinAirin} + H_{H_2OinInject} = H_{Airout} + H_{H_2OinAirOut,V} + W_e$$

The flow rates are:

Hydrogen in (Equation 5-39):

$$\dot{m}_{H_2in} = S_{H_2} \frac{M_{H_2}}{2F} I \cdot n_{cell}$$

$$S_{H_2} = 1 \text{ (dead-end mode)}$$

$$\dot{m}_{H_2in} = 1 \frac{2.0158}{2 \times 96,485} 1,428.6 = 0.0149 \text{ g s}^{-1}$$

Air in (Equation 5-42):

$$\dot{m}_{Airin} = \frac{S_{O_2}}{r_{O_2}} \frac{M_{Air}}{4F} I \cdot n_{cell} = \frac{S_{O_2}}{0.2095} \frac{28.848}{4 \times 96,485} 1,428.6 = 0.5097 S_{O_2}$$

Water vapor in air in (from water balance above):

$$\dot{m}_{H_2OinAirin} = 0.004397 S_{O_2} \text{ g}$$

Air out (from Equation 5-56):

$$\dot{m}_{Airout} = \dot{m}_{O_2Out} + \dot{m}_{N_2Out}$$

$$\dot{m}_{O_2out} = [(S_{O_2} - 1)M_{O_2}] \frac{I \cdot n_{cell}}{4F} = 0.1184 S_{O_2} - 0.1184$$

$$\dot{m}_{N_2out} = \left[ S_{O_2} \frac{1 - r_{O_2in}}{r_{O_2in}} M_{N_2} \right] \frac{I \cdot n_{cell}}{4F} = 0.3913 S_{O_2}$$

Water vapor in air out (from water balance above):

$$\dot{m}_{H_2OinAirout,V} = 0.1044 S_{O_2} - 0.02188 \text{ g s}^{-1}$$

Energy flows (enthalpies) are:

Hydrogen in (from Equation 5-64):

$$H_{H_2in} = \dot{m}_{H_2in} (c_{p,H_2} t_{in} + h_{HHV}^0)$$

Hydrogen higher heating value at 0°C is (from Equation 5-65):

$$h_{HHV}^0 = h_{HHV}^{25} - \left( c_{p,H_2} + \frac{1}{2} \frac{M_{O_2}}{M_{H_2}} c_{p,O_2} - \frac{M_{H_2O}}{M_{H_2}} c_{p,H_2O(l)} \right) \cdot 25$$

$$h_{HHV}^0 = 141,900 - \left( 14.2 + \frac{31.9988/2}{2.0158} 0.913 - \frac{18.0152}{2.0158} 4.18 \right) \cdot 25$$

$$h_{HHV}^0 = 142,298 \text{ J/gK}$$

$$H_{H_2in} = 0.0149(14.2 \times 20 + 142,298) = 2124.5 \text{ (W)}$$

Air in (from Equation 5-63):

$$H_{AirIn} = \dot{m}_{Airin} c_{p,Air} t_{in} = 0.5097 S_{O_2} \times 1.01 \times 20 = 10.296 S_{O_2}$$

Water vapor in air in (from Equation 5-66):

$$\begin{aligned} H_{H_2O\text{inAirin}} &= \dot{m}_{H_2O\text{inAirin}}(c_{p,H_2O(g)}t_{in} + h_{fg}^0) \\ H_{H_2O\text{inAirin}} &= 0.004397S_{O_2}(1.85 \times 20 + 2500) = 11.155S_{O_2}(\text{W}) \end{aligned}$$

Water injected (from Equation 5-67):

$$H_{H_2O\text{Inject}} = \dot{m}_{H_2O\text{Inject}} \times 4.18 \times 20 = 83.6 \dot{m}_{H_2O\text{Inject}}$$

Air out:

$$\begin{aligned} H_{\text{AirOut}} &= \dot{m}_{O_2\text{Out}}c_{p,O_2}t_{out} + \dot{m}_{N_2\text{in}}c_{p,N_2}t_{out} \\ &= (0.1184S_{O_2} - 0.1184) \times 0.913 \times 65 + 0.3913S_{O_2} \times 1.04 \times 65 \\ &= 33.478S_{O_2} - 7.0264 \end{aligned}$$

Water vapor in air out (from Equation 5-66):

$$\begin{aligned} H_{H_2O\text{inAirOut}} &= \dot{m}_{H_2O\text{inAirOut}}(c_{p,H_2O(g)}t_{out} + h_{fg}^0) \\ &= (0.1044S_{O_2} - 0.02188) \times (1.85 \times 65 + 2500) = 273.55S_{O_2} - 57.331 \end{aligned}$$

Electricity generated:

$$W_{el} = 1000 \text{ W}$$

Energy balance is:

$$\begin{aligned} 2124.5 + 10.296S_{O_2} + 11.155S_{O_2} + 83.6\dot{m}_{H_2O\text{Inject}} \\ = 33.478S_{O_2} - 7.0264 + 273.55S_{O_2} - 57.331 + 1000 \end{aligned}$$

After rearranging the energy balance equation becomes:

$$83.6\dot{m}_{H_2O\text{Inject}} - 285.58S_{O_2} + 1188.85 = 0 \quad (\text{Equation E2})$$

By combining with the water balance and solving the two equations, E1 and E2, with two unknowns, the result is:

$$\begin{aligned} S_{O_2} &= 4.24 \text{ and} \\ \dot{m}_{H_2O\text{Inject}} &= 0.26688 \text{ g s}^{-1} \end{aligned}$$

Therefore, by injecting  $0.26688 \text{ g s}^{-1}$  of liquid water in ambient air at fuel cell inlet, with the stoichiometry of 4.24 it is possible to maintain the desired operating temperature of  $65^\circ\text{C}$  and have just enough water at the air outlet to avoid either flooding with liquid water or drying with dry air. Note that

such a fuel cell would have to be thermally insulated. Also, operation with dry hydrogen probably would not be possible, that is, additional water may be needed to humidify hydrogen. Nevertheless, such a fuel cell would result in an extremely simple system: no need for air humidification and no need for stack cooling, probably the two bulkiest supporting system components.

## References

1. Barbir, F., M. Fuchs, A. Husar, and J. Neutzler, *Design and Operational Characteristics of Automotive PEM Fuel Cell Stacks*, *Fuel Cell Power for Transportation*, SAE SP-1505 (SAE, Warrendale, PA, 2000), pp. 63–69.
2. ASHRAE Handbook, 1981 Fundamentals (ASHRAE, Atlanta, GA, 1982).
3. Bosnjakovic, F., *Technical Thermodynamics* (Holt Rinehart and Winston, New York, 1965).

## Problems

### Problem No. 1:

A fuel cell generates 100 Amps at 0.6 V. Hydrogen flow rate in the fuel cell is 1.8 standard liters per minute (slpm); air flow rate is 8.9 slpm. Calculate:

- a) hydrogen stoichiometric ratio
- b) oxygen stoichiometric ratio
- c) oxygen concentration at the outlet (neglect water present)

### Problem No. 2:

If both gases in Problem 1 are 100% saturated at 60°C and 120 kPa, calculate:

- a) the amount of water vapor present in hydrogen (in g/s)
- b) the amount of water vapor present in oxygen (in g/s)
- c) the amount of water generated in the fuel cell reaction (in g/s)

### Problem No. 3:

In Problem 2, calculate the amount of liquid water at the cell outlet (assuming zero net water transport through the membrane). Both air and hydrogen at the outlet are at ambient pressure and at 60°C.

- a) in hydrogen outlet
- b) in air outlet

**Problem No. 4:**

For Problem 3, calculate

- a) the fuel cell efficiency
- b) rate of heat generated (W)

**Problem No. 5:**

An H<sub>2</sub>/Air fuel cell operates at 80°C and 170 kPa. Hydrogen is supplied in a dead-end mode. If the net electrochemical drag is 0.25 molecules of H<sub>2</sub>O per proton, calculate required relative humidity of hydrogen at the inlet so that there is neither water accumulation nor drying of the membrane on the hydrogen side of the fuel cell. Explain the physical meaning of your result.

**Problem No. 6:**

An H<sub>2</sub>/Air fuel cell operates with hydrogen utilization of 84% and oxygen stoichiometric ratio of 2. Both hydrogen and air must be fully saturated at the cell operating pressure and temperature. Which of the following is true?

- a) air needs approximately 4 times more water
- b) air needs approximately 2 times more water
- c) hydrogen needs approximately 2 times more water
- d) cannot say which reactant needs more water because temperature and pressure are not given

**Problem No. 7:**

Air is fully saturated with water vapor at fuel cell inlet and at fuel cell outlet (actually there is also liquid water dripping at the outlet). The air temperature is the same at the inlet and at the outlet. The fuel cell operates with oxygen stoichiometric ratio of 2. Air passes through a single-channel serpentine flow field.

Is the water vapor content (in mols of water vapor per mol of dry gas) at the outlet:

- a) higher than at the inlet
- b) lower than at the inlet
- c) same as at the inlet

Explain!

## Quiz

1. Stoichiometric ratio is:
  - a) ratio between hydrogen and oxygen at fuel cell inlet
  - b) ratio between hydrogen and oxygen consumed in fuel cell
  - c) ratio between an actual flow rate of an reactant at the fuel cell inlet and the rate of consumption of that same reactant
2. In the case of an air-breathing fuel cell, higher oxygen stoichiometric ratio:
  - a) means higher concentration of O<sub>2</sub> at the outlet
  - b) means higher concentration of O<sub>2</sub> at the inlet
  - c) has nothing to do with concentration
3. Dead-end operation means:
  - a) no hydrogen is leaving the fuel cell
  - b) fuel cell is “dead,” that is, produces no current
  - c) consumption is proportional to cell voltage
4. In a dead-end operation the stoichiometric ratio at the inlet is:
  - a) same as at the outlet
  - b) 1
  - c) 0
5. Pressure at a fuel cell air inlet:
  - a) is lower than at outlet
  - b) is higher than at the outlet
  - c) you cannot say if it higher or lower because it depends on current
6. A certain quantity of a gas at higher temperature can contain:
  - a) less water vapor than at a lower temperature
  - b) more water vapor than at a lower temperature
  - c) same amount of water vapor as at a lower temperature
7. Relative humidity is:
  - a) percentage of partial pressure of water vapor relative to saturation pressure
  - b) ratio between the amount of water vapor and the amount of dry air
  - c) percentage of water in air
8. If the air flow rate at the inlet is kept proportional to current (for example, at 2 × stoichiometry) then:

- a) concentration of O<sub>2</sub> is constant throughout the cell regardless of current
  - b) O<sub>2</sub> concentration decreases along the length of the fuel cell
  - c) O<sub>2</sub> concentration reaches zero at certain current
9. If back diffusion of water is equal to the electroosmotic drag, and both gases are saturated at the inlet:
- a) there is no net water transport across the membrane
  - b) fuel cell will flood on the air (cathode) side
  - c) fuel cell will dry out on the air (cathode) side
10. The form of water at the cathode (air) exit of the fuel cell depends on:
- a) operating pressure and temperature only
  - b) stoichiometric ratio and temperature only
  - c) stoichiometric ratio, temperature, pressure and humidity of air at the inlet

# CHAPTER 6

## 6. Stack Design

As seen in Chapter 3, the fuel cell electrochemical reactions result in theoretical cell potential of 1.23 V, and the actual potential in operation is lower than 1 V. If a single cell were required to generate 1 kW of power, it would need to generate electrical current higher than 1000 Amperes. Such a current could be generated only with a large active area ( $>1000\text{ cm}^2$ ), and it would require very thick cables between the fuel cell and the load in order to minimize the resistive losses. A more practical solution would be to have multiple cells electrically connected in series. The cell active area and the cross-sectional area of the connecting cables would decrease with a number of cells connected in series. For example, 1 kW power output may be accomplished with as many as 40 cells connected in series, each cell operating at 0.6 V and  $1\text{ A/cm}^2$ . Total current would be about 42 Amperes at 24 Volts.

### 6.1. Sizing of a Fuel Cell Stack

The first step in designing a fuel cell stack is to determine its active area and number of cells in the stack. When a stack is designed for an application, the design inputs come from the application requirements, such as desired power output, desired or preferred stack voltage or voltage range, desired efficiency, and volume and weight limitations. Some of these requirements may conflict each other, and the stack sizing and design process often results in a compromise solution that meets the key requirements (such as power output) and finds an optimum between the conflicting requirements.

Another design input is the unit performance best described by the polarization curve. The fuel cell polarization curve is the key for sizing and design of a fuel cell stack. However, as shown in Chapter 5, the fuel cell performance is determined by operational conditions (pressure, temperature, humidity of reactant gases) that must be determined based on the application requirements and constraints.

The stack power output is simply a product of stack voltage and current:

$$W = V_{st} \cdot I \quad (6-1)$$

The stack potential is simply a sum of individual cell voltages or a product of average individual cell potential and number of cells in the stack:

$$V_{st} = \sum_{i=1}^{N_{cell}} V_i = \bar{V}_{cell} \cdot N_{cell} \quad (6-2)$$

The current is a product of current density and cell active area:

$$I = i \cdot A_{cell} \quad (6-3)$$

Cell potential and current density are related by the polarization curve:

$$V_{cell} = f(i) \quad (6-4)$$

The polarization curve may be defined by a set of data ( $V_{cell}$ - $i$ ), or by any of the Equations (3-43), (3-46), or (3-52), or by linear approximation (Equation 3-68).

The fuel cell stack efficiency may be approximated with a simple Equation (3-61):

$$\eta = V_{cell}/1.482 \quad (6-5)$$

that is not valid only for the potentials close to the open circuit potentials.

The previous section represents a set of five equations with eight variables. Additional variables or constraints may be stack volume and weight, both being functions of number of cells in the stack and cell active area, in addition to stack construction and choice of materials. It is therefore a matter of simple arithmetic to calculate the remaining variables if three of them are given; for example, power output, stack voltage, and stack efficiency (a little complication is the form of the equation  $V_{cell} = f(i)$ , which may require some iterative process to calculate current density,  $i$ , when cell potential  $V_{cell}$  is given). If less than three inputs are given, then there may be an infinite number of cell active area and number of cell combinations that satisfy the previous equations, with some limitations (Figure 6-1). Both active area and number of cells in the stack, as well as their combination, have physical and/or technological limits. For example, a large number of cells with very small active area would be difficult to align and assemble. On the other hand, a small number of cells with a large active area would

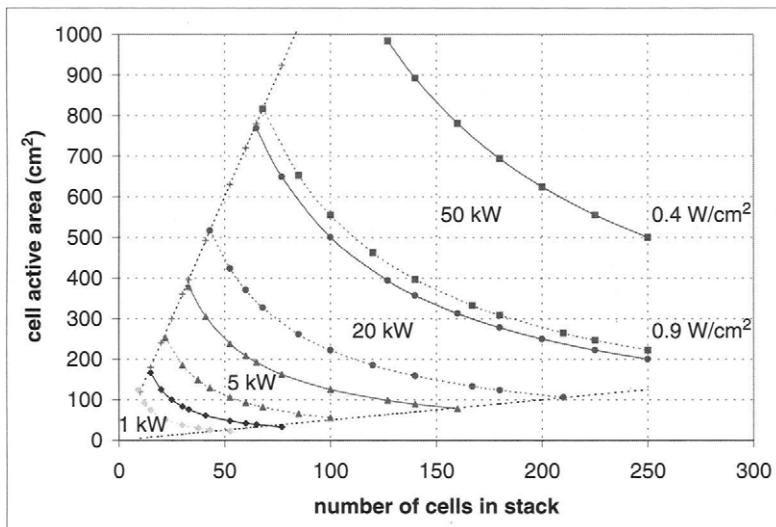


FIGURE 6-1. Fuel cell stack sizing—number of cells and cell active area for different power outputs (solid lines are for  $0.4 \text{ W/cm}^2$  and dashed lines are for  $0.9 \text{ W/cm}^2$ ).

result in high current–low voltage combination and would result in significant resistive losses in connecting cables.

Very often the number of cells in a stack is limited or determined by required stack voltage. Stacks with active area up to  $1000 \text{ cm}^2$  have been demonstrated; more typically, active area is between  $50$  and  $300 \text{ cm}^2$  depending on application and desired power output. In larger active areas it is more difficult to achieve uniform conditions, which is one of the key aspects of a successful stack design as it is discussed below. Maximum number of cells in a stack is limited by compression forces, structural rigidity, and pressure drop through long manifolds. Stacks with up to  $200$ – $250$  cells have been demonstrated.

These limits also apply to the case of the determined system, that is, with three variables given. If the solution for number of cells and cell active area falls outside the limitations, it would be necessary to reconsider and modify the requirements.

Very often, there is a need to optimize the stack efficiency and size. These are two conflicting requirements for a given power output and a given polarization curve. Typical fuel cell polarization curves are shown in Figure 6-2. Most of the published fuel cell stack polarization curves fall within these two lines.

The nominal operating point (cell voltage and corresponding current density) is the operating point at nominal power output, and it may be

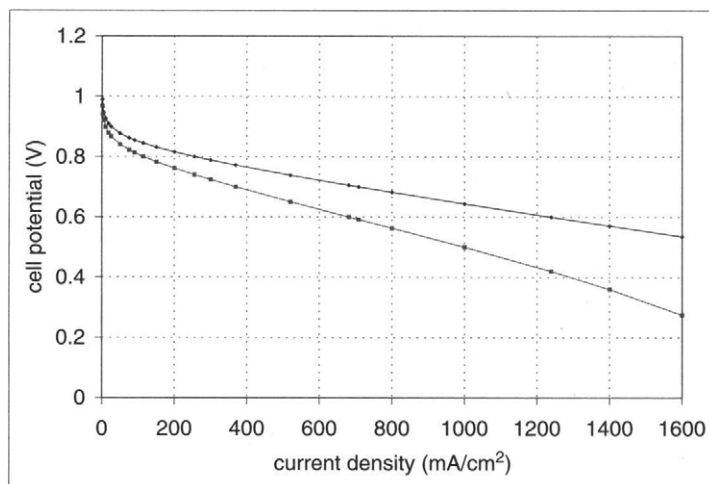


FIGURE 6-2. Typical PEM fuel cell polarization curves.

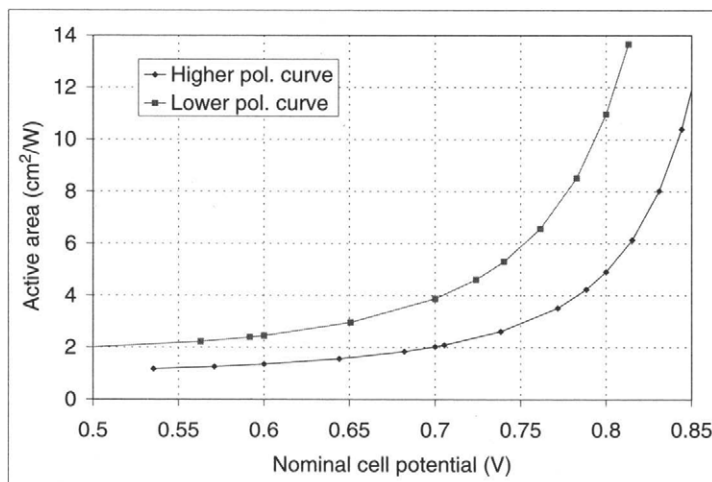


FIGURE 6-3. Stack size vs selected nominal cell potential (corresponding to polarization curves in Figure 6-2).

selected anywhere on the polarization curve. Selection of this point has a profound effect on the stack size and efficiency. Lower selected cell voltage at nominal power results in higher power density and consequently in smaller stack size for any given power output. Figure 6-3 shows the relationship between stack size (total active area per unit power output) and

nominal cell potential for the two polarization curves from Figure 6-2. From Figure 6-3, it follows that a stack with nominal cell voltage of 0.7 V would require about 40% larger active area than a stack sized at 0.6 V/cell. Selection of 0.8 V/cell at nominal power would result in more than twice the size of a stack sized at 0.7 V/cell. However, higher cell voltage means better efficiency and consequently lower fuel consumption. Currently, most fuel cell manufacturers/developers use between 0.6 V and 0.7 V as voltage at nominal power. However, in order to reach some system efficiencies goals, the fuel cells would have to be rated at 0.8 V/cell or even higher. Indeed in applications where the efficiency (which translates in reactant consumption) is critical, such as in space applications where both reactants must be carried on board, the fuel cells are rated and operated above 0.8 V. The extra fuel cell size is negligible compared with the size (and weight) of hydrogen and oxygen saved.

Optimum cell voltage at nominal power should be determined for each application based on the optimization criteria (such as the lowest cost of generated electricity, or the least expensive system, or the lowest size and weight), and it should therefore take into consideration many parameters, such as the cost of fuel cell, cost of fuel, lifetime, capacity factor, load profile, system efficiency, and so on [1]. If the stack is operated at partial load (below 20% of nominal power) most of the time, then higher selected nominal cell voltage does not necessarily mean higher operating efficiency. As shown in Figure 6-4, at 20% of nominal power there is no efficiency advantage of higher selected nominal cell voltage. This is due to operation

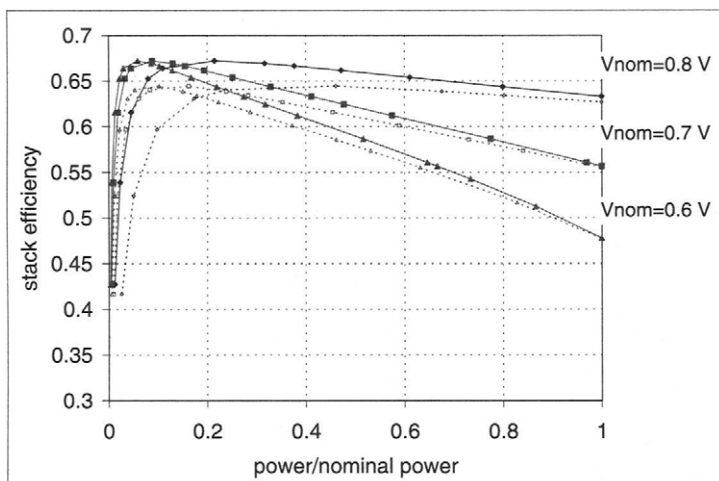


FIGURE 6-4. Stack efficiency (based on LHV) vs power output for different selected nominal cell potentials (solid lines are for the higher and dashed lines are for the lower polarization curve in Figure 6-2).

at very low current densities where parasitic losses (including gas permeation through the polymer membrane) may not be negligible.

## 6.2. Stack Configuration

A fuel cell stack consists of a multitude of single cells stacked up so that the cathode of one cell is electrically connected to the anode of the adjacent cell. In that way, exactly the same current passes through each of the cells. Note that the electrical circuit is closed with both electron current passing through solid parts of the stack (including the external circuit) and ionic current passing through electrolyte (ionomer), with the electrochemical reactions at their interfaces (catalyst layers).

The bipolar configuration is best for larger fuel cells because the current is conducted through relatively thin conductive plates, and thus travels a very short distance through a large area (Figure 6-5). This causes minimum electroresistive losses, even with a relatively bad electrical conductor such as graphite (or graphite polymer mixtures). For small cells it is possible to connect the edge of one electrode to the opposing electrode of the adjacent cell by some kind of a connector [2–4]. This is applicable only to very small active area cells, because current is conducted in a plane of very thin electrodes, thus traveling a relatively long distance through a very small cross-sectional area (Figure 6-6).

The main components of a fuel cell stack are the membrane electrode assemblies or MEAs (membranes with electrodes on each side with a catalyst layer between them), gaskets at the perimeter of the MEAs, bipolar plates, bus plates (one at each end of the active part of the stack) with electrical connections, and the end plates (one at each end of the stack), with

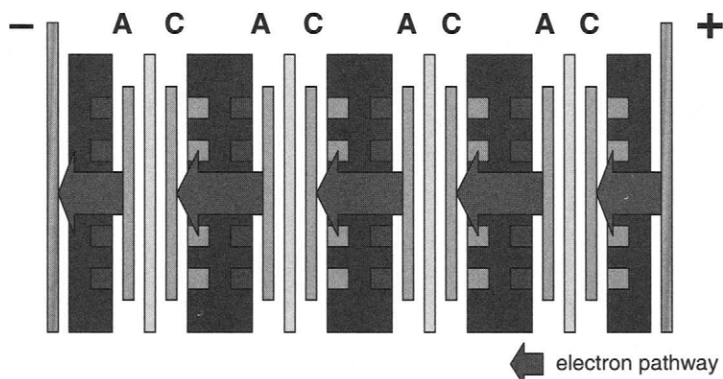


FIGURE 6-5. Bipolar configuration.

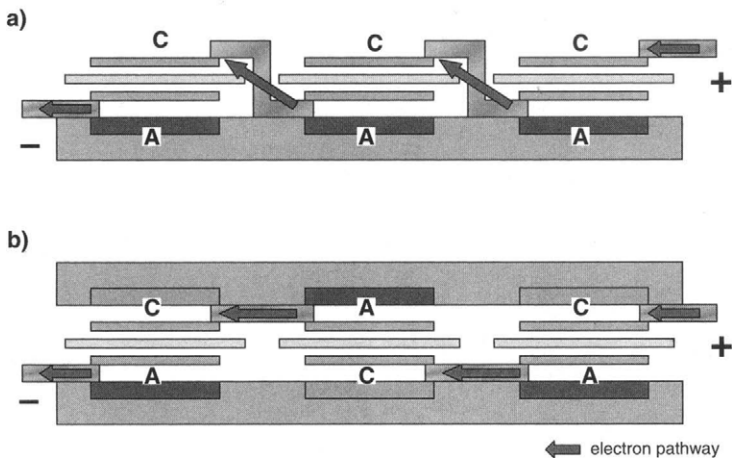


FIGURE 6-6. Examples of side-by-side stack configurations for smaller fuel cells:  
a) zig-zag connections with open air cathode; b) flip-flop configuration.

fluid connections [5]. Cooling of the stack, that is, its active cells, must be arranged in some fashion as discussed below. The whole stack must be kept together by tie-rods, bolts, shroud, or some other arrangement (Figure 6-7).

In some stack configurations, humidification of one or both reactant gases is included in the stack, either in a separate stack section or between each cell. In both cases water is used for both cooling and humidification, and the heat generated in each of the active cells is used for humidification. Figure 6-8 shows a stack configuration where the reactant gases first pass through a humidification section and then through the active cells, whereas water first passes through the active portion of the stack, gets heated up, and then passes through the humidification section, where heat and water transfer between water and the reactant gases occurs through polymer membranes [6]. The advantage of this stack configuration is in compactness of the gas humidification system and reduced heat dissipation, but this very advantage is also its main drawback—lack of versatility in controlling water and heat management and inability to separate heat from water management.

In another configuration (Figure 6-9), water passes between each cell separated by a porous graphite plate from the reactant gases [7]. Porous plate allows water transport, effectively facilitating water and heat management in each cell. Hydrogen, air, and water pressures must be carefully regulated so that water in the porous plate channels is always at slightly negative pressure compared with reactants pressure. Pore size controls bubble-point such that the reactants do not mix. Water recirculation to a radiator

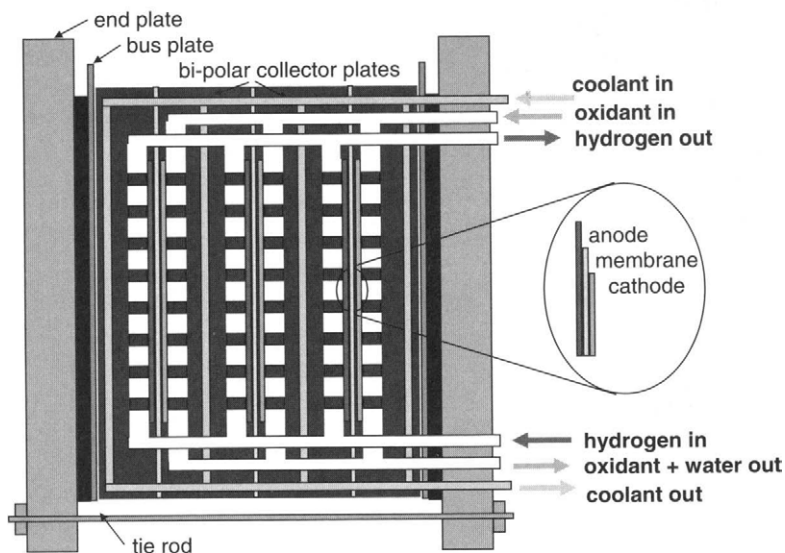


FIGURE 6-7. Stack schematic [5].

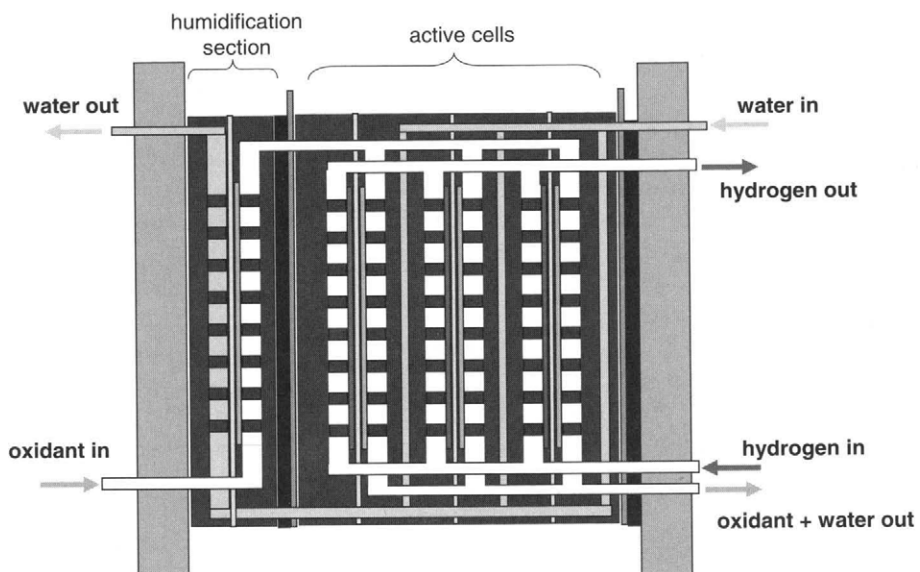


FIGURE 6-8. Stack configuration with internal humidification.

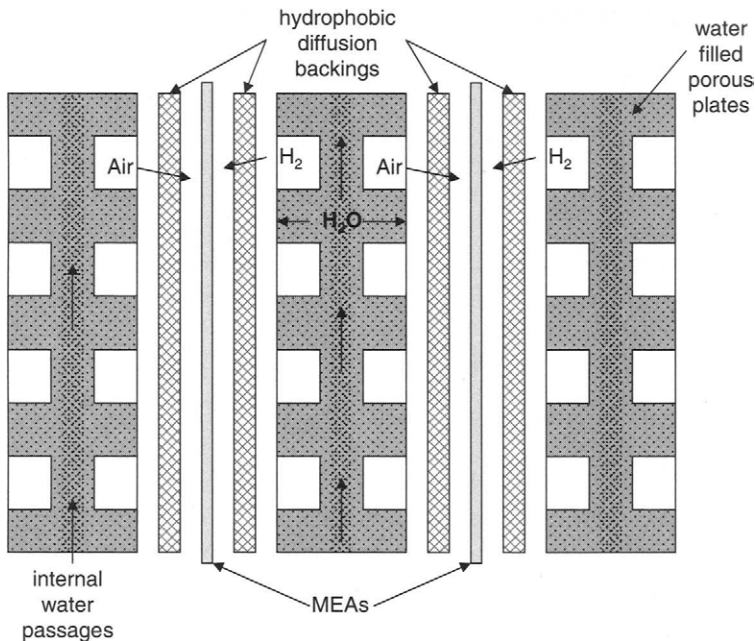


FIGURE 6-9. Stack configuration with water management through porous plate. (Adapted from [7].)

provides stack cooling. The main disadvantage of this concept is inability to separate heat from water management, but others are a very tight pressure control requirement and operation at low pressures only.

The following are the key aspects of a fuel cell stack design:

- uniform distribution of reactants to each cell,
- uniform distribution of reactants inside each cell,
- maintenance of required temperature in each cell,
- minimum resistive losses (choice of materials, configuration, uniform contact pressure),
- no leak of reactant gases (internal between the cells or external),
- mechanical sturdiness (internal pressure, including thermal expansion; external forces during handling and operation, including shocks and vibrations).

Each of these aspects is discussed in the following sections.

### 6.3. Uniform Distribution of Reactants to Each Cell

Because fuel cell performance is sensitive to the flow rate of the reactants, it is absolutely necessary that each cell in a stack receives approximately the same amount of reactant gases. Uneven flow distribution would result in uneven performance between the cells. Uniformity is accomplished by feeding each cell in the stack in parallel, through a manifold that can be either external or internal. External manifolds can be made much bigger to ensure uniformity. They result in a simpler stack design, but they can only be used in a cross-flow configuration and are, in general, difficult to seal. Internal manifolds are more often used in PEM fuel cell design, not only because of better sealing but also because they offer more versatility in gas flow configuration.

It is important that the manifolds that feed the gases to the cells and the manifolds that collect the unused gases are properly sized. The cross-sectional area of the manifolds determines the velocity of gas flow and the pressure drop. As a rule of thumb, the pressure drop through the manifolds should be an order of magnitude lower than the pressure drop through each cell in order to ensure uniform flow distribution.

The flow pattern through the stack can be either a "U" shape, where the inlet and outlet are at the same side of the stack and the flows in inlet and outlet manifolds are in opposite direction from each other, or a "Z" shape, where the inlets and outlets are on opposite sides of the stack and the flows in inlet and outlet manifolds are parallel to each other (Figure 6-10). If properly sized, both should result in uniform flow distribution to individual cells. Stacks with more than 100 cells have been successfully built.

The procedure to calculate the pressure drop through the manifolds and the entire stack, and the resulting flow distribution, involves a flow network problem consisting of  $N-1$  loops [8] where  $N$  is the number of cells in the stack. The flow in any network must satisfy the basic relations of continuity and energy conservation as follows:

1. The flow into any junction must equal the flow out of it.
2. The flow in each segment has a pressure drop that is a function of the flow rate through that segment.
3. The algebraic sum of the pressure drops around any closed loop must be zero.

The first requirement is satisfied with the following relationships:

$$Q_{in}(i) = Q_{cell}(i) + Q_{in}(i+1) \text{ in inlet manifold} \quad (6-6)$$

$$Q_{out}(i) = Q_{cell}(i) + Q_{out}(i+1) \text{ in outlet manifold, "U" configuration} \quad (6-7)$$

$$Q_{out}(i) = Q_{cell}(i) + Q_{out}(i-1) \text{ in outlet manifold, "Z" configuration} \quad (6-8)$$

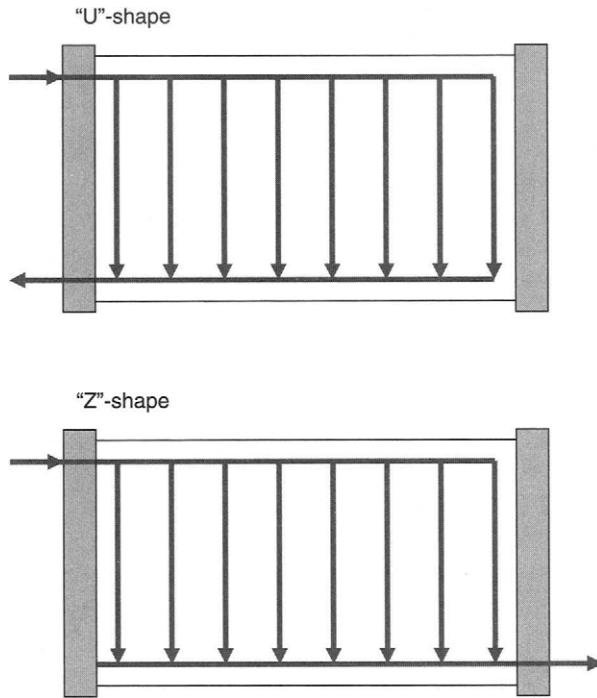


FIGURE 6-10. Stack flow configurations.

Note that by definition of the cells and flows numbering shown in Figure 6-11:

$$Q_{\text{out}}(1) = Q_{\text{stack}} \quad (6-9)$$

For a nonoperating stack, that is, one with no species consumption or generation, the flow at the stack outlet is equal to the flow at inlet:

$$Q_{\text{out}}(1) = Q_{\text{in}}(1) \text{ for "U" configuration} \quad (6-10)$$

$$Q_{\text{out}}(N) = Q_{\text{in}}(1) \text{ for "Z" configuration} \quad (6-11)$$

The pressure drop, derived directly from the Bernoulli equation, in each manifold segment is [8]:

$$\Delta P(i) = -\rho \frac{[u(i)]^2 - [u(i-1)]^2}{2} + f\rho \frac{L}{D_H} \frac{[u(i)]^2}{2} + K_f \rho \frac{[u(i-1)]^2}{2} \quad (6-12)$$

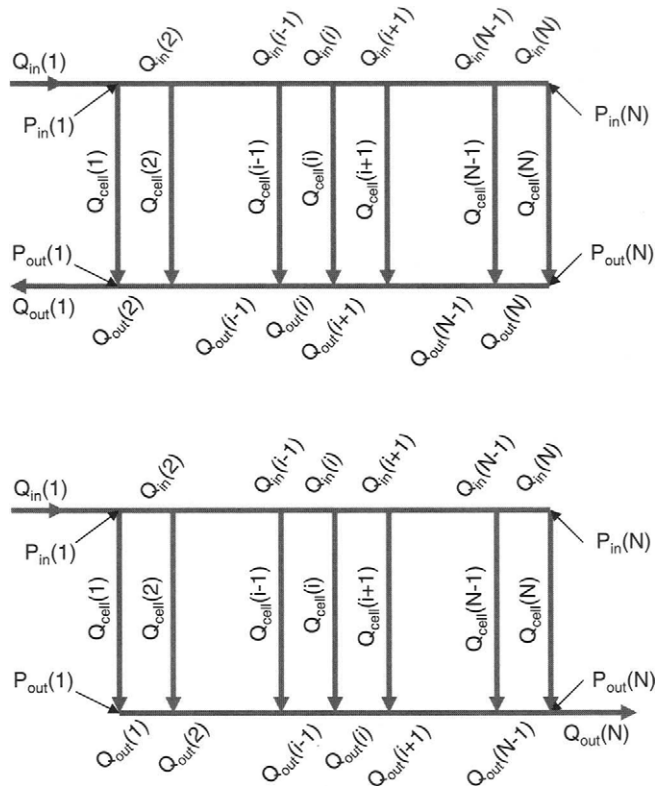


FIGURE 6-11. Designation of pressure and flow variables for "U" (above) and "Z" (below) stack flow configurations.

where:

$\rho$  = density of the gas ( $\text{kg m}^{-3}$ )

$u$  = velocity ( $\text{m s}^{-1}$ )

$f$  = friction coefficient

$L$  = length of the segment (m)

$D_H$  = hydraulic diameter of the manifold segment (m)

$K_f$  = local pressure loss coefficient

The first term on the right-hand side of Equation (6-12) represents the energy decrease along the streamline in the manifold due to velocity loss; the second term is the pressure drop due to friction with the walls; and the last term is the pressure loss due to local disturbances described by the geometric coefficient.

The loss of pressure due to local disturbances, such as flow branching out or in (tees) or sudden changes in direction (elbows), should be taken into account when calculating the pressure drop in each segment. Typically in fluid-mechanics textbooks, these losses are called "minor losses"; however, in fuel cell manifolds they may not be negligible. Koh *et al.* [8] showed that the flow distribution largely depends on the local pressure loss coefficients. Though some geometrical pressure loss coefficients are available for various pipe fittings, none fit a specific shape of the fuel cell gas flow manifolds. Koh *et al.* [8] concluded that the geometrical pressure loss coefficients should be determined experimentally for each stack design.

For laminar flow ( $Re < 2000$ ), the friction coefficient  $f$  for a circular conduit is:

$$f = \frac{64}{Re} \quad (6-13)$$

For turbulent flow, the friction coefficient is primarily a function of the wall roughness. The walls of fuel cell manifolds may be considered "rough" because they are not a smooth pipe, but consist of the bipolar plates clamped together, often with the gasket material protruding into the manifold. The relative roughness,  $\epsilon/D$ , can be as high as 0.1. In that case the friction coefficient (according to Karman [9]) is:

$$f = \frac{1}{\left(1.14 - 2 \log \frac{\epsilon}{D}\right)^2} \quad (6-14)$$

The pressure drop through the cell,  $\Delta P_{cell}$ , is discussed in the section 6.4.5. Pressure Drop through the Flow Field. In most cases it is a linear function of the flow rate through each cell.

The third requirement is that the algebraic sum of the pressure drops around any closed loop must be zero:

$$\text{For } i = 1 \text{ to } (N - 1) \quad (6-15)$$

$$\Delta P_{in}(i+1) + \Delta P_{cell}(i+1) + \Delta P_{out}(i+1) - \Delta P_{cell}(i) = 0 \text{ in "U" configuration} \quad (6-16)$$

$$\Delta P_{in}(i+1) + \Delta P_{cell}(i+1) - \Delta P_{out}(i) - \Delta P_{cell}(i) = 0 \text{ in "Z" configuration} \quad (6-17)$$

For a given flow rate at the stack entrance and a known pressure either at the stack inlet or at the stack outlet, it is possible to calculate the flow rate through each of the cells using a method of successive approximations, such as the Hardy-Cross method commonly used for pipe networks [9], or

the method suggested by Koh *et al.* [8]. The procedure in either method is similar:

1. It starts with an approximation of the flows in each of the cells  $Q_{\text{cell}} = Q_{\text{stack}} / N_{\text{cell}}$ .
2. It calculates the pressure drops in individual manifold segments and cells.
3. It checks the sum of pressure drops in each of the loops (it should be zero).
4. It adjusts the flows in each loop by a correction,  $\Delta Q$ , proportional to the error in sum of the pressure drops, and the process is repeated one loop at a time until the error is negligible.

For the same size conduits, "Z" configuration usually results in more uniform flow distribution than "U" configuration. It may be shown that for "U" configuration, uniform distribution of flows through the individual cells results when the pressure drop through the cell is at least an order of magnitude higher than the pressure drop through the stack inlet manifold (Figure 6-12). The inlet and outlet manifolds must be sized accordingly. Sometimes it is beneficial to have more than one manifold for one reactant, especially for the stacks with larger active area. In that case pressure drop through each manifold must also be balanced to ensure uniform flow

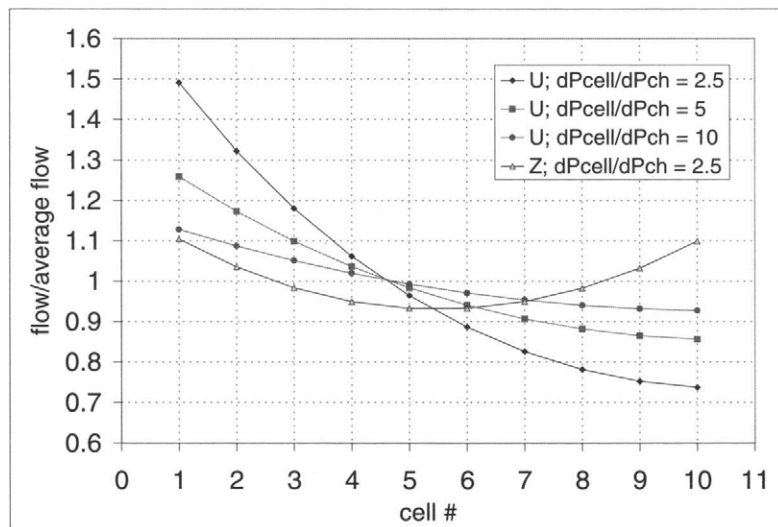


FIGURE 6-12. Flow distribution in individual cells of a 10-cell stack for "U" and "Z" configurations and for various ratios of pressure drop through individual cell and through the inlet manifold ( $dP_{\text{cell}}/dP_{\text{ch}}$ ).

distribution to each manifold. Similar methods as depicted previously may be used for that calculation.

When the stack is in operation, the change in flow rate, gas density, and viscosity due to species consumption and generation must be taken into account, although it should not significantly affect the pressure drop results (<5%).

#### 6.4. Uniform Distribution of Reactants Inside Each Cell

Once the reactant gases enter the individual cell they must be distributed over the entire active area. This is typically accomplished through a flow field, which may be in a form of channels covering the entire area in some pattern or porous structures. The following sections describe the key flow field design variables.

##### 6.4.1. Shape of the Flow Field

The flow fields come in different shapes and sizes. The size comes from the power/voltage requirements as shown in section 6. Sizing of a Fuel Cell Stack. The shape is the result of positioning the inlet and outlet manifolds, flow field design, heat management, and manufacturing constraints. The most common shapes of the flow field are square and rectangular, but circular, hexagonal, octagonal, or irregular shapes have been used or at least tried (Figure 6-13).

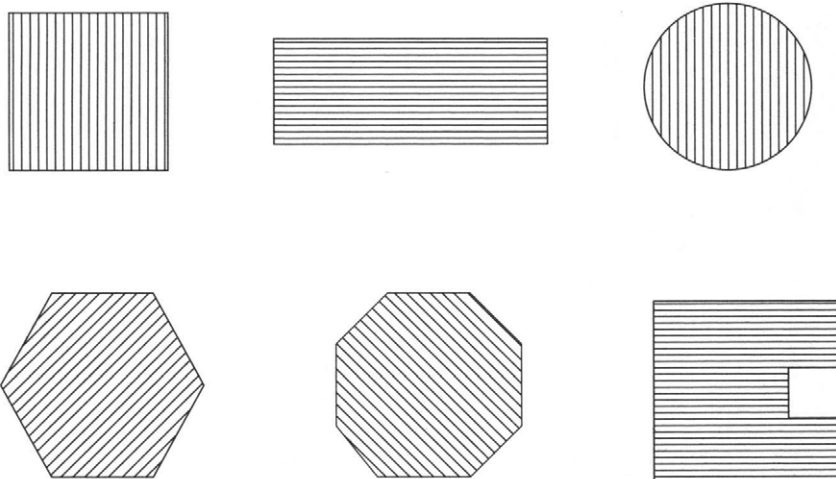


FIGURE 6-13. Various shapes of the fuel cell active area.

### 6.4.2. Flow Field Orientation

The orientation of the flow field and positions of inlet and outlet manifolds are important only because of the gravity effect on water that may condense inside the flow field (the effect of gravity on the reactant gases is negligible). Condensation may take place either during operation, depending on the choice of operational conditions, or after shutdown. Numerous combinations are possible, some of which are shown in Figure 6-14.

Anode and cathode may be oriented in the same direction, in opposite direction, or in cross-configuration. Position of anode vs cathode may have some effect on fuel cell performance because of varied concentration of reactant gases and water. In some cases the flow fields are oriented so that the cathode outlet is next to the anode inlet and vice versa, allowing water exchange through the membrane due to water concentration gradient (*i.e.*, the exiting gas has much higher temperature and water content).

The stack orientation, and so the flow field orientation, may be either vertical or horizontal. In the latter case, either anode or cathode may be facing up (Figure 6-15). Again, this may have some effect on liquid water removal, particularly after shutdown and cooling.

### 6.4.3. Configuration of Channels

There are many configurations of channels that have been tried in PEM fuel cells, all with the same goal—to ensure uniform reactant gases distribution and product water removal (see Figure 6-16). Some most common designs will be discussed next.

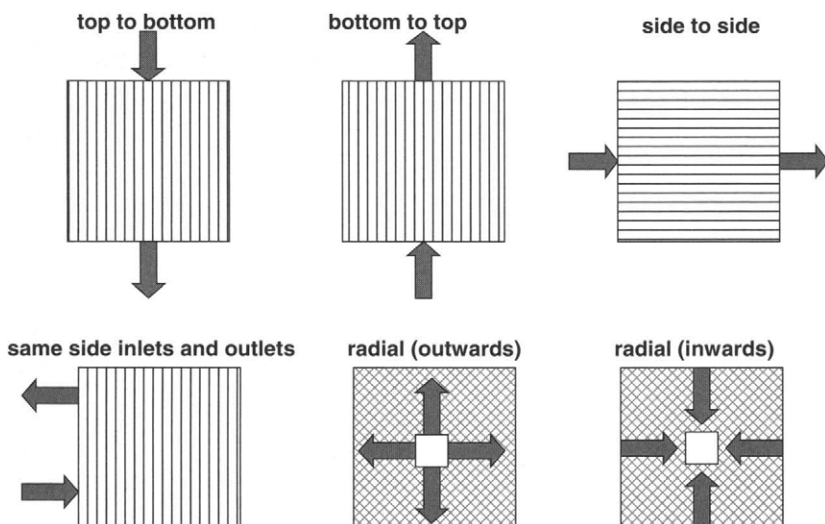


FIGURE 6-14. Possible flow field orientations.

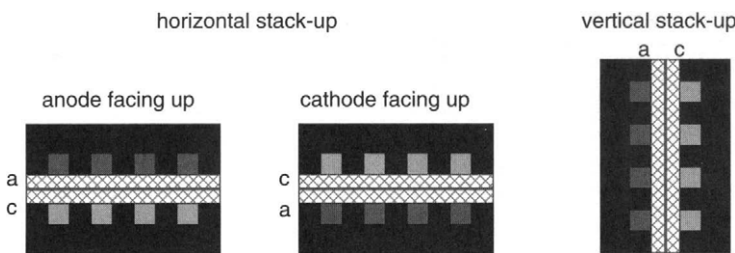


FIGURE 6-15. Stack and cell orientation options.

- Straight channels with large manifolds—Although this appears to ensure uniform distribution, it actually does not work in PEM fuel cells. Distribution is indeed uniform, but only under ideal conditions. Any water droplet that develops in a channel would effectively block the entire channel, and the velocity would not be sufficient to push the water out.
- Straight channels with small manifolds—This design has the same shortcomings and, in addition, has inherent maldistribution of reactant gases, because the channels immediately below or above the manifold receive most of the flow. The early fuel cells built with such a flow field exhibited low and unstable cell voltages.
- Crisscross configuration—This flow field attempts to eliminate the shortcomings of the straight channel flow field by introducing traversal channels allowing the gas to bypass any “trouble” spot, that is, coalescing water droplets. The problems of low velocities and uneven flow distribution due to positioning of the inlet and outlet manifolds are not reduced with this design.
- Single-channel serpentine—As described by Watkins *et al.* [10], this is the most common flow field for small active areas. It ensures that the entire area is covered, although the concentration of reactants decreases along the channel. There is a pressure drop along the channel due to friction on the walls and due to turns. The velocity is typically high enough to push any water condensing in the channel. Attention must be paid to pressure differential between the adjacent channels, which may cause significant bypassing of channel portions.
- Multichannel serpentine—A single-channel serpentine configuration would not work for the large flow field areas, because of a large pressure drop. Although a pressure drop is useful in removing the water, excessive pressure drop may generate larger parasitic energy losses. Watkins *et al.* [11] proposed a flow field that has a multitude of parallel channels meandering through the entire area in a serpentine fashion. Except the lower pressure drop, this flow field has the same features, advantages, and shortcomings of the single-

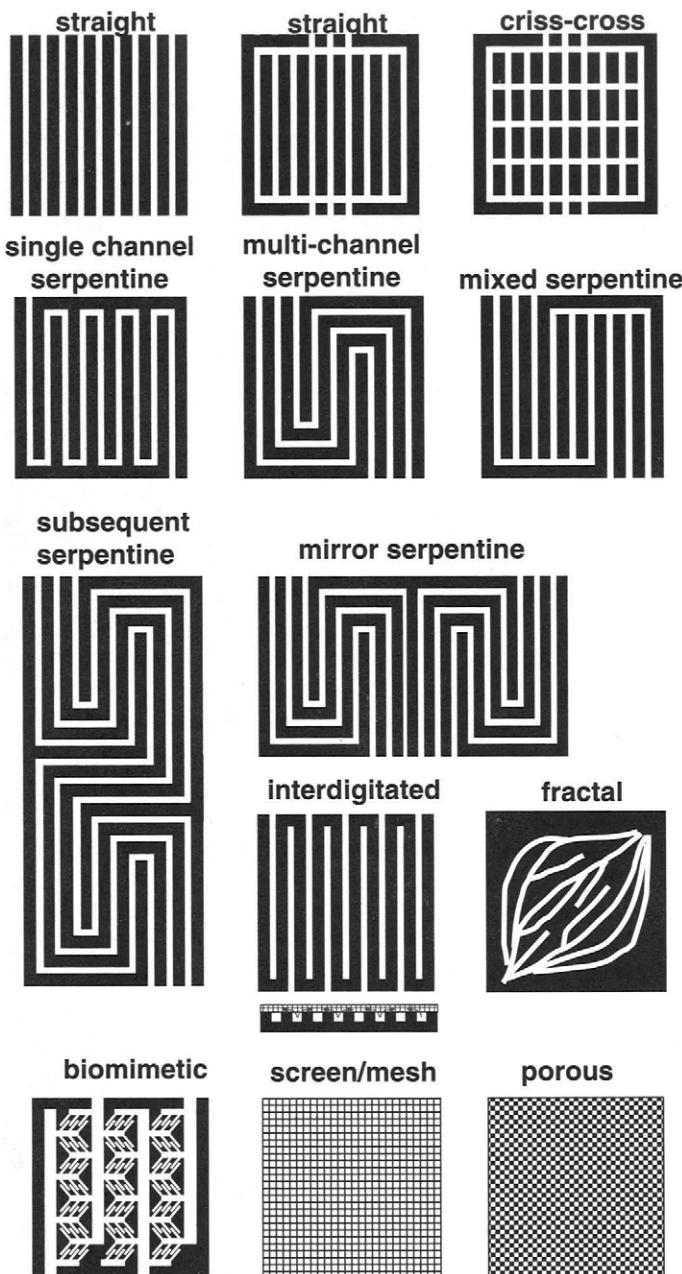


FIGURE 6-16. Various flow field configurations.

channel serpentine. The fact that there are parallel channels means that there is always a possibility that one of the channels may get blocked as discussed previously with straight channels.

- Multichannel serpentine with mixing—As suggested by Cavalca *et al.* [12], this flow field design allows gases to mix at every turn in order to minimize the effect of channel blocking. This does not reduce the chance of channel blockage, but it limits its effect only to a portion of the channel, because the flow field is divided in smaller segments, each with its own connecting channel to both the inlet and the outlet.
- Subsequent serially linked serpentine—This flow field also divides the flow field into segments in an attempt to avoid the long straight channels and relatively large pressure differentials between the adjacent sections, thus minimizing the bypassing effect [13].
- Mirror serpentine—This is another design to avoid large pressure differentials in adjacent channels, particularly suited for a larger flow fields with multiple inlets and outlets. These are arranged so that the resulting serpentine patterns in adjacent segments are mirror images of each other, which results in balanced pressures in adjacent channels, again minimizing the bypassing effect [14].
- Interdigitated—First described by Ledjeff [15], advocated by Nguyen [16], and successfully employed by Energy Partners in their NG-2000 stack series [17,18], this flow field differs from all of the above-mentioned because the channels are discontinued, that is, they do not connect inlet to the outlet manifolds. This way the gas is forced from the inlet channels to the outlet channels through the porous back-diffusion layer. Wilson *et al.* [19] suggested a variation of interdigitated flow field in which the channels are made by cutting out the strips of the gas diffusion layer. Convection through the porous layer shortens the diffusion path and helps remove any liquid water that otherwise may accumulate in the gas diffusion layer, resulting in better performance, particularly at higher current densities. However, depending on the properties of the gas diffusion layer, this flow field may result in higher pressure drops. Due to the fact that the most of the pressure drop occurs in the porous media, the uniformity of flow distribution between individual channels and between individual cells strongly depends on uniformity of gas diffusion layer thickness and effective porosity (after being squeezed). One of the problems with this flow field is inability to remove liquid water from the inlet channels. Issacci and Rehg [20] suggested the porous blocks at the end of the inlet channels allowing water to be removed.
- BioMimetic—Suggested by Morgan Carbon [21], this is a further refinement of the interdigitated concept. Larger channels branch to

smaller side channels further branching to really tiny channels interweaving with outlet channels that are arranged in the same fashion—tiny channels leading to larger side channels leading to the large channels. This type of branching occurs in nature (leaves or lungs), hence the name biomimetic.

- Fractal—This flow field suggested by the Fraunhofer Institute [22] is essentially the interdigitated flow field concept, but the channels are not straight and they have branches.
- Mesh—Metallic meshes and screens of various sizes are successfully being used in the electrolyzers. The uniformity may greatly be affected by positioning of the inlet manifolds. The researchers at Los Alamos National Lab successfully incorporated metal meshes in fuel cell design [23]. The problems with this design are introduction of another component with tight tolerances, corrosion, and interfacial contact resistance.
- Porous media flow field [24]—This is similar to mesh flow field; the difference is in pore sizes and material. The gas distribution layer must be sufficiently thick and have enough pores sufficiently large to permit a substantially free flow of reactant gas both perpendicular to and parallel to the catalyst layer. Although metallic porous materials (foams) are brittle, carbon-based ones may be quite flexible. This type of flow field may only be applicable for smaller fuel cells because of the high pressure drop.

#### 6.4.4. Channel's Shape, Dimensions, and Spacing

The flow field channels may have different shapes, often resulting from the manufacturing process rather than from functionality. For example, slightly tapered channels would be very difficult to obtain by machining, but they are essential if the bipolar plate is manufactured by molding. Channel geometry may have effect on water accumulation. In the round-bottomed channel, condensed water forms a film of water at the bottom, whereas in the channel with tapered walls, condensed water forms small droplets

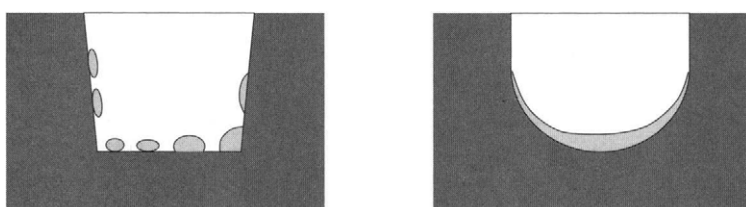


FIGURE 6-17. The shape of the channel cross-section affects the form of liquid water formation.

(Figure 6-17). The sharp corners at the bottom of the channel help to break the surface tension of the water film, resisting film formation [25].

The shape and size of the water droplets in the channels also depends on hydrophobicity of the porous media and the channel walls. Figure 6-18 shows the possible combinations of hydrophobicity and hydrophilicity of the porous gas diffusion layer and the channel walls and their effect on water droplet shape and size [26].

Typical channel dimensions are around 1 mm, but may vary from 0.4 to 4 mm. The spacing between the channels is similar. With today's advances in micromanufacturing techniques (MEMS, photolithography) it is possible to produce channels of 0.1 mm and even smaller. The dimensions of the channels and their spacing affect the reactant gas access to the gas diffusion layer and pressure drop, but also electrical current and heat conduction. Wider channels allow more direct contact of the reactants gas to the gas diffusion layer and also provide wider area for water removal from the gas diffusion layer. Figure 6-19 shows O<sub>2</sub> concentration in a cross-section of an H<sub>2</sub>/Air fuel cell with serpentine or straight channels [27]. Oxygen concentration, and therefore current density, is higher in the area directly above the channel, and it is significantly lower in the area above the land between the channels.

However, if the channels are too wide there will be no support for the MEA, which will deflect into the channel. Wider spacing enhances conduction of electrical current and heat; however, it reduces the area directly exposed to the reactants and promotes the accumulation of water in the gas diffusion layer adjacent to these regions. For a geometry shown in Figure 6-20, and with simplification of the current path in the control area (one half channel and one half spacing between the channels) the voltage loss through the control area is [28]:

$$\Delta V = \Delta V_{BP} + \Delta V_{GDL} + \Delta V_{CR} \quad (6-18)$$

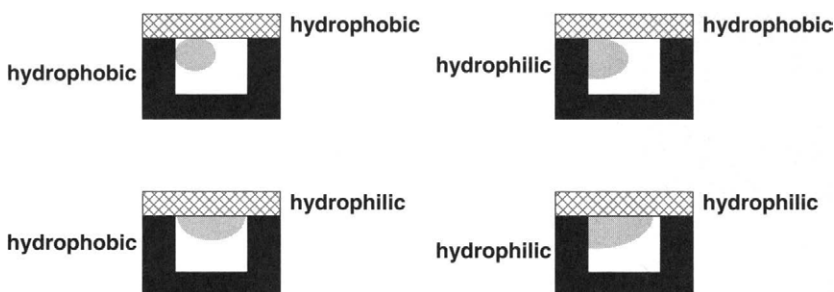


FIGURE 6-18. Possible combinations of hydrophobicity and hydrophilicity of the porous gas diffusion layer and the channel walls and their effect on droplet size and shape.

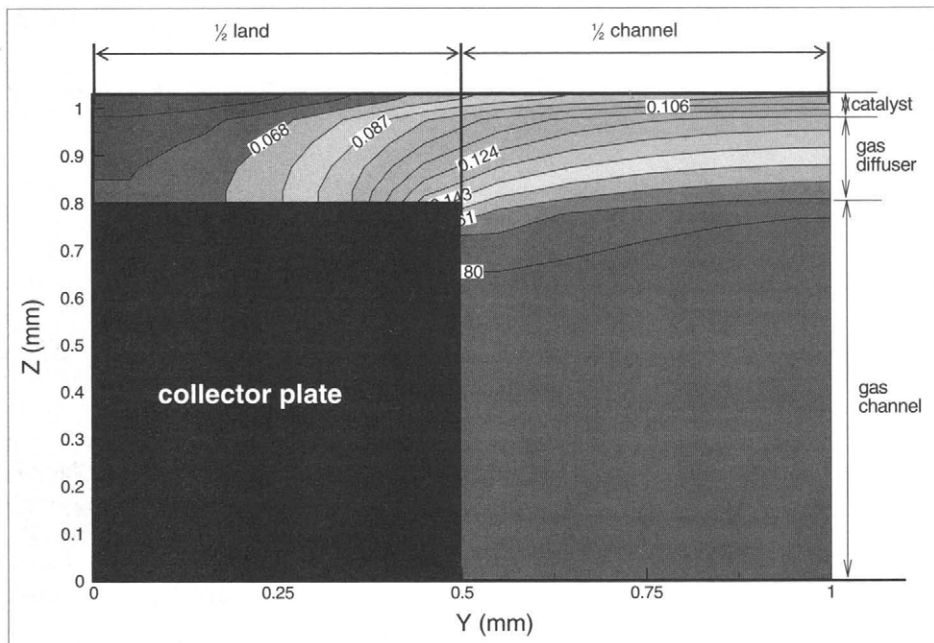


FIGURE 6-19. Oxygen concentration distribution in and above the channel. (Adapted from [27].)

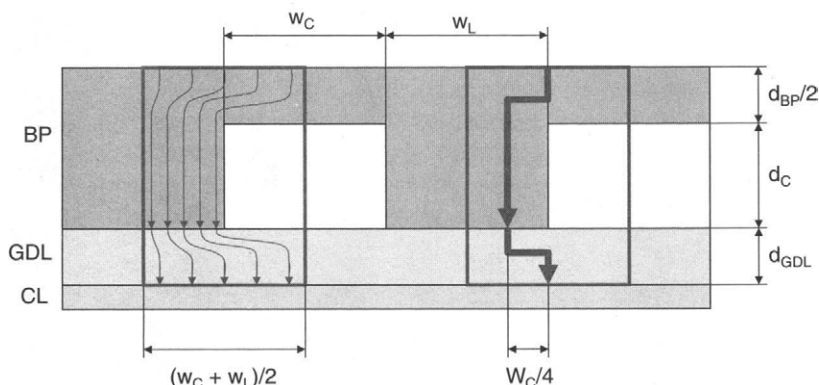


FIGURE 6-20. Current path through bipolar plate and gas diffusion layer (left, actual; right, approximation).

where:

$\Delta V_{BP}$  is the voltage drop through the bipolar plate:

$$\Delta V_{BP} = \left[ \left( \frac{w_L + w_C}{w_L} d_C + \frac{d_{BP}}{2} \right) \rho_{BP,z} + \frac{(w_L + w_C) w_C}{4d_{BP}} \rho_{BP,xy} \right] i \quad (6-19)$$

$\Delta V_{GDL}$  is the voltage drop through gas diffusion layer:

$$\Delta V_{GDL} = \left[ d_{GDL} \rho_{GDL,z} + \frac{(w_L + w_C) w_C}{8d_{GDL}} \rho_{GDL,xy} \right] i \quad (6-20)$$

and  $\Delta V_{CR}$  is the voltage drop due to interfacial contacts:

$$\Delta V_{CR} = R_{CR} \frac{w_L + w_C}{w_C} i \quad (6-21)$$

where dimensions  $w_L$ ,  $w_C$ ,  $d_{GDL}$ ,  $d_C$ , and  $d_{BP}$  are defined in Figure 6-20, and

$\rho$  = resistivity of either bipolar plate (BP) or gas diffusion layer (GDL) in either z-direction (through-plane) or xy-direction (in-plane),  $\Omega\text{cm}$

$R_{CR}$  = contact resistance between the gas diffusion layer and bipolar plate,  $\Omega\text{cm}^2$

$i$  = current density at the GDL–catalyst layer interface,  $\text{A cm}^{-2}$

Note that the voltage loss through the entire bipolar plate, two gas diffusion layers, and two interfaces is twice as much as what is calculated by Equation 6-18.

In, general, as landing width,  $w_L$ , narrows, the fuel cell performance improves, until there is either MEA deflection into the channel or the gas diffusion layer crashes because of excessive force applied. The optimum channel size and spacing is therefore a balance between maximizing the open area for the reactant gas access to the gas diffusion layer and providing sufficient mechanical support to the MEA and sufficient conduction paths for electrical current and heat.

Wilkinson and Vanderleeden [25] suggested the use of the following equation to calculate the maximum deflection of the MEA in the channel,  $d_{max}$  (mm):

$$d_{max} = \frac{0.032(1-v^2)}{t^3 \left( \frac{1}{b^4} + \frac{1}{L^4} \right)} \frac{p}{E} \quad (6-22)$$

where:

- v = Poisson's ratio
- t = MEA thickness, mm
- b = unsupported channel width, mm
- L = channel length, mm
- p = pressure, kPa
- E = Young's modulus, kPa

#### 6.4.5. Pressure Drop through the Flow Field

Most of the flow fields are arranged as a number of parallel channels [Figure 6-17]. In that case the pressure drop along a channel is also the pressure drop in the entire flow field. The pressure drop along a flow field channel may be approximated by the equation for incompressible flow in pipes and conduits with sufficient accuracy as long as the pressure drop is less than 30% of the inlet pressure:

$$\Delta P = f \frac{L}{D_H} \rho \frac{\bar{v}^2}{2} + \sum K_L \rho \frac{\bar{v}^2}{2} \quad (6-23)$$

where:

- f = friction factor
- L = channel length, m
- D<sub>H</sub> = hydraulic diameter, m
- ρ = fluid density, kg m<sup>-3</sup>
- ̄v = average velocity, m s<sup>-1</sup>
- K<sub>L</sub> = local resistance (for example in sharp turns)

Hydraulic diameter is defined as four times the channel cross-sectional area divided by its perimeter. For a typical rectangular channel with w<sub>c</sub> as width and d<sub>c</sub> as depth (Figure 6-21):

$$D_H = \frac{2w_C d_C}{w_C + d_C} \quad (6-24)$$

Channel length is:

$$L = \frac{A_{cell}}{N_{ch}(w_C + w_L)} \quad (6-25)$$

where:

$A_{cell}$  = cell active area,  $m^2$

$N_{ch}$  = number of parallel channels

$w_C$  = channel width, m

$w_L$  = space between the channels, m

The velocity in a fuel cell channel at the entrance of the cell is:

$$\bar{v} = \frac{Q_{stack}}{N_{cell} N_{ch} A_{ch}} \quad (6-26)$$

where:

$\bar{v}$  = velocity in the channel,  $m s^{-1}$

$Q_{stack}$  = air flow rate at the stack entrance,  $m^3 s^{-1}$

$N_{cell}$  = number of cells in the stack

$N_{ch}$  = number of parallel channels in each cell

$A_{ch}$  = cross-sectional area of the channel, for a rectangular channel

$A_{ch} = bd$ , as defined previously

The total flow rate at the stack entrance is (combining Equations 5-42 and 5-47, and dividing by density of humid air):

$$Q_{stack} = \frac{I}{4F} \frac{S}{r_{O_2}} \frac{RT_{in}}{P_{in} - \varphi P_{sat}(T_{in})} N_{cell} \quad (6-27)$$

where:

$Q$  = volumetric flow rate,  $m^3 s^{-1}$

$I$  = stack current, A,  $I = iA_{cell}$

$F$  = Faraday constant 96, 485, As  $mol^{-1}$

$S$  = oxygen stoichiometric ratio

$r_{O_2}$  = oxygen content in air, by volume = 0.2095

$R$  = universal gas constant =  $8.314 J mol^{-1} K^{-1}$

$T_{in}$  = temperature at stack inlet, K

$P_{in}$  = pressure at stack inlet, Pa

$\varphi$  = relative humidity

$P_{sat}$  = saturation pressure at given inlet temperature (Equation 5-25)

$N_{cell}$  = number of cells in stack

By combining the previous equations (6-24 through 6-27), the velocity at the stack inlet is:

$$\bar{v} = \frac{i}{4F} \frac{S}{r_{O_2}} \frac{(w_C + w_L)L}{w_C d_C} \frac{RT}{P - \varphi P_{sat}} \quad (6-28)$$

Reynolds number is important to determine whether the flow in the channel is laminar or turbulent. Reynolds number at the channel entrance is:

$$Re = \frac{\rho \bar{v} D_H}{\mu} = \frac{1}{\mu} \frac{i}{2F} \frac{S}{r_{O_2}} \frac{(w_C + w_L)L}{w_C + d_C} \left( M_{Air} + M_{H_2O} \frac{\varphi P_{sat(Tin)}}{P_{in} - \varphi P_{sat(Tin)}} \right) \quad (6-29)$$

The flow rate at the stack outlet is somewhat different than the flow at the inlet. It can be lower, equal, or higher, depending on the conditions at the inlet and outlet (flow rate, temperature, pressure, temperature, and humidity). Assuming that the outlet flow is saturated with water vapor, the flow rate at the stack outlet is:

$$Q_{stack}^{out} = \frac{I}{4F} \left( \frac{S}{r_{O_2}} - 1 \right) \frac{RT_{out}}{P_{in} - \Delta P - P_{sat(Tout)}} N_{cell} \quad (6-30)$$

where:

$\Delta P$  = pressure drop through the stack

The ratio between the outlet and inlet flow rate, thus velocity, is:

$$\frac{Q_{stack}^{out}}{Q_{stack}^{in}} = \frac{S - r_{O_2in}}{S} \frac{T_{out}}{T_{in}} \frac{P_{in} - \varphi P_{vs(Tin)}}{P_{in} - \Delta P - P_{sat(Tout)}} \quad (6-31)$$

The first factor is always lower than 1, the second factor is either higher than or equal to 1 (depending on the inlet temperature being lower than or equal to outlet temperature), and the third factor also depends on the inlet temperature and humidity (if the gas at the inlet is saturated at the stack temperature, then this factor is higher than 1). For all practical purposes, the difference between the inlet and outlet flow rates varies within  $\pm 5\%$ .

The values for viscosity of common fuel cell gases are shown in Table 6-1. The variation of viscosity with pressure is small for most gases, but viscosity varies with temperature [29]:

$$\mu = \mu_0 \left( \frac{T_0 + C}{T + C} \right) \left( \frac{T}{T_0} \right)^{\frac{3}{2}} \quad (6-32)$$

where  $\mu_0$  is known viscosity at temperature  $T_0$ , from Table 6-1; the coefficient,  $C$ , is also listed in Table 6-1.

TABLE 6-1  
Viscosity of Fuel Cell Gases (at 25°C)

	Viscosity $\text{kg m}^{-1} \text{s}^{-1}$	Coefficient $C$
Hydrogen	$0.92 \times 10^{-5}$	72
Air	$1.81 \times 10^{-5}$	120
Water vapor	$1.02 \times 10^{-5}$	660

Viscosity of gas mixtures, such as humidified air or humidified hydrogen, can be calculated from the following equation [30]:

$$\mu_{\text{mix}} = \frac{\mu_1}{1 + \Psi_1 \frac{M_2}{M_1}} + \frac{\mu_2}{1 + \Psi_2 \frac{M_1}{M_2}} \quad (6-33)$$

where:

$$\Psi_1 = \frac{\sqrt{2}}{4} \left( 1 + \left( \frac{\mu_1}{\mu_2} \right)^{0.5} \left( \frac{r_2}{r_1} \right)^{0.25} \right)^2 \left( 1 + \frac{r_1}{r_2} \right)^{-0.5} \quad (6-34)$$

$$\Psi_2 = \frac{\sqrt{2}}{4} \left( 1 + \left( \frac{\mu_2}{\mu_1} \right)^{0.5} \left( \frac{r_1}{r_2} \right)^{0.25} \right)^2 \left( 1 + \frac{r_2}{r_1} \right)^{-0.5} \quad (6-35)$$

and

$\mu_1, \mu_2$  are the viscosities of components 1 and 2

$r_1, r_2$  are the volume fractions of components 1 and 2 in the mixture

$M_1, M_2$  are the molecular weights of components 1 and 2

For steady laminar flow in a channel, the product of the friction factor and the Reynolds number is a constant [31]:

$$\text{Re } f = \text{constant} \quad (6-36)$$

For a circular channel,  $\text{Re } f = 64$ . For rectangular channels, the value of  $\text{Re } f$  depends on the channel aspect ratio,  $w_C/d_C$ :

$$\text{Re } f \approx 55 + 41.5 \exp\left(\frac{-3.4}{w_C/d_C}\right) \quad (6-37)$$

For a square channel,  $\text{Re } f \approx 56$ .

Though some geometrical pressure-loss coefficients,  $K_L$ , are available for various bends or elbows, none fit a specific shape of gas flow channels in fuel cell. Values as high as  $30f$  have been suggested for 90-degree bends and as high as  $50f$  for close pattern return bends [29].

For fully turbulent flow, the friction coefficient  $f$  is independent of Reynolds number and may be approximated by the Karman's equation (Equation 6-14). Note that the three walls of the channel are smooth, but the fourth one is the porous gas diffusion layer.

For the porous flow fields, the pressure drop may be determined by Darcy's Law [32]:

$$\Delta P = \mu \frac{Q_{\text{cell}}}{kA} L \quad (6-38)$$

where:

$\mu$  = viscosity of the fluid,  $\text{kg m}^{-1} \text{s}^{-1}$

$Q_{\text{cell}}$  = volumetric flow rate through a cell,  $\text{m}^3 \text{s}^{-1}$

$k$  = permeability,  $\text{m}^2$

$A$  = cross-sectional area of the flow field,  $\text{m}^2$

$L$  = length of the flow field,  $\text{m}$

The same equation may be used to approximate the pressure drop through any flow field as long as the flow is laminar. The permeability factor,  $k$ , then refers to the entire flow field, and must be determined experimentally.

In most cases the flow through the fuel cell flow field is laminar, which means that the pressure drop is linearly proportional to velocity, that is, to flow rate. However, in a fuel cell channel there are some deviations from the uniform pipe flow:

- Roughness of the GDL is different than that of the channel walls.
- The reactant gas participates in the chemical reaction and the flow rate varies along the channel, although not significantly.
- Temperature may not be uniform along the channel.
- Typically the channel is not straight but there are numerous sharp turns (90 or 180 degrees).
- Liquid water may be present inside the channel either in the form of little droplets or as a film, in both cases effectively reducing the channel cross-sectional area.

Figure 6-21 shows linear relationship between the the flow rate and the pressure drop through the cathode side of a three-cell,  $65\text{-cm}^2$  stack, when dry air at room temperature is run through the stack and no current, and thus no water, is being generated [33]. The Reynolds number at the entrance of the cathode channels was <250 at the highest flow rate. When humidified air (100% RH at  $60^\circ\text{C}$ ) is run through the stack, the pressure drop is higher because of condensation in the cold, nonoperating stack; however, as the flow rate is increased, the pressure drop approaches that of the dry air. This may be explained by improved water removal from the stack at higher channel velocities.

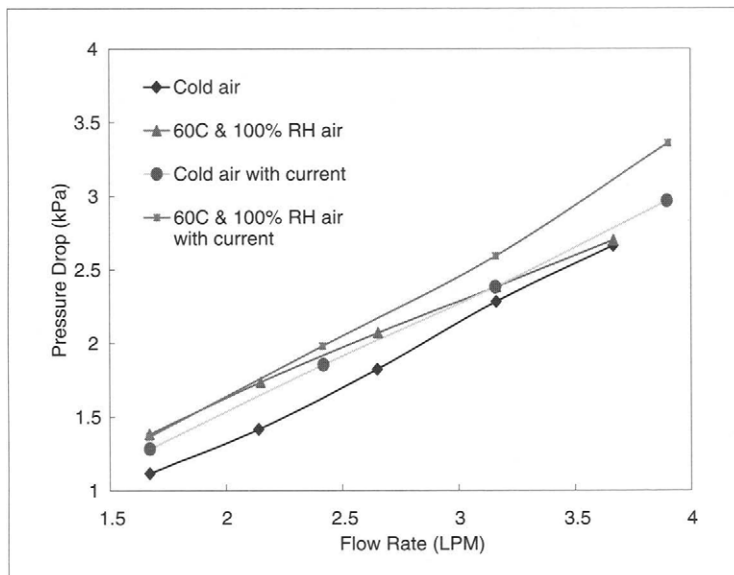


FIGURE 6-21. Pressure drop of a three-cell, 65-cm<sup>2</sup> stack as a function of flow rate [33].

When the stack is operational and generates water, the pressure drop is linearly proportional to the flow rate if the incoming air is dry, because all the product water gets evaporated in the flow of air. Note that the molar flow rate at the exit is higher than the flow rate at the inlet, because each oxygen molecule consumed is replaced by two water vapor molecules. When the incoming air is fully humidified, evaporation of the product water is no longer possible, and as the result the pressure drop starts to increase exponentially with the air flow rate (and with current, *i.e.*, water generation rate), as shown in Figure 6-21.

#### *Example*

Calculate the pressure drop through a cathode flow field of a 60-cell stack with 65-cm<sup>2</sup> cell area. The stack operates at 125 kPa (inlet), 60°C, with saturated air. The flow rate is kept proportional to current at 3 times stoichiometry. Nominal operating point is 0.4 A cm<sup>-2</sup> at 0.7 V. The cathode flow field consists of six parallel serpentine channels 0.8 mm wide, 0.8 mm deep, and 0.8 mm apart, with four 90-degree bends.

#### *Solution:*

The pressure drop is (Equation 6-23):

$$\Delta P = f \frac{L}{D_H} \rho \frac{\bar{v}^2}{2} + \sum K_L \rho \frac{\bar{v}^2}{2}$$

Hydraulic diameter is (Equation 6-24):

$$D_H = \frac{2w_C d_C}{w_C + d_C} = 2 \times 0.08 \times 0.08 / (0.08 + 0.08) = 0.08 \text{ cm}$$

Channel length is (Equation 6-25):

$$L = \frac{A_{cell}}{N_{ch}(w_C + w_L)} = \frac{65}{6 \times (0.08 + 0.08)} = 67.7 \text{ cm}$$

The flow rate at the stack entrance is (Equation 6-27):

$$\begin{aligned} Q_{stack} &= \frac{I}{4F} \frac{S}{r_{O_2}} \frac{RT_{in}}{P_{in} - \phi P_{sat(T_{in})}} N_{cell} = \frac{0.4 \times 65}{4 \times 96,485} \frac{3}{0.21} \frac{8.314 \times (273.15 + 60)}{125,000 - 19,944} 60 \\ &= 0.00152 \text{ m}^3 \text{ s}^{-1} = 1520 \text{ cm}^3 \text{ s}^{-1} \end{aligned}$$

where 19,944 Pa is the saturation pressure at 60°C.

The velocity in a fuel cell channel at the entrance of the cell is (Equation 6-26):

$$v = \frac{Q_{stack}}{N_{cell} N_{ch} A_{ch}} = \frac{1520}{60 \times 6 \times 0.08 \times 0.08} = 660 \text{ cm s}^{-1}$$

The Reynolds number at the channel entrance is (Equation 6-29):

$$Re = \frac{\rho v D_H}{\mu}$$

$$\begin{aligned} \rho &= \text{density of humidified air} = \frac{(P - P_{sat})M_{air} + P_{sat}M_{H2O}}{RT} \\ &= \frac{(125,000 - 19,944) \times 29 + 19,944 \times 18}{8314 \times (273.15 + 60)} = 1.23 \text{ kg m}^{-3} = 0.00123 \text{ g cm}^{-3} \end{aligned}$$

Viscosity of humidified air is (from Table 6-1 and Equations 6-32 through 6-35):

$$\mu = 2 \times 10^{-5} \text{ kg m}^{-1} \text{ s}^{-1} = 0.0002 \text{ g cm}^{-1} \text{ s}^{-1}$$

$$Re = \frac{\rho v D_H}{\mu} = 0.00123 \times 660 \times 0.08 / 0.0002 = 324.7$$

$$Re f \approx 55 + 41.5 \exp\left(\frac{-3.4}{b/d}\right) = 56$$

Friction factor:

$$f = 56/\text{Re} = 56/324.7 = 0.172$$

And finally, the pressure drop is:

$$\Delta P = f \frac{L}{D_H} \rho \frac{\bar{v}^2}{2} + \sum K_L \rho \frac{\bar{v}^2}{2} = 0.172 \frac{0.677}{0.0008} 1.23 \frac{6.6^2}{2} + (4 \times 30 \times 0.172) 1.23 \frac{6.6^2}{2}$$

$$= \underline{\Delta P = 4452 \text{ Pa}} \quad \underline{\text{Answer}}$$

This pressure drop has been calculated based on inlet conditions. The velocity at the outlet is somewhat lower, so the average velocity throughout the channel would be lower, and consequently, the pressure drop would be somewhat lower. The exact solution may be obtained through an iterative process.

The inlet and outlet manifolds of this 60-cell stack should be sized so that the pressure drop through a manifold is at least an order of magnitude lower than the pressure drop through individual cells, that is, less than 445 Pa (the total stack pressure drop would then be about 5300 Pa).

## 6.5. Heat Removal from a Fuel Cell Stack

To maintain the desired temperature inside the cells, the heat generated as a by-product of the electrochemical reactions must be taken away from the cells and from the stack. Different heat management schemes (Figure 6-22) may be applied, such as:

- Cooling with a coolant flowing between the cells.

Coolant may be deionized water, antifreeze coolant, or air. Cooling may be arranged between each cell, between the pair of cells (in such

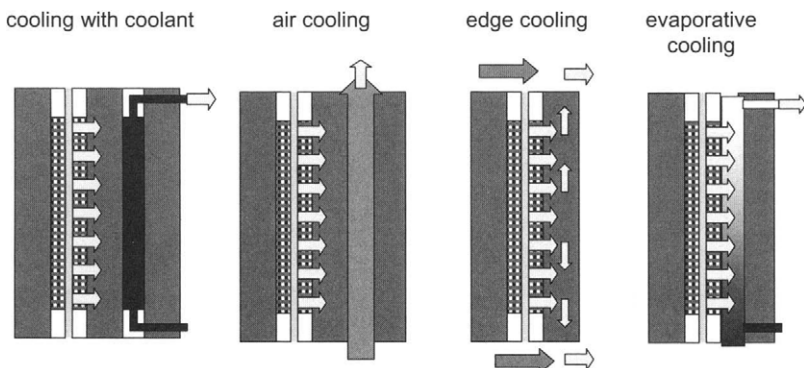


FIGURE 6-22. Different cell/stack cooling options.

configuration one cell has the cathode and other cell has the anode next to the cooling arrangement), or between a group of cells (this is feasible only for low-power densities because it results in higher temperatures in the center cells). Equal distribution of coolant may be accomplished by the manifolding arrangement similar to that of reactant gases. If air is used as a coolant, equal distribution may be accomplished by a plenum.

- Cooling with coolant at the edge of the active area (with or without fins).

The heat is conducted through the bipolar plate and then transferred to the cooling fluid, typically air. To achieve relatively uniform temperature distribution within the active area, the bipolar plate must be a very good thermal conductor. In addition, the edge surface may not be sufficient for heat transfer and fins may need to be employed. This method results in a much simpler fuel cell stack and fewer parts, but it has heat transfer limitations and is typically used for low-power outputs.

- Cooling with phase change.

Coolant may be water or another phase-change medium. Use of water simplifies the stack design, because water is already used in both anode and cathode compartments.

### 6.5.1. Stack Heat Balance

There are several ways to set the fuel cell stack energy balance. In general, energy of fuel (higher heating value) is converted into either electricity or heat:

$$\text{Energy of fuel reacted} = \text{Heat generated} + \text{Electricity generated}$$

or

$$\frac{I}{2F} H_{HHV} n_{cell} = Q_{gen} + IV_{cell} n_{cell} \quad (6-39)$$

Heat generated in a fuel cell stack is then:

$$Q_{gen} = (1.482 - V_{cell}) I n_{cell} \quad (6-40)$$

The previous equation assumes that all the product water leaves the stack as liquid at 25°C, which may be the case if the inlet is fully saturated at the stack operating temperature. If all of the product water leaves the stack as vapor, then the following equation is more appropriate:

$$Q_{\text{gen}} = (1.254 - V_{\text{cell}}) I n_{\text{cell}} \quad (6-41)$$

The previous equations (6-39 through 6-41) are just approximations. A complete stack energy balance (such as shown in Equations 5-62 through 5-67) should take into account the heat (enthalpy) brought into the stack with reactant gases, as well as the heat of the unused reactant gases leaving the stack, including both latent and sensible heat of water at the stack inlet and stack outlet:

Enthalpy of reactant gases in = electricity generated + enthalpy of unused reactant gases including heat of product water + heat dissipated to the surrounding + heat taken away from the stack by active cooling or

$$\sum Q_{\text{in}} = W_{\text{el}} + \sum Q_{\text{out}} + Q_{\text{dis}} + Q_c \quad (6-42)$$

On closer examination of this energy balance, it is clear that some of the heat generated in the stack is carried away by reactant gases and product water, some is lost to the surrounding by natural convection and radiation, and the rest must be taken away from the stack by active cooling.

Because heat generation is associated with the (voltage) losses in a fuel cell, most heat is generated in the catalyst layers, predominantly on the cathode side, then in the membrane due to ohmic losses, and also in the electrically conductive solid parts of the fuel cell (also due to ohmic losses). This heat is first carried by heat conduction through solid parts of the fuel cell, namely porous electrode structures, including the gas diffusion layer and bipolar plates (Figure 6-23). Some heat is transferred to the reactant gases (depending on their temperature), some is transferred to the cooling medium through convection, and some is conducted to the edge of the stack where it is transferred to the surrounding air through radiation and natural convection (or, in some cases, forced convection when this is the primary way of stack temperature control).

### 6.5.2. Heat Conduction

The rate of heat transferred by conduction in the x-direction through a finite cross-sectional area A is, according to the Fourier Law of Conduction, proportional to the temperature difference:

$$Q_x = kA \frac{dT}{dx} \quad (6-43)$$

where k is the thermal conductivity,  $\text{W/m}^{-1}\text{k}^{-1}$ .

The values of thermal conductivity, k, for some typical fuel cell materials are given in Table 6-2.

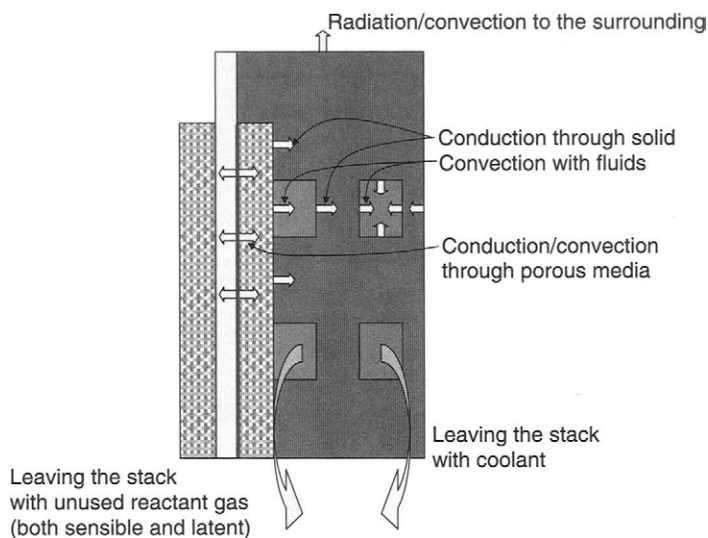


FIGURE 6-23. Heat paths in a fuel cell segment.

**TABLE 6-2**  
Thermal Conductivity of Some Fuel Cell Materials

Material	Thermal Conductivity <sup>a</sup> W m <sup>-1</sup> K <sup>-1</sup>
Aluminum	237
Copper	401
Nickel	91
Nickel alloys (Inconel, Hasteloy)	12
Titanium	22
Stainless steel 316	13
Platinum	71
Graphite	98
Graphite/polymer mix	~20 <sup>b</sup>
Carbon fiber paper	1.7 <sup>b</sup>
Teflon	0.35
Liquid water	0.611
Water vapor	0.0198
Air	0.0267
Hydrogen	0.198

<sup>a</sup>At 300K, <sup>b</sup>through-plane.

More generally, the steady state heat conduction is governed by the equation (easily obtained by differentiating Equation 6-43):

$$\frac{d^2T}{dx^2} = 0 \quad (6-44)$$

which can also easily be extended to three-dimensional steady state heat conduction:

$$\nabla \cdot (\nabla T) = 0 \quad (6-45)$$

To solve this equation, two boundary conditions (for each direction) must be given that describe the behavior of  $T$  at the system boundaries (constant  $T$  or prescribed flux).

When the heat is conducted through two adjacent materials with different thermal conductivities, the third boundary condition comes from a requirement that the temperature at the interface is the same for both materials (in cases when the contact resistance may be neglected) or there is a discontinuity in temperature distribution at the interface described by either contact resistance  $R_{tc}$  or thermal contact coefficient  $h_{tc}$ , defined by:

$$Q = h_{tc} A \Delta T \quad (6-46)$$

$$R_{tc} = \frac{1}{h_{tc} A} \quad (6-47)$$

For the case involving internal heat generation due to electrical resistance, Equation (6-44) becomes:

$$\frac{d^2T}{dx^2} + \frac{q_{int}}{k} = 0 \quad (6-48)$$

where:

$$q_{int} = \text{rate of heat generation per unit volume}$$

In the fuel cell, internal heat generation results from electrical and ionic resistance:

$$q_{int} = i^2 \rho_s \quad (6-49)$$

In porous media, an effective thermal conductivity is used that takes into account porosity of the media,  $\epsilon$ :

$$k_{\text{eff}} = -2k_s + \left[ \frac{\epsilon}{2k_s + k} + \frac{1-\epsilon}{3k_s} \right]^{-1} \quad (6.50)$$

*Example:*

A fuel cell operates at 0.6 V and  $1 \text{ A cm}^{-2}$ . Calculate the temperature distribution through a gas diffusion layer-bipolar plate sandwich on the cathode side. Assume a constant heat flux at the gas diffusion–catalyst layer interface equal to all the fuel cell losses, except those due to ionic and electrical resistance. Assume that half of the resistive losses apply to the anode side and half to the cathode. Ionic resistance through the membrane is  $0.1 \text{ Ohm}\cdot\text{cm}^2$ . At the outer edge of the bipolar plate assume that heat is removed by a cooling fluid at  $60^\circ\text{C}$ , with heat transfer coefficient,  $h = 1600 \text{ W m}^{-2} \text{ K}^{-1}$ . Electrical resistivity of the gas diffusion layer and bipolar plate is  $0.08 \text{ Ohm}\cdot\text{cm}$  and  $0.06 \text{ Ohm}\cdot\text{cm}$ , respectively. There is a contact resistance of  $0.005 \text{ Ohm}\cdot\text{cm}^2$  between the gas diffusion layer and bipolar plate. Effective thermal conductivity of GDL and bipolar plate is  $1.7 \text{ W m}^{-1} \text{ K}^{-1}$  and  $20 \text{ W m}^{-1} \text{ K}^{-1}$ , respectively. There is a thermal contact resistance between these two layers equal to  $1^\circ\text{C}/\text{W}$ . Thickness of GDL and bipolar plate is  $0.38 \text{ mm}$  and  $3.3 \text{ mm}$ , respectively.

*Solution:*

Assume one-dimensional steady state conduction.

Let  $T_1$  be the temperature at the bipolar plate-cooling fluid interface,  $T_2$  temperature of the bipolar plate facing the gas diffusion layer,  $T_3$  temperature of the gas diffusion layer facing the bipolar plate, and  $T_4$  temperature of the gas diffusion layer facing the catalyst layer.

Voltage loss through GDL is:  $V = IR = i \rho_{\text{GDL}} d_{\text{GDL}} = 1 \times 0.08 \times 0.038 = 0.00304 \text{ V}$

Voltage loss through bipolar plate =  $i \rho_{\text{BP}} d_{\text{BP}} = 1 \times 0.06 \times 0.33 = 0.0198 \text{ V}$

Voltage loss due to contact resistance =  $1 \times 0.005 = 0.005 \text{ V}$

Total electrical resistance (one side) =  $0.00304 + 0.00198 + 0.005 = 0.01 \text{ V}$

Total electrical resistance (both sides) =  $0.01 \times 2 = 0.02 \text{ V}$

Voltage loss due to ionic resistance =  $1 \times 0.1 = 0.1 \text{ V}$

Total resistive losses =  $0.12 \text{ V}$

Fuel cell voltage corrected for resistance =  $0.6 + 0.12 = 0.72 \text{ V}$

Heat generation in fuel cell (except resistance) =  $(1.254 - 0.72) \times 1^2 = 0.534 \text{ W cm}^{-2}$

Heat flux at the catalyst–gas diffusion layer interface (including  $\frac{1}{2}$  of the ionic resistance):

$$Q_4 = 0.534 + 1^2 \times 0.1/2 = 0.584 \text{ W cm}^{-2}$$

Heat generation due to resistance in GDL =  $i \times \Delta V = 1 \times 0.00304 = 0.00304 \text{ W cm}^{-2}$

Heat generation due to resistance in bipolar plate =  $1 \times 0.00198 = 0.00198 \text{ W cm}^{-2}$

Heat generation due to contact resistance =  $1 \times 0.005 = 0.005 \text{ W cm}^{-2}$

Heat flux at the bipolar plate-cooling fluid interface

$$Q_1 = 0.584 + 0.00304 + 0.00198 + 0.005 = 0.594 \text{ W cm}^{-2}$$

Heat flux at the bipolar plate-gas diffusion layer interface (on the bipolar plate side):

$$Q_2 = 0.594 - 0.00198 = 0.592 \text{ W cm}^{-2}$$

Heat flux at the bipolar plate-gas diffusion layer interface (on the GDL side):

$$Q_3 = 0.592 - 0.005 = 0.587 \text{ W cm}^{-2}$$

Convection heat flux from the bipolar plate surface to the cooling fluid (from Equation 6-52):

$$Q_1 = h(T_F - T_1)$$

The temperature  $T_1$  is then:

$$T_1 = T_F + Q_1/h = 60 + .594/0.16 = 63.71$$

The governing equation for heat flux inside the bipolar plate is (Equation 6-48):

$$\frac{d^2T}{dx^2} + \frac{q_{int}}{k} = 0$$

After two integrations, it becomes:

$$T = \frac{q_{int}}{k} \frac{x^2}{2} + C_1 x + C_2$$

The integration constants,  $C_1$  and  $C_2$ , can be determined from the boundary conditions:

$$\begin{aligned} \text{At } x = 0 & \quad T = T_1 \\ \text{At } x = d_{BP} & \quad k \frac{dT}{dx} = Q_2 \end{aligned}$$

therefore:

$$C_2 = T_1$$

and

$$C_1 = \frac{Q_2}{k} + \frac{q_{int}}{k} d_{BP}$$

Temperature distribution in bipolar plate is:

$$T = T_1 + \frac{Q_2}{k_{BP}} x + \frac{q_{int,BP}}{k_{BP}} \left( d_{BP} x - \frac{x^2}{2} \right)$$

where:

$$q_{int,BP} = 0.00198 / 0.33 = 0.006 \text{ W cm}^{-3}$$

The temperature  $T_2$  (at  $x = d_{BP}$ ) is:

$$T_2 = T_1 + \frac{Q_2}{k_{BP}} d_{BP} + \frac{q_{int,BP}}{k_{BP}} \frac{d_{BP}^2}{2} = 63.71 + \frac{0.592}{0.19} 0.33 + \frac{0.006}{0.19} \frac{0.33^2}{2} = 64.74^\circ\text{C}$$

There is a discontinuity in temperature at the gas diffusion layer–bipolar plate interface due to contact resistance. Temperature  $T_3$  is then:

$$T_3 = T_2 + R_{tc} Q_3 = 64.74 + 1 \times 0.587 = 65.33^\circ\text{C}$$

The temperature distribution inside the GDL is (applying the same equation as for bipolar plate):

$$T = T_3 + \frac{Q_4}{k_{GDL}} x + \frac{q_{int,GDL}}{k_{GDL}} \left( d_{GDL} x - \frac{x^2}{2} \right)$$

where:

$$q_{int,GDL} = 0.00304 / 0.038 = 0.080 \text{ W cm}^{-3}$$

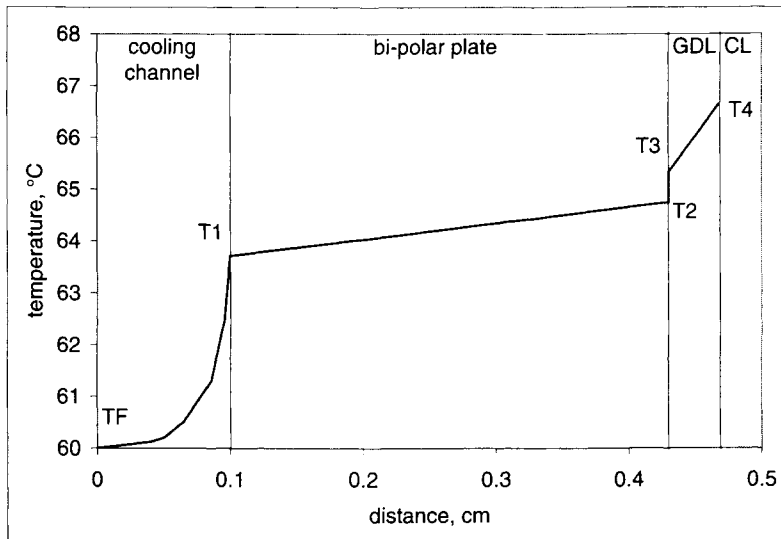


FIGURE 6-24. Temperature distribution across the bipolar plate–gas diffusion layer sandwich.

The temperature  $T_4$  (at  $x = d_{\text{GDL}}$ ) is:

$$T_4 = T_3 + \frac{Q_4}{k_{\text{GDL}}} d_{\text{GDL}} + \frac{q_{\text{int,GDL}}}{k_{\text{GDL}}} \frac{d_{\text{GDL}}^2}{2} = 65.33 + \frac{0.584}{0.017} 0.038 + \frac{0.08}{0.017} \frac{0.038^2}{2} = T_4 = 66.6-64^\circ\text{C}$$

The resulting temperature distribution across the bipolar plate–gas diffusion layer sandwich is shown in Figure 6-24.

### 6.5.3. Active Heat Removal

From the heat removal point of view, a fuel cell stack may be considered as a heat exchanger with internal heat generation. The walls of the fuel cell cooling channels may be neither at constant temperature nor have the constant heat flux, but these two cases are often used as boundary cases for heat transfer analyses.

The heat to be removed by active cooling (from equation 6-42) is:

$$Q_c = \sum Q_{\text{in}} - W_{\text{el}} - \sum Q_{\text{out}} - Q_{\text{dis}} \quad (6-51)$$

The same heat,  $Q_c$ , has to be transferred to the cooling fluid:

$$\frac{dQ_c}{dA_c} = h(T_s - T_c) \quad (6-52)$$

or integrated over the entire heat exchange surface,  $A_c$ , just as in a heat exchanger:

$$Q_c = UA_c LMTD \quad (6-53)$$

where:

$h$  = local heat transfer coefficient,  $\text{W m}^{-2} \text{C}$

$U$  = overall heat transfer coefficient,  $\text{W m}^{-2} \text{C}$

$A_c$  = heat exchange area = surface area of the cooling channels,  $\text{m}^2$

LMTD = logarithmic mean temperature difference,  $^\circ\text{C}$ , defined as

$$LMTD = \frac{(T_s - T_c)_{in} - (T_s - T_c)_{out}}{\ln \frac{(T_s - T_c)_{in}}{(T_s - T_c)_{out}}} \quad (6-54)$$

The temperature difference between the stack body,  $T_s$ , and the cooling fluid,  $T_c$ , may be constant (constant thermal flux case), or it may vary from one side of the stack to the other depending on the position of coolant inlets and outlets vs reactants inlets and outlets, internal coolant and reactants passages configuration, and current density configuration.

The same heat,  $Q_c$ , has to be "absorbed" by the cooling fluid and carried out of the fuel cell stack:

$$Q_c = \dot{m} c_p (T_{c,out} - T_{c,in}) \quad (6-55)$$

The temperature difference  $\Delta T_c = \{T_{c,out} - T_{c,in}\}$  is a design variable that has to be selected in conjunction with the coolant flow rate. As usual in fuel cell design, in selecting the temperature difference between coolant outlet and inlet there are conflicting requirements. To achieve uniform temperature distribution through the stack,  $\Delta T_c$  should be selected as small as practically possible, unless larger temperature gradients are required by stack design (for example, to facilitate water management). However, small  $\Delta T_c$  would result in large coolant flow rate, which would increase parasitic power and reduce system efficiency. On the other side, larger  $\Delta T_c$  would result in lower temperature to which the coolant must be cooled at, and there may be practical limits imposed by the ambient temperature and by the characteristics and performance of the heat rejection device.

The coefficient of convection heat transfer,  $h$ , depends on the Nusselt number, that is, properties of the coolant, geometry of the passages, and flow characteristics.

$$h = Nu \frac{k}{D_H} \quad \text{or} \quad h = Nu_L \frac{k}{L} \quad \text{or} \quad \bar{h} = \bar{Nu}_L \frac{k}{L} \quad (6-56)$$

The Nusselt number represents the ratio of convection heat transfer for fluid in motion to conduction heat transfer for a motionless layer of fluid [34]. Common expressions for the Nusselt number and for various flow characteristics (*i.e.*, developed/undeveloped, laminar/turbulent) are summarized in Table 6-3 [34], and the thermal properties of some fluids commonly found in fuel cells are given in Table 6-4.

*Example:*

Coolant (50% water and 50% ethylene glycol) flows with the velocity of 1 m/s through a 1-mm square channel at 80°C. Calculate the heat transfer coefficient for hydraulically and thermally fully developed flow under uniform wall heat flux conditions. If the heat flux is 1 W cm<sup>-2</sup>, calculate the required temperature difference between the wall and the fluid.

*Solution:*

The heat transfer coefficient is:

$$h = Nu \frac{k}{D_H}$$

$$Nu = 3.61$$

$$D_H = 4A/Pm = 4 \times 0.001^2 / 4 \times 0.001 = 0.001 \text{ m}$$

$$k \text{ for water at } 80^\circ\text{C} = 0.671 \text{ W m}^{-1} \text{ K}^{-1}$$

$$k \text{ for ethylene glycol at } 80^\circ\text{C} = 0.261$$

$$k \text{ for 50/50 mixture of water and ethylene glycol} = 0.466 \text{ W m}^{-1} \text{ K}^{-1}$$

$$h = 3.61 \times 0.466 / 0.001 = 1682 \text{ W m}^{-2} \text{ K}^{-1}$$

The average temperature difference between the wall of the cooling channel and coolant required for transfer of 1 W cm<sup>-2</sup> (or 10,000 W m<sup>-2</sup>) is:

$$T_s - T_c = \frac{Q}{Ak} = \frac{10000 \text{ W m}^{-2}}{1682 \text{ W m}^{-2} \text{ K}} = 6^\circ\text{C}$$

Equation (6-45) may be solved numerically for a variety of boundary conditions, such as constant  $T_s$  at the walls, or constant or prescribed heat flux. Because of complicated three-dimensional heat transfer pathways (shown in Figure 6-23), calculation of heat fluxes and temperature profiles in a fuel cell stack requires 3-D numerical simulation. Figure 6-25 shows temperature distribution in a representative cross-section of a fuel cell obtained by 3-D numerical simulation [28]. From Figure 6-25, it is obvious that there are significant temperature variations inside a fuel cell stack. Because most heat in a fuel cell stack is produced in the cathode catalyst layer, that layer expectedly has the highest temperature.

TABLE 6-3  
Nusselt Number for Various Internal Flow Conditions (Adapted from [34].)

Condition	Equation
Laminar flow	
Hydraulically fully developed, $x/D > 0.05 RePr$	
Thermally fully developed $x/D > 0.05 RePr$	
Uniform wall temperature	
Square tube	$Nu = 2.98$
Circular tube	$Nu = 3.66$
Uniform wall heat flux	
Square tube	$Nu = 3.61$
Circular tube	$Nu = 4.36$
Thermal entry	
Uniform wall temperature	$Nu = 3.66 + \frac{0.0668 \frac{RePr}{x/D}}{1 + 0.04 \left( \frac{RePr}{x/D} \right)^{2/3}}$
Uniform wall temperature $x/D < 0.01 RePr$	$Nu = 1.67 \left( \frac{RePr}{x/D} \right)^{1/3}$
Uniform wall heat flux $x/D < 0.01 RePr$	$Nu = 1.95 \left( \frac{RePr}{x/D} \right)^{1/3}$
Hydraulic and thermal entry $x/D < 0.01 RePr$	$Nu = 1.86 \left( \frac{RePr}{x/D} \right)^{1/3}$
Turbulent flow	
Hydraulically fully developed	
Thermally fully developed	$Nu = \frac{(f/8)RePr}{1.07 + 12.7\sqrt{f/8}(Pr^{2/3} - 1)}$ where $f = 4/(1.58 \ln Re - 3.28)^2$
Thermal entry $x/D < 60$	$Nu = Nu_{TFD} \left( 1 + \frac{1.4}{x/D} \right)$
Hydraulic and thermal entry $x/D < 60$	$Nu = Nu_{TFD} \left( 1 + \frac{6}{x/D} \right)$
Transitional turbulent flow	
	$Nu = C_{tr} Nu_{L2} + (1 - C_{tr}) Nu_{T8}$
	$Nu_{L2} = Nu$ for $Re = 2000$
	$Nu_{T8} = Nu$ for $Re = 8000$
	$C_{tr} = 1.33 - Re/6000$

TABLE 6-4

Properties of Some Fuel Cell Gases and Coolant Mediums (Upper Number Is at 20°C and Lower Is at 60°C)

Gas	Density $\text{kg m}^{-3}$	Viscosity $\text{kg m}^{-1} \text{s}^{-1}$	Thermal Conductivity $\text{W m}^{-1} \text{K}^{-1}$	Specific Heat $\text{kJ kg}^{-1} \text{K}^{-1}$
Water	998	0.001	0.602	4.18
	984	0.000466	0.654	4.18
Ethylene glycol	1116	0.0214	0.249	2.38
	1088	0.0052	0.260	2.56
Propylene glycol	1036	0.054	0.200	2.47
	1010	0.0075		2.72
Air	1.21	$18 \times 10^{-6}$	0.0257	1.005
	1.06	$20 \times 10^{-6}$	0.0287	1.008
Hydrogen	0.0841	$8.8 \times 10^{-6}$	0.178	14.2
	0.0741	$9.6 \times 10^{-6}$	0.198	14.4

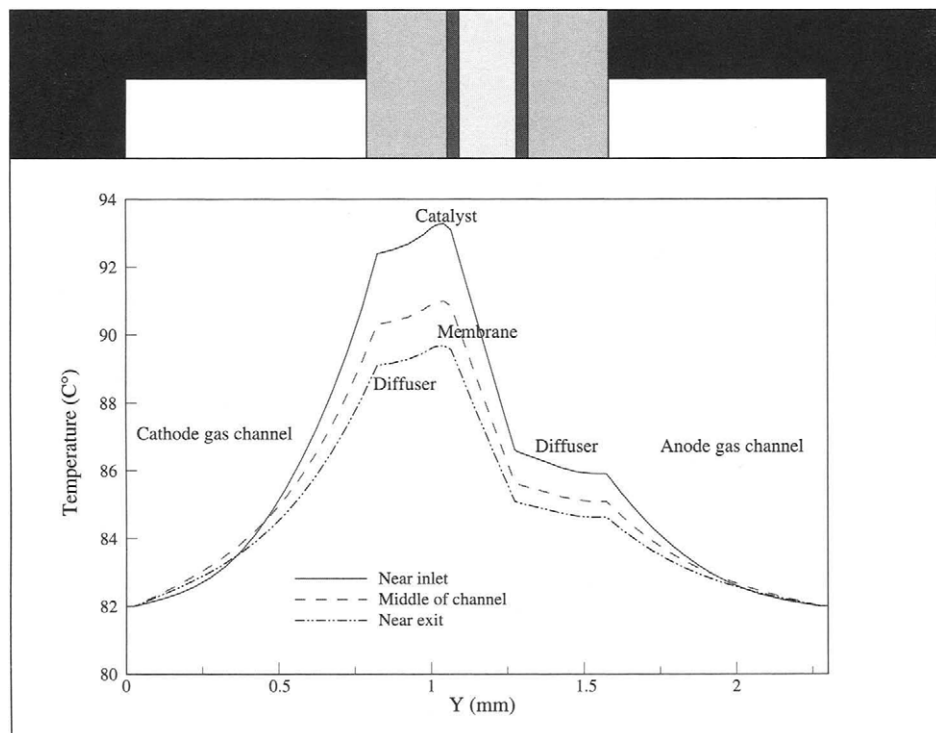


FIGURE 6-25. Temperature distribution through a fuel cell characteristic cross-section (Adapted from [28]).

### 6.5.4. Heat Dissipation from the Stack by Natural Convection and Radiation

Maximum heat that the stack may lose through natural convection and radiation to the surrounding is:

$$Q_{\text{dis}} = \frac{T_s - T_0}{R_{\text{th}}} \quad (6-57)$$

where:

$T_s$  = stack surface temperature

$T_0$  = temperature of the surrounding walls

$R_{\text{th}}$  = thermal resistance, defined as

$$R_{\text{th}} = \frac{1}{\frac{1}{R_C} + \frac{1}{R_R}} \quad (6-58)$$

where:

$R_C$  = convective thermal resistance, defined as

$$R_C = \frac{1}{hA_S} \quad (6-59)$$

and

$R_R$  = radiative thermal resistance defined as

$$R_R = \frac{1}{\sigma F A_S (T_s + T_0)(T_s^2 + T_0^2)} \quad (6-60)$$

where:

$\sigma$  = Stefan–Boltzman constant =  $5.67 \times 10^{-8} \text{ W m}^{-2} \text{ K}^{-4}$

$F$  = shape factor; for the first approximation it may be assumed as

$F = 1$

$A_S$  = stack exposed surface area,  $\text{m}^2$

For short stacks, the ratio of exposed (external) surface area and the (internal) active area,  $A_S/A_{\text{act}}$ , may be too large and the stack cannot reach the operating temperature at all, because the rate of heat dissipation is higher than the rate of heat generation. This is often the case with single cells used in laboratories that must use heat pads (or other means of temperature control) to obtain the desired operating temperature.

The heat transfer coefficient,  $h$ , in Equation (6-59) is a function of the Nusselt number,  $Nu$ :

$$h = \frac{k}{L} Nu_L \quad (6-61)$$

For vertical plates and natural convection, the Nusselt number is some empirical function of Prandtl and Rayleigh numbers,  $Nu_L = f[Pr, Ra_L]$ , such as for example:

$$Nu_L = \left\{ 0.825 + \frac{0.387 Ra_L^{1/6}}{\left[ 1 + \left( \frac{0.5}{Pr} \right)^{9/16} \right]^{8/27}} \right\}^2 \quad (6-62)$$

where:

$$Ra_L = \frac{g\beta(T_s - T_0)L^3}{\nu\alpha} \quad (6-63)$$

and

$$Pr = \frac{\nu}{\alpha} \quad (6-64)$$

where:

$g$  = gravity acceleration ( $9.81 \text{ m s}^{-2}$ )

$\beta$  = thermal expansion coefficient; for gases  $\beta = 1/T$

$L$  = characteristic length or length of travel of the fluid in the boundary layer, that is, the height of the stack, m.

$\nu$  = kinematic viscosity,  $\text{m}^2 \text{s}^{-1}$

$\alpha$  = thermal diffusivity,  $\text{m}^2 \text{s}^{-1}$

Fluid properties may be evaluated at the free stream or film (wall) temperature.

For horizontal plate:

$$Nu_L = 0.54 Ra_L^{1/4}$$

$L = A/P_m$  (area/perimeter)

Some air properties at 300 and 350K are listed in Table 6-5.

TABLE 6-5  
Air Thermal Properties

Property	@300 K	@350 K
Density, $\rho$ , $\text{kg m}^{-3}$	1.1774	0.998
Specific heat, $c_p$ , $\text{kJ kg}^{-1} \text{C}^{-1}$	1.0057	1.0090
Thermal conductivity, $k$ , $\text{W m}^{-1} \text{C}^{-1}$	0.02624	0.03003
Thermal diffusivity, $\alpha$ , $\text{m}^2 \text{s}^{-1}$	$0.2216 \times 10^{-4}$	$0.2983 \times 10^{-4}$
Thermal expansion, $\beta$ , $\text{C}^{-1}$	0.00333	0.00286
Viscosity, $\mu$ , $\text{kg m}^{-1} \text{s}^{-1}$	$1.846 \times 10^{-5}$	$2.075 \times 10^{-5}$
Kinematic viscosity, $\nu$ , $\text{m}^2 \text{s}^{-1}$	$15.68 \times 10^{-6}$	$20.76 \times 10^{-6}$
Prandtl number, Pr	0.708	0.697

### 6.5.5. Alternative Stack Cooling Options

#### Air Cooling

Air is already passing through the cathode compartment in excess of oxygen exact stoichiometry. Can the same air be used as a coolant? Theoretically, yes, although the flow rate would have to be much higher. How high? This can be found from a simple heat balance: heat generated by fuel cell must be equal to heat taken away by the flow of air.

The heat generated, assuming that the product water evaporates and leaves the stack as vapor, which actually should be the case for this cooling scheme, is {Equation 6-41}:

$$Q = (1.254 - V_{\text{cell}}) I n_{\text{cell}} \quad (6-65)$$

The heat transferred to air is:

$$\dot{Q} = \dot{m} c_p (T_{\text{Air,out}} - T_{\text{Air,in}}) \quad (6-66)$$

The mass flow rate at the stack exit is given by Equation (5-56):

$$\dot{m}_{\text{Airout}} = \left[ (S_{\text{O}_2} - 1) M_{\text{O}_2} + S_{\text{O}_2} \frac{1 - r_{\text{O}_2 \text{in}}}{r_{\text{O}_2 \text{in}}} M_{\text{N}_2} \right] \frac{i \cdot n_{\text{cell}}}{4F} \quad (6-67)$$

By combining the previous equations, an expression for required stoichiometric ratio is obtained:

$$S_{\text{O}_2} = \frac{M_{\text{O}_2} + \frac{4F(1.254 - V_{\text{cell}})}{c_p \Delta T}}{M_{\text{O}_2} + \frac{1 - r_{\text{O}_2 \text{in}}}{r_{\text{O}_2 \text{in}}} M_{\text{N}_2}} \quad (6-68)$$

The only variables in the previous equation are the cell potential,  $V_{cell}$ , and temperature difference between air at the stack inlet and outlet,  $\Delta T$ . The cell potential determines the cell efficiency, and at a lower efficiency more heat is generated (follows directly from Equation 6-65). The air temperature difference is determined by the ambient temperature and the stack operating temperature. Figure 6-26 shows the resulting cathode stoichiometric ratio as a function of two typical operating cell potentials (0.6 V and 0.7 V) and as a function of air temperature difference. The two upper curves were calculated by Equation (6-68), and the lower curve took into account the heat dissipation from the stack surface (for a 1 kW stack, with the ratio of surface area to active area  $A_s/A_{act} = 0.27$ ). Very large air flow rates are required, with stoichiometric ratio higher than 20. Product water is not sufficient to saturate these large amounts of air and therefore this cooling scheme would cause severe drying of the anode, and would not be practical. Relative humidity at the outlet may be calculated from the following equation:

$$\phi = \frac{2r_{O_2,in}}{S_{O_2} + r_{O_2,in}} \frac{P}{P_{vs}} \quad (6-69)$$

For a normal operating range of temperatures (from 40°C to 80°C), and for stoichiometric ratios above 20, relative humidity at the outlet would be below 10%, and the cell would experience severe drying.

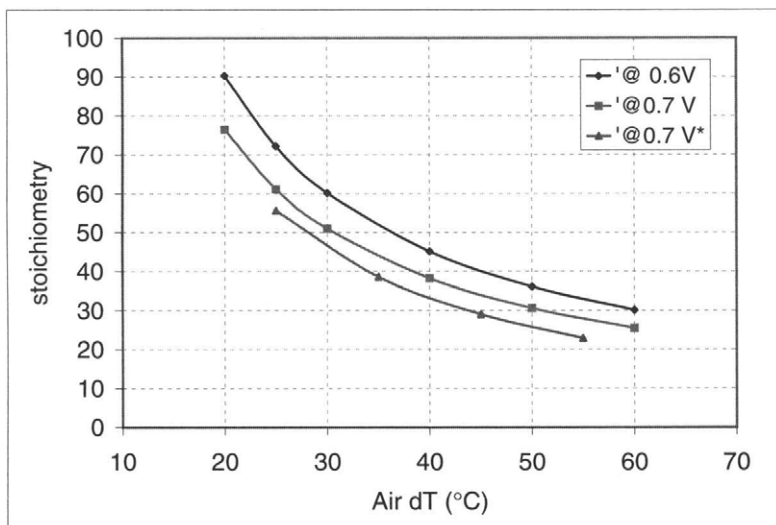


FIGURE 6-26. Required air stoichiometry for stack cooling (\*this curve takes into account heat dissipation from the stack surface).

### Evaporative Cooling

If additional liquid water is injected at the stack cathode inlet it would be possible to prevent drying and at the same time dramatically reduce the air flow rate requirement, because cooling would be achieved by evaporation of injected water. Using the mass and energy balance equation (Chapter 5), it is possible to calculate the exact amount of water and air flow rate needed to achieve saturation conditions at the outlet and provide sufficient cooling of the stack. The example in Chapter 5 shows the calculation for one set of operational conditions. Figure 6-27 shows the resulting water and air flow rate requirements for evaporative cooling over a range of operating conditions (cell potential and temperature) for an atmospheric pressure fuel cell (outlet pressure is atmospheric, and air at the inlet is at 20°C and 70% relative humidity). In addition, the conditions in Figure 6-27 assume no net water flux across the membrane, that is, electroosmotic drag equal to back diffusion. In case that electroosmotic drag is higher than back diffusion, water injection requirement would be reduced. Indeed, Wilson *et al.* [35] suggested adiabatic cooling of an atmospheric stack with water introduced on the anode side and then relying on wicking through the gas diffusion layer (using hydrophilic thread) and electroosmotic drag to saturate the ambient air on the cathode side.

### Edge Cooling

If a fuel cell flow field is made narrow enough, the heat generated may be removed on the sides of the cell instead of the more conventional way

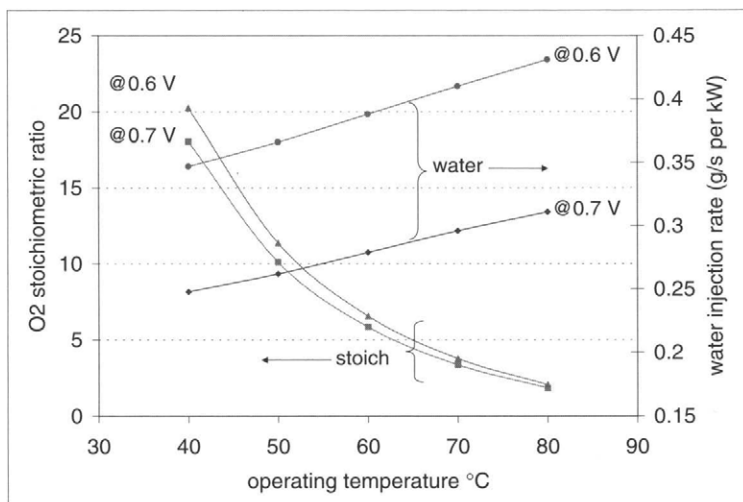


FIGURE 6-27. Air and water injection rates required for stack cooling and air saturation at the outlet.

between the cells. In this case, heat is conducted in plane of the bipolar plate rather than through it. Active cooling may still be needed at the edge of the bipolar plates. To enhance heat transfer, fins may be added, and/or high thermal conductivity material may be used.

Obviously, in this case the maximum temperature will be achieved in the center of the flow field. In a narrow and long flow field, the heat transfer may be approximated as one-dimensional (*i.e.*, heat removed through long sides is significantly larger than the heat removed at the narrow sides).

The equation that describes one-dimensional heat transfer (conduction) in a flat plate with internal heat generation is:

$$\frac{d^2T}{dx^2} + \frac{Q}{kAd_{BP}^{eff}} = 0 \quad (6-70)$$

where:

$Q$  = heat generated in the cell (either given by Equation 6-65 or by a detailed energy balance analysis), W

$k$  = bipolar plate in-plane thermal conductivity (in some cases, in-plane conductivity may be significantly different from through-plane thermal conductivity),  $\text{W m}^{-1} \text{K}^{-1}$

$A$  = cell active area,  $\text{m}^2$

$d_{BP}^{eff}$  = effective (or average) thickness of the bipolar plate in the active area, m

Although the heat is not actually generated inside the plate but rather in a thin catalyst layer above the plate, Equation (6-70) may be used with sufficient accuracy, because the thickness of the plates is very small compared with the width (*i.e.*, a few millimeters vs few centimeters). In that case, the solution of Equation (6-70) for symmetrical cooling on both sides with  $T(0) = T(L) = T_0$  is:

$$T - T_0 = \frac{Q}{kAd_{BP}^{eff}} \frac{L^2}{2} \left[ \frac{x}{L} - \left( \frac{x}{L} \right)^2 \right] \quad (6-71)$$

where:

$T_0$  = the temperature at the edge of the active area

$L$  = width of the active area

The maximum temperature difference is between the edge ( $x = 0$  or  $x = L$ ) and the center ( $x = L/2$ ):

$$\Delta T_{\max} = \frac{Q}{kA d_{BP}^{\text{eff}}} \frac{L^2}{8} \quad (6-72)$$

In addition, the heat must be conducted from the edge of the flow field to the edge of the plate or to the fin over the flow field border with width "b." The thickness of the plate at the border is  $d_{BP}$ . Because of this, the temperature will further decrease, according to the Fourier Law:

$$T_0 - T_b = \frac{Q}{2kA} \frac{L}{d_b} b \quad (6-73)$$

Where  $T_b$  is the temperature at the edge of the bipolar plate.

Therefore, the total temperature difference between the center of the plate and the edge of the plate, or the base of a fin, is:

$$\Delta T_{\max} = \frac{Q}{kA} L \left( \frac{L}{8d_{BP}^{\text{eff}}} + \frac{b}{2d_{BP}} \right) \quad (6-74)$$

Figure 6-28 shows the geometry of the narrow flat plate, and Figure 6-29 shows the maximum temperature difference in the active area (temperature in the center – temperature at the edge of the active area) as a function of flow field width and plate thermal conductivity ( $Q = 0.279 \text{ W/cm}^2$ ,  $d_{BP}^{\text{eff}} = 1.8 \text{ mm}$ ). The maximum temperature difference in the active area should be limited to  $<5-10^\circ\text{C}$ . In that case, edge cooling is limited by the

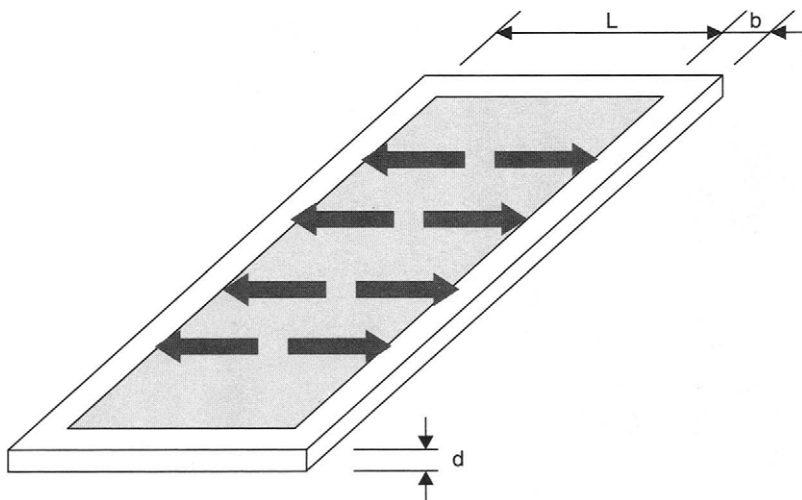


FIGURE 6-28. Geometry of narrow active area with edge cooling.

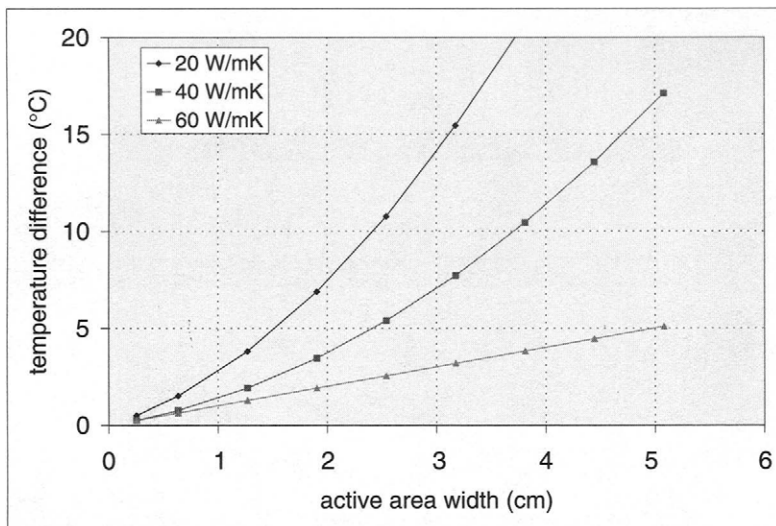


FIGURE 6-29. Maximum temperature difference in the active area (temperature in the center – temperature at the edge of the active area) as a function of flow field width and plate thermal conductivity ( $Q = 0.279 \text{ W/cm}^2$ ,  $d_{\text{BP}}^{\text{eff}} = 1.8 \text{ mm}$ ).

active area width and bipolar plate conductance. Unless a high conductivity material is used, this kind of cooling may be employed only for low-power densities (below  $0.3 \text{ W/cm}^2$ ) and narrow flow fields (2–3 cm).

## 6.6. Stack Clamping

The individual components of a fuel cell stack, namely MEAs, gas diffusion layers, and bipolar plates, must be somehow held together with sufficient contact pressure to (1) prevent leaking of the reactants between the layers and (2) to minimize the contact resistance between those layers. This is typically accomplished by sandwiching the stacked components between the two end plates connected with several tie-rods around the perimeter (Figure 6-30) or in some cases through the middle. Other compression and fastening mechanisms may be employed too, such as snap-in shrouds or straps.

The clamping force is equal to the force required to compress the gasket, plus the force required to compress the gas diffusion layer, plus internal force (for example the internal operating pressure).

The pressure required to prevent the leak between the layers depends on the gasket material and design. Various materials ranging from rubber to proprietary polymer configurations are used for fuel cell gaskets. The

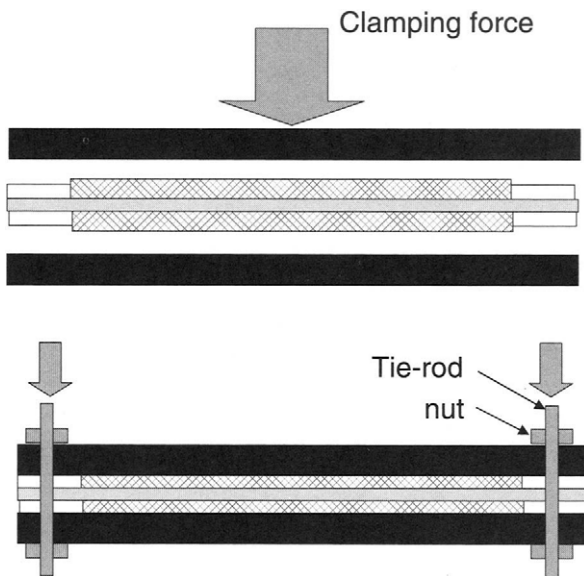


FIGURE 6-30. Compression of fuel cell components with tie-rods.

designs also vary from manufacturer to manufacturer, including flat or profile gaskets, gaskets as individual components or molded on bipolar plate, or on or around the gas diffusion layer. A so-called seven-layer MEA includes the catalyzed membrane, two gas diffusion layers—one on each side—and the gasket that keeps the entire MEA together.

The torque on the bolts required to achieve the required force may be calculated from the following equation:

$$T = \frac{FK_b D_b}{N_b} \quad (6-75)$$

where:

$T$  = tightening torque, Nm

$F$  = clamping force, N

$K_b$  = friction coefficient (0.20 for dry and 0.17 for lubricated bolts)

$D_b$  = bolt nominal diameter, m

$N_b$  = number of bolts

Too much force on the perimeters may cause bending of the end plates (as shown in Figure 6-31), which has an adverse effect on the compression over the active area. Compression distribution inside the cell may be monitored

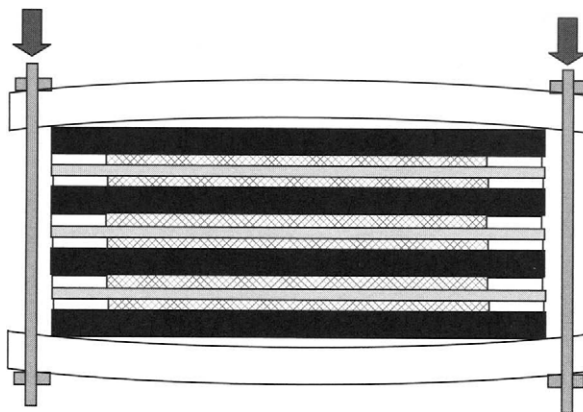


FIGURE 6-31. Bending of the end plates if too much force is applied on tie-rods around the perimeter.

by pressure-sensitive films (which register only the highest force applied), or by pressure-sensitive electronic pads, which connected to a monitor allow inspection of compression force distribution in real time throughout the assembly process. Because of the possibility of bending, the end plates must be designed with sufficient stiffness. Alternatively, end plates with a hydraulic or pneumatic piston that applies a uniform force throughout the active area may be used. Another alternative is to put the tie-rods through the center of the plate and then design the flow field around it.

Figure 6-32 shows the compressive force distribution in a cell using a pressure-sensitive film with two different end plate designs: one with inadequate stiffness that resulted in insufficient force (*i.e.*, very bad contacts) inside the active area and one with hydraulic piston that resulted in very uniform compressive force distribution inside the active area [36].

As discussed in Chapter 4 (Figure 4-22), a pressure of 1.5 to 2.0 MPa is required to minimize the contact resistance between a gas diffusion layer and a bipolar plate. The gas diffusion layer is compressible (Figure 4-17), and the required "squeeze" may be determined by the cell design, that is, by carefully matching the thicknesses of the gas diffusion layer, gaskets, and hard-stops or recesses on the bipolar plate. If the gas diffusion layer is compressed too much, it will collapse and it will lose its main function—gas and water permeability, as is very graphically illustrated in Figure 6-33. As the compression (expressed as a percentage of gas diffusion media squeeze) is increased, the cell performance improves because of the reduced interfacial resistance. If the compression is too much, the polarization curve exhibits severe mass transport problems. Optimum compression must be experimentally determined for any gas diffusion media. The test

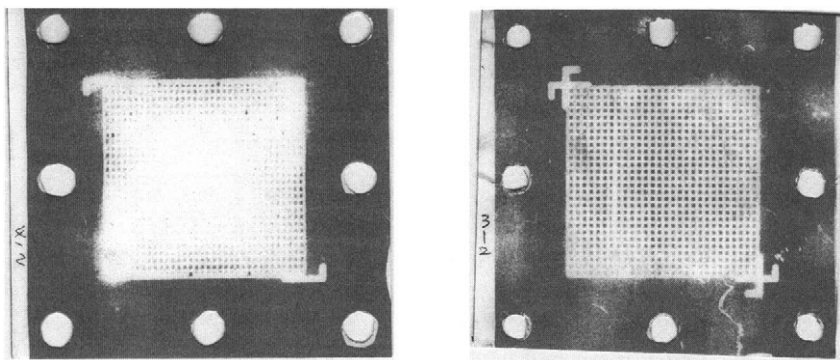


FIGURE 6-32. Compressive force distribution in a cell with inadequate stiffness of the end plates (left) and in a cell with a hydraulic piston in one of the end plates (right) [36].

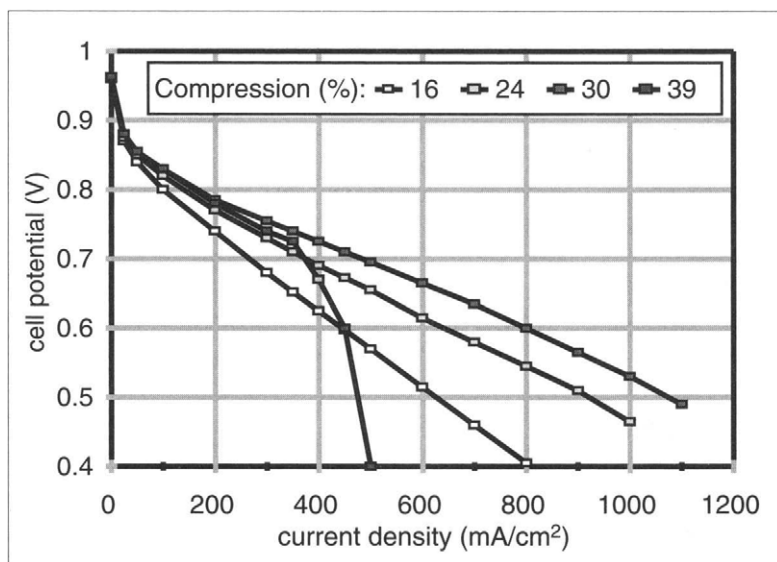


FIGURE 6-33. Effect of too much compression of the gas diffusion media on cell performance.

cells may be specially designed to allow change of compression even during the cell operation [37,38].

The stack design must also ensure that adequate clamping force is maintained during cell operation. As a result of different coefficients of thermal expansion for different materials used in a fuel cell stack, the compression force may increase or decrease when the stack reaches its operating temperature. This must be compensated by the use of coil, disc, or polyurethane springs.

## References

1. Barbir, F., PEM Fuel Cell Stack Design Considerations, in *Proc. Fuel Cell Technology: Opportunities and Challenges* (AIChE Spring National Meeting, New Orleans, LA, March 2002) pp. 520–530.
2. Barbir, F., *Development of an Air-Open PEM Fuel Cell, SBIR Phase I Final Technical Report*, A report by Energy Partners, Inc. to U.S. Army Research Laboratory, contract DAAL01-95-C-3511, 1995.
3. Ledjeff, K. and R. Nolte, New SPFC-Technology with Plastics, in O. Savadogo, P. R. Roberge, and T. N. Veziroglu (editors), *New Materials for Fuel Cell Systems* (Editions de l'Ecole Polytechnique de Montreal, Montreal, 1995) pp. 128–134.
4. Cisar, A., D. Weng, and O. J. Murphy, Monopolar Fuel Cells for Nearly Passive Operation, in *Proc. 1998 Fuel Cell Seminar* (Palm Springs, CA, November 1998) pp. 376–378.
5. Barbir, F., Progress in PEM Fuel Cell Systems Development, in *Hydrogen Energy System*, in Y. Yurum (editor), *Utilization of Hydrogen and Future Aspects*, NATO ASI Series E-295 (Kluwer Academic Publishers, Dordrecht, The Netherlands, 1995) pp. 203–214.
6. Chow, C. Y. and B. M. Wozniczka, Electrochemical fuel cell stack with humidification section located upstream from the electrochemically active section, U.S. Patent No. 5,382,478, 1995.
7. Reiser, C. A. and R. D. Sawyer, Solid polymer electrolyte fuel cell stack water management system, U.S. Patent No. 4,769,297, 1988.
8. Koh, J. -H., H. K. Seo, C. G. Lee, Y.-S. Yoo, and H. C. Lim, Pressure and Flow Distribution in Internal Gas Manifolds of a Fuel Cell Stack, *Journal of Power Sources*, Vol. 115, 2003, pp. 54–65.
9. Daugherty, R. L. and J. B. Franzini, *Fluid Mechanics with Engineering Applications*, Seventh ed. (McGraw-Hill, New York, 1977).
10. Watkins, D. S., K. W. Dircks, and D. G. Epp, Novel fuel cell fluid flow field plate, U.S. Patent No. 4,988,583, 1991.
11. Watkins, D. S., K. W. Dircks, and D. G. Epp, Fuel cell fluid flow field plate, U.S. Patent No. 5,108,849, 1992.
12. Cavalca, C., S. T. Homeyer, and E. Walsworth, Flow field plate for use in a proton exchange membrane fuel cell, U.S. Patent No. 5,686,199, 1997.
13. Rock, J. A., Serially-linked serpentine flow channels for PEM fuel cell, U.S. Patent No. 6,309,773, 2001.
14. Rock, J. A., Mirrored serpentine flow channels for fuel cell, U.S. Patent No. 6,099,984, 2000.

15. Ledjeff, K., A. Heinzel, F. Mahlendorf, and V. Peinecke, Die Reversible Membran-Brennstoffzelle, in *Elektrochemische Energiegewinnung, Dechema Monographien*, Vol. 128, 1993, p. 103.
16. Nguyen, T. V., Gas Distributor Design for Proton-Exchange-Membrane Fuel Cells, *Journal of the Electrochemical Society*, Vol. 143, No. 5, 1996, pp. L103–L105.
17. Barbir, F., J. Neutzler, W. Pierce, and B. Wynne, Development and Testing of High Performing PEM Fuel Cell Stack, in *Proc. 1998 Fuel Cell Seminar* (Palm Springs, CA, 1998) pp. 718–721.
18. Barbir, F., M. Fuchs, A. Husar, and J. Neutzler, *Design and Operational Characteristics of Automotive PEM Fuel Cell Stacks, Fuel Cell Power for Transportation*, SAE SP-1505 (SAE, Warrendale, PA, 2000) pp. 63–69.
19. Wilson, M. S., T. E. Springer, J. R. Davey, and S. Gottesfeld, Alternative Flow Field and Backing Concepts for Polymer Electrolyte Fuel Cells, in S. Gottesfeld, G. Halpert, and A. Langrebe (editors), *Proton Conducting Membrane Fuel Cells I*, The Electrochemical Society Proceedings Series, PV 95-23 (Pennington, NJ, 1995) p. 115.
20. Issacci, F. and T. J. Rehg, Gas block mechanism for water removal in fuel cells, U.S. Patent No. 6,686,084, 2004.
21. Chapman, A. R. and I. M. Mellor, Development of BioMimetic<sup>TM</sup> Flow-Field Plates for PEM Fuel Cells, in *Proc. 8<sup>th</sup> Grove Fuel Cell Symposium* (London, September 2003).
22. Tüber, K., A. Oedegaard, M. Hermann, and C. Hebling, Investigation of Fractal Flow Fields in Portable PEMFC and DMFC, in *Proc. 8<sup>th</sup> Grove Fuel Cell Symposium* (London, September 2003).
23. Zawodzinski, C., M. S. Wilson, and S. Gottesfeld, Metal Screen and Foil Hardware for Polymer Electrolyte Fuel Cells, in S. Gottesfeld and T. F. Fuller (editors), *Proton Conducting Membrane Fuel Cells II, Electrochemical Society Proceedings*, Vols. 98–27, 1999, pp. 446–456.
24. Damiano, P. J., Fuel cell structure, U.S. Patent No. 4,129,685, 1978.
25. Wilkinson, D. P. and O. Vanderleeden, Serpentine Flow Field Design, in W. Vielstich, A. Lamm, and H. Gasteiger (editors), *Handbook of Fuel Cell Technology—Fundamentals, Technology and Applications*, Vol. 3, Part 1 (John Wiley & Sons, New York, 2003) pp. 315–324.
26. Mathias, M., Design, Engineering, Modeling, and Diagnostics, NSF Workshop on Engineering Fundamentals of Low Temperature PEM Fuel Cells (Arlington, VA, November 2001) ([http://electrochem.cwru.edu/NSF/presentations/NSF\\_Mathias\\_Diagnostics.pdf](http://electrochem.cwru.edu/NSF/presentations/NSF_Mathias_Diagnostics.pdf)).
27. Mathias, M. F., J. Roth, J. Fleming, and W. Lehnert, Diffusion Media Materials and Characterization, in W. Vielstich, A. Lamm, and H. Gasteiger (editors), *Handbook of Fuel Cell Technology—Fundamentals, Technology and Applications*, Vol. 3, Part 1 (John Wiley & Sons, New York, 2003) pp. 517–537.
28. Liu, H., T. Zhou, and L. You, Development of Unified PEM Fuel Cell Models, in *DOE Fuel Cells for Transportation Program* (Annual National Laboratory R&D Meeting, Oak Ridge National Laboratory, June 6–8, 2001).
29. Crane Co., Flow of Fluids Through Valves, Fittings and Pipe, Technical Paper No. 410 (Author, New York, 1982).

30. Bird, R. B., W. E. Stewart, and E. N. Lightfoot, *Transport Phenomena* (John Wiley & Sons, New York, 1960).
31. Kee, R. J., P. Korada, K. Walters, and M. Pavol, A Generalized Model of the Flow Distribution in Channel Networks of Planar Fuel Cells, *Journal of Power Sources*, Vol. 109, Issue 1, 2002, pp. 148–159.
32. Dullien, F.A.L., *Porous Media: Fluid Transport and Pore Structure*, Second ed. (Academic Press, San Diego, CA, 1992).
33. Barbir, F., H. Gorgun, and X. Wang, Relationship Between Pressure Drop and Cell Resistance as a Diagnostic Tool for PEM Fuel Cells, *Journal of Power Sources* [in press] 2005.
34. Lindon, T. C., *Heat Transfer—Professional Version* (Prentice Hall, Englewood Cliffs, NJ, 1993).
35. Wilson, M. S., S. Moeller-Holst, D. M. Webb, and C. Zawodzinski, Efficient Fuel Cell Systems, 1999 Annual Progress Report: *Fuel Cells for Transportation* (U.S. Department of Energy, Washington D.C., 1999) pp. 80–83.
36. Wang, X. and B. Zhang, Pressurized Endplates for Uniform Pressure Distributions in PEM Fuel Cells, First International Conference on Fuel Cell Development and Deployment (Storrs, CT, March 2004).
37. Ihonen, J., F. Jaouen, G. Lindbergh, and G. Sundholm, A Novel Polymer Electrolyte Fuel Cell for Laboratory Investigations and In-Situ Contact Resistance Measurements, *Electrochimica Acta*, Vol. 46, Issue 19, 2001, pp. 2899–2911.
38. Higier, A., A. Husar, G. Haberer, and H. Liu, Design of a Single Cell, Variable Compression PEM Fuel Cell Test Fixture, in *Proc. 2002 Fuel Cell Seminar* (Palm Springs, CA, 2002) p. 45.

## Problems

### Problem No. 1:

Determine the required number of cells and cell active area for a fuel cell stack that has to generate 50kW at 120 Volts. Polarization curve may be approximated by:

$$V_{\text{cell}} = 0.85 - 0.2i \quad (\text{where } i \text{ is in } \text{A cm}^{-2}).$$

The stack should have efficiency of 0.5.

### Problem No. 2:

For an H<sub>2</sub>/O<sub>2</sub> fuel cell polarization curve determined by the following parameters:

T = 60°C, P = 101.3 kPa, i<sub>0</sub> = 0.002 A cm<sup>-2</sup>, R = 0.21 Ohm·cm<sup>2</sup>, i<sub>L</sub> = 2 A cm<sup>-2</sup>, i<sub>loss</sub> = 1.2 mA cm<sup>-2</sup>, determine the efficiency at 0.6 V and 0.7 V. Also, determine the efficiency at 20% of nominal power for both V<sub>nom</sub> = 0.6 V and V<sub>nom</sub> = 0.7 V.

**Problem No. 3:**

A fuel cell has  $100\text{-cm}^2$  active area covered by six parallel channels on the cathode. Each channel is 0.8 mm wide and 0.8 mm deep, with equal spacing between the channels of 0.8 mm. The fuel cell generates  $0.8\text{ A/cm}^2$ . Air at the inlet is fully saturated at  $60^\circ\text{C}$ . Pressure at the inlet is 200 kPa, and there is a 15-kPa pressure drop through the flow field. Oxygen stoichiometric ratio is 2.5. Calculate the velocity and Reynolds number at the air inlet and outlet (neglect liquid water at the outlet).

**Problem No. 4:**

For a fuel cell from Problem 3, calculate the heat generated at  $0.65\text{ V}$  and  $1\text{ A cm}^{-2}$  by using the Equation 6-41 and by doing a detailed mass and heat balance analysis (assume hydrogen is supplied in dead-end mode saturated at  $60^\circ\text{C}$  and that net water transport through the membrane is such that there is no water accumulation on the anode side). Explain the difference in results.

**Problem No. 5:**

Calculate the amount of liquid water produced in the cell from Problem 3. This liquid is probably dispersed in numerous droplets. However, assuming that a liquid water film is formed at the bottom of the channel, and that water in the film is moving with velocity  $\frac{1}{3}$  of the air velocity, calculate the depth of the film at the fuel cell exit, or the percentage of the channel's cross-sectional area filled with liquid water.

**Problem No. 6:**

Calculate the temperature at a center of the long, narrow flow field ( $2.2\text{ cm}$ ), of a fuel cell operating at  $0.75\text{ V}$  and  $0.33\text{ A cm}^{-2}$ . Cooling is obtained at the edge of the cell by flowing air at  $25^\circ\text{C}$  ( $h = 50\text{ W m}^{-2}\text{ K}^{-1}$ ). The bipolar plate is made out of graphite/polymer mixture with  $k = 19\text{ W m}^{-1}\text{ K}^{-1}$ , and it is 2 mm thick in the active area and 3 mm thick at the border. The border around the active area is 8 mm wide.

**Quiz**

1. A flow field is:

- a) flow channels that feed each cell in the fuel cell stack
- b) a "maze" of channels on the surface of the bipolar plate
- c) a plane in which the fuel cell electrochemical reaction takes place

2. The velocity in the flow field channel does not depend on:
  - a) channel length
  - b) channel depth
  - c) channel width
3. One of the most important features of the flow field is:
  - a) allows the flow of the reactant gases through each cell with minimum pressure drop
  - b) uniform supply of reactants over the entire active area
  - c) allows significant heat removal by circulating excess air
4. Nonuniform distribution of gases over the active area results in:
  - a) "starving" regions
  - b) high pressure drop
  - c) "hick-ups"
5. The flow in the fuel cell channels is typically:
  - a) laminar
  - b) turbulent
  - c) mixed/transient
6. A characteristic of laminar flow is:
  - a) pressure drop is minimal
  - b) pressure drop is higher than in turbulent flow
  - c) pressure drop is directly proportional to the flow rate
7. If all the product water in a fuel cell is in liquid form, its volume compared with the volume of air exiting the fuel cell would be:
  - a) an order of magnitude less
  - b) about the same
  - c) several orders of magnitude less
8. As oxygen is consumed along the channel, O<sub>2</sub> content in air:
  - a) linearly decreases
  - b) decreases faster near the entrance
  - c) decreases faster near the exit
9. Removal of heat from the fuel cell stack is:
  - a) to keep the stack at a desired temperature
  - b) to maintain a desired efficiency
  - c) to maintain some liquid water in the membrane

10. "Squeezing" the gas diffusion layer:

- a) always improves the fuel cell performance because it reduces the interfacial resistance
- b) it improves the performance only up to a certain "squeeze"; if the squeeze is excessive it has an adverse effect
- c) it has nothing to do with performance—it only prevents overboard leaks

# CHAPTER 7

## 7. Fuel Cell Modeling

Modeling plays a significant and important role in fuel cell design and development process. Because of its importance, modeling is initiated early into a fuel cell development cycle, as shown in Figure 7-1 [1]. The flowchart illustrates a typical procedure in fuel cell development, where the process begins with a set of requirements. Requirements include power and energy requirements, environmental operating conditions, size and volume limitations, safety specifications, and others. Along with the requirements, knowledge of materials, processes, and material interactions is necessary to properly construct a fuel cell stack. Once several designs are down-selected, modeling of the designs is performed to determine how well the candidate systems satisfy requirements. The modeling helps the designer further down-select designs to fabricate and test. The tests performed on the final designs can either result in a final prototype or result in an iteration of existing designs for improvement. Reliable diagnostics are needed not only to find out what is wrong with the existing design so that it can be improved, but also to calibrate and verify the models and assumptions used in developing them.

This design iteration loop can be quite lengthy and frequent, especially when stringent requirements or poor modeling capabilities exist. On the contrary, improvements in modeling capability can help the designer find and improve on existing designs that satisfy stringent requirements. Hence, modeling has a critical role in the fuel cell design and development process. A designer can use an accurate and robust model to design and develop fuel cell stacks more efficiently and often with better performance and lower manufacturing cost.

Using fuel cell modeling as a successful design tool requires the model to be robust, accurate, and able to provide usable answers quickly. In terms of robustness, the model should be able to predict fuel cell performance under a large range of operating conditions. For example, a PEM fuel cell can be operating at different temperature, humidity level, and fuel mixture. A robust model should be able to predict fuel cell performance under varying conditions. The model must also predict fuel cell performance

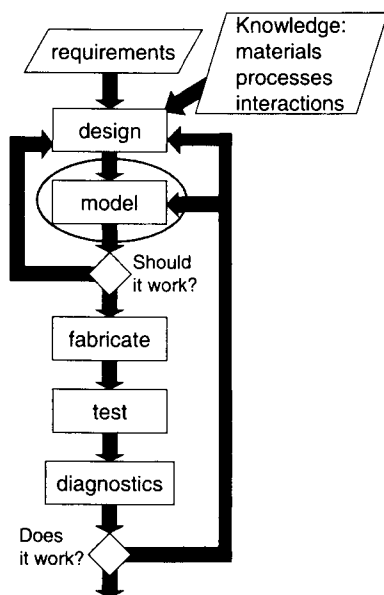


FIGURE 7-1. Role of modeling and diagnostics in the fuel cell development process.

accurately. It should be mentioned here that accuracy does not necessarily mean that a model should accurately predict the absolute value of all the physical phenomena being modeled at any point in space and time. Instead, a model should accurately predict the relative values or the trends (e.g., an increase in value of one parameter should result in either no, low, moderate, or significant increase or decrease of another parameter). Accuracy can be contributed to using the correct assumptions, using the correct properties and other numerical input parameters, predicting the correct physical phenomena by using the correct governing equations, and being able to match the modeling results with experimental data. However, enhancing model robustness and accuracy often trades off with computational efficiency. To provide answers quickly, the designer must select a model that balances robustness, accuracy, and computational effort.

## 7.1. Theory and Governing Equations

Physical phenomena occurring within a PEM fuel cell can in general be represented by the solution of conservation equations for mass, momentum, energy, species, and current transport. In addition, equations that deal specifically with phenomena in a fuel cell may be used where applicable, such as:

- Darcy's equation for fluid flow in conduits and porous media,
- Fick's Law for diffusion,
- Stefan–Maxwell equation for multispecies diffusion,
- Fourier's Law for heat conduction,
- Faraday's Law for relationship between electrical current and consumption of reactants in an electrochemical reaction,
- Butler–Volmer equation for relationship between electrical current and potential,
- Ohm's Law of electrical current conduction.

Also, empirical equations, particularly those describing water behavior in the polymer membrane and related phenomena, are often used in modeling, in absence of equations that describe the actual physical phenomena.

Any model is as good as the assumptions that it is built upon. Assumptions are needed to simplify the model. It is important to understand the assumptions in order to understand the model's limitations and to accurately interpret its results. Common assumptions used in fuel cell modeling are:

- ideal gas properties,
- ideal gas mixtures,
- incompressible flow,
- laminar flow,
- isotropic and homogeneous membrane and electrode structures,
- negligible ohmic potential drop in solid components,
- the mass and energy transport through porous structures of porosity  $\epsilon$  is modeled from macroperspective using the volume-averaged conservation equations.

### 7.1.1. Conservation of Mass

The general equation for mass conservation, which is valid for all the processes inside a fuel cell such as fluid flow, diffusion, phase change, and electrochemical reactions, is:

$$\frac{\partial \rho}{\partial t} + \nabla \cdot (\rho v) = 0 \quad (7-1)$$

where:

$\rho$  = density,  $\text{kg m}^{-3}$

$v$  = velocity vector,  $\text{m s}^{-1}$

$\nabla$  = operator,  $\frac{d}{dx} + \frac{d}{dy} + \frac{d}{dz}$

The transient term represents accumulation of mass with time, and the second term represents the change in mass flux.

### 7.1.2. Conservation of Momentum

Momentum conservation is described by the following equation:

$$\frac{\partial(\rho\mathbf{v})}{\partial t} + \nabla \cdot (\rho\mathbf{v}\mathbf{v}) = -\nabla p + \nabla \cdot (\mu^{\text{eff}}\nabla\mathbf{v}) + S_m \quad (7-2)$$

where:

$p$  = fluid pressure, Pa

$\mu^{\text{eff}}$  = mixture average viscosity,  $\text{kg m}^{-1} \text{s}^{-1}$

$S_m$  = momentum source term

The transient term in the momentum conservation equation represents the accumulation of momentum with time, and the second term describes advection momentum flux. The first two terms on the right side of the momentum conservation equation represent momentum imparted due to pressure and viscosity, respectively. The source term is different for different regions of the fuel cell, namely:

For gas channels:

$$S_m = 0 \quad (7-3)$$

For backing layers and voids of the catalyst layers:

$$S_m = -\frac{\mu}{K} \epsilon v \quad (7-4)$$

where:

$K$  = permeability of the gas diffusion layer (or the catalyst layer),  $\text{m}^2$   
 $\epsilon$  = porosity of the gas diffusion layer

This source term for the momentum conservation equation represents a pressure drop arising from Darcy's drag force imposed by the pore walls on the fluid.

For water transport in polymer phase, an additional source term is electrokinetic permeability:

$$S_m = -\frac{\mu}{K_p} \epsilon_m x_m v + \frac{K_\phi}{K_p} c_f n_f F \nabla \phi_m \quad (7-5)$$

where:

- $\epsilon_m$  = membrane water porosity
- $x_m$  = volume fraction of ionomer in the catalyst layer
- $K_\phi$  = electrokinetic permeability,  $m^2$
- $K_p$  = hydraulic permeability of the membrane,  $m^2$
- $c_f$  = concentration of fixed charge,  $mol\ m^{-3}$
- $n_f$  = charge number of the sulfonic acid ions
- $F$  = Faraday's constant
- $\phi_m$  = ionomer phase potential

### 7.1.3. Conservation of Energy

Conservation of energy for any domain in a PEM fuel cell is described by:

$$(\rho c_p)_{eff} \frac{\partial T}{\partial t} + (\rho c_p)_{eff} (\mathbf{v} \cdot \nabla T) = \nabla \cdot (k_{eff} \nabla T) + S_e \quad (7-6)$$

where:

- $c_p$  = mixture-averaged specific heat capacity,  $J\ kg^{-1}\ K^{-1}$
- $T$  = temperature,  $K$
- $k$  = thermal conductivity,  $W\ m^{-1}\ K^{-1}$
- $S_e$  = energy source term

Subscript "eff" represents effective properties for the porous media [2]:

$$(\rho c_p)_{eff} = (1 - \epsilon) \rho_s c_{p,s} + \epsilon \rho c_p \quad (7-7)$$

$$k_{eff} = -2k_s + \left[ \frac{\epsilon}{2k_s + k} + \frac{1 - \epsilon}{3k_s} \right]^{-1} \quad (7-8)$$

Where  $\rho_s$ ,  $c_{p,s}$ , and  $k_s$  represent the density, specific heat capacity, and thermal conductivity of the solid matrix, respectively.

The source term in the energy conservation equation may include heat from reactions, Ohmic heating, and/or heat of evaporation or condensation in case there is a phase change.

In gas channels, the only possible heat source or sink is phase change, that is, condensation of water vapor present in the gas streams as a heat source and evaporation of liquid water present in the channels (in the form of a film or droplets) as a heat sink.

Evaporation will happen only if both of the following conditions are satisfied:

- there is liquid water present in the gas stream,  $x_{H2O(l)} > 0$ , and
- the gas is not saturated,  $x_{H2O(g)} < x_{sat}$  (saturated gas may become unsaturated if either the pressure decreases or the temperature increases).

Condensation will happen only if the gas is already fully saturated,  $x_{H2O(g)} > x_{sat}$ , and the temperature of the gas drops (*i.e.*, in contact with cooler parts of the fuel cell). Condensation may also happen when the reactant gas or its constituents (hydrogen or oxygen) "disappear" in the electrochemical reaction, although this does not happen in the channels but rather in the catalyst layer.

The maximum rate of condensation (in  $\text{mol s}^{-1}$ ) is:

$$N_{H2O,cond} = \frac{P - P_{sat}}{P - P_{sat}} \frac{y_w}{N_{H2O(v)in}} N_{H2O(v)in} \quad (7-9)$$

where water vapor molar fraction,  $y_w$ , is:

$$y_w = \frac{N_{H2O(v)in}}{N_{H2O(v)in} + N_{gas}} \quad (7-10)$$

The same equation may be used for evaporation (when  $P_{sat}/y_w > P$ ), assuming there is liquid water present in the gas stream.

$$N_{H2O,evap} = \frac{\frac{P_{sat}}{y_w} - P}{P - P_{sat}} N_{H2O(v)in} \quad (7-11)$$

However, in case of evaporation it may be easier to deal with water content ( $x$  or  $\chi$ ), defined as mass or molar ratio of water vapor and dry gas, respectively:

$$N_{H2O,evap} = \min[N_{H2O(l)}, N_{gas}(\chi_{sat} - \chi)] \quad (7-12)$$

The actual, local rate of evaporation would depend on local conditions, particularly on water-gas interface. Bosnjakovic [3] defines the rate of heat exchange during the process of evaporation using the evaporation coefficient,  $\sigma$ , defined as the mass flow rate of dry air that must be saturated in order to evaporate  $(x_{sat} - x_{H2O(g)})$  amount of water over  $1\text{m}^2$  of contact surface. In that case:

$$S_e = -\sigma A_{fg} (x_{sat} - x_{H2O(g)}) \Delta h_{fg} \quad (7-13)$$

where:

- $\sigma$  = evaporation coefficient,  $\text{kg m}^{-2} \text{s}^{-1}$   
 $A_{fg}$  = phase-change surface area per unit volume,  $\text{m}^{-1}$   
 $x_{sat}$  = maximum mass fraction of water vapor in dry gas (at saturation),  $\text{kg}_w \text{kg}_g^{-1}$   
 $x_{H2O(g)}$  = fraction of water vapor in dry gas,  $\text{kg}_w \text{kg}_g^{-1}$   
 $\Delta h_{fg}$  = heat of evaporation,  $\text{J/kg}$

The evaporation coefficient,  $\sigma$ , may be determined from the dimensionless Lewis factor,  $\sigma c_p / \alpha$ , which is given by the following equation derived from analogy between heat and mass transport [3]:

$$\frac{\sigma c_p}{\alpha} = \left[ \frac{D \rho c_p}{k(l+x)} \right]^{l-n} \left( \frac{v_h}{v_d} \right)^{m-n} \frac{\frac{M_w}{M_g} + x}{x_{sat} - x} \ln \frac{\frac{M_w}{M_g} + x_{sat}}{\frac{M_w}{M_g} + x} \quad (7-14)$$

where:

- $\alpha$  = coefficient of heat transfer between water surface and gas,  $\text{W m}^2 \text{K}^{-1}$   
 $D$  = diffusion of water vapor through gas,  $\text{m}^2 \text{s}^{-1}$   
 $\rho$  = density of humid air,  $\text{kg m}^{-3}$   
 $c_p$  = heat capacity,  $\text{J kg}^{-1} \text{K}^{-1}$   
 $k$  = thermal conductivity of humid gas,  $\text{W m}^{-1} \text{K}^{-1}$   
 $x$  = fraction of water vapor in dry gas,  $\text{kg}_w \text{kg}_g^{-1}$   
 $v_h$  = kinematic viscosity of humid gas,  $\text{m}^2 \text{s}^{-1}$   
 $v_d$  = kinematic viscosity of dry gas,  $\text{m}^2 \text{s}^{-1}$   
 $M_w$  = molecular mass of water,  $\text{kg kmol}^{-1}$   
 $M_g$  = molecular mass of gas,  $\text{kg kmol}^{-1}$   
 $m$  = coefficient,  $\sim 0.75$  [3]  
 $n$  = coefficient,  $\sim 0.33$  [3]

In gas diffusion layers, the possible heat sources are due to Ohmic resistance through solid and phase change in pores (again, evaporation is possible only if there is liquid water present, i.e.,  $x_{H2O(l)} > 0$ , and the gas is not saturated, i.e.,  $x_{H2O(g)} < x_{sat}$ ):

$$S_e = \frac{i_e^2}{\kappa_s^{\text{eff}}} - \sigma A_{fg} (x_{sat} - x_{H2O(g)}) (\Delta h_{fg}) \quad (7-15)$$

where:

- $i_e$  = current density,  $\text{A m}^{-2}$   
 $\kappa_s^{\text{eff}}$  = effective electric conductivity of the gas diffusion layer,  $\text{S cm}^{-1}$

In catalyst layers, the source term includes the heat released by the electrochemical reaction, heat generated due to ionic and electronic resistance, and heat of water evaporation (again, only if there is liquid water present, and the gas is not saturated):

$$S_e = j \left[ |\Delta V_{act}| - \frac{T\Delta S}{nF} \right] + \left( \frac{i_m^2}{\kappa_m^{eff}} + \frac{i_e^2}{\kappa_s^{eff}} \right) - \sigma A_{fg} (x_{sat} - x_{H2O(g)}) (\Delta h_{fg}) \quad (7-16)$$

where:

$j$  = transfer current density,  $A \text{ cm}^{-3}$ , defined later by Equations 7-29 and 7-30

$\Delta V_{act}$  = activation overpotential,  $V$

$i_m$  = ionic current density,  $A \text{ cm}^{-2}$

$\kappa_m^{eff}$  = effective ionic conductivity of ionomer phase in the catalyst layer,  $S \text{ cm}^{-1}$

In the membrane, the only heat source is due to ohmic resistance:

$$S_e = \frac{i_m^2}{\kappa_m} \quad (7-17)$$

#### 7.1.4. Conservation of Species

Species conservation equations representing mass conservation for the individual gas phase species are:

$$\frac{\partial(\varepsilon\rho x_i)}{\partial t} + \nabla \cdot (\mathbf{v}\varepsilon\rho x_i) = \nabla \cdot (\rho D_i^{eff} \nabla x_i) + S_{s,i} \quad (7-18)$$

where:

$x_i$  = mass fraction of gas species,  $i = 1, 2, \dots, N$  (for example  $i = 1$  for hydrogen,  $i = 2$  for oxygen,  $i = 3$  for water vapor, etc.; liquid water may be treated as a separate species)

$S_{s,i}$  = source or sink terms for the species

The first two terms in the species conservation equation represent species accumulation and advection terms, and the first term on the right-hand side represents Fickian diffusion of species in porous medium. In the porous medium,  $D_{i,eff}$  is a function of the porosity,  $\varepsilon$ , and tortuosity,  $\tau$ . Because there is considerable lack of information for gas transport in PEM porous media, one common relationship used in literature is given by the Bruggeman model [4], where  $\tau = 1.5$ :

$$D_{i,eff} = D_i \varepsilon^\tau \quad (7-19)$$

where:

$D_i$  is the free-stream mass diffusion coefficient.

The Stefan–Maxwell equations for a multicomponent species system may be added [5] to define the gradient in mole fraction of the components:

$$\nabla y_i = RT \sum_j \frac{y_i N_i - y_j N_j}{p D_{ij}^{\text{eff}}} \quad (7-20)$$

where:

$y_i$  = gas phase mole fraction of species i

$N_i$  = superficial gas-phase flux of species i averaged over a differential volume element, which is small with respect to the overall dimensions of the system, but large with respect to the pore size [5]

$D_{ij}^{\text{eff}}$  = effective binary diffusivity of the pair i,j in the porous medium, which may be calculated for any temperature and pressure from the following equation [6]:

$$D_{ij}^{\text{eff}} = \frac{a}{p} \left( \frac{T}{\sqrt{T_{c,i} T_{c,j}}} \right)^b (p_{c,i} p_{c,j})^{1/3} (T_{c,i} T_{c,j})^{5/12} \left( \frac{1}{M_i} + \frac{1}{M_j} \right)^{1/2} \epsilon^{1.5} \quad (7-21)$$

where:

$T_c$  and  $p_c$  are the critical temperature and pressure of the species i and j

$M$  = molecular weight of species i and j

$a$  = 0.0002745 for diatomic gases,  $H_2$ ,  $O_2$ , and  $N_2$ , and  $a$  = 0.000364 for water vapor

$b$  = 1.832 for diatomic gases,  $H_2$ ,  $O_2$ , and  $N_2$ , and  $b$  = 2.334 for water vapor

The source term in the species conservation equation,  $S_{s,i}$ , is equal to zero everywhere except in the catalyst layers where the species are consumed or generated in the electrochemical reactions. In that case the source terms,  $S_{s,i}$ , for hydrogen, oxygen, water vapor, and liquid water, respectively, are:

$$S_{s,H_2} = -j_a \frac{M_{H_2}}{2F} \quad (7-22)$$

$$S_{s,O_2} = -j_c \frac{M_{O_2}}{4F} \quad (7-23)$$

$$S_{s,H_2O(g)} = \sigma A_{fg} (x_{sat} - x_{H_2O(g)}) \quad (7-24)$$

$$S_{s,H_2O(l)} = +j_c \frac{M_{H_2O}}{2F} - \sigma A_{fg} (x_{sat} - x_{H_2O(g)}) \quad (7-25)$$

In the water source term, it is assumed that water is generated as liquid and then it evaporates if the neighboring air or oxygen is not saturated.

### 7.1.5. Conservation of Charge

Current transport is described by a governing equation for conservation of charge:

$$\nabla \cdot (\kappa_s^{\text{eff}} \nabla \phi_s) = S_{\phi s} \quad (7-26)$$

for electrical current, and

$$\nabla \cdot (\kappa_m^{\text{eff}} \nabla \phi_m) = S_{\phi m} \quad (7-27)$$

for ionic current, where:

$\kappa_s^{\text{eff}}$  = electrical conductivity in the solid phase,  $\text{S cm}^{-1}$

$\kappa_m^{\text{eff}}$  = ionic conductivity in the ionomer phase (including the membrane),  $\text{S cm}^{-1}$

$\phi_s$  = solid phase potential, V

$\phi_m$  = electrolyte phase potential, V

$S_\phi$  = source term representing volumetric transfer current;  
at the anode catalyst layer  $S_{\phi s} = -j_a$  and  $S_{\phi m} = j_a$ ;

at the cathode catalyst layers  $S_{\phi s} = j_c$ ,  $S_{\phi m} = -j_c$ ; and

$S_\phi = 0$  elsewhere.

An additional complication is that the ionomer phase conductivity,  $\kappa_m$ , strongly depends on temperature and water content inside the ionomer,  $\lambda$ , which in turn is a function of conditions (relative humidity) outside the membrane, as discussed in Chapter 4 (Equations 4-3 and 4-2, respectively).

In any volume on either anode or cathode the electronic and ionic currents generated are equal, that is,  $S_{\phi s} = S_{\phi m}$ . Also the total current (of either electrons or ions) generated in the anode catalyst layer must be equal to the total current "consumed" in the cathode catalyst layer (and also must be equal to the total current going through the membrane):

$$\int_{V_a} j_a dV = \int_{V_c} j_c dV \quad (7-28)$$

The transfer currents,  $j$ , are the result of the electrochemical reactions that take place on the catalyst surface, and are driven by the surface overpotential  $\Delta V_{\text{act}}$ , which is the potential difference between the solid phase and the electrolyte membrane:

$$\Delta V_{act} = \phi_s - \phi_m - V_{ref} \quad (7-29)$$

where the subscripts s and m indicate the solid phase and electrolyte membrane–ionomer phase, respectively. The reference potential of the electrode is zero on the anode side, and it equals the theoretical cell potential at given temperature and pressure on the cathode (combination of Equations 2-18 and 2-37):

$$V_{ref} = E_{T,P} = -\left(\frac{\Delta H}{nF} - \frac{T\Delta S}{nF}\right) + \frac{RT}{nF} \ln \left[ \left( \frac{P_{H_2}}{P_0} \right) \left( \frac{P_{O_2}}{P_0} \right)^{1/2} \right] \quad (7-30)$$

If the actual reactants concentrations, that is, partial pressures, at the catalyst surface are used in the last term of Equation 7-30,  $V_{ref}$  then also includes the concentration polarization losses:

$$V_{ref} = E_{T,P} = -\left(\frac{\Delta H}{nF} - \frac{T\Delta S}{nF}\right) + \frac{RT}{nF} \ln \left[ \left( \frac{P_{H_2}^{eff}}{P_0} \right) \left( \frac{P_{O_2}^{eff}}{P_0} \right)^{1/2} \right] \quad (7-31)$$

Referring to Figure 3.9, the overpotential defined by Equation 7-29 is positive on the anode and negative on the cathode. The cell potential is then a difference between the cathode and anode solids at the two ends of the cell:

$$V_{cell} = \phi_{s,c} - \phi_{s,a} \quad (7-32)$$

The relationship between the surface overpotential and transfer current density is given by the Butler–Volmer equation. For the anode (from Equation 3-16):

$$j_a = ai^{+}_{0,a} \left\{ \exp \left[ \frac{-\alpha_a F \Delta V_{act,a}}{Rt} \right] - \exp \left[ \frac{(1-\alpha_a) F \Delta V_{act,a}}{RT} \right] \right\} \quad (7-33)$$

where:

$j_a$  = transfer current density, A m<sup>-3</sup>

$a$  = electrocatalytic surface area per unit volume, m<sup>-1</sup>

$i^{+}_{0,a}$  = anode exchange current density per unit of electrocatalytic (Pt) surface area, A m<sup>-2</sup>

and for the cathode (from Equation 3-17):

$$j_c = ai^{+}_{0,c} \left\{ \exp \left[ \frac{-\alpha_c F \Delta V_{act,c}}{Rt} \right] - \exp \left[ \frac{(1-\alpha_c) F \Delta V_{act,c}}{RT} \right] \right\} \quad (7-34)$$

The exchange current density at different pressures and temperatures (as per Equation 3-15) is defined as [7]:

$$i^{+}_0 = i_0^{\text{ref}} \left( \frac{P_r}{P_r^{\text{ref}}} \right)^{\gamma} \exp \left[ \frac{E_C}{RT} \left( 1 - \frac{T}{T_{\text{ref}}} \right) \right] \quad (7-35)$$

The average current density is the total current generated in a fuel cell divided by the geometric area:

$$i_{\text{avg}} = \frac{1}{A} \int_{V_a} j_a dV = \frac{1}{A} \int_{V_c} j_c dV \quad (7-36)$$

## 7.2. Modeling Domains

The previous set of equations is applied to a computational domain using finite difference, finite volume, or finite element methods. The input is either the cell voltage or the average current density. In addition, the flow rates and conditions at the inlet must also be prescribed, as well as the boundary conditions at the outside walls. The boundary conditions depend on the model domain. Several typical computational domains may be of interest, namely:

- 1-D model through the membrane, z-direction as defined in Figure 7-2, for analysis of fluxes, concentrations, temperatures, and potentials in the catalyst layer and the membrane for any given conditions in the channel(s).
- 2-D model of a partial cross-section, yz-direction as defined in Figure 7-2, for analysis of fluxes and concentrations in the gas diffusion and catalyst layers. This is similar to the 1-D, but it is extended in two dimensions to include the effect of the "ribs" or "lands" between the channels. This domain may include only one side (either cathode or anode) or both sides.
- 2-D model of along-the-channel cross-section, xz-direction (Figure 7-2) for analysis of changes along the channel due to reduced concentrations of reactant gases, pressure drop, and increased concentrations of water. This domain may include only one side (typically cathode), or both sides if the effects of co- or counterflow of hydrogen on the other side are of interest.
- 3-D model of a partial cross-section, essentially a combination of two 2-D models (Figure 7-3).
- 3-D model of an entire cell, needed to analyze the flow field or heat removal from the cell (Figure 7-4).
- 3-D model of an entire stack.

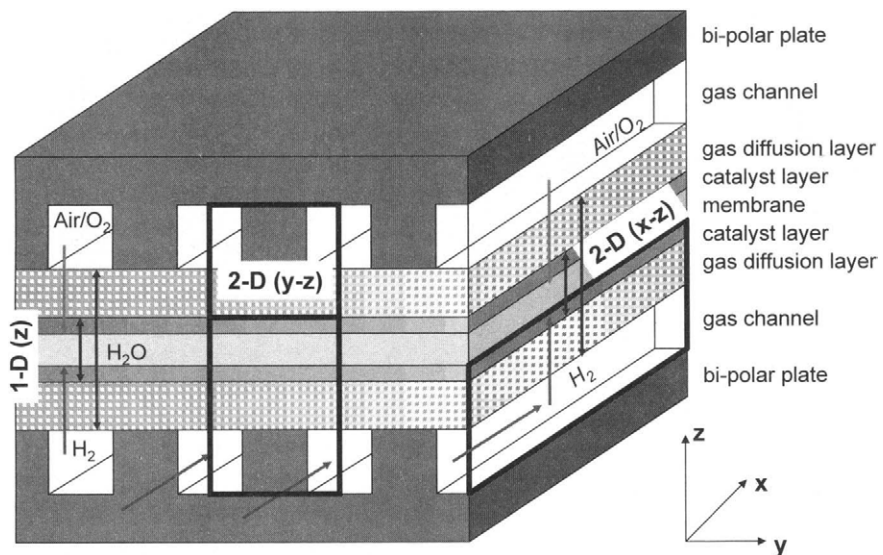


FIGURE 7-2. 1-D and 2-D modeling domains for a PEM fuel cell.

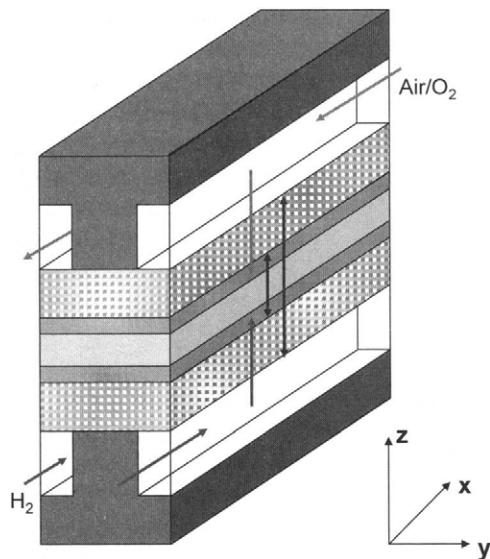


FIGURE 7-3. 3-D modeling domain for PEM fuel cell.

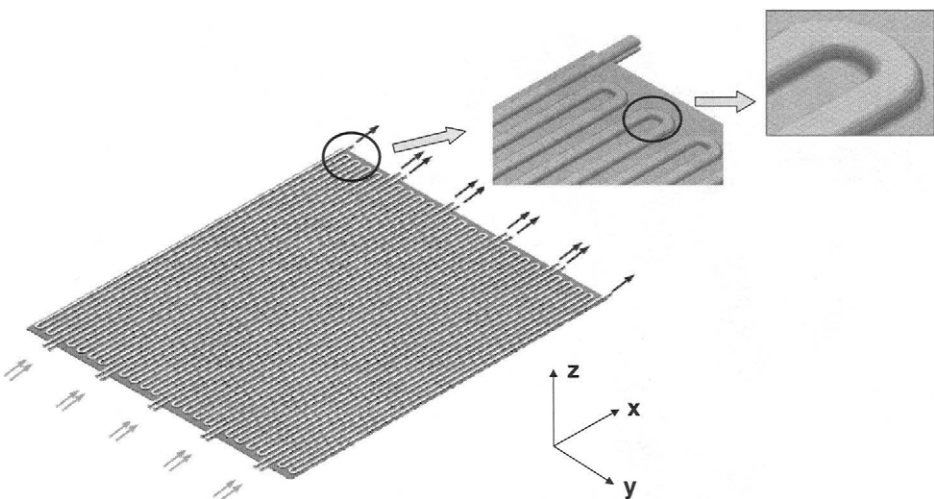


FIGURE 7-4. Entire flow field as a modeling domain [8].

Partial models (1-D or 2-D) may be very useful and may provide abundance of information with sufficient accuracy if the boundary conditions are properly selected. 3-D models are of course more comprehensive, particularly if the thermal effects are included; however, these models may be very complex and may require long computing time.

A number of numerical methods to solve this system of equations have been documented. This set of governing equations is commonly discretized using a computational grid, and solved using finite difference, finite volume or finite element methods. Numerical solution procedure, computational methods, and equation stiffness characteristics have been described in detail [9–11]. Commercial software is also becoming increasingly available, though the designer must prudently decide the best software for his or her application.

When a fuel designer decides on a solution procedure or software, care must be taken in using the model properly. Strong emphasis needs to be placed on properly validating the model before usage. Even though comparison with numerical results obtained elsewhere is acceptable, it is highly recommended to validate model predictions to experimental data as close as possible to the designer's system of interest.

### 7.3. Modeling Examples

Several examples will be used to illustrate the procedure and capability of PEM fuel cell models.

### 7.3.1. One-Dimensional through-the-Membrane Model (Bernardi–Verbrugge [5])

One of the first and most often cited PEM fuel cell models is the Bernardi–Verbrugge model [5]. This is a one-dimensional model that treats the cathode gas diffusion electrode bonded to a polymer electrolyte and transport of neutral and charged species within. The model results in a set of differential equations, which once solved allow determination of species concentration profiles, spatial dependence of the pressure and potential drop, and identification of various contributions to the total potential drop. The model is based on simplifying assumptions such as:

- Isothermal conditions throughout the domain.
- Gases behave like ideal gases.
- Total pressure within the gas diffuser is constant.
- The gases are well mixed and of uniform composition.
- Water is available on both boundaries of the domain.
- Membrane is fully hydrated as well as the pores in gas diffuser.
- Gas phase is in equilibrium with the liquid water phase.

The modeling domain includes the membrane, the catalyst layer, and the gas diffusion layer, as shown in Figure 7-5. The conditions in the gas chamber are considered to be given and do not change in z-direction (or in any direction).

The model sets the governing equations and boundary conditions for each of the three regions.

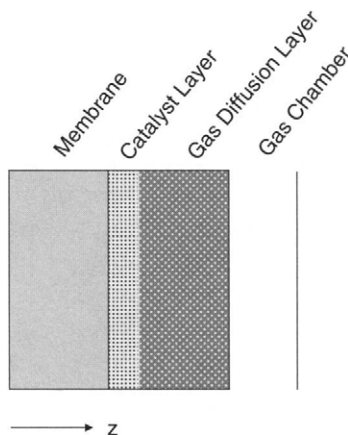


FIGURE 7-5. Modeling domain of 1-D through the membrane model (Bernardi–Verbrugge).

In the membrane, the liquid water transport inside the membrane and catalyst layers is described by a form of Schlögl's equation of motion, which in essence is a special case of Equation (7-2) with source terms as specified in Equation (7-5). According to it, the velocity of water inside the MEA is due to potential and pressure gradients:

$$u = \frac{K_\phi}{\mu} z_f c_f F \frac{d\phi_m}{dz} - \frac{K_p}{\mu} \frac{dP}{dz} \quad (7-37)$$

where:

$u$  = velocity in  $z$ -direction,  $\text{m s}^{-1}$

$K_\phi$  = electrokinetic permeability,  $\text{m}^2$

$\mu$  = viscosity,  $\text{kg m}^{-1} \text{s}^{-1}$

$z_f$  = charge number of the sulfonic acid ions inside the membrane,  $-1$

$c_f$  = concentration of sulfonic acid ions inside the membrane,  $\text{mol m}^{-3}$

$F$  = the Faraday constant

$\phi_m$  = potential in the electrolyte phase, V

$K_p$  = hydraulic permeability,  $\text{m}^2$

$P$  = pressure, Pa

The following electroneutrality in the membrane applies:

$$-z_f c_f = \sum_i z_i c_i \quad (7-38)$$

Because the only mobile ions in the membrane fluid pore are hydrogen ions:

$$-z_f c_f = c_H^+ \quad (7-39)$$

where  $c_H^+$  is proton concentration inside the membrane.

This means that the proton concentration in the membrane can be considered constant, and diffusion is not a mode of proton transport.

The potential in the membrane changes because of conduction and migration:

$$\kappa_m \frac{d\phi_m}{dz} = -i + F c_f u \quad (7-40)$$

where:

$\kappa_m$  = ionic conductivity of the membrane,  $\text{S cm}^{-1}$

$i$  = current density in the electrolyte phase,  $\text{A cm}^{-2}$

Also, current conservation in the membrane is expressed as (from Equation 7-27, with  $S_{\phi m} = 0$  and  $\kappa_m = \text{const.}$ ):

$$\frac{di}{dz} = 0 \quad (7-41)$$

The continuity equation for dissolved oxygen species (from Equation 7-18) yields:

$$u \frac{dc_{O_2}}{dz} = D_{O_2}^{\text{eff}} \frac{d^2 c_{O_2}}{dz^2} \quad (7-42)$$

The general equation of continuity for incompressible fluid flow (Equation 7-1) eliminates the velocity variable from the set of equations:

$$\frac{du}{dz} = 0 \quad (7-43)$$

In the catalyst layer, the same equations of liquid water (Equation 7-37) and charge transport (Equation 7-40) in the electrolyte phase apply, however, with effective properties,  $K_{\phi}^{\text{eff}}$ ,  $K_p^{\text{eff}}$ , and  $\kappa^{\text{eff}}$  to account for a porous nature of the catalyst layer where the electrolyte phase occupies only a portion,  $\epsilon_m$ , of the total volume.

The continuity equation for water transport in the catalyst layer accounts for water generation:

$$\rho \frac{du}{dz} = -\frac{1}{2F} \frac{di}{dz} \quad (7-44)$$

Similarly, the continuity equation for dissolved oxygen species also accounts for water production and oxygen depletion:

$$u \frac{dc_{O_2}}{dz} = D_{O_2}^{\text{eff}} \frac{d^2 c_{O_2}}{dz^2} - \left( \frac{1}{4F} - \frac{1}{2F} \frac{c_{O_2} M_{H_2O}}{\rho_{H_2O(l)}} \right) \frac{di}{dz} \quad (7-45)$$

Standard Butler–Volmer equation describes the relationship between the current generation rate and surface overpotential (Equation 7-34).

Because this model only deals with one side of the fuel cell, it is not necessary to account for the potential increase between the anode and the cathode, and in that case the overpotential is simply a difference between potentials in solid and electrolyte phases:

$$\Delta V_{\text{act},c} = \phi_s - \phi_m \quad (7-46)$$

The exchange current density takes into account the actual concentration of both oxygen and proton species at the catalyst surface:

$$i_{0,c}^+ = i_{0,c}^{\text{ref}} \left( \frac{c_{O_2}}{c_{O_2}^{\text{ref}}} \right)^{\gamma_{O_2}} \left( \frac{c_{H^+}}{c_{H^+}^{\text{ref}}} \right)^{\gamma_{H^+}} \quad (7-47)$$

The movement of electrons in the solid portion of the catalyst layer is governed by Ohm's Law:

$$i_s = -\kappa_s^{\text{eff}} \frac{d\phi_s}{dz} \quad (7-48)$$

Electroneutrality in the catalyst layer must be preserved, thus:

$$\frac{di_s}{dz} + \frac{di}{dz} = 0 \quad (7-49)$$

In the gas diffusion layer, the transport of gaseous species is described by the Stefan–Maxwell equation (7-20) for three species, namely oxygen, nitrogen, and water vapor. Although in the catalyst layer oxygen is considered to be dissolved in water present in the electrolyte phase, the amount of oxygen and nitrogen dissolved in liquid water traveling through the gas diffusion layer is negligible compared with the amount of oxygen and nitrogen in the gas phase. The equation of conservation of species then takes the form:

$$\frac{dN_{O_2,g}}{dz} = 0 \quad (7-50)$$

Because nitrogen does not participate in the reaction, there is no net movement of nitrogen in the gas diffusion layer, thus:

$$N_{N_2,g} = 0 \quad (7-51)$$

Also, water vapor in the pores of the gas diffusion layer is considered to be equilibrated with liquid water present in the pores, that is,  $y_{H_2O} = y_{H_2O}^{\text{sat}}$ , thus:

$$\frac{dy_{H_2O}}{dz} = 0 \quad (7-52)$$

where  $y_{H_2O}$  is the molar fraction of water vapor in the gas diffusion layer, that is:

$$y_{O_2} + y_{N_2} + y_{H_2O} = 1 \quad (7-53)$$

Incorporation of Equations 7-50 through 7-53 in the Stefan–Maxwell set of equations (7-20) yields:

$$\frac{P}{RT} \frac{D_{H_2O-N_2}^{\text{eff}}}{y_{N_2}} \frac{dy_{N_2}}{dz} = \frac{I}{4F} \frac{D_{H_2O-N_2}^{\text{eff}}}{D_{N_2-O_2}^{\text{eff}}} + N_{H_2O} \quad (7-54)$$

where:

$$N_{H_2O} = \frac{I}{4F} y_{H_2O}^{\text{sat}} \left[ 1 - y_{H_2O}^{\text{sat}} - y_{N_2} + y_{N_2} \frac{D_{N_2-O_2}^{\text{eff}}}{D_{H_2O-N_2}^{\text{eff}}} \right]^{-1} \quad (7-55)$$

Because there are no charged species traveling through the gas diffusion layer, water movement is solely due to pressure gradient, and Schrödiger's equation (7-37) reduces to:

$$u = -\frac{K_p^{\text{eff}}}{\mu} \frac{dP}{dz} \quad (7-56)$$

where  $K_p^{\text{eff}}$  accounts for porous nature of the gas diffusion layer including the wet-proofing.

Continuity for water species in the gas diffusion layer means:

$$\rho \frac{du}{dz} = -\frac{dN_{H_2O}}{dz} \quad (7-57)$$

Unlike the general model presented in the section 7.1. Theory and Governing Equations, the Bernardi–Verbrugge model needs the boundary conditions at the interfaces, namely membrane–catalyst layer and catalyst layer–gas diffusion layer interfaces. The general model treats all three regions as a single domain and uses the same governing equations in all the regions; only the source terms are different. As a result of such an approach, no interfacial conditions are required to be specified at internal boundaries between the regions.

At the membrane,  $z = 0$ , the boundary conditions are:

$$\phi_m = 0 \quad P = P_0 \quad c_{O_2} = 0 \quad (7-58)$$

At the membrane–catalyst layer interface,  $z = \delta_m$ , flux of liquid water, flux of dissolved oxygen and current in the electrolyte phase are continuous, and therefore the following boundary conditions apply:

$$\kappa \frac{d\phi_m}{dz} \Big|_m = \kappa^{\text{eff}} \frac{d\phi_m}{dz} \Big|_{cl} \quad (7-59)$$

and

$$u|_m = \epsilon_m u|_{cl}$$

where  $\epsilon_m$  is volume fraction of polymer in the catalyst layer, and

$$D_{O_2} \frac{dc_{O_2}}{dz} \Big|_m = D_{O_2}^{\text{eff}} \frac{dc_{O_2}}{dz} \Big|_{cl} \quad (7-60)$$

Also, at the membrane–catalyst layer interface,  $z = \delta_m$ , current in the solid phase is equal to zero:

$$\frac{d\phi_s}{dz} \Big|_{cl} = 0 \quad (7-61)$$

At the catalyst layer–gas diffusion layer interface,  $z = \delta_m + \delta_{cl}$ , the current in the solid phase and total flux of water are continuous:

$$\left. \begin{array}{l} \kappa_s^{\text{eff}} \frac{d\phi_s}{dz} \Big|_{cl} = \kappa_s^{\text{eff}} \frac{d\phi_s}{dz} \Big|_{gdl} \\ \rho \epsilon_m \epsilon_w u|_{cl} = \rho u|_{cl} + N_{H_2O} \end{array} \right\} \quad (7-62)$$

The dissolved oxygen concentration in the membrane phase of the catalyst layer is related to the oxygen gas-phase concentration in the gas diffuser by a Henry's Law constant,  $K_{O_2}$ , defined by:

$$c_{O_2}^{\text{sat}} = (1 - y_{N_2} - y_{H_2O}^{\text{sat}}) \frac{P_{in}}{K_{O_2}} \quad (7-63)$$

The ionic current at the catalyst layer–gas diffusion layer interface is equal to zero:

$$\frac{d\phi_m}{dz} \Big|_{gdl} = 0 \quad (7-64)$$

At the face of the gas diffuser,  $z = \delta_m + \delta_{cl} + \delta_{gdl}$ , which is in contact with the gas chamber:

$$p = p_{in} \quad (7-65)$$

$$y_{N2} = y_{N2}^{in}$$

Both  $p_{in}$  and  $y_{N2}^{in}$  are known.

Once the set of equations (7-37 through 7-57) with boundary conditions (Equations 7-58 through 7-65) are simultaneously solved, this model provides useful information about the spatial variation of reaction rate, current density, and oxygen concentration within the modeling domain (Figure 7-6).

The current density is constant throughout the membrane region. In the catalyst layer, the electrolyte phase gradually transfers its current to the solid, electrically conductive phase, and the membrane phase current density decreases to zero at the catalyst layer–gas diffusion layer interface. For very low current density, the reaction rate is constant throughout the catalyst layer. At higher current densities almost all the activity happens in a portion of the catalyst layer next to the gas diffusion layer, where oxygen is rapidly depleted.

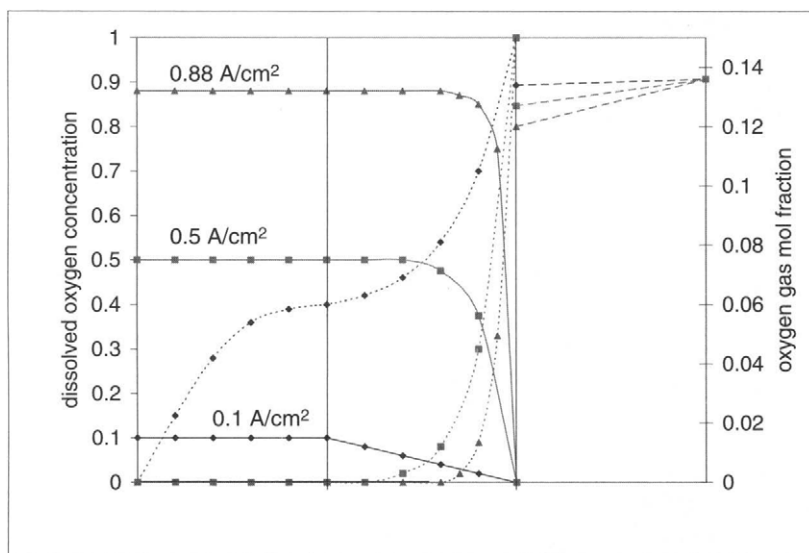


FIGURE 7-6. Sample of results generated by the Bernardi–Verbrugge model [5]—spatial distribution of current density (solid lines) and oxygen concentration (dotted line) in the electrolyte phase and oxygen mol fraction in the gas diffusion layer (dashed line).

### 7.3.2. One-Dimensional Catalyst Layer Model (You–Liu [12])

In this model, similar to Weisbrod *et al.* [13], the catalytic layer is described as a macro-pseudo-homogeneous film with the following assumptions:

- The potential drop in solid matrix is negligible as compared with the potential drop in the electrolyte phase.
- The catalyst Pt particle is uniformly distributed throughout the layer.
- The water content in the ionomer is constant.
- Oxygen diffusion coefficient is constant.
- Isothermal conditions.

The model is derived from a basic mass-current balance by the control volume approach. A relaxation method is used to solve the two-point boundary problem. The effects of different parameters on the catalyst layer are studied in detail. The discussions in this paper may help in the optimization design of cathode catalyst layer in PEM fuel cells.

The composite catalyst layer is considered to be an effective, homogeneous medium of uniform thickness. The decrease of oxygen molar flux in a control volume is balanced by the increase of proton current density:

$$\frac{di_z}{dz} = -4F \frac{dN_{O_2}}{dz} \quad (7-66)$$

When the cathode electrochemical reaction,  $O_2 + 4H^+ + 4e^- \rightarrow 2H_2O$ , takes place, the electrode potential deviates from equilibrium potential, and it is defined as:

$$\Delta V_{act} = V_{ca} - V_r = \phi_s - \phi_m \quad (7-67)$$

The kinetic expression for the oxygen reduction rate per unit volume can be described by using the Butler–Volmer expression with the assumption that reduction current is positive for negative overpotential:

$$\frac{di_z}{dz} = A_c i_{0,c}^+ \left\{ \exp \left[ \frac{-\alpha_c F \Delta V_{act,c}}{RT} \right] - \exp \left[ \frac{(1-\alpha_c) F \Delta V_{act,c}}{RT} \right] \right\} \quad (7-68)$$

where  $i_{0,c}^+$  is exchange current density at the equilibrium potential, and  $A_c$  is catalyst surface area per unit volume.

When water velocity is neglected, the proton current is related to the polymer electrolyte potential difference:

$$\frac{d\phi}{dz} = \frac{i_z}{\kappa^{eff}} \quad (7-69)$$

From Equations (7-66 and 7-69), and assuming the matrix of solid phase to be equipotential (as stated in assumption 1), changes in overpotential can be expressed as:

$$\frac{d(-\Delta V_{act,c})}{dz} = \frac{i_z}{\kappa^{eff}} \quad (7-70)$$

The oxygen flux is related to oxygen concentration according to Fick's Diffusion Law:

$$N_{O_2} = -D_{O_2}^{eff} \frac{d(C_{O_2})}{dz} \quad (7-71)$$

where  $D_{O_2}^{eff}$  is the effective oxygen diffusion coefficient as per Equation 7-19.

Thus, four unknowns,  $i_z$ ,  $\Delta V_{act}$ ,  $N_{O_2}$ , and  $C_{O_2}$  in the catalyst layer, are described by Equations 7-66, 7-68, 7-70, and 7-71.

The appropriate boundary conditions are listed next.

At  $z = 0$  (the gas diffuser–catalyst layer interface):

$$\left. \begin{array}{l} i_z = 0 \\ N_{O_2} = \frac{i_\delta}{nF} \end{array} \right\} \quad (7-72)$$

$$C_{O_2} = C_{O_2}^{z=0}$$

At  $y = \delta$  (the catalyst layer–membrane interface):

$$\frac{d(-\Delta V_{act,c})}{dz} = \frac{i_\delta}{\kappa^{eff}} \quad (7-73)$$

The governing equations with a set of boundary conditions have been solved with a relaxation approach, starting with assumed overpotential at the catalyst layer–membrane interface. The model has been verified by comparing the results with experimental data. The results, spatial variation of current density, oxygen concentration, and overpotential across catalyst layer are shown in Figure 7-7. It should be noted that the results in Figure 7-7 are expressed as dimensionless current density,  $I^*$ , and dimensionless oxygen concentration,  $\chi$ , defined as  $I^* = I/I_{lim}$  and  $\chi = C_{O_2}/C_{O_2}^{z=0}$ , respectively. The results are similar to those from the Bernardi–Verbrugge model [5], indicating that at higher overpotentials, that is, higher overall current densities, the reaction happens in a portion of the catalyst layer next to the gas diffusion layer. The model is useful to study the effect of catalyst layer parameters such as proton conductivity, effective porosity, and catalyst surface area.

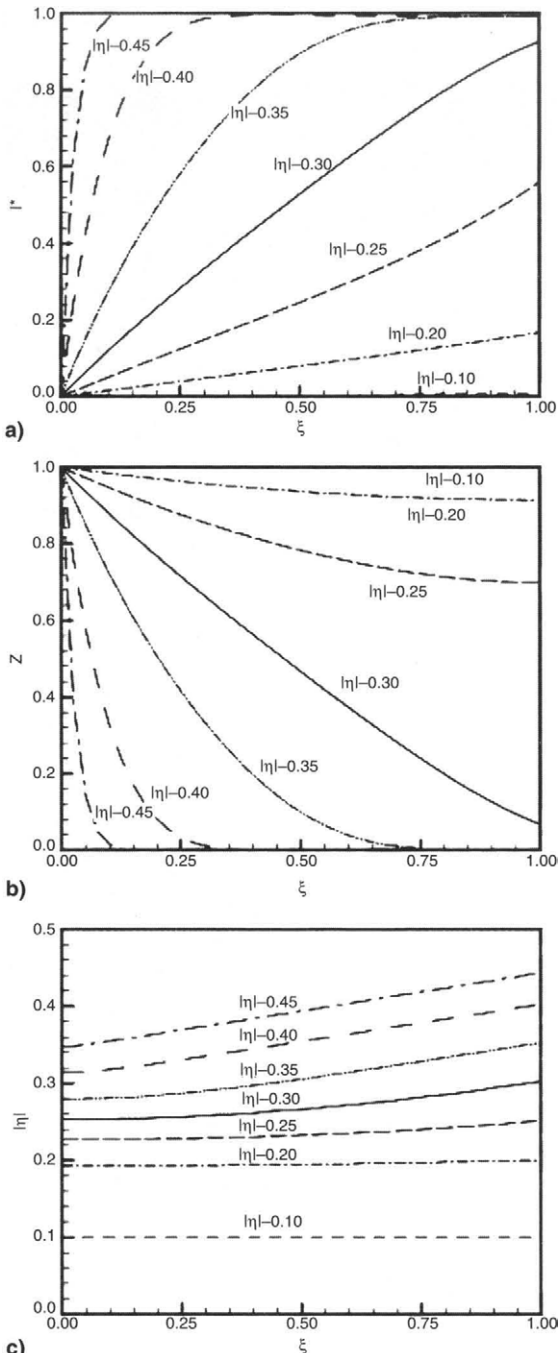


FIGURE 7-7. Sample of results generated with You-Liu model [12]: a) variation of current density with overpotential, b) variation of oxygen concentration with overpotential, c) variation of overpotential across catalyst layer ( $|\eta|$  in figures corresponds to  $\Delta V_{\text{act}}$  in equations, and  $\xi = z/\delta_c$ ). (Reprinted by permission from International Association for Hydrogen Energy.)

### 7.3.3. Two-Dimensional above-the-Channel Model (Jeng *et al.* [14])

Because the electrode portion covered by the ribs is not directly exposed to the channels, it suffers from a slow reactant gas mass transfer. The ribs can be regarded as barriers to mass transfer; however, they are necessary for electric current conduction. A complete understanding of the mass transfer phenomena within the GDL, under the influence of current collector ribs, will facilitate a proper PEM fuel cell design. West and Fuller [15] studied the effects of rib sizing and the GDL thickness on the current and water distributions within a PEM fuel cell. They found that dimensions of the ribs only slightly altered the cathode potential for a given current density, but had a significant influence on water management. Hental *et al.* [16] experimentally investigated the effects of both rib and channel widths on the performance of single PEM fuel cells. Naseri-Neshat *et al.* [17] studied the effect of gas flow channel spacing on current density through a 3-D model. Yan *et al.* [18] developed a two-dimensional mass transport model to investigate the anode gas flow channel cross-section and GDL porosity effects. They found that an increase in either the GDL porosity, channel width fraction, or the number of channels could lead to better cell performance. Nguyen and He [19], based on the modeling results, concluded that more channels and shorter rib widths are preferred for an interdigitated flow field configuration.

The two-dimensional model for the oxygen transport through the gas diffusion layer (GDL), such as the one proposed by Jeng *et al.* [14], takes the current collector ribs into account, as shown by the enlarged portion of a single cell appearing in Figure 7-8.  $L_1$  and  $L_2$  denote the midline of the GDL portion in contact with the rib and the channel, respectively. A GDL element bounded by  $L_1$ ,  $L_2$  has been selected for analysis in this two-dimensional model.

Jeng *et al.* [14] describe the two-dimensional oxygen mass transport within the GDL as:

$$N_{O_2} = -(\epsilon^{3/2} D_{O_2}) \nabla C \quad (7-74)$$

where  $N_{O_2}$  is the oxygen molar flux (a vector quantity) in the GDL. By taking divergence of both sides of Equation (7-74) and by applying the species conservation for oxygen, the Laplace's equation is obtained that governs the oxygen concentration distribution within the GDL:

$$\nabla^2 C = \frac{\partial^2 C}{\partial y^2} + \frac{\partial^2 C}{\partial z^2} \quad (7-75)$$

For this purpose, the catalyst layer can be regarded as an infinitely thin film and located on the left boundary of the GDL (Figure 7-8). The rate of the electrochemical reaction within the catalyst layer can be described using this thin-film model, yielding a Butler–Volmer rate expression. It is then

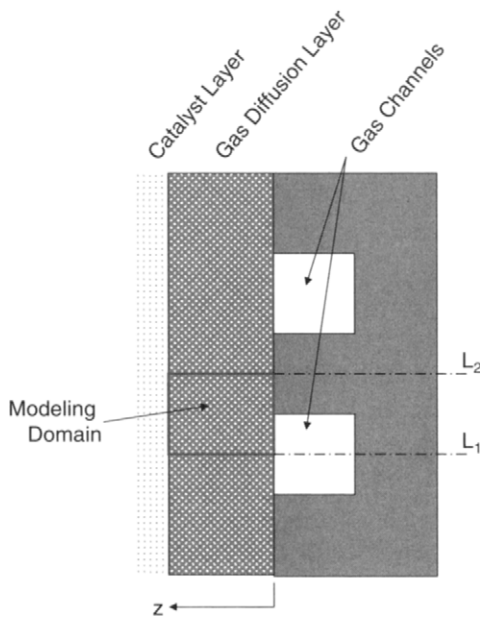


FIGURE 7-8. Modeling domain definition for the Jeng *et al.* model [14].

simplified to give a Tafel-type equation in terms of the oxygen concentration at the catalyst layer as:

$$i = A_c i_0 \delta_c \frac{C(y, z)}{C_{ref}} \exp\left(\frac{\alpha_c F \Delta V_{act,c}}{RT}\right) \quad (7-76)$$

where:

$i$  = local current density,  $\text{A cm}^{-2}$

$A_c$  = the specific area of the active surface,  $\text{cm}^2 \text{cm}^{-3}$

$i_0$  = reference exchange current density,  $\text{A cm}^{-2}$

$\delta_c$  = thickness of the catalyst layer,  $\text{cm}$

$C(y, z)$  = the oxygen concentration at the catalyst layer,  $\text{mol cm}^{-3}$

$C_{ref}$  = the reference oxygen concentration associated with  $i_0$ ,  $\text{mol cm}^{-3}$

$\alpha_c$  = cathode transfer coefficient

$\Delta V_{act,c}$  = cathode overpotential,  $\text{V}$

In this two-dimensional model, both the local current density and the oxygen concentration at the catalyst layer vary with  $y$ . Furthermore, under the steady state condition and the zero reactant crossover assumption, the

current is determined by the oxygen diffusion rate at the GDL–catalyst layer interface. This indicates that:

$$\frac{i}{4F} = N_{O_2|z=\delta_c} = -\epsilon^{3/2} D_{O_2} \left. \frac{\partial C}{\partial z} \right|_{z=\delta_c} \quad (7-77)$$

By combining Equations (7-76) and (7-77), the following boundary condition for the GDL–catalyst layer interface is obtained:

$$\left. \frac{\partial C}{\partial z} \right|_{z=\delta_c} = -\frac{A_c i_0 \delta_c}{4F\epsilon^{3/2} D_{O_2}} \frac{C(y, \delta_c)}{C_{ref}} \exp\left(\frac{\alpha_c F \Delta V_c}{RT}\right) \quad (7-78)$$

where the expression  $\frac{A_c i_0 \delta_c}{4F\epsilon^{3/2} D_{O_2} C_{ref}} \exp\left(\frac{\alpha_c F \Delta V_c}{RT}\right)$  is constant (K) for the given cathode overpotential  $\Delta V$  and the physical parameter and property values  $A_c$ ,  $i_0$ ,  $\delta_c$ ,  $\alpha_c$ ,  $T$ ,  $\epsilon$ ,  $D_{O_2}$ , and  $C_{ref}$ .

Concentration of oxygen on the boundary facing the channel is assumed to be known,  $C = C_0$ . It is also assumed that the cathode overpotential,  $\Delta V_{act,c}$ , is constant along the catalyst layer–GDL boundary.

Other boundary conditions follow from the domain geometry. Symmetrical boundary conditions on both the upper and lower boundaries of the GDL element apply; hence, the condition  $\partial C / \partial y = 0$  is imposed on both  $L_1$  and  $L_2$ . The molar flow rate across the GDL–rib interface is zero, so the  $\partial C / \partial z = 0$  condition applies to that part of the boundary.

The two-dimensional Laplace's equation (7-75) associated with the corresponding boundary conditions has been discretized using the finite-difference approach and solved using an alternating-direction explicit (ADE) method [20]. From the solution, Jeng *et al.* obtained the oxygen concentration distribution in the GDL, that is,  $C(y, z)$ . The oxygen molar flow rate at the GDL–catalyst layer interface,  $N_{O_2|z=\delta_c}$ , and the local current density,  $i$ , are then evaluated using Equation (7-77).

The average current density is simply:

$$i_{ave} = \frac{2}{w_1 + w_c} \int_0^{(w_1+w_c)/2} i(y) dy \quad (7-79)$$

The resulting oxygen concentrations inside the gas diffusion layer and current density at the GDL–catalyst layer interface are shown in Figure 7-9 for three different average current densities (0.1, 0.5, and 1.0 A cm<sup>-2</sup>). Oxygen concentration is shown in a dimensionless form as  $C/C_0$ . At low average current density, oxygen concentration is high throughout the gas diffusion layer ( $C > 0.78 C_0$ ), resulting in relatively uniform current density distribution. At high current density, oxygen is almost depleted in the

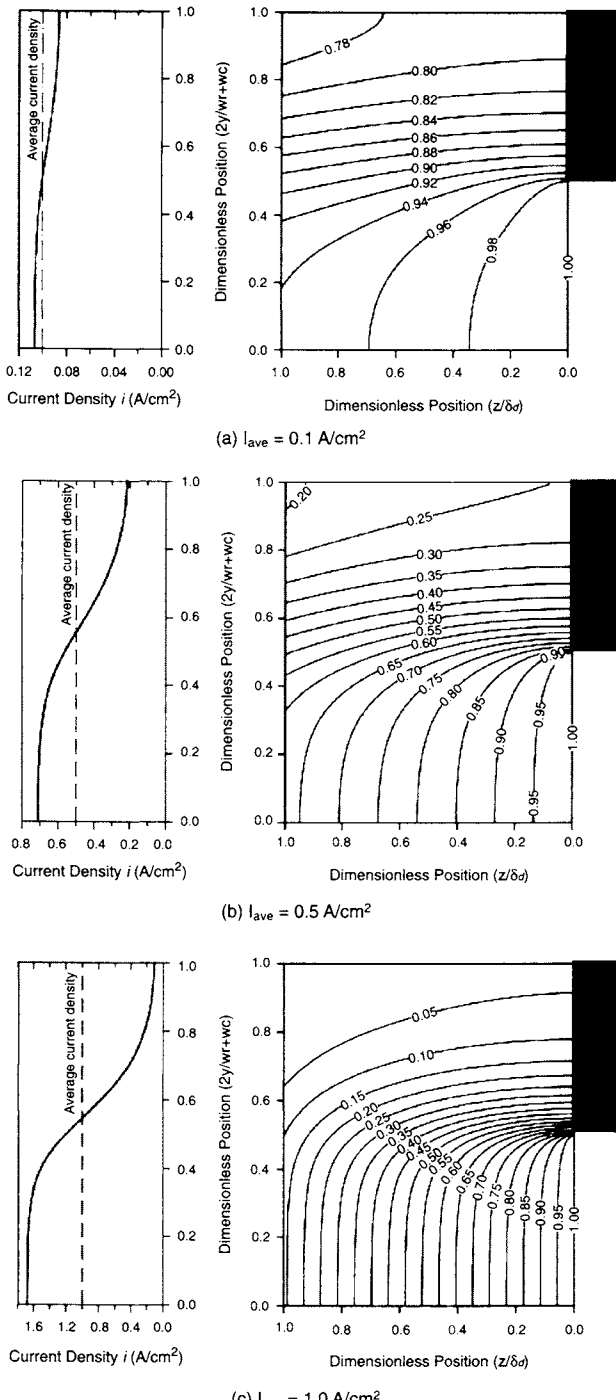


FIGURE 7-9. Oxygen concentration in gas diffusion layer and current density distribution at GDL–catalyst layer interface resulting from the Jeng *et al.* above-the-channel model [14]. (Reprinted by Permission of Elsevier.)

region of the gas diffusion layer above the rib, resulting in most of the reaction occurring directly above the channel, and very little activity ( $0.1 i_{ave}$ ) above the rib.

### 7.3.4. Two-Dimensional along-the-Channel Model (Gurau *et al.* [21,22])

All of the previous one- and two-dimensional models assumed that oxygen concentration in the gas channel, or, more specifically, at the gas diffusion layer-gas channel interface, is known. However, oxygen concentration along the channel changes as oxygen is being depleted in the electrochemical reaction. At the same time, water content along the channel increases.

Yi and Nguyen [23] developed basically a one-dimensional along-the-channel model, considering mass, species, and energy balances (not the momentum balance). The fluxes in z-direction (through the membrane electrode assembly) are taken into account as they affect the concentrations of reactants and products in the gas channel, but the changes of concentrations of reactants and products in z-direction are not considered with the exception of water flux through the membrane. An interesting aspect of this model is that the fuel cell channels are modeled as the heat exchangers, allowing temperature variation along the channel, as a function of co- or counterflow of hydrogen, air, and coolant.

Furthermore, all of the previous models consider oxygen transport in the gas diffusion layer solely as a result of concentration gradient, and they do not consider an interaction of the species in the channel with those in the gas diffuser due to velocity vector. Gurau *et al.* [21,22] presented the first unified approach by coupling the flow and transport governing equations in the flow channel and gas diffuser with no boundary conditions at the interface. The modeling domain of this model is shown in Figure 7-10, and it is different for different species, namely:

- Oxygen domain includes cathode channel, cathode gas diffusion layer, and cathode catalyst layer, with no boundary conditions required at the interfaces between these layers.
- Hydrogen domain includes anode channel, anode gas diffusion layer, and anode catalyst layer, with no boundary conditions required at the interfaces between these layers.
- Liquid water domain includes the membrane and both catalyst layers. This implies that the volume occupied by liquid water in the gas channels coming from the gas diffusers is negligible (*i.e.*, in gas channels, only gas mixtures are present).

The model is based on the following set of assumptions:

- Only the steady state case is considered.
- The gas mixtures are considered to be perfect gases.

- The flow is laminar everywhere.
- The gas mixture flows are incompressible.
- The volume occupied by liquid water in the gas channels coming from the gas diffusers is negligible (in gas channels, only gas mixtures are present).
- The dispersion of the fluids in the porous media is also disregarded. Its effects can be easily accounted in the general diffusion coefficients.
- The gas diffusers, catalyst layers, and the PEM are considered each as isotropic porous media.
- Dilation or contraction of the porous media is neglected.
- The contact electrical losses at the interfaces between different fuel cell elements are neglected.
- The catalyst layers are considered to have vanishing small thickness when the transport equations are solved, but the real values are taken into account when the membrane phase potential and current density are calculated.
- The heat generated under reversible conditions is neglected.

The distribution of the reactant concentrations along the electrodes is needed to calculate the transfer currents in electrochemical cells. The concentrations along the gas channels/gas diffusers/catalyst layers vary because of diffusion-convection transport and electrokinetics in the catalyst layers. These distributions depend therefore on the gas and medium

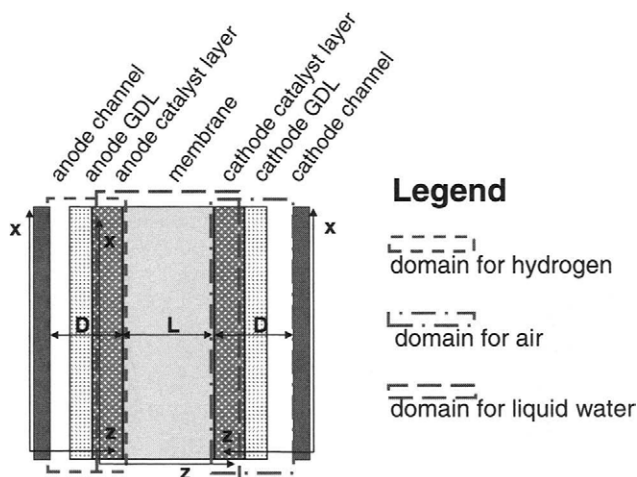


FIGURE 7-10. Domains for species in a PEM fuel cell used in Gurau *et al.* model [21].

properties, as well as on the reaction rates. These latter ones are in turn functions of the reactant concentrations, and an iterative procedure is required to predict them. A proper description of the species concentration distribution involves the use of the 2-D momentum equations in the coupled gas channel/gas diffuser/catalyst layer domain, coupled with the continuity and species concentration equations (such as the Stefan-Maxwell set of equations) and equations describing the electrochemical reactions (the Butler-Volmer equation). These latter ones are coupled with the transport equations in membrane via electroosmotic terms. The independent variables for constant geometry and material properties are the mass-flow rates, temperatures, humidities, and the pressures of the gas mixtures at the gas channel inlets, the external circuit resistance, and the temperature of the heating (cooling) medium. These are actually the only parameters that can be controlled in laboratory experiments or real-life fuel cell applications.

As already mentioned, boundary conditions for the dependent variables of the transport equations at the interfaces between different layers of the same domain are not required. At the gas channel entries, conditions of the first kind have to be prescribed for the gas mixture velocities, pressures, temperatures, and component concentrations. At the interfaces between the gas channels and the plate collectors, boundary conditions of the first kind have to be prescribed for the gas mixture velocity components (no slip condition) and for the temperature if the temperature of the cooling (heating) agent is known, or boundary conditions of the second kind are prescribed if the wall is adiabatic.

At the interfaces between the gas diffusers and the gas channels, the following boundary conditions are assumed for the liquid water velocity components:

$$\frac{\partial u}{\partial x} = \frac{\partial v}{\partial x} = 0 \quad (7-80)$$

where  $u$  and  $v$  are velocities in  $x$ - and  $z$ -directions, respectively.

Similar boundary conditions are prescribed at the lower and upper boundaries that delimit the membrane:

$$\frac{\partial u}{\partial z} = \frac{\partial v}{\partial z} = 0 \quad (7-81)$$

In the gas diffusers, water vapor is considered to be at equilibrium with the liquid water in the pores. Here also, the liquid water temperature is set equal to the temperature of the gas mixtures.

For the membrane phase potential equation, the boundary conditions are:

- at the upper and lower limits:  $\frac{\partial\phi}{\partial z} = 0$ , that is, no protonic current leaves the domain; and
- at the interface between the catalyst layer and the gas diffuser:  $\frac{\partial\phi}{\partial x} = 0$ , that is, no protonic current leaves the domain.

Solving the transport equations over domains covering more than one fuel cell element has to be done carefully. In the gas channels and in the gas diffusers, the objects of analysis are gas mixtures, whereas in the membrane, catalyst layers, and partially in the gas diffuser, it is the liquid water. The energy equation may be solved over the entire domain covering all the fuel cell elements; the continuity, momentum, and species conservation equations must be solved for each domain. It should be noted that the gas diffusers and catalyst layers each belong to two different domains.

The velocity and pressure fields for the gas mixtures are solved first in the coupled gas channel–gas diffuser domains disregarding the changes in composition of the gas mixtures. This enables one to solve the flow and pressure fields for the gas mixtures first, and once these fields are found, the equations for the other dependent variables may be solved. The gas species concentrations are dependent on the transfer current densities; therefore, the transport equations for the gas components are solved iteratively, together with the Butler–Volmer equations for anode and cathode catalyst layers. After convergence is achieved, one proceeds to solve for the transport equations related to the liquid water flow, for the membrane phase potential and current densities. Because the source terms of the energy equations are functions of the current density, a new level of iterations is needed, except for the velocity and pressure fields of the gas mixtures.

There are generally two ways of solving for the electrochemical equations: either the operating current density is given and different potential losses are calculated, or the so-called potentiostatic approach is used, when the cell potential is set and the current density is calculated. For a 2-D model, the operating current density is expressed as the average of the current density along the interface between the membrane and the catalyst layer.

Some of the results generated by the Gurau *et al.* model [21,22] are shown in Figures 7-11 and 7-12. As oxygen from air is consumed by electrochemical reaction at the catalyst layer, the oxygen mole fraction decreases along the flow direction. Because oxygen is only consumed by the catalyst layer, the model predicts a spanwise gradient of oxygen (Figure 7-11). The porous diffusion layer slows down oxygen transport to the catalyst layer, while water vapor generated at the catalyst layer further inhibits oxygen from reaching the catalyst layer. Water vapor molar fraction increases along the length of the channel, as water is being produced (Figure

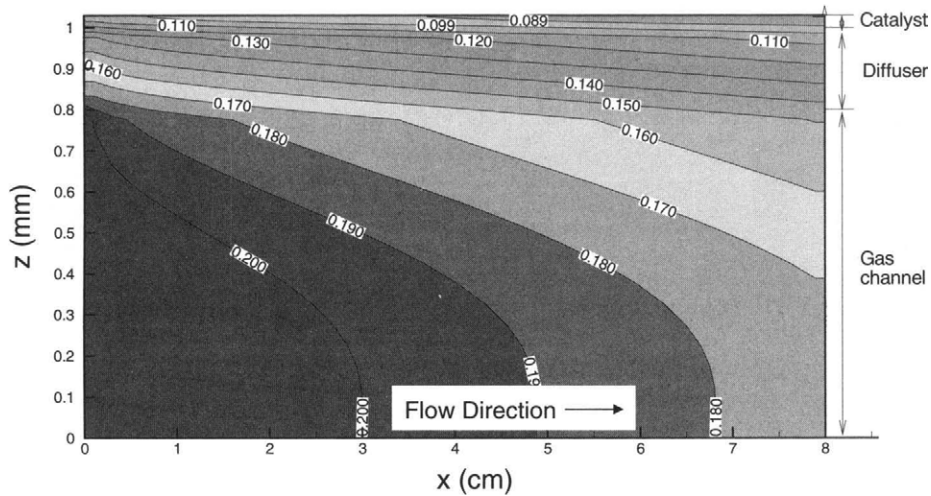


FIGURE 7-11. Oxygen mole fraction contours along cathode side gas channel (results from Gurau *et al.* 2-D along-the-channel model [21,22]).

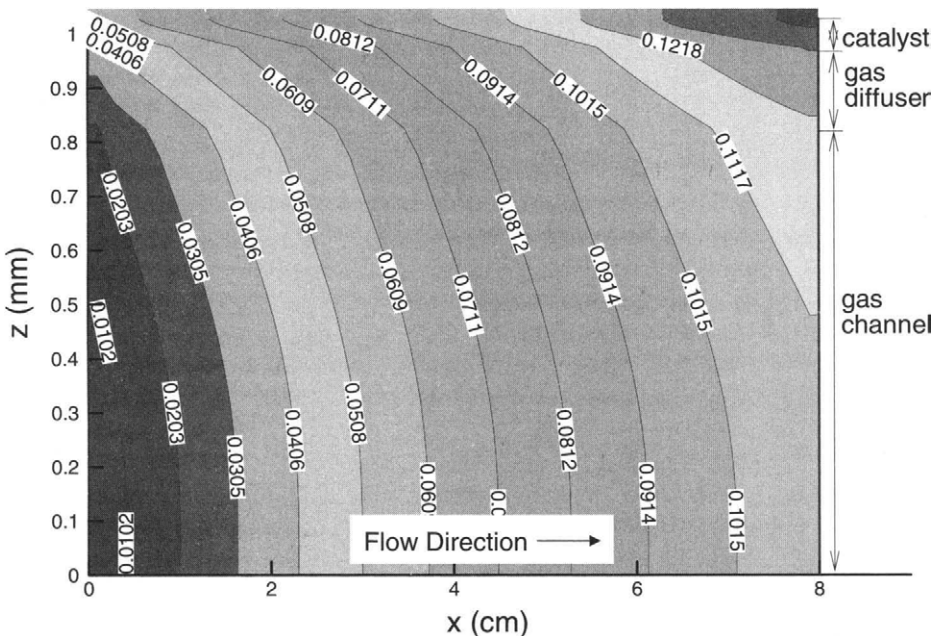


FIGURE 7-12. Water vapor mole fraction contours along cathode side gas channel (results from Gurau *et al.* 2-D along-the-channel model [21,22]).

7-12). Both oxygen and water vapor mole fraction distribution is a strong function of current, that is, reaction rate.

Note that depending on operating conditions, air in the channel may be saturated already at the inlet, and stays saturated along the channel, so any water added to the channel, such as product water, must be in liquid form. In that case a two-phase flow must be considered. The model by Gurau *et al.* does account for liquid water but only inside the membrane—liquid water presence in the gas diffusion layer and in the channels is ignored. You and Liu [24] built upon the Gurau *et al.* model [21] by accounting for liquid water in all the regions of the model domain, albeit in isothermal conditions. Liquid water presence is included through a phase saturation term defined as:

$$s_{(l)} = \frac{\rho_g g_{H2O} - \rho_l g_{H2O(g)}}{\rho_l - \rho_g g_{H2O(g)}} \quad (7-82)$$

$$s_{(g)} = 1 - s_{(l)} \quad (7-83)$$

where:

$s_{(l)}$  = volumetric fraction of the void space occupied by liquid water

$s_{(g)}$  = volumetric fraction of the void space occupied by gas mixture

$g$  = species mass fraction

$\rho$  = density ( $\text{kg m}^{-3}$ )

The two-phase mixture density is:

$$\rho = \rho_g s_{(g)} + \rho_l s_{(l)} \quad (7-84)$$

### 7.3.5. Three-Dimensional Models

Higher dimension fuel cell models can be considered to study PEM fuel cell performance. As shown previously, two-dimensional models can be used to characterize fuel cell performance along the channel length (x-z plane) or across channels (y-z plane). In the y-z plane, the model can focus on the membrane electrolyte assemble, or include the effect of gas transport in the porous diffusion layer and gas channel. In the y-z plane, several channels can be considered in order to investigate the effects such as gas mixing between the channels occurring in the diffusion layer. A three-dimensional model can be used to consider all the aforementioned phenomena, but computational limitations often limit the model's fidelity. The equations are the same as those in 1-D and 2-D models, but all the differential equations are applied in all three directions. Consequently, the boundary conditions must be applied for all three dimensions.

A three-dimensional distribution of oxygen mole fraction on the cathode side, resulting from modeling effort by Liu *et al.* [25,26], is shown in Figure 7-13. The modeling domain includes an entire length of the two halves of the adjacent gas channels separated by a "rib" of the bipolar plate (shown as an empty space in Figure 7-13) and corresponding gas diffusion layer above the channels and the rib. The channels show a typical downstream depletion of oxygen concentration in air due to consumption by electrochemical reactions at the catalyst layer. Oxygen mole fraction is low in the porous diffusion layer because of low diffusion rate of oxygen into the porous structure, water generation as a by-product of the electrochemistry occurring at the catalyst layer, and a majority of the diffusion layer being obstructed from the gas stream by the collector plate. This three-dimensional distribution of oxygen mole fraction shows that the most active catalyst layer is located directly above the gas channel. This trend is exhibited throughout the length of the channel. The trend is further validated by examining the current density distribution in the catalyst layer (Figure 7-14). The regions of high current density can be correlated to locations of high oxygen concentration on the catalyst layer. Location of highest current density is at the gas channel entrance, where the highest oxygen concentration in air provides for the largest electrochemical reaction rates.

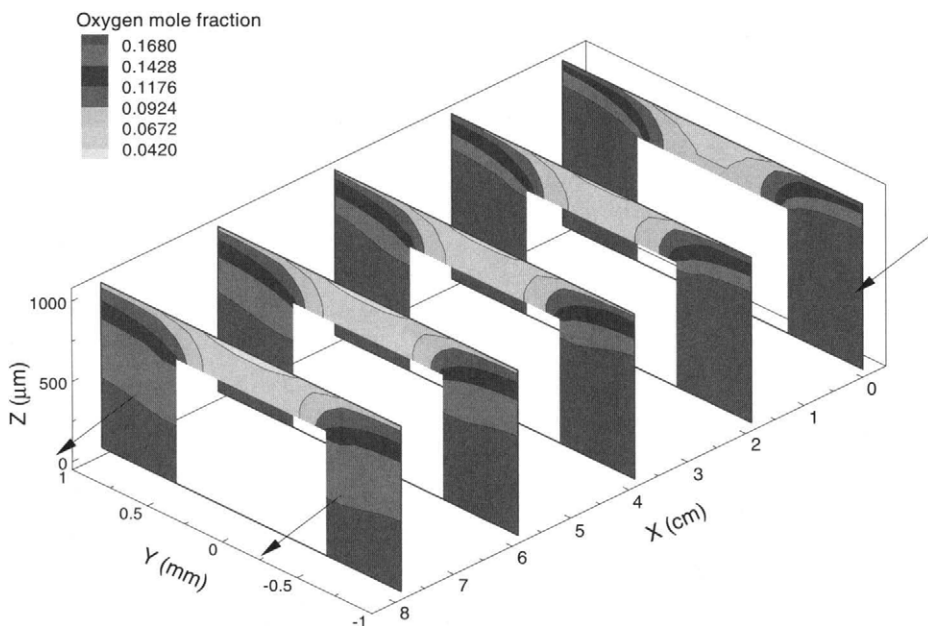


FIGURE 7-13. Three-dimensional distribution of oxygen mole fraction along cathode side gas channels (Liu *et al.* [25]).

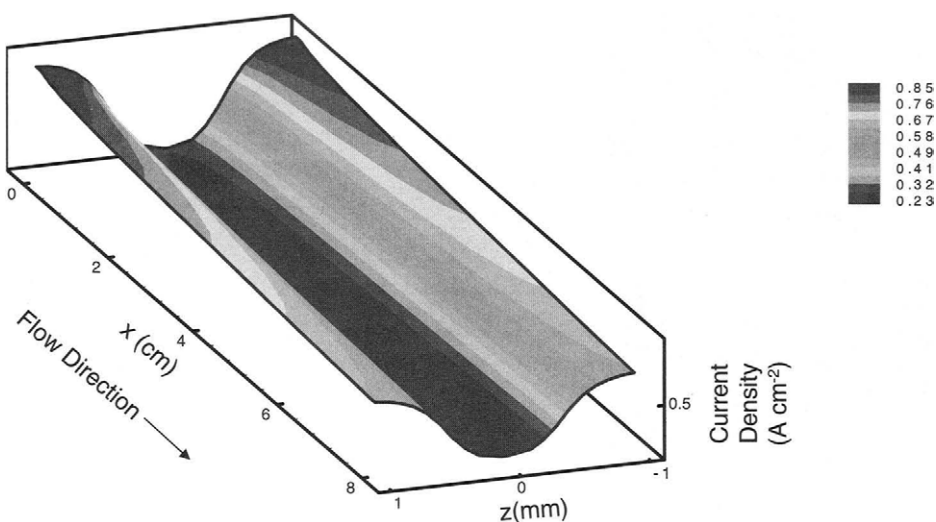


FIGURE 7-14. Current density distribution across the catalyst layer in the cathode [results of 3-D model by Liu *et al.* [25]].

The same model may be applied to a slightly different geometry, such as interdigitated flow field, where the flow is forced through the gas diffusion layer. In this case the oxygen mole fraction distribution in the channel and in the gas diffusion layer catalyst layers looks dramatically different from that in a straight or serpentine channel (Figure 7-15). Oxygen mole fraction is uniform throughout the inlet channel, and it is exhibiting significantly higher gradients in the gas diffusion layer, resulting in both higher limiting currents and more uniform distribution of current density at the gas diffusion layer–catalyst layer interface. In addition to Liu and coworkers at University of Miami [25–28], interdigitated flow field has been extensively studied by one of its first proponents, Nguyen and coworkers at the University of Kansas [19,29–33].

#### 7.4. Conclusions

Modeling has emerged to be a powerful and important tool for the fuel cell community. Several CFD software distributors, such as FemLab, FLUENT, and CFD Research (now ESI Group), have developed fuel cell modules that can be used in conjunction with the original CFD codes. Researchers, designers, and developers alike have used modeling to explore fuel cells, ranging from elucidating new fundamentals to characterizing fuel cell system performance.

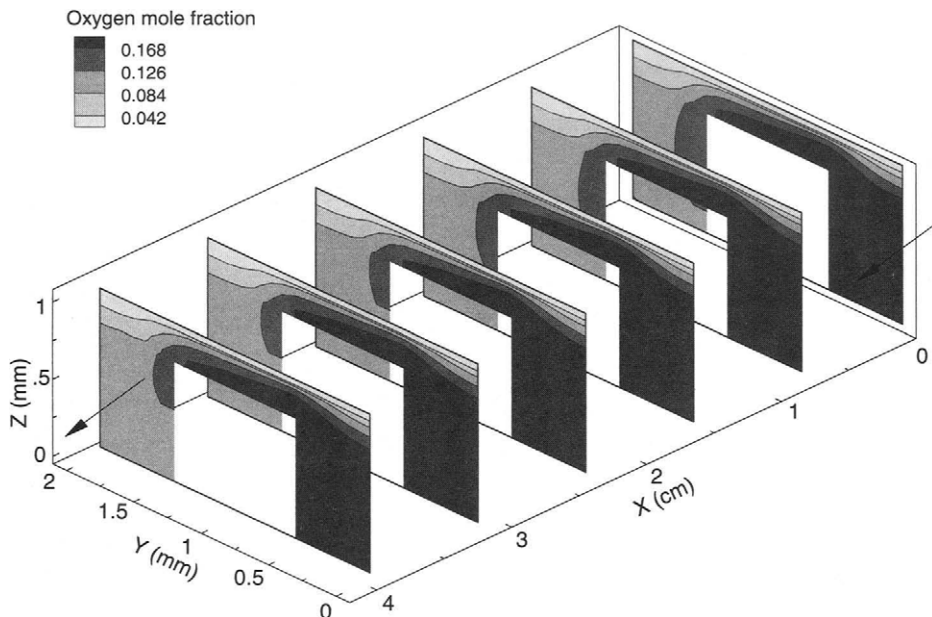


FIGURE 7-15. Three-dimensional distribution of oxygen mole fraction along cathode side gas channels for interdigitated flow field (Liu *et al.* [25]).

Two major themes arise in modeling of fuel cells:

1. The user needs to select the appropriate model that balances model capabilities, robustness, and accuracy.
2. Model accuracy is strongly dependent on its validity. The fuel cell model must be chosen such that it properly represents the problem being modeled, and it must be validated comprehensively in order to bring out its true predictive power.

This chapter is intended to provide an introduction to fuel cell modeling. The reader is encouraged to seek additional resources in this evolving field [4,5,8,12–14,17–19,21–27,31–46].

## References

1. Barbir, F. PEM Fuel Cells Design, Engineering, Modeling and Diagnostic Issues, lecture at the NSF Workshop on Engineering Fundamentals of Low Temperature PEM Fuel Cells (Arlington, VA, November 2001) ([http://electrochem.cwru.edu/NSF/presentations/NSF-Barbir\\_Diagnostics.pdf](http://electrochem.cwru.edu/NSF/presentations/NSF-Barbir_Diagnostics.pdf)).
2. Dagan, G., *Flow and Transport in Porous Formations* (Springer-Verlag, Berlin, 1989).

3. Bosnjakovic, F. *Technical Thermodynamics* (Holt Rinehart and Winston, New York, 1965).
4. Mazumder, S. and J. V. Cole, Rigorous 3-D Mathematical Modeling of PEM Fuel Cells, *Journal of the Electrochemical Society*, Vol. 150, No. 11, 2003, pp. A1503–A1509.
5. Bernardi, D. M. and M. W. Verbrugge, Mathematical Model of a Gas Diffusion Electrode Bonded to a Polymer Electrolyte, *AIChE Journal*, Vol. 37, No. 8, 1991.
6. Bird, R. B., W. E. Stewart, and E. N. Lightfoot, *Transport Phenomena*, Second ed. (John Wiley & Sons, New York, 2002).
7. Gasteiger, H. A., W. Gu, R. Makharia, and M. F. Matthias, Catalyst Utilization and Mass Transfer Limitations in the Polymer Electrolyte Fuel Cells, Tutorial (Electrochemical Society Meeting, Orlando, FL, 2003).
8. Shimpalee, S., S. Greenway, D. Spuckler, and J. W. Van Zee, Predicting Water and Current Distributions in a Commercial-Size PEMFC, *Journal of Power Sources*, Vol. 135, 2004, pp. 79–87.
9. Oran, E. S. and J. P. Boris, *Numerical Simulation of Reactive Flow*, Second ed. (Cambridge University Press, Cambridge, UK, 2001).
10. Kee, R. J., M. E. Coltrin, and P. Glarborg, *Chemically Reacting Flow: Theory and Practice* (John Wiley & Sons, New York, 2003).
11. Patankar, S. V., *Numerical Heat Transfer and Fluid Flow* (Hemisphere, New York, 1980).
12. You, L. and H. Liu, A Parametric Study of the Cathode Catalyst Layer of PEM Fuel Cells Using a Pseudo-Homogeneous Model, *International Journal of Hydrogen Energy*, Vol. 26, 2001, pp. 991–999.
13. Weisbrod, K. R., S. A. Grot, and N. Vanderborgh, Through-the-Electrode Model of a Proton Exchange Membrane Fuel Cell, in S. Gottesfeld (editor), *Proc. 1<sup>st</sup> Intl. Symp. Proton Conducting Membrane Fuel Cells*, Vols. 95–23 (Electrochemical Society, Pennington, NJ, 1995) pp. 152–166.
14. Jeng, K. T., S. F. Lee, G. F. Tsai, and C. H. Wang, Oxygen Mass Transfer in PEM Fuel Cell Gas Diffusion Layers, *Journal of Power Sources*, Vol. 138, 2004, pp. 41–50.
15. West, A. C. and T. F. Fuller, Influence of Rib Spacing in Proton-Exchange Membrane Electrode Assemblies, *Journal of Applied Electrochemistry*, Vol. 26, 1996, pp. 557–565.
16. Hental, P. L., J. B. Lakeman, G. O. Mepsted, and P. L. Adcock, New Materials for Polymer Electrolyte Membrane Fuel Cell Current Collectors, *Journal of Power Sources*, Vol. 80, 1999, p. 235.
17. Naseri-Neshat, H., S. Shimpalee, S. Dutta, W. K. Lee, and J. W. Van Zee, Predicting the Effect of Gas-Flow Channel Spacing on Current Density in PEM Fuel Cells, *Advanced Energy Systems*, Vol. 39, 1999, pp. 337–350, ASME.
18. Yan, W. M., C. Y. Soong, F. L. Chen, and H. S. Chu, Effects of Flow Distributor Geometry and Diffusion Layer Porosity on Reactant Gas Transport and Performance of Proton Exchange Membrane Fuel Cells, *Journal of Power Sources*, Vol. 125, 2004, p. 27.
19. Nguyen, T. V. and W. He, Interdigitated Flow Field Design, in W. Vielstich, A. Lamm, and H. Gasteiger (editors), *Handbook of Fuel Cell Technology—Fundamentals, Technology and Applications*, Vol. 3, Part 1 (John Wiley & Sons, New York, 2003) pp. 325–336.

20. Anderson, D. A., J. C. Tannehill, and R. H. Pletcher, *Computational Fluid Mechanics and Heat Transfer* (McGraw-Hill, New York, 1984).
21. Gurau, V., H. Liu, and S. Kakac, Two-Dimensional Model for Proton Exchange Membrane Fuel Cells, *AIChE Journal*, Vol. 44, No. 11, 1998, pp. 2410–2422.
22. Gurau, V., F. Barbir, and H. Liu, Two-Dimensional Model for the Entire PEM Fuel Cell Sandwich, in S. Gottesfeld and T. F. Fuller (editors), *Proc. Proton Conduction Membrane Fuel Cells II*, Vols. 98–27 (The Electrochemical Society, Pennington, NJ, 1999) pp. 479–503.
23. Yi, J. S. and T. V. Nguyen, An Along-the-Channel Model for Proton Exchange Fuel Cells, *Journal of the Electrochemical Society*, Vol. 145, 1998, pp. 1149–1159.
24. You, L. and H. Liu, A Two-Phase Flow and Transport Model for the Cathode of PEM Fuel Cells, *International Journal of Heat and Mass Transfer*, Vol. 45, 2002, pp. 2277–2287.
25. Liu, H., T. Zhou, and L. You, Development of Unified PEM Fuel Cell Models, in *DOE Fuel Cells for Transportation Program* (Annual National Laboratory R&D Meeting, Oak Ridge National Laboratory, June 6–8, 2001).
26. Zhou, T. and H. Liu, A General Three-Dimensional Model for Proton Exchange Membrane Fuel Cells, *Journal of Transport Phenomena*, Vol. 3, No. 3, 2001, pp. 117–198.
27. Kazim, A., H. Liu, and P. Forges, Modelling of Performance of PEM Fuel Cells with Conventional and Interdigitated Flow Fields, *Journal of Applied Electrochemistry*, Vol 29, 1999, pp. 1409–1416.
28. Wang, L. and H. Liu, Performance Studies of PEM Fuel Cells with Interdigitated Flow Fields, *Journal of Power Sources*, Vol. 134, 2004, pp. 185–196.
29. Nguyen, T. V., Gas Distributor Design for Proton-Exchange-Membrane Fuel Cells, *Journal of the Electrochemical Society*, Vol. 143, No. 5, 1996, pp. L103–L105.
30. Wood III, D. L., J. S. Yi, and T. V. Nguyen, Effect of Direct Liquid Water Injection and Interdigitated Flow Field on the Performance of Proton Exchange Membrane Fuel Cells, *Electrochimica Acta*, Vol. 43, 1998, pp. 3795–3809.
31. Yi, J. S. and T. V. Nguyen, Multicomponent Transport in Porous Electrodes of Proton Exchange Membrane Fuel Cells Using the Interdigitated Gas Distributors, *Journal of the Electrochemical Society*, Vol. 146, 1999, p. 38.
32. He, W., J. S. Yi, and T. V. Nguyen, Two-Phase Flow Model of the Cathode of PEM Fuel Cells Using Interdigitated Flow Fields, *AIChE Journal*, Vol. 46, 2000, pp. 2053–2064.
33. Natarajan, D. and T. V. Nguyen, Three-Dimensional Effects of Liquid Water Flooding in the Cathode of a PEM Fuel Cell, *Journal of Power Sources*, Vol. 115, 2003, pp. 66–80.
34. Springer, T., T. A. Zawodzinski, and S. Gottesfeld, Polymer Electrolyte Fuel Cell Model, *Journal of the Electrochemical Society*, Vol. 138, 1991, pp. 2334–2342.
35. Springer, T., M. S. Wilson, and S. Gottesfeld, Modeling and Experimental Diagnostics in Polymer Electrolyte Fuel Cells, *Journal of the Electrochemical Society*, Vol. 140, 1993, pp. 3513–3526.
36. Fuller, T. F. and J. Newman, Water and Thermal Management in Solid-Polymer-Electrolyte Fuel Cells, *Journal of the Electrochemical Society*, Vol. 140, 1993, pp. 1218–1227.

37. Divisek, J., J. Mosig, B. Steffen, and U. Stimming, Proton Exchange Membrane Fuel Cell Model, in F. Lapicque et al. (editors), *Electrochemical Engineering and Energy* (Plenum Press, New York, 1995) pp. 187–196.
38. Amphlett, J. C., R. M. Baumert, R. F. Mann, B. A. Peppley, and P. R. Roberge, Performance Modeling of the Ballard Mark IV Solid Polymer Electrolyte Fuel Cell, *Journal of the Electrochemical Society*, Vol. 142, 1995, pp. 1–8.
39. Um, S., C. -Y. Wang, and K. S. Chen, Computational Fluid Dynamics Modeling of Proton Exchange Membrane Fuel Cells, *Journal of the Electrochemical Society*, Vol. 147, 2000, pp. 4485–4493.
40. Baschuk, J. J. and X. Li, Modelling of Polymer Electrolyte Membrane Fuel Cells with Variable Degrees of Water Flooding, *Journal of Power Sources*, Vol. 86, 2000, pp. 181–186.
41. Rowe, A. and X. Li, Mathematical Modeling of Proton Exchange Membrane Fuel Cells, *Journal of Power Sources*, Vol. 102, 2001, pp. 82–96.
42. Springer, T., T. Rockward, T. A. Zawodzinski, and S. Gottesfeld, Model for Polymer Electrolyte Fuel Cell Operation on Reformate Feed, *Journal of the Electrochemical Society*, Vol. 148, 2001, pp. A11–A23.
43. Dutta, S., S. Shimpalee, and J. W. Van Zee, Numerical Prediction of Mass-Exchange Between Cathode and Anode Channels in a PEM Fuel Cell, *International Journal of Heat and Mass Transfer*, Vol. 44, 2001, pp. 2029–2042.
44. Jaouen, F., G. Lindbergh, and G. Sundholm, Investigation of Mass-Transport Limitations in the Solid Polymer Fuel Cell Cathode, I Mathematical Model, *Journal of the Electrochemical Society*, Vol. 149, 2002, pp. A437–A447.
45. Siegel, N. P., M. W. Ellis, D. J. Nelson, and M. R. von Spakovsky, Single Domain PEMFC Model Based on Agglomerate Catalyst Geometry, *Journal of Power Sources*, Vol. 115, 2003, pp. 81–89.
46. Nam, J. H. and M. Kaviani, Effective Diffusivity and Water-Saturation Distribution in Single- and Two-Layer PEMFC Diffusion Medium, *International Journal of Heat and Mass Transfer*, Vol. 46, 2003, pp. 4595–4611.

## Problems

### Problem No. 1:

For a 2-D modeling domain representing the gas diffusion layer above two halves of the channels and an entire rib between them (as shown in the figure below) representing a portion of an interdigitated flow field, write the governing equations and corresponding boundary conditions. Assume isothermal conditions. Also, assume that the catalyst layer has no thickness, that is, the reaction happens at the boundary between the gas diffusion layer and the catalyst layer. List the inputs (independent variables).

### Problem No. 2:

Write the governing equations and corresponding boundary conditions for electric current flux through the same domain as defined in Problem 1.

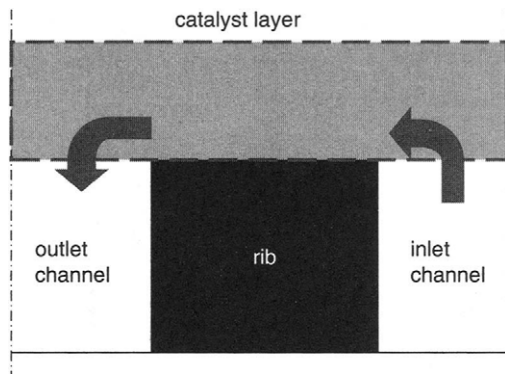


Figure with Problems 1 and 2.

### Problem No. 3:

Write the governing equations and corresponding boundary conditions for a 1-D model of a single fuel cell cathode channel (1-D means that only changes along the length of the channel should be taken into account). Assume isothermal conditions and that the reaction happens at the upper channel boundary. Also, list other assumptions needed to develop this model.

### Quiz

1. The relationship between electrical current and consumption of reactants in an electrochemical reaction is described by:
  - a) Butler–Volmer equation
  - b) Faraday's Law
  - c) Fick's Law
  
2. Which of the following is not used in fuel cell modeling:
  - a) conservation of momentum
  - b) conservation of mass
  - c) conservation of temperature
  
3. Conservation of mass applies to:
  - a) any element of a fuel cell
  - b) any element of a fuel cell except the catalyst layer, where because of the electrochemical reactions, there may be a change of mass
  - c) any element of a fuel cell except those where either evaporation or condensation takes place

4. The Stefan–Maxwell equation is used to model:
  - a) diffusion of a gas mixture through porous media
  - b) diffusion of a gas through another gas
  - c) diffusion of a gas through liquid
5. An assumption of isothermal conditions eliminates from modeling:
  - a) energy conservation equation
  - b) momentum conservation equation
  - c) temperature conservation equation
6. The cathode overpotential is:
  - a) positive
  - b) negative
  - c) it may be either positive or negative, depending on the sign of the anode overpotential
7. What is the source term in the energy conservation equation in the membrane?
  - a) heat of reaction in the cathode
  - b) ionic resistance
  - c) electronic resistance
8. In any volume of the anode, ionic current generated is always:
  - a) equal to the electronic current generated
  - b) greater than electronic current generated
  - c) same as ionic current generated in the adjacent anode volume
9. Total ionic current in the cathode is:
  - a) greater than the total ionic current in the anode
  - b) smaller than the total ionic current in the anode
  - c) same as the total ionic current in the anode
10. Symmetry boundary conditions are often used in fuel cell modeling to:
  - a) eliminate the need to model anode (if geometry of the anode is symmetrical to the cathode)
  - b) reduce number of equations used in the model and speed up the computation
  - c) simplify the modeling domain and speed up the computation

# CHAPTER 8

## 8. Fuel Cell Diagnostics

In addition to modeling, which is described in Chapter 7, diagnostics is another tool that can help elucidate the complex processes taking place in an operational fuel cell. As shown in Figure 8-1, diagnostics can be used in the fuel cell design process to determine if there is anything wrong with the fuel cell and point to possible causes, as well as to calibrate or validate the model. A PEM fuel cell in operation is always between having too much water and not having enough water. Too much water may cause flooding in either the catalyst layer or the gas diffusion layer or even in the gas channels. The result of cell flooding is loss of cell potential due to difficulty of one or both reactant gases reaching the catalyst sites (concentration polarization). Too little water is likely to cause membrane drying, which in turn increases cell resistance and reduces cell potential. A number of diagnostic techniques have been developed to identify and quantify cell flooding and drying.

### 8.1. Polarization Curve

As discussed in Chapter 3, fuel cell performance is characterized by its polarization curve, that is, a plot of cell potential vs current density. Three distinct regions of a fuel cell polarization curve are noticeable (Figure 8-2):

- At low current densities, the cell potential drops sharply as a result of the activation polarization.
- At intermediate current densities, the cell potential drops linearly with current; clearly as a result of ohmic losses (*i.e.*, cell resistance).
- At high current densities, the cell potential drop departs from linear relationship with current density, as a result of more pronounced concentration polarization.

By fitting the experimental results to one of the equations describing the polarization curve (*e.g.*, Equation 3-54 or page 65), insightful information may be gained about the parameters of the polarization curve, such as reversible cell potential,  $V_r$ ; apparent exchange current density,  $i_o$ ; Tafel

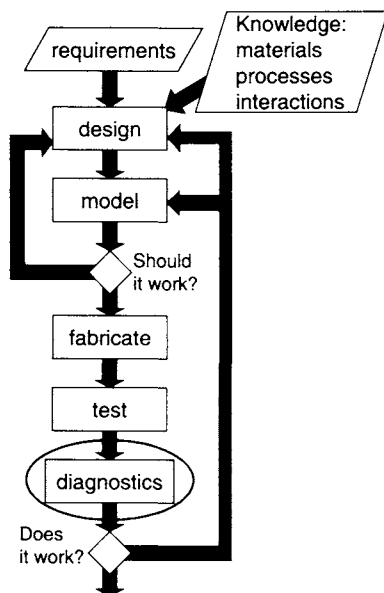


FIGURE 8-1. Role of diagnostics in fuel cell design process.

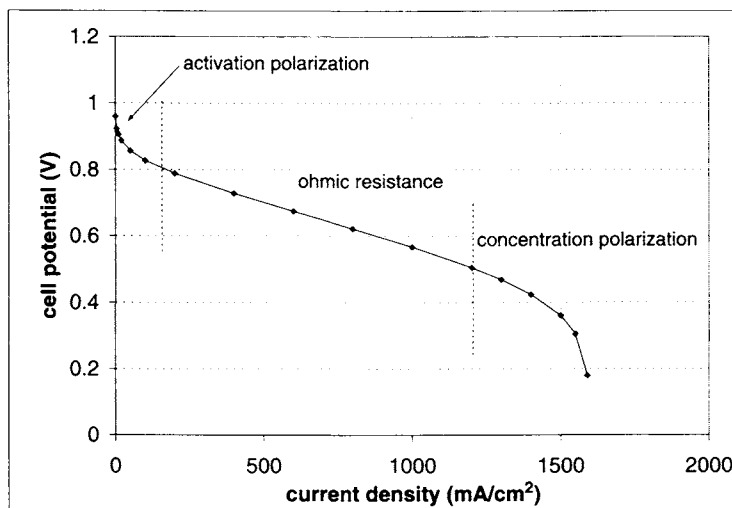


FIGURE 8-2. A fuel cell polarization curve with three distinct regions.

slope,  $b$ ; cell resistance,  $R_i$ ; or limiting current  $i_L$  (as demonstrated by Ticianelli *et al.* [1]).

Polarization curve is typically recorded by starting at the open circuit potential and then increasing current and taking measurements at prescribed potential or current intervals. The sweep may be done at different speeds

ranging from a quick sweep taking only several seconds to a slow sweep allowing the fuel cell to adjust at each operating point up to several minutes.

The reactant gases' flow rate may be kept constant at sufficiently high flow rate to allow operation at the highest current density, or the flow rate may change in proportion to current density in prescribed stoichiometry. The former is suitable for quick sweeps, whereas the later is only suitable for slow sweeps because the flow rate adjustments may take some time. Changing of the current ahead of the flow rate may result in fuel cell deprivation of reactant gases and unwanted cell potential drop.

If the polarization curve is recorded in both directions increasing and decreasing current, it may show hysteresis, that is, the two curves may not be on top of each other. This typically points to either flooding or drying in the fuel cell. For example, if the cell is flooding on the cathode side, then operation at higher current density would only make the situation worse because additional water would be produced. The polarization curve recorded with decreasing current would show lower voltage at higher currents than the previously taken polarization curve with increasing current. Conversely, if the cell is drying on the cathode side, additional water produced at high current densities would be beneficial, resulting in higher cell potential in a backward polarization curve (Figure 8-3). Similar behavior may result in a fuel cell that is drying and flooding on the anode side. In order to distinguish between the anode drying and cathode flooding, additional information is needed, such as membrane resistance.

A difference in polarization curves between the cell operating with air and pure oxygen may be used to characterize flooding or problems in water

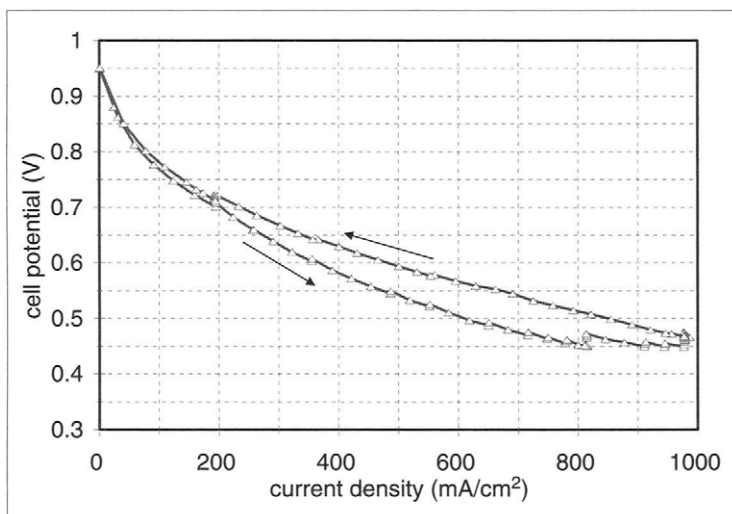


FIGURE 8-3. Fuel cell polarization curve hysteresis—cathode drying (temperature: 80°C, H<sub>2</sub>/Air humidification: 80/60°C, H<sub>2</sub>/Air stoichiometry: 1.5/5.0).

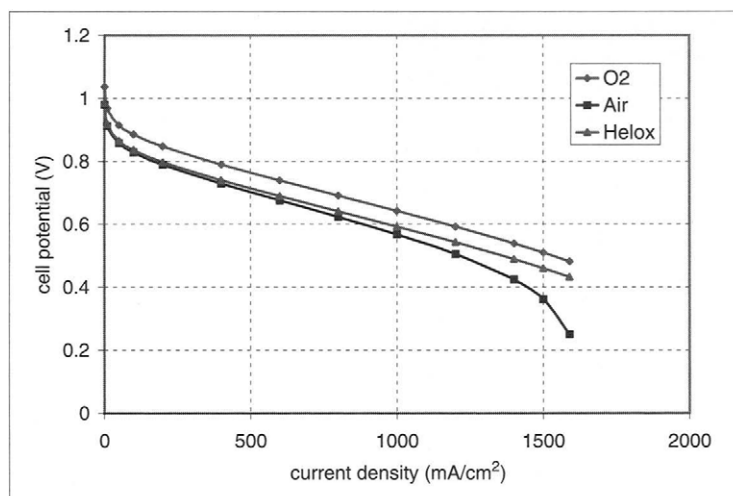


FIGURE 8-4. Comparative polarization curves (after T. Ralph *et al.* [2]).

management in the cathode compartment. The difference in cell voltage between pure oxygen and air results from the difference in concentration of oxygen at the catalyst surface (Nernst equation plus effect on exchange current density). If there are no other effects, this difference should be nearly constant at any current density. Increase in cell potential difference between oxygen and air (oxygen gain) at higher current densities points to some mass transport problems. This may be further elucidated if an additional polarization curve is recorded using a mixture of oxygen with helium (helox) at the cathode. If oxygen has to diffuse through a water film, both air and helox polarization curves should be similar (if oxygen concentration is the same). If the problem is in the gas phase diffusion, then the helox curve would show higher cell potential because the oxygen diffusion in helium is noticeably faster than oxygen diffusion in nitrogen (as shown in Figure 8-4).

## 8.2. Current Interrupt

A polarization curve provides useful but not sufficient information about fuel cell performance. For example, both flooding and drying of a cell would result in a loss of voltage, but a single polarization curve would not be able to distinguish between the two. In addition, recording of a polarization curve takes time and cannot be done during normal operation of a fuel cell. A quick measurement of the cell resistance may provide more information about the cell's performance. For example, drying of the membrane would

result in resistance increase. One of the methods to measure the resistance in an operational fuel cell is the current interrupt method. In this method, the current is interrupted for a very short period (an order of magnitude of several milliseconds) and the resulting voltage gain is observed. The difference between the cell voltage before and after the current interrupt, divided by the current, is the cell resistance.

To understand cell resistance measurement, a fuel cell may be represented by a simplified electrical circuit, such as the one shown in Figure 8-5, consisting of a couple of resistors and a capacitor. The first resistor represents the cell resistance, both electronic and ionic. The second resistor in a loop with a capacitor represents the charge transfer resistance, that is, activation polarization. When the current is interrupted, no current goes through the first resistor and the circuit's voltage jumps instantaneously, followed by much slower increase due to discharging of the capacitor (Figure 8-6). Eventually, when the capacitor is fully discharged, the cell reaches the open circuit voltage. The instantaneous voltage jump represents the cell resistance, and the remaining gain is the charge transfer resistance or the activation polarization. The difficulty with this simple method is in determining the exact point of instantaneous voltage gain. The voltage behavior may be monitored in real time with an oscilloscope, or several discreet voltage readings may be done at different interrupt times and then extrapolated back to zero time. Another difficulty is the so-called ringing

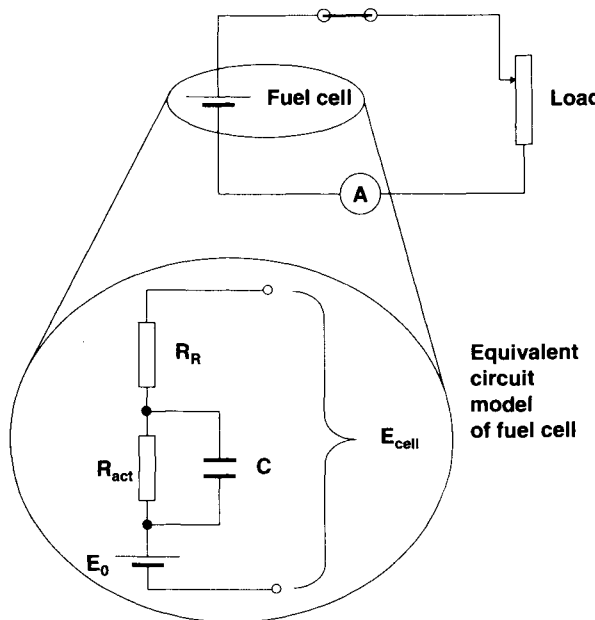


FIGURE 8-5. Equivalent circuit representing a fuel cell.

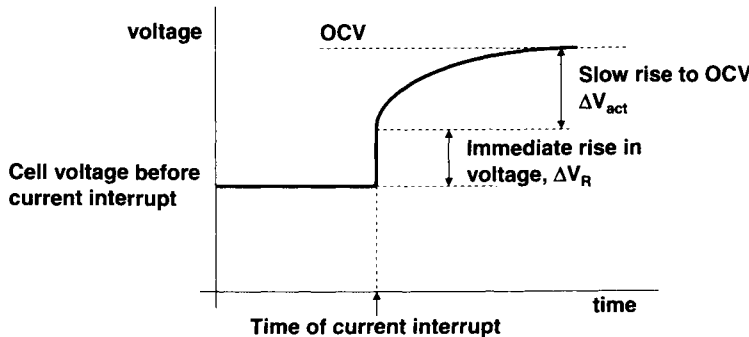


FIGURE 8-6. Cell voltage behavior after current interrupt.

effect caused by cable inductance [3], particularly at short delay times (delay time is the time between current interrupt and voltage measurement).

### 8.3. AC Impedance Spectroscopy

Even more information about the cell parameters may be obtained through AC impedance spectroscopy. In this method, an AC signal of known amplitude and frequency is sent through the cell, and the phase change and amplitude of the response is recorded. This may be repeated at different frequencies, that is, through an entire frequency spectrum.

With known amplitude and frequency, a signal is defined as:

$$I = I_{\max} \sin(\omega t) \quad (8-1)$$

where:

$I_{\max}$  = signal amplitude (A)

$\Omega = 2\pi f$ ; where  $f$  = frequency ( $s^{-1}$  or Hz)

$t$  = time (s)

The response is then:

$$V = V_{\max} \sin(\omega t - \phi) \quad (8-2)$$

where:

$V_{\max}$  = response amplitude

$\phi$  = phase angle

For a pure resistor, the phase angle  $\phi = 0$ , and the impedance  $Z = R$ .

For a capacitor, the phase angle  $\phi = \frac{\pi}{2}$ , and the impedance is:

$$Z_C = -\frac{j}{\omega C} \quad (8-3)$$

where:

$$j = \sqrt{-1}$$

C = capacitance (F)

For a fuel cell equivalent circuit, such as the one shown in Figure 8-7, the impedances are:

$$Z_R = R_R; \quad Z_{act} = R_{act}; \quad Z_C = -\frac{j}{\omega C} \quad (8-4)$$

The impedance of the entire circuit is then:

$$Z(\omega) = R_R + \frac{1}{\frac{1}{R_{act}} - \frac{\omega C}{j}} = R_R + \frac{R_{act}}{1 + j\omega CR_{act}} \quad (8-5)$$

After rearranging, it becomes a complex number:

$$Z(\omega) = R_R + \frac{R_{act}}{1 + (\omega CR_{act})^2} - j \frac{\omega CR_{act}^2}{1 + (\omega CR_{act})^2} \quad (8-6)$$

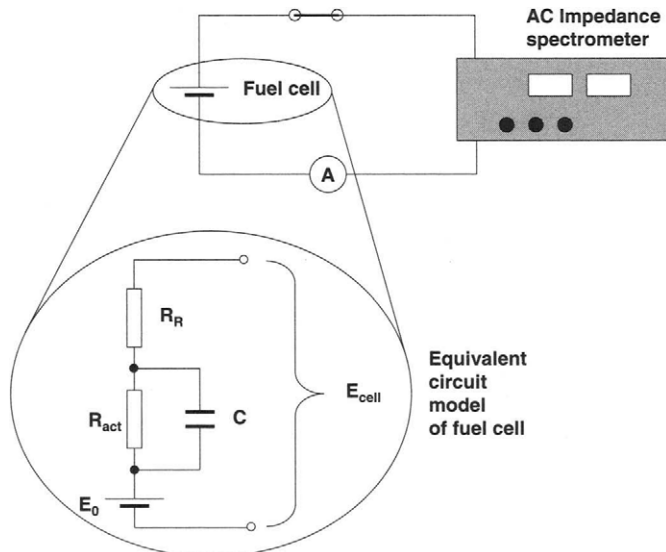


FIGURE 8-7. AC impedance spectroscopy setup and fuel cell equivalent circuit.

with the real part:

$$\text{Re } Z = R_R + \frac{R_{\text{act}}}{1 + (\omega C R_{\text{act}})^2} \quad (8-7)$$

and the imaginary part:

$$\text{Im } Z = \frac{\omega C R_{\text{act}}^2}{1 + (\omega C R_{\text{act}})^2} \quad (8-8)$$

with the absolute value of impedance:

$$|Z| = \left[ (\text{Re } Z)^2 + (\text{Im } Z)^2 \right]^{1/2} \quad (8-9)$$

and the phase angle:

$$\tan(\phi) = \frac{\text{Im } Z}{\text{Re } Z} \quad (8-10)$$

Plotted in a Nyquist diagram ( $\text{Im } Z$  vs  $\text{Re } Z$ ), the measurements of complex impedance at various frequencies of this simple fuel cell equivalent circuit result in a semicircle (Figure 8-8). At very low frequencies, the resulting impedance is  $Z = R_R + R_{\text{act}}$ , whereas at very high frequencies, the resulting impedance is  $Z = R_R$ . Sometimes, a single measurement at high frequency is used to measure the cell resistance  $R_R$ . However, the entire frequency

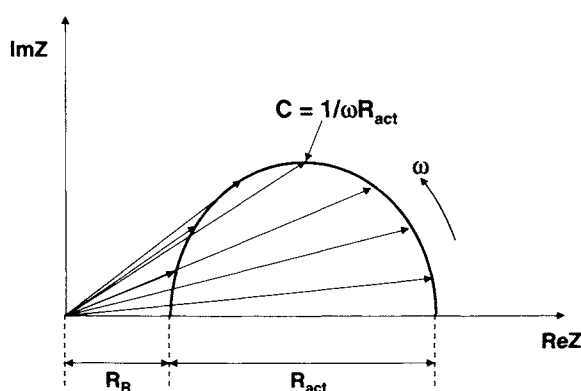


FIGURE 8-8. Resulting complex impedance at various frequencies of the fuel cell equivalent circuit from Figure 8-7.

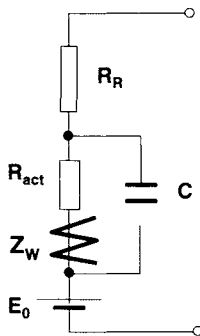


FIGURE 8-9. Modified fuel cell equivalent circuit with Warburg impedance representing concentration polarization.

spectrum may provide more useful information about the cell's inner workings [4-6].

The fuel cell equivalent circuit from Figure 8-7 may be modified by including a so-called Warburg impedance (Figure 8-9) representing the concentration polarization [7].

The Warburg impedance is described as:

$$Z_W = \frac{\sigma}{\omega^{1/2}} - j \frac{\sigma}{\omega^{1/2}} \quad (8-11)$$

where:

$$\sigma = \frac{RT}{\sqrt{2}(nF)^2 A} \left( \frac{1}{D_O^{1/2} C_O} + \frac{1}{D_R^{1/2} C_R} \right) \quad (8-12)$$

where:

$A$  = electrode area,  $\text{m}^2$

$D_O$  = diffusion coefficient for oxidized species,  $\text{m}^2 \text{s}^{-1}$

$C_O$  = concentration of oxidized species,  $\text{mol m}^{-3}$

$D_R$  = diffusion coefficient for reduced species

$C_R$  = concentration of reduced species,  $\text{mol m}^{-3}$

If the two concentrations differ widely, it is the lower concentration that determines the value of  $\sigma$  [7].

In this case the semicircle is not completed at low frequencies; instead, an extended straight line with a slope of 1 appears in the Nyquist plot (Figure 8-10). Diffusion of species is clearly a much slower process than the flow of electrons, and it is therefore detected at low frequencies.

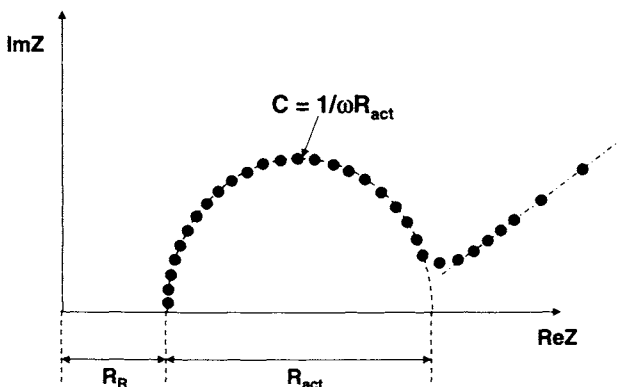


FIGURE 8-10. Resulting complex impedance at various frequencies of the fuel cell equivalent circuit from Figure 8-9.

The frequency at which a transition from a semicircle to the straight line occurs depends on the concentration of the reactants and products, on the exchange current density, and on the overpotential [7].

#### 8.4. Pressure Drop as a Diagnostic Tool

Operating conditions, such as pressure, temperature, flow rates, and humidity of reactant gases, have a great effect on PEM fuel cell performance. In general, performance of a PEM fuel cell is stable in a relatively narrow operational conditions window. This is mainly related to water management issues inside the cell. Although it is possible to select operational conditions to maintain required water balance at the inlet and outlet, flooding or drying may still take place because of uneven local conditions inside the cell. Too much water results in flooding, that is, blocking of porous passages, which in turn reduces the transport rate of reactants to the catalyst site. Flooding can occur on both anode and cathode sides. Too little water results in membrane drying, which in turn results in increased ionic resistance. The immediate result of either flooding or drying is the loss of cell potential. Without a proper diagnostic tool, that is, by monitoring only the cell potential or its resistance, very often it is difficult to distinguish between flooding and drying. To take the proper corrective action(s), it is necessary to have a simple, quick, and reliable monitoring and diagnostic tool.

General Motors patented a method and apparatus for detection of flooding in an  $\text{H}_2/\text{O}_2$  fuel cell based on monitoring the pressure drops across the  $\text{H}_2$  and  $\text{O}_2$  flow fields and comparing them with predetermined thresholds of acceptability [8]. If the pressure drop exceeds the threshold,

the corrective measures are automatically initiated, such as turning off humidification, increasing the gas mass flow rate, reducing gas pressure, and/or reducing current drain. General Motors also patented a method for controlling the humidity level based on monitoring of the cell resistance [9]. It correlated high-frequency resistance of a fuel cell to the degree of humidification in an attempt to find the optimum humidification conditions. Too much humidification resulted in cell flooding with no changes in cell resistance.

Barbir *et al.* [10] and He *et al.* [11] investigated the pressure drop as a diagnostic tool for detection of flooding in the fuel cell. They monitored the pressure drop in a fuel cell with interdigitated flow fields in a variety of operating conditions causing either flooding or drying of the fuel cell.

Rodatz *et al.* [12] studied the operational aspects of a large PEMFC stack under practical conditions. They particularly addressed the pressure drop, the effect of bends in the flow field, and two-phase flow. They observed a decrease in pressure drop when the stack current was reduced. The large time constant observed was attributed to gradual water removal from the MEA, followed by clearing out of the flow passages.

The pressure drop is a result of friction within the passages or reactant gases through the cell. Liquid water may be present inside the channel either in the form of little droplets or as a film. Formation of larger water droplets effectively reduces the channel cross-sectional area and/or diverts the flow through other channel, in either case causing an increase in pressure drop. Although a pressure drop increase is a reliable sign of increased water content in the fuel cell, it cannot be used to detect the cell drying out, because in that case the pressure drop would remain unchanged. However, by combining the pressure drop with the cell resistance measurements, it should be possible to detect either flooding or drying. The cell resistance does not change if the cell is flooding, but an increase in cell resistance would be an unambiguous sign that the cell drying is taking place. During an operational cycle a fuel cell may go through the phases of flooding and drying, and a reliable method to distinguish between the two is needed in order to take the proper corrective measures. The use of pressure drop as a diagnostic tool for cell flooding and drying is illustrated through several examples [13].

Figure 8-11 [13] shows how pressure drop reflects flooding of a stack caused by the humidification temperature being higher than the stack temperature, resulting in water condensation on the cathode side. Flooding is typically characterized by erratic cell potential behavior, such as sudden cell voltage drops and increases. The cell voltage increases suddenly when a slug of water is expelled from a channel. The cathode pressure drop increases, clearly indicating flooding conditions inside the stack. As soon as the stack temperature becomes higher than the air inlet temperature, there is no more condensation, the pressure drop starts to decline, and the cell potential becomes less erratic.

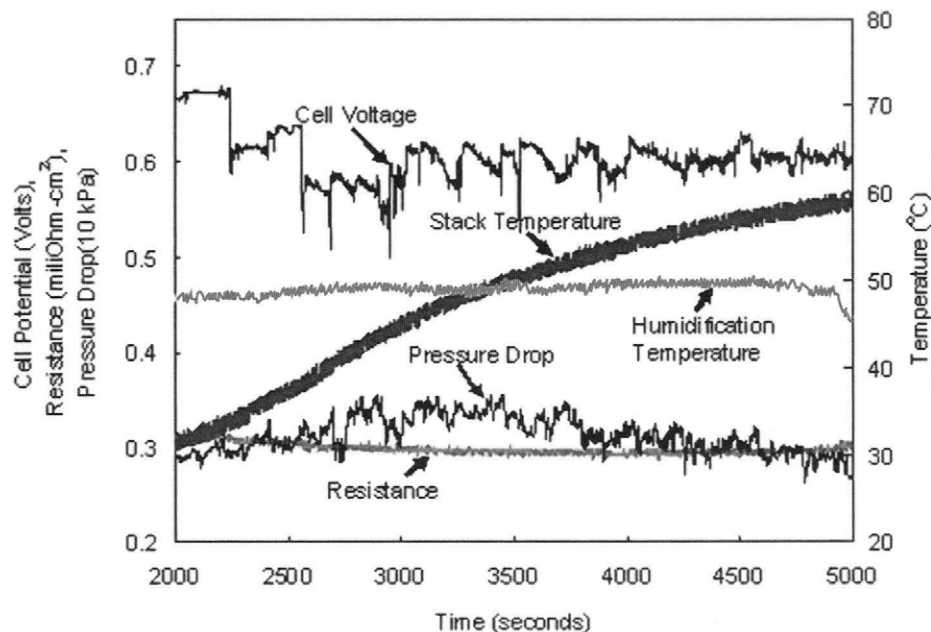


FIGURE 8-11. Example of pressure drop increase as a result of cell flooding [13] (note the erratic cell voltage pattern as a result of flooding).

In the case of inadequate humidification, the membrane may start to dry out. This is illustrated in Figure 8-12a [13]. When the humidification temperature decreases well below the stack operating temperature, the stack starts to dry out. This is indicated by a decrease in pressure drop, which levels off at a new lower value corresponding to the pressure drop of dry air, and is accompanied by a continuous increase in cell resistance. As a result, the cell potential deteriorates. When the required humidification is restored, the pressure drop increases, the cell resistance decreases, and as the result, the cell voltage recovers (Figure 8-12b).

Figure 8-13 [10] illustrates how the conditions in a cell that is first flooding, then drying, and then flooding again. Drying of the cell was caused by excess flow of dry hydrogen through the anode, which reversed the direction of the net water transport through a thin membrane and removed excess water from the cathode compartment (this method of water management was proposed by Voss *et al.* [14]).

## 8.5. Current Density Mapping

Interesting and useful information about the inner workings of a fuel cell may be obtained by current density mapping. Although this is not practi-

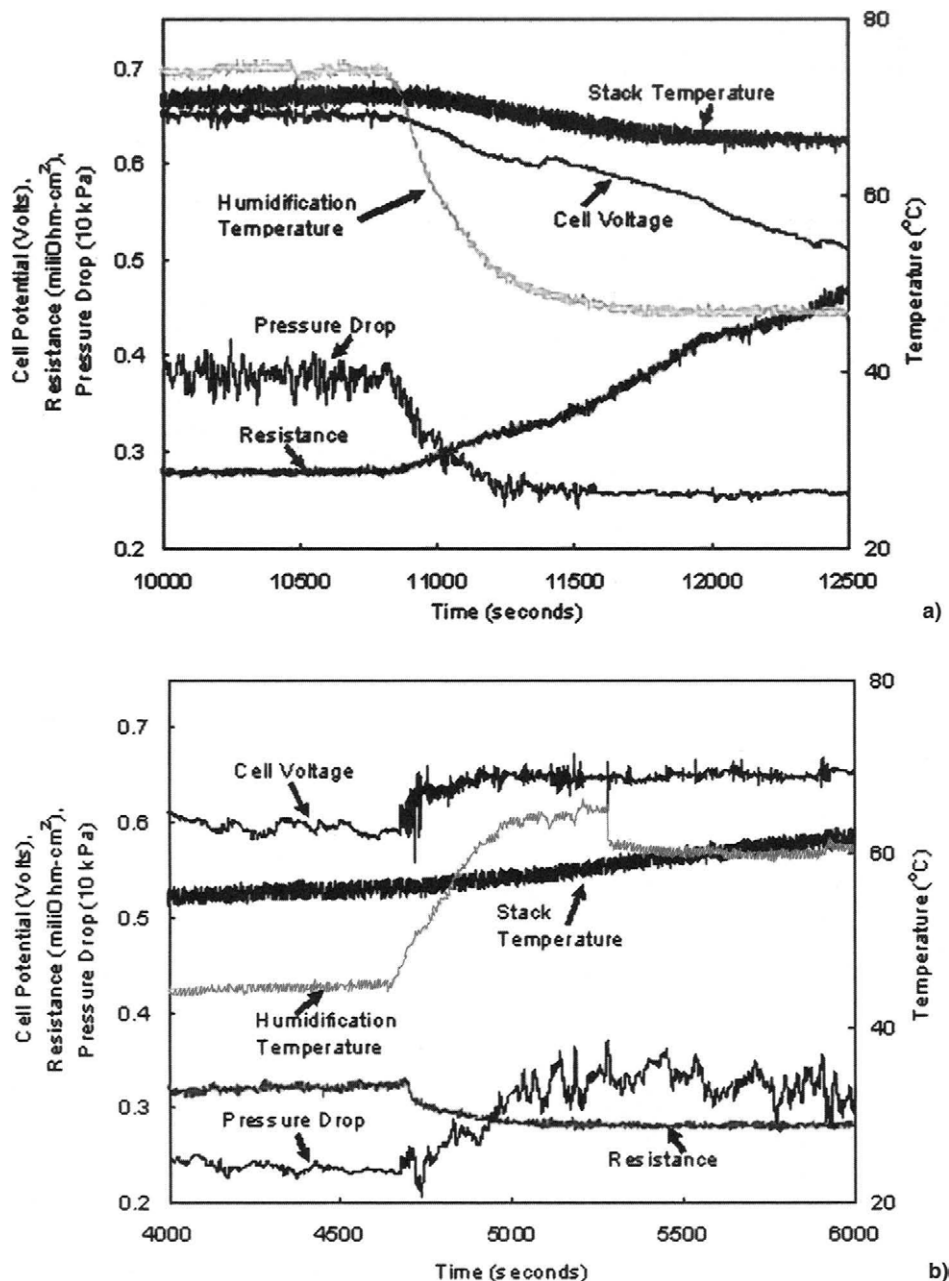


FIGURE 8-12. Illustration of stack drying caused by a) insufficient humidification and b) recovery [13].

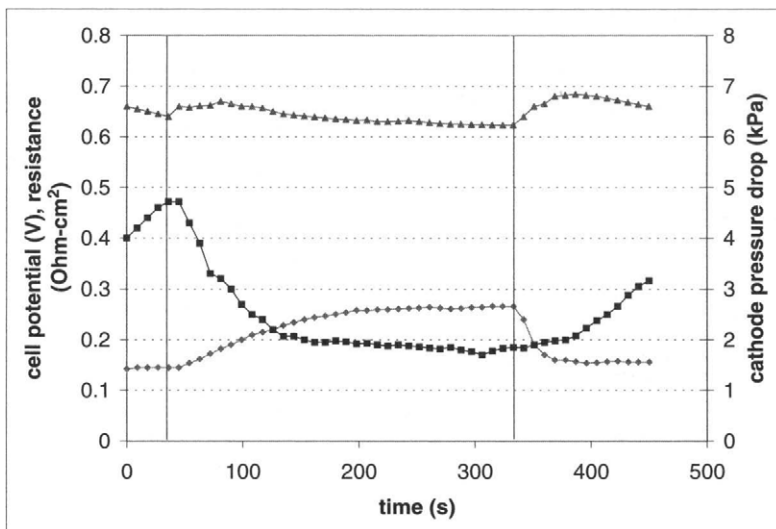


FIGURE 8-13. An example of pressure drop decrease during cell drying. (Adapted from [10]).

cal for a working fuel cell stack, it may be very useful during the cell design process and particularly for verification and calibration of the numerical models.

Because the bipolar plates are good electrical conductors, uneven current distribution resulting at the reaction sites, that is, in the catalyst layers, quickly equalizes. To map the current distribution, measurement must be taken before current gets a chance to equalize. This may be accomplished by segmenting a cell in smaller segments isolated from each other, and the current from each segment must be taken out of the cell independently.

Several approaches to current density mapping have been reported. Cleghorn *et al.* [15] pioneered current density distribution measurements on a typical 100-cm<sup>2</sup> lab scale PEM fuel cell setup, using printed circuit board technology to create a segmented current collector and flow field (Figure 8-14). This was used on the anode with segmented gas diffusion and catalyst layers, while the cathode employed regular unsegmented diffusion and catalyst layers, current collector, and flow field. The effects of anode and cathode stream humidity and stoichiometric flow rate of air on the steady state current density distribution were studied (Figure 8-15). The authors used a specially designed multiplexer to control the voltage at the various segments, which allowed only analysis of steady state behavior.

Stumper *et al.* [16] analyzed several methods for current density distribution mapping. The first approach involved the use of several different

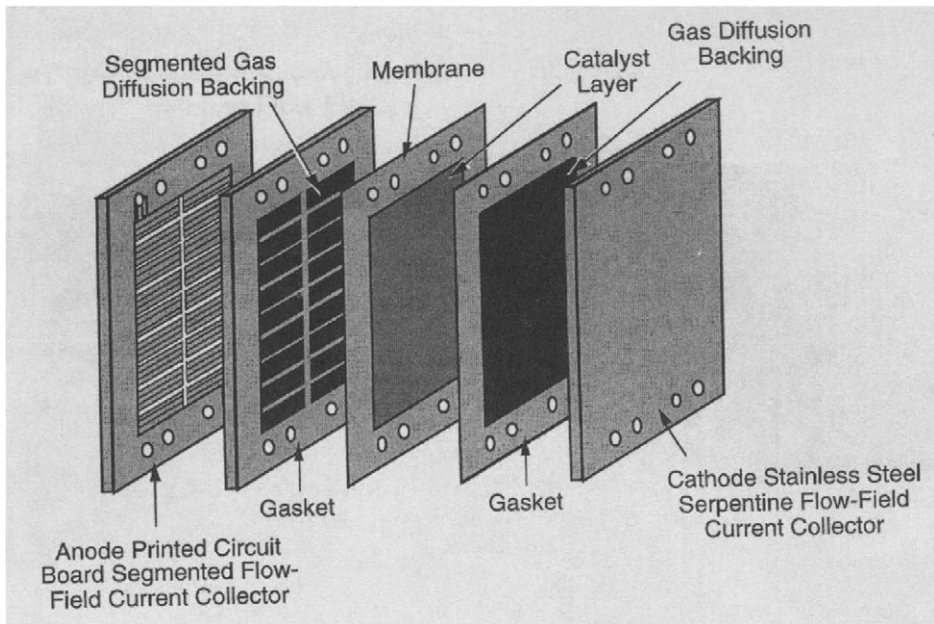


FIGURE 8-14. Segmented fuel cell design used for current density mapping [15]. (Reprinted with kind permission of Springer Science and Business Medicine.)

MEAs with a catalyzed active area of varying fractions of the total flow field area. In the second approach, the authors used a number of “subcells” at various locations along the gas flow channel that were electrically insulated from the main active MEA and controlled by a separate load. In the third approach, a network of passive graphite resistors were placed between the flow field plate and the current collecting bus plate, while the potential drop across these resistors was monitored to establish the current flowing through them. However, none of these methods provided sufficient spatial resolution, and all involved significant errors due to lateral currents and/or contact resistance.

Wieser *et al.* [17] proposed the use of an array of Hall sensors with a segmented current collector and flow field for local current density measurements. The authors used unsegmented electrodes in their study. The use of numerous Hall sensors can significantly complicate the experimental setup, making experimentation expensive and tedious. Moreover, interference from neighboring segments is also possible.

Natarajan and Nguyen [18] presented some qualitative results on hydrogen starvation effects using a segmented current collector and segmented electrode (diffusion and catalyst layers) setup on the anode side, while using a single common electrode and current collector on the cathode side. The authors employed six segments along a single straight channel

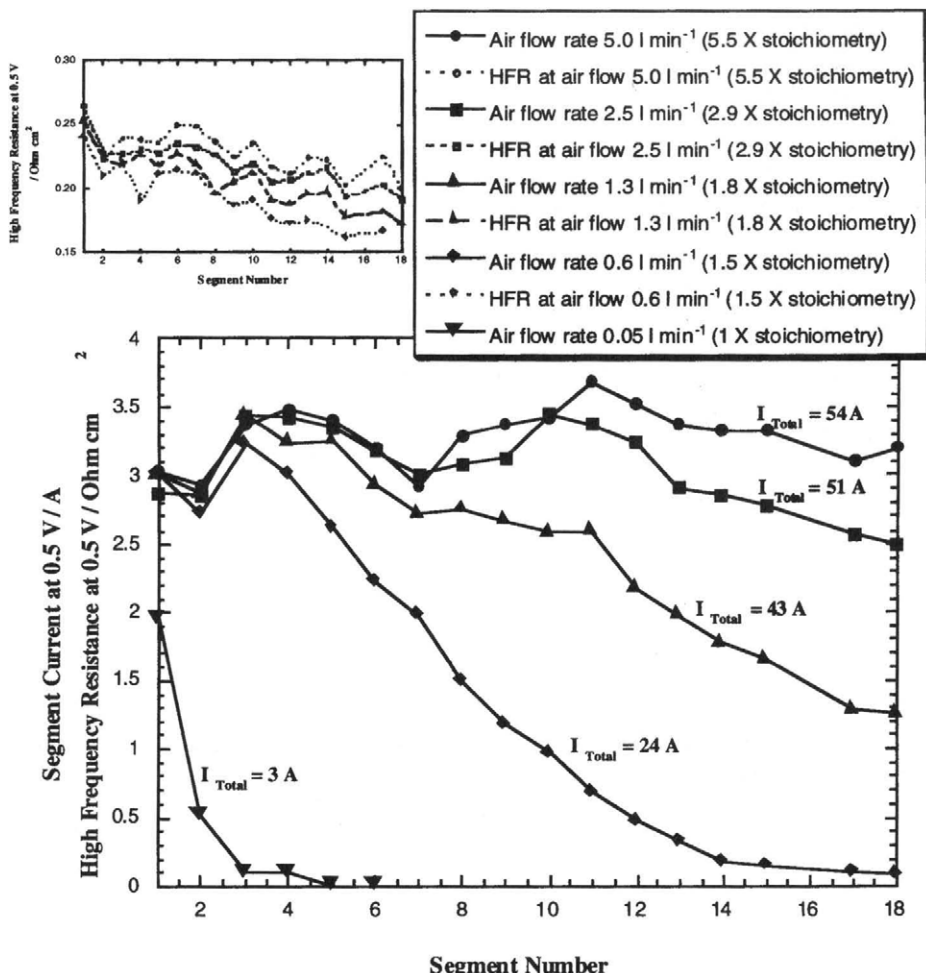


FIGURE 8-15. Current density in segments at different total currents resulting from different air flow rates (HF resistance is shown in small window) [15]. (Reprinted with kind permission of Springer Science and Business Medicine.)

(corresponding to the conventional or serpentine flow field design) that were individually controlled by a multichannel potentiostat/galvanostat to avoid the possible pitfalls associated with the use of a single load and a multiplexer.

Recently, Mench and Wang [19] used specially built segmented flow fields with serpentine flow channels for both the anode and cathode sides, where the individual segments were separately controlled by a multichannel potentiostat/galvanostat. The segmented flow fields were fabricated by embedding gold-plated stainless steel ribs in a polycarbonate block. The

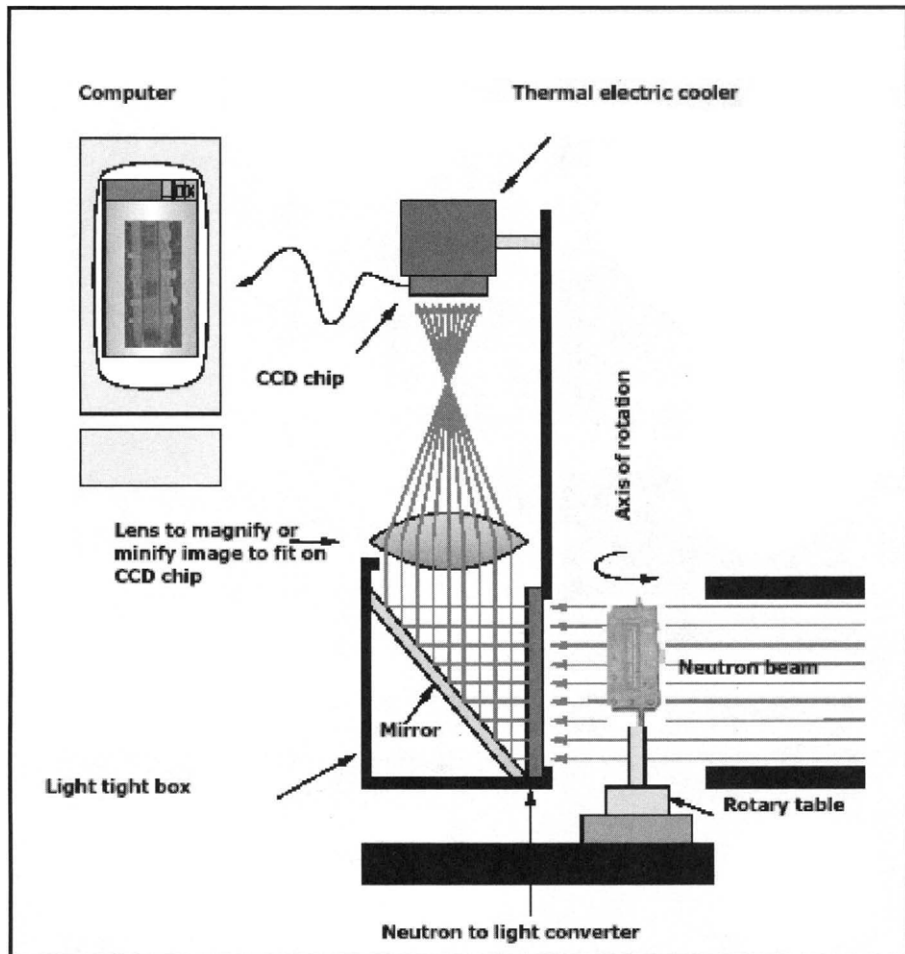


FIGURE 8-16. A setup for neutron imaging of a fuel cell [20].

authors employed commercially available MEAs where the electrodes were not segmented.

## 8.6. Neutron Imaging

For diagnostic purposes a fuel cell may be exposed to a neutron beam (Figure 8-16). Neutrons provide the contrast necessary to image the hydrogen and water in a PEMFC without suffering significant reduction while passing through the cell's metal encasement. The use of neutrons to image fuel cells was first demonstrated in 1998 by Bellows *et al.* [21].

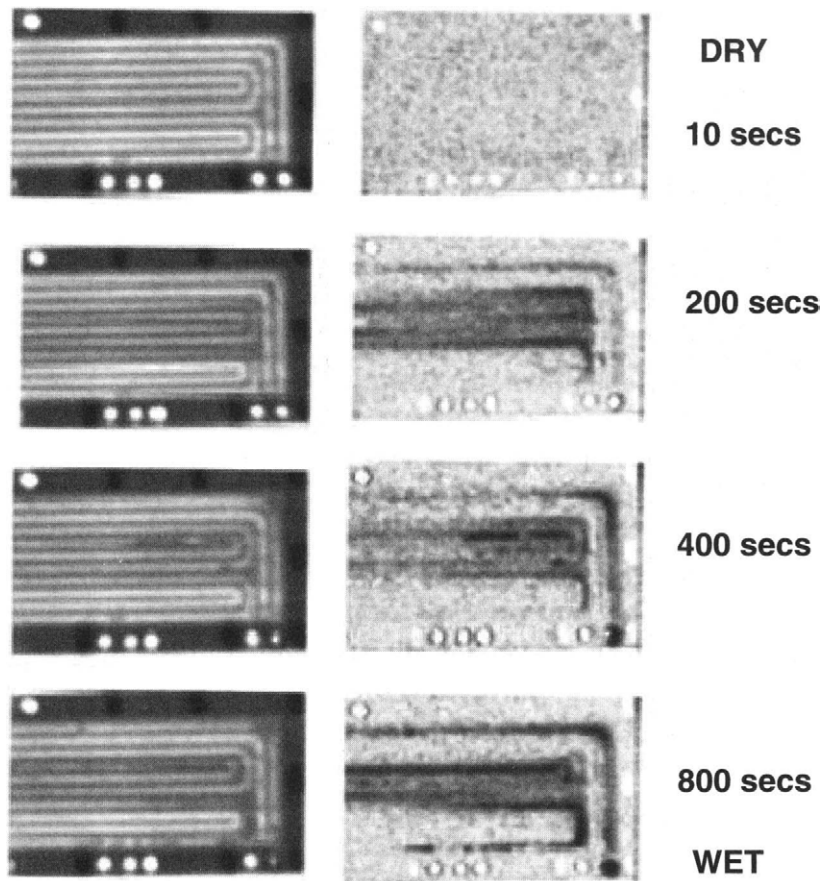


FIGURE 8-17. The results of neutron imaging of an operating fuel cells with the flow channels on the left and water only on the right, showing severe flooding in the channels after approximately 10 minutes of operation [20].

Real-time radiography produces a movie that provides an immediate qualitative evaluation of the water management system. Masking techniques can be used to determine the location of the water in the cell (Figure 8-17) [20]. Normalizing the images allows for quantification of the total cell water content, flow channel water content, and membrane/gas diffusion layer water content. In addition, the 2-D images may be combined to create a digital 3-D representation of the cell that can be manipulated to carefully examine any region of the cell for damage. Neutron imaging appears to be a viable, although expensive, method for detailed evaluation of water management in PEM fuel cells.

## References

1. Ticianelli, E. A., C. R. Derouin, A. Redondo, and S. Srinivasan, Methods to Advance Technology of Proton Exchange Membrane Fuel Cells, *Journal of the Electrochemical Society*, Vol. 135, 1998, p. 2209.
2. Ralph, T. R. and M. P. Hogarth, Catalysis for Low Temperature Fuel Cells, *Platinum Metal Review*, Vol. 46, No. 1, 2002, pp. 3–14.
3. Smith, M., D. Johnson, and L. Scribner, Electrical Test Methods for Evaluating Fuel Cell MEA Resistance, *Fuel Cell Magazine*, March 2004, p. 15.
4. Selman, J. R. and Y. P. Lin, Application of AC Impedance in Fuel Cell Research and Development, *Electrochimica Acta*, Vol. 38, No. 14, 1993, pp. 2063–2073.
5. Springer, T. E., T. A. Zawodzinski, M. S. Wilson, and S. Gottesfeld, Characterization of Polymer Electrolyte Fuel Cells Using AC Impedance Spectroscopy, *Journal of the Electrochemical Society*, Vol. 143, 1996, pp. 587–599.
6. Paganin, V. A., C. L. F. Oliveira, E. A. Ticianelli, T. E. Springer, and E. R. Gonzalez, Modelistic Interpretation of the Impedance Response of a Polymer Electrolyte Fuel Cell, *Electrochimica Acta*, Vol. 43, 1998, pp. 3761–3766.
7. Gileadi, E., *Electrode Kinetics for Chemists, Chemical Engineers and Material Scientists* (VCH Publishers, New York, 1993).
8. Bosco, A. D. and M. H. Fronk, Fuel cell flooding detection and correction, U.S. Patent No. 6, 103, 409, 2000.
9. Mathias, M. F. and S. A. Grot, System and method for controlling the humidity level of a fuel cell, U.S. Patent No. 6, 376, 111, 2002.
10. Barbir, F., A. Husar, and R. Venkataraman, Pressure Drop as a Diagnostic Tool for PEM Fuel Cells (Electrochemical Society Fall Meeting, San Francisco, September 2001).
11. He, W., G. Lin, and T. V. Nguyen, Diagnostic Tool to Detect Electrode Flooding in Proton-Exchange-Membrane Fuel Cells, *AIChE Journal*, Vol. 49, No. 12, 2003, pp. 3221–3228.
12. Rodatz, P., F. Buechi, C. Onder, and L. Guzzella, Operational Aspects of a Large PEFC Stack Under Practical Conditions, *Journal of Power Sources*, Vol. 128, 2004, pp. 208–217.
13. Barbir, F., H. Gorgun, and X. Wang, Relationship Between Pressure Drop and Cell Resistance as a Diagnostic Tool for PEM Fuel Cells, *Journal of Power Sources* (in press) 2004.
14. Voss, H. H., D. P. Wilkinson, P. G. Pickup, M. C. Johnson, and V. Basura, Anode Water Removal: A Water Management and Diagnostic Technique for Solid Polymer Fuel Cells, *Electrochimica Acta*, Vol. 40, No. 3, 1995, pp. 321–328.
15. Cleghorn, S., C. R. Derouin, M. S. Wilson, and S. Gottesfeld, A Printed Circuit Board Approach to Measuring Current Distribution in a Fuel Cell, *Journal of Applied Electrochemistry*, Vol. 28, 1998, pp. 663–672.
16. Stumper, J., S. A. Campbell, D. P. Wilkinson, M. C. Johnson, and M. Davis, In-Situ Methods for the Determination of Current Distributions in PEM Fuel Cells, *Electrochimica Acta*, Vol. 43, No. 24, 1998, pp. 3773–3783.
17. Wieser, C. H., A. Helmbold, and E. Gulzow, A New Technique for Two-Dimensional Current Distribution Measurements in Electrochemical Cells, *Journal of Applied Electrochemistry*, Vol. 30, 2000, p. 803.
18. Natarajan, D. and T. V. Nguyen, Experimental Investigation of Spatial-Temporal Current Distribution in a PEM Fuel Cell, in *Proc. of the AIChE*

*2000 Annual Meeting and Symposium on Fuel Cells, Systems and Processors II, Paper No. 4* (Los Angeles, CA, 12–17 November 2000).

19. Mench, M. M., C. Y. Wang, and M. Ishikawa, In-Situ Current Distribution Measurements in Polymer Electrolyte Fuel Cells, *Journal of the Electrochemical Society*, Vol. 150, 2003, p. A1052.
20. Arif, M., D. Jacobson, P. Huffman, and R. Satija, New Neutron Imaging Facility At The NIST Reactor For Fuel Cell Research, Fuel Cells Lab R&D Review Meeting, May 9–10, 2002, Golden, CO <http://www.eere.energy.gov/hydrogenandfuelcells/pdfs/nn0123ad.pdf> (accessed February 2005).
21. Bellows, R. J., M. Y. Lin, M. Arif, A. K. Thompson, and D. Jacobson, Neutron Imaging Technique for In Situ Measurement of Water Transport Gradients Within Nafion in Polymer Electrolyte Fuel Cells, *Journal of the Electrochemical Society*, Vol. 146, 1999, p. 1099.

## Problems

### Problem No. 1:

Approximate the polarization curve given in the below equation:

$$V_{\text{cell}} = V_0 - b \ln(i/i_0) - Ri.$$

Applying the least squares method, estimate the values for the parameters in the previous equation, namely  $V_0$ ,  $b$ ,  $i_0$ , and  $R$ .

$i$ (mA cm $^{-2}$ )	5	10	20	50	100	200	400	600	800
$V$ (V)	0.933	0.912	0.891	0.859	0.830	0.791	0.734	0.683	0.635

### Problem No. 2:

For the fuel cell equivalent circuit shown in Figure 8-9, derive the equations for real and imaginary parts of the impedance.

### Problem No. 3:

For the fuel cell equivalent circuit shown in Figure 8-7, given with  $R_R = 0.2$  mOhm,  $R_{\text{act}} = 1$  mOhm, and  $C = 5 \mu\text{F}$ , calculate real and imaginary parts of the impedance,  $\text{Re}Z$  and  $\text{Im}Z$ , and plot the Nyquist diagram.

## Quiz

1. Hysteresis of the fuel cell polarization curve is caused by:
  - a) either cell drying or flooding
  - b) cell flooding only
  - c) cell resistance

2. If a cell is flooded in the cathode catalyst layer, fuel cell polarization curve generated with helox (21% O<sub>2</sub> and 79% He) as the cathode gas will be:
- a) the same as polarization curve generated with air
  - b) above the polarization curve generated with air, particularly at higher current densities
  - c) the same as polarization curve generated with pure oxygen
3. In current interrupt technique, cell resistance is:
- a) the remaining cell voltage immediately after current interrupt
  - b) the difference between the cell voltage immediately after and before current interrupt
  - c) the difference between the cell voltage immediately after current interrupt and open circuit voltage
4. A fuel cell equivalent circuit consists of:
- a) at least one resistor and one capacitor
  - b) at least two resistors and one capacitor
  - c) at least two capacitors and one resistor
5. A Nyquist diagram plots:
- a) frequency vs phase angle
  - b) cell impedance vs cell resistance
  - c) imaginary vs real portion of the impedance
6. Cell resistance may be measured:
- a) with low-frequency AC impedance
  - b) with high-frequency AC impedance
  - c) only with the entire frequency spectrum
7. Which of the following methods cannot be used to check the cell resistance in a nonoperational fuel cell?
- a) current interrupt
  - b) high-frequency AC impedance
  - c) AC impedance spectroscopy
8. In a Nyquist diagram resulting from AC impedance spectroscopy, the cell resistance is represented by:
- a) the radius of the resulting semicircle
  - b) the distance between the origin and the semicircle's center
  - c) the distance between the origin and the closest point on the semicircle

9. Warburg impedance is added to a fuel cell equivalent circuit to represent:
- a) additional activation polarization
  - b) concentration polarization
  - c) electronic cell resistance
10. Cell flooding is likely to result in:
- a) increase in pressure drop through the cathode and no changes in cell resistance
  - b) no changes in pressure drop and decrease in cell resistance
  - c) increase in both pressure drop and cell resistance

# CHAPTER 9

## 9. Fuel Cell System Design

A system is defined as a group of units, objects, or items, so combined as to form a whole and to operate in unison. In case of a fuel cell, the system includes all the necessary components needed to operate a fuel cell stack and deliver electrical current. A fuel cell stack is obviously the heart of a fuel cell system; however, without the supporting equipment the stack itself would not be very useful. The fuel cell system typically involves the following subsystems:

- oxidant supply (oxygen or air),
- fuel supply (hydrogen or hydrogen rich gas),
- heat management,
- water management,
- power conditioning,
- instrumentation and controls.

Depending on the available or chosen fuel and oxidant, the fuel cell systems may be categorized as:

- hydrogen–oxygen systems,
- hydrogen–air systems,
- reformat–air systems.

### 9.1. Hydrogen–Oxygen Systems

Because of technical difficulties, the added size and weight of oxygen storage, and related safety concerns, pure oxygen systems are typically used only in applications where air is not available, such as in submarines and space applications.

#### 9.1.1. Oxygen Supply

Stored oxygen is already under pressure, so the supply of oxygen to a fuel cell involves a pressure regulator to reduce the pressure to the fuel cell oper-

ating pressure. Oxygen should be supplied in excess of stoichiometrically required, typically with stoichiometric ratios of 1.2 to 1.3 (i.e., 20% to 30% excess). The reason for this is that the excess oxygen has to carry the product water from the cell. Excess oxygen may be vented at the fuel cell exit, but most practical systems operate in a closed loop configuration, where excess oxygen is returned back to the stack inlet. An active (pump) or a passive (ejector) device is needed to bring the gas from the low pressure at the stack exit to a higher pressure at the stack inlet. Liquid water at the exhaust may be separated in a simple water-gas separator, and the warm, saturated gas from the exit may be mixed with a dry gas from the tank to obtain desired humidity at the stack inlet. The resulting oxygen supply system is shown in Figure 9-1.

From the mass and energy balance it is possible to calculate the achievable oxygen inlet temperatures for various combinations of operating conditions, namely temperature, pressure, and stoichiometry.

#### *Mass balance:*

Because oxygen from the tank is completely dry, the amount of water at the stack inlet is equal to the amount of water vapor at the stack outlet. This also means that the amount of liquid water separated at the stack outlet is equal to water generated in the stack, plus any net water transport from the anode through the membrane. The mass balance equation is:

$$\dot{m}_{H_2O,in(v)} + \dot{m}_{H_2O,in(l)} = \dot{m}_{H_2O,out(v)} \quad (9-1)$$

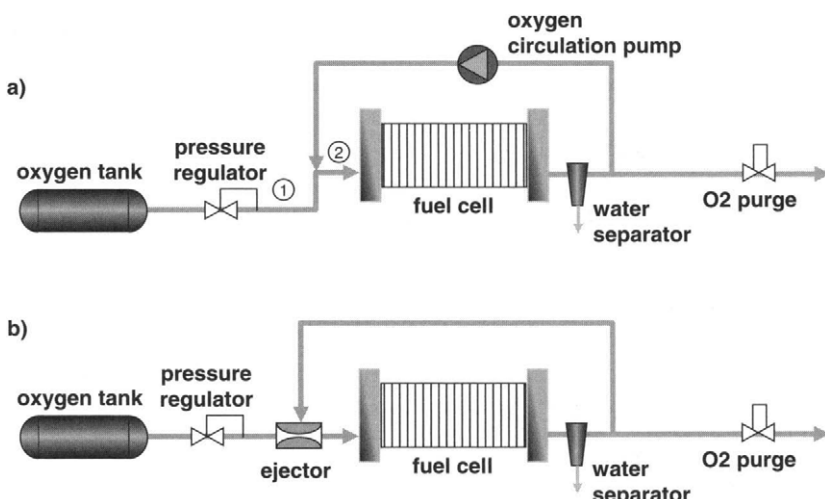


FIGURE 9-1. Closed loop oxygen supply system. a) with circulation pump; b) with ejector

where:

indexes in and out refer to in and out of the fuel cell stack, and indexes {v} and {l} refer to vapor and liquid form, respectively.

$\dot{m}_{H_2O,in(v)}$  = the mass flow of water vapor at stack inlet:

$$\dot{m}_{H_2O,in(v)} = \min \left[ \frac{IN_{cell}}{4F} M_{H_2O} S_{O_2} \frac{P_{sat}(t_{in})}{P_{out} - P_{sat}(t_{in})}, \dot{m}_{H_2O,out(v)} \right] \quad (9-2)$$

and

$\dot{m}_{H_2O,out(v)}$  = mass flow of water vapor at stack outlet:

$$\dot{m}_{H_2O,out(v)} = \frac{IN_{cell}}{4F} M_{H_2O} (S_{O_2} - 1) \frac{P_{sat}(t_{out})}{P_{out} - P_{sat}(t_{out})} \quad (9-3)$$

Depending on the pressure and temperature at the stack inlet, not all water may be in a vapor form. The amount of liquid water at the stack inlet,  $\dot{m}_{H_2O,in(l)}$ , may be calculated from Equation (9-1). However, temperature at the stack inlet,  $t_{in}$ , is unknown and must be found from the energy balance. Energy balance for mixing of two streams is (the numbers correspond to those in Figure 9-1):

$$H_1 + H_4 = H_2 \quad (9-4)$$

where:

$H_1$  = enthalpy of oxygen from the tank:

$$H_1 = \frac{IN_{cell}}{4F} M_{O_2} c_{p,O_2} t_{tank} \quad (9-5)$$

$H_4$  = enthalpy of oxygen and water vapor at the stack outlet:

$$H_4 = \frac{IN_{cell}}{4F} (S_{O_2} - 1) \left[ M_{O_2} c_{p,O_2} t_{st,out} + M_{H_2O} \frac{P_{sat}(t_{st,out})}{P_{out} - P_{sat}(t_{st,out})} (c_{p,H_2O(v)} t_{st,out} + h_{fg}^0) \right] \quad (9-6)$$

$H_2$  = enthalpy of the mix, that is, oxygen and water at the stack inlet:

$$H_2 = \frac{IN_{cell}}{4F} S_{O_2} M_{O_2} c_{p,O_2} t_{st,in} + \dot{m}_{H_2O,in(v)} (c_{p,H_2O(v)} t_{st,in} + h_{fg}^0) + \dot{m}_{H_2O,in(l)} c_{p,H_2O(l)} t_{st,in} \quad (9-7)$$

The results are shown in Figure 9-2. Oxygen from the tank is assumed to be at 20°C and dry. It should be noted that for the points above the saturation line the oxygen at the stack inlet is oversaturated, that is, it contains liquid water, but below the saturation line the oxygen is undersaturated. In either case the resulting temperature at oxygen inlet is below the stack operating temperature.

If this simple humidification scheme is not sufficient, active humidification of oxygen must be applied, using the liquid water collected from the stack exhaust and the heat from the stack (Figure 9-3). This way it is possible to reach saturation at a temperature closer to the stack operating temperature. Sometimes, humidification is accomplished in a separate section of the stack, also using the stack heat, as shown in Chapter 6.

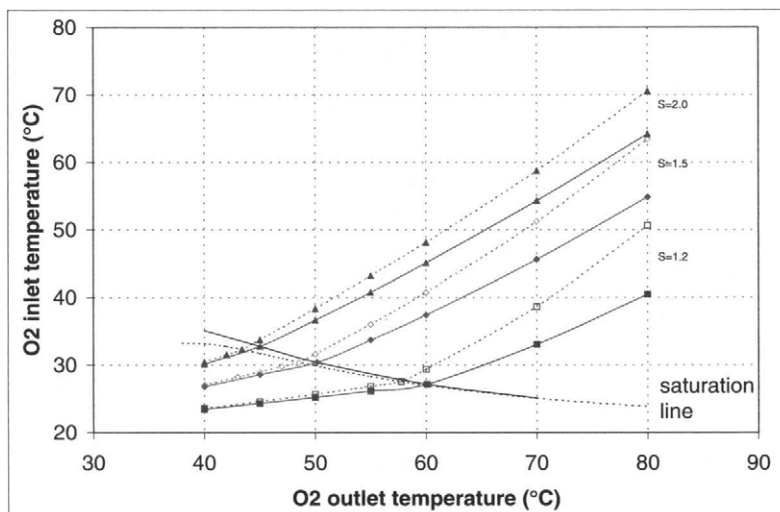


FIGURE 9-2. Achievable oxygen temperature at the stack inlet when the oxygen exhaust is recirculated back to the inlet, as shown in Figure 9-1; dashed lines are for atmospheric pressure and solid lines are for 300 kPa.

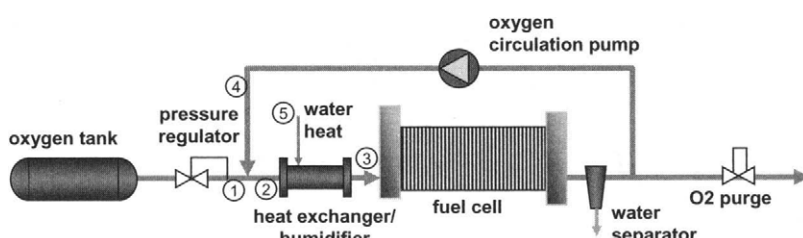


FIGURE 9-3. Closed loop oxygen supply system with humidifier.

The amount of water needed to be added in the humidifier can be calculated from the mass balance:

$$\dot{m}_{H_2O,in} = \frac{IN_{cell}}{4F} M_{H_2O} \left[ S_{O_2} \frac{\varphi P_{sat}(T_{in})}{P_{in} - \varphi P_{sat}(T_{in})} - (S_{O_2} - 1) \frac{P_{sat}(T_{out})}{P_{out} - P_{sat}(T_{out})} \right] \quad (9-8)$$

The amount of heat needed to ensure that all the water at the fuel cell entrance is in vapor form can be calculated from the energy balance (the numbers correspond to those in Figure 9-3):

$$H_{in} = H_3 - H_1 - H_4 - H_5 \quad (9-9)$$

where:

$H_3$  = enthalpy of oxygen and water vapor at the stack inlet:

$$H_3 = \frac{IN_{cell}}{4F} S_{O_2} \left[ M_{O_2} c_{p,O_2} t_{st,in} + M_{H_2O} \frac{\varphi P_{sat}(t_{st,in})}{P_{in} - \varphi P_{sat}(t_{st,in})} (c_{p,H_2O(v)} t_{st,in} + h_{fg}^0) \right] \quad (9-10)$$

$H_1$  = enthalpy of oxygen from the tank as defined previously (Equation 9-5)

$H_4$  = enthalpy of oxygen and water vapor at the stack outlet, also defined previously (Equation 9-6)

$H_5$  = enthalpy of liquid water added to the humidifier:

$$h_5 = \dot{m}_{H_2O,in} c_{p,H_2O(l)} t_w \quad (9-11)$$

### 9.1.2. Hydrogen Supply

The fuel for PEM fuel cells is hydrogen. Hydrogen is the lightest and most abundant element in the universe; however, on Earth it is not present in its molecular form, but in many chemical compounds, such as water or hydrocarbons. Hydrogen is therefore not an energy source but a synthetic fuel that must be produced. For fuel cell systems, hydrogen may be produced elsewhere and then stored as a part of the system, or hydrogen generation may be a part of a fuel cell system. The systems with hydrogen storage are typically much simpler and more efficient, but hydrogen storage requires a lot of space even when hydrogen is compressed to very high pressures or even liquefied. Table 9-1 shows some hydrogen properties.

The most common way of storing hydrogen is in high-pressure cylinders. Typical storage pressures are between 200–450 bars (3000 or 6600 psi), and even 690 bar (10,000 psi) has been reported [4]. Table 9-2 shows the required volume to store 1 kg of hydrogen at different pressures (1 kg of hydrogen happens to be the energy equivalent of 1 gallon of gasoline).

**TABLE 9-1**  
Hydrogen Properties (Compiled from [1-3])

Property	Unit	Value
Molecular weight	$\text{kg kmol}^{-1}$ ( $\text{g mol}^{-1}$ )	2.016
Density	$\text{kg m}^{-3}$ ( $\text{g l}^{-1}$ )	0.0838
Higher heating value	$\text{MJ kg}^{-1}$	141.9
	$\text{MJ m}^{-3}$	11.89
Lower heating value	$\text{MJ kg}^{-1}$	119.9
	$\text{MJ m}^{-3}$	10.05
Boiling temperature	K	20.3
Density as liquid	$\text{kg m}^{-3}$	70.8
Critical temperature	K	32.94
Critical pressure	bar	12.84
Critical density	$\text{kg m}^{-3}$	31.40
Self ignition temperature	K	858
Ignition limits in air	(vol. %)	4–75
Stoichiometric mixture in air	(vol. %)	29.53
Flame temperature in air	K	2318
Diffusion coefficient	$\text{m}^2 \text{s}^{-1}$	0.61
Specific heat	$\text{kJ kg}^{-1} \text{K}^{-1}$ ( $\text{J g}^{-1} \text{K}^{-1}$ )	14.89

**TABLE 9-2**  
Required Volume to Store 1 kg of Hydrogen as Compressed Gas

Pressure kPa	Volume liters
100	128.8
200	68.7
340	43.9
480	33.5
690	26.0

Hydrogen storage in conventional steel cylinders (at 2200psi) is not practical for almost any application because those are too heavy (although a fuel cell-powered submarine built by Perry Technologies in 1989 used those for storage of both hydrogen and oxygen [5]). Lightweight composite tanks constructed with an aluminum body wrapped by composite fiber and epoxy resin have been developed for storage of hydrogen in automotive application, allowing storage density as high as 5% hydrogen (by weight). However, when the tank support, valves, and pressure regulators are taken into account, practical storage densities are between 3% and 4% hydrogen by weight. These tanks come in different sizes, ranging from 30 to 300 liters (for up to 8 kg of hydrogen at 450 bar [6]).

Another option is to store hydrogen in a liquid form. Hydrogen is liquid at 20.3 K. This is a common way to store relatively large quantities of hydrogen. Smaller tanks for use in automobiles have been developed and demonstrated by BMW [7]. They can reach storage efficiency of 14.2% hydrogen by weight and require about 22 liters to store 1 kg of hydrogen. These tanks must be specially constructed and heavily insulated to minimize hydrogen boil-off. A relatively simple evaporator is sufficient to produce gaseous hydrogen needed for fuel cell applications.

Yet another way of storing hydrogen is in metal hydrides. Some metals (such as various alloys of magnesium, titanium, iron, manganese, nickel, chromium, and others) form metal hydrides when exposed to hydrogen. Hydrogen atoms are packed inside the metal lattice structure, and because of that, higher storage densities may be achieved than with compressed hydrogen (1 kg hydrogen can be stored in 35–50 liters). The problem with this storage is that the metals are intrinsically heavy; storage efficiency of 1.0% to 1.4% hydrogen by weight can be achieved. Higher storage efficiencies have been reported with some metal hydrides, but those are typically high-temperature metal hydrides (above 100°C) and thus not practical with low-temperature PEM fuel cells. To release hydrogen from metal hydrides, heat is required. Waste heat from the fuel cell, in both water-cooled and air-cooled systems, is sufficient to release hydrogen from low-temperature metal hydrides. Because hydrogen is stored in basically solid form, this is considered one of the safest hydrogen storage methods.

Several chemical ways of storing hydrogen have been proposed and some practically demonstrated, such as hydrazine, ammonia, methanol, ethanol, lithium hydride, sodium hydride, sodium borohydride, lithium borohydride, diborane, calcium hydride, and so forth. Although attractive because most of them are in liquid form and offer relatively high hydrogen storage efficiencies (up to 21% by weight for diborane), they require some kind of a reactor to release hydrogen. In addition, some of them are toxic and some can cause severe corrosion problems.

Once hydrogen is released from the storage tank, the simplest way to supply hydrogen to a fuel cell is in the dead-end mode (Figure 9-4a). Such a system would only require a preset pressure regulator to reduce the pressure from the stack to the fuel cell operating pressure. The long-term operation in a dead-end mode may be possible only with extremely pure gasses, both hydrogen and oxygen. Any impurities present in hydrogen will eventually accumulate in the fuel cell anode. This also includes water vapor that may remain (when the back diffusion is higher than the electroosmotic drag), which may be the case with very thin membranes and when operating at low current densities. In addition, inerts and impurities may diffuse from the air side until an equilibrium concentration is established. To eliminate this accumulation of inerts and impurities, purging of the hydrogen compartment may be required (Figure 9-4b). This may be programmed either as a function of cell voltage or as a function of time.

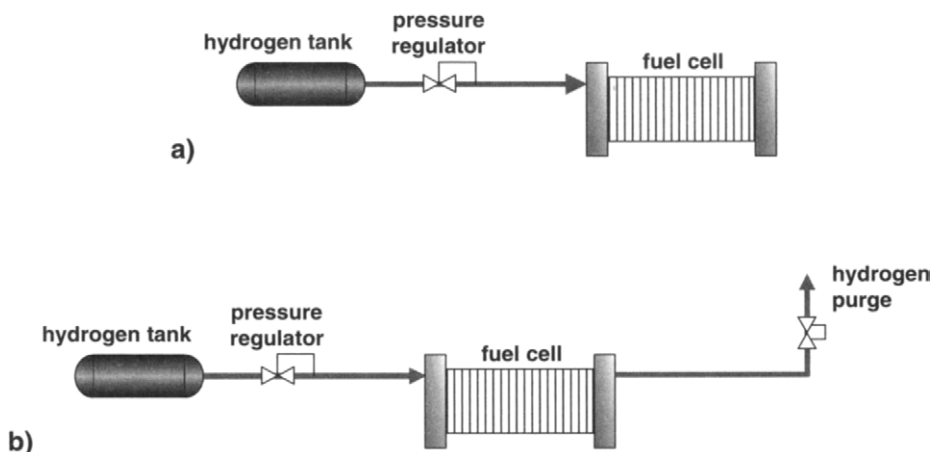


FIGURE 9-4. Hydrogen supply schemes: a) dead-end; b) dead-end with intermittent purging.

If purging of hydrogen is not possible or preferred because of safety, mass balance, or system efficiency reasons, excess hydrogen may be flown through the stack ( $S > 1$ ) and unused hydrogen returned to the inlet, either by a passive (ejector) or an active (pump or compressor) device (Figure 9-5). In either case, it is preferred to separate and collect any liquid water that may be present at the anode outlet. The amount of liquid water to be collected depends on operating conditions and membrane properties. In thinner membranes, back diffusion may be higher than the electroosmotic drag, and some of the product water may exit the stack at the anode side.

Hydrogen typically must be humidified up to 100% relative humidity before entering the fuel cell stack, in order to avoid drying of the membrane due to electroosmotic drag. In that case a humidifier/heat exchanger is needed at the stack inlet (Figure 9-6). Hydrogen may be humidified by water injection and simultaneously or subsequently heated to facilitate evaporation of water, or by membrane humidification, that allows water and heat exchange.

### 9.1.3. Water and Heat Management—System Integration

In addition to supplying the reactants to the fuel cell stack, the fuel cell system also must take care of the fuel cell by-products—water and heat. Water plays an important role in fuel cell operation. As discussed in Chapter 4, water is essential for proton transport across the polymer membrane. Because of that, in principle, both cathode and anode reactants must be humidified before entering a fuel cell stack. Water must be collected at the fuel cell exhaust for reuse.

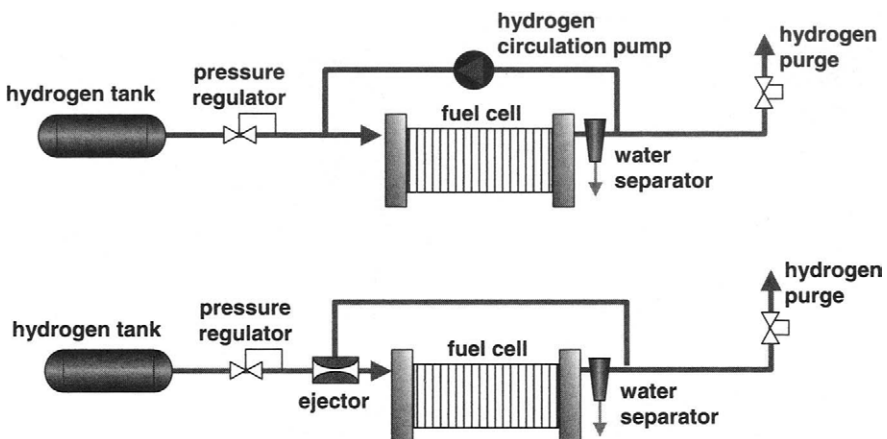


FIGURE 9-5. Closed loop hydrogen supply system with pump (above) and ejector (below).

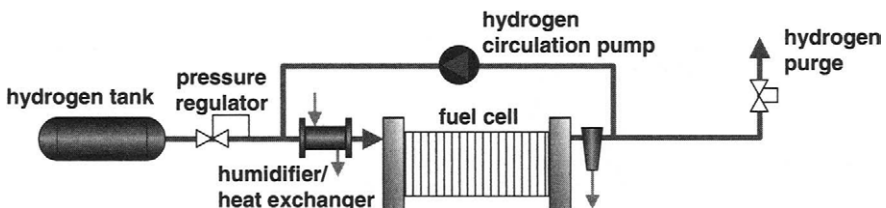


FIGURE 9-6. Closed loop hydrogen supply system with humidifier.

In a closed loop configuration, the system is always operating in the water production mode. Both reactant gases are stored dry, humidified at the inlet, and unused gases are recirculated from the outlet back to the inlet after the liquid water has been removed and collected in a tank. The tank must be sized so that it can store the produced water. On a system level, including hydrogen and oxygen storage tanks, the mass of the system does not change, that is, hydrogen and oxygen are converted to water. The mass of water increases with time as the mass of hydrogen and oxygen in the tanks decreases.

The same water may be used for humidification and to remove the heat from the stack. Heat is discharged from the system through a radiator or a liquid/liquid heat exchanger (depending on the application). Figure 9-7 shows an example of a hydrogen-oxygen closed loop system [8].

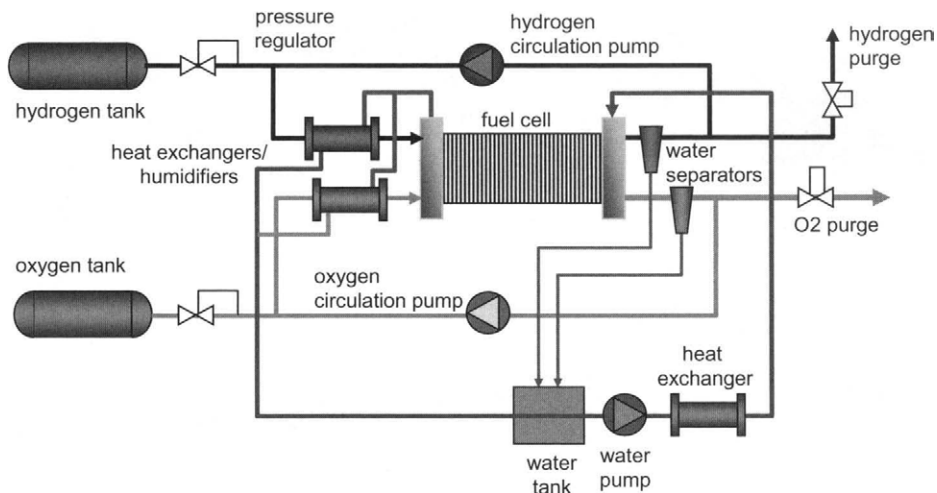


FIGURE 9-7. An example of closed loop hydrogen-oxygen fuel cell system.

## 9.2. Hydrogen–Air Systems

For most terrestrial systems it is more practical to use oxygen from air than to carry oxygen as a part of the fuel cell system. Oxygen content in air is 20.95% by volume. This dilution has a penalty on fuel cell voltage (about 50 mV), as shown in Chapter 3. Additional penalty in both power output and efficiency is because oxygen and almost 4 times that of nitrogen must be somehow pumped through the fuel cell.

### 9.2.1. Air Supply

In hydrogen-air systems, air is supplied by a fan or a blower (for low-pressure systems) or by an air compressor (for pressurized systems). In the former case, the exhaust from the fuel cell is opened directly into the environment (Figure 9-8a), whereas in a pressurized system, pressure is maintained by a preset pressure regulator (Figure 9-8b).

In any case, a fan, blower, or compressor is run by an electric motor that requires electrical power and thus represents power loss or parasitic load. Compression may be either isothermal or adiabatic. The former implies an infinitesimally slow process allowing temperature equilibration with the environment. The latter implies quite the opposite—a process so fast that no heat is exchanged with the environment during the compression. This is much closer to real life where the speed of compression is such that it does not allow heat exchange with the environment.

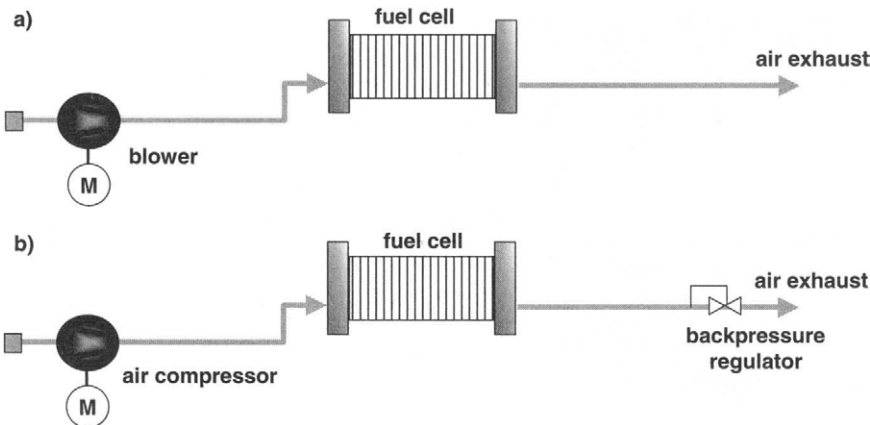


FIGURE 9-8. Air supply for a fuel cell system: a) ambient pressure; b) pressurized system.

The ideal power needed for adiabatic compression of air from pressure  $P_1$  to pressure  $P_2$  is:

$$W_{\text{comp,ideal}} = \dot{m}_{\text{Airin}} \cdot c_p \cdot T_1 \left[ \left( \frac{P_2}{P_1} \right)^{\frac{k-1}{k}} - 1 \right] \quad (9-12)$$

where:

$\dot{m}_{\text{Airin}}$  = air flow rate,  $\text{g s}^{-1}$

$c_p$  = specific heat,  $\text{J g}^{-1} \text{K}^{-1}$

$T_1$  = temperature before compression, K

$P_2$  = pressure after compression, Pa

$P_1$  = pressure before compression, Pa

$k$  = ratio of specific heats (for diatomic gases  $k = 1.4$ )

However, no compression is ideal, that is, there are inefficiencies associated with the compression process that result in more power needed:

$$W_{\text{comp}} = \frac{\dot{m}_{\text{Airin}} \cdot c_p \cdot T_1}{\eta_{\text{comp}}} \left[ \left( \frac{P_2}{P_1} \right)^{\frac{k-1}{k}} - 1 \right] \quad (9-13)$$

where the efficiency,  $\eta_{\text{comp}}$ , is defined as a ratio between ideal (adiabatic) and actual compression power.

From the energy balance it is possible to calculate the temperature at the end of compression:

$$T_2 = T_1 + \frac{T_1}{\eta_{\text{comp}}} \left[ \left( \frac{P_2}{P_1} \right)^{\frac{k-1}{k}} - 1 \right] \quad (9-14)$$

The actual electric power draw for compression is even larger than  $W_{\text{comp}}$  from Equation (9-13) because of additional mechanical and electrical inefficiencies:

$$W_{\text{EM}} = \frac{W_{\text{comp}}}{\eta_{\text{mech}} \cdot \eta_{\text{EM}}} \quad (9-15)$$

At higher pressures, above 150 kPa, a compressor's electric motor may consume a significant portion of the fuel cell power output, depending not only on the compressor efficiency but also on the stoichiometric ratio and cell operating voltage, as shown in Figure 9-9.

The net power output,  $W_{\text{net}}$ , is the fuel cell power,  $W_{\text{FC}}$ , less the power delivered to the auxiliary components,  $W_{\text{aux}}$ , which includes the compressor or the blower:

$$W_{\text{net}} = W_{\text{FC}} - W_{\text{aux}} \quad (9-16)$$

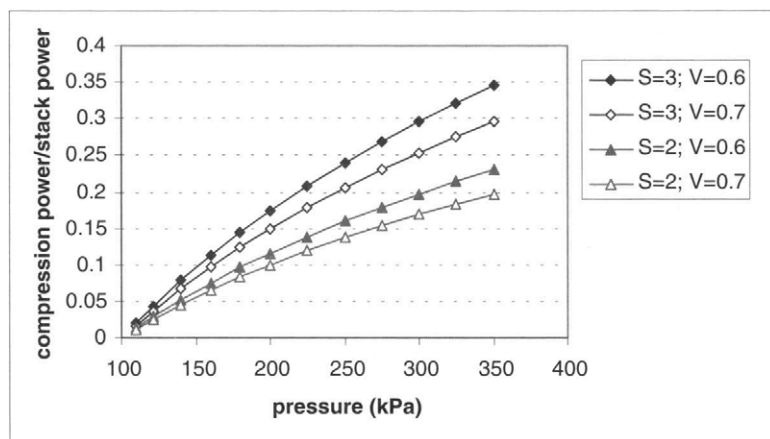


FIGURE 9-9. Compression power as a function of pressure (assuming inlet pressure is atmospheric, inlet temperature of 20°C, and compressor efficiency of 70%).

The net system efficiency is then:

$$\eta_{\text{sys}} = \eta_{\text{FC}} \frac{W_{\text{net}}}{W_{\text{FC}}} = \eta_{\text{FC}} (1 - \xi_{\text{aux}}) \quad (9-17)$$

Where  $\xi_{\text{aux}}$  is the ratio between auxiliary power (also called parasitic losses) and fuel cell power output,  $W_{\text{aux}}/W_{\text{FC}}$ .

One of the main reasons for operating a fuel cell at an elevated pressure is to get more power out of it. However, when compression power is taken into account, operation at higher pressure may not result in more power, as is illustrated in the following example.

*Example 9-1.*

Consider a fuel cell stack that can operate at either 300 kPa or 170 kPa (inlet pressure) with oxygen stoichiometric ratio of 2. The stack performance (polarization curve) is shown in Figure 5.1. Calculate the net power output and the net efficiency at both pressures. Assume current density of 800 mA/cm<sup>2</sup>.

*Solution:*

Operation at higher pressure (300 kPa) would yield 0.66 V per cell (from the polarization curve).

Resulting power density is:  $0.8 \times 0.66 = 0.528 \text{ W cm}^{-2}$

Air flow rate is (Equation 5-42):

$$\dot{m}_{\text{Airin}} = \frac{S_{\text{O}_2}}{r_{\text{O}_2}} \frac{M_{\text{Air}}}{4F} i = \frac{2}{0.21} \frac{29}{4 \times 96485} 0.8 = 5.725 \times 10^{-4} \text{ g s}^{-1} \text{ cm}^{-2}$$

Compression power (from Equation 9-13 or from Figure 9-9, assuming the compressor total efficiency of 0.7):

$$W_{\text{comp}} = \frac{\dot{m}_{\text{Airin}} \cdot c_p \cdot T_1}{\eta_{\text{comp}}} \left[ \left( \frac{P_2}{P_1} \right)^{\frac{k-1}{k}} - 1 \right] = \frac{5.725 \times 10^{-4} \times 1 \times 293}{0.7} \left[ \left( \frac{300}{101.3} \right)^{\frac{1.4-1}{1.4}} - 1 \right]$$

$$= 0.088 \text{ W cm}^{-2}$$

Net power density (Equation 9-16):  $0.528 - 0.088 = 0.440 \text{ W cm}^{-2}$

System efficiency (Equation 9-17):  $\frac{0.66}{1.482} \left( 1 - \frac{0.088}{0.528} \right) = 0.37$

Similar calculation for low-pressure operation (170 kPa) would yield the following results:

Cell potential: 0.60 V per cell

Power density:  $0.480 \text{ W cm}^{-2}$

Compression power:  $0.040 \text{ W cm}^{-2}$

Net power density:  $0.480 - 0.040 = 0.440 \text{ W cm}^{-2}$

System efficiency: 0.37

Therefore, for this particular case there is no apparent advantage in operating this fuel cell at elevated pressure, that is, both systems result in same net power output and same system efficiency. If the voltage difference between these two pressures were less than 60 mV, low pressure would result in more power output and better system efficiency. However, there may be other determining factors, such as operating temperature, which may impact system complexity and performance at different pressures.

The desired air flow rate is maintained by regulating the speed of the compressor. For low-pressure systems, with insignificant compressor power draw, it may be convenient to operate at a constant flow rate, that is, at the constant compressor speed. For high-pressure operating systems, operation at constant flow rate would have a detrimental effect on the system efficiency at partial loads, as shown in the following example.

*Example 9-2.*

For the fuel cell from Example 9-1, calculate the ratio between auxiliary power and fuel cell power output,  $W_{\text{aux}}/W_{\text{FC}}$ , at nominal power, at 50% net power output and at 25% net power output, if the compressor operates at constant speed, that is, providing constant air flow rate.

*Solution:*

At nominal power ( $440 \text{ mW/cm}^2$ ):

$$W_{\text{aux}}/W_{\text{FC}} = 88/528 = 0.167 \text{ at } 300 \text{ kPa}$$

$$W_{\text{aux}}/W_{\text{FC}} = 40/480 = 0.083 \text{ at } 170 \text{ kPa}$$

At 50% nominal power ( $220 \text{ mW/cm}^2$ ):

$$W_{\text{aux}}/W_{\text{FC}} = 88/(220 + 88) = 0.286 \text{ at } 300 \text{ kPa}$$

$$W_{\text{aux}}/W_{\text{FC}} = 40/(220 + 40) = 0.145 \text{ at } 170 \text{ kPa}$$

At 25% nominal power ( $110 \text{ mW/cm}^2$ ):

$$W_{\text{aux}}/W_{\text{FC}} = 88/(110 + 88) = 0.444 \text{ at } 300 \text{ kPa}$$

$$W_{\text{aux}}/W_{\text{FC}} = 40/(110 + 40) = 0.267 \text{ at } 170 \text{ kPa}$$

The system efficiency at 25% nominal power output at 300 kPa would drop to 0.3, because of high parasitic losses, as opposed to 0.485 that would have been if the flow rate were kept proportional to current.

From the previous example it follows that in pressurized systems it is important to regulate the air flow rate in proportion to current being generated.

In general, there are two types of compressors that may be used in pressurized fuel cell systems, namely:

- positive displacement compressors, such as piston, diaphragm, scroll, screw, or rotary vane compressors, or
- centrifugal compressors, radial or axial.

Because of their pressure-flow characteristics, the flow regulation is different for these two types of compressors.

For a positive displacement compressor, the flow rate may be changed without the need to change the back pressure (Figure 9-10), by simply reducing the speed of the motor,  $N_p$ . The pressure is somewhat higher at higher flow rates as a function of pressure drop through the stack. Note that the compressor efficiency may not be the same along the operation line. The compressor efficiency at both partial load and nominal power should be taken into account when selecting the compressor for a fuel cell system.

However, the centrifugal compressors have different pressure-flow rate characteristics. The centrifugal compressors must not be operated in the low-flow region, left of the surge line. In fuel cell systems, this means that the flow regulation must be accompanied by the pressure regulation as well, in order to keep the operating point right of the compressor surge line (Figure 9-11). This happens to be beneficial in terms of compressor efficiency. By changing both flow rate and pressure, it is possible to operate with high efficiencies through a wide range of flow rates.

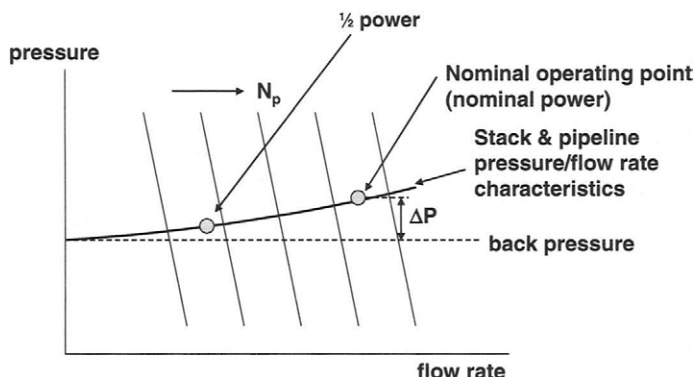


FIGURE 9-10. Reduction of flow rate does not need a change in back pressure for positive displacement compressors.

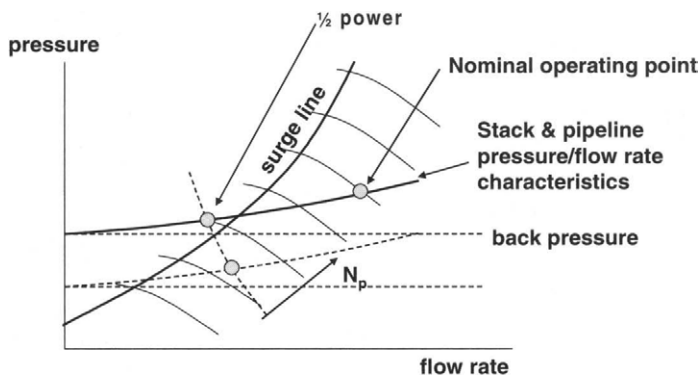


FIGURE 9-11. Reduction of flow rate requires reduction of pressure for centrifugal compressors.

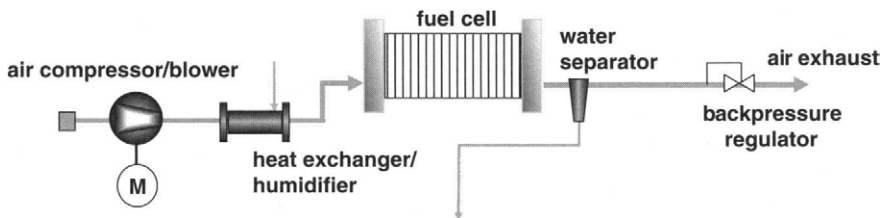


FIGURE 9-12. Schematic diagram of air supply for a fuel cell system.

Air typically has to be humidified before entering the fuel cell stack. Various humidification schemes are discussed in section 9.2.4. *Humidification Schemes*. At the stack outlet, typically there is some liquid water that may be easily separated from the exhaust air, in a simple, off-the-shelf gas/liquid separator. Water collected at the exhaust may be stored and reused, either for cooling or for humidification (Figure 9-12).

In a pressurized system, air at the exhaust is warm and still pressurized at somewhat lower pressure than it is at the inlet. This energy may be utilized in an expander or a turbine, to generate work that may offset some of the work needed to compress the air. The compressor and the turbine may be installed on the same shaft, creating a turbo-compressor (Figure 9-13).

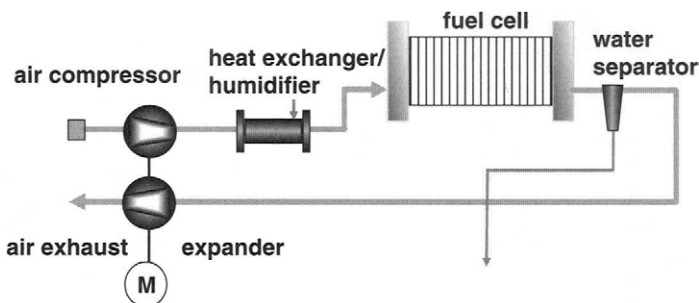


FIGURE 9-13. Schematic diagram of a fuel cell system with an expander at the exhaust.

The amount of work that may be extracted from the hot warm air at the fuel cell exhaust, by expanding it from the pressure at the fuel cell exhaust,  $P_{out}$ , to the atmospheric pressure,  $P_0$ , is:

$$W_{exp} = \dot{m}_{Airout} \cdot c_p \cdot T_{out} \left[ 1 - \left( \frac{P_0}{P_{out}} \right)^{\frac{k-1}{k}} \right] \eta_{exp} \quad (9-18)$$

The expander efficiency,  $\eta_{exp}$ , is a ratio between actual work and ideal isentropic work between these two pressures.

Because the air at the exhaust also carries some water vapor, the mass flow rate, specific heat, and the coefficient  $k$  (ratio of specific heats) have to be adjusted accordingly. This adjustment typically results in a power increase of less than 5%.

The temperature at the end of expansion is:

$$T_{end} = T_{out} - T_{out} \left[ 1 - \left( \frac{P_0}{P_{out}} \right)^{\frac{k-1}{k}} \right] \eta_{exp} \quad (9-19)$$

Because of the inefficiencies of both compression and expansion processes and because of the pressure drop through the stack, an expander may recover only a portion of the compression work, as shown in Figure 9-14. However, if the temperature of the exhaust is increased, for example by combustion of excess hydrogen at the stack anode outlet, expansion may generate all the power needed for compression.

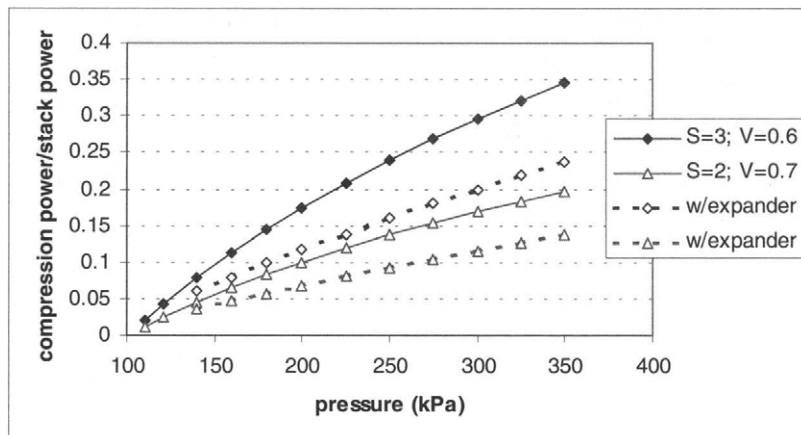


FIGURE 9-14. Compression power as a function of fuel cell operating pressure for a system with compressor/expander (assuming ambient pressure of 101.3 kPa and ambient temperature of 20°C, and both compressor and expander efficiency of 70%).

### 9.2.2. Passive Air Supply

For very small power outputs it is possible to design and operate a fuel cell with passive air supply, relying only on natural convection due to concentration gradients. Such a fuel cell typically has the front of the cathode directly exposed to the atmosphere, therefore without the bipolar plates, or it is in bipolar configuration, where the cathode flow field has openings to the atmosphere on the side (Figure 9-15). In either case an oxygen concentration gradient is formed between the open atmosphere and the catalyst layer where oxygen is being consumed in the electrochemical reaction. The performance of such fuel cells is typically not limited only by the oxygen diffusion rate, but also by water and heat removal, both dependent on the temperature gradient. Maximum current density that can be achieved with free-convection fuel cells is typically limited to about  $0.1\text{--}0.15\text{ A cm}^2$ .

These ambient or free-convection fuel cells result in a very simple system, needing only hydrogen supply (Figure 9-16). Several cells may be connected sideways in series (anode of one cell electrically connected to the cathode of the adjacent cell) to get the desired voltage output. Figure 9-16 shows such a multicell configuration where the free-convection cathodes are employed on both sides (and hydrogen flow field is contained in the middle). It is interesting that this fuel cell can generate power at either 6 V or 12 V, depending on how the two sides are electrically connected (in parallel or in series, respectively).

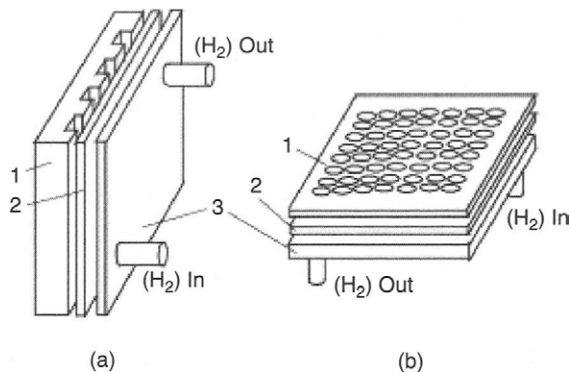


FIGURE 9-15. Examples of free-convection fuel cells [9].

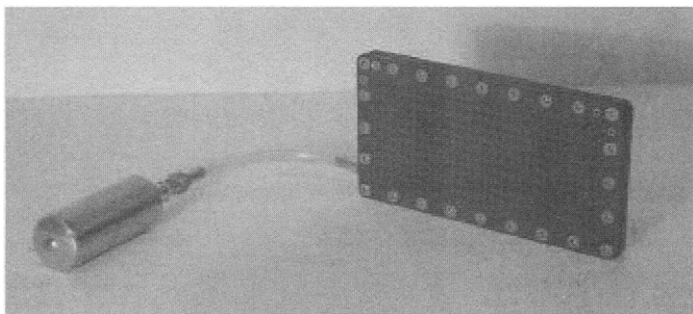


FIGURE 9-16. Simple fuel cell system based on passive air supply [10].

### 9.2.3. Hydrogen Supply

Hydrogen supply for hydrogen-air systems does not differ from hydrogen supply for hydrogen-oxygen systems, described previously in the section Hydrogen Supply. Design options include dead-end or flow through with recirculation of unused hydrogen. However, operation in a closed loop system without intermittent purging would not be possible for an extended period because of accumulation of inert gases, either those present in hydrogen or nitrogen that would over time permeate through the fuel cell membrane because of concentration gradient.

One additional option in hydrogen-air systems is to use hydrogen from the fuel cell exhaust in a burner to generate more heat, which then may be converted into work in a turbine/expander (Figure 9-17). The turbine/expander mounted on the same shaft with the air compressor may minimize, or under some conditions eliminate, the parasitic losses associated with powering the air compressor.

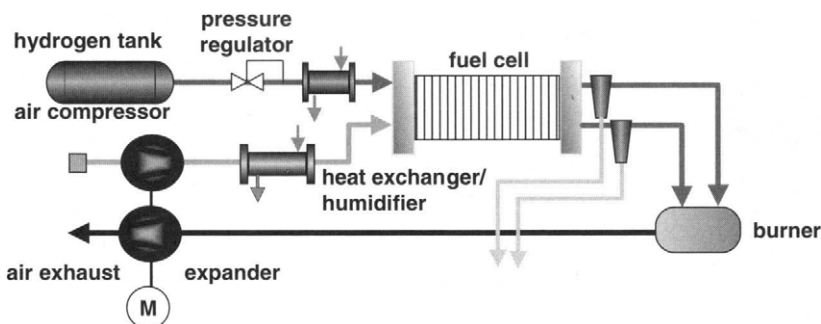


FIGURE 9-17. Use of hydrogen exhaust in a burner to enhance operation of the expander/turbine.

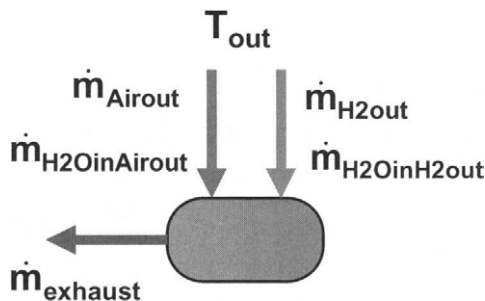


FIGURE 9-18. Mass balance of a tail gas burner.

The amount of work that can be extracted from the exhaust gas in the turbine is:

$$W_{\text{exp}} = \dot{m}_{\text{exh}} \cdot c_{\text{pexh}} \cdot T_B \left[ 1 - \left( \frac{P_0}{P_{\text{out}}} \right)^{\frac{k-1}{k}} \right] \eta_{\text{exp}} \quad (9-20)$$

The composition of the exhaust gas, its specific heat, mass flow rate, and temperature may be calculated from the burner mass and energy balance, as shown in Figure 9-18.

The mass flow rate out of the burner consists of unburned oxygen, nitrogen, and water vapor:

$$\dot{m}_{\text{exh}} = \dot{m}_{\text{O}_2\text{Bout}} + \dot{m}_{\text{N}_2\text{Bout}} + \dot{m}_{\text{H}_2\text{OBout,V}} \quad (9-21)$$

Oxygen mass flow is equal to the mass flow of oxygen before the burner minus oxygen that was used for combustion of hydrogen (assuming complete combustion):

$$\dot{m}_{\text{O}_2\text{Bout}} = \dot{m}_{\text{O}_2\text{FCout}} - \frac{1}{2} \dot{m}_{\text{H}_2\text{FCout}} \frac{M_{\text{O}_2}}{M_{\text{H}_2}} \quad (9-22)$$

where:

$$\begin{aligned} M_{O_2} &= \text{molecular weight of oxygen} \\ M_{H_2} &= \text{molecular weight of hydrogen} \end{aligned}$$

Nitrogen mass flow should not change:

$$\dot{m}_{N2Bout} = \dot{m}_{N2FCout} = \dot{m}_{N2FCin} \quad (9-23)$$

In case of complete combustion, there should be no hydrogen in the exhaust:

$$\dot{m}_{H2Bout} = 0 \quad (9-24)$$

Water vapor mass flow rate includes water vapor present in both hydrogen and air outlet from the fuel cell, plus water generated by combustion of hydrogen in the burner:

$$\dot{m}_{H2OBout,V} = \dot{m}_{H2OinAirout,V} + \dot{m}_{H2OinH2out,V} + \dot{m}_{H2FCout} \frac{M_{H2O}}{M_{H2}} \quad (9-25)$$

The energy balance requires that the sum of the enthalpies of all the flows coming into the burner must be equal to the sum of enthalpies leaving the burner:

$$\sum H_{FCout} = \sum H_{Bout} \quad (9-26)$$

The sum of enthalpies coming into the burner includes hydrogen and oxygen exhaust from the fuel cell together with water vapor present:

$$\begin{aligned} \sum H_{FCout} &= t_{out} [\dot{m}_{Airout} C_{pAir} + \dot{m}_{H2out} C_{pN2} + (\dot{m}_{H2OinAirout,V} + \dot{m}_{H2OinH2out,V}) C_{pH2O,V}] \\ &\quad + (\dot{m}_{H2OinAirout,V} + \dot{m}_{H2OinH2out,V}) h_{fg}^0 \end{aligned} \quad (9-27)$$

The sum of enthalpies at the burner outlet is:

$$\sum H_{Bout} = t_B (\dot{m}_{O2Bout} C_{pO2} + \dot{m}_{N2FCout} C_{pN2} + \dot{m}_{H2OBout,V} C_{pH2O,V}) + \dot{m}_{H2OBout,V} h_{fg}^0 \quad (9-28)$$

By combining Equations (9-21 through 9-28), one may obtain the resulting temperature of the exhaust gas.

Obviously, a higher hydrogen stoichiometry ratio would leave more hydrogen in the fuel cell exhaust and consequently would result in more

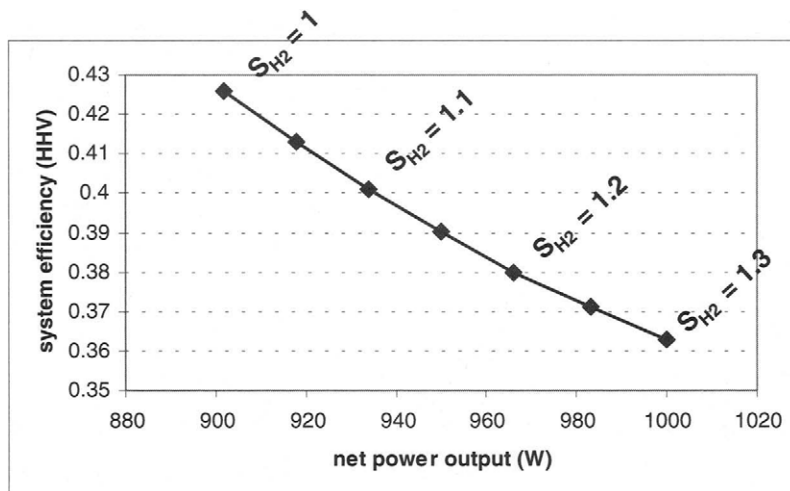


FIGURE 9-19. Net power output and system efficiency of a fuel cell system with a tail gas burner and an expander/turbine for various hydrogen utilization (stack power output 1 kW at 0.7 V/cell, 60°C, 300 kPa; compressor and expander efficiencies 0.70).

work produced from the turbine, reducing the parasitic load, and therefore increasing the fuel cell net power output. However, burning excess hydrogen results in lower fuel cell system efficiency (as shown in Figure 9-19).

#### 9.2.4. Humidification Schemes

In principle, both air and hydrogen streams must be humidified at the fuel cell inlet. Hydrogen must be humidified to ensure that the electroosmotic drag does not dry out the anode side of the membrane. Air must be humidified in spite of water produced on the cathode side to ensure that the excess of dry gas, particularly in the entrance region, does not remove water at a rate higher than water is being generated in the electrochemical reaction.

Several humidification methods and schemes can be applied for air humidification. Humidification of a gas can be achieved by:

- a) bubbling of gas through water,
- b) direct water or steam injection,
- c) exchange of water (and heat) through a water permeable medium,
- d) exchange of water (and heat) on an adsorbent surface (enthalpy wheel).

Bubbling is often used in laboratory settings for relatively low flow rates (corresponding to small, single cells), but rarely in practical systems. In this

method, air is dispersed through a porous tube immersed in heated liquid water. In this way, bubbles of air in water form a relatively large contact area between gas and liquid water where the evaporation process can take place. The desired level of humidification is achieved by controlling the temperature of liquid water, in laboratory settings typically with electrical heaters. If the device is sized properly, the gas emerging at the liquid surface is saturated at a desired, preset temperature. The efficiency of humidification depends on the water level, so the required water level must be maintained. The device must be designed so that the outgoing humidified air does not carry water droplets. In practical systems this method is rarely used because of its size and cumbersome controls (temperature, water level) and the need to collect liquid water at the fuel cell outlet, which in some cases may require not only gas/liquid separators, but a condensing heat exchanger as well. In addition, pushing of air through a porous medium results in additional pressure drop, which then must be overcome by the air supply device, resulting in higher pumping power, that is, higher parasitic power and lower system efficiency.

Direct water injection is a more elegant, more compact, and easier-to-control method (Figure 9-20a). The required amount of water to be injected can be easily calculated for any combination of operating conditions (temperature, pressure, gas flow rate, and desired relative humidity):

$$\dot{m}_{H_2O} = \dot{m}_{Air} \frac{M_{H_2O}}{M_{Air}} \left( \frac{\varphi P_{sat}(T)}{P - \varphi P_{sat}(T)} - \frac{\varphi_{amb} P_{sat}(T_{amb})}{P_{amb} - \varphi_{amb} P_{sat}(T_{amb})} \right) \quad (9-29)$$

where  $\varphi$ , T, P, and  $\varphi_{amb}$ ,  $T_{amb}$ ,  $P_{amb}$  are relative humidity, temperature, and pressure at the fuel cell inlet and of the ambient air, respectively.

The exact amount of water may be dosed by a metering pump. It is important that water is injected in the form of fine mist, so that a large contact area between water and air facilitates evaporation. However, simple injection of liquid water in the gas stream may not be sufficient to actually humidify the gas, because humidification also requires heat for evaporation. The enthalpy of water, even if the water is hot, is usually not sufficient and additional heat is required. The sources of heat may be the air compressor (obviously applicable only in pressurized systems) and the fuel cell stack itself. In most of the operating conditions, there is sufficient amount of heat generated in the fuel cell stack. It is the duty of the system to transfer a portion of that heat to the humidification process (Figure 9-20b).

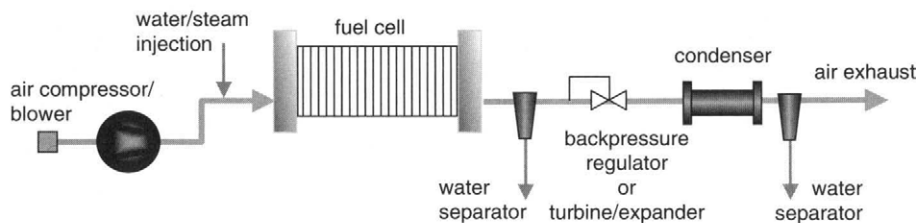
Water injection during the compression process may actually improve the efficiency of the compression process by simultaneously cooling the compressed gas; however, this method is not applicable for all kinds of compressors.

Direct steam injection eliminates the need for additional heat exchange; however, steam must be generated somewhere in the system,

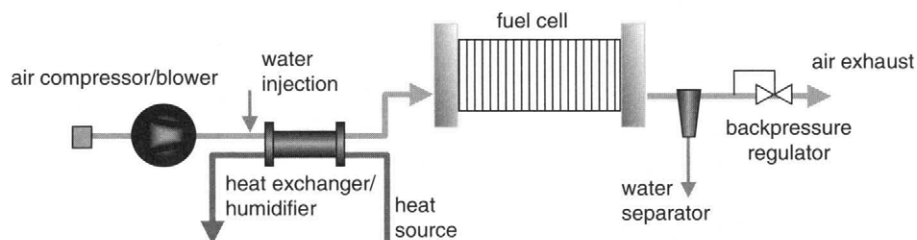
which means that this method is applicable only for the systems where heat is generated at a temperature above the water boiling temperature (100°C at 101.3 kPa).

Exchange of heat and water from the cathode exhaust with incoming air is an elegant way of taking advantage of water and heat produced in the fuel cell stack (Figure 9-20c). This can be achieved through a water-

a)



b)



c)

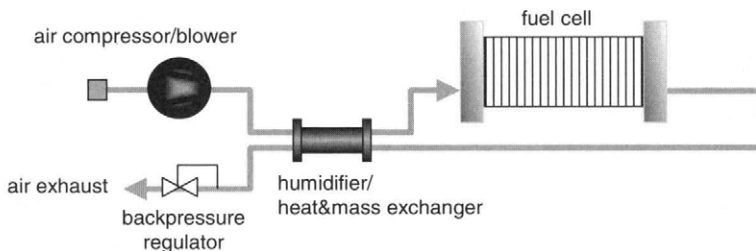


FIGURE 9-20. Practical air humidification schemes: a) water/steam injection, b) water injection with heat exchange, c) exchange of water and heat with the cathode exhaust.

permeable medium, such as porous plate (metal, ceramic, or graphite), or a water-permeable membrane (such as Nafion), or through an enthalpy wheel. These devices are essentially mass and heat exchangers, allowing both heat and water to be exchanged between warm and oversaturated fuel cell exhaust and dry incoming air. The heat and water fluxes in a humidifier at low fuel cell operating pressure are in the same direction (from fuel cell exhaust to inlet), whereas at elevated pressure due to compression, the inlet gas may be hot, and in that case the heat and water flow in opposite directions. In either case, it is not possible to humidify the incoming gas to 100% relative humidity at stack operating temperature with this method, because of finite temperature and water concentration differences between the two sides of the humidifier needed for heat and mass transfer.

### 9.2.5. Water and Heat Management—System Integration

Water and heat are the by-products of the fuel cell operation, and the supporting system must include the means for their removal. Both water and heat from the fuel cell stack may be at least partially reused, for example for humidification of the reactant gases, or for facilitating hydrogen release from metal hydride storage tanks.

Water and heat handling may be integrated into a single subsystem if deionized water is used as a stack coolant. In that case water removes the heat from the stack and the same water and heat are used to humidify the reactant gases. The remaining heat has to be discarded to the surrounding through a heat exchanger; for hydrogen-air systems that is typically a radiator. The amount of heat to be discarded must be calculated from the stack and humidifier energy balances.

The flow rate of the coolant is

$$\dot{m}_{\text{coolant}} = \frac{Q}{c_p \cdot \Delta T} \quad (9-30)$$

$\Delta T$  is typically a design variable. Most typically,  $\Delta T$  is below 5°C, and rarely above 10°C. Smaller  $\Delta T$  results in more uniform stack temperature distribution, but it requires larger coolant flow rate, which in turn increases parasitic losses. Sometimes larger stack temperature variations are needed to maintain the water in the desired state [11]; in that case, the coolant  $\Delta T$  is dictated by the stack temperature requirements.

The size of the radiator heat exchanger depends on the temperature difference between the coolant and the ambient air. For that reason, it is preferred to operate the fuel cell system at a higher temperature, for systems where the size of the components is critical. However, the operating pressure and water balance must be taken into account when deciding on the operating temperature.

It should be noted that smaller stacks may be air cooled. In that case a fan replaces the coolant pump. Reuse of waste heat collected by air as coolant is not practical, but it may be convenient to blow the warm exhaust over the metal hydride tanks.

Even smaller stacks, with relatively large outside surface area (relative to the active area inside), may be passively cooled by natural convection and radiation. If necessary, the surface area may be enlarged by fins.

A hydrogen-air fuel cell system must be designed so that it does not need any backup water supply. Water is generated inside the stack, but water is needed for humidification of one or both reactant gases. Sometimes, depending on the intended operation of the fuel cell system, and depending on the stack's capabilities of recirculating water internally (e.g., with the use of thinner membranes and with hydrogen and air in counter-flow), humidification of only one of the reactants may be sufficient. Water for humidification must be collected at the stack exhaust, on the cathode side (although sometimes it is necessary on both cathode and anode exhausts). Depending on the fuel cell operating conditions (pressure, temperature, and flow rates), water at the exhaust may be in either liquid or gaseous form. Liquid water is relatively easily separated from the gaseous stream in liquid/gas separators. If liquid water collected at the stack exhaust is not sufficient for humidification, the exhaust must be cooled so that additional water may condense and be separated.

On the system level, water balance is very simple: the amount of water entering the system in ambient air, plus water generated inside the fuel cell, must be larger than or equal to the amount of water leaving the system with exhaust air and hydrogen. Hydrogen exhaust can be either continuous (flow-through mode) or periodic stream (dead-end or recirculation with periodic purging).

System water balance is given with the following equation:

$$\dot{m}_{H_2O,Airin} + \dot{m}_{H_2O,gen} = \dot{m}_{H_2O,Airout} + \dot{m}_{H_2O,H2out} \quad (9-31)$$

where:

$\dot{m}_{H_2O,Airin}$  = water entering the system with ambient air intake:

$$\dot{m}_{H_2O,Airin} = \frac{S_{O_2}}{r_{O_2}} \frac{\varphi_{amb} P_{vs}(T_{amb})}{P_{amb} - \varphi_{amb} P_{vs}(T_{amb})} \frac{M_{H_2O}}{4F} I \cdot n_{cell} \quad (9-32)$$

$\dot{m}_{H_2O,gen}$  = water generated inside the stack:

$$\dot{m}_{H_2O,gen} = \frac{M_{H_2O}}{2F} I \cdot n_{cell} \quad (9-33)$$

$\dot{m}_{H_2O,Airout}$  = water (vapor) leaving the system with air exhaust:

$$\dot{m}_{H_2O,Airout} = \frac{S_{O_2} - r_{O2in}}{r_{O2in}} \frac{P_{vs}(T_{st})}{P_{ca} - \Delta P_{ca} - P_{vs}(T_{st})} \frac{M_{H_2O}}{4F} I \cdot n_{cell} \quad (9-34)$$

$\dot{m}_{H_2O,H_2out}$  = water leaving the system with hydrogen exhaust:

$$\dot{m}_{H_2O,H_2out} = (S_{H_2} - 1) \frac{P_{vs}(T_{st})}{P_{an} - \Delta P_{an} - P_{vs}(T_{st})} \frac{M_{H_2O}}{2F} I \cdot n_{cell} \quad (9-35)$$

Water balance therefore depends on:

- the oxygen (and hydrogen) flow rate, that is, stoichiometric ratio,
- stack operating temperature, that is, temperature of the exhaust,
- stack operating pressure, or more precisely the stack outlet pressure, that is, the pressure at which the liquid water is separated from the exhaust gases,
- ambient conditions (pressure, temperature, and relative humidity).

It should be noted that water balance on the system level does not depend on current and number of cells (because  $I \cdot n_{cell}$  product appears in each of the previous equations, it gets cancelled when Equations (9-32) through (9-35) are introduced in Equation 9-31).

Figure 9-21 shows the required exhaust temperature that results in neutral water balance as a function of air flow rate and operating pressure (ambient conditions are assumed to be 20°C, 101.3 kPa, and 60% relative humidity). For the ambient pressure operation and oxygen stoichiometry of 2.0, the stack should not be operated above 60°C. If it is necessary to operate at a higher temperature, then a higher operating pressure should be selected or additional heat exchanger may be needed to achieve neutral water balance (which may defeat the purpose of operating at a higher temperature).

It should be noted that hydrogen does not carry much water out of the system. The dashed lines in Figure 9-21 take into account water taken away from the system by hydrogen exhaust assuming hydrogen stoichiometry of 1.2.

Presence of water in the system makes fuel cell systems susceptible to freezing if used outdoors in cold climate. In such case, the coolant loop is separated from the water system, which allows for antifreeze coolants (such as aqueous solutions of ethylene-glycol or propylene-glycol) to be used instead of deionized water. Nevertheless, water cannot be completely eliminated from the system; after all, the PSA membrane contains up to 35% water. Operation, or actually, survival and start-up, of a fuel cell system in a cold environment is an issue that must be addressed by the

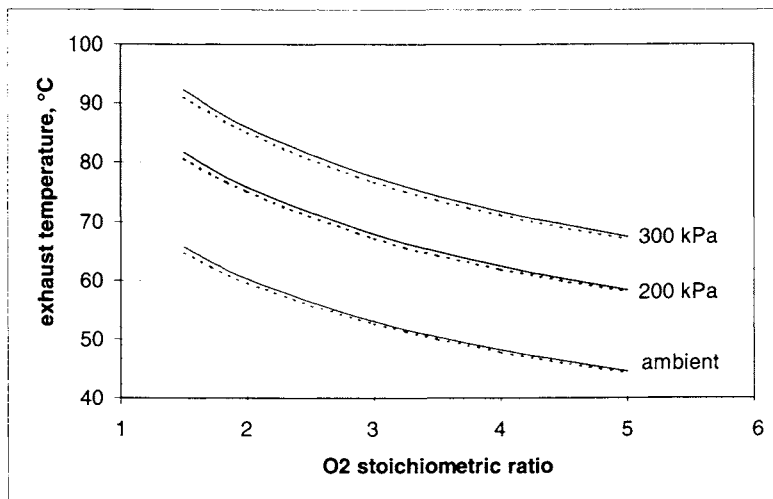


FIGURE 9-21. Required stack exhaust temperature to achieve neutral system water balance.

system design. The system, when operational, can keep itself at operating temperature. Therefore, one way to keep the system warm is to operate it either periodically or constantly at some very low power level, which may significantly affect the overall system efficiency and may not be practical for long periods. Another way to avoid freezing is to drain the water from the system at shutdown. In systems that are used in backup power applications, small electric heaters may be used to keep the system above freezing and ready for quick start-up.

The system configuration greatly depends on application. In some cases a very simple system, consisting of nothing more than a bottle of hydrogen and a fuel cell (such as the one shown in Figure 9-16), may be sufficient. In other cases the system needs most of the components and subsystems discussed earlier. Figure 9-22 shows a schematic diagram of an actual hydrogen-air fuel cell system employed in a fuel cell utility vehicle [12]. Figure 9-23 shows the actual layout in the vehicle.

### 9.3. Fuel Cell Systems with Fuel Processor

To bring fuel cells to the marketplace even before hydrogen becomes a readily available fuel, conventional fuels such as natural gas for stationary applications, gasoline for transportation, and methanol for portable power may be used, if hydrogen generation from these fuels is made a part of the

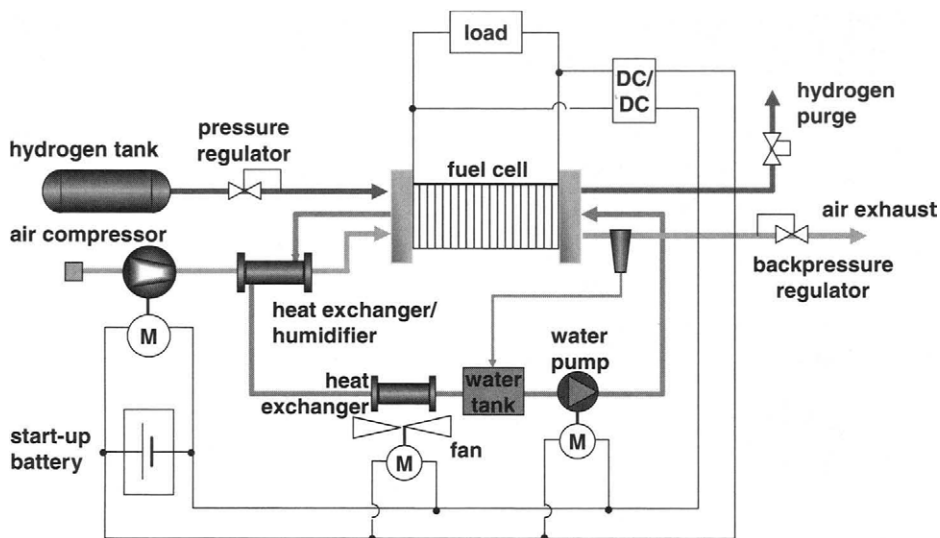


FIGURE 9-22. An example of a complete hydrogen-air fuel cell system.

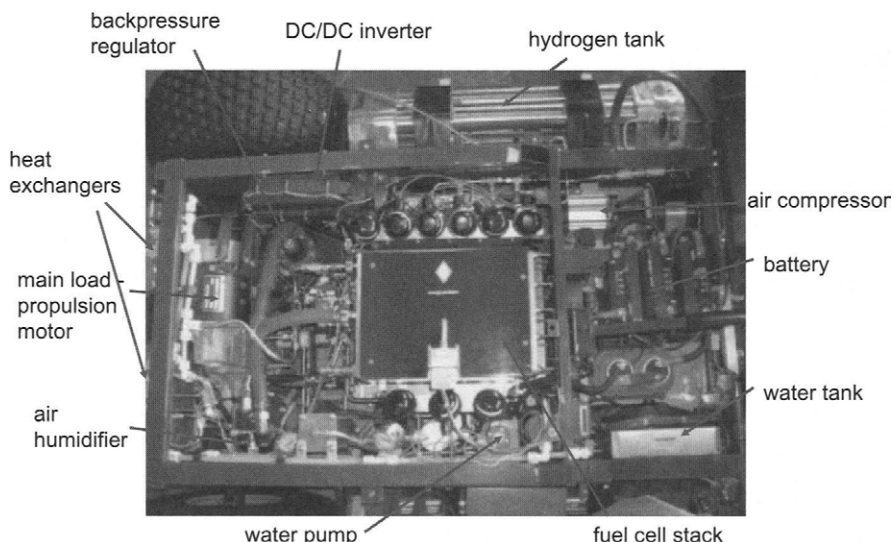


FIGURE 9-23. An actual fuel cell system installed in a John Deere Gator utility vehicle showing all the components from the schematic diagram in Figure 9-22.

fuel cell system. Hydrogen can be generated from hydrocarbon fuels, such as natural gas, gasoline, or methanol, by several processes, such as:

- steam reformation,
- partial oxidation,
- autothermal reformation, which is essentially a combination of steam reformation and partial oxidation.

In addition, several other processes must be employed to produce hydrogen pure enough to be used in PEM fuel cells, such as:

- desulfurization—to remove sulfur compounds present in fuel,
- shift reaction—to reduce the content of CO in the gas produced by the fuel processor,
- gas clean-up, involving preferential oxidation, methanation, or membrane separation—to further minimize the CO content in the reformatte gas.

### 9.3.1. Basic Processes and Reactions

Table 9-3 summarizes the basic processes and reactions used in fuel processing. In addition to general equation, examples are given for methane,

TABLE 9-3  
Basic Processes and Reactions in Fuel Reforming

Combustion	$C_mH_nO_p + (m + n/4 - p/2)O_2 \rightarrow mCO_2 + (n/2)H_2O + \text{heat}$
water vapor generated	$\left\{ \begin{array}{l} CH_4 + 2O_2 \rightarrow CO_2 + 2H_2O(g) + 802.5 \text{ kJ} \\ C_8H_{18} + 12.5O_2 \rightarrow 8CO_2 + 9H_2O(g) + 5063.8 \text{ kJ} \\ CH_3OH + 1.5O_2 \rightarrow CO_2 + 2H_2O(g) + 638.5 \text{ kJ} \end{array} \right.$
liquid water generated	$\left\{ \begin{array}{l} CH_4 + 2O_2 \rightarrow CO_2 + 2H_2O(l) + 890.5 \text{ kJ} \\ C_8H_{18} + 12.5O_2 \rightarrow 8CO_2 + 9H_2O(l) + 5359.8 \text{ kJ} \\ CH_3OH + 1.5O_2 \rightarrow CO_2 + 2H_2O(l) + 726.5 \text{ kJ} \end{array} \right.$
Partial Oxidation	$C_mH_nO_p + (m/2)O_2 \rightarrow (m - p)CO + pCO_2 + (n/2)H_2 + \text{heat}$ $CH_4 + \frac{1}{2}O_2 \rightarrow CO + 2H_2 + 39.0 \text{ kJ}$ $C_8H_{18} + 4O_2 \rightarrow 8CO + 9H_2 + 649.8 \text{ kJ}$ $CH_3OH + \frac{1}{2}O_2 \rightarrow CO_2 + 2H_2 + 154.6 \text{ kJ}$
Steam Reforming	$C_mH_nO_p + mH_2O + \text{heat} \rightarrow (m - p)CO + pCO_2 + (m + n/2)H_2$ $CH_4 + H_2O(g) + 203.0 \text{ kJ} \rightarrow CO + 3H_2$ $C_8H_{18} + 8H_2O(g) + 1286.1 \text{ kJ} \rightarrow 8CO + 17H_2$ $CH_3OH + H_2O(g) + 87.4 \text{ kJ} \rightarrow CO_2 + 3H_2$ $CH_4 + H_2O(l) + 247.0 \text{ kJ} \rightarrow CO + 3H_2$ $C_8H_{18} + 8H_2O(l) + 1638.1 \text{ kJ} \rightarrow 8CO + 17H_2$ $CH_3OH + H_2O(l) + 131.4 \text{ kJ} \rightarrow CO_2 + 3H_2$
Gas Shift Reaction	
water vapor used	$CO + H_2O(g) \rightarrow CO_2 + H_2 + 37.5 \text{ kJ}$
liquid water used	$CO + H_2O(l) + 6.5 \text{ kJ} \rightarrow CO_2 + H_2$
Preferential Oxidation	$CO + 0.5 O_2 \rightarrow CO_2 + 279.5 \text{ kJ}$
Water Evaporation	$H_2O(l) + 44.0 \text{ kJ} \rightarrow H_2O(g)$

isooctane, and methanol. Methane may be used as a good representative of natural gas (natural gas contains up to 95% methane), and octane may be used as a representative of liquid hydrocarbon fuels. Gasoline is actually a blend of various hydrocarbons and cannot be represented with a single chemical formula.

Each reaction either needs energy (endothermic) or generates heat (exothermic). In the equations in Table 9-3, endothermic heat is shown on the left side of the equation whereas exothermic heat is shown on the right-hand side as a result of the reaction. The heats of the reactions were calculated from the heat of formation of participating species (shown in Table 9-4), and therefore refer to 25°C. Because the reactions take place at considerably higher temperatures, additional heat must be brought to the process to bring the reactants to the reaction temperature, and a significant amount of heat leaves the system with the products. For the reactions involving water, the form in which water participates may have a significant impact on the heat required or generated. In most of the processes steam is used, and therefore it would be appropriate to use the equations with water vapor. However, for system-level analyses such as those presented in this chapter, energy for steam generation must also be taken into account. In that case the equations with liquid water are used. This is also convenient when dealing with the efficiencies. As discussed in Chapter 2, the use of higher heating value for efficiency calculation is more appropriate, although in all combustion processes water leaves the system as vapor and has no chance to contribute to the process efficiency.

### 9.3.2. Steam Reforming

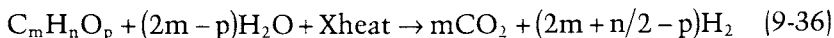
Steam reforming is an endothermic process, which means that heat must be brought to the reactor. This heat is typically generated by combustion of an additional amount of fuel. The two reactions are physically separated

TABLE 9-4  
Heat of Formation of Some Common Fuel Cell Gases and Liquids (from [13])

	Molecular Mass g/mol	Heat of Formation kJ/mol
Hydrogen, H <sub>2</sub>	2.016	0
Oxygen, O <sub>2</sub>	31.9988	0
Nitrogen, N <sub>2</sub>	14.0067	0
Carbon monoxide, CO	28.0106	-113.8767
Carbon dioxide, CO <sub>2</sub>	44.010	-393.4043
Water vapor, H <sub>2</sub> O (g)	18.0153	-241.9803
Water, liquid, H <sub>2</sub> O (l)	18.0153	-286.0212
Methane, CH <sub>4</sub>	16.043	-74.85998
Methanol, CH <sub>3</sub> OH	32.0424	-238.8151
Octane, C <sub>8</sub> H <sub>18</sub>	114.230	-261.2312

by a thermally conductive wall. Because of that, the resulting gas does not include any nitrogen. The steam reformation reaction is reversible, and the product gas is a mixture of hydrogen, carbon monoxide, carbon dioxide (some shift reaction also taking place), water vapor, and unconverted fuel. Figure 9-24 shows a schematic diagram of the steam reforming process. The actual composition is a function of temperature, pressure, and composition of the feed gas. Figure 9-25 shows equilibrium concentrations of methane steam reformation as a function of temperature. Because the product gas still contains a significant amount of carbon monoxide, it is taken to the shift reactor where CO reacts with additional steam and is converted to more hydrogen and CO<sub>2</sub>. Depending on the desired CO content and applied catalyst, the shift reaction may be split into a high-temperature and a low-temperature shift reaction. The resulting gas still contains about 1% of CO, which would be detrimental to PEM fuel cell. The CO content is further reduced in the preferential oxidation process where CO is catalytically oxidized with oxygen from air. Selection of the catalyst and control of operating conditions is critical, in order to avoid, or at least minimize, combustion of hydrogen present in the gas.

The overall equation for steam reforming including the shift reaction is:



The heat needed for the process, Xheat, is obtained by combustion of an additional amount of fuel, k:

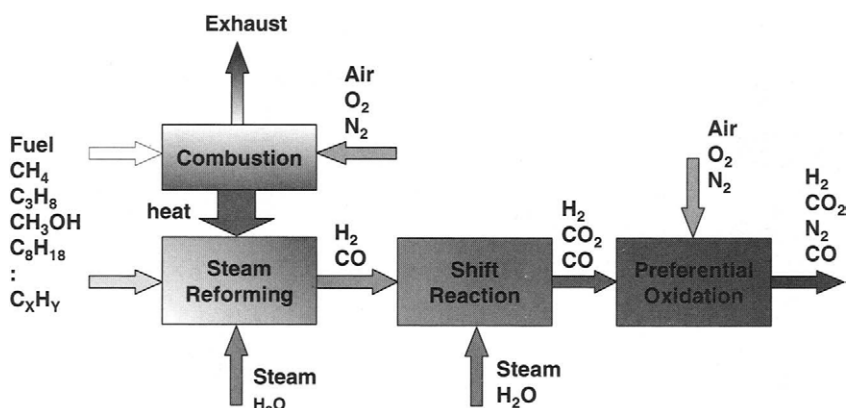


FIGURE 9-24. Schematic representation of a steam reforming process.

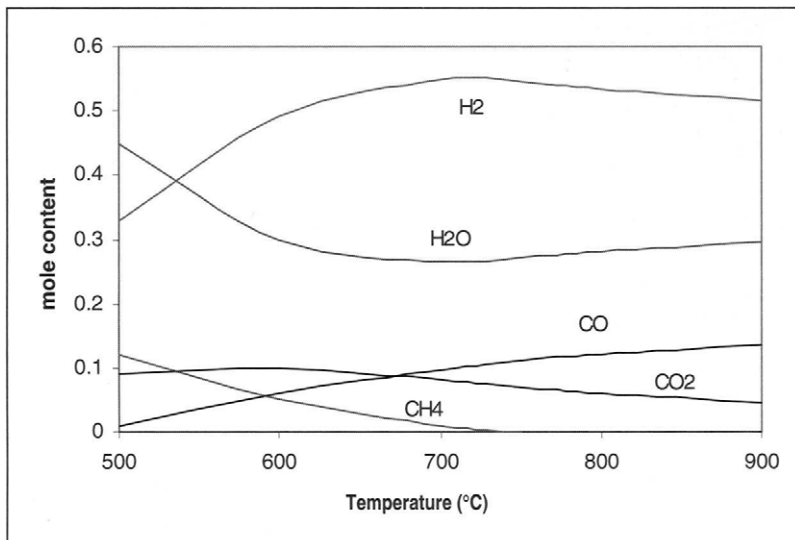


FIGURE 9-25. Equilibrium concentrations of methane steam reformation as a function of temperature (at atmospheric pressure).

where  $k$  is the ratio between the absolute values of heat of the steam reforming reaction and heat of the combustion reaction:

$$k = \frac{\Delta H_{SR} + (m - p)\Delta H_{shift}}{\Delta H_{comb}} \quad (9-38)$$

Note that  $\Delta H_{comb}$  is also the heating value of particular fuel used in the combustion process (Table 9-3).

The theoretical efficiency of the steam reforming process is then a ratio between the heating value of hydrogen produced and the heating value of fuel consumed in both reactions:

$$\eta = \frac{\left(2m + \frac{n}{2} - p\right)}{(1+k)} \frac{\Delta H_{H_2}}{\Delta H_{fuel}} \quad (9-39)$$

It can be easily shown that the theoretical efficiency of the steam reforming process is 100%, if the heating values are replaced by the heats of formation of the constituents of the corresponding reactions (*i.e.*, hydrogen combustion, fuel combustion, steam reforming, and shift reaction). The actual efficiency is always lower because of:

- heat losses in the process, including both heat dissipated to the environment and heat taken away by the gases (both, exhaust gases from combustion reaction and product gases from the shift reaction), and
- incomplete reactions, including all three reactions involved.

### *Steam Reforming with Membrane Separation*

Another elegant way of avoiding shift reaction and selective oxidation is to use a metal membrane to separate hydrogen from the reformate produced by steam reforming. These membranes allow only hydrogen to go through, so the product is high-purity hydrogen. Carbon monoxide and unconverted fuel, and other by-products of steam reformation, are brought back into the combustion chamber (Figure 9-26), reducing the amount of fuel that has to be burned to produce the heat for the steam reforming process. Such a process can be very efficient. However, filtration through the membrane requires relatively high pressure. Because of that, such a process is more suitable for liquid fuels, such as methanol, or for fuels that already come compressed, such as propane. Compression of natural gas would take a significant toll on the overall system efficiency.

#### 9.3.3. Partial Oxidation and Autothermal Reforming

Unlike steam reforming, partial oxidation is an exothermic process. Essentially, it is a combustion, but with a less-than-stoichiometric amount of oxygen, so that the products are carbon monoxide and hydrogen (instead of carbon dioxide and water vapor produced in full combustion). Similar to steam reforming, the reformate gas must go through shift reaction to

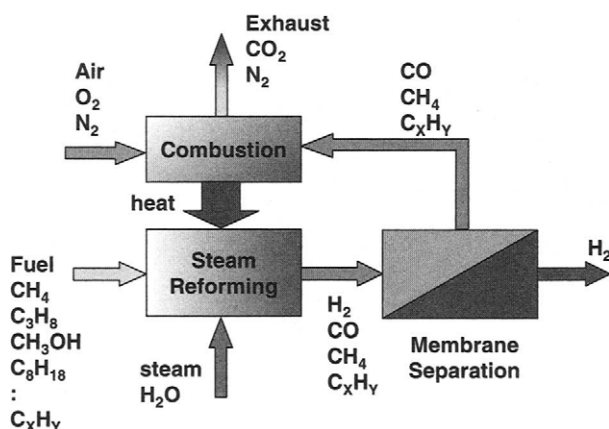


FIGURE 9-26. Schematic representation of the steam reforming process with metal membrane separation.

produce more hydrogen and through preferential oxidation to reduce the CO content to an acceptable level.

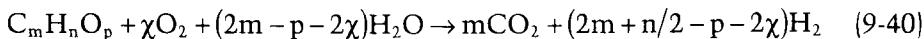
Partial oxidation produces less hydrogen per mole of fuel. In the case of methane, partial oxidation would generate only 2 moles of hydrogen per mole of methane, as opposed to 3 moles of hydrogen produced by steam reforming. In the case of octane, this ratio is even worse, that is, 9 moles vs 17 moles.

In addition, unlike the product gas from steam reforming, which contains only hydrogen and carbon dioxide (with minute amounts of CO after preferential oxidation), the product gas from partial oxidation contains relatively large amounts of nitrogen. In other words, hydrogen content in the gas is much lower (about 40% vs 80% from steam reforming), and that may have some impact on fuel cell performance.

Figure 9-27 shows a schematic diagram of the partial oxidation process.

Because partial oxidation is an exothermic process (*i.e.*, produces heat), and steam reforming is an endothermic process (*i.e.*, needs heat), these two processes can actually be combined in the so-called autothermal reforming process. Instead of external combustion and heat transfer to the steam reforming reactor, in an autothermal reformer, heat is generated internally by partial oxidation, and the heat is then carried by the reacting gases and partial oxidation products (hydrogen and carbon monoxide) to the steam reforming zone (Figure 9-28).

The overall equation of an autothermal process with shift reaction is:



Where  $\chi$  is the number of moles of oxygen per mole of fuel.

For methane, octane, and methanol, respectively, the overall equation is:

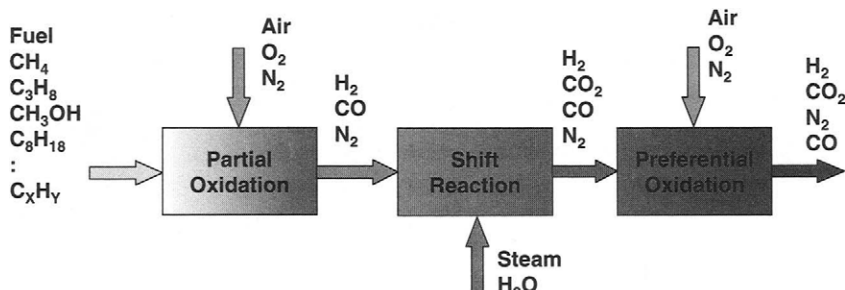


FIGURE 9-27. Schematic representation of the partial oxidation process.

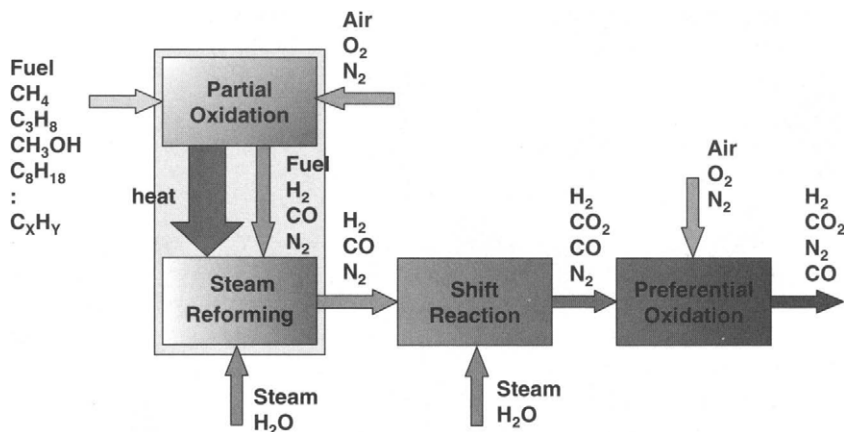
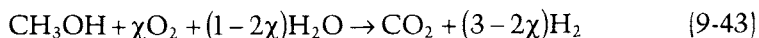


FIGURE 9-28. Schematic representation of an autothermal reforming process.



The previous reaction may be endothermic, exothermic, or thermoneutral, depending on the amount of oxygen brought into the system,  $\chi$ . Note that this is exactly the same overall equation as the overall equation for steam reforming with external combustion. However, the difference is that in the steam reforming, the two processes, combustion and reforming, are physically separated, whereas in autothermal reforming these processes follow each other in the same reactor.

If  $\chi$  in the equation is selected so that no heat is needed and no heat is generated, this process is autothermal, and its theoretical efficiency is 100%. The efficiency, defined as the heating value of hydrogen produced and the heating value of fuel consumed, is:

$$\eta = \left( 2m + \frac{n}{2} - p - 2\chi \right) \frac{\Delta H_{\text{H}_2}}{\Delta H_{\text{fuel}}} \quad (9-44)$$

For 100% efficiency,  $\eta = 1$ ,  $\chi$  is:

$$\chi_{\eta=1} = m + \frac{n}{4} - \frac{p}{2} - \frac{\Delta H_{\text{fuel}}}{\Delta H_{\text{H}_2}} \quad (9-45)$$

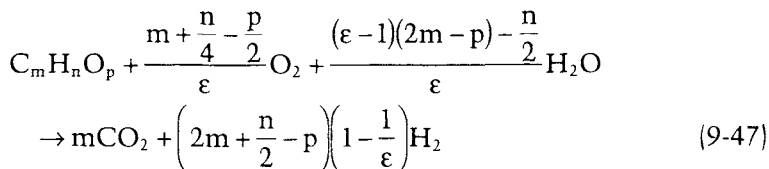
For natural gas, for example:

$$\chi_{\eta=1} = 1 + \frac{4}{4} - \frac{890.5}{2 \times 286} = 0.443$$

Similarly, for octane  $\chi_{\eta=1} = 3.19$ , and for methanol  $\chi_{\eta=1} = 0.23$ . Because  $\chi$  is different for every fuel, very often an equivalence ratio is used instead. The equivalence ratio,  $\epsilon$ , is defined as a ratio between the theoretical amount of oxygen needed for complete combustion and the actual amount of oxygen,  $\chi$ :

$$\epsilon = \frac{m + \frac{n}{4} - \frac{p}{2}}{\chi} \quad (9-46)$$

In that case the overall equation for autothermal reforming becomes:



The ideal efficiency of the autothermal reforming is then:

$$\eta = \left( 2m + \frac{n}{2} - p \right) \left( 1 - \frac{1}{\epsilon} \right) \frac{\Delta H_{H2}}{\Delta H_{fuel}} \quad (9-48)$$

Note that for  $\epsilon = 1$  the reaction becomes regular combustion and no hydrogen is being produced. As the equivalence ratio increases, the amount of hydrogen, and therefore the efficiency, increases. Figure 9-29 shows the theoretical efficiency of the reforming process as a function of equivalence ratio for methane, octane, and methanol. However, there are both theoretical and practical limits to the equivalence ratio. The theoretical limit corresponds to the 100% efficiency, based on the higher heating value (for both hydrogen and fuel). An increase of the equivalence ratio means that less oxygen is used in the process. At the equivalent ratios approaching the theoretical limit, there is a risk of carbon formation in the fuel processor, through the following reactions:



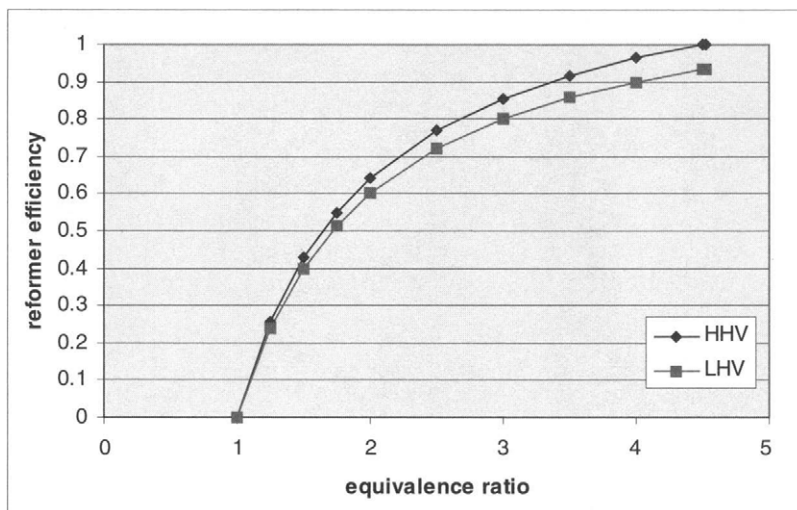
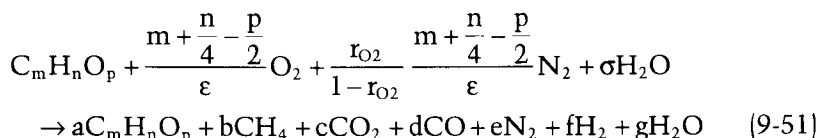


FIGURE 9-29. Relationship between reformer efficiency and equivalence ratio.

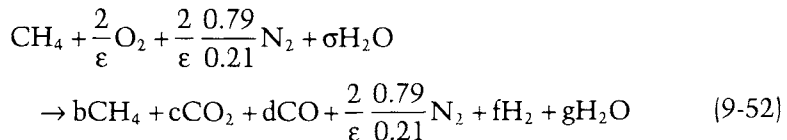
To reduce the risk of carbon formation, the equivalence ratio is always selected somewhat below the theoretical value, and steam is added to the reaction in excess of that theoretically required, typically at a rate corresponding to the steam-to-carbon ratio,  $\sigma$ , of 2.0–3.0 (moles of steam to moles of carbon in fuel).

The actual fuel reforming reaction is then:



Nitrogen appears in the reaction, because it comes with air. Because nitrogen practically does not participate in the reaction, the coefficient  $e$  on the right side of the equation is equal to the nitrogen coefficient on the left side. Other coefficients on the right side, that is, the exact composition of the reformate gas, with given feed on the left side, will depend on the catalyst, reactor design, temperatures, pressure, and process control. Fuel appearing on the right side represents fuel slip through the reactor, obviously unwanted.  $\text{CH}_4$  appears on the right side as a result of incomplete reactions.

For example, in the case of natural gas the previous reaction becomes:



With some assumptions and with known feed parameters,  $\epsilon$  and  $s$ , it is possible to calculate the composition of the resulting reformate gas from the species balance.

From carbon balance:

$$b + c + d = 1 \quad (9-53)$$

From oxygen balance:

$$\frac{4}{\epsilon} + \sigma = 2c + d + e \quad (9-54)$$

From hydrogen balance:

$$4 + 2\sigma = 4b + 2f + 2e \quad (9-55)$$

From nitrogen balance:

$$e = \frac{2}{\epsilon} \frac{0.79}{0.21} \quad (9-56)$$

These are four equations, but there are six coefficients on the right side of Equation (9-52). The remaining two equations may be derived from the requirements for maximum CO content in the produced reformate gas (typically around 1% by vol. in dry gas) and from the efficiency requirement.

The CO content (by vol.) in the dry reformate gas is:

$$r_{\text{CO}} = \frac{d}{b+c+d+e+f} = \frac{d}{1 + \frac{2}{\epsilon} \frac{0.79}{0.21} + f} \quad (9-57)$$

Similarly, hydrogen content in the dry reformate gas is:

$$r_{\text{H}_2} = \frac{f}{b+c+d+e+f} = \frac{f}{1 + \frac{2}{\epsilon} \frac{0.79}{0.21} + f} \quad (9-58)$$

The actual efficiency of the reforming process is:

$$\eta_{\text{actual}} = f \frac{\Delta H_{H_2}}{\Delta H_{\text{fuel}}} \quad (9-59)$$

Hydrogen content in the reformate gas is directly related to the actual efficiency. From Equations (9-58) and (9-59) it follows:

$$\eta_{\text{actual}} = \frac{r_{H_2} \frac{\Delta H_{H_2}}{\Delta H_{\text{fuel}}} \left( 1 + \frac{2}{\varepsilon} \frac{0.79}{0.21} \right)}{1 - r_{H_2}} \quad (9-60)$$

Figure 9-30 shows the relationship between hydrogen content and the reformer efficiency for an autothermal natural gas reformer. It should be noted that for each equivalence ratio there is a limit that the efficiency can reach (from Equation 9.48 or Figure 9-29).

A typical composition of the reformate gas from an autothermal natural gas reformer is shown in Table 9-4. Similar analysis may be performed for other fuels.

The previous reactions include both the fuel reforming and shift reaction as they occur simultaneously, although they take place in separate reactors using different types of catalysts. The high temperature in the fuel processor does not favor the shift reaction. Sometimes, the shift reaction is divided in two steps—high-temperature shift reaction (400–500°C) and low-temperature reaction (200–250°C), also using different types of catalysts, typically iron and copper based. Recently, precious metal catalysts,

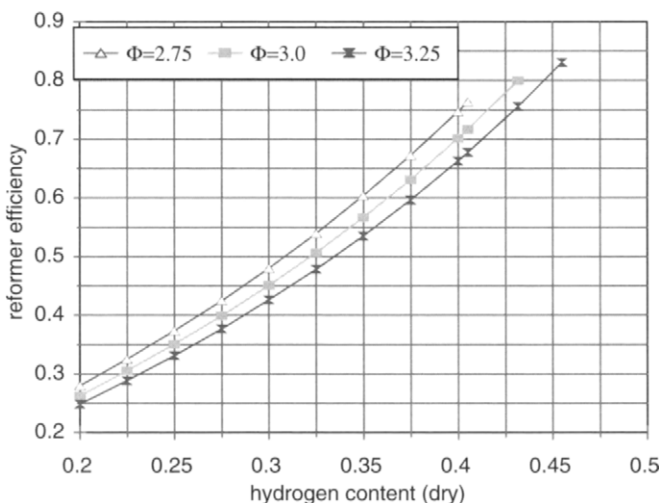


FIGURE 9-30. Relationship between hydrogen content in dry reformate gas (by vol.) and autothermal natural gas reformer efficiency (CO content 1%).

TABLE 9-5

Reformate Gas Composition for Various Equivalence Ratios and Efficiencies (for Natural Gas)

Equivalence ratio	3.0	3.0	3.20
Carbon to steam ratio	2.0	2.0	2.0
Theoretical efficiency (HHV)	0.85	0.85	0.88
Actual efficiency (HHV)	0.75	0.80	0.80
Actual efficiency (LHV)	0.70	0.75	0.75
CO <sub>2</sub>	0.150	0.152	0.153
H <sub>2</sub>	0.401	0.416	0.428
N <sub>2</sub>	0.428	0.417	0.402
CO	0.010	0.010	0.010
CH <sub>4</sub>	0.011	0.004	0.008

such as Pt on ceria or gold on ceria, show more promise, not only because they are more tolerant to sulphur, but more important, because they allow higher space velocities, thus resulting in smaller reactors.

Shift reaction can reduce the CO content typically to below 1% (by vol. in dry gas). This would still be too high for a PEM fuel cell, which has very low tolerance to CO (typically below 100 ppm, depending on the operating temperature). Further CO cleanup is achieved by an additional step—preferential or selective oxidation. This is essentially a controlled catalytic combustion of CO on noble metal catalyst that at a given temperature has higher affinity to CO than to H<sub>2</sub>. The reaction is simply:



However, to ensure almost complete elimination of CO (below 100 ppm), oxygen must be provided in excess, typically 2.0–3.5 higher than the stoichiometric ratio. Excess oxygen in presence of noble metal catalyst reacts with hydrogen present in the reformate gas. The efficiency of the preferential oxidation process is then defined as a ratio between the amount of hydrogen at the outlet and the amount of hydrogen at the inlet. Figure 9-31 shows the efficiency of a typical PROX reactor. In addition, air supply and PROX temperature must be carefully controlled to avoid hazardous situations, particularly if the gas flow rate is highly variable.

In general, control of the fuel processing is not an easy task. Fuel processing consists of a series of reactors, each operating at its own relatively narrow operating temperature window. The composition of the gas at the exit of each of those reactors highly depends on the composition of the inlet gas, plus oxygen and steam feed, and the reactor temperature. If any of the parameters is even slightly out of the operating window even for a very short period, the result is higher CO content at the outlet, which as shown below, may have a detrimental effect on fuel cell performance.

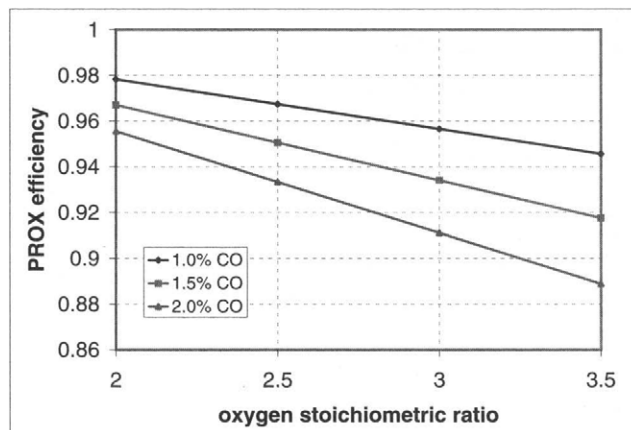


FIGURE 9-31. Efficiency of a PROX reactor as a function of oxygen stoichiometric ratio and CO content at the inlet.

TABLE 9-6

Typical Reformate Compositions for Various Fuels and Various Reforming Processes (It Includes Preferential Oxidation as Well)

	$H_2$	$CO_2$	$N_2$
Natural gas Autothermal	0.42	0.16	0.42
Gasoline Autothermal	0.40	0.20	0.40
Methanol Autothermal	0.50	0.20	0.30
Natural gas Steam reforming	0.75	0.24	0.01
Methanol Steam reforming	0.70	0.29	0.01

### 9.3.4. Effect of Reformate on Fuel Cell Performance

The composition of the reformate gas coming out of the reformer depends on the type of fuel, type of reformer, and the operating fuel processor efficiency. Table 9-6 gives approximate composition for some typical cases. In addition, not shown in the table, the reformate gas contains up to 100 ppm CO, unconverted fuel, and other hydrocarbons (methane, ethane, ethylene), and it may contain traces of other by-products, such as hydrogen sulfide, ammonia, aldehydes, and so forth.

The reformate gas has several effects on PEM fuel cell performance, such as:

- loss of potential due to hydrogen's low content,
- catalyst poisoning with CO,
- catalyst and membrane poisoning with other constituents (such as ammonia and hydrogen sulfide) even at very small concentrations.

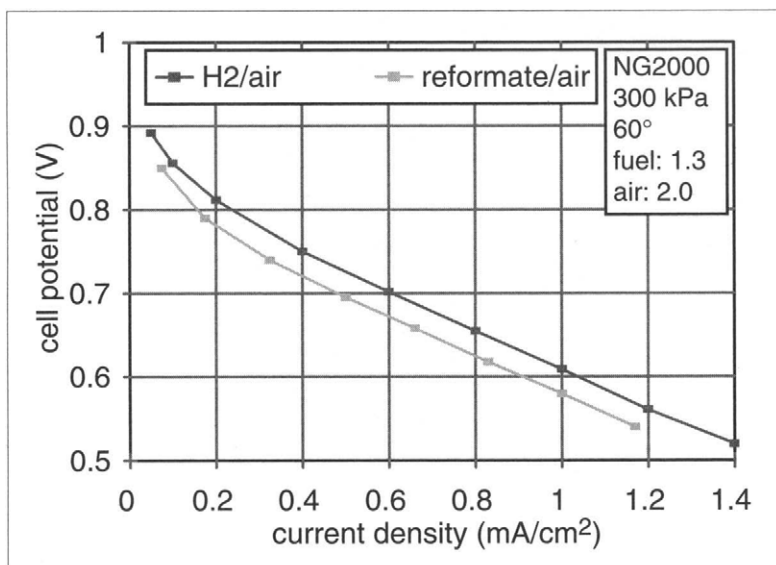


FIGURE 9-32. Effect of reduced hydrogen concentration in reformate on fuel cell performance [14].

Hydrogen content of 40% results in 2.5 times lower concentration than in pure hydrogen. The result is a lower cell voltage due to the Nernst equation. Typically, the voltage loss is less than 30 mV (Figure 9-32).

Carbon monoxide has a much more severe impact, even at very low concentrations. At low temperatures (below 100°C), Pt has higher affinity toward CO than toward hydrogen, and as a result most of the catalyst sites get occupied with CO [15], even at concentrations as low as 100 ppm, resulting in practically no current-generating capability (Figure 9-33). It is well documented that in PEM fuel cells at 80°C, PtRu catalyst has much higher tolerance to CO [16]. Figure 9-34 shows significant improvement in cell performance with PtRu anode catalyst as compared with regular Pt catalyst. This is probably due to water activation by Ru and subsequent CO electrooxidation on a neighboring Pt atom [17], or due to weakening of the pt-CO bond strength [15].

In addition, a little bit of air (typically about 2%) injected on the anode side of the fuel cell (called air bleed) helps oxidize the CO. With PtRu catalyst and with 2% air bleed it is possible to operate a fuel cell with reformate containing up to 100 ppm with virtually no loss in performance (Figure 9-34) [18].

Better tolerance to CO would be possible at higher temperatures (>120–130°C); however, regular PSA membranes cannot operate at those temperatures. There are significant research efforts dedicated to development of the membranes that can operate at higher temperatures. Although some show promise [19–21], none has been put in practical applications

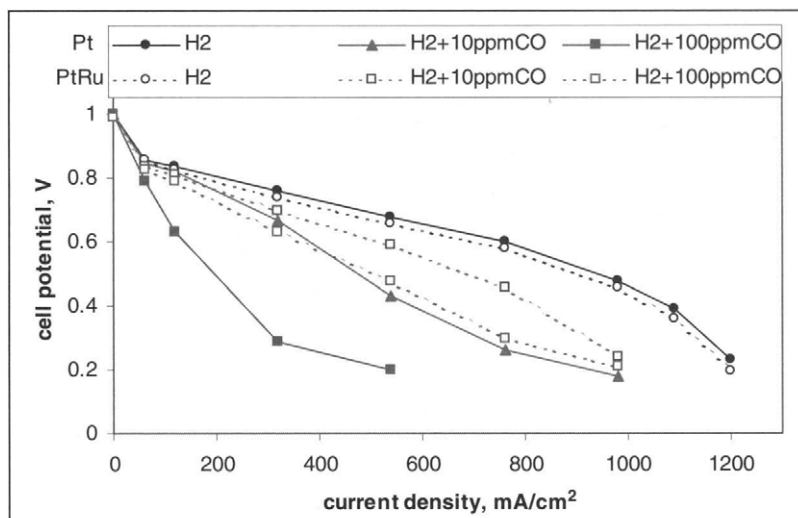


FIGURE 9-33. CO tolerance of Pt and PtRu catalyst (308 kPa, 80°C, 1.3/2.0 hydrogen/air stoichiometry) [15].

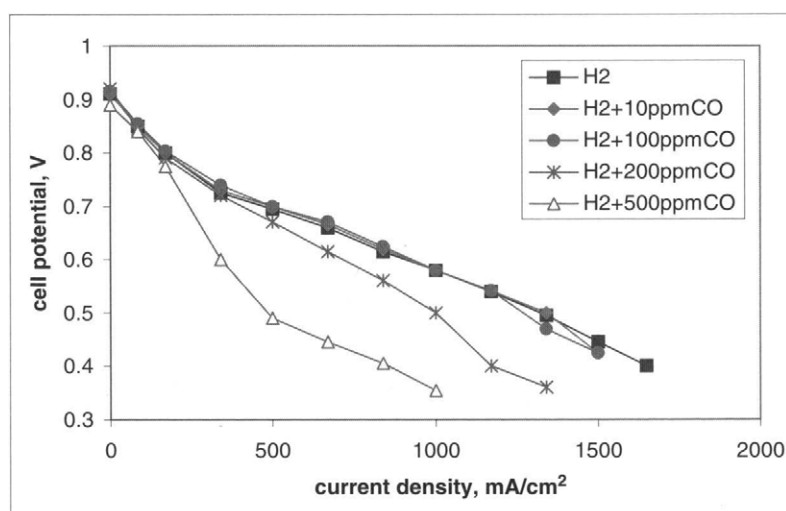


FIGURE 9-34. Effect of 2% air bleed on CO tolerance of PtRu catalyst (reformate/air, reformate composition 40% H<sub>2</sub>, 40% N<sub>2</sub>, 20% CO<sub>2</sub>; 308 kPa, 60°C, 1.3/2.0 hydrogen/air stoichiometry) [18].

yet. An additional benefit of operation at a higher temperature would be smaller size of the heat rejection equipment.

Other possible by-products in the reformate may have a detrimental effect on PEM fuel cell performance. Figure 9-35 shows what happens when a small quantity (13 to 130 ppm) of ammonia is injected in the anode fuel stream [22]. The cell current at given cell potential steadily declines. It seems that this poisoning is reversible, that is, after the flow of ammonia is disconnected, the cell performance slowly improves. Note that the performance did not return to its original value even after several hours. Ammonia may be generated in the autothermal reformer under certain

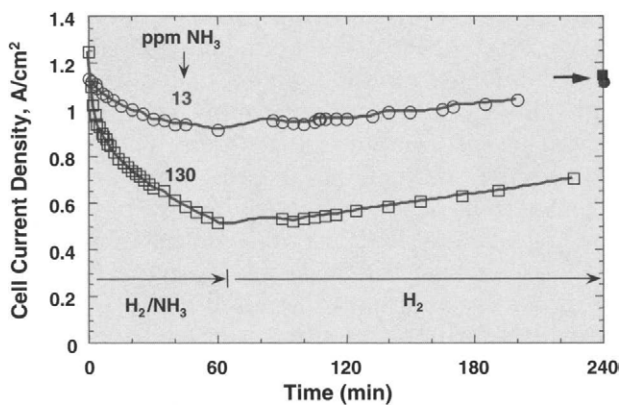


FIGURE 9-35. Effect of two concentrations of  $\text{NH}_3$  on fuel cell performance at  $80^\circ\text{C}$  [22]. (Reprinted by permission from the Electrochemical Society.)

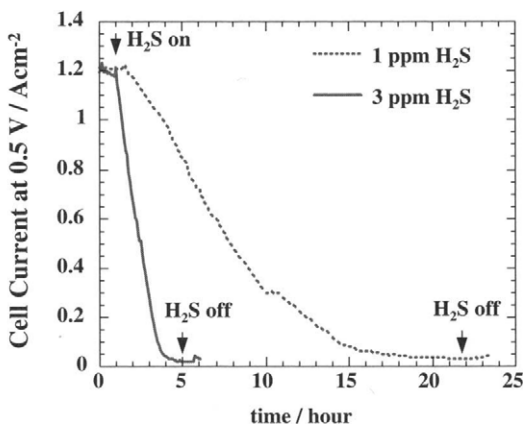


FIGURE 9-36. Effect of 1 ppm and 3 ppm  $\text{H}_2\text{S}$  burp on fuel cell performance operating at 0.5 V and  $80^\circ\text{C}$ . Humidified  $\text{H}_2/\text{H}_2\text{S}$  mix is injected directly to the anode [23]. (Reprinted by permission from the Electrochemical Society.)

conditions (after all, the main constituents, hydrogen and nitrogen, are present).

Poisoning with H<sub>2</sub>S, which also may be formed in the reformer in the case that the fuel desulfurization step is not working properly, seems more fatal to the fuel cell performance (Figure 9-36) [23]. As low as 1–3 ppm of H<sub>2</sub>S was sufficient to practically “kill” the cell, and performance does not seem to improve after H<sub>2</sub>S feed has been discontinued, that is, the damage was permanent.

### 9.3.5. System Integration

As discussed earlier, a fuel processor encompasses several processes, each taking place in a separate reactor/vessel. In addition, some of them require air supply, some require steam supply, and all require some kind of temperature control. The equipment for air supply, steam supply, and temperature control must be incorporated in the fuel processor subsystem. There are numerous ways the components and the flows between them can be arranged. The goal is to have a system with highest possible efficiency (*i.e.*, hydrogen yield), lowest possible CO content in the produced gas, minimum harmful by-products (such as ammonia and hydrogen sulfide), and flexibility enough that it can respond to the fuel cell hydrogen needs. Figure 9-37 shows some possible reformer subsystem configurations. Although the two systems in Figure 9-37 contain the same components, they are arranged in slightly different ways. One, for example, uses the heat from the fuel cell tail gases burner to preheat the fuel and water, whereas the other uses this heat entirely to generate steam, and uses the heat from the main reactor to preheat fuel. In the case of liquid fuel (such as gasoline or methanol), preheating also includes fuel evaporation. Both natural gas and gasoline, and particularly diesel fuel, contain sulphur, which must be removed, typically as the first step in fuel processing. Additional heat exchangers may be needed in the systems that intend to recuperate waste heat.

The fuel processor needs to be fully integrated with the fuel cell system. It not only provides fuel to the fuel cell, and uses the heat from the fuel cell exhaust gases, but it also shares air, water, coolant, and control subsystems as illustrated in Figure 9-38.

The reformatte coming out of the fuel processor is hot and oversaturated with water. This eliminates the need for anode humidifier, but it requires a cooler to bring the anode gas to the fuel cell operating temperature. Condensed water is separated before entering the fuel cell stack.

The fuel processor and the fuel cell typically operate at the same pressure, so they may share the same air supply. It is important to distribute the air flow to where it is needed, namely, fuel cell stack, fuel processor reactor, and preferential oxidation reactors; an additional air bleed may be required at the stack anode inlet. To avoid expensive mass flow controllers

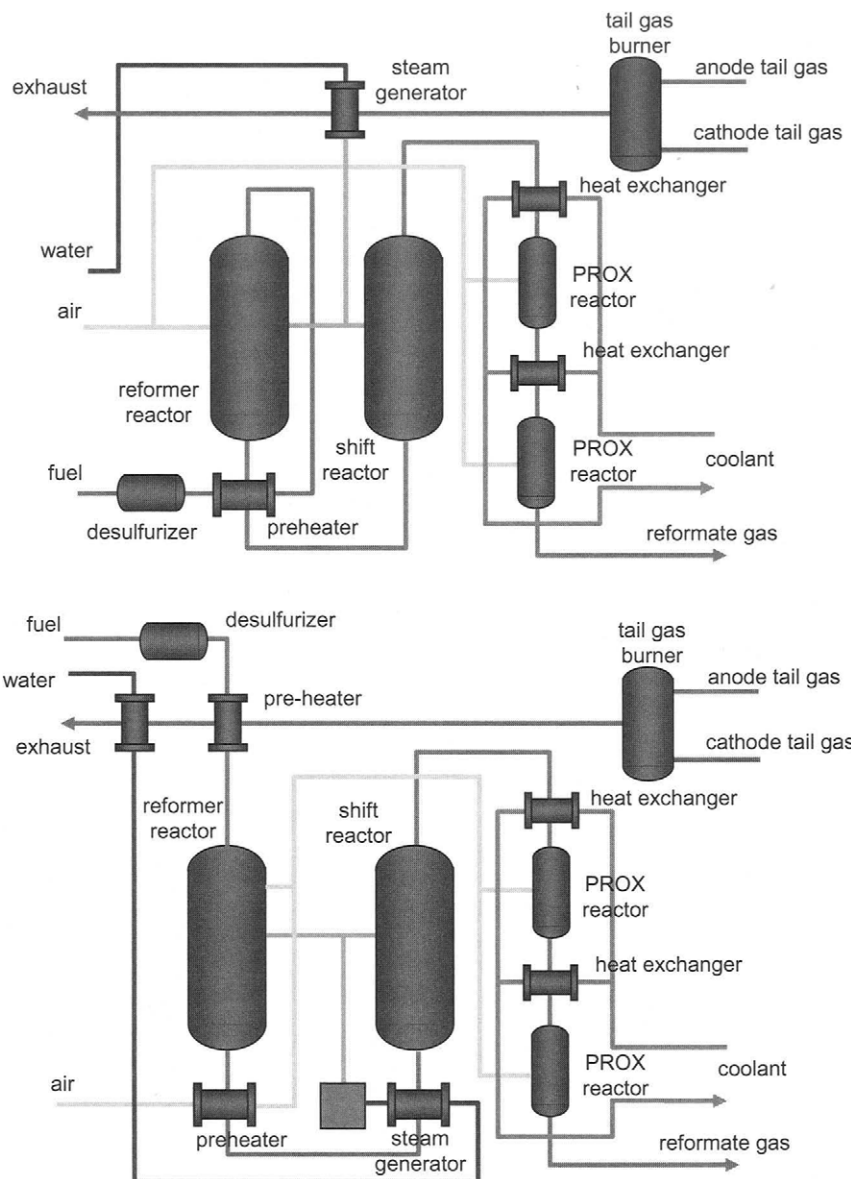


FIGURE 9-37. Schematic diagrams of two versions of an autothermal reformer.

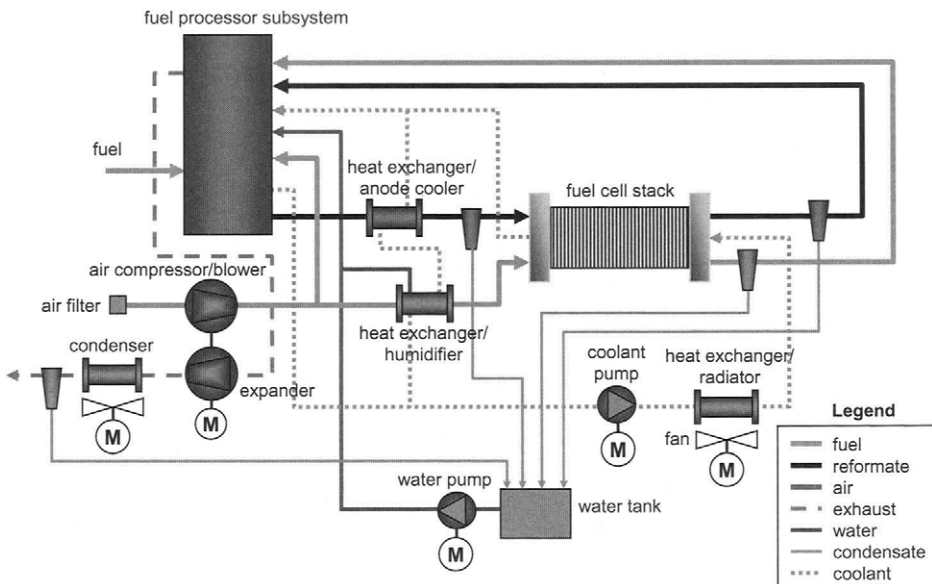


FIGURE 9-38. A complete fuel cell system integrated with fuel processor.

(which also may require much higher pressures to operate properly), passive devices such as orifices are often used.

Water is needed by the fuel processor to generate steam for the fuel processor and shift reactors, and by the fuel cell for humidification of the cathode inlet. Various cathode humidification schemes have been discussed. Typically, high-pressure water is required for both steam generation and injection in the humidifier. Fuel cell systems, regardless of application, may be designed to operate without need for makeup water. Water enters the system with ambient air and leaves the system with exhaust. Water is created as a product in the fuel cell, in the tail gas burner, and small quantities are produced in the preferential oxidation (as a result of unwanted hydrogen oxidation). At the same time, water is consumed in the fuel processor (both in steam reforming and in gas shift reactions).

The system water balance is therefore given by the following equation:

$$\dot{m}_{H_2O}^{air,in} + \dot{m}_{H_2O}^{FC} + \dot{m}_{H_2O}^{TGC} + \dot{m}_{H_2O}^{PROX} = \dot{m}_{H_2O}^{FP,cons} + \dot{m}_{H_2O}^{exh,out} \quad (9-62)$$

where:

$\dot{m}_{H_2O}^{air,in}$  = amount of water (humidity) that enters the system with ambient air

$$\dot{m}_{H_2O}|_{in}^{air} = \dot{m}_{Airin} \frac{M_{H_2O}}{M_{air}} \frac{\varphi_{amb} P_{vs}(T_{amb})}{P_{amb} - \varphi_{amb} P_{vs}(T_{amb})} \quad (9-63)$$

where  $\dot{m}_{Airin}$  is the total amount of dry air needed by the fuel cell system, which includes, air for the fuel cell, air for the fuel processor, air for preferential oxidation, and air for air bleed:

$$\dot{m}_{Airin} = \dot{m}_{Air}|_{in}^{FC} + \dot{m}_{Air}|_{in}^{FP} + \dot{m}_{Air}|_{in}^{PROX} + \dot{m}_{Air}|_{Airbleed} \quad (9-64)$$

Air for the fuel cell is given by Equation (5-42):

$$\dot{m}_{Air}|_{in}^{FC} = \frac{S_{O_2}}{r_{O_2}} \frac{I \cdot n_{cell}}{4F} M_{Air} \quad (9-65)$$

Air for the fuel processor may be calculated from Equations (5-39, 9-51, and 9-59):

$$\dot{m}_{Air}|_{in}^{FP} = S_{H_2} \frac{I \cdot n_{cell}}{2F} \frac{\Delta H_{fuel}}{\eta_{FP} \Delta H_{H_2}} \frac{m + n/4 - p/2}{\epsilon} \frac{M_{Air}}{r_{O_2}} \quad (9-66)$$

Air for preferential oxidation may be calculated from Equations (5-39, 9-51, 9-57, 9-59, and 9-61):

$$\begin{aligned} \dot{m}_{Air}|_{in}^{PROX} &= S_{H_2} \frac{I \cdot n_{cell}}{2F} \frac{\Delta H_{fuel}}{\eta_{FP} \Delta H_{H_2}} r_{CO} \\ &\left( 1 + \frac{m + n/4 - p/2}{\epsilon} \frac{1 - r_{O_2}}{r_{O_2}} + \eta_{FP} \frac{\Delta H_{H_2}}{\Delta H_{fuel}} \right) \frac{S_{PROX}}{2} \frac{M_{Air}}{r_{O_2}} \end{aligned} \quad (9-67)$$

Air bleed is usually about 2% of the anode flow:

$$\dot{m}_{Air}|_{Airbleed} = 0.02 \cdot \frac{S_{H_2}}{r_{H_2}} \frac{I \cdot n_{cell}}{2F} M_{Air} \quad (9-68)$$

$\dot{m}_{H_2O}|_{gen}^{FC}$  = amount of water generated in fuel cell (from Equation 5-7):

$$\dot{m}_{H_2O}|_{gen}^{FC} = \frac{In_{cell}}{2F} M_{H_2O} \quad (9-69)$$

$\dot{m}_{H_2O}|_{gen}^{TGC}$  = amount of water generated in tail gas combustor:

$$\dot{m}_{H_2}|_{gen}^{TGC} = (S_{H_2} - 1) \frac{I \cdot n_{cell}}{2F} M_{H_2O} \quad (9-70)$$

$\dot{m}_{H_2O}|_{gen}^{PROX}$  = amount of water generated in preferential oxidation of CO (from Equations 9-51, 9-57, 9-59, and 9-61):

$$\dot{m}_{H_2O}|_{gen}^{PROX} = S_{H_2} \frac{I \cdot n_{cell}}{2F} \frac{\Delta H_{fuel}}{\eta_{FP} \Delta H_{H_2}} r_{CO} \\ \left( 1 + \frac{m + n/4 - p/2}{\epsilon} \frac{1 - r_{O_2}}{r_{O_2}} + \eta_{FP} \frac{\Delta H_{H_2}}{\Delta H_{fuel}} \right) (S_{PROX} - 1) M_{H_2O} \quad (9-71)$$

$\dot{m}_{H_2O}|_{cons}^{FP}$  = amount of water consumed in the fuel processor (from Equations 9-47, 9-57, and 9-59):

$$\dot{m}_{H_2O}|_{cons}^{FP} = S_{H_2} \frac{I \cdot n_{cell}}{2F} \frac{\Delta H_{fuel}}{\eta_{FP} \Delta H_{H_2}} \frac{(\epsilon - 1)(2m - p) - n/2}{\epsilon} M_{H_2O} \quad (9-72)$$

$\dot{m}_{H_2O}|_{out}^{exh}$  = amount of water that exits the system with exhaust gases

$$\dot{m}_{H_2O}|_{out}^{exh} = \dot{m}_{exh} \frac{M_{H_2O}}{M_{exh}} \frac{P_{vs}(T_{exh})}{P_{amb} - P_{vs}(T_{exh})} \quad (9-73)$$

where  $\dot{m}_{exh}$  is the mass flow of exhaust gases, which may be easily calculated from the system mass balance:

$$\dot{m}_{exh} = \dot{m}_{fuelin} + \dot{m}_{Airin} - \dot{m}_{H_2O}|_{gen}^{FC} - \dot{m}_{H_2O}|_{gen}^{TGC} - \dot{m}_{H_2O}|_{gen}^{PROX} + \dot{m}_{H_2O}|_{cons}^{FP} \quad (9-74)$$

$$\dot{m}_{fuelin} = S_{H_2} \frac{I \cdot n_{cell}}{2F} \frac{\Delta H_{fuel}}{\eta_{FP} \Delta H_{H_2}} M_{fuel} \quad (9-75)$$

Note that in Equations (9-65) through (9-72) and (9-75),  $I \cdot n_{cell}$  may be replaced by  $W/V_{cell}$ , where  $W$  is the fuel cell power output.

Equation (9-62) is satisfied and neutral water balance is accomplished by condensing the exhaust gases to a required temperature,  $T_{exh}$ . In systems where neutral water balance is not critical, the condenser at the exhaust may be omitted.

Water presence in the system makes the fuel cell systems susceptible to freezing if used in a cold environment. Various engineering solutions have been proposed and a few tried in the field to prevent freezing, ranging from draining the water from the system at shutdown to keeping the system warm either by electric heaters or having the system run (constantly or periodically) at very low power. The former requires changes in both system and stack design, whereas the latter may have a significant impact on overall system efficiency.

Deionized water may be used as coolant, but in the systems susceptible to freezing, the coolant loop is separated from the water loop, which allows for antifreeze coolants to be used, such as aqueous solutions of ethylene-glycol or propylene-glycol. Another option is to have an

air-cooled system, which is typically employed for low-power applications (below 3–4 kW).

In addition to taking the heat away from the fuel cell stack, the cooling loop also cools down the reformate gas coming from the fuel processor and provides heat, if needed, in the air humidification process. Moreover, temperature control of the preferential oxidation process is needed (as shown in Figures 9-37 and 9-38). The heat is then rejected from the system to the environment by the heat exchanger, typically of a radiator type. Some heat may be rejected from the system in the condenser just before the exhaust gases leave the system. The condenser is needed to condense and save the water in the exhaust to maintain a neutral water balance in the system.

The heat load distribution on the radiator and condenser depends on the operating pressure and temperature. Figure 9-39 shows the heat loads on the radiator and condenser as a function of operating pressure and temperature [24]. Higher operating temperatures and lower operating pressures result in the shifting of heat load from the radiator to the condenser. While at high pressure (300 kPa) and low temperature (60°C) almost all the heat is rejected in the radiator, at low pressure (170 kPa) and high temperature almost all the heat is rejected in the condenser. The major difference between the radiator and the condenser is that the radiator is a liquid/gas heat exchanger and the condenser is a gas/gas heat exchanger (some heat transfer is used for phase change, that is, condensation of water, but the amount of water is orders of magnitude lower than the amount of gas). The heat transfer coefficients are significantly lower for gas/gas heat exchangers, which means that for the same amount of heat load these heat exchangers require a much larger heat exchange area.

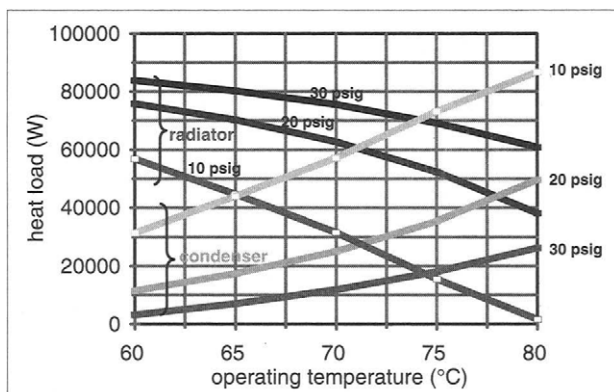


FIGURE 9-39. Radiator and condenser heat load as a function of operating pressure and temperature of a 50-kWe net system operating at 32.5% system efficiency [24].

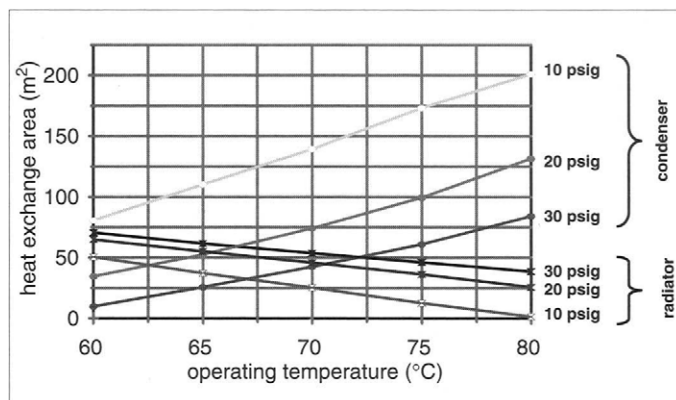


FIGURE 9-40. Required heat exchange area for a 50-kW<sub>c</sub> net system operating at 32.5% system efficiency (liquid/gas heat transfer coefficient = 60 W/m<sup>2</sup>/°C, air/air heat transfer coefficient 15 W/m<sup>2</sup>/°C, fin area/tube area = 10) [24].

Figure 9-40 compares the heat exchange areas for the radiator and condenser at different operating temperatures and pressures [24]. Although the automotive heat exchangers are typically densely packed ( $>1000\text{ m}^2/\text{m}^3$ ) the size of the heat exchangers may very well be a limiting factor for the automotive fuel cell systems. Higher operating temperature does not necessarily mean smaller heat exchanger size, if water balance is to be maintained. For this particular analysis [24], the smallest heat exchangers resulted in a system that operates at high pressure (308 kPa) and low temperature (60°C). At the operating temperature below 60°C at sufficiently high operating pressure (above 300 kPa), there is no need for a condenser, and all the heat can be rejected in the radiator.

#### 9.4. Electrical Subsystem

An electrical subsystem is needed to deliver power produced by a fuel cell to the user (load); this subsystem typically does not just deliver, but it modifies the fuel cell electrical output so that it matches the load requirements in terms of voltage, type of current, power quality, and transients. Obviously, the configuration and characteristics of such a subsystem strongly depend on the load requirements, which vary with application.

Fuel cells generate direct current (DC) at a voltage that depends on the number of cells connected in series, and on the current being generated (remember, fuel cell voltage and current are related by the fuel cell's polarization curve). The fuel cell voltage, therefore, changes with current. The fuel cell open circuit voltage is around 1 V per cell (a little bit above 1 V for hydrogen–oxygen, and a little bit below for hydrogen–air systems). The cell potential at nominal power is a design variable and it is typically selected

at a value between 0.6 and 0.7 V. Therefore, any fuel cell stack will have a voltage swing between 0.6:1.0 and 0.7:1.0. A very few loads could tolerate such voltage swings.

Voltage regulation is one of the most common functions of the electrical subsystem. Depending on where the fuel cell swing potential is relative to the required load potential, the electrical subsystem must either reduce the fuel cell voltage (so-called buck converter) or increase it (so-called boost converter). In the case that the load voltage is inside the fuel cell voltage range, a buck-boost converter is needed (Figure 9-41).

Voltage regulation is accomplished using switching or chopping circuits [25] that use electronic switches, such as:

- thyristors and GTO (gate-turn-off) thyristors
- MOSFET (metal oxide semiconductor field effect transistor), used typically in low-voltage systems up to approximately 1 kW
- IGBT (insulated gate bipolar transistor) for high-current applications (>50 A)

When arranged in electronic circuits with diodes, capacitors, and inductors (as shown in Figure 9-42), these electronic switches can provide the desired voltage output of the circuit, by switching on and off certain parts of the circuit. The output voltage is a function of input voltage and switching time.

For a step-down or buck converter:

$$V_{\text{out}} = DV_{\text{in}} \quad (9-76)$$

Where D is defined as a switching function,  $D = \frac{t_{\text{on}}}{t_{\text{on}} + t_{\text{off}}}$

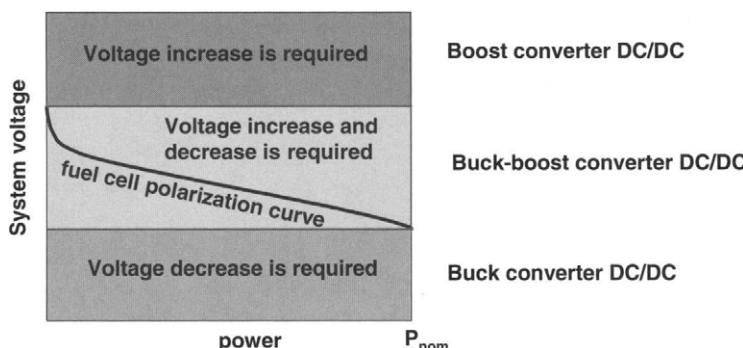


FIGURE 9-41. Fuel cell polarization curve determines the type of converter needed to match the load voltage.

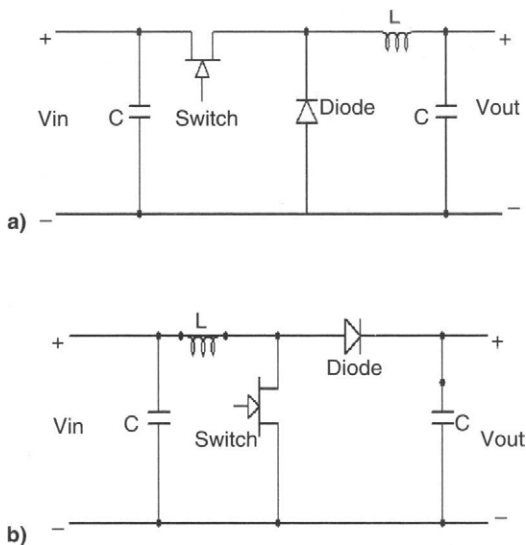


FIGURE 9-42. Switching circuits used in DC converters: a) step-down or buck converter; b) step-up or boost converter.

For a step-up or boost converter:

$$V_{\text{out}} = \frac{V_{\text{in}}}{1 - D} \quad (9-77)$$

The actual voltage is always somewhat lower than that given by Equations 9.76 and 9.77, because of energy losses in the circuit, which include switching losses, power loss in the switch while it is turned on, power loss due to the resistance of the inductor, and losses in the diode. In practice, these losses are very low [25]. The efficiencies of step-down converters are typically more than 90%, and in high-voltage systems ( $V_{\text{in}} > 100 \text{ V}$ ) can be as high as 98%. The efficiencies of the step-up converters are somewhat lower because of a different duty cycle (in high-voltage systems can be as high as 95%). It should be mentioned that the efficiency is a function of current through different elements of the circuit, as well as of switching function, and therefore it is not constant throughout the power range.

Fuel cells generate direct current (DC), but some loads or applications require alternating current (AC). For those applications, the electrical subsystem must also include a step of converting DC to AC of a fixed frequency (60 or 50 Hz). This is also accomplished by the electronic switching devices arranged in electrical circuits as shown in Figure 9-43. The fuel cell system may be connected to a single AC voltage (typically in domestic applications) or to a three-phase supply (in larger industrial systems).

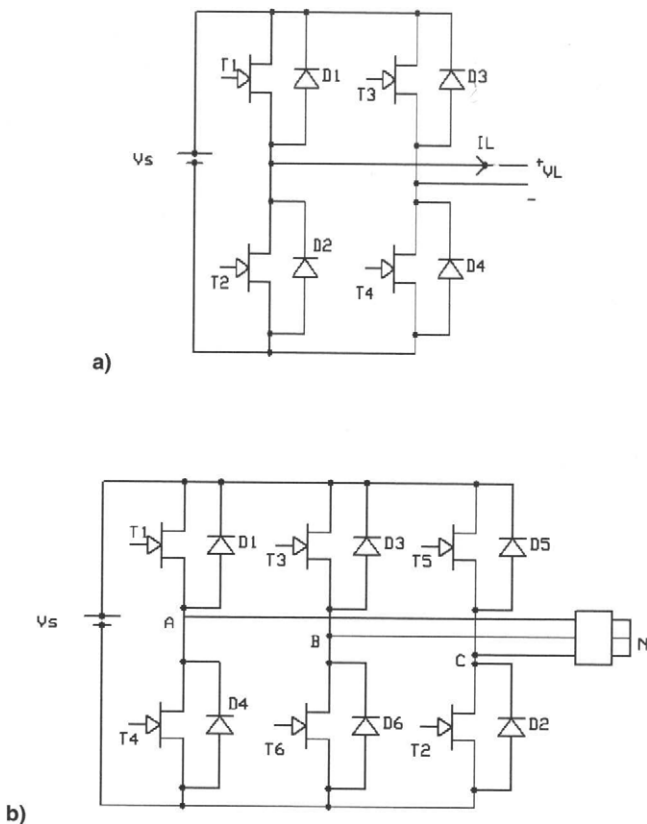


FIGURE 9-43. Configurations of typical DC/AC inverters: a) H-Bridge for single phase; b) three-phase inverter.

The resulting current from AC inverters is in a square wave shape. For some applications, this may be sufficient; however, for most applications, and particularly for the grid-connected applications, the square wave output is not acceptable. In that case modulation is required to generate the output closer to the pure sine-wave. Typically, pulse-width modulation (PWM), or more recently, tolerance-bend pulse method is used. The efficiency of commercially available DC/AC inverters varies between 70% and 90%, and it is a strong function of the required power quality (*i.e.*, how close to the true sine wave the output has to be).

A fuel cell system has several electric power-driven components, such as pumps, fans, blowers, solenoid valves, instruments, and so on. These components may operate with either DC or AC. The electrical subsystem must also provide power for these components at certain voltage and current.

Very often, a fuel cell system is equipped with a battery for start-up or for peaking. A start-up battery must match the voltage of the critical components to be started before the fuel cell is operational, or an additional voltage converter may be needed. The batteries or other peaking devices, such as ultracapacitors, can respond to sudden changes in power much faster than a fuel cell system. A fuel cell itself can respond to the changes in load as quickly as a battery, providing it has sufficient supply of reactant gases. The gases, particularly air or fuel other than hydrogen, are supplied by mechanical devices, which, by their nature, cannot respond as quickly as electrical demand may change. In that case the batteries or ultracapacitors provide power until the fuel cell can match it. The fuel cell then can also recharge the batteries/ultracapacitors.

In some cases, in applications with highly variable power, the fuel cell is intentionally sized at a power level between average and peak power. A fuel cell provides power up to its nominal power. An increase in demand above this power level further drops the fuel cell potential and in that case the battery steps in and covers the difference in power. In this case, the battery must be sized not only to match the power requirements, but also to match the energy requirements during those periods when the power demand exceeds the fuel cell nominal power. The fuel cell automatically recharges the battery when the load power goes below the fuel cell nominal power.

A control subsystem is needed not only to control the fuel cell operating parameters (flow rates, temperature, humidity, *etc.*) but also to communicate with the load and other electrical components of the system. This is particularly critical for applications where a fuel cell operates integrated within an electrical grid. The functioning of the electric and control subsystems depends on application (*e.g.*, stand-alone, grid integrated, combined with another power source, backup power).

Figure 9-44 shows a configuration of a typical fuel cell electrical subsystem configuration with the following main components:

- fuel cell stack that generates DC current at certain voltage
- converter to step down or to boost up the voltage level that is produced by fuel cell, depending on the load requirements
- battery or peaking device, such as ultracapacitor, that supplies power during periods when the demand exceeds fuel cell capabilities
- diode, to prevent current flow back to the fuel cell;
- capacitor just before the DC/DC converter to filter out the ripple
- controller to ensure efficient and reliable working of the system by monitoring current and voltages in the subsystem and determining and providing respective control signals
- power supply (DC) for auxiliary fuel cell equipment (fan, blower, pumps, solenoid valves, instruments, *etc.*)

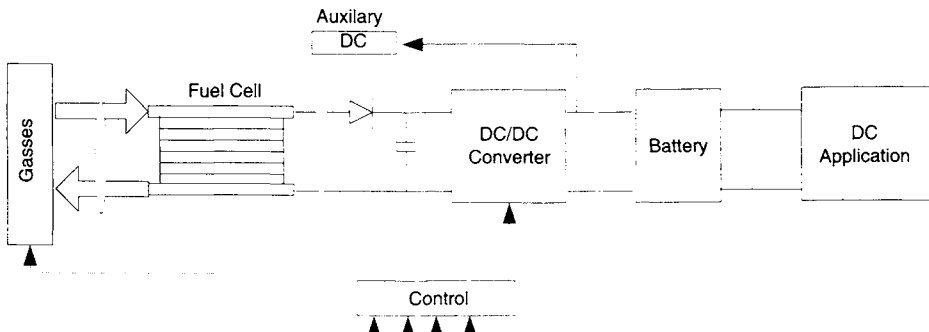


FIGURE 9-44. Schematic diagram of a fuel cell electric subsystem for DC power application.

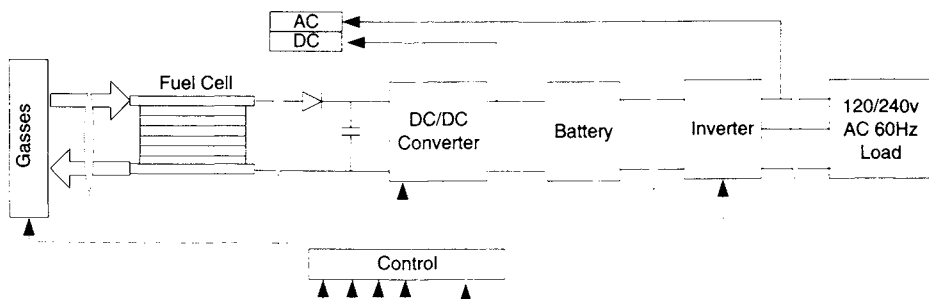


FIGURE 9-45. Schematic diagram of a fuel cell electric subsystem for stand-alone AC power application.

In case the load requires AC current (120/240 V) at certain frequency (50 or 60 Hz), an additional component of the electrical subsystem is needed—an inverter that generates AC current from a DC input (Figure 9-45). Depending on application, the system may operate as stand-alone (as shown in Figure 9-45) or it may operate parallel with the grid. In the latter case, an extra unit—a transfer switch—is needed to be connected to, and to guarantee synchronizing with the grid (Figure 9-46).

There are certain regulations for power-generating devices connected to the grid such as: (1) they must have the same voltage level and frequency as the grid, (2) they must be in phase with the grid, (3) they must have total

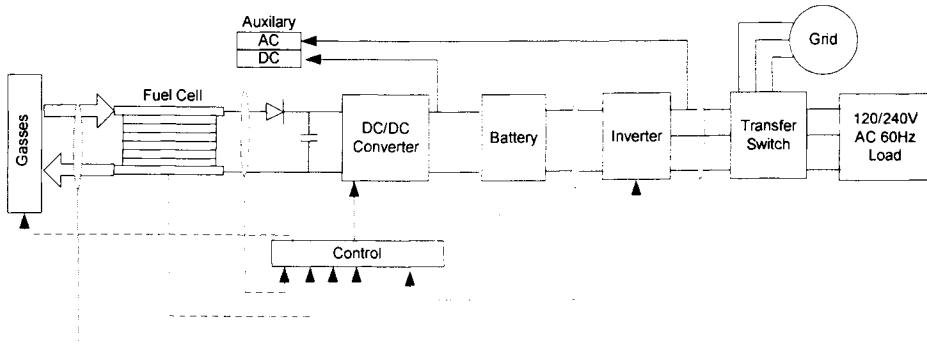


FIGURE 9-46. Schematic diagram of a fuel cell electric subsystem for grid parallel AC power application.

harmonic distortion as good or better than the grid, and (4) for safety reasons, they must automatically disconnect themselves from the grid in case the grid is down. In addition, for a system that “exports” at least a portion of its power to the grid, net metering may also be included.

## 9.5. System Efficiency

The fuel cell theoretical efficiency is 83% (Equation 2-43), based on the hydrogen’s higher heating value. The actual fuel cell efficiency in operation is much lower because of various losses (heat, electrode kinetics, electric and ionic resistance, mass transport). Additional components, such as fuel processor, power conditioning, and balance of plant, cause additional losses on the system level. Figure 9-47 shows a block diagram of a very generic fuel cell system with the flows of energy used to define the efficiencies of the individual steps.

The system efficiency is defined as a ratio between the output electrical energy,  $E_{\text{net}}$ , and the energy in fuel fed to the system,  $F_{\text{in}}$ :

$$\eta_{\text{sys}} = \frac{E_{\text{net}}}{F_{\text{in}}} \quad (9-78)$$

This efficiency is actually a product of several efficiencies of the individual components:

$$\eta_{\text{sys}} = \frac{H}{F_{\text{in}}} \frac{H_{\text{cons}}}{H} \frac{E_{\text{FC}}}{H_{\text{cons}}} \frac{E_{\text{net}}}{E_{\text{FC}}} \quad (9-79)$$

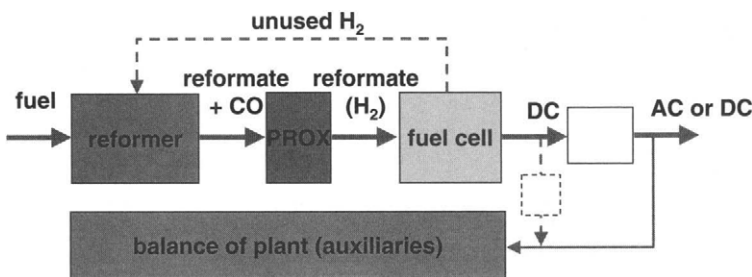


FIGURE 9-47. Simplified block diagram of a generic fuel cell system.

where:

$H$  = energy of hydrogen produced by the fuel processor (product of flow rate and heating value resulting in Watts)

$H_{\text{cons}}$  = energy of hydrogen consumed in fuel cell electrochemical reaction (also a product of flow rate and heating value resulting in Watts)

$E_{\text{FC}}$  = power produced by fuel cell (W)

Note that by definition, hydrogen fed to the fuel cell and hydrogen consumed in the fuel cell are related:

$$H = S_{\text{H2}} H_{\text{cons}} \quad (9-80)$$

Reformer efficiency is defined as a ratio between the energy in produced hydrogen and energy in fuel fed to the system.

$$\eta_{\text{ref}} = \frac{H}{F_{\text{in}}} = \frac{S_{\text{H2}} H_{\text{cons}}}{F_{\text{in}}} \quad (9-81)$$

The reformer efficiency typically does not include the efficiency of the preferential oxidation (PROX), which as shown previously is a function of the amount of air used in the process. Optimum oxygen stoichiometry that results in the lowest CO output is between 2 and 3. As shown in Figure 9-31, the PROX efficiency in that case is about 95%.

Fuel cell efficiency has two parts, fuel efficiency and voltage efficiency. Fuel efficiency is defined with the stoichiometric ratio. Because hydrogen is diluted at the fuel cell entrance, it has to be supplied in excess of the stoichiometric amount, so that hydrogen concentration at the exit is higher than zero. Typically, the reformate fuel cells operate with hydrogen stoichiometric ratios between 1.1 and 1.2. The fuel efficiency, defined

as the ratio between hydrogen consumed in the fuel cell and hydrogen actually supplied to the fuel cell is:

$$\eta_{\text{fuel}} = \frac{H_{\text{cons}}}{H} = \frac{H_{\text{cons}}}{S_{\text{H}_2} H_{\text{cons}}} = \frac{1}{S_{\text{H}_2}} \quad (9-82)$$

Unused hydrogen, however, is rarely just discarded into the atmosphere. Typically, unused hydrogen from the fuel cell stack is used to generate power in a turbine/expander or in the fuel processing process (to preheat the fuel or to generate steam, or in the steam reforming process it may be used as fuel, thus reducing the amount of fuel needed, *i.e.*, improving the overall efficiency). Fuel consumption is:

$$F_{\text{in}} = \frac{S_{\text{H}_2} H_{\text{cons}}}{\eta_{\text{ref}}} \quad (9-83)$$

Fuel consumption reduced by the recirculated hydrogen is:

$$F_{\text{in}} = \frac{S_{\text{H}_2} H_{\text{cons}}}{\eta_{\text{ref}}} - (S_{\text{H}_2} - 1)H_{\text{cons}} \quad (9-84)$$

The effective reformer efficiency, defined, as shown previously as a ratio between the energy in produced hydrogen and energy in fuel fed to the system, is:

$$\eta_{\text{ref}}^{\text{eff}} = \frac{H}{F_{\text{in}}} = \frac{S_{\text{H}_2} H_{\text{cons}}}{\frac{S_{\text{H}_2} H_{\text{cons}}}{\eta_{\text{ref}}} - (S_{\text{H}_2} - 1)H_{\text{cons}}} = \frac{1}{\frac{1}{\eta_{\text{ref}}} + \frac{1}{S_{\text{H}_2}} - 1} \quad (9-85)$$

The voltage efficiency of a fuel cell is:

$$\eta_{\text{FC}} = \frac{E_{\text{FC}}}{H_{\text{cons}}} = \frac{V_{\text{cell}}}{1.482} \quad (9-86)$$

Power produced by a fuel cell goes through power conditioning where it is brought to a desired constant voltage and desired current type, that is, direct or alternate. Some power is needed to run the system's ancillary components. This equipment may use either AC or low-voltage DC (typically 12, 24, or 42 V), in which case an additional DC/DC converter is needed, as shown in Figure 9-47. The resulting power conversion and parasitic loss efficiency is:

$$\eta_{PC} = \frac{E_{net}}{E_{FC}} = (\eta_{DC} - \xi) \quad (9-87)$$

for the case when the parasitic load runs on same voltage and current as the main load, with the efficiency of DC/DC or DC/AC power conversion  $\eta_{DC}$ . Coefficient  $\xi$  is a ratio between power needed to run the parasitic load and fuel cell gross power:

$$\xi = \frac{E_{aux}}{E_{FC}} \quad (9-88)$$

$$\eta_{PC} = \frac{E_{net}}{E_{FC}} = \eta_{DC} \left( 1 - \frac{\xi}{\eta_{DCaux}} \right) \quad (9-89)$$

for the case when the parasitic load runs on low-voltage DC and requires an additional power conversion with the efficiency  $\eta_{DCaux}$ . If the two power conversions have the same efficiency, Equation (9-89) becomes Equation (9-87).

The overall system efficiency is then:

$$\eta_{sys} = \eta_{ref} \eta_{PROX} \eta_{fuel} \eta_{FC} \eta_{PC} \quad (9-90)$$

Obviously, hydrogen–oxygen and hydrogen–air systems do not include the reforming step. In that case the system efficiency is:

$$\eta_{sys} = \eta_{fuel} \eta_{FC} \eta_{PC} \quad (9-91)$$

So, what would be a reasonable fuel cell system efficiency? Table 9-7 lists some ranges of components' efficiency and the resulting system efficiency.

**TABLE 9-7**  
Range of Efficiencies and Operating Parameters of Fuel Cell and Supporting Components and Resulting System Efficiencies

	$\eta_{ref}$	$\eta_{PROX}$	$S_{H2}$	$V_{cell}$	$\eta_{DC}$	$\xi$	$\eta_{sys} (HHV)$	$\eta_{sys} (LHV)$
<b>Hydrogen–oxygen systems</b>								
Low			1.01	0.8	0.93	0.05	0.48	0.56
High			1.01	0.85	0.96	0.03	0.53	0.62
<b>Hydrogen–air systems</b>								
Low			1.05	0.7	0.93	0.10	0.37	0.44
High			1.01	0.8	0.96	0.05	0.49	0.57
<b>Systems with fuel processor</b>								
Low	0.80	0.95	1.2	0.7	0.93	0.10	0.25	0.27
High	0.90	0.97	1.1	0.8	0.96	0.05	0.40	0.44

"Low" efficiencies should be achievable with today's technology, whereas "high" efficiencies may require some advances in reforming technology, power conditioning, and system integration.

An obvious solution for improvement of the system efficiency is to operate a fuel cell at a higher voltage. Because of the power-voltage fuel cell characteristic, higher voltage means lower power density, which in turns means a larger fuel cell for the same power output. Improvements in fuel cell catalysts, catalyst layer design, membrane materials, and fuel cell design should result in higher and less steep polarization curves, which should allow selection of higher operating voltages while still operating with considerable power densities. There seems to be room for improvements of the fuel cell efficiency, that is, operating potential, because current operating potentials are far below the theoretical potential.

## References

1. Justi, E. W., *A Solar-Hydrogen Energy System* (Plenum Press, New York, 1987).
2. Winter, C.-J. and J. Nitsch (editors), *Hydrogen as an Energy Carrier* (Springer-Verlag, Berlin Heidelberg, 1988).
3. McCarty, R. D., J. Hord, and H. M. Roder, Selected Properties of Hydrogen (Engineering Design Data), U.S. Department of Commerce, National Bureau of Standards, Monograph 168 (U.S. Government Printing Office, Washington, D.C., 1981).
4. Quantum Technologies website: [http://www.qtww.com/core\\_competencies/gf\\_storage.shtml](http://www.qtww.com/core_competencies/gf_storage.shtml) (accessed February 2005).
5. Blomen, L. J. M. J. and M. N. Mugerwa, *Fuel Cell Systems* (Plenum Press, New York, 1993).
6. Dynetek Industries website: <http://www.dynetek.com> (accessed February 2005).
7. Michel, F., H. Fieseler, G. Meyer, and F. Theissen, Onboard Equipment for Liquid Hydrogen Vehicles, in T. N. Veziroglu, C.-J. Winter, J. P. Baselt, and G. Kreysa (editors), *Hydrogen Energy Progress XI*, Vol. 2, in *Proc. of the 11th World Hydrogen Energy Conference* (Stuttgart, Germany, 1996), pp. 1063–1078.
8. Perry, Jr., J. H., A. Person, S. M. Misiaszek, and D. P. Alessi, Jr., Closed loop reactant/product management system for electrochemical galvanic energy devices, U.S. Patent No. 5,047,298, 1991.
9. Li, P.-W., T. Zhang, Q.-M. Wang, L. Schaefer, and M. K. Chyu, The Performance of PEM Fuel Cells Fed with Oxygen through the Free-Convection Mode, *Journal of Power Sources*, Vol. 114, No. 1, 2003, pp. 63–69.
10. PaxiTech website: <http://www.paxitech.com> (accessed February 2005).
11. Wilkinson, D. P. and J. St-Pierre, In-Plane Gradients in Fuel Cell Structure and Conditions for Higher Performance, *Journal of Power Sources*, Vol. 113, No. 1, 2003, pp. 101–108.

12. Barbir, F., M. Nadal, and M. Fuchs, Fuel Cell Powered Utility Vehicles, in Buchi, F. (editor), *Proc. of the Portable Fuel Cell Conference* (Lucerne, Switzerland, June 1999), pp. 113–126.
13. Weast, R. C., *CRC Handbook of Chemistry and Physics* (CRC Press, Boca Raton, FL, 1988).
14. Neutzler, J. and F. Barbir, Development of Advanced, Low-Cost PEM Fuel Cell Stack and System Design for Operation on Reformate Used in Vehicle Power Systems, *Fuel Cells for Transportation, FY1999 Annual Progress Report* (U.S. Department of Energy, Office of Advanced Automotive Technologies, Washington, D.C., October 1999), pp. 71–76.
15. Ralph, T. R. and M. P. Hogarth, Catalysis for Low Temperature Fuel Cells, *Platinum Metal Review*, Vol. 46, No. 3., 2002, pp. 117–135.
16. Gottesfeld, S. and T. A. Zawodzinski, Polymer Electrolyte Fuel Cells, in R. C. Alkire, H. Gerischer, D. M. Kolb, and C. W. Tobias (editors), *Advances in Electrochemical Science and Engineering*, Vol. 5 (Wiley-VCH, New York, 1997), p. 219.
17. Gasteiger, H. A., N. Markovic, P. N. Ross, and E. J. Cairns, CO Electrooxidation on Well-Characterized Pt-Ru Alloys, *Journal of Physical Chemistry*, Vol. 98, No. 2, 1994, pp. 617–625.
18. Barbir, F., Short Course on Automotive Fuel Cell System Engineering, in *Proc. of the Intertech Conference Commercializing Fuel Cell Vehicles 2000* (Berlin, Germany, April 2000).
19. Sumner, M. J., W. L. Harrison, R. M. Weyers, Y. S. Kim, J. E. McGrath, J. S. Riffle, A. Brink, and M. H. Brink, Novel Proton Conducting Sulfonated Poly(Arylene Ether) Copolymers Containing Aromatic Nitriles, *Journal of Membrane Science*, Vol. 239, No. 2, 2004, pp. 199–211.
20. Pawlik, J. and C. Henschel, Membrane-Electrode-Assemblies for Reformed Hydrogen Fuel Cells, in *Proc. of the 2004 Fuel Cell Seminar* (San Antonio, TX, 2004), pp. 93–96.
21. Herring, A., S. Dec, J. Malers, F. Meng, J. Horan, J. Turner, M.-A. Sweikart, J. Pern, and D. Vernon, The Use of Heteropoly Acids in Composite Membranes for Elevated Temperature PEM Fuel Cell Operation; Lessons Learned from Three Different Approaches, in *Proc. of the 2004 Fuel Cell Seminar* (San Antonio, TX, 2004), pp. 97–100.
22. Uribe, F. A., S. Gottesfeld, and T. A. Zawodzinski, Jr., Effect of Ammonia as Potential Fuel Impurity on Proton Exchange Membrane Fuel Cell Performance, *Journal of the Electrochemical Society*, Vol. 149, 2002, p. A293.
23. Uribe, F. A. and T. A. Zawodzinski, Effects of Fuel Impurities on PEM Fuel Cell Performance, in *The Electrochemical Society Meeting Abstracts* (San Francisco, September 2001), Vol. 2001–2, Abstract No. 339.
24. Barbir, F., B. Balasubramanian, and J. Neutzler, Trade-off Design Study of Operating Pressure and Temperature in PEM Fuel Cell Systems, *Advanced Energy Systems*, Vol. 39, 1999, pp. 305–315, ASME.
25. Larminie, J. and A. Dicks, *Fuel Cell Systems Explained*, Second ed. (John Wiley, Chichester, England, 2003).

## Problems

### Problem No. 1:

- a) Calculate the temperature at the end of compression in a single-stage compressor used to provide air for a fuel cell system. Ambient air is at 15°C and 101.3 kPa and (for the sake of this exercise) assume it is completely dry. Delivery pressure is 300 kPa. The fuel cell generates 50 kW at 0.7 V/cell and operates with oxygen stoichiometric ratio of 2. Assume adiabatic compression with efficiency of 0.7.
- b) Calculate the power (in kW) needed to run the compressor. Mechanical efficiency of the compressor is 93% and the efficiency of the electric motor and controller is also 93%.
- c) How much power can be recovered if the exhaust air is run through a turbine? The exhaust gas is fully saturated with water vapor at 60°C after liquid water has been removed. The pressure drop through the fuel cell is 25 kPa. The turbine efficiency is 70%.

### Problem No. 2:

For the fuel cell system from Problem 1 calculate:

- a) The amount of water (in g/s) needed to fully saturate the air at the fuel cell entrance at 60°C.
- b) Heat (in Watts) needed to be brought in the air humidification process (other than the heat of the incoming fluids, *i.e.*, air and water—assume water for humidification is available at 55°C).

### Problem No. 3:

A 10-kW, hydrogen-air fuel cell operates at 0.7 V/cell at 70°C and ambient pressure, with oxygen stoichiometry of 2.25. Liquid water is separated from the cathode exhaust. Ambient conditions are 23°C, 101.3 kPa, and 75% relative humidity. Calculate how much water would have to be stored for 7 days' operation. Propose a solution to make this system water neutral (*support your proposal with calculation showing the resulting water balance*).

### Problem No. 4:

Calculate the maximum theoretical LHV efficiency for reforming isoctane C<sub>8</sub>H<sub>18</sub>. What equivalence ratio does this efficiency correspond to?

### Problem No. 5:

Calculate composition (in vol. % of dry gas) of a reformatte gas obtained by reforming methane CH<sub>4</sub> in an autothermal fuel processor with gas shift

reactors, operating with equivalence ratio of 3.0, and LHV efficiency of 75%. CO content is 1% (by vol. dry).

### Problem No 6:

Hydrogen content in a reformate gas from a gasoline (assume octane) autothermal reformer is 41%. CO content is 1.2. Assume that in addition to products ( $H_2$ ,  $CO$ ,  $CO_2$ ), the only other by-product is  $CH_4$ .

- a) Calculate the reformer efficiency if the equivalence ratio is 3.13.
- b) Calculate the reformate generation rate (in standard liters per minute) for a 50-kW fuel cell operating at 0.66 V/cell with  $H_2$  stoichiometry of 1.15.
- c) Calculate the fuel consumption rate (in g/s).

### Problem No. 7:

The goal for the efficiency of an 85-kW fuel cell system using gasoline as fuel is 40% or higher (based on the lower heating value). The available reformer is 90% efficient, and the preferential oxidation has efficiency of 97%. The system uses power conditioning that is 94% efficient, for both main and parasitic loads. The ancillary components operate at 24 Volts DC and consume 7500W. What should be the nominal fuel cell operating potential (in Volts per cell)? How much power would the fuel cell generate? What would be fuel consumption (in g/s)? Discuss what would happen with the system efficiency at partial load, that is, 15-kW net power output.

## Quiz

1. In a fuel cell system, compressor power consumption:
  - a) is higher at higher fuel cell voltage
  - b) is lower at higher fuel cell voltage
  - c) does not depend on fuel cell voltage
2. A positive displacement compressor:
  - a) needs certain backpressure to operate
  - b) delivers air at a pressure higher than the fuel cell backpressure
  - c) delivers air at a pressure equal to the fuel cell backpressure
3. Humidification of air in a fuel cell system:
  - a) always needs additional heat
  - b) does not need additional heat in pressurized systems
  - c) may need additional heat depending on operating pressure and temperature

4. An expander may generate enough power to run the compressor:
  - a) only if the fuel cell system operates at high pressure and high temperature
  - b) if the pressure drop is sufficiently low
  - c) only if additional hydrogen is burned and this hot gas is used to run the expander
5. In a fuel cell system with hydrogen recirculation:
  - a) hydrogen flow rate at the stack inlet has stoichiometric ratio of 1
  - b) hydrogen flow rate at the stack inlet has stoichiometric ratio higher than 1
  - c) hydrogen consumption is higher than in dead-end mode operation
6. The difference between reformate produced by steam reforming and reformate produced by autothermal reforming is:
  - a) reformate from steam reforming does not contain nitrogen
  - b) reformate from authothermal reforming contains no water vapor
  - c) there is no difference
7. Shift reactor:
  - a) improves the efficiency of the reforming process
  - b) improves the yield of hydrogen
  - c) improves both yield and the efficiency
8. Equivalence ratio is:
  - a) ratio of air to fuel
  - b) ratio of theoretical air flow rate in the reformer (needed for complete reformation) and actual air flow rate
  - c) ratio of theoretical air to fuel ratio at the reformer inlet (needed for complete combustion) and actual air to fuel ratio
9. Air bleed is process of adding additional air to eliminate CO:
  - a) at the stack inlet
  - b) in the last stage of the reforming process
  - c) during the reformer process
10. Unused hydrogen from the fuel cell outlet may be used to reduce the fuel requirement at the steam reformer inlet, thus:
  - a) resulting in higher fuel processing efficiency
  - b) resulting in higher hydrogen concentration at the outlet
  - c) having no effect on the reformer efficiency

## CHAPTER 10

# 10. Fuel Cell Applications

Fuel cells can generate power from a fraction of Watt to hundreds of kilowatts. Because of that, they may be used in almost every application where local electricity generation is needed. Applications such as automobiles, buses, utility vehicles, scooters, bicycles, and submarines have been already demonstrated. Fuel cells are ideal for distributed power generation at the level of individual home, building, or community, offering tremendous flexibility in power supply. In some cases both power and heat produced by a fuel cell may be utilized resulting in very high overall efficiency. As a backup power generator, fuel cells offer several advantages over either internal combustion engine generators (noise, fuel, reliability, maintenance) or batteries (weight, lifetime, maintenance). Small fuel cells are attractive for portable power applications, either as replacement for batteries (in various electronic devices and gadgets) or as portable power generators.

Fuel cell system design is not necessarily the same for each of these applications. On the contrary, each application, in addition to power output, has its own specific requirements, such as efficiency, water balance, heat utilization, quick start-up, long dormancy, size, weight, and fuel supply. Some of those application-specific requirements and corresponding design variations will be discussed in this chapter.

### 10.1. Transportation Applications

#### 10.1.1. Automobiles

Almost all major car manufacturers have demonstrated prototype fuel cell vehicles and announced plans for production and commercialization in the near to midterm future (see Table 10-1 and Figure 10-1). The race to develop a viable fuel cell vehicle and bring it to market began during the 1990s and continues in the first decade of the twenty-first century.

The major drivers for development of automotive fuel cell technology are their efficiency, low or zero emissions, and fuel that could be produced from indigenous sources rather than imported. The main obstacles for fuel

TABLE 10-1  
Prototype Fuel Cell Vehicles by Major Car Manufacturers (compiled from HyWeb [1] and Fuel Cells 2000 [2])

<i>Manufacturer</i>	<i>Vehicle</i>	<i>Type</i>	<i>Fuel</i>	<i>Range (km)</i>	<i>Fuel Cell Supplier</i>	<i>Power (kW)</i>	<i>Year</i>
Daimler Chrysler	Necar2	FC	Compressed H <sub>2</sub>				
	Necar3	FC					
	Necar4 (Mercedes Class A)	FC	liquid H <sub>2</sub>	450	Ballard	75	1999
	Necar5 (Mercedes Class A)	FC	methanol	480	Ballard	75	2000
	Jeep Comandeer2	Hybrid with Ni-MH battery	methanol	NA	Ballard	50	2000
	Natrium	Hybrid with Li-ion battery	sodium-borohydride	500	Ballard	75	2001
	Necar5.2 (Mercedes Class A)	FC	methanol	480	Ballard	75	2001
	Sprinter	FC	compressed H <sub>2</sub>	>150	Ballard	75 (55)	2001
	F-cell	FC	compressed H <sub>2</sub>	150	Ballard	85 (65)	2002
	Sprinter UPS	FC	NA	>150	Ballard	55	2003
Ford	P2000 FCEV	FC	compressed H <sub>2</sub>	160	Ballard	75	1999
	Focus FCV	FC	compressed H <sub>2</sub>	160	Ballard	75	2000
	Think FCV	FC	compressed H <sub>2</sub>	NA	Ballard	75	2001
	FCV Hybrid	Hybrid	compressed H <sub>2</sub>	320	Ballard	85 (68)	2002
General Motors	Opel Zafira	Hybrid with MH battery	methanol	NA	GM(?)	50	1998
	Precept	Hybrid with Li-polymer and Ni-MH battery	H <sub>2</sub> in Me-H	800	GM	100 (85)	2000
	HydroGen1 (Opel Zaphira)	FC	liquid H <sub>2</sub>	400	GM	75 (55)	2000
	HydroGen 3 liquid (Zafira)	FC	liquid H <sub>2</sub>	400	GM	94	2001
	HydroGen 3 compressed 700 (Zafira)	FC	compressed H <sub>2</sub>	270	GM	94 (60)	2001

	HydroGen 3 liquid 2004	FC	compressed H <sub>2</sub>	400	GM	94 {60}	2004
	Sequel	Hybrid with Li-ion battery	compressed H <sub>2</sub>	480	GM(?)	73 + 65	2005
Toyota	FCEV (Rav4)	FC	H <sub>2</sub> in Me-H	175	Toyota	20 {45}	1996
	FCEV (Rav4)	FC	methanol	500	Toyota	25 {50}	1997
	FCHV-3	Hybrid with battery	H <sub>2</sub> in Me-H	300	Toyota	90 {80}	2001
	FCHV-4	Hybrid with NI-MH battery	compressed H <sub>2</sub>	>250	Toyota(?)	90 {80}	2001
	FCHV-5	Hybrid with NI-MH battery	gasoline	NA	Toyota(?)	90 {80}	2001
	Ovonic "H2 Prius"	Hybrid	H <sub>2</sub> in Me-H	200	NA	NA	2003
Honda	FCX-V2 {Twin Solid}	FC	methanol	NA	Honda(?)		1999
	FCX-V3	FC	compressed H <sub>2</sub>	180	Ballard	62 {60}	2000
	FCX-V4	Hybrid with ultra capacitor	compressed H <sub>2</sub>	300	Ballard	78 {60}	2001
	FCX	Hybrid with ultra capacitor	compressed H <sub>2</sub>	355	Ballard	78 {60}	2002
	FCX {Honda Stack}	Hybrid with ultra capacitor	compressed H <sub>2</sub>	395	Honda	86 {80}	2003
Nissan	FCV {R'nessa}	NA	methanol	NA	Ballard	NA	1999
	Xterra FCV	FC	H <sub>2</sub> in Me-H	NA	Ballard	75	2000
	X-trail FCV 3	Hybrid with Li-ion battery	compressed H <sub>2</sub>	NA	UTC	58	2002
	X-trail FCV 2003	Hybrid with Li-ion battery	compressed H <sub>2</sub>	350	UTC	63	2003
Mazda	Demio	FC	H <sub>2</sub> in Me-H	NA	Ballard(?)		1999
	Premacy FC-EV	FC	methanol	NA	Ballard	75	2000
Volkswagen	Bora HyMotion {Jetta}	FC	liquid H <sub>2</sub>	350{?}	Ballard		2000
	Bora HyPower—Paul Scherer Institut	Hybrid with super capacitor	NA	150	Paul Scherer Institute	28	2002

TABLE 10-1  
*Continued*

<i>Manufacturer</i>	<i>Vehicle</i>	<i>Type</i>	<i>Fuel</i>	<i>Range (km)</i>	<i>Fuel Cell Supplier</i>	<i>Power (kW)</i>	<i>Year</i>
	Touran "Hy-motion"	Hybrid with NI-MH battery	compressed H <sub>2</sub>	160	Ballard	80	2004
Renault	FEVER (Laguna)	Hybrid with NI-MH battery	liquid H <sub>2</sub>	400	DeNora	30	1998
Peugeot	Fuel Cell Cab	Hybrid with battery	compressed H <sub>2</sub>	200–300	H-Power	5.5 (22)	2001
Fiat	Seicento Elettra H2 Fuel Cell	Hybrid with battery	compressed H <sub>2</sub>	140	NA	7	2001
	Seicento	NA	compressed H <sub>2</sub>	220	Nuvera	40	2003
Hyundai	Santa Fe FCEV	FC	compressed H <sub>2</sub>	160	IFC	75	2001
	Tucson FCEV	NA	compressed H <sub>2</sub>	300	UTC	80	2004
Mitsubishi	FCV Grandis	Hybrid with Ni-H battery	compressed H <sub>2</sub>	150	Ballard	85 (65)	2003
Suzuki	WagonR-FCV	FC	compressed H <sub>2</sub>	130	GM	50 (33)	2003
	WagonR-FCV 70Mpa	FC	compressed H <sub>2</sub>	200	GM	38	2004
Lada	Avtovaz Lada ANTEL-2	Hybrid with Ni-MH battery	compressed H <sub>2</sub>	350	NA	90	2003
Audi	A2	Hybrid with Ni-MH battery	compressed H <sub>2</sub>	220	Ballard	66	2004
Kia	Sportage FCEV	Hybrid with Li-ion battery	compressed H <sub>2</sub>	300	UTC	80	2004

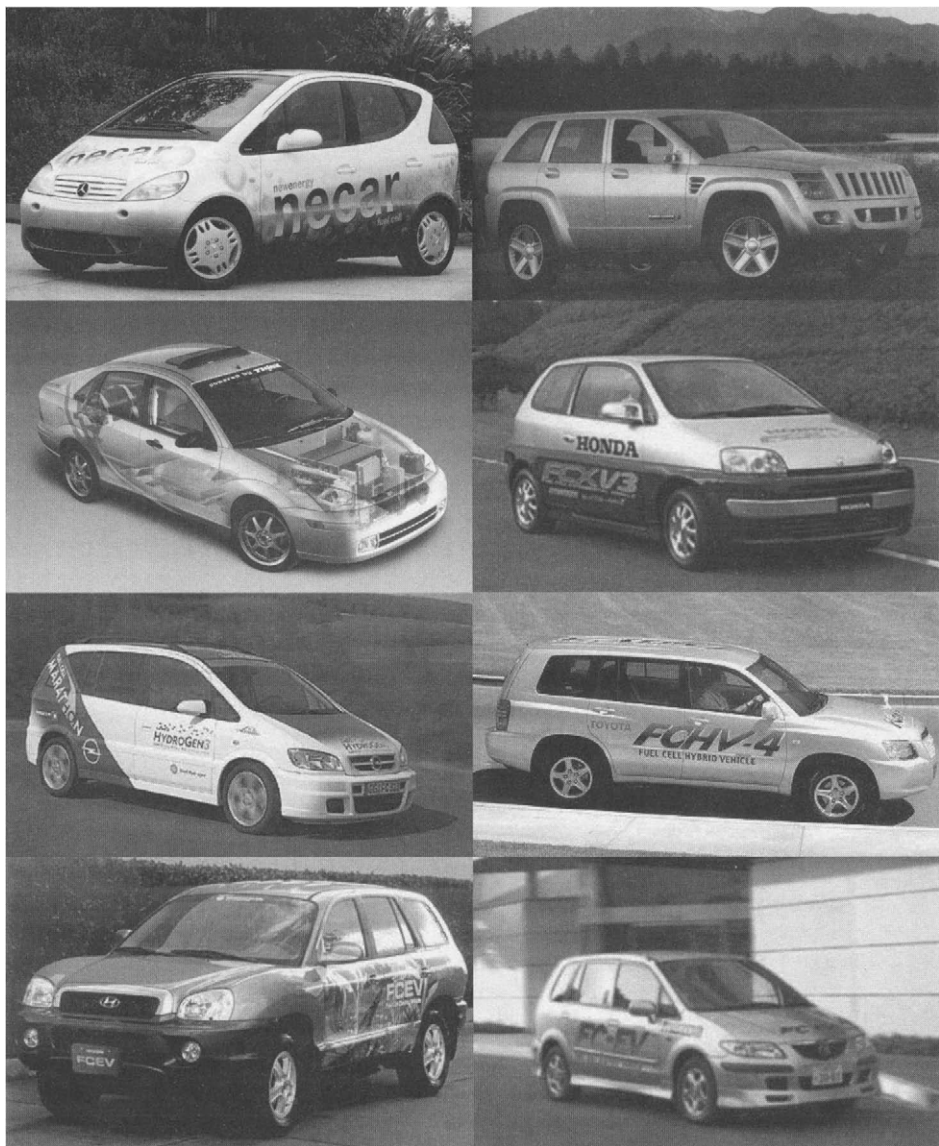


FIGURE 10-1. Fuel cell vehicles demonstrated by major car manufacturers (from top to right: DaimlerChrysler, Jeep, Ford, Honda, GM (Opel), Toyota, Hyundai and Mazda).

cell commercialization in automobiles are the cost of fuel cells and the cost and availability of hydrogen.

#### *Configurations of Automotive Fuel Cell Systems*

The fuel cell may be connected to the propulsion motor in several ways [3], namely:

1. Fuel cell is sized to provide all the power needed to run the vehicle. A battery may be present but only for start-up (such as a 12-V battery). This configuration is typically possible only with direct hydrogen fuel cell systems. A system with a fuel processor would not have as good a dynamic response. Also, a small battery would not be sufficient to start up a system with a fuel processor.
2. Fuel cell is sized to provide only the base load, but the peak power for acceleration of the vehicle is provided by the batteries or similar peaking devices (such as ultracapacitors). This may be considered a parallel hybrid configuration because the fuel cell and the battery operate in parallel—the fuel cell provides cruising power, and the battery provides peak power (such as for acceleration). The presence of a battery in the system results in much faster response to load changes. The vehicle can be started without preheating of the fuel cell system, particularly the fuel processor, and operated as purely a battery-electric vehicle until the fuel cell system becomes operational. A battery allows for recapturing of the braking energy, resulting in a more efficient system. The disadvantages of having the battery are extra cost, weight, and volume.
3. Fuel cell is sized only to recharge the batteries. The batteries provide all the power needed to run the vehicle. This may be considered a serial hybrid configuration (fuel cell charges the battery and battery drives the electric motor). The same advantages and disadvantages of having a battery apply as for the parallel hybrid configuration. The fuel cell nominal power output depends on how fast the batteries would have to be recharged. A smaller battery would have to be recharged faster and would result in a larger fuel cell.
4. Fuel cell serves only as an auxiliary power unit, that is, another engine is used for propulsion, but the fuel cell is used to run part of or the entire vehicle electrical system [4]. This may be particularly attractive for the trucks, because it would allow operation of an air-conditioning or refrigeration unit while the vehicle is not moving without the need to run the main engine.

#### *Power Demand and Efficiency (Fuel Economy)*

Power requirement of an automotive engine depends on many parameters, such as vehicle mass, frontal cross-sectional area, drag coefficient, rolling

resistance coefficient, and the efficiency of the drive train, and it changes with the vehicle speed, acceleration, and the road slope.

The efficiency of an automobile engine is more often expressed as specific fuel consumption ( $\text{g kWh}^{-1}$ ):

$$f_c = \frac{3.6 \times 10^6}{\eta_{sys} H_{LHV}} \quad (10-1)$$

where:

$H_{LHV}$  = lower heating value of fuel ( $\text{kJ/kg}$ )

$\eta_{sys}$  = the vehicle efficiency, which is a product of the fuel cell system efficiency (including the fuel processor, if any, fuel cell, and power converter), traction efficiency (typically about 93%), and electric drive efficiency (typically 90% or higher).

For a gasoline internal combustion engine at its most favorable point of operation, the specific fuel consumption is about  $240 \text{ g kWh}^{-1}$  [5], which corresponds to the system efficiency of 34%. Diesel engines have a higher efficiency of about 40%. A fuel cell engine, depending on system configuration, may have the efficiency at its most favorable operating point well above 50%, corresponding to a specific fuel consumption of below  $60 \text{ g kWh}^{-1}$ . Note that 1 g of hydrogen contains the same amount of energy as 2.73 g of gasoline, based on their lower heating value. It should also be noted that the lower heating value efficiencies are used for comparison with internal combustion engines.

The efficiency of fuel cells vs an internal combustion engine should not be compared at their most favorable operating point. These two technologies are intrinsically different and have very different efficiency-power characteristics. Although an internal combustion engine has the maximum efficiency at or near its maximum power [6], a fuel cell system has its maximum efficiency at partial load [7] (Figure 10-2). Because of this, the efficiency of a hydrogen-fueled fuel cell propulsion system in a typical driving schedule (such as the one shown in Figure 10-3), where an automobile engine operates most of the time at partial load, can be about twice that of an internal combustion engine [8–10]. The hydrogen fuel cell system efficiency in a driving schedule can be upwards of 40% and above 50%. The efficiency of a fuel cell propulsion system with an onboard fuel processor is lower than the efficiency of a hydrogen fuel cell system, but still higher than the efficiency of an internal combustion engine. The fuel cell efficiency advantage diminishes if both a fuel cell and an internal combustion engine are used in a hybrid configuration.

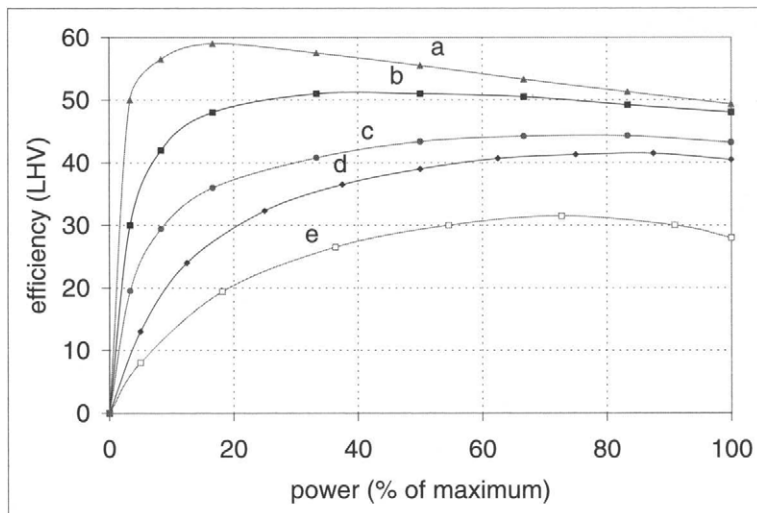


FIGURE 10-2. Comparison of the efficiency of fuel cells and internal combustion engines:

- fuel cell system operating at low pressure and low temperature;
- fuel cell system operating at high pressure and high temperature;
- fuel cell system with an onboard fuel processor;
- compression ignition internal combustion engine (diesel);
- spark ignition internal combustion engine (gasoline).

(Compiled from [6] and [7].)

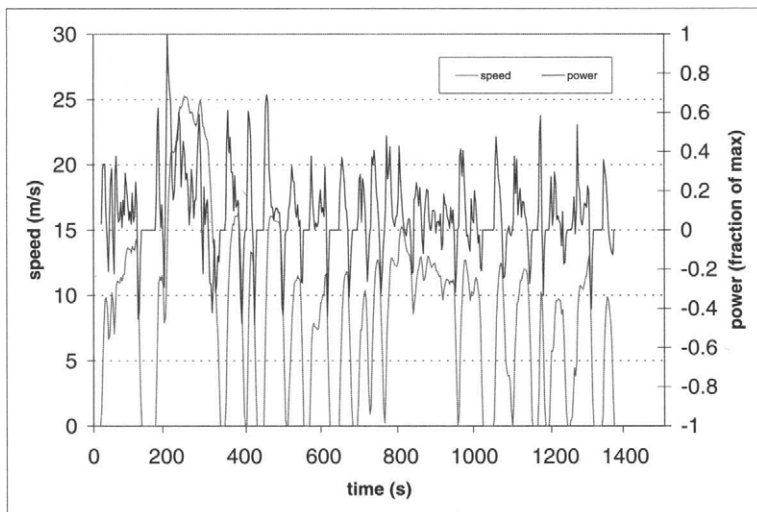


FIGURE 10-3. U.S. EPA Urban Dynamometer Driving Schedule (UDDS) [11]: average speed =  $8.7 \text{ m s}^{-1}$ , average power = 12% of maximum power.

The vehicle fuel economy (in  $\text{gm}^{-1}$ ) is [5]:

$$B_e = \frac{\int f_c v \sum F dt}{3.6 \times 10^6 \int v dt} \quad (10-2)$$

where:

$f_c$  = specific fuel consumption in  $\text{gkWh}^{-1}$  as defined by Equation (10-1)

$v$  = vehicle speed ( $\text{m s}^{-1}$ )

$\Sigma F$  = sum of the forces to be overcome (N), such as:

- air resistance  $F_a = 0.5 C_d A_v \rho v^2$
- rolling resistance:  $F_r = C_r m_v g$
- inertial forces:  $F_i = m_v a$
- gravitational force:  $F_g = m_v g \sin \theta$

where:

$C_d$  = drag coefficient (typically 0.25 to 0.4)

$A_v$  = vehicle frontal area (typically 1.5 to  $2.5 \text{ m}^2$ )

$\rho$  = air density ( $\text{kg m}^{-3}$ )

$C_r$  = rolling resistance coefficient, which is a function of tire radius and tire distortion and thus a function of vehicle speed (typically between 0.008 and 0.02) [5]

$m_v$  = vehicle mass (varies from 1000 to more than 2000 kg depending on the class of the vehicle)

$a$  = vehicle acceleration ( $\text{m s}^{-2}$ )

$g$  = gravity acceleration ( $9.81 \text{ m s}^{-2}$ )

$\theta$  = road slope angle

For a given driving schedule, such as the one shown in Figure 10-3, the vehicle speed is a function of time, and so are the system efficiency,  $\eta_{sys}$ , and the sum of forces,  $\Sigma F$ .

### Emissions

A hydrogen fuel cell does not generate any pollution. The only by-product is pure water, which leaves the system as both liquid and vapor, depending on the operating conditions (temperature and pressure) and system configuration. The amount of water produced by a fuel cell propulsion system in a typical driving schedule is comparable to the amount of water produced by an internal combustion engine. If another fuel is used (such as methanol or gasoline) and reformed onboard, the propulsion system has some emissions generated in the reforming process, but those emissions are in general still much lower than the emissions from an internal combustion engine, and such vehicles would typically qualify as ultralow emission vehicles (ULEV).

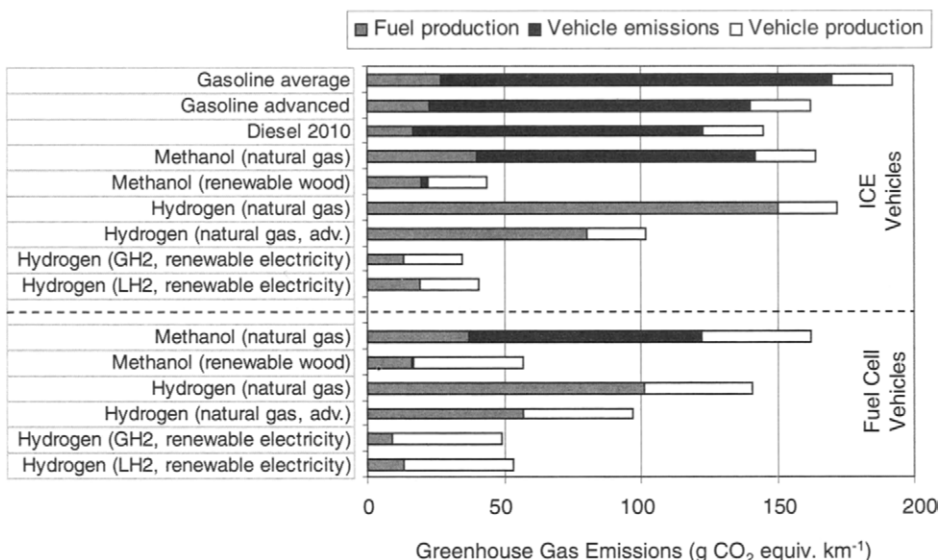


FIGURE 10-4. The results of a life-cycle analysis: greenhouse gas emissions for different power train and fuel options. (Adapted from [12].)

In an emission analysis, it is important to take into account the entire fuel cycle (well to wheels), otherwise skewed results may be generated. In general, if hydrogen is produced from fossil fuels, the emissions resulting from that process (particularly the CO<sub>2</sub> emissions) should be taken into account, regardless of whether the hydrogen generation takes place in a refinery, at the refueling station, or on the vehicle. Figure 10-4 shows the results of one such well-to-wheels life-cycle study [12]. Note that the fuel cell vehicles generate significantly less greenhouse emissions than the comparable gasoline-, diesel-, or methanol-powered internal combustion engine vehicles. The lowest emissions in this study were attributed to the hydrogen-powered internal combustion engines. This is the result of higher emissions assigned to the process of fuel cell vehicle production. Hydrogen production from renewable energy sources and water does not generate any direct emissions (Figure 10.4 does show some emissions, which are the result of manufacturing of the equipment for utilization of renewable energy), and that is the path that takes full advantage of the fuel cell technology. More about hydrogen as a fuel of the future may be read in Chapter 11.

### Cost

Automobile engines, although relatively complex, particularly compared with fuel cells, are relatively inexpensive (\$35–\$50 per kW). This is mainly because of mass production techniques employed in their manufacturing.

There are millions of cars (and of course, engines) produced annually. Fuel cells, being an immature technology and manufactured on a prototype level, are far more expensive than the internal combustion engines. However, several studies conducted by or on behalf of the major car manufacturers have shown that the fuel cells could be produced cost-competitively, assuming mass production manufacturing techniques are applied [13,14]. The major high-cost contributing components are the catalyst (precious metal, Pt, or Pt-alloys) and the ionomer membrane.

Typical platinum loading in PEM fuel cells is about  $0.4\text{ mg per cm}^2$  of each electrode active area. Assuming power density of  $0.7\text{ W/cm}^2$  (for example  $0.7\text{ V}$  and  $1\text{ A cm}^{-2}$ ), this corresponds to approximately  $1\text{ mg W}^{-1}$  or  $1\text{ g kW}^{-1}$ . The price of platinum varies on the market, but at say \$20 per gram this corresponds to about \$20 per kW, thus a significant portion of the total fuel cell system cost allowance.

The other expensive component is the ionomer membrane (Nafion or similar fluoropolymers). At \$500 per  $\text{m}^2$  this is prohibitively expensive, resulting in more than \$70 per kilowatt. Membrane manufacturers estimate that for every two orders of magnitude increase in manufacturing volume the price may be cut in half.

The cost targets (\$35 to \$50 per kW) therefore require improvements in fuel cell performance (more Watts per unit active area); reduction in catalyst loading or alternative, less expensive catalyst without sacrificing the performance; and novel, less expensive membranes.

#### *Fuel Issues (Availability, Cost, Storage)*

An automotive fuel cell system configuration greatly depends on the choice of fuel. Possible fuels for the fuel cell vehicles are hydrogen, gasoline, or methanol, each with its own advantages and disadvantages. The selection of the fuel depends on several factors:

- fuel supply infrastructure, and the cost of establishing a new one,
- the cost of fuel, per energy content, but more importantly per mile,
- environmental implications (*i.e.*, well-to-wheels emissions),
- complexity and the cost of onboard storage and processing,
- safety, both real and perceived,
- national security and related national energy policy.

Lack of hydrogen infrastructure is considered the biggest obstacle for introduction of fuel cell vehicles, although this may be a classic chicken-and-egg problem (*i.e.*, there are no fuel cell vehicles because there are no hydrogen refueling stations, but there are no hydrogen refueling stations because there is no demand for hydrogen as transportation fuel). Establishing necessary hydrogen infrastructure (hydrogen production and distribution) would require significant capital cost. Nevertheless, there are

already hundreds of hydrogen refueling stations in the United States, Japan, and Germany. California recently announced plans to build about 200 hydrogen refueling stations along its major highways [15].

Hydrogen produced from natural gas, either in a central facility or at the refueling station, can be cheaper than gasoline. The wholesale price of natural gas is 2–3 times lower than the retail price of gasoline, so at the efficiency of 70% to 80% hydrogen could be produced cost-competitively. However, the retail price of gasoline includes a hefty tax burden, but a discussion about the tax policy is certainly beyond the scope of this book. Hydrogen produced from water and electricity (via electrolysis) is in general more expensive than gasoline, unless low-cost off-peak electricity is used from the power plants that have low or zero fuel cost (nuclear and renewable power plants).

Hydrogen is the only fuel that results in a zero-emissions vehicle, particularly if hydrogen is produced from renewable energy sources. Also, hydrogen from renewable energy sources as transportation fuel could reduce dependency on imported oil. A fuel cell system that runs on pure hydrogen is relatively simple, has the best performance, runs more efficiently, and has the longest stack life. Hydrogen is nontoxic and, despite its reputation, has some very safe features (as discussed in section 11.5.4. Safety Aspects of Hydrogen as Fuel).

One of the biggest problems related to hydrogen use in passenger vehicles is its onboard storage. Hydrogen can be stored as compressed gas, as cryogenic liquid, or in metal hydrides. Tanks for compressed gaseous hydrogen are bulky, even if hydrogen is compressed to 450 bar. It takes about 40 to 50 liters of space to store 1 kg of hydrogen. The amount of fuel to be stored onboard depends on the vehicle fuel efficiency and required range. The fuel efficiency of vehicles is measured in miles per gallon (in the United States) or in liters per 100 km. The average fuel efficiency of new cars is between 20 and 30 mpg (7.9 and 11.8 l/100 km), and even better in smaller European and Japanese cars. The range is typically above 300 miles (480 km). A typical vehicle thus has about 10 to 16 gallons of gasoline onboard, taking space of 30 to 45 liters. Assuming that hydrogen fuel cell vehicles have twice the efficiency of gasoline vehicles, they will have to store between 5 and 8 kg of hydrogen, which would take anywhere between 200 and 400 liters of space, almost 10 times larger than current gasoline tanks. Further improvements in vehicle design and use of lightweight materials could improve the fuel efficiency by a factor of 2 (bringing hydrogen onboard storage requirement down to 2.5–4.0 kg), but that would apply to both hydrogen and gasoline vehicles.

Liquid hydrogen tanks are less bulky (about 30 liters per 1 kg of hydrogen), but liquid hydrogen is a cryogenic fuel (at 20 K), and its use would be associated with significant handling challenges. Hydrogen liquefaction is an energy-intensive process, requiring energy equal to about 30% of lique-

fied hydrogen's higher heating value, and therefore more expensive than compressed hydrogen. (It should be mentioned that hydrogen compression to 450 bars consumes energy in the amount equal to about 10% of compressed hydrogen's higher heating value.) In addition, storing of hydrogen at such a low temperature would result in significant boil-off losses. Well-insulated, large-volume liquid hydrogen containers (such as those used by NASA) typically have loss rates of less than 0.1% per day [16]. Modern automotive liquid hydrogen tanks can realize energy densities of 22 MJ/kg and evaporation rates of approximately 1% per day [17].

The difficulty of storing hydrogen onboard a vehicle, as well as lack of hydrogen infrastructure has forced car manufacturers to consider other, more conveniently supplied fuels for fuel cells. In that case a fuel cell system must be integrated with a fuel processor. From the infrastructure point of view, gasoline would be a logical choice, because it would allow quick penetration of fuel cell vehicles into the market. However, gasoline is not an easy fuel to reform. Because gasoline is a heavily processed fuel optimized specifically for combustion in the internal combustion engine, gasoline suppliers are also considering alternative and relatively easy-to-reform fuels such as hydrotreated naptha, hydrocrackate, alkylate/isomerate, or liquid fuels generated from natural gas [18].

Onboard reforming has an obvious advantage—the vehicle may use a liquid fuel such as methanol, but eventually uses gasoline or some other hydrocarbon fuel. This eliminates the problems of hydrogen onboard storage and nonexistence of hydrogen infrastructure. However, onboard reforming is not easy, and in spite of several more or less successfully demonstrated prototype vehicles, it does not appear to be a likely path for bringing fuel cell vehicles to market. There are numerous engineering issues with successfully integrating a fuel processor with a fuel cell:

1. Vehicles with an onboard fuel processor are not zero-emissions vehicles.
2. Onboard reforming reduces the efficiency (fuel to wheels) of the propulsion system. The reformers are typically 80% to 90% efficient (fuel to hydrogen). Use of diluted hydrogen reduces fuel cell voltage, which has a direct impact on either the efficiency or the size of the fuel cell. In addition, fuel utilization of diluted hydrogen is much lower, which further reduces the system efficiency.
3. Onboard reforming increases complexity, size, weight, and cost of the entire propulsion system.
4. Fuel processors need time to start producing hydrogen, that is, to warm up to their operating temperature. In the first prototypes the start-up time was between 15 and 30 minutes, clearly not acceptable for practical applications. Significant engineering efforts are

required to reduce the start-up time [19]. This issue may be avoided in hybrid configurations because the batteries may provide power during the fuel processor warm-up.

5. The long-term effects of fuel impurities on reformer lifetime and reformer by-products on fuel cell lifetime are not well known at present. Researchers at Los Alamos National Laboratory have reported on negative impacts of small concentrations of  $\text{NH}_3$  and  $\text{H}_2\text{S}$  possibly present in the reformat from partial oxidation [20,21].

Another fuel considered by car manufacturers is methanol. Methanol can be reformed (relatively easier than gasoline) or it can be used directly in fuel cells as diluted (1–2 M) aqueous solution (so-called direct methanol fuel cells). Although methanol infrastructure does not exist either, arguably it could be established easier than a hydrogen infrastructure, because methanol is liquid. However, methanol's corrosiveness, lethal toxicity, and solubility in water make it an unlikely fuel for widespread use in transportation.

#### *Lifetime*

The average lifetime of a vehicle is about 10 to 12 years, but the actual operating time is only in the order of 3000 to 5000 hours. Therefore, the fuel cells for automotive applications are expected to have a similar lifetime. Limited laboratory testing to date has confirmed that the PEM fuel cells can meet these expectations, although the effect of real-life conditions (numerous start-ups and shutdowns, impurities in fuel and in air) on the fuel cell and fuel cell system components' life has yet to be determined.

#### *Heat Rejection, Water Balance, and Freezing*

Automotive fuel cells must survive and operate in extreme weather conditions (−40 to +40°C). This requirement has a tremendous effect on system design. Survival and start-up in extremely cold climate requires specific engineering solutions, such as use of antifreeze coolant and water management. Water cannot be completely eliminated from the system, because water is essential for the membrane ionic conductivity.

The fuel cell heat-rejecting equipment (radiator and condenser) must be sized for heat rejection in extremely hot weather (typically from 32°C to 40°C [6]). Although a fuel cell system is more efficient than an internal combustion engine, it has similar or larger cooling loads. More important, because of the fuel cell's low operating temperature (60°C to 80°C) the heat rejection equipment is typically much larger than that for a comparable internal combustion engine [6,22].

Water balance requirement results in additional cooling loads [6,22]. Although water is produced in a fuel cell, water is needed for humidification of reactant gases and for fuel processing (in case of an onboard fuel processor), and it has to be reclaimed from the exhaust gases.

### *Size and Weight*

An automotive fuel cell system replacing an internal combustion engine must be of a similar size and weight. The size of the stack greatly depends on the selected nominal cell voltage, that is, the stack voltage efficiency. The stack specific volume ( $\text{m}^3$  per kW) is:

$$V_s = 0.1 \frac{n_{\text{cells}} d_{\text{cell}} + 2d_{\text{ep}}}{\alpha_{\text{act}} n_{\text{cells}} V_{\text{cell}} i} \quad (10-3)$$

where:

$n_{\text{cells}}$  = number of cells in a stack

$d_{\text{cell}}$  = individual cell thickness, including the cooling arrangements (m)

$d_{\text{ep}}$  = thickness of the end-plates, and the bus plates if their function is not included in the bus plates (m)

$\alpha_{\text{act}}$  = ratio of cell active area and bipolar plate area including the perimeters reserved for manifolds and seals; typical values for larger stacks are in the range of 0.80 to 0.86 [5]

$V_{\text{cell}}$  = cell potential at nominal power (V)

$i$  = current density at nominal power ( $\text{A cm}^{-2}$ )

Note that the cell potential,  $V_{\text{cell}}$ , and current density,  $i$ , are connected by the cell polarization curve. The product of cell potential and current density is the fuel cell-specific power (per unit active area):

$$P_f = V_{\text{cell}} i \left( \text{W cm}^{-2} \right) \text{ or } P_f = 10 V_{\text{cell}} i \left( \text{kW m}^{-2} \right) \quad (10-4)$$

Obviously, a lower stack specific volume results with thinner cells, better utilization of bipolar plate area, and higher performance.

The stack specific mass (in kg/kW) is then simply:

$$m_s = V_s \rho_s \quad (10-5)$$

where  $\rho_s$  is the stack density ( $\text{kg/m}^3$ ), a function of stack design and materials used. Typical fuel cell stacks have density below  $2000 \text{ kg/m}^3$ .

From the parameters in Equations (10-5) and (10-6), a new parameter may be derived, the so-called design factor,  $D_f$  ( $\text{kg/m}^2$ ), which is simply the stack mass divided by the active area. This factor is useful in comparisons of various stack designs. A good fuel cell stack design, which means a stack

with thin cells, high utilization of bipolar plate area, and selection of light-weight materials, should result in a design factor below  $10\text{ kg/m}^2$ . From a known design factor and specific performance it is easy to calculate the stack specific mass:

$$m_s = \frac{D_f}{P_f} \quad (10-6)$$

The stacks with weight and volume less than  $1\text{ kg kW}^{-1}$  and  $11\text{ kW}^{-1}$ , respectively, have already been demonstrated. The goals for the complete fuel cell system, excluding hydrogen storage, are (from Table 10-2)  $1.5\text{ kg kW}^{-1}$  and  $1.51\text{ kW}^{-1}$ . Table 10-2 lists the U.S. DOE technical targets [23] for an integrated direct hydrogen automotive fuel cell system (stack, air management, thermal subsystem).

### 10.1.2. Buses

Buses for city and regional transport are considered the most likely type of vehicles for an early market introduction of the fuel cell technology. Most of the issues discussed in the previous section, Automobiles, also apply to fuel cell applications in buses. The major differences are in power requirements, operating regimen and resulting lifetime requirements, space available for hydrogen storage, and refueling sites.

Buses require more power than passenger automobiles, typically about  $250\text{ kW}$  or more. They operate in a more demanding operating regimen with frequent starts and stops. Nevertheless, the average fuel economy of a bus fuel cell system is roughly 15% better than that of a diesel engine [24].

TABLE 10-2  
U.S. DOE Targets for Automotive Fuel Cell System [23]

	Units	Year 2010 Target
Maximum power	kW	50
Efficiency at 25% peak power	%	60
Efficiency at peak power	%	50
Power density	$\text{W l}^{-1}$	650
Specific power	$\text{W kg}^{-1}$	650
Cost	\$ $\text{kW}^{-1}$	45
Transient response (10–90% power)	s	1
Cold start-up at $-20^\circ\text{C}$ to maximum power	s	30
Cold start-up at $20^\circ\text{C}$ to maximum power	s	15
Durability	h	5000
Survivability	$^\circ\text{C}$	-40

Buses are almost always operated in a fleet and refueled in a central facility. This makes refueling with hydrogen much easier. In addition, storing larger quantities of hydrogen onboard (typically above 20kg) is less of a problem. Fuel cell buses typically store hydrogen in composite compressed gas cylinders at 250 to 300 bar, located on the roof. Because hydrogen is much lighter than air, the roof location is considered very safe.

The hydrogen fuel cell buses have a major advantage over competition (diesel buses) because they produce zero emissions. This is particularly important in already heavily polluted, densely populated cities. Under the Clean Urban Transport for Europe (CUTE) program, hydrogen fuel cell buses are being employed in major European cities such as Amsterdam, Barcelona, Hamburg, London, Luxembourg, Madrid, Porto, Reykjavik, Stockholm, and Stuttgart [25]. Sunline Transit Authority in Palm Springs, California, has been operating fuel cell buses in regular service for several years. United Nations Development Program (UNDP) and Global Environment Facility (GEF) are funding and coordinating an international program that aims to introduce fuel cell buses in major cities around the world, such as Sao Paolo, Mexico City, New Delhi, Cairo, Shanghai, and Beijing [25]. When hydrogen is produced from clean renewable energy sources, the fuel cell buses could make a significant contribution toward cleaner air in these cities. Table 10-3 presents a list of fuel cell buses already demonstrated, some of which are shown in Figure 10-5.

The main obstacles for commercialization of fuel cell buses are fuel cell cost and durability. Because of the smaller manufacturing series, the cost of the bus engines per kilowatt is somewhat higher than the cost of the automobile engines. The expected lifetime is also higher, because a typical city bus may be in operation more than 6000 hours per year. This, combined with highly intermittent operation with a lot of starts and stops, poses a challenge to fuel cell durability with current technology.

### 10.1.3. Utility Vehicles

Utility vehicles, such as forklifts, material-handling industrial vehicles, airport ground-support tow vehicles, lawn maintenance vehicles, golf carts, and airport people movers, may be another early adapter of the fuel cell technology. This application is not as demanding as passenger vehicles or buses. The competing technology is typically batteries, most often the lead acid batteries, that require often and lengthy charging and pose significant maintenance problems. Early demonstrations of fuel cell-powered utility vehicles have shown that such vehicles offer lower operating cost, reduced maintenance, lower downtime, and extended range [27]. In most cases, these vehicles are operated indoors and therefore freezing is not an issue. Because fuel cell vehicles generate zero emissions they are suitable for indoor use. In cases where the weight is actually desirable, such as in forklifts, hydrogen can be safely stored in metal hydrides.

TABLE 10-3  
Fuel Cell Buses Demonstrated to Date (Compiled from Hy Web [1] and Fuel Cell 2000 [26])

Manufacturer	Vehicle	Type	Fuel	Range (km)	Fuel Cell Supplier	Power (kW)	Year
Ballard	P4 ZEbus	NA	compressed H <sub>2</sub>	400	Ballard	260	1999
DaimlerChrysler	NeBus	NA	compressed H <sub>2</sub>	250	Ballard	250	1997
	Citaro	NA	compressed H <sub>2</sub>	200	Ballard	250	2002
MAN	Fuel Cell City Bus	NA	compressed H <sub>2</sub>	>250	Siemens	120 (150)	2000
	Low Floor Bus with FC and LH <sub>2</sub>	NA	compressed H <sub>2</sub>	300	De Nora	120 (150)	2001
	Argemuc-Man Fuel Cell Bus	Hybrid with Ni-MH battery	compressed H <sub>2</sub>	>300	Ballard	68 + 100 (150)	2004
Proton Motors	Bayern Bus II	NA	compressed H <sub>2</sub>	150–250	Proton Motors	80 (280)	2000
Toyota/Hino	Fuel Cell Bus	Hybrid with Ni-MH battery	compressed H <sub>2</sub>	>300	Toyota	90 (160)	2001
	FCHV Bus 2	Hybrid with Ni-MH battery	compressed H <sub>2</sub>	350	Toyota	180 (80)	2002
Neoplan	Midi FC Bus	Hybrid with Ni-MH battery	compressed H <sub>2</sub>	600	De Nora	40 + 100	1999

Scania, Air Liquide	FC Midi City Bus	Hybrid with battery	compressed H <sub>2</sub>	250	De Nora	60	2001
Irisbus	City Class FC	Hybrid with battery	compressed H <sub>2</sub>	NA	NA	60 (160)	2001
	CITYCELL Madrid	Hybrid with lead acid battery	compressed H <sub>2</sub>	NA	UTC	60	2003
	Turin FC Bus	Hybrid with battery	compressed H <sub>2</sub>	NA	UTC	60	2004
Thor	ThunderPower Bus	Hybrid with battery	compressed H <sub>2</sub>	320	UTC	60 (85)	2001
Autotram	Autotram	Hybrid with flywheel	compressed H <sub>2</sub>	NA	Ballard	80 (325)	2005
Dalian University	Fuel Cell Bus China	NA	compressed H <sub>2</sub>	NA	Dalian University	30	2002
Tsinghua University	DICP FCB 60kW	NA	compressed H <sub>2</sub>	NA	Tsinghua University	60	2003
	DICP FCB 100kW	NA	compressed H <sub>2</sub>	NA	Tsinghua University	100	2004



FIGURE 10-5. Some prototype fuel cell buses: Ballard P4 (1999), Thor Thunder-Power (2001), Toyota Hino (2002), Daimler Citaro (2002), Irisbus CITYCELL (2003), ARGEMUC-MAN (2004). (Courtesy of Hy-Web, Hydrogen and Fuel Cell Information System, [www.hydrogen.org/h2cars/index.html](http://www.hydrogen.org/h2cars/index.html).)

#### 10.1.4. Scooters and Bicycles

Scooters and bicycles may be a significant market for fuel cell technologies, particularly in developing countries. Despite the stringent requirements relating to weight, size, and low cost, fuel cells have been successfully demonstrated in various scooters and bicycles [27]. The power requirement is considerably less than that for automobiles—up to 3 kW for scooters and up to 1 kW for bicycles. Although the range may be smaller than for automobiles too, the volume of hydrogen storage is one of the critical issues. Some prototypes were demonstrated with direct methanol fuel cell systems. The fuel cells for scooters and bicycles are almost always air cooled. The refueling issue of these vehicles in mass markets is as complex as the issue of automobile refueling. However, because of significantly

smaller quantities of hydrogen to be stored onboard, additional options are possible, such as distribution of metal hydride tanks or home refueling devices (probably electrolyzers).

## 10.2. Stationary Power

Although development and demonstrations of fuel cells in automobiles usually draw more attention, applications for stationary power generation offer even greater market opportunity. The drivers for both market sectors are similar—higher efficiency and lower emissions. The system design for both applications is also similar in principle. The main differences are in the choice of fuel, power conditioning, and heat rejection [28]. There are also some differences in requirements for automotive and stationary fuel cell systems. For example, size and weight requirements are very important in automotive application, but not so significant in stationary applications. The acceptable noise level is lower for stationary applications, especially if the unit is to be installed indoors. The fuel cell itself of course does not generate any noise; noise may be coming from air- and fluid-handling devices. Automobile systems are expected to have a very short start-up time (fraction of a minute), whereas the start-up of a stationary system is not time limited, unless operated as a backup or emergency power generator. Both automotive and stationary systems are expected to survive and operate in extreme ambient conditions, although some stationary units may be designed for indoor installation only. And finally, the automotive systems for passenger vehicles are expected to have a lifetime of 3000 to 5000 operational hours, systems for buses and trucks somewhat longer, but the stationary fuel cell power systems are expected to operate 40,000 to 80,000 hours (5 to 10 years).

Stationary fuel cell power systems will enable the concept of distributed generation, allowing the utility companies to increase their installed capacity following the increase in demand more closely, rather than anticipating the demand in huge increments by adding gigantic power plants. Presently, obtaining the permissions and building a conventional power plant have become very difficult tasks. Fuel cells, on the other hand, do not need special permitting and may be installed virtually everywhere—inside the residential areas, even inside the residential dwellings. To the end users the fuel cells offer reliability, energy independence, “green” power, and ultimately, lower energy costs.

### 10.2.1. Classification of Stationary Fuel Cell Systems

A variety of stationary fuel cell systems are being developed. Design options of stationary fuel cell power systems with respect to application, grid connection, nominal power output, load following, choice of fuel, installation, and cogeneration capabilities are discussed next.

### *Application and Grid Connection*

Stationary fuel cells may be used in different applications, namely:

- as the only power source, thus competing with or replacing the grid, or providing electricity in areas not covered by the grid,
- as a supplemental power source working in parallel with the grid covering either the base load or the peak load,
- in combined systems with intermittent renewable energy sources (such as photovoltaics or wind turbines) generating power in periods when these energy sources cannot meet the demand,
- as a backup or emergency power generator providing power when the grid (or any other primary power source) is down.

Accordingly, the fuel cell system, and particularly its power conditioning and interconnect module, may be designed as:

- Grid parallel—allowing power from the grid to the consumer when needed, but not allowing power from the fuel cell back to the grid. The fuel cell system may be sized to provide most of the consumer's energy needs, but the grid is used to cover the short-term demand peaks. Such a system essentially does not need batteries (except for start-up when the grid is down) and does not need interconnect standards.
- Grid interconnected—allowing power flow in both directions, namely power from the grid to the consumer when needed, and power from the fuel cell back to the grid. Such a system may be designed as load following or as constant power, because excess fuel cell power can be exported to the grid. Of course, this design option requires interconnect standards.
- Stand-alone—providing power without a grid. The system must be capable of load following. Very often a sizeable battery bank is used to enable load following.
- Backup or emergency generator—the system must be capable of quick start-up and is also often combined with the batteries or other peaking device. Batteries are typically superior for low-power/low-duration backup power, but a fuel cell system becomes competitive for higher power (several kW) and longer duration (more than 30 minutes). A backup power system may be equipped with an electrolyzer-hydrogen generator and hydrogen storage [29]. In that case the unit generates its own fuel during periods when electricity from the grid is available.

### *Nominal Power Output*

With respect to power output, the fuel cell power systems may be divided in several classes, namely:

- 1–10kW with applications in individual houses, trailers, recreational vehicles, and for portable power
- 10–50kW with applications in larger homes, mansions, groups of homes, and small commercial uses such as small businesses, restaurants, warehouses, and shops.
- 50–250kW with applications in small communities, office buildings, hospitals, hotels, military bases, and so on.
- For applications higher than 250kW, PEM fuel cells may not be competitive with other high-temperature fuel cell technologies.

#### *Load Following*

Depending on its application and nominal power output, the fuel cell system may be designed to operate in load following or in constant load modes. Load following requires that the fuel cell system is sized to generate the maximum required load of the user, or that it follows the load only up to its nominal power output and the load peaks are covered by either a peaking device (such as battery or ultracapacitor) or by the grid. The latter requires that the system must be designed as grid parallel. Although a fuel cell is electrically capable of load following, its functioning in this mode depends on reactants supply, both oxygen and hydrogen, which are supplied by means of mechanical devices (pumps, blowers, or compressors) and have certain inertia and time lag in responding to change of rate. It is particularly difficult to operate a fuel processor in a transient/variable load mode while keeping the quality of generated hydrogen sufficient for fuel cell operation.

A stationary fuel cell power system may be designed to operate at constant/nominal power output all the time. Such a system is either sized to cover only the base load or it is grid interconnected and thus allowed to export excess power back to the grid.

#### *Choice of Fuel*

The PEM fuel cells run on hydrogen. However, hydrogen as a fuel is not readily available, particularly not for residential applications, except if the system is to be used as a backup power system, in which case it may be equipped with an electrolytic hydrogen generator [29]. To facilitate market acceptance, fuel cell developers are forced to add a fuel processing section to the fuel cell system. For residential and commercial applications, natural gas is a logical fuel choice because its distribution is widely developed. The majority of stationary power fuel cell systems developed to date use natural gas as fuel. Propane may be an alternative fuel for those users that are not connected to the natural gas supply line. Fuel processing of propane and natural gas is similar and usually can be accomplished with the same fuel processing catalysts and hardware. For some applications liquid fuels may be preferable such as fuel oil, gasoline, diesel, methanol, or ethanol. All of

these fuels also require fuel processing. If hydrogen is available (such as in various industrial applications or in renewable energy installations equipped with an electrolytic hydrogen generator), the system may be significantly simplified.

### *Installation Location*

The stationary fuel cell power systems may be designed for installation either outdoors or indoors. Installation indoors is more demanding in respect to codes and standards, many of which currently do not exist, therefore leaving fuel cell installers at the mercy of local authorities. On the other side, outdoor installation requires weatherproof system design, especially with respect to exposure to extreme weather conditions. Another possibility is to design a fuel cell system as a split system, where the gas processing and power generation sections of the fuel cell system are installed outdoors and the control and power conditioning sections are installed indoors.

### *Cogeneration*

Any fuel cell system generates waste heat. The major sources of heat are the fuel cell stack, fuel processor, and tail gas burner (where the hydrogen that went through the fuel cell stack unused is catalytically combusted). The heat is rejected from the system via the heat exchangers or simply dissipated to the surrounding through radiation and convection. The heat from the fuel cell system may be captured and used for heating/preheating domestic hot water, or for heating the heating medium in the space heating system combined with a natural gas boiler, or combined with a heat pump. The cogeneration systems may have more favorable economics because the overall efficiency (electrical plus thermal) may approach 90%. Figure 10-6 shows a schematic diagram of a cogeneration-capable fuel cell power system.

#### 10.2.2. System Configuration

Unless hydrogen is available as a fuel for distributed electricity generation, fuel cells must use readily available fuels such as natural gas or propane. Natural gas is available in most densely populated areas, whereas propane may be available in remote areas. A fuel cell system for stationary power generation therefore must include a fuel processor. The efficiency of the system is even more important than in an automobile, and because of that, system integration and optimization is necessary for achieving high efficiencies. Larger systems ( $>100\text{ kW}$ ) can achieve the efficiencies above 40%, whereas the efficiency of smaller systems ( $<10\text{ kW}$ ) is typically somewhat lower (36–40%). Size and weight of stationary systems is not as critical as it is in automotive systems. Also, the cost targets for stationary systems

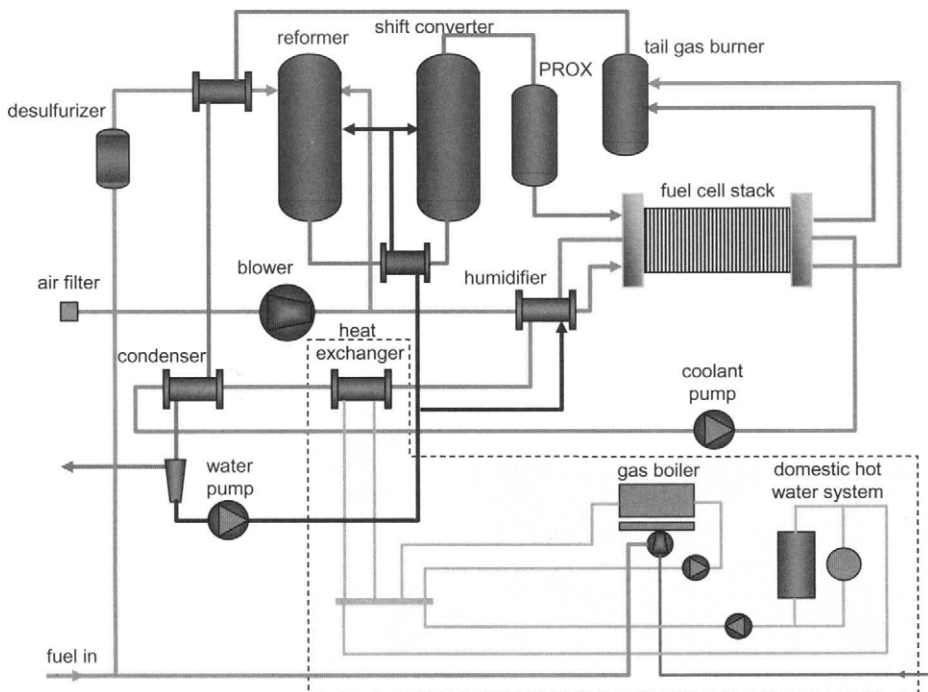


FIGURE 10-6. Schematic diagram of a cogeneration-capable fuel cell power system; a cogeneration subsystem, within dashed lines (from [30]) combined with a fuel cell system from Figure 9-38.

are at least an order of magnitude higher than the cost targets of automotive systems. A stationary fuel cell can be sized at a higher cell voltage, resulting in a more efficient, but larger and more expensive stack. Higher efficiencies can be achieved with systems operating at ambient pressure. Water balance, although preferable, is not critical as it is in an automotive system, and neither is the size of the heat rejection equipment. An automotive system can utilize the air impinging on the moving vehicle, whereas the heat rejection system of a stationary system must completely rely on fans.

The biggest difference between automotive and stationary fuel cell systems is in the electric subsystem—power conditioning. The architecture of the power conditioning system greatly depends on the system operating mode, as discussed in the section 9.4. Electrical Subsystem. An automotive system is practically a stand-alone system, a stationary fuel cell power system may operate as stand-alone, grid parallel, grid interactive, or as backup power.

A stand-alone system will require another auxiliary power source, such as batteries or supercapacitors, to provide peak power demands and to compensate for the system's inability to track rapid load changes. The fuel cell and the auxiliary power source must be sized to operate at the maximum continuous load and have the ability to handle start-up load requirements, which for motors may be several times their rated capacity. Thus, the power conditioning system must be designed to handle the combined power outputs from fuel cell and auxiliary power sources on a continuous basis, in addition to start-up load demands. The auxiliary power source is charged by the fuel cell stack during periods of low-power demands.

In a grid-tied system the power conditioning system is simplified because the grid may replace the auxiliary power source and also provide start-up power. However, the system must now be capable of synchronizing with the grid, and disconnecting in the event of a grid outage or if the signal quality from the utility is not within acceptable standards. A system designed to operate in both stand-alone and grid-tied modes is more complex because it must operate as a current source if tied to the grid and as a voltage source if operating independently. If a grid failure occurs while the fuel cell system is tied to the grid, it must disconnect quickly and maintain power to the loads without exceeding its maximum power rating. The excess loads that are dropped are the ones that are considered nonessential. The system must then monitor the grid and reconnect when the grid is operational. An efficient power management system is thus desirable for this architecture, which may be implemented by a programmable power distribution panel. An additional option for a grid-interactive system is ability to transfer electricity in both directions. A fuel cell may be sized for peak power of an individual user, and in that case it may be preferred to export excess electricity generated during low-power periods back to the grid. Metering both incoming and outgoing electricity, or net metering, may also be a part of the electrical subsystem.

Other issues that impact the architecture and design of the power conditioning system are the amount of ripple tolerated by the fuel cell, and the ability to carry unbalanced loads [31]. The ripple current on the fuel cell is the result of the switching characteristics of the electronics of the power conditioning system. Typically, two components are generated: a low-frequency component (usually 100Hz or 120Hz), which is twice the output AC frequency, and a high-frequency component (in the kHz range), which is due to the internal switching characteristics of the electronics. The amount of ripple can be filtered by the capacitors at the output of the fuel cell. Unbalanced loads result from the unequal load distribution on the individual lines of a multiple line system. For example, for residential homes in the United States the standard three-wire system provides two 120-V lines and a neutral. The power conditioning system should be designed so that each of the 120-V lines can handle the full current rating of the system.

### 10.2.3. Efficiency of Entire Fuel Cell System

The efficiency of the entire fuel cell power system is a product of efficiencies of individual components, as discussed in the section 9.5. System Efficiency:

$$\eta_{sys} = \eta_{fp} \cdot \eta_{fc} \cdot (\eta_{pc} - \xi_p) \quad (10-7)$$

where  $\xi_p$  is defined as ratio of parasitic power and fuel cell gross power output, and  $\eta_{pc}$  is the power conditioning efficiency, defined as a ratio between AC power output and DC power input in the power.

If the system has parasitic loads running on DC (typically 24 V or more recently 42 V), and the efficiencies of DC/AC and DC/DC conversions are different, then the Equation (10-7) is slightly different:

$$\eta_{sys} = \eta_{fp} \cdot \eta_{fc} \cdot \eta_{AC} \left( 1 - \frac{\xi_p}{\eta_{DC}} \right) \quad (10-8)$$

The efficiency at partial load may be slightly higher than at nominal power, primarily because the fuel cell efficiency, that is, voltage, is higher at lower power levels. However, this may be offset by a lower efficiency of fuel processor due to relatively higher thermal losses, and by relatively higher share of parasitic power. Figure 10-7 shows the efficiency power curve of a 3-kW residential fuel cell power unit [32]. The efficiency of more than 30% may be maintained throughout the operating range above approximately one-sixth or one-fifth of nominal power. Below that threshold the efficiency sharply drops. This means that it would not be desirable or feasible to operate such a fuel cell at a very low-power level.

In case of cogeneration a much higher total system efficiency may be achieved (up to 90%). In this case the total efficiency is defined as:

$$\text{total efficiency} = \frac{\text{electric power output} + \text{thermal output}}{\text{fuel consumption}} \quad (10-9)$$

### 10.2.4. Economics of Fuel Cell Systems

Economics of automotive fuel cell power systems is fairly simple: they must compete with the internal combustion engine in terms of initial cost and efficiency. Although the efficiency is important, it has a little impact on economics. The initial cost is far more critical.

Economics of residential fuel cells is more complex. Here the purchase price must be justified with sufficient savings in expenditures for energy over the lifetime of the power system. One method that may be used to evaluate feasibility of residential fuel cell power systems is a simple payback time. This is simply a ratio between purchase price and annual savings in electricity expenditures. The result suggests to the potential user

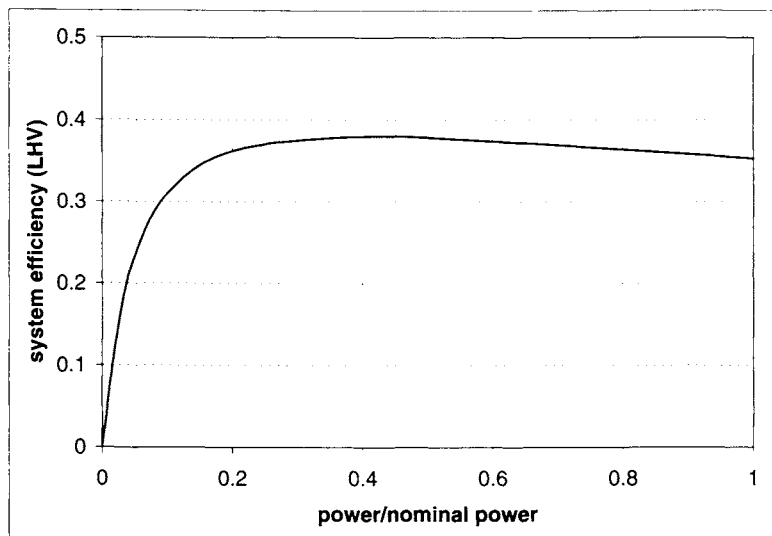


FIGURE 10-7. Efficiency (LHV) of small, residential, natural gas-fueled fuel cell system [32].

how soon his investment will pay back. This simple method does not take into account the interest lost or spent during that period, inflation, and changes in electricity and natural gas prices, but it gives a quick reference. Simple payback time is:

$$\text{SPT} = \frac{\text{purchase price of fuel cell power system}}{\text{annual savings on electricity}}, \quad (10-10)$$

or

$$\text{SPT} = \frac{P_{fc,nom} \cdot C_{fc}}{\text{AEP} \cdot \left( C_{el} - \frac{C_{ng}}{\bar{\eta}_{fc}} \right)} \quad (10-11)$$

where:

$P_{fc,nom}$  = fuel cell power system nominal power (kW)

$C_{fc}$  = specific cost of fuel cell power system per kW of nominal power ( $\$/\text{kW}^{-1}$ )

AEP = annual electricity produced by the fuel cell system ( $\text{kWh yr}^{-1}$ )

$\bar{\eta}_{fc}$  = average annual efficiency of the fuel cell system

$C_{el}$  = cost of electricity ( $\$/\text{kWh}^{-1}$ )

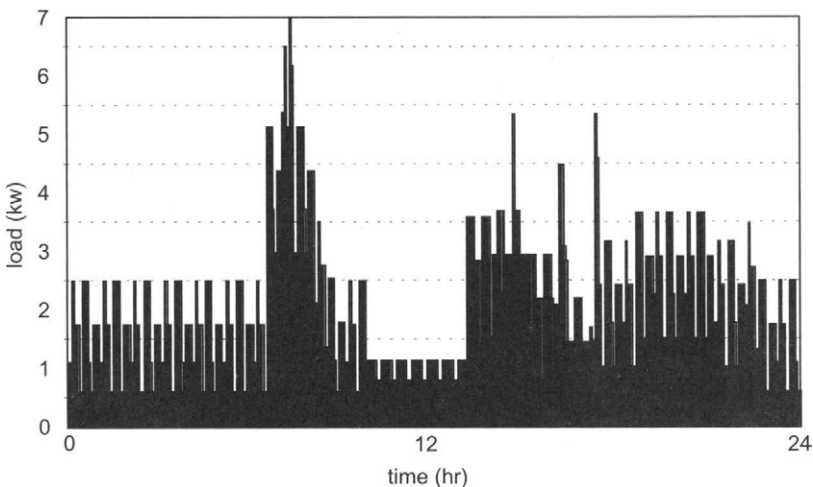


FIGURE 10-8. An example of a household daily electric load profile.

$$C_{ng} = \text{cost of natural gas } (\$/\text{kWh}^{-1}) \text{, using lower heating value of natural gas } (1000 \text{ Btu ft}^{-3}) \text{ and } 3412 \text{ Btu kWh}^{-1} \text{ conversion factor}$$

Both AEP, annual electricity produced, and  $\bar{\eta}_{fc}$ , average annual efficiency, are functions of the load profile. Load profile varies from user to user, it varies depending on the day of the week, and it varies from season to season. The main characteristic of most residential users is high variability, that is, the load varies from almost zero to several kilowatts. The average household power varies from about 1 kW in Europe and Japan to more than 2 kW in the United States. Figure 10-8 illustrates a daily load profile of a household, with power (minute average) ranging from 0.7 to 7 kW. For this particular example the total annual power consumption would be 16,000 kWh.

A fuel cell power system may be sized to generate any power between minimum and maximum load power. Obviously, if it is sized at a lower end of this range it would work with a very high capacity factor, but it would cover only a portion of the power needs. The rest would have to be supplied from the grid. If it is sized to cover all the power needs it would provide grid independence, but it would operate with a very low-capacity factor.

The amount of electricity annually produced (in kWh) by a fuel cell system is:

$$AEP = \int_{\text{year}} P_{fc} dt \quad (10-12)$$

where:

$P_{fc}$  = fuel cell power (kW) at any given time (t)

$P_{fc} = P_{load}$  for  $P_{load} < P_{nom}$ , and

$P_{fc} = P_{nom}$  for  $P_{load} \geq P_{nom}$

However, Equation (10-12) may only be used when the load profile is known. A capacity factor, CF, defined as a ratio between actually produced electricity in a time period (typically a year) and electricity that could have been produced if the system operated at nominal power for the entire period, may be easier estimated. In that case, the amount of electricity annually produced, AEP, (in kWh), is:

$$AEP = 8760 \cdot CF \cdot P_{fc,nom} \quad (10-13)$$

where:

8760 is the number of hours in a year, and

CF is the capacity factor previously defined.

A load itself has a certain capacity factor (*i.e.*, a ratio between the average and peak power). For the load profile shown in Figure 10-8, the capacity factor is 25%. A fuel cell that is sized to provide all the power required by the load would therefore operate with a 25% capacity factor. If a fuel cell were sized to a lower power, it would have a considerably higher capacity factor. A fuel cell sized to cover only a base load would operate with 100% capacity factor (providing no maintenance would be required during that period). Figure 10-9 shows the capacity factor as a function of fuel cell nominal power for the load profile given in Figure 10-8, ranging from 100% at base load (0.7 kW) to 25% at peak (7.0 kW).

Figure 10-9 also shows the average efficiency of the fuel cell system in annual operation. The average annual efficiency of a fuel cell system is defined as:

$$\bar{\eta}_{fc} = \frac{\int_{\text{year}} P_{fc} dt}{\int_{\text{year}} \frac{P_{fc}}{\eta_{fc}} dt} \quad (10-14)$$

where  $P_{fc}$  and  $\eta_{fc}$  are the fuel cell system power output and system efficiency at any given time, t, respectively.

Equation (10-14) may be used only if the annual load profile is known. Instead of the exact annual load profile, which varies greatly from household to household, or from user to user, an annual power distribution curve may be used.

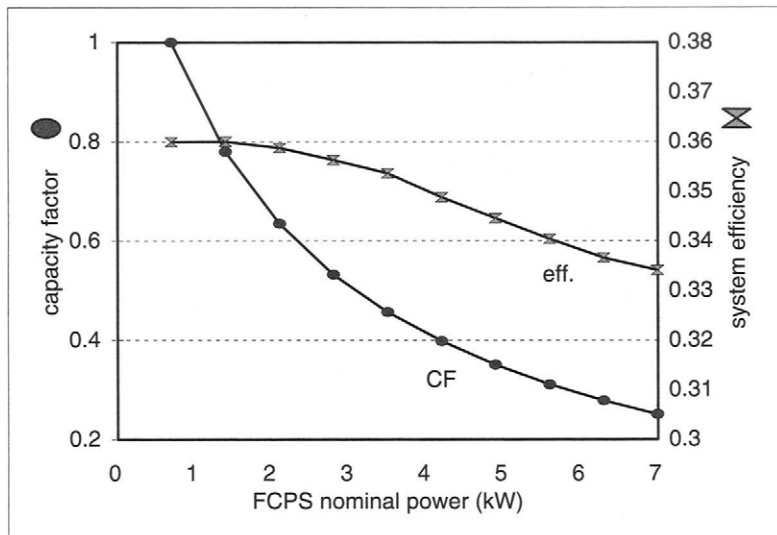


FIGURE 10-9. Capacity factor and efficiency of residential fuel cell power system as a function of nominal power [for a fuel cell system efficiency in Figure 10-7 and a load profile in Figure 10-8].

A fuel cell that operates 100% of the time at nominal power has the highest efficiency (36% in this case, corresponding to 0.75 V/cell). The fuel cell with the lowest capacity factor also has the lowest annual efficiency (33%), because most of the time it operates in the inefficient region (below 20% nominal power).

Substituting Equation (10-13) into Equation (10-11), the simple payback time is:

$$SPT = \frac{C_{fc}}{8760 \cdot CF \cdot \left( C_{el} - \frac{C_{ng}}{\bar{\eta}_{fc}} \right)} \quad (10-15)$$

In some cases, instead of fuel savings and the payback time it is necessary to calculate the cost of electricity produced by a fuel cell. From Equation (10-15) it follows:

$$C_{el} = \frac{C_{fc}}{8760 \cdot CF \cdot SPT} + \frac{C_{ng}}{\bar{\eta}_{fc}} \quad (10-16)$$

For larger installations it is more common, instead of simple payback time, to use a capital recovery factor, CRF, which takes into account the lifetime of the fuel cell system and the interest rate:

$$C_{el} = \frac{C_{fc} \cdot CRF}{8760 \cdot CF} + \frac{C_{ng}}{\bar{\eta}_{fc}} \quad (10-17)$$

where:

$$CRF = \frac{d(1+d)^L}{(1+d)^L - 1} \quad (10-18)$$

where:

$d$  = discount rate and

$L$  = fuel cell system lifetime (yr)

Capital recovery factor, CRF, has unit  $\text{yr}^{-1}$ . Note that for  $d \rightarrow 0$ ,  $CRF \rightarrow 1/L$ , and in that case  $L = SPT$ .

A more complete economic analysis should also take into account the maintenance cost:

$$C_{el} = \frac{C_{fc} \cdot CRF + AMC}{8760 \cdot CF} + \frac{C_{ng}}{\bar{\eta}_{fc}} \quad (10-19)$$

where  $AMC$  is the annual cost of maintenance per kW of installed power ( $\$/\text{kW}^{-1}\text{yr}^{-1}$ ), which at this time is difficult to predict because not that many fuel cell systems are in real-life operation.

The economics of stationary fuel cells greatly depends on the prices of electricity and natural gas. From Equation (10-15) it is clear that the simple payback time has a positive value only for  $C_{el} > \frac{C_{ng}}{\bar{\eta}_{fc}}$ , which means that the ratio between the price of electricity and the price of natural gas (both expressed in same units,  $\$/\text{kWh}^{-1}$ )  $\frac{C_{el}}{C_{ng}}$ , must be larger than  $\frac{1}{\bar{\eta}_{fc}}$ . For the fuel cell system efficiencies between 0.30 and 0.40, the electricity/natural gas price ratio must be higher than 3.33 and 2.50, respectively. The higher this ratio, the shorter the payback time would be.

The prices of electricity and natural gas vary over time, and they vary from region to region. Figure 10-10 shows how since the year 2000 the price of natural gas in the United States has risen sharply, which caused the average residential price ratio  $C_{el}/C_{ng}$  to drop from 4 to about 2.5 [33]. The residential price ratio varies significantly from region to region, as shown in Figure 10-11 for the United States and selected countries around the world [33]. Clearly, a residential fuel cell concept may be feasible only in selected countries and regions. The price of natural gas to the utility sector is somewhat lower than the price for the residential sector, which makes the fuel cells attractive for distributed generation.

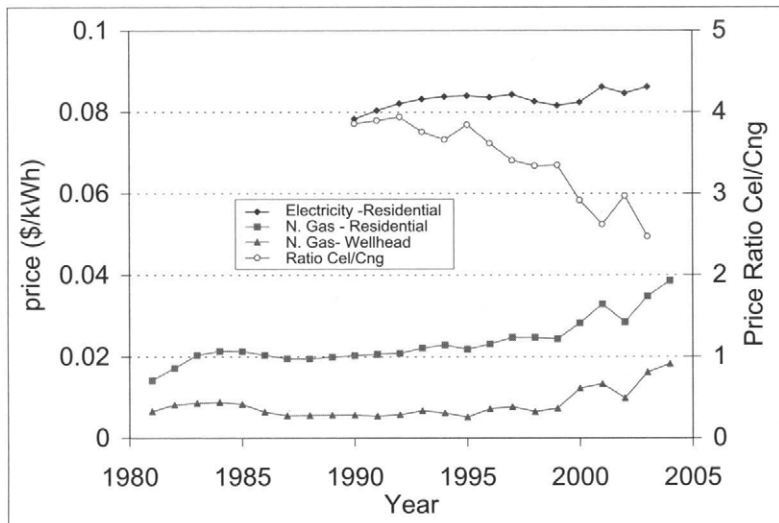


FIGURE 10-10. Price of electricity and natural gas in various regions of the United States (based on data in [33]).

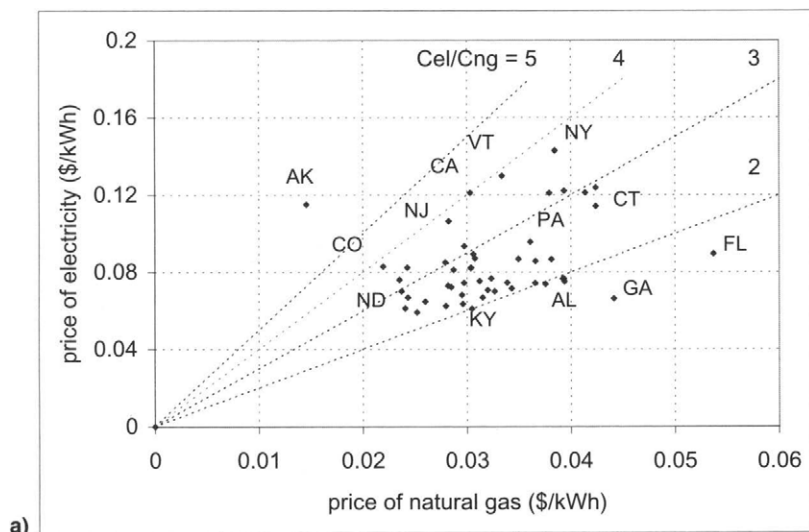


FIGURE 10-11. Price of electricity relative to price of natural gas for residential customers: a) United States (2003); b) selected world countries (2002) (based on data in [33]).

(Continued on next page.)

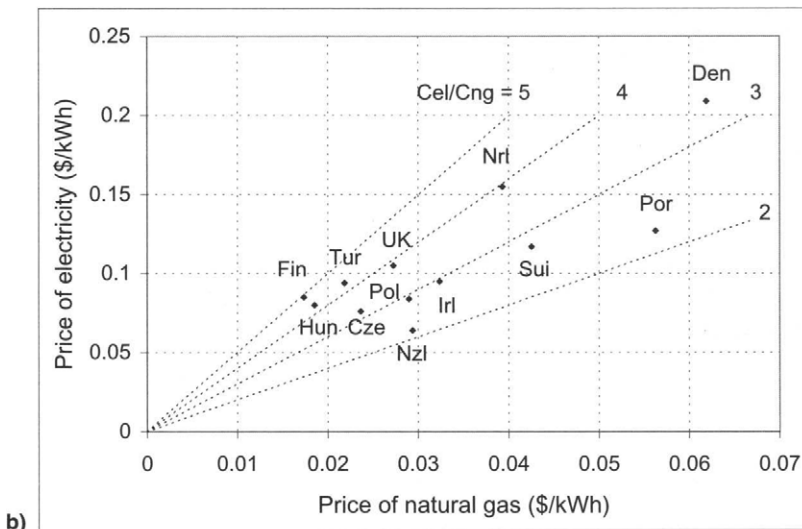
FIGURE 10-11. *Continued*

TABLE E1  
Example of a Household Simplified Load Profile

kW	%time
10.0	5
5.0	10
2.0	15
1.2	40
0.733	30
Sum	100

*Example:*

A load profile of a household may be approximated by a power distribution curve as shown in Table E1. The cost of grid electricity is \$0.15 per kWh and the price of natural gas is \$0.32 per m<sup>3</sup>. Calculate the simple payback time for a fuel cell that is sized to cover the maximum load and compare it with the payback time for a fuel cell that is sized for an average power. The fuel cell cost is \$1000 per kW. Fuel cell system efficiency is as shown in Figure 10-7.

The payback time is given by Equation (10-17). The missing parameters are the annual electricity produced and the average annual efficiency. The annual electricity produced is:

$$AEP = \sum P_{fc} t$$

**TABLE E2**  
The Results for the Case When the Fuel Cell Is Sized at Maximum Power

kW	%time	kWh/yr	%power	eff	kWh/yr
10	5	4,380.0	100	0.34	12,882.4
5	10	4,380.0	50	0.35	12,514.3
2	15	2,628.0	20	0.33	7,963.6
1.2	40	4,204.8	12	0.28	15,017.1
0.7333	30	1,927.1	7.333	0.23	8,378.7
Sum	100	17,519.9			56,756.2

$$\bar{\eta}_{fc} = \frac{\sum P_{fc} t}{\sum \frac{P_{fc}}{\eta_{fc}} t}$$

For the case where the fuel cell is sized at maximum power,  $P_{fc,nom} = 10 \text{ kW}$ , the results are shown in Table E2:

From the Table E2:

Annual electricity produced:

$$AEP = 17,519.9 \text{ kWh yr}^{-1}$$

Average power:

$$\bar{P} = \frac{AEP}{8760} = 2.0 \text{ kW}$$

Annual capacity factor:

$$CF = \frac{AEP}{8760P_{fc,nom}} = \frac{17,519.9}{8760 \times 10} = 0.2$$

Average annual efficiency:

$$\bar{\eta}_{fc} = \frac{17,519.9}{56,756.2} = 0.308$$

Cost of natural gas:

$$C_{ng} = 0.32 \text{ \$m}^{-3} / 38,300 \text{ kJ m}^{-3} \times 3600 \text{ s h}^{-1} = 0.03 \text{ \$ kWh}^{-1}$$

Simple payback time:

$$\text{SPT} = \frac{C_{fc}}{8760 \cdot CF \cdot \left( C_{el} - \frac{C_{ng}}{\bar{\eta}_{fc}} \right)} = \frac{1000}{8760 \times 0.2 \left( 0.15 - \frac{0.03}{0.308} \right)} = \underline{10.8 \text{ years}}$$

For the case where the fuel cell is sized at average power,  $P_{fc,nom} = 2.0 \text{ kW}$ , the results are shown in Table E3:

From the Table E3:

Annual electricity produced:

$$\text{AEP} = 11,387.9 \text{ kWh yr}^{-1}$$

Annual capacity factor:

$$CF = \frac{\text{AEP}}{8760P_{fc,nom}} = \frac{11,387.9}{8760 \times 2} = 0.65$$

Average annual efficiency:

$$\bar{\eta}_{fc} = \frac{11,387.9}{33,058.4} = 0.344$$

Simple payback time:

$$\text{SPT} = \frac{C_{fc}}{8760 \cdot CF \cdot \left( C_{el} - \frac{C_{ng}}{\bar{\eta}_{fc}} \right)} = \frac{1000}{8760 \times 0.65 \left( 0.15 - \frac{0.03}{0.34} \right)} = \underline{2.8 \text{ years}}$$

A 2-kW fuel cell is therefore more likely to be economical for this case. A payback time of 2.8 years will likely be appealing to an average residential customer.

TABLE E3  
The Results for the Case When the Fuel Cell Is Sized at Average Power

kW	%time	kWh/yr	%power	eff	kWh/yr
2	30	5,256.0	100	0.34	15,458.8
1.2	40	4,204.8	60	0.35	12,013.7
0.733	30	1,927.1	36.67	0.345	5,585.8
Sum	100	11,387.9			33,058.4

The economics of a fuel cell from the previous example may be improved by either exporting excess electricity back to the grid or utilizing the heat produced by the fuel cell. In the former case the price of electricity exported back to the grid may not be the same as the price of purchased electricity. In that case, the simple payback time is:

$$SPT = \frac{P_{fc,nom} \cdot C_{fc}}{AEP_{int} \cdot \left( C_{el} - \frac{C_{ng}}{\bar{\eta}_{fc}} \right) + AEP_{exp} \cdot \left( C_{el,exp} - \frac{C_{ng}}{\bar{\eta}_{fc}} \right)} \quad (10-20)$$

where:

$AEP_{int}$  = amount of electricity consumed internally ( $\text{kWh yr}^{-1}$ )

$AEP_{exp}$  = amount of electricity exported back to the grid ( $\text{kWh yr}^{-1}$ )

$C_{el,exp}$  = price of electricity exported back to the grid ( $\$/\text{kWh}^{-1}$ )

For the previous example:

$$AEP_{int} = 17,519.9 \text{ kWh yr}^{-1}$$

$$AEP_{exp} = P_{fc,nom} \times 8760 - AEP_{int} = 87,600 - 17,519.9 = 70,080.1 \text{ kWh yr}^{-1}$$

$\bar{\eta}_{fc}$  = 0.34 {because the fuel cell would operate 100% of the time at nominal power}

Assuming that the price of electricity exported back to the grid will be 90% of the electricity purchase price, the simple payback time will be:

$$SPT = \frac{10 \times 1000}{17,519.9 \times \left( 0.15 - \frac{0.03}{0.34} \right) + 70,080.1 \times \left( 0.15 \times 0.9 - \frac{0.03}{0.34} \right)} = 2.3 \text{ years}$$

The economics in this case greatly depends on the price of electricity exported to the grid. In some countries this price is regulated and the utilities are mandated to purchase electricity from the individual producers. The economics of grid-interactive stationary power fuel cells may be further improved if they are operated by a utility company paying a lower rate for natural gas. In fact, a natural gas utility company may become an electricity producer.

In cases where the waste heat generated by the fuel cell system is utilized, the payback time must take into account the savings in heating fuel. Heating fuel may be natural gas, heating oil, or even electricity. The efficiency of the heating systems is typically well above 80% and in the case of condensing boilers it may be 100% or more (see section 2.3. Higher and Lower Heating Value of Hydrogen for an explanation of an efficiency greater than 100%).

The total fuel cell efficiency (both thermal and electrical) is defined with Equation (10-9). The amount of heat used per year (AHP) is then:

$$AHP = AEP \left( \frac{\eta_{tot}}{\eta_{el}} - 1 \right) \times f_{hu} \quad (10-21)$$

Note that not all the heat may be utilized over the year. Although the heat for domestic hot water is needed throughout the year, heat for space heating is needed only during the heating season, whose duration depends on climate. A ratio between the heat actually utilized and the heat produced by a fuel cell system is included in Equation (10-21) as a heat utilization factor,  $f_{hu}$ . In some cases, fuel cell systems for cogeneration of heat and power may be used in a heat following mode, and either using or exporting generated electricity.

Simple payback time for combined heat and power generation is:

$$SPT = \frac{C_{fc} \cdot P_{fc}}{AEP \left[ C_{el} - \frac{C_{ng}}{\eta_{el}} + \left( \frac{\eta_{tot}}{\eta_{el}} - 1 \right) f_{hu} \frac{C_{fuel}}{\eta_{heat}} \right]} \quad (10-22)$$

where:

$C_{fuel}$  = cost of fuel ( $\$/kW^{-1}$ ) used for heating (natural gas, heating oil, or electricity)

$\eta_{heat}$  = efficiency of conventional heat generation

#### Example:

If the fuel cell from the previous example also generates heat with the combined total energy efficiency of 75%, and two-thirds of that heat can be utilized, calculate the payback time. The heat was otherwise generated by burning natural gas in a 90% efficient furnace.

From Equation (10-22):

$$SPT = \frac{1000 \times 10}{17519.9 \times \left[ 0.15 - \frac{0.03}{0.308} + \left( \frac{0.75}{0.308} - 1 \right) \frac{2}{3} \frac{0.03}{0.9} \right]} = 6.8 \text{ years}$$

Therefore, combined heat and power generation results in further savings and the payback time is reduced from 10.8 years for a system that generates only electricity to 6.8 years.

As shown in the previous examples, the economics of stationary fuel cells depends greatly on how those units are being used. Several different scenarios are possible, namely:

1. *Fuel cell system for individual user (residential or commercial) sized to cover the entire load.* Such a system would have a low capacity factor and relatively low average efficiency, and because of that, the payback time will be unacceptably high. Nevertheless, this scenario may be acceptable where the user is willing to pay premium price for being grid independent. In addition, this may pass in the new homes market, where the buyer pays for an oversized and not very efficient fuel cell, but the high cost is masked by the cost of the entire purchase.
2. *Fuel cell system sized to cover the entire load, but excess electricity sold to the grid.* This scenario may work only if the utility wants to buy excess electricity at a reasonable price, or if the utility actually owns the fuel cell system and operates it as a distributed generator. The user would not see the difference in either power supply or cost, although there should be some incentives for the individual users to accept "mini power plants" in their homes or businesses. This scenario may be attractive for utilities in heavily populated urban areas, where building new large power plants is out of question. Because of their modularity, small size, ultralow emissions, and low noise, the fuel cell power systems may be installed in buildings. In such a way, the utility companies would be able to gradually increase their capacity without large investments. Of course, the premise is that the fuel cell power systems are cost-effective, that is, they have a reasonable payback time.
3. *Fuel cell system sized to cover part of the load.* In this case the fuel cell system operates with high capacity factor and high efficiency, and is more likely to be cost-competitive. A downside of this option is that the user depends on the grid for peak power. In case of grid power outage the user may be able to use the fuel cell but only for some critical loads if the wiring is arranged that way.
4. *Fuel cell system in combination with batteries (or ultracapacitors) for short-term peak power.* In this case the fuel cell may be sized to operate with a very high capacity factor providing baseline load and charging the batteries during off-peak hours. However, analysis of such a system would have to include the economics and lifetime of the batteries.
5. *Fuel cell cogeneration system.* Economics of all of the previous scenarios may be significantly improved if waste heat generated by the fuel cell system can be utilized. In that case the payback time must take into account the amount of heat that may be recovered and fuel that would have been used to generate that amount of heat (Equation 10-22). The system may be designed and sized for either electric load following or thermal load following. Such a system would be combined with a boiler heating system.

6. *Fuel cell as standby or emergency generator.* This may be an ideal niche market for fuel cell power systems for several reasons:
  - The efficiency is not important.
  - The expected lifetime is only about 1000 hours (200 hours/year for 5 years)—what should be achievable with today's systems.
  - Quick start-up is not required (batteries or ultracapacitors may be used to provide power during the fuel cell start-up period).
  - The fuel cell system is better than batteries in terms of size and weight (and probably cost) for applications that require more than 5 kWh of backup.
  - The fuel cell system is superior to gasoline or diesel generators in terms of noise and emissions.
  - Combined with an electrolyzer, such a system generates its own fuel. This application is discussed in greater detail in the following section.

### 10.3. Backup Power

Backup power is defined as any device that provides instantaneous, uninterruptible power. The term UPS (uninterruptible power supply) is an often used term, but can sometimes refer to systems that supply A/C power, or systems that supply power for no more than 30 to 60 minutes. A more general definition includes all types of power outputs and all backup times. Typical applications for backup power include telecommunications systems, information technology and computer systems, manufacturing processes, security systems, utility substations, and railway applications. Backup power systems are employed in cases where the loss of power results in a significant reduction in productivity or financial loss.

Fuel cell system requirements for backup power applications significantly differ from requirements for such systems in automotive and stationary (primary) power generation markets. As Table 10-4 shows, there are only a few common characteristics between the backup power on one side and automotive and stationary (primary) power on the other.

Fuel cell backup power can use hydrogen as fuel. Hydrogen can be provided in tanks that would have to be replaced after they are emptied (which may be a logistic problem or may create new business opportunities—refilling of hydrogen bottles). A more elegant solution would be for the fuel cell to generate its own hydrogen via an electrolysis process during periods when electricity is available and the fuel cell is dormant. A combination of fuel cell and electrolyzer is often referred to as a reversible fuel cell (see the Section 10.5. Regenerative Fuel Cells and Their Applications). A backup power fuel cell thus does not depend on hydrogen infrastructure and therefore may be commercialized before the automotive and stationary fuel cells.

TABLE 10-4  
Summary of Market Requirements for Fuel Cell Systems [29]

	<i>Automotive</i>	<i>Stationary (Primary Power)</i>	<i>Stationary (Backup Power)</i>
Power output	50–100 kW	1–10 kW & 200 kW	1–10 kW
Fuel	Reformate/H <sub>2</sub>	Reformate	Hydrogen
Life (operational)	5000 hours	>40,000 hrs	<2000 hrs
High efficiency	Critical	Critical	Not critical
Instant start	Very important	Not important	Very important
Output mode	Highly variable	Variable	Constant
Operation	Intermittent	Constant	Intermittent
Preferred voltage	>300 V	>110 V	24 V or 48 V
Heat recovery	Not needed	Very important	Not needed
Water balance	Very important	Very important	Not critical
Size and weight	Critical	Not critical	Not critical
Extreme conditions	Critical	Not critical	Important
Cost	<\$100/kW	<\$1000/kW	\$1000–\$3000/kW

The operational lifetime requirement for a fuel cell in backup power application is less than 2000 hours. Such a fuel cell operates with continuous load requirements during the power outage, but never longer than 8 hours. This duty cycle is achievable with today's fuel cell technology. Operational lifetimes of several thousand hours have been demonstrated by almost all the major membrane electrode assembly (MEA) suppliers/developers.

The system efficiency is critical for both stationary and automotive applications. For backup power there is no imposed efficiency goal, but the fuel cell efficiency directly translates in the size and cost of both the electrolyzer and hydrogen storage. Because the fuel cell efficiency is "tradeable" with its size, and thus cost, an optimization study is needed to determine an optimal fuel cell efficiency. However, with hydrogen as fuel the system parasitic losses could be minimized, resulting in high achievable efficiency (up to 50%).

One of the most important system requirements for backup power applications (especially for telecommunications) is ability to start instantly upon power outage. The required response time is in the order of milliseconds. The fuel cell itself can meet this requirement, as long as the supply of reactants is uninterrupted, otherwise a bridge power may be needed (such as batteries or ultracapacitors). System engineering solutions could significantly reduce or even eliminate the need for bridge power. For example, the fuel cell may be kept in a "ready" mode. Most of the time the backup power system is in the "idle" or "ready" mode and the operation is highly intermittent. It may only operate up to 50–200 hours per year.

Although the fuel cell generates water, the system may lose water over time. In a regenerative fuel cell system, water is lost from the system through oxygen exhaust when the system is operating in the electrolysis mode and through air exhaust when the system is operating in the fuel cell mode. However, with a proper system design the water loss is minimal and an adequately sized water tank (for at least a full year of operation) may be a more economical solution than water recovery.

Although system size and weight are absolutely critical for automotive applications, they are less important for stationary applications. However, a backup power unit must typically fit in place of the technology that it replaces (usually batteries). For some locations, the weight advantage of the fuel cell system over conventional batteries may improve its competitiveness. In those cases, the weight may be tradeable with other system elements such as efficiency and cost. Fuel cell backup power systems, including hydrogen storage for more than a few kWh, are in general much lighter than conventional batteries (lead acid) and may be lighter than most advanced batteries, too.

Clearly, the fuel cells designed for automotive or stationary power application do not meet existing backup power requirements. In some cases they indeed exceed the requirements, but some of the system features that drive these designs to exceed current requirements often negatively affect system cost and complexity. Therefore, a fuel cell stack and system specifically designed for backup power applications is more likely to meet the requirements at minimum cost.

For fuel cells to be offered at reasonable prices, there must be sufficient production volume with which to drive down the costs. This implies a market large enough to support the purchase of thousands or tens of thousands of units per year at a minimum. Although the automotive market holds the ultimate promise of high volume with tens of millions of units per year, the backup power market offers a significant opportunity for fuel cell commercialization in its own right.

At power levels between 1 and 100kW, the backup power market worldwide is far in excess of 100,000 units annually. Large and increasing numbers of backup power systems are sold for support of computer systems, telecom systems, and other applications. These units represent both new and replacement systems. One of the positive aspects of existing technology used in backup power systems, lead acid batteries, is that the expected life is generally 3 to 7 years. This means the replacement market is a steady and growing segment of the market. To put this in perspective, in the United States alone there are more than 100,000 cellular sites, all using backup power systems. Assuming a 5-year replacement cycle, this would suggest that 20,000 replacement systems are needed each year [29].

In addition, long-term growth rates for telecommunications and computer technology well exceed average economic growth projections. Thus,

the backup power market offers more than enough unit volume to make it economically viable and financially attractive for fuel cell developers.

A fuel cell backup power system must be equipped with hydrogen storage sufficient for the system operation for the required period. Empty hydrogen bottles may be replaced, or a more elegant solution is to equip the system with a hydrogen generator (electrolyzer or a reformer). Because the system is used where electricity is available and not necessarily natural gas or propane, an electrolyzer appears to be a better option. The electrolyzer must be sized to generate the required amount of hydrogen in a given time period (typically much longer than the backup time).

The required electrolyzer power is:

$$P_{EL,nom} = \frac{P_{FC,nom} \cdot \tau_{FC} \cdot CF_{FC}}{\eta_{FC,sys} \cdot \eta_{EL,sys} \cdot \tau_{EL} \cdot CF_{EL}} \quad (10-23)$$

where:

- $P_{FC,nom}$  = fuel cell nominal power (kW)
- $\tau_{FC}$  and  $\tau_{EL}$  = duration of operation in fuel cell and electrolyzer modes, respectively (hours)
- $CF_{FC}$  and  $CF_{EL}$  = capacity factors of fuel cell and electrolyzer, respectively, defined as a ratio between average power and nominal power
- $\eta_{FC,sys}$  and  $\eta_{EL,sys}$  = system efficiency of fuel cell and electrolyzer, respectively

The electrolyzer efficiency is the reverse of fuel cell efficiency:

$$\eta_{EL} = \frac{1.482}{V_{cell}} \frac{i - i_{loss}}{i} \quad (10-24)$$

where:

$V_{cell}$  = electrolyzer cell voltage; similarly to fuel cell nominal voltage, electrolyzer cell nominal voltage is an arbitrary value; typically the electrolyzers operate at below 2 V per cell.

$i$  = electrolyzer current density, A cm<sup>-2</sup>

$i_{loss}$  = current and hydrogen loss, A cm<sup>-2</sup>; this is typically negligible at low pressures and high operating current densities; however, it may become significant at very high pressures due to hydrogen crossover permeation.

The electrolyzer system efficiency is:

$$\eta_{EL,sys} = \frac{1.482}{V_{cell}} \frac{i - i_{loss}}{i} \frac{\eta_{DC}}{1 + \zeta} \quad (10-25)$$

where:

$\eta_{DC}$  = efficiency of power conversion (either AC/DC or DC/DC)

$\zeta$  = ratio between parasitic power and net power consumed by the electrolyzer

An important feature of the fuel cell backup power system is that it separates power from energy from recharging. In batteries, all three features are tied to the battery itself. The power output of a fuel cell backup power system depends on the size of the fuel cell. The amount of energy stored is a function of the size of the hydrogen storage. This can be changed independent of the fuel cell size, thus providing incremental increase in energy storage at a fraction of the cost of the batteries that would be needed to provide that increase. The recharging time is a function of the electrolyzer size, which again can be tailored to fit the requirement without changing the size of the energy storage or the power output. Figure 10-12 shows a prototype 1-kW backup power system where these three features are built into three modules [29].

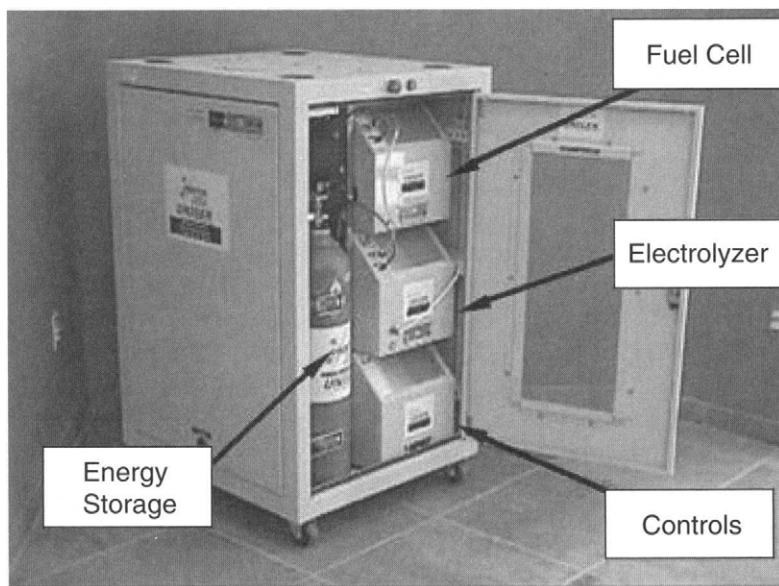


FIGURE 10-12. A prototype 1-kW backup power system. (Courtesy of Proton Energy Systems.)

In applications where the fuel cells are used as energy storage devices and compete with the batteries, specific energy is an important parameter. Specific energy or gravimetric energy density is defined as the amount of electrical energy stored (in kWh) per unit mass (kg) of the entire system. For a fuel cell system, specific energy,  $\epsilon_d$ , may be defined as:

$$\epsilon_d = \frac{\tau \cdot CF}{\frac{D_f}{P_f} \left( \frac{K_f}{P_{FC}} + S_f \right) + \frac{\tau}{\eta_{FC} H_{HV} \sigma_{st}}} \quad (10-26)$$

where:

- $\tau$  = duration of operation (hours); for backup power this is typically up to 8 hours
- CF = capacity factor during operation (if the load is constant then CF = 1)
- $D_f$  = stack design factor ( $\text{kg m}^{-2}$ ) as defined in Equation (10-6)
- $P_f$  = fuel cell specific power per unit active area ( $\text{kW m}^{-2}$ )
- $K_f$  and  $S_f$  = fuel cell system mass factors;  $K_f$  is the mass of the system (kg) independent of power output, and  $S_f$  is the mass of the system proportional to power output ( $\text{kg kWh}^{-1}$ )
- $P_{FC}$  = fuel cell system nominal power output (kW)
- $\eta_{FC}$  = fuel cell system efficiency
- $H_{HV}$  = hydrogen heating value ( $\text{kWh kg}^{-1}$ ); lower or higher heating value depending on how the fuel cell system efficiency is expressed
- $\sigma_{st}$  = hydrogen storage efficiency (kg H<sub>2</sub> per kg of total storage system mass)

Figure 10-13 shows the achievable hydrogen fuel cell system energy density for a 1-kW system. For duration of 8 hours, energy density is 0.27 kWh kg<sup>-1</sup>, several times better than energy density of lead acid batteries and comparable to that of most advanced rechargeable batteries. The assumptions used for variables in Equation (10-26) are conservatively achievable with today's fuel cells and hydrogen storage tanks.

Assumptions: CF = 1;  $D_f = 30 \text{ kg m}^{-2}$ ;  $P_f = 3 \text{ kW m}^{-2}$ ;  $K_f = 2 \text{ kg}$ ;  $S_f = 5 \text{ kg kWh}^{-1}$ ;  $P_{FC} = 1 \text{ kW}$ ;  $\eta_{FC} = 0.5$  (LHV);  $\sigma_{st} = 3\%$ .

#### 10.4. Fuel Cells for Small Portable Power

The term "portable power system" is not sharply defined. Hoogers [34] attempted to define it as "a small grid-independent electric power unit ranging from a few watts to roughly one kilowatt, which serves mainly a purpose of convenience rather than being a primarily a result of environ-

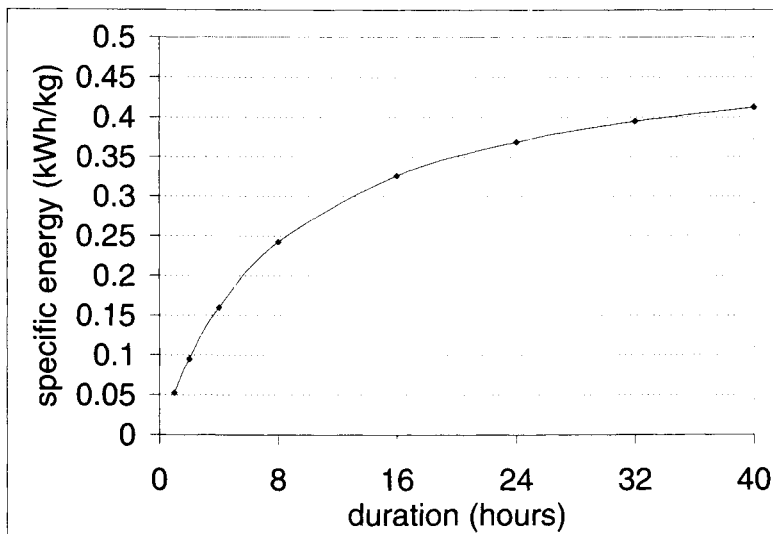


FIGURE 10-13. Achievable hydrogen fuel cell system energy density.

mental or energy-saving considerations." These devices may be divided into two main categories:

1. Battery replacements, typically well under 100 Watts
2. Portable power generators, up to 1 kW

The key feature of small fuel cells to be used as battery replacements is a running time without recharging. Obviously, by definition the size and weight are also important. Power units with either significantly higher power densities or larger energy storage capacities than those of existing secondary batteries may find applications in portable computers, communication and transmission devices, power tools, remote meteorological or other observation systems, and in military gadgets. In addition to the size of the fuel cell itself, the critical issue is the fuel and its storage. Hydrogen, although a preferred fuel for PEM fuel cells, is rarely used because of bulkiness or weight of its storage, even in small quantities required by those small devices. Hydrogen may be stored in room temperature metal hydride storage tanks. Some chemical hydrides offer higher energy density; however, they must be equipped with suitable reactors where hydrogen is released in controlled chemical reaction [35]. Most portable fuel cells use methanol as fuel, or more precisely methanol aqueous solutions, either directly (so-called direct methanol fuel cells) or via microreformers.

The military market is particularly attractive as it often can be a sympathetic early adopter of new technologies, willing to accept high prices and limited performance if other application-specific requirements can be met (such as low noise, low thermal signature, long duration both in oper-

ation and dormant, size and weight, safety) [36]. The range of interest in small fuel cells from the military is difficult to categorize. Some examples of early military fuel cell products or prototypes include [36]:

- battery chargers,
- soldier power,
- telecommunications,
- navigation systems,
- computers,
- various tools,
- exoskeletons,
- auxiliary power unit for vehicles,
- unmanned aerial vehicles,
- small autonomous robot vehicles,
- unattended sensors and munitions,
- ocean sensors and transponders.

Although a preferred fuel for military applications would be logistic fuel (JP-8), because of difficulties in reforming this fuel, particularly on such a small size, the same fuels used for nonmilitary applications, such as hydrogen, metal hydrides, chemical hydrides methanol, are acceptable as long as they are supplied in closed canisters or cartridges and do not have to be dispensed.

Development of small fuel cells for portable power applications has resulted in a myriad of stack configurations. Some stacks are miniaturized replicas of the larger automotive or stationary power fuel cells with the same components, MEAs, gas diffusion layers, bipolar plates, and end plates. Some use planar configuration where the cells are connected with conductive strips. Recently, microfluidic cells manufactured on silicon-based chips are emerging [37,38].

The fuel cell systems for these applications are extremely simplified. The simplicity of the system is more important than the cell/stack size. Power density generated is often below  $0.1 \text{ W/cm}^2$ . These cells/stacks do not need active cooling; those using hydrogen mainly operate in a dead-end mode, and air is often supplied passively.

## 10.5. Regenerative Fuel Cells and Their Applications

A regenerative fuel cell (RFC) is a device that can operate alternately as an electrolyzer and as a fuel cell. The electrolyzer and fuel cell functions can be integrated into a single stack of cells (unitized), or two separate (discrete) stacks may be used, one as a fuel cell and one as an electrolyzer. In an electrolysis mode, the stack generates hydrogen (and oxygen) from electricity, and in a fuel cell mode it generates electricity from stored hydrogen (and oxygen, possibly extracted from air). It is therefore an energy storage device

(similar to a rechargeable battery) with hydrogen as a storage medium. The regenerative fuel cell has the highest achievable specific energy of all rechargeable energy storage options. Theoretical specific energy of H<sub>2</sub>/O<sub>2</sub> fuel cell systems is 3600 Wh/kg (accounting only for the mass of reactants and assuming theoretical fuel cell efficiency), but when the masses of storage tanks and the fuel cell system are taken into account with practical fuel cell efficiencies, specific energy in excess of 400 Wh/kg may be achieved [39]. As such, it may be used in applications where relatively large amounts of electricity need to be stored, such as:

- energy storage for remote off-grid power sources;
- in conjunction with highly intermittent renewable energy sources (solar and wind);
- emergency or backup power generation (as discussed in the section Backup Power);
- unmanned underwater vehicles;
- high-altitude, long-endurance solar rechargeable aircraft;
- hybrid energy storage/propulsion systems for spacecraft.

Regenerative fuel cells generate their own hydrogen and therefore do not depend on hydrogen infrastructure. Because of that they may be commercialized in the niche applications listed earlier.

### 10.5.1. Design Trade-offs

Several trade-offs must be considered in the design of an RFC system, such as oxygen vs air feed operation, unitized vs discrete stack approach, pumped vs static feed, and selection of operating pressure [40]. These trade-offs are discussed next.

#### Oxygen vs Air

Because oxygen is produced in the electrolysis process it may be advantageous to store it and use it later in the fuel cell reaction. The fuel cell operation with pure oxygen results in higher voltage than its operation with air. The gain due to a higher partial pressure of oxygen is usually higher than that predicted solely by the Nernst equation, particularly because of the higher diffusion rates of pure oxygen as compared with a oxygen/nitrogen mixture. In addition, a fuel cell operating with air requires a device for pumping of air through the fuel cell, resulting in additional parasitic losses. Passive air supply, based on natural convection due to temperature and concentration gradients, may be used only for very low-power applications.

The decision whether to store oxygen or vent it strongly depends on application. Systems that use oxygen may be totally closed to the environment, which is critical in applications where maintenance is difficult

or costly. Obviously for space applications oxygen storage is the only option. For many terrestrial applications the gains in fuel cell performance (or efficiency) and reduction in maintenance cost may not be sufficient to justify the capital cost and safety issues of storing high-pressure oxygen. For some applications, there is merit to accumulating a small portion of the oxygen generated during electrolysis, which is subsequently available for short-term fuel cell performance enhancement, by mixing with the air stream. Often cost, efficiency, and duty cycle considerations provide a significant driver toward choice of oxidant for a given application.

### *Unitized vs Discrete*

In the unitized regenerative fuel cell (URFC), the functions of both the electrolyzer and the fuel cell are carried out by a single stack that can operate alternately in each mode. The URFC has important advantages in space applications where weight is critical. For terrestrial applications, especially those that do not include oxygen storage, separate electrolyzer and fuel cell units are generally more applicable. There are inevitably fewer design constraints on devices designed to operate in only one mode. If, for example, a separate electrolyzer can operate at higher output pressure than a URFC, there may be sufficient savings associated with reduced tank volume to justify separate components. In some applications there is a big difference between charge and discharge power. Operation of a URFC in such a regime may not be feasible, that is, it may be outside of operational range, whereas the discrete components may be better optimized for respective charge/discharge powers. Design of an electrolyzer electrode is inherently different than design of a fuel cell electrode. Although the electrolyzer oxygen electrode (anode) is generally designed to be flooded, the fuel cell oxygen electrode (cathode) must repel produced water. Operation with pure oxygen in flooded or partially flooded electrodes may be feasible, particularly at elevated pressure, but operation with air may show severe mass transport limitations even at very low current densities. Because of that, design of a URFC may be easier for applications where oxygen is stored and used, and discrete units may be a better choice when air is used in the fuel cell operating mode, unless flooding issues are mitigated in the URFC design.

### *Pumped vs Static Feed*

Many PEM electrolyzer cell designs require high-pressure or circulating pumps, but static water feed electrolysis can generate high-pressure gases without pumps. Static feed electrolysis transports water (by osmosis and diffusion) between the water supply and the oxygen electrode, where electrolysis occurs. Static feed systems can eliminate all moving parts (except the poppets inside valves and water expulsion containers) by suitable modifications to the electrolysis cell itself. A URFC system that employs static feed electrolysis and stores oxygen can be completely closed to the envi-

ronment and has the potential to be a “maintenance-free” system. Such a system has clear advantages in locations where maintenance is expensive or prohibitive. Thermal management of static feed systems (without pumps) is a challenge, so high-performance operation can be difficult to achieve.

Although supply of reactant gases in a static mode during fuel cell operation is feasible, particularly using pure hydrogen and oxygen, removal of water requires special cell designs.

### *Operating Pressure*

A PEM fuel cell operates better at elevated pressure, that is, operation in higher pressure results in higher cell voltage. However, if air is used instead of pure oxygen, then it must be pressurized by a compressor. Power needed to run the compressor may very well offset the voltage gain, and because of that, pressurized fuel cell systems are, in general, less efficient than the ambient pressure systems. However, if pressurized hydrogen and oxygen are available there is no parasitic power consumption for pressurization, and that is why operation of hydrogen/oxygen fuel cells at higher pressure is preferred. PEM fuel cells operating at pressures up to 150 psig (1.0 MPa) have been demonstrated [41].

Pressurized electrolyzers result in a simpler system because there is no compressor required for the storing of reactant gases at high pressures. PEM electrolyzers that operate at greater than 2000 psi (>14 MPa) have been successfully demonstrated, and pressures up to 6000 psi (41 MPa) appear to be achievable [42]. Operation at high pressure demands use of thicker polymer membranes (to minimize loss of hydrogen and oxygen due to diffusion), but thicker membranes result in higher ionic resistance. Although operation at higher current densities results in lower efficiency, in high-pressure systems, where efficiency losses may be dominated by diffusion, there is an efficiency argument to operate at higher current densities in order to reduce the active area. Selection of operating pressure, for both electrolyzer and fuel cell, is a complex issue and must be considered in conjunction with other trade-off analyses.

#### 10.5.2. Regenerative Fuel Cell Applications

##### *Backup Power/UPS*

Fuel cell use in backup power applications has been discussed in the section Backup Power. Batteries and diesel or gasoline generators currently used in these applications have severe drawbacks and limitations, such as maintenance requirements, reliability, noise, (in)convenience, and cost. The RFC may alleviate these problems. This technology has a clear advantage over batteries in applications requiring higher power outputs for longer periods. It provides greater flexibility in design because, unlike batteries, it sepa-

rates charging time, storage capacity, and power output. Charging time can be varied by the size of the electrolyzer, storage capacity by the size of hydrogen storage, and power output by the fuel cell size. Therefore, various combinations are possible. The RFC also has an advantage over diesel or gasoline generators because it does not require a fuel supply—it generates its own fuel. These units generate hydrogen when grid power is available, store it, and then produce power when the grid is unavailable.

Depending on the application, hydrogen may be generated at high pressure or it may be pressurized with a compressor. Hydrogen can be stored in either high-pressure cylinders or metal hydrides. A regular bottle of hydrogen can store 0.5 kg of hydrogen at 2000 psi (14 MPa), sufficient to operate a 1-kW fuel cell for 7 to 8 hours [40]. The size of hydrogen storage depends on desired system autonomy and fuel cell efficiency, although there is no explicit efficiency requirement for a backup power unit. The value of delivered electricity (when there is a power outage) by far surpasses the value of electricity used to generate hydrogen. Reliability is therefore a much more important characteristic of a backup power system than efficiency. The unit must also be capable of quick start and rapid response to load variations, and because of that it is often combined with ultracapacitors.

The capacity of the electrolyzer is determined by allowed "recharge" time, which may be shorter, equal to, or longer than the "discharge" time, depending on the application. Consequently, the electrolyzer nominal power input could be larger or smaller than the fuel cell nominal power output.

Theoretically, the same amount of water used to generate hydrogen should be replenished by recombining that hydrogen in fuel cell reaction. However, some water leaves the system with venting oxygen from the electrolyzer and cathode exhaust from the fuel cell.

The power conditioning subsystem consists of a regulated voltage power supply for the electrolyzer and a DC/DC or DC/AC inverter that matches the fuel cell output voltage with that of the load, which again varies with application. Depending on the number of cells in the fuel cell stack, either "boost" or "buck" voltage regulators must be a part of the power conditioning subsystem.

Backup power systems usually operate less than 200 hours per year. Both PEM fuel cells and PEM electrolyzers have demonstrated continuous and discontinuous operation well in excess of 3000 hours. Therefore, from that aspect, PEM technology can meet the demands of this application, offering longer than a 10-year life.

### *Renewable Power*

Renewable energy sources, such as solar and wind, are inherently intermittent. The capacity factor, defined as a ratio between average power over

a period of time and maximum or nominal power, is about 20% for solar and about 30% for wind installations. An RFC may be used to store the excess energy when the renewable sources are available, by converting electricity to hydrogen, and then generate electricity from hydrogen when these renewable sources are not available.

The interface between the renewable source and RFC system must match their current and voltage, which differ for solar and wind systems. Photovoltaic solar systems generate direct current, which may be used directly by the electrolyzer if their polarization curves are well matched, otherwise a DC/DC converter may be needed. Wind generators typically generate AC, so the interface must include an AC/DC inverter, similar to the electrolyzer's regulated voltage power supply.

Electrolyzer's power input vs fuel cell power output depends on the capacity factors of both source and load, and on the efficiencies of both electrolyzer and fuel cell as well as the efficiency of hydrogen storage. If the load requires constant power then the electrolyzer connected to a solar power source may have power input up to 10 times higher than the fuel cell power output [43].

The size of hydrogen storage depends on the dynamics of hydrogen production and consumption. However, if the storage must account for not only daily but also seasonal variations in renewable source availability, then required hydrogen storage may be quite large. Hydrogen produced by the RFC may be used as a fuel for cooking, heating, or transportation. In that case, both electrolyzer and renewable power source must be sized accordingly. Such a system would provide energy independence for a device, house, farm, or a community in a remote area (Figure 10-14). This technology also has a great potential in developing countries where the energy/power needs are relatively small and the power infrastructure is insufficient or nonexistent. The RFC is an enabling technology that may make the renewable energy sources more practical.

### *High-Altitude Aircraft*

NASA's Helios, a prototype solar-powered aircraft, set an altitude record for all propeller-driven aircraft on August 13, 2001, when it flew to 96,863 feet (29.52 km) [44]. Such aircraft may replace some of the satellites for a fraction of the cost. The RFC is an enabling technology that could extend the range of a high-altitude solar-powered aircraft and theoretically make it an "eternal" airplane that never has to land. During the day the aircraft would be propelled by electricity produced by a photovoltaic array located on the top of the wings. The excess electricity would be used to generate hydrogen and oxygen, which are then stored in the lightweight pressure vessels that would also serve as the structural elements of the wings. During the night the aircraft would be propelled by electricity generated by recombining hydrogen and oxygen in RFC. Energy storage systems with

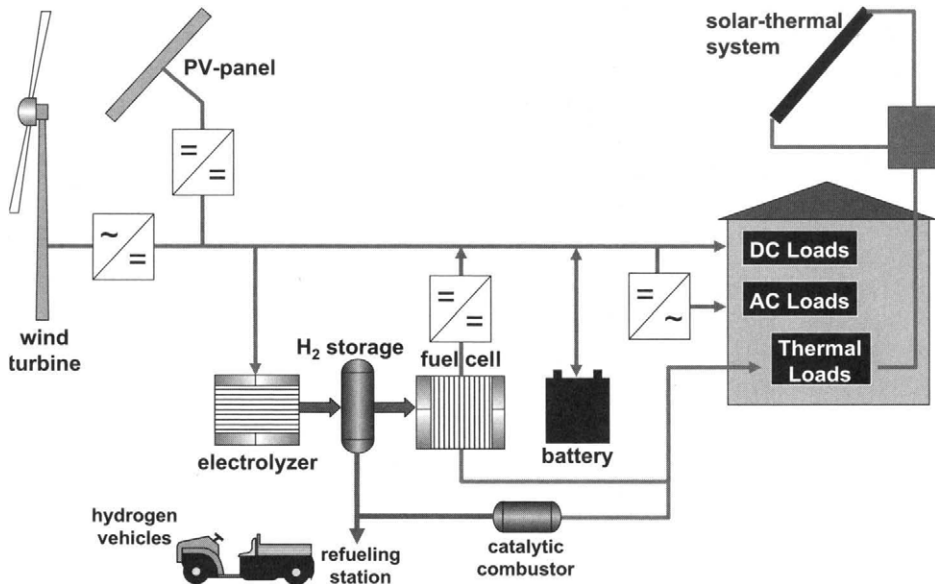


FIGURE 10-14. Regenerative fuel cell as a part of a renewable energy stand-alone system.

extremely high specific energy (>400 Wh/kg) based on RFCs have been designed to be used in high-altitude, long-endurance solar rechargeable aircraft [45–48].

#### *Space Applications—Water Rocket*

Applications of a URFC energy storage system specifically designed for zero gravity operation are of interest to NASA for solar-powered aircraft, satellite propulsion, space stations, and planetary bases. Water-based technology for space applications is generically called Water Rocket, which is the collective name for an integrated set of technologies that offer new options for spacecraft propulsion, power, energy storage, and structure. Low-pressure water stored on the spacecraft is electrolyzed to generate, separate, and pressurize gaseous hydrogen and oxygen. These gases, stored in light-weight pressure tanks, can be used for cold gas thrusters, burned to generate high thrust, or recombined to produce electric power (Figure 10-15). As a rocket propulsion system, Water Rocket provides the highest feasible chemical-specific impulse (~400 seconds) [48,49]. With innovative pressure tank technology as a part of the vehicle's structural elements, Water Rocket's specific energy (Wh kg<sup>-1</sup>) can exceed that of the best foreseeable batteries by an order of magnitude. For pulsed power applications, Water

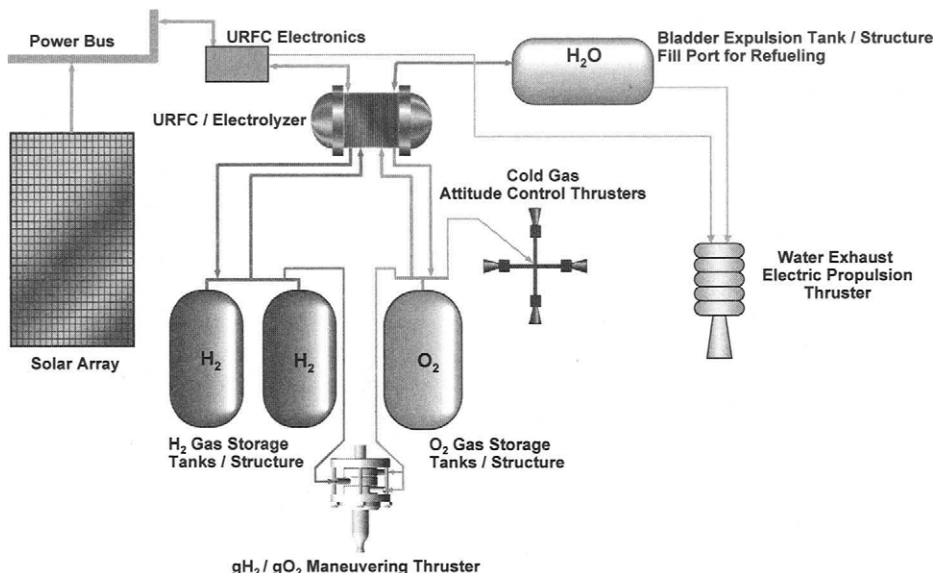


FIGURE 10-15. Water Rocket concept [48,49]. (Courtesy of Proton Energy Systems.)

Rocket propellants can be used to drive very high power density generators, such as MHD devices or detonation-driven pulse generators. A space vehicle using Water Rocket propulsion can be totally inert and nonhazardous during assembly and launch. These features are particularly important for the timely development and flight qualification of new classes of spacecraft, such as microsatellites, nanosatellites, and refuelable spacecraft.

## References

1. HyWeb information: <http://www.hydrogen.org/h2cars/overview/index.html> (accessed February 2005).
2. Fuel Cell 2000: <http://www.fuelcells.org/info/charts/carchart.pdf> (accessed February 2005).
3. Rajashekara, K., Propulsion System Strategies for Fuel Cell Vehicles, SAE Paper No. 2000-01-0369 (Society of Automotive Engineers, Warrendale, PA, 2000).
4. Tachtler, J., T. Dietsch, and G. Goetz, Fuel Cell Auxiliary Power Unit—Innovation for the Electric Supply of Passenger Cars, SAE Paper No. 2000-01-0374, in *Fuel Cell Power for Transportation 2000* (SAE SP-1505) (SAE, Warrendale, PA, 2000), pp. 109–117.
5. Konrad, G., M. Sommer, B. Loschko, A. Schell, and A. Docter, System Design for Vehicle Applications: DaimlerChrysler, in W. Vielstich, A. Lamm, and

- H. Gasteiger (editors), *Handbook of Fuel Cell Technology—Fundamentals, Technology and Applications*, Vol. 4 (J. Wiley, New York, 2003), pp. 693–713.
- 6. Masten, D. A., and A. D. Bosco, System Design for Vehicle Applications: GM/Opel, in W. Vielstich, A. Lamm, and H. Gasteiger (editors), *Handbook of Fuel Cell Technology—Fundamentals, Technology and Applications*, Vol. 4 (J. Wiley, New York, 2003), pp. 714–724.
  - 7. Stone, R., Competing Technologies for Transportation, in G. Hoogers (editor), *Fuel Cell Technology Handbook* (CRC Press, Boca Raton, FL, 2003).
  - 8. Thomas, C. E., B. D. James, F. D. Lomax, Jr., and I. F. Kuhn, Jr., Fuel Options for the Fuel Cell Vehicle: Hydrogen, Methanol or Gasoline? *International Journal of Hydrogen Energy*, Vol. 25, No. 6, 2000, pp. 551–568.
  - 9. Well-to-Wheel Energy Use and Greenhouse Gas Emissions of Advanced Fuel/Vehicle Systems, North American Analysis. Report by General Motors in cooperation with Argonne National Laboratory, BP Amoco, ExxonMobil and Shell, 2001.
  - 10. Weiss, M. A., J. B. Heywood, E. M. Drake, A. Schafer, and F. F. AuYeung, *On the Road in 2020. A Life-Cycle Analysis of New Automobile Technologies* (Massachusetts Institute of Technology, Boston, 2000).
  - 11. EPA Urban Dynamometer Driving Schedule (UDDS): <http://www.epa.gov/otaq/emisslab/methods/uddsdds.gif> (accessed February 2005).
  - 12. Pehnt, M., Life-Cycle Analysis of Fuel Cell System Components, in W. Vielstich, A. Lamm, and H. Gasteiger (editors), *Handbook of Fuel Cell Technology—Fundamentals, Technology and Applications*, Vol. 4 (J. Wiley, New York, 2003), pp. 1293–1317.
  - 13. Allison Gas Turbine Division, *Research and Development of Proton Exchange Membrane (PEM) Fuel Cells for Transportation Applications, Initial Conceptual Design*, Report to U.S. DOE, Contract No. DE-AC02-90CH10435, Report No. EDR 16194, 1994.
  - 14. Lomax, Jr., F. D., B. D. James, G. N. Baum, and C. E. Thomas, *Detailed Manufacturing Cost Estimates for Polymer Electrolyte Membrane (PEM) Fuel Cells for Light Duty Vehicles, Directed Technologies*, Report to U.S. DOE, Contract No. DE-AC02-94CE50389, 1998.
  - 15. California's Governor Executive Order S-7-04, 2004: [http://www.joinarnold.com/pdf/hydrogen\\_highway\\_eo.pdf](http://www.joinarnold.com/pdf/hydrogen_highway_eo.pdf) (accessed February 2005).
  - 16. Carpetis, C., Storage, Transport and Distribution of Hydrogen, in J. Nitsch (editor), *Hydrogen As an Energy Carrier* (Springer-Verlag, Berlin Heidelberg New York, 1988).
  - 17. Michel, F., H. Fieseler, G. Meyer, and F. Theissen, Onboard Equipment for Liquid Hydrogen Vehicles, in T. N. Veziroglu *et al.* (editors), *Hydrogen Energy Progress XI*, Vol. 2 (International Association for Hydrogen Energy, Coral Gables, FL, 1996), pp. 1063–1077.
  - 18. Berlowitz, P. J., and C. P. Darnell, Fuel Choices for Fuel Cell Powered Vehicles, SAE Paper No. 2000-01-0003, in *Fuel Cell Power for Transportation 2000* (SAE SP-1505) (SAE, Warrendale, PA, 2000), pp. 15–25.
  - 19. Sadler, M., R. P. G. Heath, and R. H. Thring, Warm-up Strategies for a Methanol Reformer Fuel Cell Vehicle, SAE Paper No. 2000-01-0371, in *Fuel Cell Power for Transportation 2000* (SAE SP-1505) (SAE, Warrendale, PA, 2000), pp. 95–100.

20. Uribe, F. A., S. Gottesfeld, and T. A. Zawodzinski Jr., Effect of Ammonia as Potential Fuel Impurity on Proton Exchange Membrane Fuel Cell Performance, *Journal of Electrochemical Society*, Vol. 149, 2002, p. A293.
21. Uribe, F. A., and T. A. Zawodzinski, Effects of Fuel Impurities on PEM Fuel Cell Performance, in *Proc. 201st ECS Meeting*, Vol. 2001-2, Abstract No. 339 (San Francisco, 2001).
22. Fronk, M. H., D. L. Wetter, D. A. Masten, and A. Bosco, PEM Fuel Cell System Solutions for Transportation, SAE Paper No. 2000-01-0373, in *Fuel Cell Power for Transportation 2000* (SAE SP-1505) (SAE, Warrendale, PA, 2000), pp. 101–108.
23. U.S. Department of Energy, Office of Advanced Transportation Technologies, *2001 Annual Progress Report: Fuel Cell for Transportation* (Washington, D.C., December 2001).
24. Hoogers, G., Automotive Applications, in G. Hoogers (editor), *Fuel Cell Technology Handbook* (CRC Press, Boca Raton, FL, 2003).
25. Adamson, K.-A., Fuel Cell Market Survey: Buses, *Fuel Cell Today*, Article 916, November 2004: [http://www.fuelcelltoday.com/FuelCellToday/FCTFiles/FCTArticleFiles/Article\\_916\\_BusSurvey%20Final%20Version.pdf](http://www.fuelcelltoday.com/FuelCellToday/FCTFiles/FCTArticleFiles/Article_916_BusSurvey%20Final%20Version.pdf) (accessed February 2005).
26. Fuel Cell 2000: <http://www.fuelcells.org/info/charts/buses.pdf> (accessed February 2005).
27. Croper, M., Fuel Cell Market Survey: Niche Transport, *Fuel Cell Today*, Article 823, June 2004: [http://www.fuelcelltoday.com/FuelCellToday/FCT-Files/FCTArticleFiles/Article\\_823\\_NicheTransport0604.pdf](http://www.fuelcelltoday.com/FuelCellToday/FCT-Files/FCTArticleFiles/Article_823_NicheTransport0604.pdf) (accessed February 2005).
28. Barbir, F., System Design for Stationary Power Generation, in W. Vielstich, A. Lamm, and H. Gasteiger (editors), *Handbook of Fuel Cell Technology—Fundamentals, Technology and Applications*, Vol. 4 (J. Wiley, New York, 2003), pp. 683–692.
29. Barbir, F., T. Maloney, T. Molter, and F. Tombaugh, Fuel Cell Stack and System Development: Matching Market to Technology Status, in *Proc. 2002 Fuel Cell Seminar* (Palm Springs, CA, November 18–21, 2002), pp. 948–951.
30. Hoogers, G., Stationary Power Applications, in G. Hoogers (editor), *Fuel Cell Technology Handbook* (CRC Press, Boca Raton, FL, 2003).
31. Lester, L. E., Fuel Cell Power Electronics, *Fuel Cells Bulletin*, No. 25, 2001, pp. 5–9.
32. Barbir, F., G. C. Joy, and D. J. Weinberg, Development of Residential Fuel Cell Power Systems, in *Proc. 2000 Fuel Cell Seminar* (Portland, OR, 2000), pp. 483–486.
33. U.S. Energy Information Administration, Department of Energy: <http://www.eia.doe.gov> (accessed February 2005).
34. Hoogers, G., Portable Applications, in G. Hoogers (editor), *Fuel Cell Technology Handbook* (CRC Press, Boca Raton, FL, 2003).
35. Heinzel, A., and C. Hebling, Portable PEM Systems, in W. Vielstich, A. Lamm, and H. Gasteiger (editors), *Handbook of Fuel Cell Technology—Fundamentals, Technology and Applications*, Vol. 4 (J. Wiley, New York, 2003), pp. 1142–1151.
36. Geiger, S., and D. Jollie, Fuel Cell Market Survey: Military Applications, *Fuel Cell Today*, Article 756, April 2004: <http://www.fuelcelltoday.com/>

- FuelCellToday/FCTFiles/FCTArticleFiles/Article\_756\_MilitarySurvey0404.pdf (accessed February 2005).
- 37. Shah, K., W. C. Shin, and R. S. Besser, A PDMS Micro Proton Exchange Membrane Fuel Cell by Conventional and Non-Conventional Microfabrication Techniques, *Sensors and Actuators B: Chemical*, Vol. 97, No. 2–3, 2004, pp. 157–167.
  - 38. Yamazaki, Y., Application of MEMS Technology to Micro Fuel Cells, *Electrochimica Acta*, Vol. 50, No. 2–3, 2004, pp. 659–662.
  - 39. Barbir, F., T. Molter, and L. Dalton, Efficiency and Weight Trade-off Analysis of Regenerative Fuel Cells as Energy Storage for Aerospace Applications, *International Journal of Hydrogen Energy*, Vol. 30, No. 4, 2005, pp. 231–238.
  - 40. Barbir, F., M. Lillis, F. Mitlitsky, and T. Molter, Regenerative Fuel Cell Applications and Design Options, in *Proc. of (CD) 14th World Hydrogen Energy Conference* (Montreal, June 2002).
  - 41. Murphy, O. J., G. D. Hitchens, and D. J. Manko, High Power Density Proton Exchange Fuel Cells, *Journal of Power Sources*, Vol. 47, 194, pp. 353–368.
  - 42. Mitlitsky, F., B. Myers, A. H. Weisberg, and A. Leonida, Applications and Development of High Pressure PEM Systems, Portable Fuel Cells International Conference (Lucerne, Switzerland, 1999) pp. 253–268.
  - 43. Barbir, F., Integrated Renewable Hydrogen Utility System, in *Proc. 1999 DOE Hydrogen Program Annual Review Meeting* (Lakewood, CO, May 4–6, 1999).
  - 44. NASA Dryden Research Center Press Release: 01-58, NASA Solar Aircraft Sets Altitude Record; Communications and Environmental Breakthroughs Expected, August 14, 2001: <http://www.dfrc.nasa.gov/PAO/PressReleases/2001/01-58.html> (accessed February 2005).
  - 45. Mitlitsky, F., N. J. Colella, B. Myers, and C. J. Anderson, Regenerative Fuel Cells for Solar Powered Aircraft, 28th Intersociety Energy Conversion Engineering Conference (IECEC) (Atlanta, GA, 1993).
  - 46. Mitlitsky, F., N. J. Colella, and B. Myers, Unitized Regenerative Fuel Cells for Solar Rechargeable Aircraft and Zero Emission Vehicles, 1994 Fuel Cell Seminar (San Diego, CA, 1994).
  - 47. Mitlitsky, F., B. Myers, and A. H. Weisberg, Lightweight Pressure Vessels and Unitized Regenerative Fuel Cells, 1996 Fuel Cell Seminar (Orlando, FL, 1996).
  - 48. Mitlitsky, F., A. H. Weisberg, P. H. Carter, B. Myers, and J. T. Kare, Applications of Water Refuelable Spacecraft, Final Report to DARPA/TTO, Agreement No. 99-G527, January 5, 2000.
  - 49. Mitlitsky, F., A. H. Weisberg, P. H. Carter, M. D. Dittman, B. Myers, R. W. Humble, and J. T. Kare, Water Rocket—Electrolysis Propulsion and Fuel Cell Power, AIAA-99-4609, AIAA Space Technology Conference (Albuquerque, NM, September 28–30, 1999).

## Problems

### Problem No. 1:

The average speed and power of an automotive fuel cell system over a 400-km range are 9 m/s and 9 kW, respectively, and the average fuel cell effi-

ciency (LHV) during that ride is 53%. Calculate the amount of hydrogen that has to be stored onboard. What is the corresponding fuel efficiency (in miles per gallon of gasoline equivalent)?

#### Problem No. 2:

A power profile of a 75-kW fuel cell vehicle, and corresponding drive train efficiencies are given in the following table:

Time	Power	Efficiency
3.0%	100.0%	49%
7.0%	50.0%	55%
27.5%	25.0%	57%
27.5%	12.5%	58%
35.0%	0%	

Calculate the average efficiency over such driving schedule for the following two cases:

- a) During idle periods the fuel cell is shut off and does not consume any fuel.
- b) During idle periods the fuel cell is kept running to supply the parasitic load, which is estimated at 2.5 kW. The fuel cell efficiency during that period is 50%.

#### Problem No. 3:

From your home energy bills find the price of electricity and natural gas. Also find information on the heating fuel (electricity, natural gas, or heating oil). Estimate the payback time for a 5-kW fuel cell system that operates with 50% capacity factor and average efficiency of 35% with and without cogeneration (assume total efficiency of 75%). The fuel cell system costs \$4400, including installation. How could the feasibility of this system be improved?

#### Problem No. 4:

A utility company pays \$6 per 1000 cubic feet of natural gas and wants to install a fuel cell to generate electricity during peak hours. The fuel cell costs \$1200 per kW, including installation. The capacity factor will be 33% and the average efficiency also 33%. Assuming a 5-year lifetime with 5% discount rate, estimate what should be the cost of generating electricity (in

\$/kWh). What if the same fuel cell were used as a base load operating with 95% capacity factor and 38% average efficiency?

### Problem No. 5

A 5-kW hydrogen/oxygen fuel cell system is proposed for space application. Hydrogen is stored at 300 bar in the tanks that provide 5% storage density (0.05 kg H<sub>2</sub> per kg of full tank). Assume that oxygen is stored in similar tanks with the same weight/volume ratio. The fuel cell operates at 0.75 V and 1 A/cm<sup>2</sup>. The design factor is 12 kg/m<sup>2</sup>. The efficiency of DC/DC power conversion is 95%. The parasitic power is 400 W. The supporting system weighs 16 kg. Estimate the specific energy (in kWh/kg), and compare it with the best available batteries. How could the specific energy be further improved?

### Problem No. 6

A regenerative fuel cell is installed to provide constant 2-kW power output from a PV array. The fuel cell system efficiency is 50% (LHV) and the electrolyzer system efficiency is 75% (also LHV). The fuel cell operates 12 hours during the night. During the day the PV array provides 2 kW for the load and it runs the electrolyzer. During these 12 hours the electrolyzer operates with 22% capacity factor. Calculate:

- a) The amount of hydrogen to be stored (in kg) and the size of the storage if the electrolyzer is capable of pressurizing hydrogen up to 100 bar.
- b) The power input to the electrolyzer system.
- c) The nominal power of the PV array (assuming 140 W/m<sup>2</sup>); calculate the size of the PV array.

### Quiz

1. An automotive fuel cell system is more efficient than an internal combustion engine at:
  - a) maximum power only
  - b) partial load only
  - c) any load
2. An automobile needs to store approximately:
  - a) 0.5 kg of hydrogen
  - b) 5 kg of hydrogen
  - c) 50 kg of hydrogen

3. One kilogram of hydrogen pressurized at 200 bar takes approximately:
  - a) 6 liters
  - b) 16 liters
  - c) 60 liters
4. A pressurized fuel cell system with a turbine/expander:
  - a) is more efficient than a low-pressure system
  - b) has about same efficiency as a low-pressure system
  - c) is less efficient than a low-pressure system
5. The economics of fuel cells for stationary generation of electricity depends on:
  - a) a difference in price between electricity and natural gas
  - b) a ratio of prices of electricity and natural gas
  - c) price of natural gas only
6. Capacity factor is:
  - a) number of hours a fuel cell system operates divided by 8760 (number of hours in a year)
  - b) a ratio between kilowatthours of electricity produced in a year and kilowatthours that would have been produced if the system operated at full power the entire year
  - c) a ratio between the fuel cell average power and average power required by the load
7. Annual average efficiency of a fuel system:
  - a) is always smaller than the efficiency at nominal power
  - b) is always higher than the efficiency at nominal power
  - c) may be smaller or larger depending on how the system is operated throughout the year
8. What would be the effect of an increase in the price of natural gas on the economics of a fuel cell system that is used in cogeneration (heat and power mode)?
  - a) it will make the fuel cell less economical
  - b) it will make the fuel cell more economical
  - c) it is hard to say; it depends on the ratio of electricity and heat utilization and respective efficiencies
9. The power needed to run an electrolyzer in a regenerative fuel cell with discrete fuel cell and electrolyzer stacks:

- a) is always larger than the nominal fuel cell power
  - b) is always smaller than the nominal fuel cell power
  - c) depends on the required charging time and therefore can be either larger or smaller than the nominal fuel cell power
10. Specific energy of a regenerative fuel cell power system depends on:
- a) efficiency of fuel cell
  - b) efficiency of electrolyzer
  - c) efficiency of both fuel cell and electrolyzer

# CHAPTER 11

## 11. Fuel Cells and Hydrogen Economy

### 11.1. Introduction

PEM fuel cells need hydrogen as fuel. Hydrogen is not a source of energy, and hydrogen is not a readily available fuel. Hydrogen is more like electricity—an intermediary form of energy or an energy carrier. Just like electricity, it can be generated from a variety of energy sources, be delivered to the end users, and at the user end, it can be converted to useful energy efficiently and cleanly. However, although electricity infrastructure is already in place, hydrogen infrastructure is practically nonexistent. It is this lack of hydrogen infrastructure that is considered one of the biggest obstacles to fuel cell commercialization. Commercialization of fuel cells, particularly for transportation and stationary electricity-generation markets, must be accompanied by commercialization of hydrogen energy technologies, that is, technologies for hydrogen production, distribution, and storage. In other words, hydrogen must become a readily available commodity (not as a technical gas but as an energy carrier) before fuel cells can be fully commercialized. On the other hand, it may very well be that the fuel cells will become the driving force for development of hydrogen energy technologies. Fuel cells have many unique properties, such as high energy efficiency, no emissions, no noise, modularity, and potentially low cost, which may make them attractive in many applications even with a limited hydrogen supply. This creates what is often referred to as a “chicken and egg problem”—does the development and commercialization of fuel cells come before development of hydrogen energy technologies or must hydrogen infrastructure be in place before fuel cells can be commercialized?

### 11.2. Transitions in Energy Supply

Many scientists consider hydrogen the fuel of the future in the post-fossil fuel era. When and how hydrogen energy technologies will be commer-

cialized is probably beyond the scope of this book. Nevertheless, some clues may be obtained by looking into the history of energy use and transitions in energy supply.

Figure 11-1 shows the ever-growing global demand for energy, and how it has been met by a variety of energy sources. At present, more than 85% of world energy demand is met by fossil fuels—coal, petroleum, and natural gas [1]. These fuels are readily available and convenient to use. Humankind has learned to exploit them relatively efficiently to satisfy its energy needs. The tremendous economic growth of modern industrialized society has been based on utilization of fossil fuels.

However, energy technologies, particularly those related to fossil fuel extraction, transportation, processing, and end use (which is almost always combustion), have harmful impacts on the environment, which in turn cause direct and indirect adverse effects on the global economy. Those environmental impacts may be on a local level, such as air pollution due to emissions, water and soil pollution due to spills and leaks, or on a regional level because of pollutants dispersion and acid rains, and even on a global level as a result of carbon dioxide accumulation in the atmosphere with threatening consequences such as global warming, climate changes, and rising sea level.

If environmental stress does not force a shift to other, cleaner energy sources and fuels, the finite supply of fossil fuels will mandate such a change eventually. Reserves of fossil fuels are finite—that is an indisputable

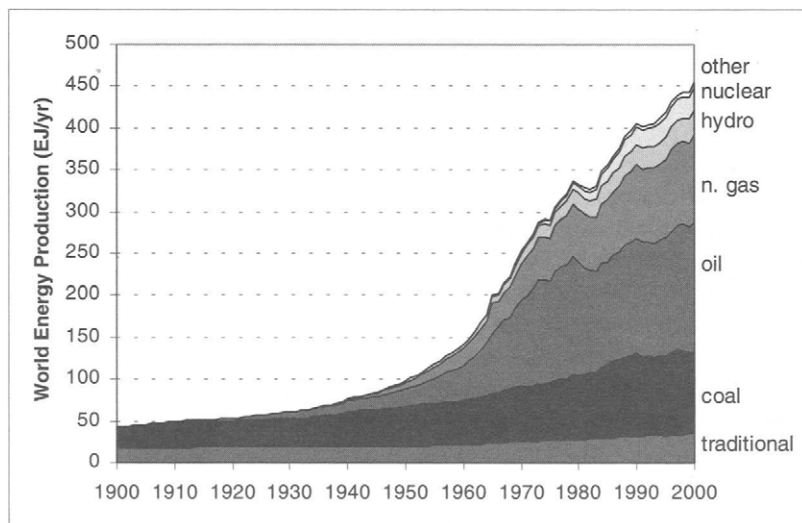


FIGURE 11-1. History of world energy production [1].

fact—yet it is often a subject of vigorous arguments. What is arguable is not whether the reserves are finite, but rather when they will be depleted, or at what level of depletion the global economy will become noticeably affected. Furthermore, the demand for energy will continue to rise because of the continuing increase in world population and the growing demand on energy resources by the developing countries in order to improve their standard of living. Figure 11-2 shows a gap between the energy demand and fossil fuels availability. This gap represents an opportunity for non-fossil fuel energy sources.

The present energy system, based on utilization of fossil fuels, is clearly not in balance with the environment, and therefore cannot be sustainable. It relies on a finite source of stored energy, converts that energy into useful forms primarily through a combustion process, and discharges the products of combustion, such as CO<sub>2</sub> and a myriad of pollutants, into the environment (Figure 11-3). From Figure 11-3 it is obvious that such a system can only run as long as there is enough stored energy or as long as the environment is capable of absorbing pollution, whichever event occurs first.

It is clear that our civilization is facing an unavoidable transition from convenient but environmentally not so friendly, and ultimately scarce

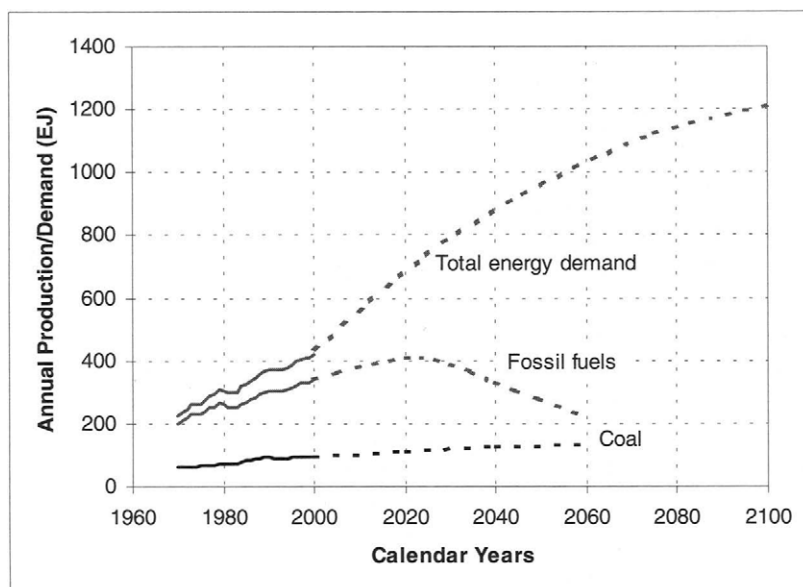


FIGURE 11-2. Projections of energy demand and supply. (Sources: Historical data from [1]; World energy demand forecast from [2]; Fossil fuels and coal forecasts extrapolated from [3] and [4].)

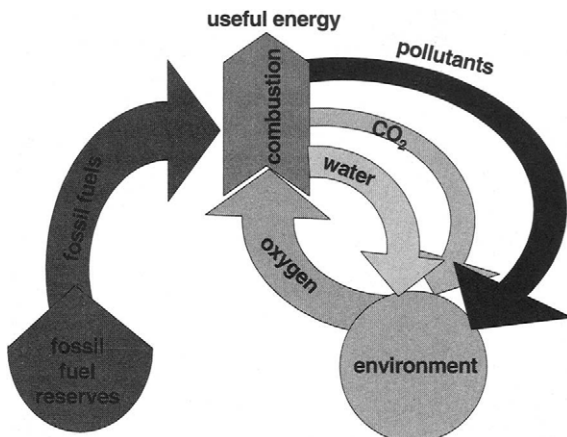


FIGURE 11-3. Present unsustainable energy system.

energy sources to less convenient, but preferably clean and nonexhaustable ones. There are several known energy sources that satisfy cleanliness and abundance requirements, such as direct solar radiation, various forms of indirect solar energy (wind, waves, ocean currents, ocean thermal, biomass), and geothermal, tidal, and nuclear energy. Technologies for utilization of these sources are at various stages of development and their (direct economic) competitiveness with existing energy technologies varies from case to case. Human ingenuity may add new sources to this list in the future.

Regardless of the energy sources of the future, there will always be a need for convenient, clean, safe, efficient, and versatile energy carriers or forms of energy that can be delivered to the end users. One such carrier is electricity, which is already being used worldwide. Electricity is a convenient form of energy—it can be produced from various sources, it can be transported over large distances, it can be distributed to the end users, it is clean (although its production from fossil fuels is not), and at the user end it may be very efficiently used in a variety of applications.

Hydrogen is another clean, efficient, and versatile energy carrier, which supplements electricity very well. Together, these two carriers may be able to satisfy all future energy needs, and form a permanent energy system that would be independent of individual primary energy sources. Hydrogen has some unique properties that make it an ideal energy carrier, namely:

- It can be produced from and converted into electricity at relatively high efficiencies.

- Raw material for hydrogen production is water, which is available in abundance. Hydrogen is a completely renewable fuel, because the product of hydrogen utilization (either through combustion or through electrochemical conversion) is pure water or water vapor.
- It can be stored in gaseous form (convenient for large-scale storage), in liquid form (convenient for air and space transportation), or in the form of metal or chemical hydrides (convenient for surface vehicles and other relatively small-scale storage requirements).
- It can be transported over large distances through pipelines or via tankers (in some cases more efficiently and economically than electricity).
- It can be converted into other forms of energy in more ways and more efficiently than any other fuel, that is, in addition to flame combustion (like any other fuel), hydrogen may be converted through catalytic combustion, electrochemical conversion, and hydriding.
- Hydrogen as an energy carrier is environmentally compatible, because its production from electricity or directly from solar energy, its storage, transportation, and end use do not produce any pollutants (except small amounts of NO<sub>x</sub> if hydrogen is burned with air at high temperatures), greenhouse gases, or any other harmful effects on the environment. Hydrogen itself is not toxic.
- Hydrogen is a relatively safe fuel if handled properly. Several in-depth studies suggest that hydrogen has many properties that make it at least as safe as other fuels used today (gasoline, natural gas, or propane) [5,6]. More on hydrogen safety can be read in the section 11.5. Hydrogen Energy Technologies.

### 11.3. History of Hydrogen as Fuel

The first vision of the energy system based on hydrogen was provided by science fiction writer Jules Verne in his novel *The Mysterious Island* [7]:

Water decomposed into its primitive elements... and decomposed doubtless, by electricity... will one day be employed as fuel, ... hydrogen and oxygen which constitute it, used singly or together, will furnish an inexhaustible source of heat and light, of an intensity of which coal is not capable, ... Water will be the coal of the future.

After investigating the electrochemical process first described by Sir William Grove in 1839, Ostwald in 1894 predicted that the twentieth century would become the Age of Electrochemical Combustion, with the replacement of steam Rankine cycle heat engines by much more efficient, pollution-free fuel cells [8].

In 1923 Haldane predicted that hydrogen—derived from wind power via electrolysis, liquefied, and stored—would be the fuel of the future [9]. This view was repeated in more technical detail, some 15 years later, by Sikorski [10], who realized hydrogen's potential as aviation fuel. He predicted that introduction of hydrogen would bring about a profound transformation of aeronautics.

Lawaczek [11] in the early 1920s outlined the concepts for hydrogen-powered cars, trains, and engines; collaborated in developing of an efficient pressurized electrolyzer; and was probably the first to suggest that energy could be transported via hydrogen-carrying pipelines, similar to natural gas. In the 1920s and 1930s, Erren and his team of engineers converted more than 1000 cars and trucks to multifuel systems using both hydrogen and gasoline as fuel [12].

The concept of a solar-originated hydrogen economy was first set down by Bockris (1962), developed and diagrammed by Justi (1965), named a Hydrogen Economy by Bockris and Triner (1970), formulated by Bockris (1971) and Bockris and Appleby (1972), and quantified by Gregory (1972) and Marchetti (1972) [13].

Bockris proposed a general plan of supplying American cities with solar-based energy via hydrogen. He suggested the use of floating platforms containing photovoltaic devices, producing hydrogen by the electrolysis of seawater, and piping hydrogen to land [14].

A similar concept, but for Japan, called PORSHE (Planned Ocean Raft System for the Hydrogen Economy) was later proposed and elaborated by Ohta [15].

Justi [16] made the first diagram of the solar hydrogen economy. He proposed the thermoelectric conversion of solar energy into hydrogen in the Mediterranean area, and transportation of hydrogen to Germany through a pipeline. He envisioned hydrogen as a fuel for households and industry, large-scale and localized electricity generation and transportation (in electric vehicles).

Bockris and Veziroglu [17] outlined the solar hydrogen energy system and discussed the real economics of potentially competitive energy systems of the future. They showed that if hydrogen utilization efficiency advantage and total fuel costs (*i.e.*, cost of production plus the cost of environmental damage done in every step of the fuel cycle) are taken into account, the solar hydrogen energy system is the most economical energy system possible.

Scott and Hafele [18] addressed the issue of the global climatic disruption caused by excessive use of carbon fuels and concluded that hydrogen energy system is a practical technological pathway that can mitigate and then reverse energy-sector contributions to greenhouse gas climatic disruption, and at the same time bring economic growth and improvements to the quality of life. They provided a vision of the transition to the

hydrogen energy system as two sequential but overlapping waves: integrated energy systems (*i.e.*, the mix of fossil fuel and hydrogen) and neat hydrogen technologies.

Winter feared that the point of transition to hydrogen and solar energy could be another “lost moment of history” [19]. Timely transition to these clean forms of energy would lead toward new direction in development of human civilization, qualitatively and quantitatively different than the path based on utilization of fossil fuels.

#### 11.4. Hydrogen Energy System

Hydrogen is not just a fuel. Hydrogen is a fuel that will allow the imminent transition from fossil fuel economy. The energy system in which hydrogen has a prominent role is often referred to as the Hydrogen Economy (although a title such as Electricity and Hydrogen Economy would be more accurate).

A global energy system in which electricity and hydrogen are produced from available energy sources and used in every application where fossil fuels are being used today—in transportation, residential, commercial, and industrial sectors—is depicted in Figure 11-4. In such a system, electricity and hydrogen are produced in large industrial plants as well as

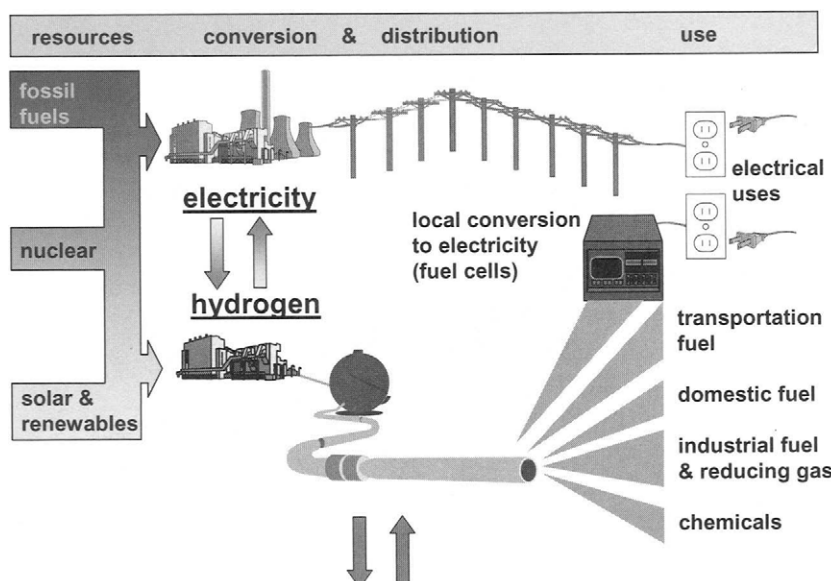


FIGURE 11-4. Hydrogen/electricity energy system.

in small, decentralized units, wherever the primary energy source (solar, nuclear, and even fossil) is available. Electricity is used directly or transformed into hydrogen. For large-scale storage, hydrogen can be stored underground in ex-mines, caverns, or aquifers. Energy transport to the end users, depending on distance and overall economics, is in the form of either electricity or hydrogen. Hydrogen may be transported, by means of pipelines or supertankers. It is then used in transportation, industrial, residential, and commercial sectors as a fuel. Some of it may be used in fuel cells to generate electricity, depending on demand, geographical location, or time of day.

Production of hydrogen from fossil fuels may be justified only in cases where it results in higher efficiency or lower emissions, or where fossil fuels cannot be used at all. These technologies will not help reduce dependency on fossil fuels and will not reduce CO<sub>2</sub> generation. They may be used in a transition period and help in bringing hydrogen to the market cost-effectively and in establishing hydrogen infrastructure.

Full benefits of hydrogen will be realized only in conjunction with renewable energy sources. Both hydrogen and electricity complement the renewable energy sources and allow their indirect utilization in almost every imaginable application. Such a system is in complete balance with the environment, as shown in Figure 11-5, and can run as long as the energy source is available.

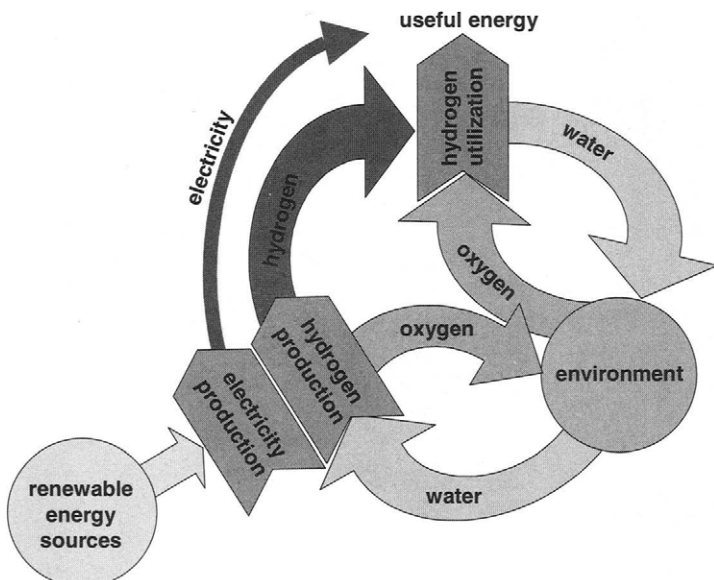


FIGURE 11-5. A sustainable energy system based on renewable energy sources.

## 11.5. Hydrogen Energy Technologies

A hydrogen economy requires technologies for hydrogen production, storage, distribution, and utilization. Most of these technologies have already been developed, although very few of them to a level where they could compete with the existing energy technologies. The following is a brief review of technologies for hydrogen production, storage, and utilization.

### 11.5.1. Technologies for Hydrogen Production

Production of hydrogen requires feedstock (logical sources being hydrocarbon fuels,  $C_xH_y$ , and water,  $H_2O$ ) and energy. The amount of energy required to produce hydrogen is always greater than the energy that can be released by hydrogen utilization.

Presently, hydrogen is mostly being produced from fossil fuels (natural gas, oil, and coal). Hydrogen is used in refineries to upgrade crude oil (hydrotreating and hydrocracking), in the chemical industry to synthesize various chemical compounds (such as ammonia, methanol), and in metallurgical processes (as a reduction or protection gas). The only statistically significant use of hydrogen as a fuel is for the space programs.

Technologies for hydrogen production from fossil fuels have been developed and are used to produce industrial hydrogen. These include steam reforming of natural gas, partial oxidation of hydrocarbons, and coal gasification. Depending on the cost of fuel, hydrogen can be produced for \$6 to \$14 per GJ [20]. However, as mentioned earlier, these technologies will not help reduce dependency on fossil fuels and will not reduce  $CO_2$  generation. The only method that can generate hydrogen from fossil fuels without generation of  $CO_2$  is direct thermal (and catalytic) cracking of hydrocarbons. This method has been used to produce carbon, but for cost-effective hydrogen generation it is in a rather early development phase, barely showing technical feasibility in the labs [21].

Water electrolysis is a mature technology and was developed for hydrogen production capacities ranging from a few  $cm^3/min$  to thousands  $m^3/hr$ . It is relatively efficient (>70%), but because it needs high-quality energy (electricity), hydrogen produced by water electrolysis is expensive (>\$20/GJ). There is also potential to generate relatively inexpensive hydrogen from hydropower and nuclear plants during off-peak hours.

Water electrolysis is particularly suitable for use in conjunction with photovoltaics (PVs). In general, there is a good match between the polarization curves of PVs and electrolyzers, and experience from a handful of PV/electrolysis pilot plants shows that they can be matched directly (with no power-tracking electronics) with relatively high efficiency (>93% coupling efficiency) [22]. Electricity produced from photovoltaics is expensive and hydrogen produced from such electricity is even more expensive. Nevertheless, this technology is mature enough that it could eventually be

used on a large scale for electricity and hydrogen generation. The cost of PV cells in the 1990s did not change significantly in spite of a multifold increase in production volume. Projections from the late 1980s were that the cost could be as low as \$0.2/W<sub>p</sub> [23], but the price of PV modules is still more than \$4/W<sub>p</sub>. It would be prohibitively expensive to generate electricity and hydrogen on a large scale at such prices.

Many other methods for hydrogen production, suitable for coupling with solar or other renewable energy technologies, have been investigated and developed to at least a pilot demonstration stage. These include direct thermal decomposition or thermolysis [24], thermochemical cycles [25], and photolysis (photochemical, photoelectrochemical, and photobiological processes) [26,27]. Unfortunately, all of these processes have severe technical difficulties, many of them have been abandoned, and all of them are far from industrial use.

### 11.5.2. Technologies for Hydrogen Storage

Hydrogen as an energy carrier must be stored to overcome daily and seasonal discrepancies between energy source availability and demand. Hydrogen can be stored either as a pressurized gas or as a liquid. It can also be stored in chemical or physical combinations with other materials, such as metal hydrides, chemical hydrides, glass microspheres, and cryoabsorbers.

*Large underground hydrogen storage* in caverns, aquifers, depleted petroleum and natural gas fields, and man-made caverns resulting from mining and other activities is likely to be technologically and economically feasible [28]. Hydrogen storage systems of the same type and the same energy content as natural gas storage systems will be more expensive by approximately a factor of 3, due to hydrogen's lower volumetric heating value. Technical problems, specifically for the underground storage of hydrogen, other than expected losses of the working gas in the amount of 1–3% per year, are not anticipated. In fact, there are several instances of hydrogen being kept in large underground storages. The city of Kiel's public utility has been storing town gas with a hydrogen content of 60–65% in a gas cavern with a geometric volume of about 32,000 m<sup>3</sup> and a pressure of 80 to 160 bar at a depth of 1330 m since 1971 [29]. Gaz de France, the French National Gas Company, has stored hydrogen-rich refinery by-product gases in an aquifer structure near Beynes, France. Imperial Chemical Industries of Great Britain stores its hydrogen in the salt mine caverns near Teeside, United Kingdom [30].

*Aboveground pressurized gas storage systems* are used today in natural gas business in various sizes and pressure ranges, from standard pressure cylinders (50 l, 200 bar) to stationary high-pressure containers (>200 bar) or low-pressure spherical containers (>30,000 m<sup>3</sup>, 12 to 16 bar). This application range may be similar for hydrogen storage.

Vehicular pressurized hydrogen tanks made of ultralight but strong new composite materials that allow pressures in excess of 200 bars have been developed and used in prototype automobiles and buses. Storage density of above 0.05 kg of hydrogen per 1 kg of total weight is easily achievable [31]. However, storage of hydrogen as compressed gas results in relatively large tanks, that is, ~60 liters/kg H<sub>2</sub> at 200 bars and ~35 liters/kg H<sub>2</sub> at 400 bars.

Liquid hydrogen storage: Production of liquid hydrogen or liquefaction is an energy-intensive process, typically requiring amounts of energy equal to about one-third of the energy in liquefied hydrogen. Hydrogen liquefaction and use of liquid hydrogen is usually practiced only where achieving high storage density is absolutely essential, such as in aerospace applications. Some prototype hydrogen-powered automobiles also use specially developed liquid hydrogen tanks [32].

Metal hydride storage: Hydrogen can form metal hydrides with some metals and alloys. During the formation of the metal hydride, hydrogen molecules are split and hydrogen atoms are inserted in spaces inside the lattice of suitable metals or alloys. In such a way, an effective storage is created comparable to the density of liquid hydrogen. However, when the mass of the metal or alloy is taken into account, then the metal hydride gravimetric storage density is comparable to storage of pressurized hydrogen. The best achievable gravimetric storage density is about 0.07 kg of H<sub>2</sub>/kg of metal, for a high temperature hydride such as MgH<sub>2</sub>. During the storage process (charging or absorption) heat is released, which must be removed in order to achieve the continuity of the reaction. During the hydrogen release process (discharging or desorption), heat must be supplied to the storage tank. An advantage of storing hydrogen in hydriding substances is the safety aspect. A serious damage to a hydride tank (e.g., collision) would not pose a fire hazard because hydrogen would remain in the metal structure.

Novel hydrogen storage methods: Several novel hydrogen storage methods are being investigated that offer potential for higher energy densities than the conventional methods listed earlier. These include hydrogen storage in activated carbon at cryogenic temperatures and elevated pressures [33], storage in carbon nanotubes [34,35], storage in glass microspheres [36], or storage in polyhydride chemical complexes [37]. Although some of these methods are very promising, none has been demonstrated to date on a level that would guarantee acceptable practicality, cost, or safety.

### 11.5.3. Technologies for Hydrogen Utilization

Technologies for hydrogen conversion into other useful energy forms have already been developed and demonstrated. In almost all cases hydrogen is converted more efficiently than any other fuel, and more important, hydro-

gen conversion creates little or no emissions (mainly water or water vapor). These technologies are the driving force for development of technologies for hydrogen production and storage.

*Combustion of hydrogen in internal combustion engines and turbines:*

Hydrogen is a very good fuel for internal combustion engines. Hydrogen-powered internal combustion engines are on average about 20% more efficient than comparable gasoline engines. The thermal efficiency of an engine can be improved by increasing either the compression ratio or the specific heat ratio. In hydrogen engines both ratios are higher than in a comparable gasoline engine because of hydrogen's lower self-ignition temperature and ability to burn in lean mixtures. However, the use of hydrogen in internal combustion engines results in ~15% loss of power due to lower energy content in a stoichiometric mixture in the engine's cylinder. The power output of a hydrogen engine can be improved by using advanced fuel-injection techniques or liquid hydrogen [38].

One of the most important advantages of hydrogen as a fuel for internal combustion engines is that hydrogen engines emit far fewer and far less pollutants than comparable gasoline engines. Basically, the only products of hydrogen combustion in air are water vapor and small amounts of nitrogen oxides. However, the emissions of  $\text{NO}_x$  in hydrogen engines are typically one order of magnitude smaller than emissions from comparable gasoline engines. Small amounts of unburned hydrocarbons,  $\text{CO}_2$ , and CO have been detected in hydrogen engines due to lubrication oil [38].

Hydrogen use in turbines and jet engines is similar to that of conventional jet fuel. The use of hydrogen avoids problems of sediments and corrosion on turbine blades, and therefore it prolongs life and reduces maintenance. Gas inlet temperatures can be pushed beyond normal gas turbine temperatures of 800°C, thus increasing the overall efficiency. The only pollutants resulting from the use of hydrogen in turbines and jet engines are nitrogen oxides.

*Direct steam generation by hydrogen/oxygen combustion:* Hydrogen combusted with pure oxygen results in pure steam, that is,  $2\text{H}_2 + \text{O}_2 \rightarrow 2\text{H}_2\text{O}$ . This reaction would develop temperatures in the flame zone above 3000°C; therefore, additional water has to be injected so that the steam temperature can be regulated at a desired level. Both saturated and superheated vapor can be produced. The German Aerospace Research Establishment (DLR) has developed a compact hydrogen/oxygen steam generator [39]. Such a device is close to 100% efficient, because there are no emissions other than steam and little or no thermal losses. It can be used to generate steam for spinning reserve in power plants, for peak load electricity generation, in industrial steam supply networks, and as a micro steam generator in medical technology and biotechnology.

*Catalytic combustion of hydrogen:* Hydrogen and oxygen in the presence of a suitable catalyst may be combined at temperatures significantly lower than flame combustion (from ambient to 500°C). Catalytic burners

require considerably more surface area than conventional flame burners. Therefore, the catalyst is typically dispersed in a porous structure. The reaction rate and resulting temperature are easily controlled by regulating the hydrogen flow rate. The only product of catalytic combustion of hydrogen is water vapor. Because of low temperatures, there are no nitrogen oxides formed. The device is inherently safe because the reaction cannot migrate into the hydrogen supply, because there is no flame and hydrogen concentration is above the higher flammable limit (75%). Possible applications of catalytic burners are in household appliances such as cooking ranges and space heaters. Fraunhofer Institute for Solar Energy Systems, Germany, has developed and demonstrated several household appliances using catalytic burners [40].

*Electrochemical electricity generation (fuel cells):* Fuel cells are one of the most attractive and most promising hydrogen technologies. In a fuel cell, hydrogen combines with oxygen without combustion in an electrochemical reaction and produces direct current (DC) electricity. Depending on the type of the electrolyte used, there are several types of fuel cells. Alkaline fuel cells have been used in the space program (Apollo and Space Shuttle) since the 1960s. Phosphoric acid fuel cells are already commercially available in container packages for stationary electricity generation. PEM fuel cells are a serious candidate for automotive applications, but also for small-scale distributed stationary power generation, backup power, and portable power generation, as described in Chapter 10. High-temperature fuel cells, such as molten carbonate and solid oxide fuel cells, have been developed to a precommercial/demonstration stage for stationary power generation.

*Metal hydrides applications:* Hydrogen's ability to form metal hydrides may be used not only for hydrogen storage but also for various energy conversions. When a hydride is formed by the chemical combination of hydrogen with a metal, an element, or an alloy, heat is generated, that is, the process is exothermic. Conversely, in order to release hydrogen from a metal hydride, heat must be supplied. The heat generated during the charging process and the heat needed for discharging are functions of the hydriding substance, the hydrogen pressure, and the temperature at which the heat is supplied or extracted. Using different metals and by forming different alloys, different hydriding characteristics can be obtained. In other words, it is possible to make or to find hydriding substances, which are more suitable for a given application, such as refrigeration, compression, pumping, waste heat storage, electricity generation, hydrogen purification, and isotope separation. However, most of these technologies are far from commercial applications.

#### 11.5.4. Safety Aspects of Hydrogen as Fuel

Like any other fuel or energy carrier, hydrogen poses risks if not properly handled or controlled. The risk of hydrogen, therefore, must be considered

relative to the common fuels such as gasoline, propane, or natural gas. The specific physical characteristics of hydrogen are quite different from those common fuels. Some of these properties make hydrogen potentially less hazardous, whereas other hydrogen characteristics could theoretically make it more dangerous in certain situations. Table 9-1 shows relevant hydrogen properties, and Figure 11-6 compares hydrogen properties with other fuels and ranks their effect on safety.

Nevertheless, hydrogen's safety record has been unjustly tainted by the Hindenburg accident and the hydrogen bomb, although the former is essentially a proof of how safe hydrogen is, and the latter has nothing to do with either gaseous or liquid hydrogen use as fuel. Careful investigation of the Hindenburg disaster proved that it was the flammable aluminum powder-filled paint varnish that coated the infamous airship, not the hydrogen, that started the fire [41]. The hydrogen that the airship was filled with caught on fire considerably after the Hindenburg's surface skin started to burn and was over in less than 1 minute. The flames from hydrogen combustion traveled upward, far away from the crew and passengers in the cabins below. What fell to the ground with the passengers were burning shrouds from the exterior fabric, a large inventory of diesel fuel, and combustible materials that were in the cabins. Thirty-three persons were killed in the Hindenburg fire; however, 62 persons lived through the disaster by

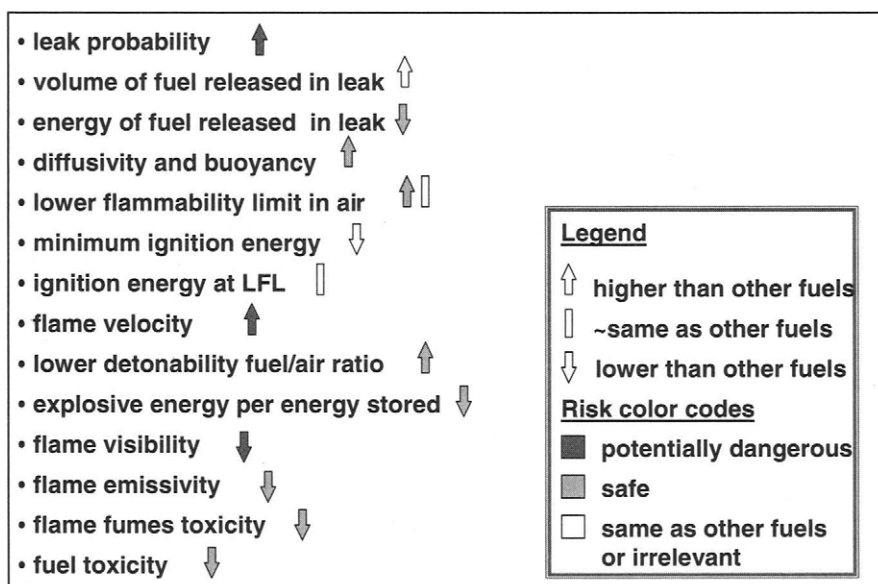


FIGURE 11-6. Summary of hydrogen safety related properties compared with other fuels.

being fortunate enough to ride the Hindenburg down and escape the flames and wreckage that fell to the ground.

Because hydrogen has the smallest molecule, it has a greater tendency to escape through small openings than other liquid or gaseous fuels. Based on properties of hydrogen such as density, viscosity, and its diffusion coefficient in air, the propensity of hydrogen to leak through holes or joints of low pressure fuel lines may be only 1.26 to 2.8 times faster than a natural gas leak through the same hole (and not 3.8 times faster as frequently assumed based solely on diffusion coefficients). Experiments have indicated that most leaks from residential natural gas lines are laminar [5]. Because natural gas has energy density per unit volume over 3 times higher than hydrogen, the natural gas leak would result in more energy release than a hydrogen leak.

For very large leaks from high-pressure storage tanks, the leak rate is limited by sonic velocity. Because of a higher sonic velocity (1308 m/s), hydrogen would initially escape much faster than natural gas (sonic velocity of natural gas is 449 m/s). Again, because natural gas has more than 3 times the energy density of hydrogen, a natural gas leak will always contain more energy.

If a leak should occur for whatever reason, hydrogen will disperse much faster than any other fuel, thus reducing the hazard levels. Hydrogen is both more buoyant and more diffusive than gasoline, propane, or natural gas. Table 11-1 compares some properties and leak rates for hydrogen and natural gas [5].

Hydrogen/air mixture can burn in relatively wide volume ratios, between 4% and 75% of hydrogen in air. Other fuels have much lower flammability ranges, viz., natural gas 5.3–15%, propane 2.1–10%, and gasoline 1–7.8%. However, this range has little practical value. In many actual leak situations the key parameter that determines if a leak would ignite is the

TABLE 11-1  
Properties and Leak Rates of Hydrogen and Natural Gas [5]

	<i>Hydrogen</i>	<i>Natural Gas</i>
Flow parameters		
Diffusion coef. (cm <sup>2</sup> /s)	0.61	0.16
Viscosity ( $\mu$ -poise)	87.5	100
Density (kg/m <sup>3</sup> )	0.0838	0.651
Sonic velocity(m/s)	1308	449
Relative leak rates		
Diffusion	3.80	1
Laminar flow	1.23	1
Turbulent flow	2.83	1
Sonic flow	2.91	1

lower flammability limit, and hydrogen's lower flammability limit is 4 times higher than that of gasoline, 1.9 times higher than that of propane, and slightly lower than that of natural gas.

Hydrogen has a very low ignition energy (0.02 mJ), about one order of magnitude lower than other fuels. Ignition energy is a function of the fuel/air ratio, and for hydrogen it reaches a minimum at about 25–30% hydrogen content in air. At the lower flammability limit, hydrogen ignition energy is comparable to that of natural gas [6].

Hydrogen has a flame velocity 7 times faster than that of natural gas or gasoline. A hydrogen flame would therefore be more likely to progress to a deflagration or even a detonation than other fuels. However, the likelihood of a detonation depends in a complex manner on the exact fuel/air ratio, the temperature, and particularly the geometry of the confined space. Hydrogen detonation in open atmosphere is highly unlikely.

The lower detonability fuel/air ratio for hydrogen is 13–18%, which is two times higher than that of natural gas and 12 times higher than that of gasoline. Because the lower flammability limit is 4%, an explosion is possible only under the most unusual scenarios, for example, hydrogen would first have to accumulate and reach 13% concentration in a closed space without ignition, and at that point an ignition source would have to be triggered.

Should an explosion occur, hydrogen has the lowest explosive energy per unit of stored energy of any fuel, and a given volume of hydrogen would have 22 times less explosive energy than the same volume filled with gasoline vapor.

Hydrogen flame is nearly invisible, which may be dangerous, because people in the vicinity of a hydrogen flame may not even realize there is a fire. This may be remedied by adding chemicals that will provide the necessary luminosity. The low emissivity of hydrogen flames means that nearby materials and people will be much less likely to ignite or be hurt by radiant heat transfer. The fumes and soot from a gasoline fire pose a risk to anyone inhaling the smoke, whereas hydrogen fires produce only water vapor (unless secondary materials begin to burn).

Liquid hydrogen presents another set of safety issues, such as risk of cold burns, and the increased duration of leaked cryogenic fuel. A large spill of liquid hydrogen has some characteristics of a gasoline spill; however, it will dissipate much faster. Another potential danger is a violent explosion of a boiling liquid expanding vapor in case of a pressure relief valve failure.

Hydrogen onboard a vehicle may pose a safety hazard. Such hazards should be considered in situations when the vehicle is inoperable, when the vehicle is in normal operation, and in collisions. Usually, potential hazards are due to fire, explosion, or toxicity. The latter can be ignored, because neither hydrogen nor its fumes in case of fire are toxic. Hydrogen as a source of fire or explosion may come from the fuel storage, from the fuel supply lines, or from the fuel cell itself. The fuel cell poses the least

hazard, although in a fuel cell hydrogen and oxygen are separated by a very thin (~20–30 µm) polymer membrane. In case of membrane rupture hydrogen and oxygen would combine, and the fuel cell would immediately lose its potential, which should be easily detected by a control system. In such a case the supply lines would be immediately disconnected. The fuel cell operating temperature (60–90°C) is too low to be a thermal ignition source; however, hydrogen and oxygen may combine on the catalyst surface and create ignition conditions. Nevertheless, the potential damage would be limited because of a small amount of hydrogen present in the fuel cell and fuel supply lines.

The largest amount of hydrogen at any given time is present in the tank. Several tank failure modes may be considered in both normal operation and collision, such as:

- a catastrophic rupture, due to a manufacturing defect in the tank, a defect caused by abusive handling of the tank or a stress fracture, a puncture by a sharp object, or external fire combined with failure of a pressure relief device to open;
- a massive leak, due to a faulty pressure relief device tripping without cause or a chemically induced fault in the tank wall; a puncture by a sharp object, or operation of a pressure relief device in case of a fire (which is exactly the purpose of the device); and
- a slow leak due to stress cracks in the tank liner, a faulty pressure relief device, or faulty coupling from the tank to the feed line, or impact-induced openings in the fuel line connection.

In a study conducted on behalf of Ford Motor Company, Directed Technologies, Inc. has performed a detailed assessment of probabilities of the abovementioned failure modes [6]. The conclusion of the study is that a catastrophic rupture is a highly unlikely event. However, several failure modes resulting in a large hydrogen release or a slow leak have been identified both in normal operation and in collisions.

Most of the failure modes discussed previously may either be avoided or have their occurrence and consequences minimized by:

- leak prevention through proper system design, selection of adequate equipment (some further testing and investigation may be required), allowing for tolerance to shocks and vibrations, locating a pressure relief device vent, protecting the high-pressure lines, installing a normally closed solenoid valve on each tank feed line, and so on;
- leak detection either by a leak detector or by adding an odorant to the hydrogen fuel (this may be a problem for fuel cells); and
- ignition prevention, through automatically disconnecting battery bank, thus eliminating a source of electrical sparks which are the

cause of 85% gasoline fires after a collision, by designing the fuel supply lines so that they are physically separated from all electrical devices, batteries, motors, and wires to the maximum extent possible, and by designing the system for both active and passive ventilation (such as an opening to allow the hydrogen to escape upward).

Risk is typically defined as a product of probability of occurrence and consequences. The abovementioned study by Directed Technologies, Inc. [6] includes a detailed risk assessment of the several most probable or most severe hydrogen accident scenarios, such as:

- fuel tank fire or explosion in unconfined spaces,
- fuel tank fire or explosion in tunnels,
- fuel line leaks in unconfined spaces,
- fuel leak in a garage,
- refueling station accidents.

The conclusion of this study is that in a collision in open spaces, a safety-engineered hydrogen fuel cell car should have less potential hazard than either a natural gas or gasoline vehicle. In a tunnel collision, a hydrogen fuel cell vehicle should be nearly as safe as a natural gas vehicle, and both should be potentially less hazardous than a gasoline or propane vehicle, based on computer simulations comparing substantial postcollision release of gasoline and natural gas in a tunnel. The greatest potential risk to the public appears to be a slow leak in an enclosed home garage, where an accumulation of hydrogen could lead to fire or explosion if no hydrogen-detection or risk-mitigation devices or measures are applied (such as passive or active ventilation).

In conclusion, hydrogen appears to pose risks of the same order of magnitude as other fuels. In spite of public perception, in many aspects hydrogen is actually a safer fuel than gasoline and natural gas.

## **11.6. Predicting the Future**

As discussed earlier, hydrogen is considered a fuel that will make a transition from fossil fuels possible. When will this transition happen? Is it imminent? Hydrogen technologies seem to be technically feasible. When will they become economically feasible? To answer these questions, we would have to take a peek at the future.

Predicting the future is, of course, impossible. However, all systems behave in accordance with established laws of physics, and if enough information is available, their future behavior may be predicted, at least to some extent. For example, if we throw a ball in the air, we can with great cer-

tainty predict that the ball will initially go up, reach its peak, and then come back down. If we want to predict how high the ball will fly and when and where it will fall down, more information is needed.

All systems in nature require energy. Their behavior, therefore, may be studied and predicted based on their energy use and available energy resources. The same applies to the global economy. As mentioned before, the tremendous economic growth of modern industrialized society has been based on utilization of fossil fuels, a convenient and concentrated form of energy. Although all economic models are based on growth, from a thermodynamic point of view it is clear that no system based on finite energy sources can continue to grow forever. Such a system does go through exponential growth during periods when the resources are plentiful, but eventually reaches its peak and then declines as the resources become depleted, as shown in Figure 11-7. If we want to calculate how high the peak will be and when it will happen, much more information about the system and its energy use would be needed. The diagram in Figure 11-7 and accompanying equations are based on Odum's energy language [42–44], originally developed to describe energy flows in ecological systems, but subsequently applied to any complex system, including human economic systems on a global, national, or regional scale.

A system based on utilization of a constant flow of incoming energy (such as solar energy) behaves differently. It does not go through a peak, but continues to grow and eventually it reaches a steady state (Figure 11-8). The rate of growth and the steady state level, which a system can obtain, depend on the rate of utilization of available solar energy and the effort required to convert solar energy into more useful forms of energy (hydrogen and electricity being only the intermediary steps, *i.e.*, energy carriers).

Human civilization is actually a system that is based on both renewable and nonrenewable energy sources (Figure 11-9). The renewable energy

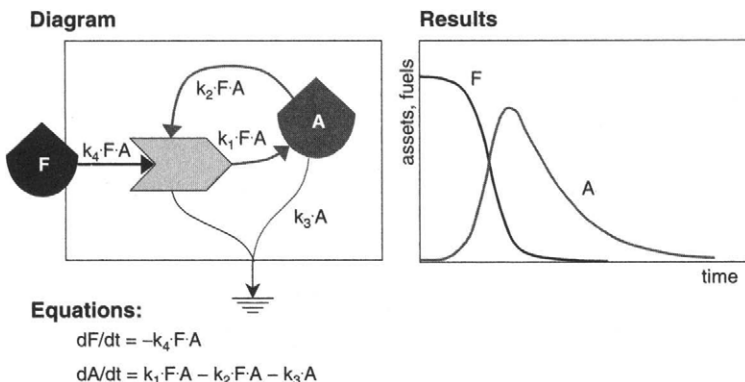


FIGURE 11-7. A simple model of a system based on nonrenewable energy sources.

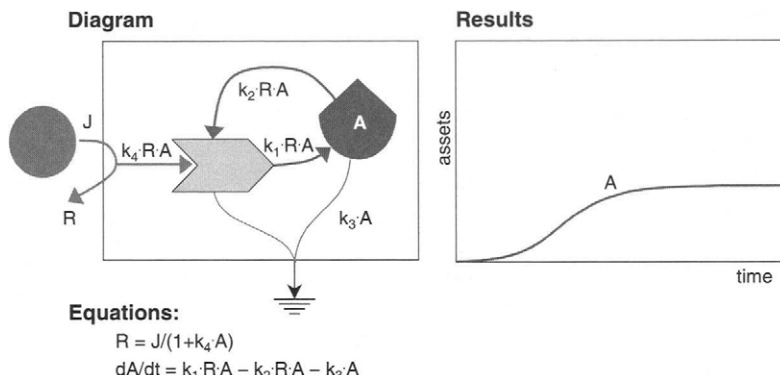


FIGURE 11-8. A simple model of a system based on a constant flow (renewable) energy source.

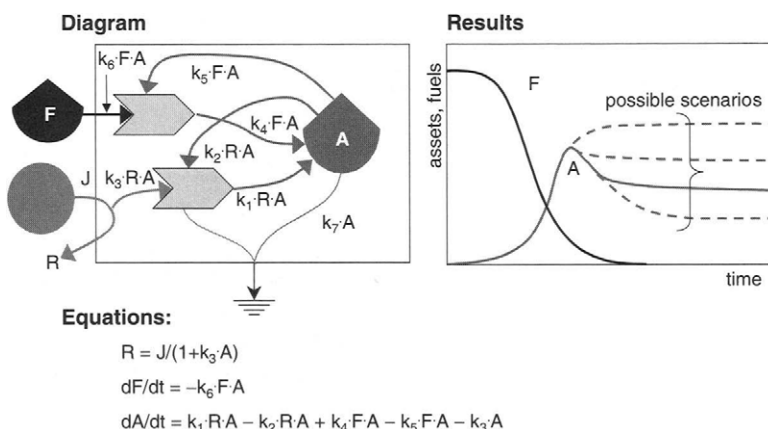


FIGURE 11-9. A simple model of a system based on renewable and nonrenewable energy sources.

sources could have never provided the growth enabled by the use of fossil fuels. The problem is that the finite reserves of fossil fuels cannot perpetuate this growth indefinitely. What cannot be predicted by such a simple model is at which level the system would reach a steady state after the nonrenewable, stored energy has been depleted. The steady state level depends on the effort required to convert renewable energy into more useful forms of energy, that is, net energy gain from renewable energy sources.

Various modeling studies, such as those conducted by an MIT team [45,46], indicate that the global economy will peak sometime in the first

half of the twenty-first century, and after that will continue to decline. The main reasons for that would be environmental stress and depletion of natural resources (including fluid fossil fuels). A modeling study conducted at the University of Miami [2] has come up with similar results, although using a different method. Both studies, however, concluded that it would be possible to reverse the negative trends by timely introduction of clean, new technologies that will ease, and actually reverse the burden on the environment, and that will not depend on exhaustible natural resources. Although the MIT study was not specific about those technologies, the University of Miami researchers have identified hydrogen economy based on renewable energy sources as a solution to global economic and environmental problems [2]. This study indicated that the timing and the rate of introduction of a new energy system might be critical. As shown in Figures 11-10 and 11-11, early introduction of the solar hydrogen energy system will have long-term beneficial effects on both the global economy and the environment. If this transition starts when the economy begins to decline, it may be too late to reverse the trend, because the economy would no longer be able to afford investing in a long-term project such as establishing a new energy system.

Historically, in the context of a longer time span, the fossil fuels era may well be considered just a short interlude between the solar past and the solar future. In that short period (about 300 years) fossil fuels made possible a tremendous development of human civilization. If fossil fuels are used to support the establishment of a permanent energy system such as the solar hydrogen energy system, they could be considered a spark that provided a transition from the low-level solar energy past to the higher-

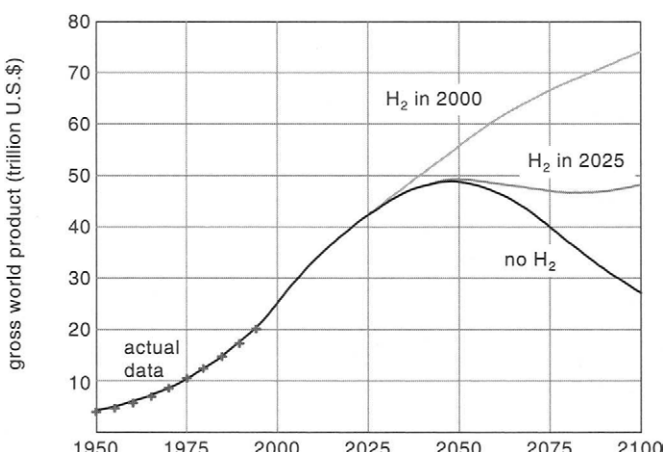


FIGURE 11-10. Effect of timeliness of transition to hydrogen energy system on global economy (1990 US \$) [2].

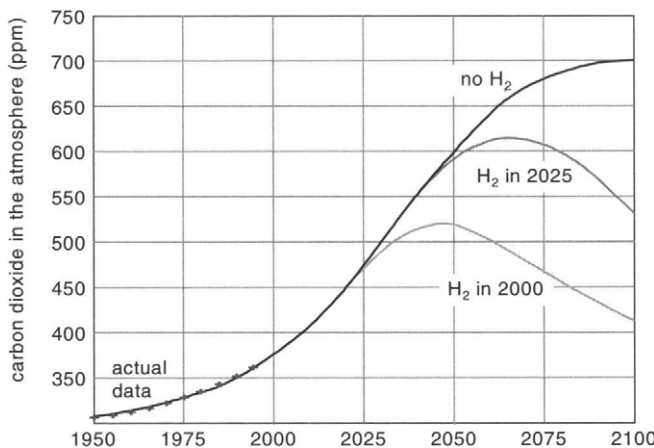


FIGURE 11-11. Effect of timeliness of transition to hydrogen energy system on CO<sub>2</sub> concentration in the atmosphere [2].

level solar energy future. Solar energy is steadily available in quantity that exceeds human needs by several orders of magnitude. However, solar energy (both direct and indirect) is so dispersed that it requires a lot of effort (high-quality energy) to convert it to usable energy forms. The rate at which renewable energy can support the growth of the economy and the eventual steady state depends on the magnitude of efforts required to harvest it and present it to the end users. In economic terms this is equivalent to the cost of energy at the user end. More studies are required to determine the net energy gain of solar electricity and solar hydrogen technologies.

## 11.7. Transition to Hydrogen Economy

A transition from convenient but environmentally not so friendly, and ultimately scarce energy sources (fossil fuels) to less convenient, but clean and nonexhaustable ones (renewable energy sources) seems to be imminent. Hydrogen may play a significant role in this transition by allowing renewable energy sources to be used in virtually any application.

Replacement of a global energy system will not and cannot happen overnight. There is an enormous capital tied in the existing energy system. Building another energy system that would compete with the existing one is out of the question. The new energy system must gradually replace the existing one. Because businesses are too often concerned with short-term profits, governments and international organizations must realize the long-term benefits of the hydrogen energy system and support the transition both legislatively and financially. Introduction of "real economics" and

elimination of subsidies for the existing energy system would help in that transition. The term "real economics" refers to economics that takes into account past, present, and future environmental damage, associated with use of particular energy source or fuel, depletion of environmental resources, military expenses for keeping energy resources accessible, and other hidden external costs.

The most difficult would be the initial penetration of hydrogen energy technologies in the existing energy markets. First, hydrogen as fuel cannot compete in today's market with the very fuels it is produced from (including electricity). Also, as with any new technology, hydrogen energy technologies, such as fuel cells, are in most cases initially more expensive than the existing mature technologies, even when real economics is applied. Hydrogen energy technologies are expensive because the equipment for hydrogen production and utilization is not mass-produced. It is not mass-produced because there is no demand for it, and there is no demand because it is too expensive. This is a closed circle, or another chicken-and-egg problem. The only way for hydrogen energy technologies to penetrate into the major energy markets is to start with those technologies that may have niche markets, where the competition with the existing technologies is not as fierce or where they offer clear advantage over the existing technologies regardless of the price. Another push for commercialization may be gained through governmental or international subsidies for technologies that offer some clear advantages. Once developed, these technologies may help reduce the cost of other related hydrogen technologies, and initiate and accelerate their widespread market penetrations. One example is fuel cell buses in major third-world cities, where hydrogen can be produced from clean and renewable energy sources. These buses replace heavy-polluting diesel buses in regular service, and the difference in price between a fuel cell bus and a regular bus is covered by the World Bank's Global Environment Facility.

Another major difficulty is interrelation and interdependence between hydrogen technologies. For example, it is extremely difficult if not impossible to introduce hydrogen-powered automobiles or hydrogen-powered airplanes into the market without reliable and economically feasible technologies for hydrogen production, distribution, storage, and refueling. On the other hand, significant development of hydrogen production, distribution, and storage technologies will never happen without a large demand for hydrogen.

## **11.8. Coming Energy Revolution?**

Recent history of human civilization is characterized by technological revolutions (Figure 11-12). The industrial revolution started with the invention of the steam engine, which allowed utilization of coal and

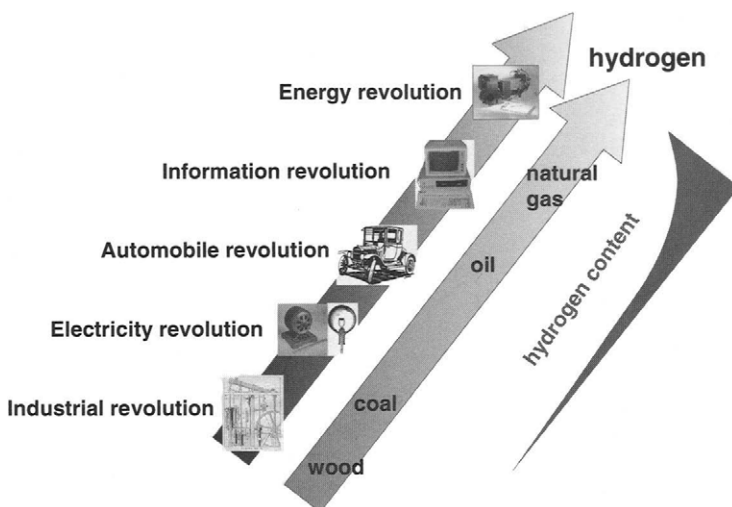


FIGURE 11-12. History of technological revolutions and history of fuels.

revolutionized manufacturing with a profound effect on economic and social systems. The electricity revolution brought convenient energy to almost every home and allowed the development of many electrical devices and gadgets, which in turn caused remarkable changes in lifestyle. The automobile revolution started with Ford's mass-manufactured, affordable Model T automobile. Automobiles changed city layout, and the way of living. Most recently, the information revolution, which is still ongoing, started with the invention of computers. Although originally invented for computing only, computers are now being used in everyday life for storing and disseminating information, communication, entertainment, art, and so forth. In a short time, life without a computer has become unimaginable.

What is common to all of these revolutions is that each started with a technological invention so powerful that it made changes in everyday life, and allowed development of new products and services unimaginable before its implementation. The fuel cell is likely one of those powerful technologies that could create the next revolution—the energy revolution. It will change the way energy is converted to useful power. It will allow greater utilization of renewable energy sources, it will promote rational use of energy, it will decentralize power generation, and it will allow power generation at various scales, while at the same time without harming the environment.

At the same timescale, it should be noted that different fuels have been used alongside the technological revolutions. Before the industrial revolution, the main fuels were wood and other traditional forms of energy.

With the coming of the industrial revolution, coal became the main fuel for more than a century until it was replaced by oil, the main energy source that fueled the automobile revolution. In recent years, natural gas has become more and more significant. The trend is clear—each fuel has been substituted by a fuel with higher hydrogen to carbon ratio. Whereas wood is primarily carbon, coal has the ratio of hydrogen to carbon ~1:1, oil or gasoline ~2:1, and natural gas 4:1. Therefore, it can be extrapolated that the logical choice for an ultimate fuel is pure hydrogen—the fuel of the energy revolution.

## 11.9. Conclusions

- Transition from the fossil fuel-based energy system seems to be inevitable, due to depletion of liquid fossil fuels (oil and natural gas), and due to environmental concerns.
- Hydrogen and electricity are the most probable energy carriers of the future, because they can be produced from any energy source, and they are clean and versatile. Produced from renewable energy sources, they result in a permanent energy system.
- Hydrogen technologies, that is, technologies for hydrogen production, storage, and utilization, have been developed. Although these technologies are not mature, there are no major technological obstacles for widespread utilization of hydrogen.
- Transition to a hydrogen energy system will be difficult for a variety of reasons, such as competition with an established infrastructure, lack of policies favoring “real” economics, interdependence of hydrogen technologies, dependency on the renewable energy technologies, and so forth.
- More analyses of solar hydrogen and solar electricity net energy gain are required.
- Fuel cells may be the first hydrogen technologies commercialized on a large scale, with applications ranging from power generation to transportation. This technology has a potential to revolutionize the energy business.

## References

1. Energy Information Administration, *International Energy Annual 2001* (DOE/EIA-0219, 2001, Washington D.C., 2003).
2. Barbir, F., H. J. Plass, Jr., and T. N. Veziroglu, Modeling of Hydrogen Penetration in the Energy Market, *International Journal of Hydrogen Energy*, Vol. 18, No. 3, 1993, pp. 187–195.
3. Energy Information Administration, *System for the Analysis of Global Energy Markets* (DOE/EIA, Washington D.C., 2003).

4. Campbell, C. J. and J. H. Laherrere, The End of Cheap Oil, *Scientific American*, March 1998.
5. Swain, M. R. and M. N. Swain, A Comparison of H<sub>2</sub>, CH<sub>4</sub>, and C<sub>3</sub>H<sub>8</sub> Fuel Leakage in Residential Settings, *International Journal of Hydrogen Energy*, Vol. 17, No. 10, 1992, pp. 807–815.
6. Thomas, C. E., Hydrogen Vehicle Safety Report, prepared by Directed Technologies, Inc. for Ford Motor Company, Contract No. DE-AC02-94CE50389 (U.S. Department of Energy, Washington, D.C., 1996).
7. Verne, J., *The Mysterious Island* (Airmont Publishing Company, New York, 1965).
8. Ostwald, W. Z., *Elektrochemie*, Vol. 1, p. 122, 1894. Cited by A. J. Appleby, From Sir William Grove to Today: Fuel Cells and the Future, lecture at the Grove Anniversary Fuel Cell Symposium (The Royal Institution, London, 1989).
9. Haldane, J.B.S., *Daedalus or Science and the Future* (Kega, Paul, Trench, Truber and Company, Ltd., London, 1923).
10. Sikorsky, I. I., *Science and the Future of Aviation*, Steinmitz Memorial Lectures (Schenectady Section, A.I.E.E., 1938).
11. Lawaczek, F., *Technik und Wirtschaft im Dritten Reich* (Eher Verlag, Munich, 1932).
12. Erren, R. A. and W. H. Compell, Hydrogen: A Commercial Fuel for Internal Combustion Engines and Other Purposes, *Journal of the Institute of Fuels*, Vol. 6, No. 29, 1933.
13. Bockris, J. O'M., *Energy: The Solar-Hydrogen Alternative* (Australia and New Zealand Book Co., Sydney, 1975).
14. Bockris, J. O'M., Memorandum to Westinghouse Company (C. Zenner, 1962).
15. Escher, W.J.D. and T. Ohta. Direct Solar Energy Conversion at Sea, in T. Ohta (editor), *Solar-Hydrogen Energy Systems* (Pergamon Press, Oxford, 1979), pp. 225–248.
16. Justi, E., *Conduction Mechanisms and Energy Transformation in Solids* (Verlag Vandenhoeck and Ruprecht, Göttingen, 1965).
17. Bockris, J. O'M. and T. N. Veziroglu, A Solar-Hydrogen Energy System for Environmental Compatibility, *Environmental Conservation*, Vol. 12, No. 2, 1985, pp. 105–118.
18. Scott, D. S. and W. Hafele, The Coming Hydrogen Age: Preventing World Climatic Disruption, *International Journal of Hydrogen Energy*, Vol. 15, No. 10, 1990, pp. 727–738.
19. Winter, C.-J., Hydrogen and Solar Energy—Ultima Ratio Avoiding a “Lost Moment in the History of Energy,” in T. N. Veziroglu and P. K. Takahashi (editors), *Hydrogen Energy Progress VIII*, Vol. 1 (Pergamon Press, New York, 1990), pp. 3–47.
20. Steinberg, M. and H. C. Cheng, Modern and Prospective Technologies for Hydrogen Production from Fossil Fuels, in T. N. Veziroglu and A. N. Protsenko (editors), *Hydrogen Energy Progress VII*, Vol. 2 (Pergamon Press, Oxford, 1988), pp. 699–740.
21. Muradov, N. Z., CO<sub>2</sub> Free Production of Hydrogen by Catalytic Pyrolysis of Hydrocarbon Fuels, in J. C. Bolcich and T. N. Veziroglu (editors), *Hydrogen Energy Progress XII*, Vol. 1 (International Association of Hydrogen Energy, Coral Gables, FL, 1998), pp. 523–532.

22. Steeb, H., A. Brinner, H. Bubmann, and W. Seeger, Operation Experience of a 10kW PV-Electrolysis System in Different Power Matching Modes, in T. N. Veziroglu and P. K. Takahashi (editors), *Hydrogen Energy Progress VIII*, Vol. 2 (Pergamon Press, New York, 1990), pp. 691–700.
23. Ogden, J. M. and R. H. Williams, *Solar Hydrogen: Moving beyond Fossil Fuels* (World Resources Institute, Washington, D.C., 1989).
24. Baykara, S. Z. and E. Bilgen, An Overall Assessment of Hydrogen Production by Solar Water Thermolysis, *International Journal of Hydrogen Energy*, Vol. 14, No. 12, 1989, pp. 881–889.
25. Yalcin, S., A Review of Nuclear Hydrogen Production, *International Journal of Hydrogen Energy*, Vol. 14, No. 8, 1989, pp. 551–561.
26. Willner, I. and B. Steinberger-Willner, Solar Hydrogen Production through Photo-Biological, Photochemical and Photoelectrochemical Assemblies, *International Journal of Hydrogen Energy*, Vol. 13, No. 10, 1988, pp. 593–604.
27. Das, D. and T. N. Veziroglu, Hydrogen Production by Biological Processes: A Literature Survey, *International Journal of Hydrogen Energy*, Vol. 26, No. 1, 2001, pp. 13–28.
28. Taylor, J. B., J.E.A. Anderson, K. M. Kalyanam, A. B. Lyle, and L. A. Philips, Technical and Economic Assessment of Methods for the Storage of Large Quantities of Hydrogen, *International Journal of Hydrogen Energy*, Vol. 11, No. 1, 1986, pp. 5–22.
29. Carpetis, C., Storage, Transport and Distribution of Hydrogen, in C.-J. Winter and J. Nitsch (editors), *Hydrogen as an Energy Carrier* (Springer-Verlag, Berlin Heidelberg, 1988), pp. 249–289.
30. Pottier, J. D. and E. Blondin, Mass Storage of Hydrogen, in Y. Yurum (editor), *Hydrogen Energy System, Utilization of Hydrogen and Future Aspects*, NATO ASI Series E-295 (Kluwer Academic Publishers, Dordrecht, The Netherlands, 1995), pp. 167–180.
31. Mitlitsky, F., Development of an Advanced, Lightweight, High Pressure Storage Tank for On-Board Storage of Compressed Hydrogen, in *Proc. of Fuel Cells for Transportation TOPTEC* (Alexandria, VA, SAE, Warrendale, PA, 1996).
32. Braess, H.-H. and W. Strobl, Hydrogen as a Fuel for Road Transport of the Future: Possibilities and Prerequisites, in T. N. Veziroglu *et al.* (editors), *Hydrogen Energy Progress XI*, Vol. 2 (International Association of Hydrogen Energy, Coral Gables, FL, 1996), pp. 1363–1404.
33. Schwartz, J. A. and K.A.G. Amankwah, Hydrogen Storage Systems, in D. G. Howell (editor), *The Future of Energy Gases*, U.S. Geological Survey Professional Paper 1570 (U.S. Government Printing Office, Washington, D.C., 1993), pp. 725–736.
34. Chambers, A., C. Park, R.T.K. Baker, and N. M. Rodriguez, Hydrogen Storage in Graphite Nano-Fibers, *Journal of Physical Chemistry, B*, Vol. 102, No. 22, 1998, pp. 4253–4259.
35. Dillon, A. C., K. M. Jones, and M. J. Heben, Carbon Nanotube Materials for Hydrogen Storage, in *Proc. 1996 U.S. DOE Hydrogen Program Review, Vol. II* (NREL, Golden, CO, 1996), pp. 747–763.
36. Rambach, G. and C. Hendriks, Hydrogen Transport and Storage in Engineered Glass Microspheres, in *Proc. 1996 U.S. DOE Hydrogen Program Review, Vol. II* (NREL, Golden, CO, 1996, pp. 765–772).

37. Jensen, C., Hydrogen Storage via Polyhydride Complexes, in *Proc. 1996 U.S. DOE Hydrogen Program Review*, Vol. II (NREL, Golden, CO, 1996), pp. 787–794.
38. Nornbeck, J. M., J. W. Heffel, T. D. Durbin, B. Tabbara, J. M. Bowden, and M. C. Montano, *Hydrogen Fuel for Surface Transportation* (SAE, Warrendale, PA, 1996).
39. Sternfeld, H. J. and P. Heinrich, A Demonstration Plant for the Hydrogen/Oxygen Spinning Reserve, *International Journal of Hydrogen Energy*, Vol. 14, 1989, pp. 703–716.
40. Ledjeff, K., New Hydrogen Appliances, in T. N. Veziroglu and P. K. Takahashi (editors), *Hydrogen Energy Progress VIII*, Vol. 2 (Pergamon Press, New York, 1990), pp. 1429–1444.
41. Bain, A., *The Freedom Element: Living with Hydrogen* (Blue Note Books, Cocoa Beach, FL, 2004).
42. Odum, H. T., *Systems Ecology* (John Wiley & Sons, New York, 1983).
43. Odum, H. T., Simulation Models of Ecological Economics Developed with Energy Language Methods, *Simulation*, August 1989, pp. 69–75.
44. Odum, H. T. and E. C. Odum, *Modeling for All Scales: An Introduction to System Simulation* (Academic Press, San Diego, CA, 2000).
45. Meadows, D. H., D. L. Meadows, J. Randers, and W. W. Behrens, *Limits to Growth* (Universe Books, Publishers, New York, 1972).
46. Meadows, D. H., D. L. Meadows, and J. Randers, *Beyond the Limits* (Chelsea Green, Post Mills, VT, 1991).

# Index

- AC Impedance spectroscopy 254–258  
Aciplex 75  
activation energy 38  
activation losses 40–44, 48, 49  
activation overpotential 214  
activation polarization 40–44, 48, 250  
active area 147, 150  
adiabatic compression 281  
adiabatic cooling 194  
air bleed 313, 319  
air cooling 192–193, 296, 321  
air flow rate 133, 135, 283  
alkaline fuel cell 6, 8  
ammonia 315  
anode 10, 17, 33, 48, 162, 216  
Apollo 4  
applications 13, 337–390  
Asahi Chemical 75  
Asahi Glass 75  
Audi 340  
automobiles 13, 337–352  
autothermal reformation 300, 304–312, 315, 317  
auxiliary power 283  
auxiliary power unit 342  
Avogadro's number 21  
  
back diffusion 74, 83, 134, 194, 277, 278  
back pressure regulator 116  
backup power 326, 358, 376–381, 384, 386–387  
Bacon 4  
Ballard 5, 7, 13, 15, 16, 338–340, 354, 355, 356  
  
Barrer 84, 86  
battery 299, 326, 342, 375  
Bernardi-Verbrugge model 221–227, 244  
Bernoulli equation 157  
bicycles 356  
binary diffusivity 215  
biomimetic 164, 165  
bipolar configuration 152  
bipolar plate 93, 99–108, 152, 262  
bipolar plate materials 100–102  
bipolar plate properties 100, 102  
blower 115, 280, 326  
BMW 277  
Boltzmann's constant 35  
boost converter 323, 324  
Bosnjakovic 212, 244  
buck converter 323, 324  
bulk conductivity 103–105  
bulk resistivity 103–105  
burner 289–291, 318  
bus plate 152  
buses 352–356  
Butler-Volmer equation 36, 37, 40, 209, 217, 223, 228, 231  
  
capacitor 323  
capacity factor 151, 365–367, 371, 372, 379, 381  
capital recovery factor 368  
carbon balance 309  
carbon cloth 10, 92, 93, 107  
carbon fiber paper 10, 92, 93, 107  
carbon formation 307, 308  
Carnot Efficiency 2, 26–28

- Carnot Engine 2  
 catalyst 10, 88–93  
 catalyst layer 44, 73, 74, 88–93, 216,  
   227, 233, 234, 236  
 catalyst loading 38, 89, 347  
 catalyst poisoning 312, 314–316  
 catalyst specific area 38, 89  
 catalyst support 89  
 catalyst surface 88, 89  
 cathode 10, 17, 33, 48, 162, 216  
 cell potential 47–48, 62, 148, 194, 254,  
   260, 277, 284, 351  
 charge number 222  
 charge transfer 34  
 chemical hydrides 277, 382  
 clamping force 197  
 clamping pressure 107  
 Clean Urban Transport for Europe  
   (CUTE) 353  
 closed loop system 274, 279, 280  
 CO tolerance 312–316  
 cogeneration 360, 361, 375  
 collector/sePARATOR plate 73, 99  
 combined heat and power (CHP) 360,  
   374, 375  
 combustion 300, 303, 304, 410  
 compression power 281–283  
 compressive force 199, 200, 201  
 compressor 115, 121, 280, 285–286,  
   387  
 concentration gradient 45, 83  
 concentration polarization 45, 48, 57,  
   250  
 condensation 212, 321  
 condenser 321, 322  
 conservation of charge 216–218  
 conservation of energy 211–214  
 conservation of mass 209, 214  
 conservation of momentum 210–211  
 conservation of species 214  
 contact resistance 105–108, 169, 197  
 coolant 177, 178, 294, 297, 320  
 cooling 153, 177, 178  
 cost, electricity 364, 367–370  
 cost, fuel cell 12, 151, 346, 352, 353,  
   360, 378  
 cost, natural gas 364, 367–370, 371,  
   374  
 crisscross configuration 164  
 crossover 39, 42–44, 48, 49, 54, 55  
 current density 33, 44, 47, 48, 60, 61,  
   83, 148, 169, 213, 218, 227, 232, 241,  
   249, 260, 262–264, 288, 351  
 current density distribution 227, 234,  
   242, 262  
 current density mapping 260,  
   262–264  
 current efficiency 60  
 current interrupt 252  
 DaimlerChrysler 13, 338, 341, 354,  
   356  
 Darcy coefficient 98  
 Darcy's drag force 210  
 Darcy's Law 98, 174, 209  
 DC/AC inverter 324, 325, 327, 328,  
   388  
 DC/DC converter 323–327, 388  
 dead-end mode 120, 121, 277, 278  
 deflection of MEA 169  
 DeNora 13, 340, 354, 355  
 density 189, 192, 276  
 desulfurization 300  
 dew point 127  
 diagnostics 249–266  
 diffusion coefficient 257  
 diffusion rate 47  
 diode 323, 326  
 direct methanol fuel cell 382  
 distributed power generation 15  
 Dow Chemical 75  
 Dow membrane 75, 77  
 driving schedule 344  
 drying 249, 251–252, 258–262  
 Dupont 75, 92  
 durability 352, 353  
 economics 363–376  
 edge cooling 194  
 efficiency 2, 11, 24, 25, 29, 58, 62, 121,  
   148, 151, 281, 283, 284, 292, 303,  
   306, 310, 324, 328–332, 337,  
   342–345, 352, 360, 363, 366, 371,  
   372, 377  
 ejector 121, 272  
 electrical conductivity 216  
 electrical subsystem 322–328  
 electrochemical drag 74

- electrochemical reactions 9, 10, 33, 35, 39, 44, 45, 88, 216  
 electrode 73, 88–93  
 electrokinetic permeability 222  
 electrolysis 376, 407  
 electrolyte phase potential 216, 224, 237  
 electrolyzer 379, 380, 383, 386, 388  
 electron 10  
 electroneutrality 222  
 electroosmotic drag 81, 83, 134, 194, 277, 278  
 emissions 12, 337, 345, 346, 348, 357  
 end plate 152  
 energy balance 137–142, 179, 273, 291, 294  
 Energy Partners 7  
 enthalpy, combustible gas 137  
 enthalpy, dry gas 126, 137  
 enthalpy, liquid water 126, 138, 275  
 enthalpy, moist gas 126  
 enthalpy, oxygen 273, 275  
 enthalpy, reaction 18, 20, 23  
 enthalpy, water vapor 126, 138, 273, 275  
 entropy 20, 23, 179  
 equilibrium 35  
 equivalence ratio 307–312  
 equivalent electrical circuit 253, 255  
 equivalent weight 76  
 ethylene glycol 189, 297, 320  
 evaporation 211, 212, 214, 278, 300  
 evaporation coefficient 213  
 evaporative cooling 194  
 exchange current density 35–40, 49, 52, 54, 56, 58, 217, 218, 224, 228, 232, 250, 258  
 expander 286, 287, 289, 290, 292  
 Faraday's constant 21, 35, 52, 211  
 Faraday's Law 33, 59, 118, 209  
 Fiat 340  
 Fick's Law 45, 209, 229  
 Flemion 75  
 flip-flop configuration 153  
 flooding 95, 249, 250–252, 258–261, 266  
 flow distribution 156, 160  
 flow field 93, 161–166, 170  
 flow field channels 93, 99, 162, 236  
 flow field orientation 162  
 flow field shape 162  
 flow pattern 156  
 flow-through mode 120, 121  
 Ford 338, 341, 415  
 Fourier Law of conduction 179, 196, 209  
 four-point probe method 103–104  
 fractal 164, 166  
 free convection 288  
 freezing 297, 298, 320, 350  
 frequency 254–258  
 friction coefficient 158, 159, 170, 176  
 fuel cell sizing 64–69, 149  
 fuel cell system 271–300, 318, 327–329, 337, 342, 360, 361, 375, 383  
 fuel economy 342, 343  
 fuel efficiency 348  
 fuel processor 298–312, 316–318, 329, 342, 349, 360  
 fuel utilization 60, 120, 329, 330  
 gas diffusion layer (GDL) 74, 93–98, 200, 210, 227, 231, 233, 234, 236  
 gas diffusion layer compressibility 97, 98  
 gas diffusion layer electrical conductivity 97, 213  
 gas diffusion layer permeability 97–99  
 gas diffusion layer porosity 96, 97  
 gas permeation 84–88  
 gaskets 197  
 gasoline 298, 301, 349, 359  
 Gemini 4  
 General Motors 5, 13, 258, 338–341  
 geometrical pressure loss coefficient 159, 173  
 Gibbs free energy 20–24, 28, 29, 33, 35  
 Gore-Select 78  
 graphite 100  
 graphite/composite 100–102  
 gravimetric energy density 381, 382  
 grid-integrated system 326, 362  
 Grove 4  
 Gurau, *et al.*, model 235, 245  
 Gurley number 98

- Hall sensor 263  
 Hardy-Cross method 159  
 heat balance 117, 178  
 heat conduction 179–185, 195–197  
 heat conduction through porous media 181–182  
 heat convection 179, 180, 186  
 heat dissipation 190  
 heat exchanger 278, 294, 295, 321, 322  
 heat generated 178, 192, 214  
 heat generation 181, 185  
 heat management 153, 271, 278, 294  
 heat of formation 18, 301  
 heat of reaction 17  
 heat rejection 350, 357  
 heat removal 177, 185–187  
 heat transfer 74  
 heat transfer coefficient 186, 187, 213, 321  
 heating value 18, 20, 25, 59, 60, 137, 138, 343, 381  
 helium 58, 252  
 helox 252  
 Henry's Law 226  
 high altitude aircraft 384, 388  
 high-pressure cylinder 275, 276, 348, 353, 409  
 Honda 339, 341  
 humidification 127, 129, 153, 259, 260, 274, 278, 279, 286, 292–295, 318, 321  
 humidifier 275, 278, 294, 318  
 humidity ratio 124, 125  
 hydraulic diameter 158, 170, 176  
 hydraulic permeability 211, 222  
 hydraulic permeation 83  
 hydrogen 3, 10, 18, 35, 40, 52, 121, 138, 189, 271, 275, 288, 347, 382, 387, 402–416  
 hydrogen balance 309  
 hydrogen consumption rate 59, 119  
 hydrogen economy 405–406, 420, 421  
 hydrogen energy system 405–406  
 hydrogen flow rate 133, 134  
 hydrogen permeation 44  
 hydrogen production 407  
 hydrogen solubility 85  
 Hydrogen storage 408–409  
 hydrogen sulfide 315, 316, 350  
 hydrogen, properties 276, 413, 414  
 hydrogen, safety aspects 411–416  
 Hydrogenics 15  
 hydrophilic 167  
 hydrophobic 167  
 hysteresis 251  
 Hyundai 340, 341  
 impedance 254–258  
 inductor 323  
 insulated gate bipolar transistor (IGPT) 323  
 interdigitated channels 164, 165  
 interdigitated flow field 164, 165, 242, 243  
 interfacial contact 105, 169  
 internal combustion engine 25, 343–345, 410  
 internal current 39, 42–44, 48, 49, 55, 60  
 internal humidification 154  
 isoctane 301  
 Jeng, *et al.*, model 231, 244  
 John Deere 15, 299  
 Johnson Matthey 92  
 Karman's equation 159, 174  
 Kia 340  
 Lada 340  
 laminar flow 159, 187, 188, 209  
 Laplace's equation 231, 233  
 Lewis factor 213  
 life cycle analysis 346  
 lifetime 151, 350, 377  
 limiting current density 47, 52, 55, 56, 250  
 liquid hydrogen 277, 248, 349, 414  
 Liu, H. 242, 243, 244, 245  
 load profile 151, 365, 366, 370  
 local pressure loss coefficient 159, 173  
 logarithmic mean temperature difference (LMTD) 186  
 manifold 156, 158–160, 177  
 mass balance 132, 136, 272, 278, 290  
 Mazda 339, 341  
 MEA 73, 92, 152  
 membrane 75–88

- membrane electrode assembly 73, 91, 152  
 membrane separation 300, 304  
 mesh 164, 166  
 metal hydrides 277, 248, 353, 382, 409, 411  
 metallic plates 101, 102  
 methanation 300  
 methane 300  
 methanol 298, 300, 301, 349, 350, 359  
 microporous layer 95, 96  
 Mitsubishi 340  
 Mollier diagram 127–128  
 molten carbonate fuel cells 9  
 MOSFET 323  
  
 Nafion 75–88  
 natural convection 179, 190  
 natural gas 298, 301, 308, 348, 359, 360, 407  
 Nernst equation 29, 45, 55, 252  
 net metering 328  
 neutron imaging 265–266  
 neutron magnetic resonance 82  
 Nissan 339  
 nitrogen balance 309  
 nominal cell voltage 151, 351  
 nominal operating point 149,  
 nominal power output 149, 351, 358, 379  
 Nusselt number 187–188, 191  
 Nuvera 340  
 Nyquist diagram 256, 257  
  
 Ohm's Law 44, 209, 224  
 Ohmic resistance 213, 250  
 open circuit potential 39, 50, 250  
 operating conditions 115–142, 194  
 operating pressure 115, 116, 123, 272, 284, 294, 295, 386  
 operating temperature 115–117, 178, 193, 194, 272, 274, 284, 294, 295  
 overpotential 37, 39, 40, 217, 232, 258  
 oxidation 34, 35, 40, 89  
 oxygen 3, 10, 35, 40, 57, 86, 87, 121, 138, 271, 274, 384  
 oxygen balance 309  
 oxygen concentration 122, 168, 227, 230–234, 239, 241  
 oxygen consumption rate 119  
 oxygen content 123  
 oxygen flow rate 133, 135  
 oxygen solubility 85  
  
 parasitic losses 283, 363  
 partial load 151, 363  
 partial oxidation 300, 304–312, 407  
 partial pressure 45, 124  
 perfluorocarbon-sulfonic acid ionomer 75  
 permeability 44, 84–88, 210  
 Perry Energy Systems 5  
 Perry Technologies 16, 276  
 Peugeot 340  
 phase angle 256  
 phosphoric acid fuel cell 8  
 pipe network 159  
 Planck's constant 35  
 platinum 89–93  
 platinum alloys 92  
 platinum-ruthenium catalyst 313  
 Plugpower 6  
 Poisson's ratio 170  
 polarization curve 47–59, 61–69, 147, 150, 249–252  
 polymer membrane 10  
 porous media flow field 164, 166  
 porous plate 155  
 portable power 15, 381  
 potential 20, 21, 29, 39  
 potential distribution 50–51  
 power conditioning 271, 322–328, 357, 361, 387  
 power density 61, 283, 284  
 Prandtl number 191, 192  
 preferential oxidation (PROX) 300, 311, 312, 316, 321, 329  
 pressure 28, 29, 38, 52, 56, 57, 130, 210, 218, 258, 281  
 pressure drop 131, 135, 156, 159, 160, 164, 170, 172, 174–177  
 pressure regulator 271, 277  
 propane 359  
 propylene glycol 189, 297, 320  
 Proton Energy Systems 15, 380, 390  
 proton-conductive membrane 73, 75–88,  
 protonic conductivity 76, 78–80

- pulsed field gradient 82  
 purging 120, 277, 278
- radiation 179, 180, 190  
 radiator 321, 322  
 radiotracer technique 82  
 rate determining step 36  
 Rayleigh number 191  
 reactant flow rates 118–124, 132–136  
 reactants humidity 124–132  
 reaction constant 35  
 reaction rate 33  
 recirculation mode 120, 121  
 reduction 34, 35, 40, 89, 92  
 reference electrode 40  
 reformate gas composition 311, 312, 315, 316  
 refueling station 348  
 regenerative fuel cell 383–390  
 relative humidity 124, 193, 216, 278, 293, 294  
 Renault 340  
 renewable energy 387, 389  
 resistance 39, 44, 45, 54, 55, 250–257  
 resistive losses 44–45  
 reversible fuel cell 376  
 reversible potential 36, 50, 250  
 Reynolds number 159, 172–174, 176  
 saturation pressure 124, 129  
 Schrödiger equation of motion 222  
 Schroeder's paradox 77  
 Scooters 13, 356  
 segmented cell 262–265  
 selective oxidation 311, 312  
 serpentine channels 163, 164  
 Sessile drop method 95  
 shape factor 190  
 shift reaction 300, 302–305, 311  
 Shoenbein 4  
 Siemens 16, 354  
 simple payback time 364, 367, 370–374  
 size 13, 351, 357, 378  
 solid oxide fuel cells 9  
 solid phase potential 216, 224  
 solubility 85  
 specific energy 381–383, 389  
 specific heat 22, 23, 138, 189, 192, 211, 281  
 specific power 381  
 stack number of cells 149  
 stack clamping 197  
 stack configuration 152–155  
 stack design 147–201, 351  
 stack design factor 351, 352, 381  
 stack potential 148  
 stack sizing 147–151  
 stack volume 147, 148  
 stack weight 147, 148  
 stand-alone system 362, 389  
 start-up time 357  
 static feed 385  
 stationary power 357  
 steam reformation 300–304, 407  
 Stefan-Boltzman constant 190  
 Stefan-Maxwell equations 209, 215, 224, 228  
 stoichiometric ratio 60, 119, 120, 123, 272, 282, 291, 329  
 stoichiometry 60, 121, 135, 272, 314  
 submarine 5, 16, 271, 276  
 sulphonic acid 75, 76  
 surface topography 107  
 survivability 352  
 Suzuki 340  
 Switching 323  
 symmetry factor 35  
 system design 271, 337
- Tafel equation 40, 232  
 Tafel slope 41, 52, 53, 58, 249  
 Teflon (PTFE) 75, 95  
 temperature 22, 23, 29, 38, 52, 58, 59, 76, 130, 196, 211, 218, 258, 281, 287, 298  
 temperature distribution 184, 185  
 tetrafluoroethylene 75  
 theoretical fuel cell potential 20, 21, 23  
 thermal conductivity 180, 181, 189, 192, 213  
 thermoneutral potential 60  
 three-phase boundary 89  
 thyristor 323  
 tie-rod 153, 198, 199

- Toray 97, 98  
torque 198  
Toyota 339, 341, 354, 356  
transfer coefficient 35, 37, 52, 232  
transfer current density 214, 216,  
  217  
turbine 286, 289, 290, 292  
turbulent flow 159, 187, 188  
two-phase flow 74, 240
- ultracapacitor 326, 342, 375  
Umicore 92  
uninterruptible power supply (UPS)  
  376  
UTC Fuel Cells 8, 13, 100, 339, 340,  
  355  
utility vehicles 353
- vapor content 125, 136  
velocity in channel 171, 176  
viscosity 172–174, 176, 189, 191, 192,  
  210, 213, 222  
Volkswagen 339  
voltage efficiency 60, 330  
voltage losses 39–47, 179  
voltage regulation 322–328
- W.L. Gore and Associates 75, 78, 92  
Warburg impedance 257  
water 4, 10, 76–83, 189  
water balance 138–141, 258, 295–298,  
  318–320, 350, 361  
water content 76, 79, 80, 216  
water diffusion 82  
water film 166  
water generation rate 119, 130, 131,  
  175  
water management 153, 260, 271, 278,  
  294  
water rocket 389–390  
water self-diffusion coefficient 82  
water transport 74, 80–84, 134, 210  
water uptake 76–78,  
weight 13, 351, 352, 357, 378  
Wilhemly method 95  
World energy demand forecast 400  
World energy production 400
- You-Liu model 228, 244  
Young's modulus 170
- Zawodzinski 76, 80–81, 82, 83, 90, 108  
zig-zag configuration 153